METABOLIC FLUX ANALYSIS OF MAMMALIAN CELL METABOLISM USING MULTIPLE ISOTOPIC TRACERS AND MASS SPECTROMETRY

by

Woo Suk Ahn

A dissertation submitted to the Faculty of the University of Delaware in partial fulfillment of the requirements for the degree of Doctor of Philosophy in Chemical Engineering

Summer 2012

METABOLIC FLUX ANALYSIS OF MAMMALIAN CELL METABOLISM USING MULTIPLE ISOTOPIC TRACERS AND MASS SPECTROMETRY

by

Woo Suk Ahn

Approved: _____
Abraham M. Lenhoff, Ph.D.
Chair of the Department of Chemical and Biomolecular Engineering

Approved: _____
Babatunde A. Ogunnaike, Ph.D.
Interim Dean of the College of Engineering

Approved: _____
Charles G. Riordan, Ph.D.
Vice Provost for Graduate and Professional Education

I certify that I have read this dissertation and that in my opinion it meets the academic and professional standard required by the University as a dissertation for the degree of Doctor of Philosophy.

Signed: _____

Maciek R. Antoniewicz, Ph.D.
Professor in charge of dissertation

I certify that I have read this dissertation and that in my opinion it meets the academic and professional standard required by the University as a dissertation for the degree of Doctor of Philosophy.

Signed: _____

Eleftherios T. Papoutsakis, Ph.D.
Member of dissertation committee

I certify that I have read this dissertation and that in my opinion it meets the academic and professional standard required by the University as a dissertation for the degree of Doctor of Philosophy.

Signed: _____

Kelvin H. Lee, Ph.D.
Member of dissertation committee

I certify that I have read this dissertation and that in my opinion it meets the academic and professional standard required by the University as a dissertation for the degree of Doctor of Philosophy.

Signed: _____

Michael J. Betenbaugh, Ph.D.
Member of dissertation committee

ACKNOWLEDGMENTS

This dissertation is the results for four years in Department of Chemical Engineering, University of Delaware. It was a great honor that I studied in the top school. I give great thanks to the department. A lot of people supported this study. First, I would like to thank Prof. Maciek Antoniewicz for his wonderful mentoring and support. He is one of the best advisors who I have met. Prof. Eleftherios Papoutsakis and Prof. Kelvin Lee gave valuable advice to me and help for successful completion of PhD degree, and I always feel happy to meet great three mentors in this department. And, it is a great fortune that I met Prof. Michael Betenbaugh, top leader of cell culture engineering. I am sincerely grateful for his support and interests. I acquired valuable insights in this field through vivid discussion and questioning with lab members, Jungik Choi, Robert Leighty, Scott Crown, Aditi Swarup and Jennifer Au and I am very thankful to them.

My family has been my strong motivation and supporters in my life. My wife, Eunhye Ha is a wonderful woman as a wife, mother for two boys, excellent singer and pianist with great talents, and wonderful friend in life. I am pleased to see my two boys, Hyunjun Ahn and Minjun Ahn. They are always good boys to parents and show brilliant achievements in US. Every day our families in Korea always pray to God for us: Dr. Youngwoong Ha, Kyunghee Lee and Ilkuk Ha in Won-ju city. Eunhyun Ha and Byungwon Choi in In-cheon city, and Donghyun Ahn and Yongsook Lee, in Yang-ju city. Kiesoon Ahn, Dr. Jaedoe Nam, and Yoonhwan Ahn in Seoul city. All is my lovely families. Always God guides me right way.

TABLE OF CONTENTS

LIST OF TABLES

LIST OF FIGURES

ABSTRACT

Metabolic flux analysis (MFA) is a powerful technology to characterize intracellular metabolism in living cells using isotopic tracers and mass spectrometry. Therefore, in the past two decades, MFA techniques have been developed to study biological systems. However, the applications of MFA for mammalian cells have been limited due to the complexity of cellular metabolism even though mammalian cells are key platforms for biopharmaceutical production and biomedical research. Here, we present two applications for glycolysis and gluconeogenesis systems. First, we describe the analysis of metabolic fluxes in CHO metabolism at fed-batch mode. We established two metabolic models of CHO cells for non-stationary and stationary ^{13}C-MFA. It was found that cellular metabolism in CHO cells were significantly rewired from exponential growth to stationary phases during culture. The results provide a solid foundation for applications such as cell line development and medium optimization. Second, we describe gluconeogenesis metabolism of Fao rat hepatoma cells perturbed by transcription factors. Using multiple isotopic tracers and combined ^{13}C-MFA, we observed the regulations of metabolic fluxes by transcriptional activators and inhibitors for gluconeogenesis metabolism. The discovery and the applied MFA techniques can allow us to evaluate the pharmaceutical drug for metabolic disease, e.g. Type II diabetes. And finally, we provide the comprehensible procedures to be considered for ^{13}C-MFA technique: isotopic and metabolic stationarity, isotopic tracer design, key measurements, multiple isotopic tracers and model validation.

Chapter 1

INTRODUCTION

In this thesis, ^{13}C-metabolic flux analysis (^{13}C-MFA) was applied to elucidate mammalian cell metabolism of Chinese hamster ovary (CHO) and Fao rat hepatoma cells. To provide background on the estimation techniques used and cellular metabolism in general, ^{13}C-MFA and mammalian cell metabolism are reviewed in this chapter. First, the technology of MFA is divided into classical MFA based on stoichiometric balancing and ^{13}C-MFA based on stoichiometric and isotopomer balancing. ^{13}C-MFA is classified into isotopic stationarity of labeled metabolites and metabolic stationarity of cellular fluxes. Second, general metabolism of mammalian cells is reviewed using a representative cell line, CHO cells, which is the main platform to produce bio-therapeutics (Walsh, 2010).

1.1 Methods for Metabolic Flux Analysis (MFA)

In the past decade, a number of new MFA techniques have become available to the scientific community for estimating *in vivo* metabolic fluxes. Here, we provide an overview of these different MFA techniques. Figure 1.1 shows the classifications of the various MFA methods that have been developed, or are currently under development. The two main distinguishing characteristics between the different MFA methods are: i) whether stable-isotope tracers (such as ^{13}C) are applied or not; and ii) whether metabolic steady state is assumed for the system or not.

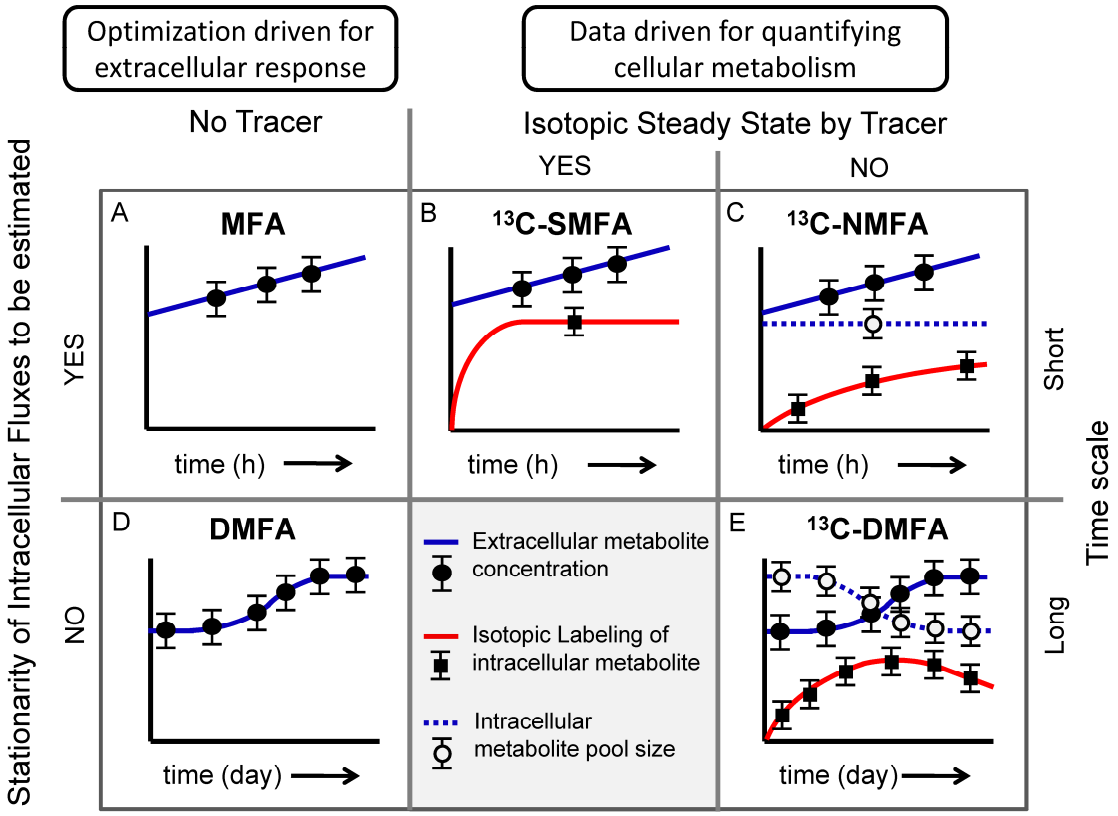

Figure 1.1 Classifications of metabolic flux analysis. They were separated by two assumptions of metabolic (blue line) and isotopic stationarity (red line) according to time and required measurement points. Under metabolic steady-state; (A) classical MFA, (B) ^{13}C-MFA on isotopic steady state and (C) ^{13}C-NMFA on isotopic non-stationarity. Under metabolic and isotopic non-stationarity: (D) DMFA using extracellular time-course measurements and (E) ^{13}C-DMFA using time-course measurements of extracellular fluxes and ^{13}C-labeled isotopomers

1.1.1 Flux Analysis at Metabolic Steady State Using MFA

The key point to calculate metabolic fluxes in living cells using classical MFA (Figure 1.1A) is that the biological system can be characterized with an integrated biochemical network model, rather than a set of individual reactions. The MFA method relies on balancing fluxes around metabolites within an assumed metabolic network model. The first step in the analysis is to express the biochemical network model as a stoichiometric matrix in which rows represent balanced intracellular metabolites and columns represent metabolic fluxes in the model. By assuming metabolic (pseudo) steady state for intracellular metabolites, fluxes are constrained by the stoichiometry matrix:

$$S \times v = 0 \tag{1.1}$$

To estimate metabolic fluxes, the stoichiometric constraints are complemented with measurements of external metabolic rates such as substrate uptake and product accumulation rates:

$$R \times v = r \tag{1.2}$$

The combined system of equations 1 and 2 is then solved using simple linear least-squares regression. Using MFA, metabolic fluxes can be estimated in systems that are fully determined (i.e. containing all the necessary external rate measurements), or overdetermined (i.e. with redundant external flux measurements). The main advantage of MFA is that it is easy to apply and accessible to most researchers, since it only requires simple linear algebra (Bonarius et al., 1997; Vallino and Stephanopoulos, 1993; Zupke and Stephanopoulos, 1995) and relies on relatively robust measurements of extracellular metabolites. A limitation of MFA for analysis of most biological systems, however, is that the number of constraints (stoichiometric and rate measurements) is often insufficient to observe all important intracellular

metabolic pathway fluxes (Bonarius et al., 1997; Klamt et al., 2002). To make the system fully determined additional assumptions are needed, for example, by leaving out specific pathways that are assumed to carry little or no flux, or by including cofactor balances (e.g. NADH, NADPH and ATP balances) as additional constraints. The use of cofactor balances, however, is generally not encouraged for MFA. The presence of several isoenzymes that have alternative cofactor requirements, e.g. NADH- and NADPH-dependent malic enzymes, and uncertainties regarding transhydrogenase activity and futile cycles renders these cofactor balances uninformative. In some studies, NADH and NADPH were lumped together (Bonarius et al., 1996; Nyberg et al., 1999b) and rates of CO_2 and NH_3 production and O_2 consumption were used as additional constraints to make the system observable (Nyberg et al., 1999b; Zupke and Stephanopoulos, 1995). The classical MFA technique has been successfully applied to study metabolism of many mammalian cell lines, including murine hybridoma (Bonarius et al., 1998b; Follstad et al., 1999; Gambhir et al., 2003; Paredes et al., 1998; Zupke and Stephanopoulos, 1995), CHO (Altamirano et al., 2001), baby hamster kidney (BHK) (Cruz et al., 1999), and human kidney fibroblasts (Henry et al., 2005; Nadeau et al., 2000).

1.1.2 Flux analysis at Metabolic and Isotopic Steady State Using ^{13}C-MFA

^{13}C-MFA is a more advanced technique for estimating metabolic fluxes at metabolic steady state (Figure 1.1B) that makes use of ^{13}C-labeled tracers, isotopomer and metabolite balancing, and ^{13}C-labeling measurements using techniques such as NMR (Marx et al., 1999; Szyperski, 1995), mass spectrometry (Antoniewicz et al., 2011; Antoniewicz et al., 2007c; Christensen and Nielsen, 2000; Dauner and Sauer, 2000; Hofmann et al., 2008; Klapa et al., 2003), and tandem mass spectrometry (Choi

and Antoniewicz, 2011; Jeffrey et al., 2002; Kiefer et al., 2007). In ^{13}C-MFA, cells are cultured for an extended period of time (typically >3 h) in the presence of a specifically labeled ^{13}C-tracer, e.g. [1,2-^{13}C]glucose, which results in the incorporation of ^{13}C-atoms into metabolic intermediates and metabolic products. The measured ^{13}C-labeling distributions is highly dependent on the relative values of intracellular metabolic fluxes because mass isotopomer distributions labeled by tracers are changed by atom transition in reaction network such as reversible reactions containing forward and backward fluxes, reactions for branch point and parallel reactions. Therefore, these ^{13}C-labeling measurements can be used as additional constraints to estimate fluxes, which are called isotopomer balances. In ^{13}C-MFA, a non-linear least-squares regression problem is solved:

$$\min \mathrm{SSR} = \sum \frac{(x-x_m)^2}{\sigma_x^2} + \sum \frac{(r-r_m)^2}{\sigma_r^2} \qquad (1.3)$$

$$\text{s.t.} \quad f_{\text{isotopomer model}}(v, x) = 0$$

The goal of ^{13}C-MFA is to find a set of feasible intracellular metabolic fluxes that minimize the variance-weighted sum of squared residuals (SSR) between the measured and predicted values of ^{13}C-labeling data from intracellular metabolites and extracellular input and output rates. Fundamental assumptions for ^{13}C-MFA are metabolic and isotopic steady states; that is, metabolic fluxes and isotopic distributions are assumed to be constant in time. The time required to reach isotopic steady state in a system depends on several factors: (i) the metabolic activity of cells; (ii) metabolite pools to be sampled, (iii) substrates to be used as tracers, and (iv) media metabolites to be interacted with cellular metabolites. For example, glycolytic intermediates may reach isotopic steady state within 3 h following the introduction of ^{13}C-labeled glucose, but TCA cycle intermediates may require more than 24 h to approach isotopic

steady state (Maier et al., 2008; Sengupta et al., 2011; Young et al., 2008). On the other hand, for [U-^{13}C]glutamine, TCA cycle intermediates typically reach isotopic steady state within 3 h, but it may take much longer for glycolytic intermediates to approach isotopic steady state. In Chapter 4 of this study, most of glycolytic metabolites were not labeled during 12 h culture after addition of [U-^{13}C]glutamine. The reason is that key catabolic enzymes between TCA cycle and glycolysis, phophoenolpyruvate carboxykinase (PEPCK) were not active in CHO cells. In contrast, glycolytic metabolites reached isotopic steady state within 4 h after addition of [U-^{13}C]glutamine using Fao rat hepatoma cells in Chapter 6. This suggests that dynamics for labeling is highly dependent on the applied system.

The main advantage of ^{13}C-MFA is the large number of redundant measurements that can be obtained for flux estimation. For example, using GC-MS one can easily obtain more than 100 isotopomer measurements to estimate on the order of ~5-10 unknown net fluxes in the model. Thus, with so many redundant measurements, the accuracy and precision of flux estimates are greatly improved, and level of confidence in the final flux result is much higher compared to classical MFA. Furthermore, more complex metabolic network models can be composed and investigated using ^{13}C-MFA (Boghigian et al., 2010; Wittmann, 2007). For example, it is possible to estimate parallel metabolic pathways (e.g. pentose phosphate pathway and glycolysis), cyclic pathways (e.g. pyruvate cycling), and bidirectional reversible fluxes (Bonarius et al., 1998a; Schmidt et al., 1998; Wiechert, 2001). The reversible reaction consists of forward and backward fluxes in ^{13}C-MFA. Wiechert proposed net and exchange fluxes (Eq. 1.4) instead of forward and backward fluxes (Wiechert and de Graaf, 1997). This definition of reversible flux was used for this study.

$$v_n^{net} = v_n^{\rightarrow} - v_n^{\leftarrow} \quad (1.4)$$

$$v_n^{exch} = \min(v_n^{\rightarrow}, v_n^{\leftarrow})$$

Additional applications of the ^{13}C-MFA technique include validation of proposed network models and elucidation of stereochemistry of unknown metabolic reactions (Beste et al., 2011; Crown et al., 2011; Moxley et al., 2009).

While ^{13}C-MFA is certainly more powerful for estimating *in vivo* metabolic fluxes than classical MFA, it is also much more computationally intensive. Solving large sets of non-linear isotopomer balances for intracellular metabolites is not trivial, and the non-linear nature of the least-squares regression problem requires iterative algorithms. In the past decade, several mathematical approaches have been developed to reduce the computational burden of ^{13}C-MFA. The first modeling framework for simulating intracellular ^{13}C-labeling distributions was proposed by Zupke and Stephanopoulos based on atom mapping matrices (Zupke and Stephanopoulos, 1994). In subsequent years improved modeling approaches were introduced based on isotopomer balancing (Schmidt et al., 1997), cumomer balancing (Wiechert et al., 1999), bondomer balancing (van Winden et al., 2002), and most recently, elementary metabolite units (EMU) balancing (Antoniewicz et al., 2007b). Currently, the EMU modeling approach is the most advanced and computationally efficient method for simulating isotopic labeling distributions in metabolic network models. It was shown that EMU simulations are typically several orders of magnitude more efficient than equivalent isotopomer and cumomer simulations (Antoniewicz et al., 2007b). For statistical analysis of flux results, flux confidence intervals must be calculated using advanced statistical analysis methods that consider the inherent system nonlinearities (Antoniewicz et al., 2006a), or alternatively using computationally intensive Monte Carlo simulations (Yang et al., 2005). Several powerful software packages were

recently developed for ^{13}C-MFA based on the EMU modeling framework, such as Metran (Yoo et al., 2008) and OpenFlux (Quek et al., 2009).

The ^{13}C-MFA technique also requires precise and unbiased ^{13}C-labeling measurements. Since small errors in labeling measurements can translate to large errors in the estimated fluxes, the ^{13}C-labeling measurements must be as accurate and precise as possible and Antoniewicz et al. suggested that the measurement errors of mass isotopomer distribution (MID) should be less than 0.5 mol% (Antoniewicz et al., 2007a). In the early years of ^{13}C-MFA, the NMR technique was often used for measuring ^{13}C-labeling, however, in recent years, mass spectrometry based techniques such as GC-MS and LC-MS have gained more attention due to their higher sensitivity, lower capital cost and lower operational cost (Wittmann, 2002). In the past years, ^{13}C-MFA has been successfully applied in several mammalian cell lines, including CHO (Goudar et al., 2010), hybridoma (Bonarius et al., 1998a; Zupke and Stephanopoulos, 1995), HEK-293 (Henry and Durocher, 2011), adipocytes (Yoo et al., 2008), and hepatocytes (Maier et al., 2008).

1.1.3 Flux Analysis at Isotopic Non-steady State Using ^{13}C-NMFA

The requirement of isotopic steady state places significant limitations on the use of ^{13}C-MFA for studying mammalian cell metabolism. As indicated above, the time required to reach isotopic steady state can be on the order of hours, or even days in mammalian cells (Maier et al., 2008; Sengupta et al., 2011; Young et al., 2008). To solve this issue, Young et. al. developed the isotopic non-stationary ^{13}C-NMFA method (Figure 1.1C) (Young et al., 2008). In ^{13}C-NMFA, metabolic fluxes are estimated at metabolic (pseudo) steady state, i.e. assuming constant fluxes and metabolite pools, and using transient ^{13}C-labeling data (Wiechert and Nöh, 2005):

$$\min \mathrm{SSR} = \sum \frac{(x(t) - x(t)_m)^2}{\sigma_x^2} + \sum \frac{(r - r_m)^2}{\sigma_r^2} \quad (1.5)$$

$$\text{s.t.} \quad C \times \frac{dx}{dt} = f_{\text{isotopomer model}}(v, x)$$

$$S \times v = 0$$

As part of the parameter estimation procedure, ordinary differential equations (ODE) of isotopomer balances are numerically integrated to simulate isotopomer distributions as a function of time. The non-linear least-squares regression techniques employed for parameter estimation in ^{13}C-NMFA are similar to ^{13}C-MFA. In addition to estimating metabolic fluxes, metabolite pool sizes are fitted in ^{13}C-NMFA to account for the observed labeling transients. The computational time for ^{13}C-NMFA is significantly increased compared to ^{13}C-MFA. Fortunately, the application of EMU modeling framework has reduced the computational time to less than an hour for typical metabolic networks of central metabolism, which is about a 5000-fold improvement compared to equivalent isotopomer/cumomer simulations (Young et al., 2008). ^{13}C-NMFA was recently successfully applied to study CHO cell metabolism in a fed-batch culture in Chapter 3 (Ahn and Antoniewicz, 2011).

1.1.4 Flux Analysis at Metabolic Non-steady State Using DMFA

The next generation in flux analysis is to estimate dynamic metabolic fluxes at metabolic non-steady state (Figure 1.1D). In recent years, initial attempts have been undertaken to develop techniques for dynamic metabolic flux analysis (DMFA) of systems that are not at metabolic steady state (Lequeux et al., 2010; Llaneras and Picó, 2007; Niklas et al., 2011b). The objective of DMFA is to determine metabolic shifts during a culture from analysis of time-series of extracellular measurements. Current DMFA methods generally assume that flux transients are slow, i.e. on the order of

hours, compared to the time required to reach (pseudo) steady state for intracellular metabolites, which is typically on the order of seconds to minutes. With this assumption, three steps are needed to determine flux transients from time-series of extracellular measurements: (i) the experiment is divided into discrete time intervals; (ii) average external rates are calculated for each time interval by taking derivatives of external concentration measurements; and (iii) fluxes are calculated for each time interval using classical MFA. The results of these steady state models, evaluated at different time points, are then combined to obtain a time profile of flux transients during a culture. An alternative to the step (i) is to apply data smoothing on extracellular measurements using, for example, splines (Niklas et al., 2011b), linear (Provost and Bastin, 2004), or polynomial fitting (Lequeux et al., 2010), and then take derivatives of the smoothed data to increase time resolution of the estimated flux dynamics (Niklas et al., 2011b).

The main advantage of DMFA is that it provides information on metabolic shifts that cannot be obtained using classical MFA, with only modest additional experimental effort. The computational effort is also relatively low, especially compared to ^{13}C-MFA. However, since DMFA is based on metabolite balancing alone, the method carries the same limitations as MFA for resolving intracellular pathway fluxes. As such, DMFA cannot resolve parallel pathways, cyclic pathways and reversible reactions. Recently, DMFA was successfully applied to study metabolic shifts in CHO cells (Provost and Bastin, 2004) and in a human cell line (Niklas et al., 2011b).

1.1.5 Flux Analysis at Metabolic and Isotopic Non-steady State Using ^{13}C-DMFA

A logical extension to the DMFA framework is to incorporate dynamic isotope labeling measurements to allow estimation of intracellular fluxes of cyclic pathways, parallel pathways and reversible reactions that cannot be determined using extracellular measurements alone. Methods for ^{13}C-DMFA (Figure 1.1E) are still underdeveloped and there is an obvious need for more research and development in this area to acquire more accurate solutions and more practical applications. An example of ^{13}C-DMFA was reported that dynamic fluxes were analyzed for a fed-batch fermentation of *E. coli* that overproduced 1,3-propanediol (Antoniewicz et al., 2007c). In that study, metabolic fluxes were determined at 20 time points during the culture using local external rate measurements and ^{13}C-labeling dynamics of proteinogenic amino acids. To account for transients in isotopic labeling of ^{13}C-glucose in the medium and proteinogenic amino acids, two dilution parameters were introduced, termed D- and G-parameters, in analogy with the isotopomer spectral analysis (ISA) modeling framework (Kelleher and Masterson, 1992). Using this approach, metabolic flux distributions were estimated and it was identified the metabolic shifts during the fed-batch fermentation. However, this technique projected dynamic fluxes combining discrete data by numerous flux estimations in time series by stationary ^{13}C-MFA under the assumption of pseudo isotopic and metabolic steady sate. Thus, it is limited to biological systems with high metabolic activity such as *E.coli*. A general ^{13}C-DMFA technique applicable for intrinsic non-stationary systems has not been reported yet.

1.2 Overview of Metabolism in Mammalian Cells

In this section, we provide on the overview of the central metabolic pathways in CHO cells and related mammalian cells. The following pathways are reviewed: glycolysis and lactate production; anaplerosis and cataplerosis; pentose phosphate pathway; glutaminolysis and TCA cycle; and amino acid metabolism.

1.2.1 Glycolysis and Lactate Production

Mammalian cells can utilize glycolysis, TCA cycle and oxidative phospholylation to generate energy from glucose with a maximum yield of 36 mol ATP per mol glucose. Normally under hypoxic conditions, the carbon flow at the pyruvate branch point can be diverted to lactate production, as redox neutral is controlled by conversion of glucose to lactate, i.e. there is no net production or consumption of NADH or NADPH. However, most of mammalian production cells lines such as CHO cells or cancer cells metabolize glucose to lactate regardless of the level of oxygen supply, which has been termed “the Warburg Effect”, or aerobic glycolysis (Warburg, 1956). Aerobic glycolysis is an inefficient metabolic phenotype, since only 4 mol ATP per mol glucose are generated in the conversion of glucose to lactate (Vander Heiden et al., 2009). Vander Heiden et al. hypothesized that proliferating cells utilize excess lactate production as a more effective means of achieving fast growth under nutrient rich conditions (Vander Heiden et al., 2009). The typical yield of lactate on glucose ranges between 1 to 2 (mol/mol) in human (Maranga and Goochee, 2006), BHK (Cruz et al., 1999), hybridoma (Ozturk and Palsson, 1991) and CHO cells (Yoon et al., 2005). A high concentration of glucose in the medium tends to increase glucose consumption and leads to increased lactate production (Ljunggren and Häggström, 1994; Wheeler and Hinkle, 1985). In cell

cultures, high levels of accumulated lactate can inhibit cell growth and product formation (Cruz et al., 2000; Lao and Toth, 1997). It was reported that lactate inhibition is related to acidification of the medium and to elevated osmolarity (Omasa et al., 1992; Ozturk et al., 1992). To reduce lactate formation, glucose-limiting feeding strategies have been employed (Europa et al., 2000; Kurokawa et al., 1994; Ljunggren and Häggström, 1994). Zhou et al. reported that cellular metabolism was improved in fed-batch cultures when glucose feeding was controlled by on-line measurement of oxygen uptake rate (Zhou et al., 1995). The yield of lactate produced per glucose consumed ($\Delta L/\Delta G$) decreased from 1.16 mol/mol to 0.16 mol/mol, which dramatically reduced by-product accumulation and improved process performance (Europa et al., 2000; Gambhir et al., 2003). Similar metabolic shifts were investigated at the transcriptional and translational levels (Korke et al., 2004; Seow et al., 2001). Comparison of high and low $\Delta L/\Delta G$ conditions revealed that glucose-related genes were down-regulated when lactate production was low. It was concluded that the metabolic shifts were likely an adaptation of cellular metabolism to new environmental conditions through a yet unknown regulatory mechanism.

The rate of glycolysis also depends on other environmental factors. For example, stimulation by growth factors can regulate glucose transporter (GLUT), hexokinase (HK) and phosphofructokinase (PFK) activity via PI3K/AKT activation (Vander Heiden et al., 2009). HK is the initial step in the conversion of glucose to glucose-6-phosphate (G6P), which is a key branch point for glycolysis, pentose phosphate pathway and glycogen storage (Wilson, 2003). Since intracellular glucose and lactate concentrations, i.e. at the two end points of glycolysis, are much higher than the intermediates G6P, fructose 6-phosphate (F6P), phosphoenolpyruvate (PEP),

and pyruvate, hexokinase has been considered one of the rate-limiting steps in glycolysis (Fitzpatrick et al., 1993; Neermann and Wagner, 1996). Recently, HK2 was identified as a key mediator of aerobic glycolysis (Wolf et al., 2011). In cancer cells, the Warburg Effect has been attributed to the activity of an alternative splice isoform of pyruvate kinase M2-PK (Christofk et al., 2008).

1.2.2 Reactions Connecting Glycolysis and TCA Cycle

Neermann and Wagner determined cell specific enzyme activities of glucose metabolism in BHK-21, CHO-K1 and hybridoma cell lines (Neermann and Wagner, 1996), and Fitzpatrick et al. measured metabolic activities in batch cultures of murine hybridoma cells (Fitzpatrick et al., 1993). None of the cell lines showed activities of PEPCK, PC and PDH that connect glycolysis and the TCA cycle. It appears that these three enzymes have low activities in most mammalian production cell lines. Since most of the glucose carbons flow to lactate via LDH, and low activity of PC (Fitzpatrick et al., 1993; Neermann and Wagner, 1996; Petch and Butler, 1994; Vriezen and van Dijken, 1998) hampers the catabolic carbon flow to the TCA cycle, knock-down of LDH and overexpression of PC were natural targets for cell engineering (Dinnis and James, 2005). Irani et al. introduced cytosolic pyruvate carboxylase from *S. cerevisiae* (PYC2) into BHK-21 cell lines, achieving higher intracellular ATP levels and lower yield of lactate on glucose (Irani et al., 1999), and a 2-fold improvement in human erythropoietin (EPO) production (Irani et al., 2002). The PYC2 gene was also introduced into human HEK-293 (Elias et al., 2003) and CHO-K1 cells (Fogolín et al., 2004), and a human PC gene was introduced into CHO-DG44 cells (Kim and Lee, 2007b), all resulting in improved cell culture performance. To further reduce lactate secretion the LDH-A gene was disrupted in hybridoma cells

(Chen et al., 2001), and partially suppressed using RNAi techniques in CHO cells (Jeong et al., 2006; Kim and Lee, 2007a).

1.2.3 Pentose Phosphate Pathway

The pentose phosphate pathway (PPP) has two distinct branches, the oxidative branch (oxPPP), and non-oxidative branch (noxPPP) (Vander Heiden et al., 2009). In oxPPP, G6P is converted to ribose-5-phoshpate (R5P) via glucose-6-phosphate dehydrogenase (G6PD) and phophogluconate dehydrogenase (6PD), which generate CO_2 and 2 NADPH. In noxPPP, R5P is also synthesized via transketolase (TK) and transaldolase (TA) without generating CO_2 or NADPH. The metabolic intermediate R5P is a key precursor for nucleotide synthesis. Thus, G6PD and TK are important enzymes for proliferating cells located at the branch point between oxPPP and noxPPP (Furuta et al., 2010). G6PD is a rate-limiting enzyme for oxPPP and is controlled by the NADPH redox status (Tian et al., 1998). Tuttle et al. reported that G6PD-deficient CHO cells were susceptible to apoptosis (Tuttle et al., 2000), and Fico et al. showed that embryonic stem (ES) cells with G6PD-deficiency were more sensitive to oxidative stress (Fico et al., 2004). Thus, oxPPP was shown to be important not only for biosynthesis but also for responding to oxidative stress (Vander Heiden et al., 2009). Interestingly, the p53 regulatory gene has two roles related to apoptosis and response to oxidative stress. In order to reduce reactive oxygen species (ROS), it stimulates oxPPP shunt for NADPH production via *TIGAR* expression that activates oxPPP by inhibition of phosphofructokinase (PFK) (Bensaad et al., 2006). The generated NADPH is used for reducing oxidized glutathione (GSSH) to glutathione (GSH) to remove ROS (Bensaad et al., 2006; Fico et al., 2004; Tian et al., 1999). At the same time, TK is also up-regulated in proliferating cell (Furuta et al., 2010). Using

TK inhibitor oxythiamine (Brin, 1962) and [1,2-^{13}C]glucose tracer (Lee et al., 1998), ribose isolated from RNA in pancreatic adenocarcinoma cells was analyzed by GC-MS. The results indicated that 85% of *de novo* ribose synthesis was derived from noxPPP (Boros et al., 1997). Recently, it was also reported that transketolase-like gene 1 (TKTL1) has an important role in nucleic acid synthesis through noxPPP (Chen et al., 2009). Taken together, these studies demonstrate that both oxPPP and noxPPP play a significant role in proliferating mammalian cells.

1.2.4 Glutaminolysis and TCA Cycle

In addition to glycolysis, glutaminolysis plays a central role in energy generation and anaplerosis in mammalian cell lines. Glutaminolysis is defined as the conversion of glutamine to pyruvate via TCA cycle, malate-aspartate shuttle and malic enzyme. The first step in glutaminolysis is the conversion glutamine to glutamate by glutaminase (GLNase) (Curthoys and Watford, 1995). Glutamate is then converted to α-ketoglutarate via deamination or transamination. Alanine aminotransferase (AlaAT) transfers the amine group of glutamate to pyruvate to form α-ketoglutarate and alanine, and aspartate aminotransferase (AspAT) catalyzes the conversion of glutamate and oxaloacetate to α-ketoglutarate and aspartate. Metabolism of glutamine to AKG can produce two ammonium molecules. Street et al. showed that almost all of the ammonium produced by HeLa and CHO cells was released from the amide group of glutamine and most of alanine and glutamate were labeled from the amine group of glutamine, using glutamine tracers with ^{15}N-labeled amide or amine groups (Street et al., 1993). These findings suggest that a significant fraction of accumulated ammonium is generated from glutamine decomposition and by glutaminase reaction and that most of α-ketoglutarate is derived via transamination rather than by glutamate

dehydrogenase (GDH). In contrast, Martinelle et al. reported that metabolism via GDH was increased 5- to 8-fold in hybridoma cultures under glucose-starved condition using $^{1}H/^{15}N$ NMR and ^{15}N-labeled glutamine, thus suggesting that regulation of GLNase and GDH is sensitive to glucose availability (Martinelle et al., 1998).

Glutamine is an unstable medium component, where it easily decomposes to pyrrolidone-carboxylic acid and ammonium (Tritsch and Moore, 1962). The decomposition rate is dependent on the pH (Lin and Agrawal, 1988; Ozturk and Palsson, 1990), temperature (Tritsch and Moore, 1962) and phosphate concentration (Bray et al., 1949). For example, Ozturk and Palsson showed that the actual uptake of glutamine in hybridoma cell culture was 3-fold lower than the apparent uptake (Ozturk and Palsson, 1990). Ammonium that is released via glutaminolysis and glutamine decomposition is a toxic by-product in mammalian cell cultures. Ammonium can accumulate to levels up to 2-10 mM in batch cultures (Ozturk et al., 1992), and can negatively affect cell growth (Hassell et al., 1991; McQueen and Bailey, 1990; Singh et al., 1994; Yang and Butler, 2000a), protein production (Hansen and Emborg, 1994) and protein glycosylation (Andersen and Goochee, 1995; Borys et al., 1994; Thorens and Vassalli, 1986; Yang and Butler, 2000b; Yang and Butler, 2002). Schneider et al. suggested that alanine aminotransferase (AlaAT) and aspartate aminotransferase (AspAT) reactions act as a detoxification process via ammonium removal (Schneider et al., 1996). In support of this, it was observed that under ammonium-stressed conditions fluxes of AlaAT and AspAT were increased, proline production was increased, and glutamate production was reduced (Bonarius et al., 1998b). To reduce ammonium accumulation by cell engineering efforts, glutamine synthetase (GS) gene

has been overexpressed in CHO (GS-CHO) and NS0 (GS-NS0) cells (Bebbington et al., 1992; Cockett et al., 1990). GS activity is normally relatively low in CHO, hybridoma, BHK and HeLa cell lines (Fitzpatrick et al., 1993; Jenkins et al., 1992; Neermann and Wagner, 1996; Street et al., 1993; Yallop et al., 2003). Cell lines overexpressing GS can be successfully cultured in glutamine-free media (Birch and Racher, 2006).

1.2.5 Amino Acid Metabolism

Mammalian cells depend on uptake of essential amino acids for protein biosynthesis and cell growth, and in theory can utilize all amino acids for catabolism. Insight into amino acid metabolism can be obtained from direct measurements of the uptake and production rates and from ^{13}C-labeling experiments. Assuming that the biomass composition for a cell line is known, one can easily calculate the fractions of amino acids utilized for catabolism and anabolism, respectively (Martens, 2007). Recently, we studied amino acid metabolism in CHO-K1 cells using [U-^{13}C]glucose and [U-^{13}C]glutamine tracers. From ^{13}C-labeling measurement of intracellular and extracellular amino acids we identified several amino acids that acquired ^{13}C-labeling, including alanine, serine, glycine, aspartate, glutamate, glutamine and proline. Using ^{13}C-MFA and additional ^{13}C-labeling measurements from TCA cycle intermediates, it was possible to establish detailed flux map of amino acid metabolism in CHO cells as explained in Chapter 3.

1.3 Aim and Outline of Thesis

As highlighted in this introduction chapter, ^{13}C-MFA has been well established based on GC-MS measurements, isotopic tracer experiments and mathematical framework of isotopomer matrix for computation. However, real application of ^{13}C-MFA is still challenging to estimate metabolic fluxes in mammalian cell due to the complexity of cellular metabolism (Ahn and Antoniewicz, 2012). To advance the frontiers of ^{13}C-MFA, two topics were selected in this thesis to evaluate mammalian cell metabolism using ^{13}C-MFA, to suggest metabolic models and experimental methods using multiple isotopic tracers and GC-MS analysis, and significantly to apply to industrial and biomedical relevant problems. First, as a glycolysis system, the metabolism of CHO cells was investigated during culture and compared at the exponential and stationary (non-growth) phases. The reason for CHO study is that CHO cells are a key platform to produce bio-therapeutics in biotechnology and pharmaceutical industry and also metabolic change during culture is an interesting topic to maximize protein production in cell culture engineering field. Second, as a gluconeogenesis system, Fao rat hepatoma cell line was cultured in the glucose-free media to produce glucose. This system mimicked glucose production in liver and was developed for the study of Type II diabetes. As such, metabolic model of ^{13}C-MFA can be used for biomedical and pharmaceutical applications, e.g. evaluation for the disease and drug screening for diabetes remediation.

In addition to applications for cell culture engineering and biomedical research, the second aim of this thesis research is to provide fundamental procedures to evaluate mammalian cell metabolism using ^{13}C-MFA. First, in this study, I suggest experimental methods for quantification of cellular and media metabolites, which were used as input parameters for ^{13}C-MFA for specific consumption and production rates

of metabolites or isotopic non-stationary ^{13}C-MFA for quantification of intracellular metabolites. Second, extraction procedures to isolate specific metabolites are developed and key intracellular metabolites were identified by GC-MS analysis using target-based metabolomics. Furthermore, appropriate mass fragments of intracellular metabolites are screened to be used as mass isotopomer distribution (MID) data for ^{13}C-MFA. As a result, the final goal of this thesis is the achievement of good flux observability and best flux solution close to real metabolism. For this goal, I suggested appropriate tracers, combined ^{13}C-MFA with multiple data from multiple tracer experiments, introduced key measurements for GC-MS and validated metabolic models using the ^{13}C-MFA technique.

The outline of this thesis is as follows:

In Chapter 2, examples of MFA and ^{13}C-MFA for studying CHO metabolism are reviewed. I found that traditional MFA for CHO cells was well established, but ^{13}C-MFA applications were not as numerous. In addition, it is suggested that isotopic non-stationarity of labeled metabolites after introduction of isotopic tracer of glucose results from exchange flux between intracellular and extracellular metabolites, i.e. lactate and amino acids and compartmentalized pools of intracellular metabolites.

Chapter 3 describes experimental procedures and isotopic non-stationary ^{13}C-MFA during CHO culture at growth and stationary phases. This is the first report about application of isotopic non-stationary ^{13}C-MFA for CHO metabolism. Key findings were that anabolic fluxes and lactate production increased at the exponential phase and oxidative pentose phosphate pathway was activated at the stationary phase.

Thus, it is observed that metabolic rewiring from growth to non-growth phase was significant during fed-batch culture of CHO cells.

Chapter 4 describes experimental procedures for combined analysis of multiple labeling experiments for ^{13}C-MFA applied to CHO culture at exponential and stationary phases. This is the first report about application of combined ^{13}C-MFA for CHO metabolism with two data sets of [1,2-^{13}C]glucose and [U-^{13}C]glutamine by parallel labeling experiments instead non-stationary ^{13}C-MFA. In this work, lipid metabolism was quantified for the first time during the culture. We find high metabolic activity of lipid metabolism at all growth states even when cell culture was at stationary phase.

Chapter 5 describes quantification of pentose phosphate pathway fluxes. In this part, we solve the key problem that the solution ranges for estimated fluxes of oxidative pentose phosphate pathway is not overlapping for different kinds of isotopic tracers. In addition, we provide key measurements to achieve good flux observability for non-oxidative pentose phosphate pathway.

Chapter 6 describes study of metabolic regulation of gluconeogenesis metabolism by transcriptional activators and inhibitors. We provide a comprehensible network model and flux maps estimated by combined ^{13}C-MFA using multiple isotopic tracers. From this study, novel findings were reported about metabolic regulations by transcriptional factors. Specifically, we find that dexamethasone activated glycolytic enzyme, i.e. pyruvate kinase as well as gluconeogenic enzyme, i.e.

phosphoenolpyruvate carboxykinase. Furthermore, we find that other glycolytic enzymes were also involved to the dexamethasone effects. In addition, even though 8-bromo-cAMP and dibutyryl-cAMP are both cAMP analogues and transcription activators for gluconeogenesis, they showed differential regulation of intracellular metabolism. Finally, we show that insulin resulted in strong down-regulation of gluconeogenesis and also enhanced amino acid metabolism for albumin production.

Chapter 2

OVERVIEW OF METABOLIC FLUX ANALYSIS OF CHINESE HAMSTER OVARY METABOLISM

Chinese hamster ovary (CHO) cells are the most popular mammalian cell line for biopharmaceutical production. In the pharmaceutical industry, CHO cells are cultivated in fed-batch mode for antibody production, where cellular metabolism is characterized by high uptake rates of glucose and glutamine and high rates of lactate secretion and ammonium generation in media. The metabolism of CHO cells shifts dramatically during culture as cells continually adapt to a changing environment from exponential growth phase to stationary phase. As a result, it has been challenging to estimate metabolic flux during cell cultures using conventional metabolic flux analysis (MFA) techniques that were developed by simple stoichiometric balances of lumped reactions and limited measurements of extracellular fluxes. In this chapter, metabolic models for CHO cells are discussed in terms of MFA techniques. Also, we review two decades of progress on conventional MFA in CHO cells and recent advances for ^{13}C-MFA. Though ^{13}C-MFA is a powerful technique for estimation of cellular metabolism, the application was significantly limited by isotopic non-stationarity of labeled metabolites after addition of isotopic tracers. The reasons for this, e.g. slow dynamics and compartmentalization are discussed in this chapter. This chapter was adapted from a published paper by Ahn and Antoniewicz (2012).

2.1 Introduction

Chinese hamster ovary (CHO) cell lines have become the most important host cell lines for the production of biotherapeutics in the biotechnology and pharmaceutical industries (Walsh, 2010). Currently, 60-70% of all recombinant biotherapeutics are produced in CHO cells, with the total global market approaching $100 billion per year (Wurm, 2004). In the past two decades, development of cell lines and optimization of culture process have been key focuses for maximizing product yield. As a result, the product yield of monoclonal antibody has increased >100-fold and the production levels approached 5 g/L (Birch and Racher, 2006). In addition, large bioreactors of 10,000 L or more are common capacities to satisfy the growing worldwide needs for therapeutic proteins (Birch and Racher, 2006; Wurm, 2004; Xie et al., 2003). However, intracellular metabolism of mammalian cells in cell culture is relatively little known despite rigorous study on CHO cell lines and cell culture process. This limited knowledge on *in vivo* metabolism and regulation under industrially relevant culture conditions limits the potential application for modern techniques such as metabolic engineering, which it is more smarter way to improve product yield, product quality and overall process performance rather than robotic technology with high throughput and trial-and-error approaches.

The metabolism of CHO cells in cell culture is characterized by high glucose and glutamine uptake rates in combination with high rates of ammonium generation and lactate production (Lao and Toth, 1997; Neermann and Wagner, 1996; Schneider et al., 1996; Yang and Butler, 2000b). It was reported that two by-products, ammonium and lactate inhibit cell growth and protein production, and furthermore deteriorate glycosylation quality of therapeutic proteins (Ozturk et al., 1992; Yang and Butler, 2000b). Thus, various strategies have been employed to reduce the levels of

by-products. For example, process parameters such as pH, temperature, CO_2 and osmolarity have been optimized (Ahn et al., 2008; Yoon et al., 2003; Zhu et al., 2005), and nutrient feeding strategies have been devised using limited feeding of glucose and glutamine, or combination feeding with slow metabolites, e.g. galactose (Altamirano et al., 2000; Altamirano et al., 2004; Chee Furng Wong et al., 2005; Khattak et al., 2010). Moreover, metabolically engineered CHO cells has been built by amplification of glutamine synthetase gene (Kingston et al., 2002), overexpression of pyruvate carboxylase gene (Kim and Lee, 2007b) and anti-apoptotic genes such as Bcl-2 (Dorai et al., 2009).

In past two decades, metabolic flux analysis (MFA) has been a powerful technology to characterize intracellular metabolism in living cells (Boghigian et al., 2010). It provides quantitative information in the cellular metabolism by determining *in vivo* fluxes (Bonarius et al., 1997). For example, MFA can be used to decipher regulation of metabolic pathways, identify bottlenecks in primary and secondary metabolic pathways for product formation, and obtain fundamental understanding about catabolic and anabolic processes, and homeostasis (Wiechert, 2001). Classical MFA can estimate flux map with small network size by stoichiometric mass balance and flux balance analysis (FBA) expands it to genome-scale size by omics database and linear optimization which is called as optimization-driven method (Boghigian et al., 2010). ^{13}C-MFA utilizes isotopic tracers to acquire relative flux values of branch point pathways inside cells by analyzing atom transitions of intracellular metabolites with mass spectrometry (MS) or nuclear magnetic resonance (NMR) and finally allows us to estimate flux distributions from direct measurement data as mass isotopomer distribution (MID) or positional isotopomer distribution (PID). Therefore,

it is called as data-driven method (Boghigian et al., 2010). For CHO cells, classical MFA was applied and flux map was estimated with extracellular metabolites (Altamirano et al., 2001). The method can be successfully adapted in bioprocess easily, while due to simplification of network model and usage of indirect measurement data as extracellular fluxes, the estimated flux map is hard to reflect real cellular metabolism. Therefore, ^{13}C-MFA is best technique to elucidate CHO cell metabolism and give information of key cellular fluxes before application of optimization purposes as conventional MFA and FBA. Recently, CHO metabolism is studied by ^{13}C isotopic tracers (Deshpande et al., 2009) and flux map is estimated by isotopic stationary or non-stationary ^{13}C-MFA (Ahn and Antoniewicz, 2011; Sengupta et al., 2011). ^{13}C-MFA of CHO metabolism shows in-depth information on intracellular metabolic fluxes, but it contains technical and computational limitations; first, large reversible fluxes from external metabolites such as lactate and amino acids dilute significantly ^{13}C-labeling of intracellular metabolites. To enhance ^{13}C-labeling power of them, the culture media before tracer experiment has been replaced by fresh media without by-products. But, it hampers the acquisition of real metabolic information because it is well known that cell physiology is responded to outside nutrient concentrations. Second, TCA metabolites in CHO cells in ^{13}C-labeling experiment show isotopic non-stationarity. The non-stationary ^{13}C-MFA requires additional measurements (time course MID data and intracellular pool size of metabolites) and rigorous computation. Third, most challenging issue in MFA field is subcellular compartments within cell. It indicates that the same metabolites exist in different places. However, any current techniques have not been applied for metabolite separation without contamination yet. Finally, real cellular metabolism is dynamically

changed by cell phases and response to environmental conditions. The classical MFA , ^{13}C-MFA techniques were developed to study systems based on the assumption of metabolic steady state, i.e. biological systems where intracellular fluxes do not change in time (Stephanopoulos et al., 1998). The assumption of time-invariant fluxes is approximated, for example, during early exponential growth in batch cultures and in steady state continuous cultures. However, industrial bioprocesses are predominantly fed-batch and these systems are inherently dynamic in nature. Therefore, additional assumptions and approximations are needed to observe fluxes in fed-batch cultures using MFA (Antoniewicz et al., 2007c). To address these limitations, initial attempts have been undertaken in recent years to develop new and improved tools and techniques for dynamic metabolic flux analysis (DMFA) for measuring *in vivo* metabolic fluxes in systems that are not at metabolic steady state. These techniques promise to identify intracellular metabolic changes as a function of time. Therefore, these methods could be used to detect intracellular metabolic bottlenecks at specific stages in CHO cell cultures and lead to novel strategies for improving CHO cell metabolism (Niklas et al., 2010).

In this chapter, we provided an overview of recent developments and applications in MFA techniques and the metabolic model for CHO cell metabolism. By highlighting important challenges in MFA, we concluded that MFA still need to be developed, e.g. related to slow labeling dynamics and compartmentalization of metabolism, and the need for further development of dynamic metabolic flux analysis.

2.2 Metabolic Model for MFA of CHO Cell Metabolism

Figure 2.1 shows a schematic diagram of central metabolic pathways in CHO cells used for metabolic flux analysis. The pathways contain; glycolysis, oxidative and non-oxidative pentose phosphate pathway (PPP), TCA cycle, anaplerotic and cataplerotic reactions, lumped pathways of amino acid metabolism and biosynthesis of biomass precursors. The fluxes shown with dotted lines can be directly calculated from measured extracellular uptake and accumulation rates, growth rate and biomass composition. With these measurements as constraints, the network model only has a few unknown fluxes left that must be determined using ^{13}C-tracers, or from additional assumptions (e.g. using cofactor balances, or fixing flux values). The key unknown free fluxes in the model, shown highlighted with boxes in Figure 2.1, are: 1) oxidative pentose phosphate pathway (oxPPP); 2) anaplerosis from pyruvate to oxaloacetate catalyzed by pyruvate carboxylase (PC); 3) gluconeogenesis from oxaloacetate to phosphoenolpyruvate catalyzed by phosphoenolpyruvate carboxykinase (PEPCK); 4) mitochondrial malic enzyme (MEm); 5) fatty acid oxidation (FAox); 6) cytosolic aconitase (ACONc); 7) cytosolic isocitrate dehydrogenase (IDHc); 8) threonine degradation to glycine and acetyl-CoA via threonine aldolase (ThrAL); and 9) glycine degradation to C1-pool and CO_2 via the glycine cleavage system (GCS).

Most flux analysis work on CHO cells has been classical MFA, and in most cases only one specific metabolic phenotype was considered, e.g. exponential growth phase or stationary phase. Table 2.1 lists important flux analysis studies on CHO cells. The first column shows the analysis method that was employed. Of the sixteen studies listed in Table 2.1, nine used stationary MFA, four used stationary MFA combined with a kinetic model, and three studies used ^{13}C-based MFA. Table 2.2 shows the scope of the metabolic network models used in MFA studies. For stationary MFA,

simplified network models were often used to ensure that the system was not underdetermined. The common assumption was to eliminate the unknown free fluxes highlighted in Figure 2.2, i.e. essentially assuming that these reactions carried little or no flux. Several studies did include oxPPP in the network model, but the oxPPP pathway was linked to nucleotide biosynthesis and/or NADPH balance without considerations of non-oxPPP by reversible reactions. As such, these studies only provided a lower estimate of the actual flux through oxPPP. In the next three sections we briefly review key results obtained from the studies listed in Table 2.2, and highlight some of the challenges that still remain for estimating metabolic fluxes in mammalian cell lines.

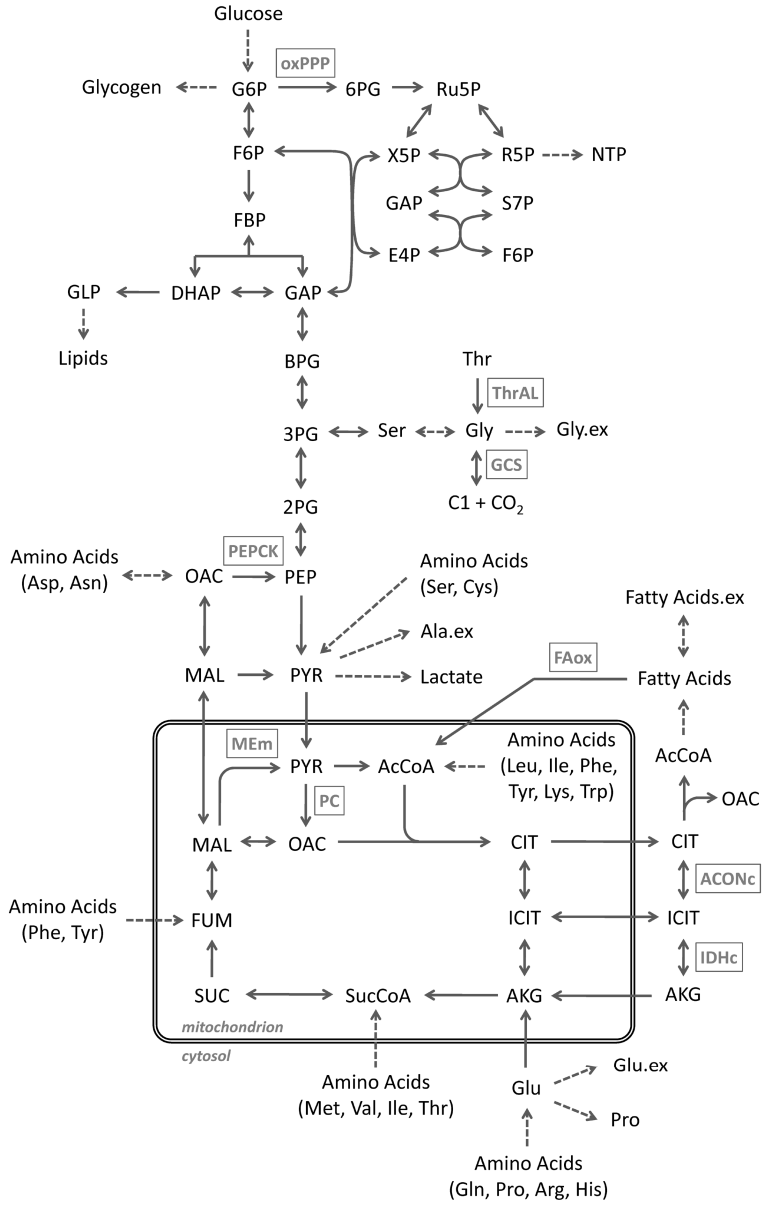

Figure 2.1 Diagram of central metabolic pathways in CHO cells. The fluxes with dotted lines can be directly calculated from measured extracellular uptake and accumulation rates and growth rate. The fluxes that cannot be determined from extracellular measurements alone are shown highlighted in boxes: oxPPP, oxidative pentose phosphate pathway; PC, pyruvate carboxylase; PEPCK, phosphoenolpyruvate carboxykinase; FAox, fatty acid oxidation; MEm, mitochondrial malic enzyme; ACONc, cytosolic aconitase; IDHc, cytosolic isocitrate dehydrogenase; ThrAL, threonine aldolase; GCS, glycine cleavage system. This figure was adapted from a published paper by Ahn and Antoniewicz (2012).

Table 2.1 Overview of MFA studies in CHO cells.

Cell line	Culture method	Flux analysis method	Major achievements	Year *[Ref.]
γ-CHO	Continuous	MFA	MFA validated the metabolism of amino acids derived from peptide in serum-free media.	1999 [1]
γ-CHO	Continuous	MFA	Carbon utilization efficiency was estimated by MFA. IFN-γ glycosylation was related to TCA cycle flux, not glycolysis.	1999 [2]
CHO TF 70R	Continuous	MFA	The efficiency of carbon utilization was estimated by MFA and linked to reduced production rate of t-PA.	2001 [3]
CHO-320	Batch	MFA + kinetic model	Macroscopic dynamical modeling approach was linked to a simplified network model for MFA.	2004 [4]
CHO-320	Batch	MFA + kinetic model	Dynamic modeling was linked to MFA to estimate fluxes during cell growth, transition and stationary phase.	2006 [5]
CHO TF 70R	Batch	MFA	Co-feeding of glucose and galactose resulted in metabolic shift from lactate production to consumption.	2006 [6]
Unknown	Perfusion	MFA	Intracellular fluxes were estimated by quasi real-time MFA in perfusion culture.	2006 [7]
Unknown	Perfusion	MFA	Error propagation from measurements to metabolic fluxes was determined for MFA.	2009 [8]
Unknown	Perfusion	^{13}C-MFA	MFA and ^{13}C-MFA were compared. Flux agreement required oxPPP and PC fluxes to be set by ^{13}C-MFA data.	2010 [9]
Super-CHO	Batch	MFA	Differences in CHO cell metabolism and hybridoma cell metabolism were identified using MFA.	2010 [10]
CHO-320	Batch	MFA	To improve flux observability, the number and type of available measurements were optimized for MFA.	2010 [11]

Table 2.1 continued

GS-CHO SF18	Fed-batch	MFA and ^{13}C-MFA	oxPPP flux was estimated by ^{13}C-MFA. MFA was used to estimate fluxes in the rest of network model.	2011 [12]
Unknown	Fed-batch and continuous	MFA	Amino acid composition of culture medium was optimized using MFA. By-product levels were reduced and cell density and antibody production were enhanced.	2011 [13]
CHO-K1	Fed-batch	MFA + kinetic model	MFA was integrated with a kinetic model to simulate metabolic dynamics in fed-batch cultures.	2011 [14]
dhfr-CHO	Fed-batch	MFA + kinetic model	Kinetic models for growing and non-growing subpopulations of cells were integrated with a simplified MFA model.	2011 [15]
CHO-K1	Fed-batch	^{13}C-MFA and ^{13}C-NMFA	Metabolic fluxes were determined for growth phase and stationary phase in a fed-batch culture using ^{13}C-based MFA.	2011 [16]

*[Ref.]: [1], (Nyberg et al., 1999b); [2], (Nyberg et al., 1999a); [3], (Altamirano et al., 2001); [4], (Provost and Bastin, 2004); [5], (Provost et al., 2006); [6], (Altamirano et al., 2006); [7], (Goudar et al., 2006); [8], (Goudar et al., 2009); [9], (Goudar et al., 2010); [10], (Quek et al., 2010); [11], (Zamorano et al., 2010); [12], (Sengupta et al., 2011); [13], (Xing et al., 2011); [14], (Nolan and Lee, 2011); [15], (Naderi et al., 2011); [16], (Ahn and Antoniewicz, 2011)

This table was adapted from a published paper by Ahn and Antoniewicz (2012).

Table 2.2 Overview of metabolic network models for MFA studies in CHO cells

Flux analysis method	Reaction in model	Reactions considered in metabolic network model						
		oxPPP	PC	PEPCK	MEc & MEm	IDHc & ACONc	FAox	Ref.
MFA	33	-	-	-	-	-	-	[1]
MFA	33	-	-	-	-	-	-	[2]
MFA	45	Yes[(a)]	-	-	-	-	-	[3]
MFA + kinetic	18+5[(b)]	Yes[(a)]	-	-	-	-	-	[4]
MFA + kinetic	24+11[(b)]	Yes[(a)]	-	-	-	-	-	[5]
MFA	24	Yes[(a)]	-	-	-	-	-	[6]
MFA	n/a	-	-	-	-	-	-	[7]
MFA	33	-	-	-	-	-	-	[8]
^{13}C-MFA	87	Yes	Yes	Yes	-	-	-	[9]
MFA	272	Yes[(c)]	-	-	Yes[(c)]	-	-	[10]
MFA	100	Yes[(d)]	-	-	-	-	-	[11]
MFA and ^{13}C-MFA	58	Yes	-	-	-	-	-	[12]
MFA	23	-	-	-	-	-	-	[13]
MFA + kinetic	34	-	-	-	-	-	-	[14]
MFA + kinetic	34+8[(b)]	-	-	-	-	-	-	[15]
^{13}C-MFA and ^{13}C-NMFA	73	Yes	Yes	-	-	-	Yes	[16]

(a) Flux of oxPPP was linked to nucleotide requirement for cell growth.
(b) Macroscopic reactions/expressions used for dynamic modeling.
(c) Fluxes of oxPPP and of cytosolic NADPH-malic enzyme were linked to nucleotide and NADPH requirements for cell growth.
(d) Only upper and lower bounds were determined.
This table was adapted from a published paper by Ahn and Antoniewicz (2012).

2.3 Applications of Classical MFA in CHO Cells

Stationary MFA has been applied in CHO cells for a variety of applications, including medium optimization (Xing et al., 2011), quantification of peptide consumption rate (Nyberg et al., 1999b), recombinant protein production rate (Altamirano et al., 2001; Nyberg et al., 1999a), co-substrate metabolism (Altamirano et al., 2006), and analysis of error propagation in flux analysis (Goudar et al., 2009). For example, Xing et al. optimized medium composition of amino acids through MFA using different concentrations of medium components (Xing et al., 2011). Nyberg et al. demonstrated that MFA can be used as a tool to validate consistency of extracellular measurements. Using MFA, Nyberg et al. showed that peptide consumption in complex media should be included in MFA modeling to obtain statistically acceptable results (Nyberg et al., 1999b). Altamirano et al. obtained good agreement between simulated and MFA estimated values for the respiratory quotient (ratio of CO_2 production to O_2 consumption) in a series of glucose-limited continuous cultures (Altamirano et al., 2001). Classical MFA was also used to provide insights into different contributions of cellular pathways for recombinant protein glycosylation. For example, Nyberg et al. reported that glycosylation site occupancy in interferon-γ was closely related to TCA efficiency, but was not sensitive to glycolysis flux (Nyberg et al., 1999a). Altamirano et al. evaluated the use of multiple substrates including glucose, galactose and glutamate to reduce accumulation of by-products such as lactate, alanine and glycine (Altamirano et al., 2006; Altamirano et al., 2000). Batch cultures of CHO cells showed two distinctive phases of lactate production and consumption and it was reported that the oxidative activity of TCA cycle in the lactate consumption phase was underestimated using MFA simulations (Altamirano et al., 2006). Recently, Goudar et al. described a procedure for determining error

propagation in flux analysis from extracellular metabolite measurements to estimated fluxes (Goudar et al., 2009). In a separate study, Goudar et al. also described the application of real-time MFA using on-line measurements (Goudar et al., 2006). To allow estimation of fluxes in underdetermined systems, Llaneras and Picó (Llaneras and Picó, 2007) and Zamorano et al. (Zamorano et al., 2010) proposed an extension to classical MFA for calculating upper and lower bounds of unresolved fluxes. The extended MFA technique was termed flux spectral analysis (FSA). Recently, Quek et al. applied a similar strategy to estimate fluxes in a large-scale model for CHO cell metabolism, consisting of 272 reactions and 228 metabolites, which was used to compare metabolism of CHO cells and hybridoma cells (Quek et al., 2010). Although not all fluxes in the model could be uniquely determined using MFA, the authors did establish upper and lower bounds for key branch points in central metabolism.

2.4 Applications of MFA in Combination with a Kinetic Model

In recent years, several studies have appeared where stationary MFA was combined with a kinetic model to describe metabolic flux dynamics in batch and fed-batch cultures of CHO cells (Goudar et al., 2006; Llaneras and Picó, 2007; Nolan and Lee, 2011; Provost and Bastin, 2004; Zamorano et al., 2010). The dynamic modeling framework was based a lumped network model derived from the CHO model by Provost and Bastin (Provost and Bastin, 2004). Recently, Nolan and Lee used a similar kinetic modeling approach and successfully traced changes in intracellular and extracellular metabolic fluxes in fed-batch cultures of CHO cells (Nolan and Lee, 2011).

2.5 Applications of ^{13}C-Tracers for Flux Analysis in CHO Cells

To our best knowledge, there are currently only three studies where ^{13}C-tracers have been applied for metabolic flux analysis in CHO cells. Goudar et al. used a mixture of [1-^{13}C]glucose and [U-^{13}C]glucose and measured ^{13}C-labeling in amino acids from hydrolyzed biomass using 2D [^{13}C, ^{1}H] NMR and ^{13}C-labeling of lactate in the medium using LC-MS for flux analysis. The key findings from this ^{13}C-MFA study were that both oxPPP and PC were active in CHO cells. About 40% of glucose was metabolized via oxPPP (remaining 60% via glycolysis), and 10% of pyruvate was converted to oxaloacetate by PC (remaining 90% was converted to acetyl-CoA by PDH). Goudar et al. demonstrated that results obtained using classical MFA only agreed with ^{13}C-MFA results when the fluxes of oxPPP and PC reactions were fixed at the values obtained from ^{13}C-MFA analysis (Goudar et al., 2010). Sengupta et al. also used a mixture of [1-^{13}C]glucose and [U-^{13}C]glucose tracers and measured ^{13}C-labeling in four metabolites of the pentose phosphate pathway using LC-MS (Sengupta et al., 2011). Sengupta et al. estimated oxPPP fluxes using ^{13}C-MFA in four CHO cell cultures at the late stationary phase. Classical MFA was then applied to estimate metabolic fluxes in the rest of the metabolic network, since no significant ^{13}C-labeling was detected in other intracellular metabolites and thus ^{13}C-MFA could not be applied. The key finding from this study was that oxPPP was very active in CHO cells at the late stationary phase. Recently, Ahn and Antoniewicz established detailed metabolic flux maps for CHO cells at two metabolic phases during a fed-batch culture, i.e. at the exponential growth phase and early stationary phase (Ahn and Antoniewicz, 2011). For this study, Ahn and Antoniewicz used [1,2-^{13}C]glucose and measured ^{13}C-labeling dynamics for 13 intracellular metabolites in the glycolysis pathway and TCA cycle using GC-MS. Ahn and Antoniewicz estimated oxPPP flux

using ^{13}C-MFA, and estimated fluxes in the rest of the model using non-stationary ^{13}C-NMFA. The key findings from this study were that PC was active at the exponential growth phase and that oxPPP was active at the early stationary phase, but not during exponential growth.

All three ^{13}C-MFA studies discussed above have concluded that the previous assumptions employed in classical MFA of CHO cells, i.e. that oxPPP and PC fluxes are negligible, are not valid. This has significant consequences for future use of classical MFA. As inclusion of oxPPP and PC reactions in MFA models creates underdetermined systems, MFA based on metabolite balancing alone cannot provide a unique solution. Methods such as flux spectrum analysis can be used to estimate upper and lower bounds for fluxes in underdetermined models, however, flux confidence intervals may become too large to derive any statistically significant conclusions from MFA studies. Thus, it appears that future studies on CHO cell metabolism should include at least some type of ^{13}C-labeling data to help constrain the flux solution.

2.6 Challenges in Estimating Fluxes due to Slow Labeling Dynamics

In contrast with bacterial cells, where labeling of intracellular metabolites approaches isotopic steady state within several minutes (Noack et al., 2011; Schaub et al., 2008; Young et al., 2008), mammalian cells generally display slow labeling incorporation into intracellular metabolites, i.e. on the order of hours (Deshpande et al., 2009). In practice, this means that ^{13}C-based flux analysis in mammalian cells requires more rigorous experimental and computational work. Instead of applying relatively well-established ^{13}C-MFA, one must perform non-stationary ^{13}C-NMFA that is computationally much more intensive and includes additional model parameters that must be estimated (i.e. metabolite pool sizes) (Young et al., 2008). Furthermore,

instead of collecting a single sample at isotopic steady state, multiple samples must be collected over time to obtain accurate profiles of ^{13}C-labeling dynamics. A key concern in these studies is ensuring that metabolic steady state is maintained during the labeling experiment. For example, Sengupta et al. did not detect any significant labeling in TCA metabolites from ^{13}C-glucose after 6 h in CHO cells (Sengupta et al., 2011), and Ahn and Antoniewicz reported that at least 24 h were needed to accumulate ~10% labeling in TCA cycle metabolites in a fed-batch culture of CHO cells. It may be challenging to maintain metabolic steady state for extended periods of time.

There are several reasons for the slow labeling dynamics in mammalian cells as shown in Figure 2.2. One reason is the fact that complex media are used in mammalian cell cultures, i.e. containing glucose, glutamine, other amino acids, fatty acids and organic acids. In some studies 5-10% serum was added to the medium (Metallo et al., 2009; Yoo et al., 2008), while serum-free media containing non-animal derived hydrolysates are commonly used in the industry (Grillberger et al., 2009; Zhou et al., 2008). As was shown by Nyberg et al., consumption of peptides from complex media should be included in MFA modeling (Nyberg et al., 1999b). Metabolism of multiple non-enriched carbon sources may dilute labeling of intracellular metabolites and slow down labeling incorporation (Figure 2.2A). Furthermore, large extracellular metabolite pools may act as buffers for labeling incorporation (i.e. the cellular volume is small compared to medium volume), especially if there is significant exchange between intracellular and extracellular metabolites (Figure 2.2B). For example, non-enriched lactate in the medium can exchange with intracellular lactate and slow down labeling dynamics of pyruvate, even under conditions where there is a large net

production of lactate, such as during exponential growth of CHO cells (Ahn and Antoniewicz, 2011).

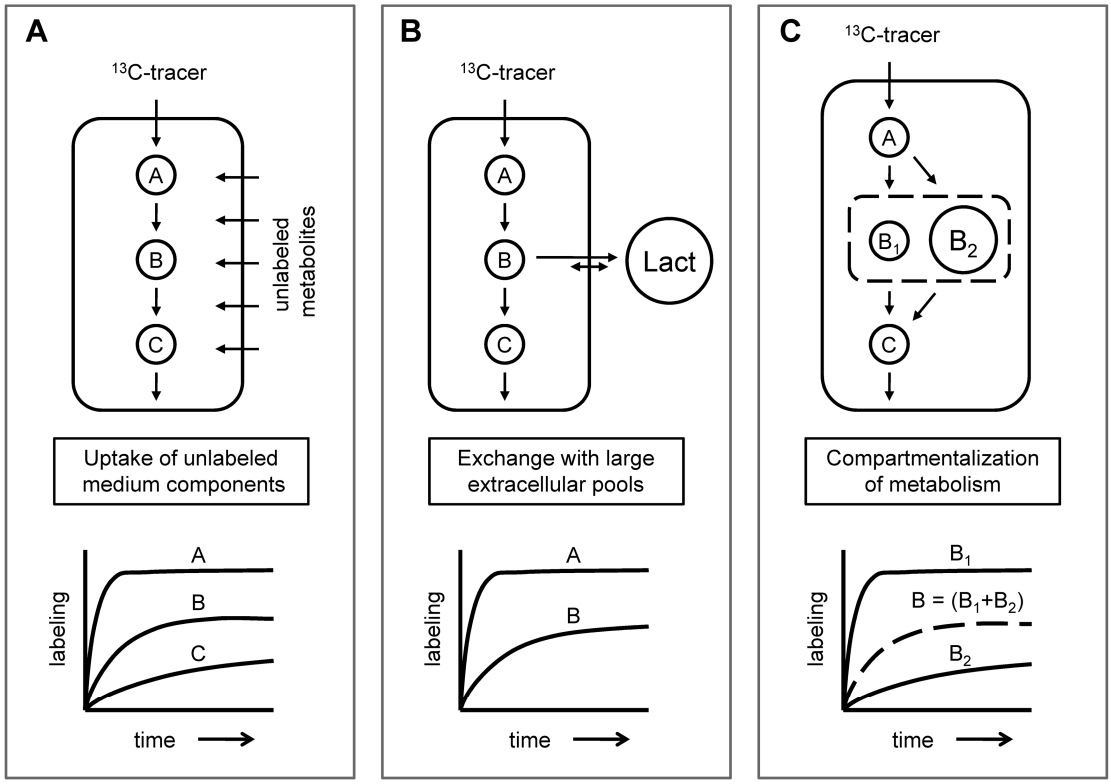

Figure 2.2 Challenges in MFA of mammalian cells due to slow ^{13}C-labeling dynamics. (A) Uptake of unlabeled medium components dilutes isotopic labeling of intracellular metabolites and increases the time needed to reach isotopic steady state. (B) Large extracellular metabolites pools like lactate can reduce intracellular labeling by rapid exchange between intracellular and extracellular lactate, even when there is a large net production of lactate. (C) Compartmentalization of metabolism. Metabolites such as pyruvate, citrate, malate and amino acids are present in multiple compartments; however, current metabolite extraction protocols cannot provide compartment-specific ^{13}C-labeling of metabolite pools. Instead, only the combined labeling of multiple metabolite pools is available. This figure was adapted from a published paper by Ahn and Antoniewicz (2012).

2.7 Challenges in Estimating Flux due to Compartmentalization of Metabolism

A final complicating factor for determining metabolic fluxes in mammalian cells, which can also slow down labeling incorporation, is related to compartmentalization of metabolism as described in Figure 2.2C (Niklas et al., 2011a). For analysis of central metabolic fluxes in CHO cells, at least two compartments must be considered, cytosol and mitochondrion in Figure 2.2C. While some metabolic pathways are restricted to a single compartment, e.g. pentose phosphate pathway in the cytosol, other pathways span multiple compartments. As an example, the gluconeogenesis pathway depends on reactions in both the cytosol and mitochondrion. Mammalian cells have many isoenzymes that can catalyze analogous reactions in multiple compartments, e.g. cytosolic and mitochondrial malic enzyme. In MFA studies, the presence of isoenzymes produces parallel pathways and metabolic cycles that cannot be resolved using metabolite balancing alone, and in many cases can even be difficult to resolve using ^{13}C-MFA techniques. There is strong evidence, however, that parallel pathways and metabolic cycles such as pyruvate cycling play a key role in regulating important events in mammalian cells, and thus should be investigated in more detail. For example, Jensen et al. identified three potential pyruvate cycles in pancreatic cells that are believed to play a role in insulin secretion (Jensen et al., 2008). Finally, transport across the mitochondrial membrane is possible only for a select number of metabolites for which specific transporters exist. These transports must therefore be shared by multiple metabolic pathways and in addition transport reducing equivalents across the mitochondrial membrane, since cofactors NADH and NADPH cannot cross the mitochondrial membrane.

It has been hypothesized that cytosolic and mitochondrial pools may be differently labeled and have different labeling time scales *in vivo*. For example,

Munger et al. showed differential labeling patterns for metabolically related metabolites using [U-^{13}C]glucose and [U-^{13}C]glutamine tracers. The results provided strong evidence of compartmentalized metabolism in fibroblast cells (Munger et al., 2008). Lu et al. also suggested the existence of two pyruvate pools based on ^{13}C NMR measurements in INS-1 β cells (Lu et al., 2002). Ideally, we would like to obtain accurate measurements of compartment-specific labeling patterns for ^{13}C-MFA. However, current extraction techniques are not well suited to separate different intracellular metabolite pools without metabolite leakage. Thus, only the combined mitochondrial and cytosolic pools of pyruvate, malate, citrate, and amino acids can be measured (Figure 2.2C) (Zamboni, 2011). Advances in metabolite extraction techniques would greatly increase the potential of using ^{13}C-MFA to resolve compartment specific fluxes in mammalian cells.

2.8 Conclusion

In this chapter, we reviewed metabolic flux analysis studies related to CHO cell metabolism and highlighted recent advanced in techniques for MFA. Classical MFA has been applied extensively to study CHO cell metabolism and metabolism of other mammalian cell lines. Initial flux maps were established using simplified network models and extracellular metabolite measurements. Recently, CHO cell metabolism was investigated in more detail using ^{13}C-based techniques. These new studies revealed several key assumptions used in previous MFA work that may not be valid in CHO cells, especially regarding activities of oxidative pentose phosphate pathway and anaplerosis from pyruvate to oxaloacetate by pyruvate carboxylase. Future studies on CHO cells should make more use of ^{13}C-tracers to better constrain flux solutions and validate other modeling assumptions.

However, metabolic flux analysis using ^{13}C-trcers in mammalian cells remains a challenging process that requires significant experimental and modeling efforts. The analysis is especially complicated by difficulties in maintaining metabolic steady state, slow labeling dynamics in ^{13}C-tracer experiments, and compartmentalized metabolism. A key factor contributing to slow labeling dynamics is the exchange of intra- and extracellular metabolites. Intracellular compartmentalization of metabolism may also contribute to this problem. Although ^{13}C-MFA is a relatively well-established technique, it has limitations for studying CHO cell metabolism due to the slow labeling incorporation. ^{13}C-NMFA overcomes isotopic non-stationarity by shorter labeling experiments. However, ^{13}C-NMFA requires additional measurements, i.e. multiple samples in time, and more advanced algorithms for parameter fitting and statistical analysis.

The difficulties in MFA related to compartmentalization of metabolism have not been properly addressed. Currently, there are no well-established methods to estimate compartment specific fluxes in eukaryotic systems, and it is still an open question whether isotopic tracers provide the best strategy to resolve these fluxes. Without reliable extraction techniques for isolating compartment specific metabolite pools and ^{13}C-labeling, it may be too difficult to elucidate parallel pathways in multiple compartments and metabolic cycles, such as pyruvate cycling, with current measurements. Novel approaches are also needed for optimal tracer experiment design and new analytical techniques to complement current ^{13}C-labeling measurements for determining fluxes in compartmentalized network models. Finally, ^{13}C-DMFA methods should be developed to fully integrate dynamic metabolite data and ^{13}C-labeling data in systems that are not at metabolic and isotopic steady state.

Chapter 3

METABOLIC FLUX ANALYSIS OF CHO CELLS AT GROWTH AND NON-GROWTH PHASES USING ^{13}C-NMFA FOR ISOTOPIC NON-STEADY STATE

Chinese hamster ovary (CHO) cells are a popular host system for production of biotherapeutics in the pharmaceutical industry. However, relatively little is known about CHO metabolism in cell culture. Thus, using ^{13}C-metabolic flux analysis (^{13}C-MFA) technique, metabolism of CHO cells was studied at the growth phase and early stationary phase using isotopic tracers and mass spectrometry in order to elucidate metabolic shift according to the change of cell growth phases. CHO cells were grown in fed-batch culture over a period of six days. On days 2 and 4, [1,2-^{13}C]glucose was introduced and the labeling of intracellular metabolites was measured by gas chromatography-mass spectrometry (GC-MS) at 6, 12 and 24 h following the addition of tracer. Intracellular metabolic fluxes were estimated from measured extracellular rates and ^{13}C-labeling dynamics of intracellular metabolites using non-stationary ^{13}C-MFA technique. The flux results indicated significant rewiring of intracellular metabolic fluxes in the transition from growth to non-growth, including changes in energy metabolism, redox metabolism, oxidative pentose phosphate pathway and anaplerosis. At the exponential phase, CHO cell metabolism was characterized by a high flux of glycolysis from glucose to lactate, anaplerosis from pyruvate to oxaloacetate and from glutamate to α-ketoglutarate, and cataplerosis though malic enzyme. At the stationary phase, the flux map was characterized by a reduced flux of glycolysis, net lactate uptake, oxidative pentose phosphate pathway flux, and reduced

rate of anaplerosis. The fluxes of pyruvate dehydrogenase and TCA cycle were similar at the exponential and stationary phase. The results presented here provide a solid foundation for future studies of CHO cell metabolism for applications such as cell line development and medium optimization for high-titer production of recombinant proteins. This chapter was adapted from a published paper by Ahn and Antoniewicz (2011).

3.1 Introduction

Mammalian cell culture has a key role for biopharmaceutical companies for the production of recombinant proteins as monoclonal antibodies and vaccines. In recent approvals in US and EU, most of biotherapeutics were produced by mammalian cell lines which were mostly used with Chinese hamster ovary (CHO) cells (Walsh, 2010). Metabolism of CHO cells is characterized by high rates of glycolysis and glutaminolysis (Quek et al., 2010). As a result, large amounts of by-products, lactate and ammonium are accumulated in media in the course of culture, which they come from the conversion of glucose to lactate and decomposition and metabolism of glutamine (Altamirano et al., 2000; Ozturk and Palsson, 1990). It was reported that the by-products inhibit cell growth and protein production and can deteriorate the glycosylation quality of the proteins (Chen and Harcum, 2005; Hossler et al., 2009). To maximize productivity and acquire good quality of products, process parameters such as pH and temperature have been optimized in the past (Ahn et al., 2008; Clark et al., 2004; Trummer et al., 2006) and metabolism of CHO cells has been modified by genetic engineering, e.g. by enhancing pyruvate carboxylase (PC) flux (Kim and Lee, 2007b) and overexpressing anti-apoptotic genes such as Bcl-2 (Mastrangelo et al., 2000).

While these approaches resulted in improved process performance, detailed knowledge on cell physiology and in particular at the level of cellular metabolism is still lacking for CHO cells due to difficulties in measuring *in vivo* metabolic fluxes in mammalian cells. Intracellular metabolic fluxes can be estimated by flux balance analysis (FBA) and metabolic flux analysis (MFA) (Boghigian et al., 2010; Chen et al., 2011; Covert et al., 2001). In FBA, fluxes are estimated in underdetermined systems (i.e. fewer measurements than estimated fluxes) under the assumption of, e.g. maximum cell growth. FBA has been successfully applied to large-scale microbial networks and used for process optimization (Boghigian et al., 2010). In ^{13}C-MFA, fluxes are estimated from isotopic labeling measurements combined with extracellular uptake and excretion rates. After the addition of an isotopic tracer, e.g. [1,2-^{13}C]glucose, ^{13}C-atoms are incorporated into intracellular metabolites that can then be detected by NMR, mass spectrometry or tandem mass spectrometry (Antoniewicz et al., 2007a; Choi and Antoniewicz, 2011; Szyperski, 1995). Flux distributions are determined from these isotopomer data by nonlinear least square regression techniques and elementary metabolite units (EMU) modeling (Antoniewicz et al., 2007b; Niklas and Heinzle, 2012; Schmidt et al., 1997; Wiechert et al., 1999). In addition to quantifying intracellular metabolic fluxes, ^{13}C-MFA can be used for validating biochemical network models and elucidating the stereochemistry of biochemical reactions (Antoniewicz et al., 2006b; Boghigian et al., 2010; Crown et al., 2011; Moxley et al., 2009; Quek et al., 2010). ^{13}C-MFA can be classified into three types according to the dynamics of ^{13}C enrichment and the assumption regarding metabolic steady state of cells (Wahl et al., 2008): (1) stationary ^{13}C-MFA: metabolic and isotopic steady state are assumed; (2) non-stationary ^{13}C-MFA: metabolic steady state

and isotopic non-steady state (Maier et al., 2008; Young et al., 2008); and (3) dynamic ^{13}C-MFA: metabolic and isotopic non-steady state (Antoniewicz et al., 2007c).

In this study, the metabolism of CHO cells was investigated at the growth phase and early stationary phase using non-stationary ^{13}C-MFA. This is the first time that metabolic fluxes have been determined at the two phases for CHO cells using isotopic tracers and mass spectrometry analysis of intracellular metabolites. It was found the significant rewiring of intracellular metabolic fluxes in the transition from growth to non-growth, including changes in energy metabolism, redox metabolism, oxidative pentose phosphate pathway and anaplerosis. At the same time, the TCA cycle flux did not change significantly during this transition. Here, using isotopic labeling experiments and mass spectrometry, the fluxes that cannot be estimated by classical MFA were observed in this study, e.g. pyruvate carboxylase (PC), oxidative pentose phosphate pathway (oxPPP) and all reversible reactions. In fact, the fluxes have been largely ignored in the previous studies that relied on metabolite balancing alone.

3.2 Materials and Methods

3.2.1 Materials

Culture materials were purchased from Cellgro (Mediatech, Manassas, VA). [1,2-^{13}C]glucose (99%), [U-^{13}C]glutamine (98%), and [U-^{13}C]algal amino acids (97~99%) were purchased from Cambridge Isotope Laboratories (Andover, MA). Free amino acids and amino acid standard H were purchased from Pierce Sci. (Rockford, IL). [U-^{13}C]Algal hydrolysate was solubilized in 0.1 N HCl at 10 mg/mL. Stocks

solutions of amino acids were kept at -85°C. Glucose stock solutions were prepared at 250 g/L in phosphate buffer saline (PBS).

3.2.2 Cell Culture

CHO-K1 cells (ATCC Cat. No. CCL-61) were grown as a monolayer culture in T-25 flasks (Corning, NY) in humidified 5% CO_2 incubator at 37°C. Cells were subcultured every three days at a split ratio of 1:10. The medium was Dulbecco's modified Eagle medium (DMEM, Cat. No. 10-013-CV) supplemented with 10% fetal bovine serum (FBS, Cat. No. 35-011-CV) and 1% penicillin-streptomycin (PS).

3.2.3 Isotopic Tracer Experiments

For isotopic tracer studies, CHO cells were grown in fed-batch culture with glucose feeding. First, cells were grown to confluency to be used as the seed. After cells were detached with trypsin EDTA (0.25% trypsin, Cat. No. 25-053-CV), they were washed once with fresh growth medium and re-suspended in growth medium at 0.60×10^6 cells/mL and seeded in T-25 flasks (5 mL/flask). The growth medium was DMEM base (1 g/L glucose and 4 mM glutamine, Cat. No. 10-014-CV) supplemented with 10% FBS, 1% PS and glucose (6.7 mM initial glucose). Twelve T-25 flasks were seeded with CHO cells: six flasks were used for cell counting and quantification of media metabolites, three flasks were used for ^{13}C-analysis at the exponential phase, and three flasks were used for analysis of stationary phase. An additional nine flasks were prepared without cells to estimate evaporation rates and concentration profiles of amino acids in time. During the six day cultivation, a bolus of glucose was added twice, on day 2 and 4, to a final glucose concentration of ~10 mM. For the study of the growth phase, glucose added on day 2 was [1,2-^{13}C]glucose and the flasks were

harvested one-by-one after 6, 12 and 24 h. For the study of the stationary phase, glucose added on day 2 was natural glucose and glucose added on day 4 was [1,2-^{13}C]glucose. The T-25 flasks were harvested after 6, 12 and 24 h. Cells were extracted as described below to obtain intracellular metabolites for analysis of ^{13}C-labeling by GC-MS. All samples were stored at -85°C.

3.2.4 Viable Cell Number, Glucose, Lactate and Ammonia Analysis

Cell numbers were measured using a hemocytometer and viability was determined by trypan blue exclusion method. Cell numbers were measured three times per sample. Concentrations of glucose and lactate were measured by YSI 2700 biochemistry analyzer (YSI, Yellow Springs, OH), and ammonium concentration was measured by Bioprofile 100^{plus} analyzer (Nova biomedical, Waltham, MA). Glucose and lactate concentrations were measured three times per sample. The results were shown in Table 3.1

3.2.5 Gas Chromatography Mass Spectrometry (GC-MS) Analysis

GC-MS analysis was performed using an Agilent 7890A GC equipped with a DB-5ms (30 m × 0.25 mm i.d. × 0.25 μm; Agilent J&W Scientific) capillary column, interfaced with a Waters Quattro Micro GC-MS/MS (Milford, MA) operating under ionization by electron impact at 70 eV and 200°C ion source temperature. The injection port and interface temperatures were both 250°C. Helium flow was maintained at 1 mL/min via electronic pressure control. Mass spectra were recorded in selected ion recording (SIR) mode with 30 ms dwell time. Mass isotopomer distributions were obtained by integration of ion chromatograms (Antoniewicz et al., 2007a) and corrected for natural isotope abundances (Fernandez et al., 1996).

Table 3.1 Measurements of viable cell number (10^6 cells/mL) and concentrations of extracellular metabolites (mM).

	Time (day)						
	0	1	2	3	4	5	6
Cell number ($\times 10^6$)	n/a	0.21	0.37	1.32	2.25	2.34	2.09
Glucose	6.68	4.59	2.54	5.32	2.21	7.04	4.49
Lactate	0.95	2.59	5.75	12.67	16.71	17.28	16.44
NH_3	0.83	1.09	1.51	2.00	2.38	2.96	3.21
Alanine	0.11	0.17	0.19	0.26	0.33	0.39	0.46
Glycine	0.42	0.51	0.52	0.63	0.74	0.77	0.85
Valine	0.66	0.75	0.67	0.66	0.69	0.65	0.70
Leucine	0.76	0.84	0.75	0.72	0.76	0.72	0.77
Ileucine	0.76	0.83	0.72	0.72	0.75	0.71	0.76
Proline	0.04	0.08	0.09	0.11	0.12	0.14	0.17
Methionine	0.17	0.18	0.16	0.14	0.14	0.13	0.14
Serine	0.35	0.38	0.29	0.21	0.14	0.07	0.06
Threonine	0.67	0.72	0.64	0.65	0.67	0.64	0.68
Phenylalanine	0.36	0.40	0.36	0.36	0.38	0.36	0.39
Aspartate	0.03	0.07	0.08	0.10	0.11	0.10	0.10
Glutamate	0.10	0.21	0.30	0.39	0.45	0.44	0.47
Tyrosine	0.32	0.36	0.32	0.34	0.34	0.32	0.34
Glutamine	2.69	2.61	1.96	1.51	1.24	0.85	0.73

* A bolus of glucose was added on day 2 to increase glucose concentration from 2.5 mM to 10.0 mM, and on day 4 to increase glucose concentration from 2.2 mM to 9.7 mM.

This table was adapted from a published paper by Ahn and Antoniewicz (2011).

3.2.6 Extraction of Intracellular Metabolites

At the sampling times, culture medium was carefully collected from the T-25 flasks and briefly centrifuged to remove debris. The attached cells were washed twice with 5 mL of cold saline water (9 g/L NaCl). Metabolism was quenched by addition of 1.5 mL of cold methanol (-20°C). After incubation on ice for 5 min, cells were collected with a cell scraper and the cell suspension was transferred into a glass tubes with Teflon-sealed caps. 1.5 mL of chloroform was added and the tubes were vortexed vigorously for 10 sec. Next, 1.5 mL of water was added and the tubes were vortexed vigorously for 1 min. All tubes were stored overnight at 4°C. The next day, the tubes were centrifuged at 2,000 rpm and 4°C for 20 min, which resulted in a clear phase separation. The upper aqueous phase (methanol and water) contained polar metabolites and lower organic phase (chloroform) contained non-polar metabolites. 3 mL of the aqueous phase was carefully transferred into two 1.5 mL microcentrifuge tubes using a glass pipette and evaporated to dryness at 37°C with air using an evaporator (Reacti-Vap/Reacti-Therm III; Fierce, Rockford, IL). During the drying process, the contents of the two tubes were combined. Dried metabolites were kept at -85°C prior to derivatization and GC-MS analysis.

3.2.7 Derivatization and GC-MS Analysis of Intracellular Metabolites

The extracted metabolites were dissolved in 50 µL of 2wt% methoxylamine hydrochloride in pyridine and incubated at 37°C for 90 min on a heating block. Next, 80 µL of N-methyl-N-(tert-butyldimethylsilyl)-trifluoroacetamide (MTBSTFA) + 1% tert-butyldimetheylchlorosilane (TBDMCS) (Thermo Scientific, Bellefonte, PA) was added and the samples were incubated for 30 min at 60°C. After an overnight incubation at room temperature, the derivatized samples were centrifuged for 2 min at

14,000×g, to remove debris, and the clear liquid was transferred into GC vials for GC-MS analysis. The injection volume was 1 μL and samples were injected in splitless or split mode depending on the peak intensities. GC oven temperature was held at 70°C for 2 min, increased to 140°C at 3°C/min, increased to 150°C at 1°C/min, increased to 280°C at 3°C/min and held for 6.33 min. The total run time was 85 min. Mass spectra of selected metabolite fragments (Table 3.2) were collected in SIR mode.

3.2.8 Derivatization and GC-MS Analysis of Extracellular Metabolites

For quantification of extracellular metabolites, 200 μL of culture medium was supplemented with 30 μL of 10 mg/mL of [U-^{13}C]algal hydrolysate, 10 μL of 60 mM [U-^{13}C]glutamine and 30 μL of 0.1 N NaOH. Three replicates were prepared for all samples. 1 mL of cold acetone (-20°C) was then added and the samples were vortexed vigorously. After centrifugation at 14,000×g for 5 min, the supernatants were evaporated to dryness under air flow at 37°C. 50 μL of pyridine was added to the samples and mixed by pipetting. 50 μL of MTBSTFA + 1% TBDMCS was added and the samples were derivatized at 60°C for 30 min. After an overnight incubation at room temperature, the derivatized samples were centrifuged for 2 min at 14,000×g, to remove debris, and the clear liquid was transferred into GC vials for GC-MS analysis. The injection volume was 1 μL and samples were injected in split mode with split ratio ranging from 1:5 to 1:20. GC oven temperature was held at 80°C for 2 min, increased to 280°C at 7°C/min and held for 9.43 min. The total run time was 40 min. Mass spectra of selected metabolite fragments (Table 3.2) were collected in SIR mode.

Table 3.2 Metabolite fragments measured by GC-MS

Metabolite	Mass (*m/z*)	Carbon atoms	Fragment formula
Organic acids			
Pyruvate	174	1-2-3	$C_6H_{12}O_3NSi$
Lactate	233	2-3	$C_{10}H_{25}O_2Si_2$
Lactate	261	1-2-3	$C_{11}H_{25}O_3Si_2$
Succinate	289	1-2-3-4	$C_{12}H_{25}O_4Si_2$
Fumarate	287	1-2-3-4	$C_{12}H_{23}O_4Si_2$
AKG	346	1-2-3-4-5	$C_{14}H_{28}O_5NSi_2$
Malate	419	1-2-3-4	$C_{18}H_{39}O_5Si_3$
PEP	453	1-2-3	$C_{17}H_{38}O_6Si_3P$
GAP	484	1-2-3	$C_{18}H_{43}O_6NSi_3P$
GLP	571	1-2-3	$C_{23}H_{56}O_6Si_4P$
Citrate	459	1-2-3-4-5-6	$C_{20}H_{39}O_6Si_3$
3PG	585	1-2-3	$C_{23}H_{54}O_7Si_4P$
Amino acids			
Alanine	232	2-3	$C_{10}H_{26}ONSi_2$
Alanine	260	1-2-3	$C_{11}H_{26}O_2NSi_2$
Glycine	246	1-2	$C_{10}H_{24}O_2NSi_2$
Valine	260	2-3-4-5	$C_{12}H_{30}ONSi_2$
Leucine	274	2-3-4-5-6	$C_{13}H_{32}ONSi_2$
Isoleucine	274	2-3-4-5-6	$C_{13}H_{32}ONSi_2$
Proline	258	2-3-4-5	$C_{12}H_{28}ONSi_2$
Methionine	320	1-2-3-4-5	$C_{13}H_{30}O_2NSi_2S$
Serine	390	1-2-3	$C_{17}H_{40}O_3NSi_3$
Threonine	404	1-2-3-4	$C_{18}H_{42}O_3NSi_3$
Phenylalanine	302	1-2	$C_{14}H_{32}O_2NSi_2$
Aspartate	302	1-2	$C_{14}H_{32}O_2NSi_2$
Aspartate	390	2-3-4	$C_{17}H_{40}O_3NSi_3$
Aspartate	418	1-2-3-4	$C_{18}H_{40}O_4NSi_3$
Glutamate	330	2-3-4-5	$C_{16}H_{36}O_2NSi_2$
Glutamate	432	1-2-3-4-5	$C_{19}H_{42}O_4NSi_3$
Glutamine	431	1-2-3-4-5	$C_{19}H_{43}O_3N_2Si_3$
Tyrosine	302	1-2	$C_{14}H_{32}O_2NSi_2$

This table was adapted from a published paper by Ahn and Antoniewicz (2011).

3.2.9 Derivatization and GC-MS Analysis of Glucose

Labeling of glucose in the medium was determined by GC-MS analysis of the aldonitrile pentapropionate derivative of glucose (Antoniewicz et al., 2011). In short, 100 μL of medium was deproteinized with cold acetone (-20°C) and the samples were evaporated to dryness under air flow. Next, 50 μL of hydroxylamine hydrochloride solution (20 mg/mL in pyridine) was added to the samples. The samples were heated at 90°C for 60 min, followed by addition of 100 μL of propionic anhydride. After 30 min incubation at 60°C, the samples were evaporated to dryness, dissolved in 100 μL of ethyl acetate and transferred into GC vials for GC-MS analysis. The injection volume was 1 μL and samples were injected at 1:40 split ratio. GC oven temperature was held at 80 °C for 1 min, increased to 280 °C at 15 °C/min, and held for 6 min. Glucose eluted at 13.4 min. Labeling of glucose was determined from mass isotopomer distribution of the fragment at *m/z* 370, which contains carbon atoms C1-C5 of glucose.

3.2.10 Preparation of Amino Acids Standards

To determine concentrations of amino acids in the [U-^{13}C]algal hydrolysate solution, which was used for amino acid quantification, amino acid standard H (1.25 μmol/mL for L-cystine, and 2.5 μmol/mL for all other amino acids) was diluted with 0.1 N HCl. Next, 0, 6.25, 12.5, 25 and 50 μL of the amino acid standard was added to 30 μL of 10 mg/mL of [U-^{13}C]algal hydrolysate. All samples were then dried under air, derivatized by TBDMS and analyzed by GC-MS. From the analysis of mass isotopomer distributions, the concentrations of all amino acids in the [U-^{13}C]algal hydrolysate solution were determined. The characterized internal standard solution

was then used for quantification of amino acids in medium samples. The quantification results of amino acids were shown in the previous Table 3.1.

3.2.11 Determination of Biomass Specific Rates

Specific growth rate (μ), specific glutamine uptake rate (q_{Gln}) and specific ammonium production rates (q_{Amm}) were defined as follows;

$$\frac{dX}{dt} = \mu X \quad (3.1)$$

$$\frac{d[Gln]}{dt} = -k[Gln] - q_{Gln}X \quad (3.2)$$

$$\frac{d[NH_3]}{dt} = k[Gln] + q_{NH_3}X \quad (3.3)$$

The differential equations were solved using the method by Glacken et al (Glacken et al., 1988). For glutamine, the spontaneous degradation to pyroglutamate and ammonium was taken into account (Ozturk and Palsson, 1990). The glutamine decomposition rate constant (k) was determined to be 0.0020 h^{-1} in control experiments without cells. In addition, we determined the accumulation rates of amino acids in the medium in control experiments without cells in Table 3.3. The accumulation was assumed to be due to hydrolysis of proteins/ peptides in the medium and due to evaporation effects. The biomass specific consumption and production rates of amino acids were calculated from time course data after correction for the accumulation rates in the control experiments. For stationary phase, an average cell number of $2.23 \pm 0.13 \times 10^6$ cells/mL (days 4-6) was used to calculate biomass specific rates.

Table 3.3 Accumulation rates of amino acids in the medium in a control experiment without CHO cells (μM/h).

	Rate (μM/h)	R^2
Alanine	0.62	0.98
Glycine	0.56	0.99
Valine	0.58	0.99
Leucine	0.96	0.99
Ileucine	0.63	0.96
Proline	0.47	0.93
Methionine	0.09	0.81
Serine	0.44	0.99
Threonine	0.49	0.95
Phenylalanine	0.42	0.98
Aspartate	0.35	0.97
Glutamate	0.53	0.99
Tyrosine	0.37	0.98

This table was adapted from a published paper by Ahn and Antoniewicz (2011).

3.2.12 Metabolic Network Model

A compartmentalized metabolic network model of CHO cell metabolism was constructed for metabolic flux analysis. The complete network model is given in Table 3.5 at the end of this chapter. The model consists of 73 reactions and 77 metabolites and includes reactions for glycolysis, pentose phosphate pathway, TCA cycle, anaplerotic and cataplerotic reactions, amino acid metabolism, lactate metabolism, fatty acid metabolism, and a lumped reaction for cell growth (v_{73}). The lumped biomass equation was based on anabolic requirements for biosynthesis of proteins, lipids, RNA, DNA, and carbohydrates (Sheikh et al., 2005). For the conversion of growth rate to the flux of the lumped biomass reaction, a dry weight for CHO cells of 0.315 mg/10^6cells was assumed (Altamirano et al., 2001). As an example, a growth rate of 0.033 h^{-1} corresponds to a flux value of 99.6 nmol/10^6cells/h for reaction v_{73} in

the model. Three compartments were considered in the model: cytosol, mitochondrion and extracellular medium. We did not include cofactor balances in the model to avoid biases resulting from uncertainties regarding fluxes of isoenzymes with alternative cofactor requirements, e.g. NADH and NADPH dependent malic enzymes and isocitrate dehydrogenase. In the model, CO_2 was treated as an unbalanced metabolite, and oxygen was not included in the model because the rate of oxygen uptake was not measured in this study and could not be estimated from ^{13}C-labeling data.

3.2.13 Metabolic Flux Analysis

^{13}C-MFA at isotopic steady state was performed using Metran software (Yoo et al., 2008), a flux analysis package based on the elementary metabolite units (EMU) framework (Antoniewicz et al., 2007b). Isotopic non-stationary ^{13}C-MFA was performed using the tools described by Young et al. (Young et al., 2008). In short, fluxes and metabolite pools sizes were estimated by minimizing the variance-weighted sum of squared residuals (SSR) between the experimentally measured and model predicted extracellular uptake and production rates, and mass isotopomer distributions of intracellular metabolites, using non-linear least-squares regression (Antoniewicz et al., 2006a; Antoniewicz et al., 2007b). In all cases, flux estimation was repeated at least 100 times starting with random initial values for all fluxes to find a global solution. The fitting results were subjected to a χ^2 statistical test to assess the goodness-of-fit, and accurate 95% confidence intervals were computed for all estimated parameters by evaluating the sensitivity of the sum of squared residuals to flux variations (Antoniewicz et al., 2006a).

3.3 Results

3.3.1 Cell Growth

CHO cells were grown in fed-batch culture over a period of six days. Figure 3.1 shows the time profiles of viable cell density, glucose and lactate concentrations. The viable cell density increased from 0.2×10^6 cells/mL on day 1 to a maximum cell density of 2.3×10^6 cells/mL on day 5. On day 6, the cell density decreased slightly to 2.1×10^6 cells/mL. Cell viability was >95% during the entire culture (data not shown). The cell growth rate at the exponential phase was 0.033 h^{-1} between days 1 and 2.

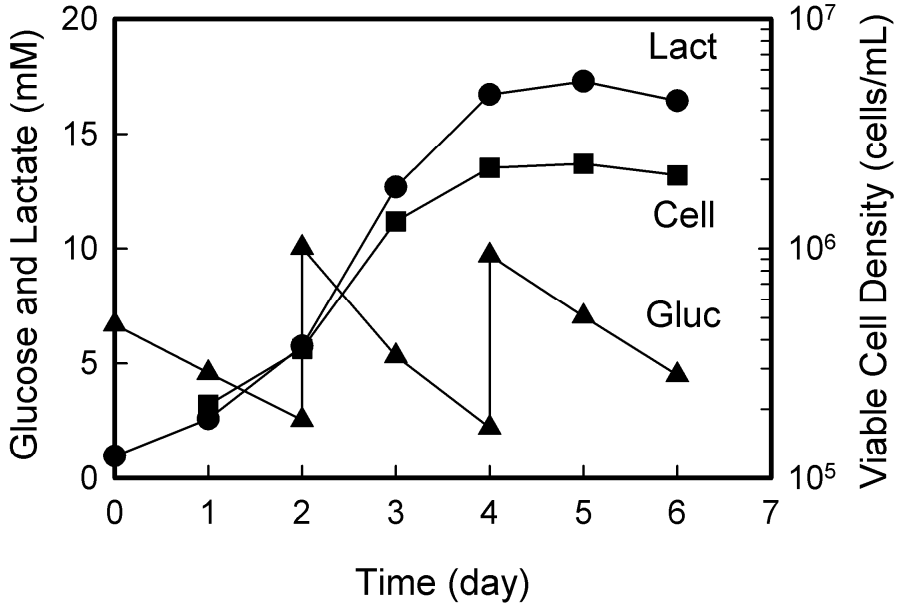

Figure 3.1 Time profiles of viable cell density and glucose and lactate concentrations in the medium (lactate, ●; viable cell density, ■; glucose, ▲). Standard deviations of glucose and lactate measurements were within 5%. Standard deviations of cell density measurements were within 7%. This figure was adapted from a published paper by Ahn and Antoniewicz (2011).

3.3.2 Glucose and Lactate Metabolism

The fed-batch experiment was designed such that the glucose concentration was above 2 mM at all times, which in preliminary studies was determined to be the minimum glucose concentration that didn't affect cell growth. During the culture, glucose concentration decreased from 6.7 mM on day 0 to 2.5 mM on day 2. On day 2, a bolus of glucose was added to a final concentration of 10.0 mM. On day 4, a second bolus of glucose was added to a final concentration of 9.7 mM. The concentration of lactate rapidly increased during the exponential growth phase from 1.0 mM on day 0 to a maximum concentration of 17.3 mM on day 5, which then slightly decreased to 16.4 mM on day 6. Figure 3.2A shows the plot of cumulative glucose and lactate concentrations. Between days 0 and 4, the amount of lactate produced per glucose consumed was constant at 1.50 mol/mol. The theoretical maximum yield of lactate from glucose is 2 mol/mol. Thus, about 75% of glucose consumed was converted to lactate during the exponential growth phase, i.e. assuming contributions from other sources are ignored.

3.3.3 Glutamine Metabolism

Figure 3.2B shows time profiles of medium metabolites related to glutamine metabolism. The biomass specific glutamine consumption rate (corrected for glutamine degradation) was 36.1 nmol/10^6cells/h at the exponential growth phase (days 2-3) and 4.2 nmol/10^6cells/h at the stationary phase (days 4-5). The biomass specific ammonium production rate was 27.0 nmol/10^6cells/h at exponential phase and 7.8 nmol/10^6cells/h at the stationary phase. Thus, the amount of ammonium produced per glutamine consumed shifted from 0.75 mol/mol at the exponential growth phase to 1.86 mol/mol at the stationary phase. The concentration of alanine increased during

the culture at a relatively constant rate from 0.11 mM on day 0 to 0.46 mM on day 6. Glutamate increased during the exponential growth phase from 0.10 mM on day 0 to 0.45 mM on day 4, but then remained relatively constant during the stationary phase. Proline increased slightly from 0.04 mM on day 0 to 0.17 mM on day 6. The concentration profiles for all measured extracellular metabolites are giving in the previous Table 3.1. Table 3.4 shows the calculated extracellular uptake and excretion rates at both phases

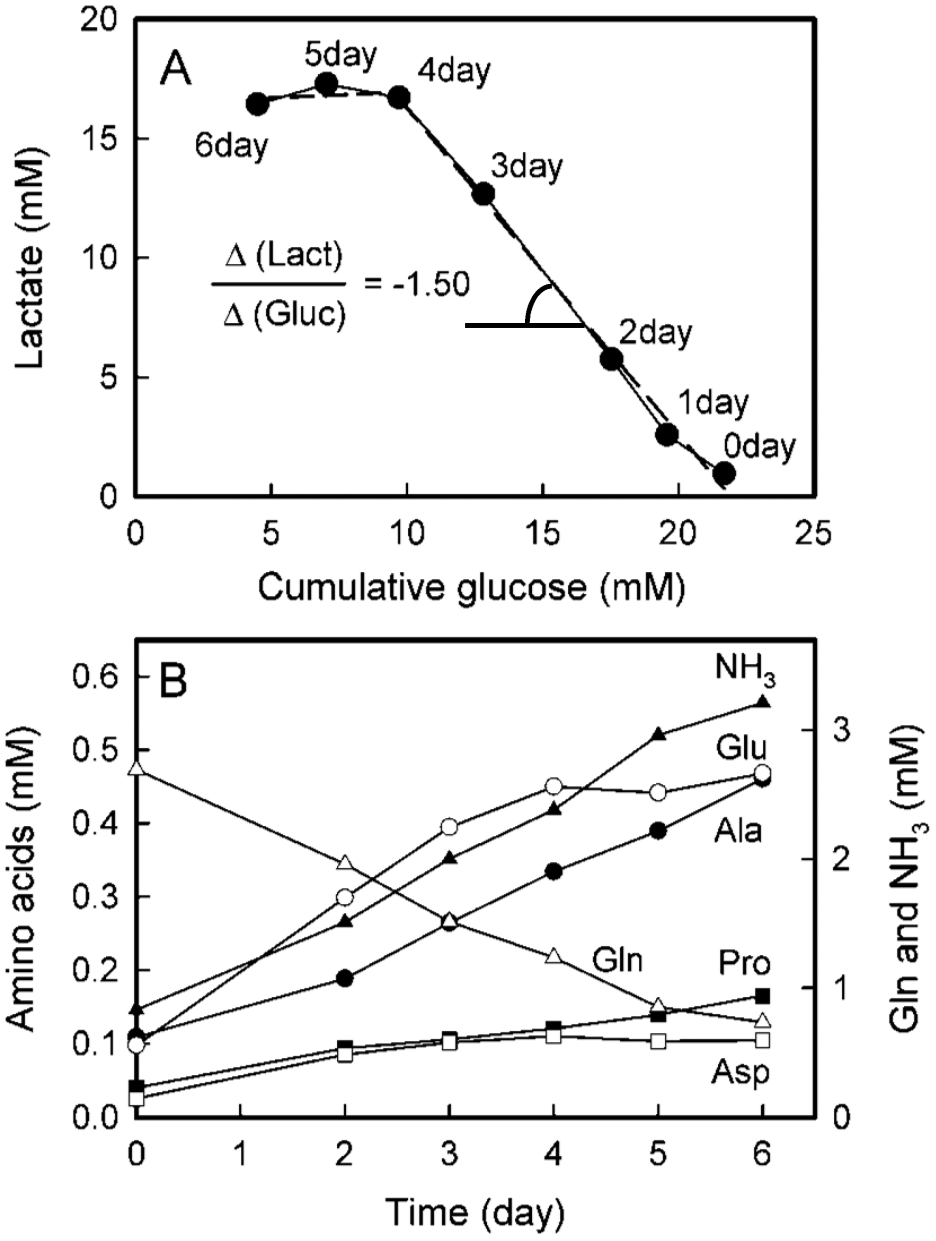

Figure 3.2 (A) Plot of cumulative glucose consumed and lactate produced during the culture. (B) Concentration profiles of free amino acids and ammonium in the medium (Ala, ●; Glu, ○; Pro, ■; Asp, □; NH_4^+, ▲; Gln, △). Standard deviations of amino acid measurements were within 5%. This figure was adapted from a published paper by Ahn and Antoniewicz (2011).

Table 3.4 Biomass specific uptake and excretion rates of extracellular metabolites (nmol/10^6cells/h).

	Exponential Phase	Stationary Phase
Glucose	-201.1	-48.8
Lactate	299.5	-2.5
NH_3	27.0	7.8
Alanine	2.1	0.6
Glycine	2.9	0.5
Valine	-5.3	-0.3
Leucine	-6.9	-0.5
Isoleucine	-6.4	-0.4
Proline	-0.3	0.1
Methionine	-1.7	-0.1
Serine	-7.5	-0.9
Threonine	-4.3	-0.3
Phenylalanine	-2.9	-0.2
Aspartate	-0.4	-0.5
Glutamate	5.2	-0.8
Tyrosine	-2.2	-0.2
Glutamine	-36.1	-4.2

This table was adapted from a published paper by Ahn and Antoniewicz (2011)

3.3.4 ^{13}C-Labeling Dynamics of Intracellular Metabolites

Isotopic tracers were applied in this study to investigate intracellular metabolism of CHO cells at the growth phase (days 2-3) and stationary phase (days 4-5). Specifically, we used [1,2-^{13}C]glucose as the tracer, which was previously identified as the best tracer for analysis of overall cellular metabolism of mammalian cells by GC-MS (Antoniewicz et al., 2006a; Metallo et al., 2009). Figure 3.3 shows the time profiles of ^{13}C-labeling of intracellular metabolites after the addition of [1,2-^{13}C]glucose on day 2 (exponential phase) and day 4 (stationary phase). The percentage

of labeled isotopomers for each metabolite (100%-M0) was determined from the measured mass isotopomer distributions (MIDs) after correction for natural isotope abundances. The composition of extracellular glucose on days 2 and 4 was 75% [1,2-^{13}C]glucose and 25% natural glucose, which was verified by GC-MS analysis. As shown in Figure 3.3A and B, metabolites in the glycolysis pathway, glyceraldehyde 3-phosphate (GAP), 3-phosphoglycerate (3PG) and phophoenolpyruvate (PEP), reached isotopic steady state within 6 h at both phases. The steady-state labeling of GAP, 3PG and PEP were 38%, 34% and 32% at the exponential phase and 36%, 32% and 30% at the stationary phase, respectively. The maximum expected labeling of glycolytic intermediates was 37.5% (=75%/2). This corresponded well with the measured values for GAP. The labeling dynamics of glycerol-3-phosphate (GLP) were significantly slower at both phases compared to glycolytic intermediates. We estimated that at 24 h GLP reached about 95% of isotopic steady-state labeling, which was 32% at the exponential phase, but only 16% at the stationary phase. The reduced enrichment at the stationary phase suggests the presence of other pathways contributing to GLP production from non-labeled sources.

The labeling dynamics related to pyruvate metabolism are shown in Figure 3.3C and D. The labeling of intracellular pyruvate, lactate and alanine were about 3-fold higher at the exponential phase than at the stationary phase. The 24 h labeling of intracellular pyruvate, lactate and alanine were 22%, 24% and 10% at the exponential phase and 7.5%, 7.9% and 5.0% at the stationary phase, respectively. The reduced labeling at the stationary phase is consistent with the metabolic shift from lactate production to lactate consumption (Figure 3.2A). At the stationary phase, the large pool of non-enriched lactate in the medium would have diluted the labeling of

intracellular pyruvate and alanine. The approach to isotopic steady state was similar at the two phases for pyruvate and lactate. We estimated that at 24 h pyruvate and lactate reached ~90% of isotopic steady-state labeling. The labeling dynamics for alanine were much slower. The labeling of alanine increased linearly over 24 h and did not approach isotopic steady-state.

The labeling dynamics of TCA metabolites are shown in Figure 3.3E-H. At 24 h, the ^{13}C-labeling of most TCA metabolites was less than 15%, which was a significant reduction from ~30% labeling of PEP. This lower level of labeling is partially explained by the slow approach to isotopic steady-state for most TCA metabolites. At 24 h, none of the TCA metabolites had reached isotopic steady-state. In fact, most of the TCA metabolites were still in the initial stages of isotopic labeling accumulation, where the labeling increases linearly with time. At 24 h, the labeling of citrate at the exponential phase (28%) was about 2-fold higher than at the stationary phase (15%). Surprisingly, the labeling of α-ketoglutarate (AKG) at both phases was similar, i.e. 20% at the exponential phase and 16% at the stationary phase, and glutamate labeling was also similar at the stationary phase (12%) and exponential phase (11%). The labeling dynamics of malate, fumarate and aspartate are shown in Figure 3.3G and H. The 24 h labeling of malate, fumarate and aspartate were 12%, 11% and 10% at the exponential phase and 11%, 7% and 9% at the stationary phase, respectively.

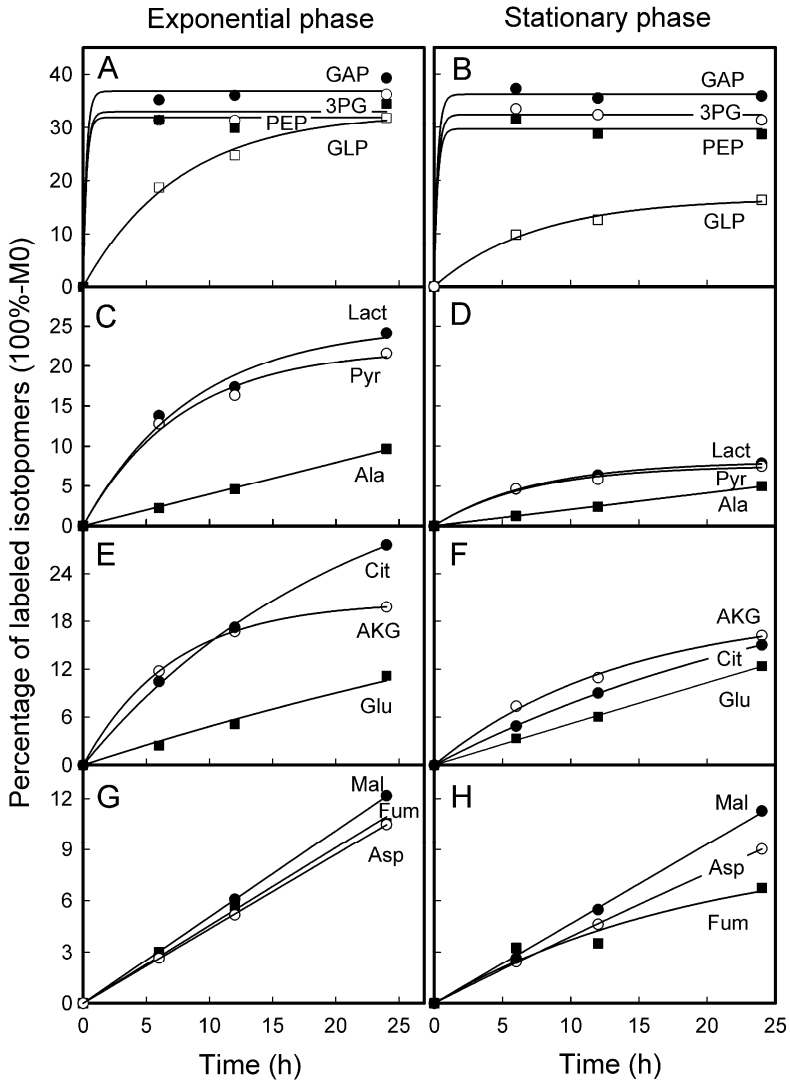

Figure 3.3 Time profiles of isotopic labeling of intracellular metabolites. They were analyzed after the introduction of [1,2-^{13}C]glucose at the exponential phase (day 2) and stationary phase (day 4). Percentages of ^{13}C-labeled mass isotopomers (100%-M0) of intracellular metabolites were determined after correction for natural isotope abundances. (A, B) metabolites related to glycolysis at exponential and stationary phases, respectively (GAP, ●; 3PG, ○; PEP, ■; GLP, □); (C, D) metabolites related to pyruvate metabolism (Lact, ●; Pyr, ○; Ala, ■); (E, F) metabolites at the beginning of TCA cycle (Cit, ●; AKG, ○; Glu, ■); (G, H) metabolites at the end of TCA cycle (Mal, ●; Asp, ○; Fum, ■). Standard deviations of isotopic labeling measurements were within 0.5 mol%. The solid lines illustrate the measured labeling trends. This figure was adapted from a published paper by Ahn and Antoniewicz (2011).

3.3.5 Mass Isotopomer Distributions (MIDs) of Intracellular Metabolites

Figure 3.4 shows the time evolution of mass isotopomers for three representative metabolites of glycolysis and TCA cycle (PEP, malate and citrate) at the exponential and stationary phases. For PEP, the distribution of mass isotopomers was relatively constant at 6, 12 and 24 h at both phases, indicating that metabolic and isotopic steady state was reached. At the exponential phase, PEP was predominantly M2 labeled with less than 3% M1 and M3 mass isotopomers. Similar labeling patterns were observed for the other glycolytic intermediates, e.g. GAP and 3PG in Figure 3.5 at 24 h after addition of tracers. The low abundance of M1 mass isotopomer indicated that oxidative pentose phosphate pathway was inactive at the exponential growth phase, i.e. there was no loss of ^{13}C from [1,2-^{13}C]glucose. At the stationary phase, the distribution of M1, M2 and M3 mass isotopomers was 17%, 74%, and 9%, respectively. Thus, the presence of M1 and M3 mass isotopomers suggested that the pentose phosphate pathway was active at the stationary phase.

In contrast to the glycolytic metabolites, the mass isotopomer distributions of TCA metabolites changed significantly with time. Thus, these metabolites were at isotopic non-steady state. At both phases, the abundances of M2 mass isotopomers decreased with time and the abundances of M1, M3 and M4 mass isotopomers increased. This pattern can be explained as follows: (i) at each turn of the TCA cycle, labeled malate was produced from labeled citrate, and since some of the ^{13}C-labeling of citrate was lost as $^{13}CO_2$, the formation of M1-labeled malate from M2-labeled citrate was expected; (ii) as the relative enrichments of TCA metabolites increased with time in Figure 3.3, the probability that two labeled molecules of AcCoA and oxaloacetate would condense also increased. Thus, the relative abundances of M3 and M4 mass isotopomers of citrate were expected to increase with time.

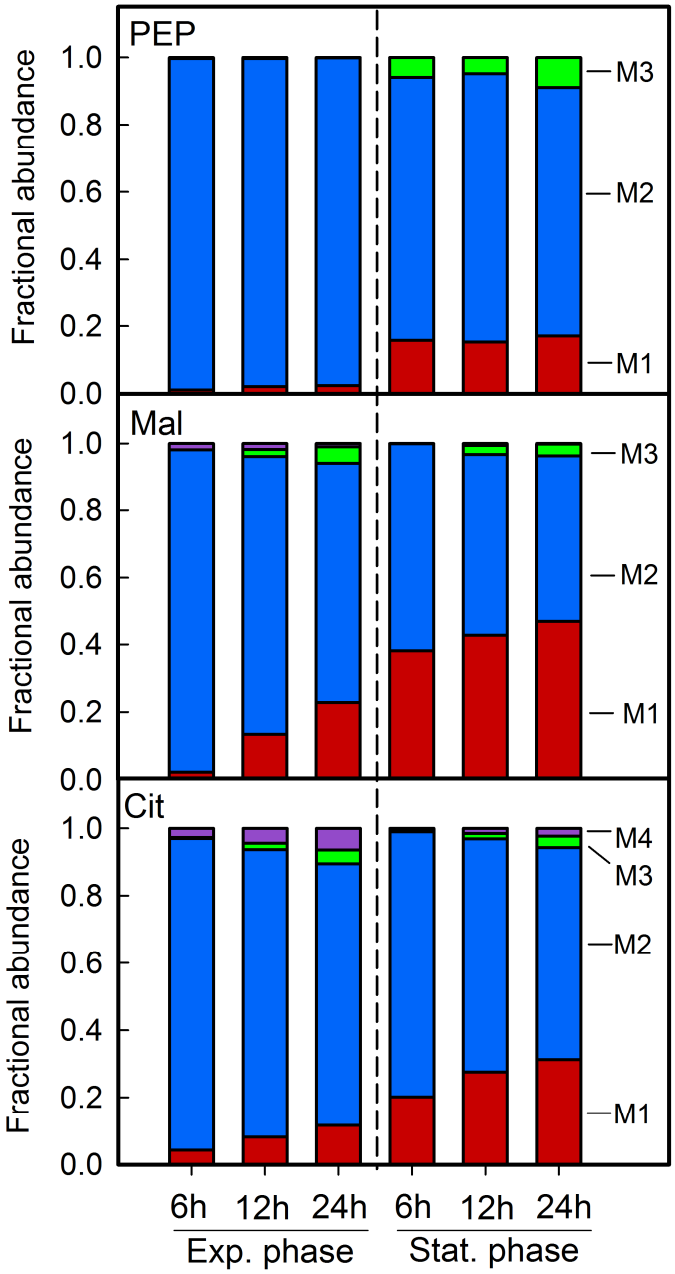

Figure 3.4 Fractional abundances of labeled mass isotopomers at 6, 12 and 24 h after the addition of isotopic tracers. It was suggested three representative metabolites in the glycolysis pathway and TCA cycle: PEP (*m/z* 453), malate (*m/z* 419) and citrate (*m/z* 459). This figure was adapted from a published paper by Ahn and Antoniewicz (2011).

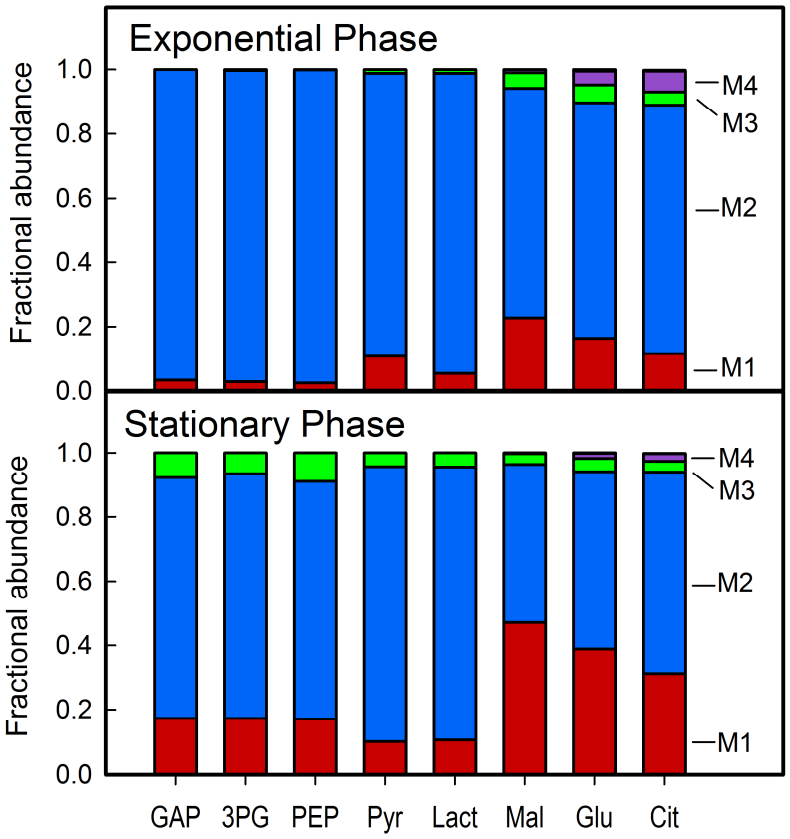

Figure 3.5 Fractional abundances of labeled mass isotopomers at 24 h after the addition of isotopic tracers at the exponential phase (A) and stationary phase (B). Shown are the data for the following metabolite fragments: GAP (*m/z* 484), 3PG (*m/z* 585), PEP (*m/z* 453), pyruvate (*m/z* 174), lactate (*m/z* 261), malate (*m/z* 419), glutamate (*m/z* 432), and citrate (*m/z* 459). This figure was adapted from a published paper by Ahn and Antoniewicz (2011).

3.3.6 Metabolic Flux Analysis

Since glycolytic metabolites reached isotopic steady-state, traditional stationary ^{13}C-MFA could be applied to determine the split ratio at the branch point between glycolysis and pentose phosphate pathway. For stationary ^{13}C-MFA we used a simplified model consisting of the reactions for glycolysis and PPP (Table 3.5, reactions 1-15), and we fitted the mass isotopomer distributions of GAP and 3PG, together with the measured glucose uptake rate, to determine the flux of oxidative pentose phosphate pathway (oxPPP). The oxPPP flux was 1.8 ± 0.2 nmol/10^6cells/h at the exponential phase and 10.1 ± 0.8 nmol/10^6cells/h at the stationary phase. Thus, the absolute oxPPP flux increased 5.6-fold at the stationary phase. The oxPPP flux normalized to glucose uptake was 0.9 ± 0.1 (mol/100 mol glucose) at the exponential phase and 20.7 ± 1.6 at the stationary phase. The normalized oxPPP flux corresponded well with the ratio of M1/M2 mass isotopomers in the glycolytic intermediates, i.e. the first ^{13}C-carbon of glucose is lost in oxPPP resulting in the formation of M1 mass isotopomers. The averaged ratio of M1/M2 mass isotopomers for GAP, 3PG, PEP and lactate was 3.3 ± 1.3 % at the exponential phase and 19.5 ± 1.9 % at the stationary phase in Figure 3.6.

3.3.7 Non-stationary Metabolic Flux Analysis

Since metabolites of the TCA cycle and related pathways did not reach isotopic steady state, stationary ^{13}C-MFA could not be applied to determine fluxes in the rest of the model. Instead, we applied non-stationary ^{13}C-MFA using the tools developed by Young et al (2008) to determine metabolic fluxes in the complete network model. Fluxes were determined by fitting the measured uptake and consumption rates of external metabolites in Table 3.4, the measured cell growth rate,

the estimated oxPPP flux, and MID data at 6, 12 and 24 h for the following intracellular metabolites: GLP (*m/z* 571), lactate (*m/z* 233, 261), malate (*m/z* 419), GAP (*m/z* 484), citrate (*m/z* 459), alanine (*m/z* 232, 260), aspartate (*m/z* 418) and glutamate (*m/z* 330, 432). For simplicity, we assumed that intracellular lactate and cytosolic pyruvate pool were equilibrated. Non-stationary ^{13}C-MFA analysis was performed for the exponential phase and the stationary phase independently. Over the three time points (6, 12, and 24 h) we collected 216 mass isotopomer measurements at each phase. The system possessed 144 redundant measurements and the expected lower and upper bounds for the 95% confidence region of SSR were 112 and 179, i.e. assuming the minimized sum of squared residual followed a χ^2-distribution. We obtained statistically acceptable fits for both phases, with minimized SSR values of 111 and 86 for the exponential and stationary phases, respectively. The complete flux results at both phases, including 95% confidence intervals for all estimated parameters, are given in Appendix A (see Tables A.1 and A.2). The estimated fluxes at both phases are shown schematically in Figure 3.6.

The most active metabolic pathway at the exponential phase was glycolysis (406 ± 34 nmol/10^{6}cells/h). The majority of pyruvate produced via glycolysis was secreted as lactate (290 ± 25 nmol/10^{6}cells/h). The TCA cycle flux was ~38% of glycolysis flux (154 ± 36 nmol/10^{6}cells/h for citrate synthase). Pyruvate dehydrogenase (PDH) was the main reaction contributing to mitochondrial AcCoA production (138 ± 35 nmol/10^{6}cells/h), with negligible contribution from fatty acid oxidation. There were two important anaplerotic reactions at the exponential phase: glutamate dehydrogenase (GDH, 24 ± 4 nmol/10^{6}cells/h) and pyruvate carboxylase (PC, 25 ± 9 nmol/10^{6}cells/h). Malic enzyme (ME) was the most significant

cataplerotic reaction (53 ± 11 nmol/10^6cells/h), with negligible flux through citrate lyase.

At the stationary phase, the glycolysis flux (97 ± 7 nmol/10^6cells/h) was reduced 4-fold compared to the exponential phase, and most of the pyruvate produced was oxidized in the TCA cycle. The PDH (106 ± 7 nmol/10^6cells/h) and citrate synthase fluxes (109 ± 7 nmol/10^6cells/h) were similar to the fluxes at the exponential phase. In contrast, anaplerosis was drastically reduced at the stationary phase, with 4.9 ± 0.4 nmol/10^6cells/h for glutamate dehydrogenase (i.e. 5-fold lower compared to the exponential phase) and 12 ± 5 nmol/10^6cells/h for pyruvate carboxylase (2-fold lower). As a result, malic enzyme flux (18 ± 5 nmol/10^6cells/h) was about 3-fold lower compared to the exponential phase. The fluxes of citrate lyase and fatty acid oxidation were negligible, consistent with the results for the exponential phase.

In addition, Figure 3.7 shows the metabolism of amino acids at both phases. Overall levels of Gln, Ser, Leu, Ile, Val, Thr, Phe, Pro, Met and Tyr were the measured values of uptake rates and the each stacked bars estimated by ^{13}C-MFA indicated the utilization for biomass production, catabolism for energy generation and conversion to other amino acids. Thus, the fates of consumed amino acids in cells were successfully observed by ^{13}C-MFA. This is one of strong applications, e.g. media formulation or cell engineering for mammalian cell culture.

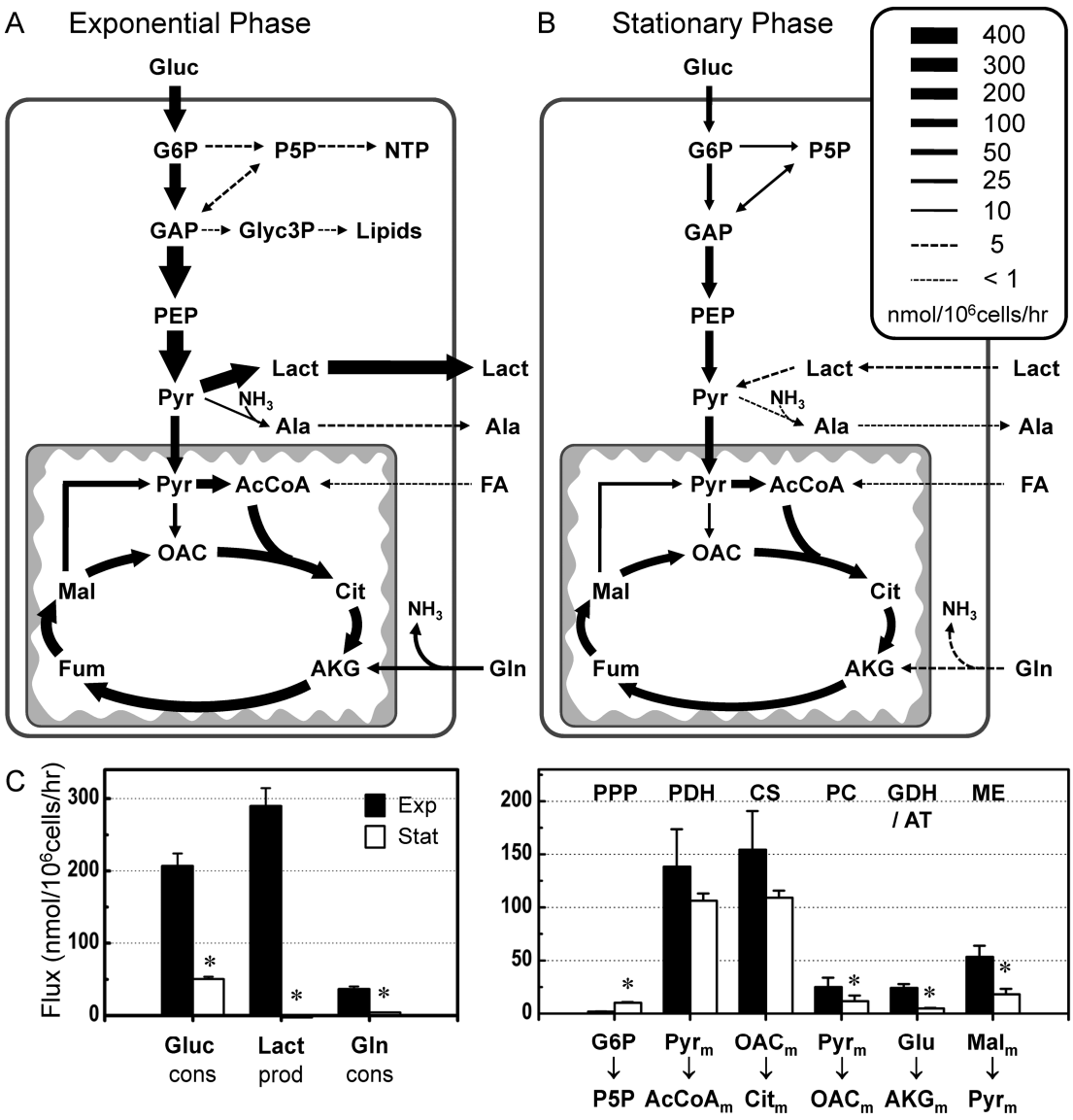

Figure 3.6 Metabolic flux maps for CHO cells at the exponential growth phase (A) and stationary phase (B) from non-stationary ^{13}C-MFA. (C) Comparison of key extracellular uptake and excretion rates. (D) Comparison of key intracellular metabolic fluxes. Asterisk (*) denotes statistically significant difference ($P < 0.01$). Abbreviations: PPP, oxidative pentose phosphate pathway; PDH, pyruvate dehydrogenase; CS, citrate synthase; PC, pyruvate carboxylase; GDH/AT, glutamate dehydrogenase /aminotransferase; ME, malic enzyme. This figure was adapted from a published paper by Ahn and Antoniewicz (2011).

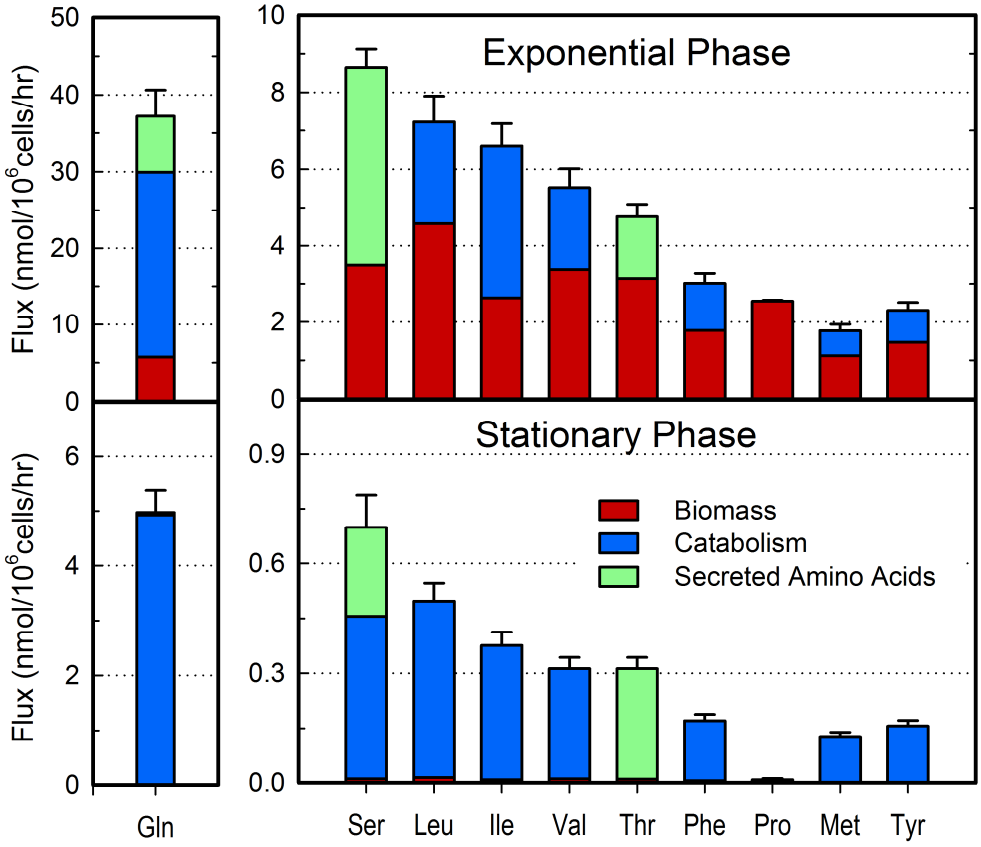

Figure 3.7 Amino acid metabolism of CHO cells at the exponential and stationary phases. Amino acids were metabolized to biomass, catabolism or other amino acids by biochemical reactions within cells.

3.4 Discussion

In this study, CHO cell metabolism was characterized at the growth phase and stationary phase by extracellular uptake and production rates, intracellular isotope labeling dynamics, and intracellular metabolic fluxes. CHO cells were grown as a monolayer culture on DMEM medium supplemented with serum, with glucose and glutamine as the main carbon sources. The growth rate and viable cell density corresponded well with results from other CHO cell and hybridoma cell cultures (Ozturk and Palsson, 1991; Yoon et al., 2003). Glucose was replenished twice during

the culture, on days 2 and 4, to maintain glucose concentration above 2 mM. It was reported previously that maintaining glucose concentration above 1 mM is important in mammalian cell culture (Kurokawa et al., 1994; Vriezen and van Dijken, 1998). This corresponded well with our preliminary results. In this study, the time points of glucose additions were carefully chosen to coincide with the mid exponential growth phase and the beginning of the stationary phase to allow the introduction of ^{13}C-labeled glucose at these time points. In previous ^{13}C-MFA studies, a pre-incubation step was sometimes applied before the addition of ^{13}C-tracers, e.g. by replacing the medium with fresh medium to re-vitalize cell activity and remove extracellular by-products such as lactate that can be taken up by the cells (Hofmann et al., 2008; Metallo et al., 2009), while in other studies chemically defined media were used to reduce the number of extracellular metabolites that can be taken up by the cells (Deshpande et al., 2009). An advantage of these approaches is that higher ^{13}C-enrichments of intracellular metabolites may be achieved due to reduced dilution of ^{13}C-labeling by external metabolites. However, the goal of this study was to establish realistic maps of cell metabolism that reflects typical CHO cell cultures at the growth and stationary phases. Therefore, we decided not to include a pre-incubation step, or refresh the medium before the addition of tracers.

As indicated above, a significant challenge in estimating intracellular metabolic fluxes in mammalian cells is the complex composition of the medium, which typically includes many carbon sources (e.g. glucose and amino acids), various growth factors and other uncharacterized nutrients from the serum. In this study, we attempted to directly measure the uptake rates of key carbon sources and the production rates of key products of metabolism. In general, if unlabeled metabolites

that are taken up by the cells, this will dilute the labeling of intracellular metabolites. In our current model, the main entry points of unlabeled material were via lactate and amino acids, which we quantified directly. If other unlabeled metabolites are taken up by the cells, the model will account for this by increasing the uptake rates of the metabolites that are metabolically closest to the entry points into central metabolism.

In this study, the transition from growth phase to stationary phase was evident from the growth curve in Figure 3.1, and correlated with a dramatic shift in glucose and lactate uptake and production rates, glutamine uptake rate, and amino acid uptake rates, all of which could be directly observed from extracellular measurements in Figure 3.2 and Table 3.4. It is well known that key intracellular metabolic fluxes such as pentose phosphate pathway and anaplerosis from pyruvate cannot be observed from extracellular measurements alone (Goudar et al., 2010). Therefore, isotopic tracers and mass spectrometry were applied in this study to investigate intracellular metabolism of CHO cells in further detail. Mass isotopomer distributions were measured for intracellular metabolites in the glycolysis pathway, TCA cycle, and amino acid metabolism. Glycolytic intermediates GAP, 3PG and PEP reached isotopic steady-state within 6 h in Figure 3.3. Other researchers also reported rapid metabolic and isotopic steady-state for glycolytic metabolites in mammalian cells (Maier et al., 2008; Sengupta et al., 2011). In this study, metabolites of the TCA cycle were significantly less labeled than glycolytic metabolites. Previously, Sengupta et al. (2011) reported no significant accumulation of ^{13}C-labeling in TCA cycle metabolites after 4 h following the introduction of ^{13}C-glucose. Here, we chose longer time points for measuring isotopic labeling of intracellular metabolites, i.e. 6, 12 and 24 h. At 24 h, most of the TCA cycle metabolites were 10-20% labeled. Even though intracellular metabolites

did not reach isotopic steady-state, non-stationary ^{13}C-MFA was successfully applied to quantify intracellular metabolic fluxes. This is the first time that fluxes in the TCA cycle and related pathways were quantified in CHO cells using isotopic tracers and intracellular metabolite labeling measurements.

Important metabolic fluxes that were determined from ^{13}C-labeling measurements were the flux of oxidative pentose phosphate pathway (oxPPP), the flux of anaplerosis from pyruvate to oxaloacetate, the flux of TCA cycle, citrate lyase flux, and the rate of fatty acid oxidation. We observed that citrate lyase and oxidation of fatty acids were negligible compared other fluxes in the model at both phases. At the exponential phase, the metabolic flux map was characterized by a negligible flux of oxPPP, high flux from glucose to lactate, and significant anaplerotic flux from pyruvate to oxaloacetate and from glutamate to AKG. The negligible oxPPP flux suggested that CHO cells did not require significant amounts of NADPH for growth. In other words, our results suggest that CHO cells rely mainly on uptake of extracellular amino acids for cell growth and not on *de novo* biosynthesis of these precursors. An alternative explanation is that CHO cells preferentially use malic enzyme for generation of NADPH instead of oxPPP. In fact, we observed a significant flux of malic enzyme at the growth phase. However, because it was not possible to distinguish between NADH-dependent and NADPH-dependent malic enzyme fluxes using ^{13}C-tracers, it difficult to evaluate redox metabolism of CHO cells in detail from the results of this study.

At the stationary phase, the metabolic flux map was characterized by a reduced flux of glycolysis, net lactate uptake, significant oxPPP flux, and reduced rate of anaplerosis. The TCA fluxes at the stationary phase were similar to the fluxes at the

exponential phase. This indicates that at the stationary phase CHO cells rely for a large part on oxidative phosphorylation for ATP generation, whereas at the exponential phase glycolysis also contributes significantly to ATP production via substrate level phosphorylation. The significant flux of oxPPP indicates that CHO cells require additional NADPH at the stationary phase. In a similar study, Sengupta et al. also reported high flux of oxPPP at the late stationary phase (Sengupta et al., 2011). The relative oxPPP fluxes, i.e. as a fraction of glucose uptake rate, reported by Sengupta et al. were much higher compared to what was observed in this study. This difference could be explained by the fact that we measured fluxes in the early stationary phase, whereas Sengupta et al. measured fluxes in the late stationary phase. However, it is still unknown what the fate is of this additional NADPH. This should be investigated in more detail in future studies. One hypothesis is that NADPH is needed to combat oxidative stress at the stationary phase (Sengupta et al., 2011).

3.5 Conclusion

^{13}C-MFA allows the estimation of multiple intracellular fluxes that cannot be observed from external uptake and excretion rates. Therefore, ^{13}C-MFA provides inherently a more realistic representation of *in vivo* cellular metabolism. In previous studies of CHO cell metabolism that relied on metabolite balancing, fluxes of oxidative pentose phosphate pathway and anaplerosis from pyruvate to oxaloacetate have been ignored, i.e. these fluxes cannot be observed from external rate measurements. However, in this study, it was found that these were some of the key fluxes that most clearly distinguished the growth phase from the stationary phase. As we discussed above, the differential activation of these pathways has implications for energy and redox homeostasis in CHO cells.

Table 3.5 Metabolic network model for non-stationary ^{13}C-MFA of CHO metabolism.

Glycolysis			
v1	Gluc.ext (abcdef)	→	G6P (abcdef)
v2	G6P (abcdef)	↔	F6P (abcdef)
v3	F6P (abcdef)	→	DHAP (cba) + GAP (def)
v4	DHAP (abc)	↔	GAP (abc)
v5	GAP (abc)	↔	3PG (abc)
v6	3PG (abc)	↔	PEP (abc)
v7	PEP (abc)	→	Pyr (abc)
Pentose Phosphate Pathway			
v8	G6P (abcdef)	→	P5P (bcdef) + CO2 (a)
v9	P5P (abcde)	↔	X5P (abcde)
v10	P5P (abcde)	↔	R5P (abcde)
v11	X5P (abcde)	↔	EC2 (ab) + GAP (cde)
v12	F6P (abcdef)	↔	EC2 (ab) + E4P (cdef)
v13	S7P (abcdefg)	↔	EC2 (ab) + R5P (cdefg)
v14	F6P (abcdef)	↔	EC3 (abc) + GAP (def)
v15	S7P (abcdefg)	↔	EC3 (abc) + E4P (defg)
Pyruvate and Lactate Metabolism			
v16	Pyr (abc)	↔	Lact (abc)
v17	Lact (abc)	↔	Lact.snk (abc)
v18	Lact (abc)	→	Lact.ext (abc)
v19	Pyr (abc)	↔	Pyr.m (abc)
TCA Cycle			
v20	Pyr.m (abc)	→	AcCoA.m (bc) + CO2 (a)
v21	AcCoA.m (ab) + OAC.m (cdef)	→	Cit.m (fedbac)
v22	Cit.m (abcdef)	↔	AKG.m (abcde) + CO2 (f)
v23	½ AKG.m (abcde) + ½ AKG.m (fghij)	→	½ Suc.m (bcde) + ½ Suc.m (jihg) + ½ CO2 (a) + ½ CO2 (f)
v24	½ Suc.m (abcd) + ½ Suc.m (efgh)	↔	½ Fum.m (abcd) + ½ Fum.m (hgfe)
v25	½ Fum.m (abcd) + ½ Fum.m (efgh)	↔	½ Mal.m (abcd) + ½ Mal.m (hgfe)
v26	Mal.m (abcd)	↔	OAC.m (abcd)

Table 3.5 continued

Anaplerosis and Gluconeogenesis			
v27	Mal.m (abcd)	→	Pyr.m (abc) + CO2 (d)
v28	Pyr.m (abc) + CO2 (d)	→	OAC.m (abcd)
v29	Mal.m (abcd)	↔	Mal.c (abcd)
v30	Mal.c (abcd)	↔	OAC.c (abcd)
Fatty Acid Metabolism			
v31	Cit.m (abcdef)	↔	Cit.c (abcdef)
v32	Cit.c (abcdef)	→	AcCoA.c (ab) + OAC.c (cdef)
v33	AcCoA.c (ab)	→	FA.c (ab)
v34	FA.ext (ab)	→	FA.c (ab)
v35	FA.c (ab)	↔	FA.m (ab)
v36	FA.m (ab)	→	AcCoA.m (ab)
Glycerol-3-phosphate Metabolism			
v37	DHAP (abc)	→	GLP (abc)
v38	GLP.ext (abc)	→	GLP (abc)
Amino Acid Metabolism			
v39	Ala (abc)	↔	Pyr (abc)
v40	Ser (abc)	→	Gly (ab) + C1 (c)
v41	Ser (abc)	→	Pyr (abc)
v42	AKG.m (abcde)	↔	Glu (abcde)
v43	Glu (abcde)	→	Pro (abcde)
v44	Gln (abcde)	→	Glu (abcde)
v45	Asp (abcd)	↔	OAC.m (abcd)
v46	Asp (abcd)	→	Asn (abcd)
v47	Thr (abcd)	→	AcCoA.c (cd) + Gly (ab)
v48	Met (abcde) + CO2 (f)	→	Suc.m (bcdf) + CO2 (a) + C1 (e)
v49	Val (abcde) + CO2 (f)	→	Suc.m (dcef) + CO2 (a) + CO2 (b)
v50	Ile (abcdef) + CO2 (g)	→	Suc.m (bcdg) + AcCoA.m (ef) + CO2(a)
v51	Phe (abcdefghi)	→	Fum.m (defg) + AcCoA.m (bc) + AcCoA.m (hi) + CO2 (a)
v52	Tyr (abcdefghi)	→	Fum.m (defg) + AcCoA.m (bc) + AcCoA.m (hi) + CO2 (a)

Table 3.5 continued

v53	Leu (abcdef) + CO2 (g)	→	AcCoA.m (bc) + AcCoA.m (de) + AcCoA.m (gf) + CO2 (a)
v54	Ala (abc)	→	Ala.ext (abc)
v55	Gly (ab)	→	Gly.ext (ab)
v56	Pro.ext (abcde)	→	Pro (abcde)
v57	Glu (abcde)	→	Glu.ext (abcde)
v58	Asp.ext (abcd)	→	Asp (abcd)
v59	Gln.ext (abcde)	→	Gln (abcde)
v60	Ile.ext (abcdef)	→	Ile (abcdef)
v61	Leu.ext (abcdef)	→	Leu (abcdef)
v62	Met.ext (abcde)	→	Met (abcde)
v63	Phe.ext (abcdefghi)	→	Phe (abcdefghi)
v64	Ser.ext (abc)	→	Ser (abc)
v65	Tyr.ext (abcdefghi)	→	Tyr (abcdefghi)
v66	Val.ext (abcde)	→	Val (abcde)
v67	Thr.ext (abcd)	→	Thr (abcd)
v68	Arg.ext (abcdef)	→	Arg (abcdef)
v69	Cys.ext (abc)	→	Cys (abc)
v70	His.ext (abcdef)	→	His (abcdef)
v71	Lys.ext (abcdef)	→	Lys (abcdef)
v72	Trp.ext (abcdefghijk)	→	Trp (abcdefghijk)

Biomass reaction			
v73	0.0624 Ala + 0.0392 Arg + 0.0374 Asp + 0.0300 Asn + 0.0151 Cys + 0.0335 Glu + 0.0402 Gln + 0.0560 Gly + 0.0149 His + 0.0337 Ile + 0.0587 Leu + 0.0593 Lys + 0.0144 Met + 0.0228 Phe + 0.0326 Pro + 0.0447 Ser + 0.0402 Thr + 0.0046 Trp + 0.0189 Tyr + 0.0433 Val + 0.0290 G6P + 0.0242 P5P + 0.2335 FA.c + 0.0113 GLP	→	Biomass

Complete metabolic network model for CHO cells used for metabolic flux analysis, along with carbon atom transitions. For each metabolite carbon atoms are identified using letters to represent successive carbon atoms. This table was adapted from a published paper by Ahn and Antoniewicz (2011).

Chapter 4

METABOLIC FLUX ANALYSIS OF CHO CELLS USING ^{13}C-MFA FOR ISOTOPIC STEADY STATE AND PARALLEL LABELING EXPERIMENTS WITH [1,2-^{13}C]GLUCOSE AND [U-^{13}C]GLUTAMINE

We applied a parallel labeling strategy using two isotopic tracers, [1,2-^{13}C]glucose and [U-^{13}C]glutamine, to determine metabolic fluxes in Chinese hamster ovary (CHO) cells. CHO cells were grown in parallel cultures over a period of six days with glucose and glutamine feeding. On days 2 and 5, isotopic tracers were introduced and ^{13}C-labeling of intracellular metabolites was measured by gas chromatography-mass spectrometry (GC-MS). Metabolites in glycolysis pathway reached isotopic steady state for [1,2-^{13}C]glucose within 1.5 h, and metabolites in the TCA cycle reached isotopic steady state for [U-^{13}C]glutamine within 3 h. Combined analysis of the data sets for ^{13}C-metabolic flux analysis (MFA) produced detailed flux maps at two metabolic phases, exponential growth phase (day 2) and early stationary phase (day 5). Flux results revealed significant rewiring of intracellular metabolism in the transition from growth to non-growth, including changes in oxidative pentose phosphate pathway, anaplerosis, amino acid metabolism, and fatty acid biosynthesis. At the growth phase, *de novo* fatty acid biosynthesis flux correlated well with the lipid requirements for cell growth. However, surprisingly, at the non-growth phase the fatty acid biosynthesis flux remained high even though no new lipids were needed for growth. Additionally, we identified a discrepancy in the estimated TCA cycle flux obtained using traditional stoichiometric flux balancing and ^{13}C-metabolic flux analysis. Our results suggested that CHO cells produced additional metabolites from

glucose that were not accounted for in the model. Follow-up experiments with [U-^{13}C]glucose confirmed accumulation of ^{13}C-labeling in previously unidentified metabolites in the medium.

4.1 Introduction

Chinese hamster ovary (CHO) cell lines are the preferred host system to produce biotherapeutics in the pharmaceutical industry (Birch and Racher, 2006; Walsh, 2010). While CHO cells have been studied for many years, there is still much unknown about the metabolism of CHO cells in culture (Ahn and Antoniewicz, 2012). In CHO cell and other mammalian cell line cultures, glucose and glutamine generally serve as the main carbon and energy sources. Consumption of these substrates results in significant accumulation of by-products such as lactate and ammonium (Quek et al., 2010) that can induce the transition from growth phase to stationary phase and have additional effects on cell viability, cell productivity and product quality (Ahn et al., 2008; Cruz et al., 2000; Lao and Toth, 1997). Understanding metabolic phenotypes at different stages in a culture, e.g. exponential growth and stationary phases can provide new avenues for improving productivity of CHO cells through targeted genetic engineering and improved process monitoring and control.

Metabolic flux analysis (MFA) is the preferred technique for obtaining quantitative information on *in vivo* metabolism. Flux information can be used, for example, to optimize medium composition (Xing et al., 2011), identify targets for cell engineering (Henry and Durocher, 2011), and validate metabolic pathways and stereochemistry of biochemical reactions (Crown et al., 2011; Moxley et al., 2009). MFA methods can be classified into two main categories: methods that rely solely on balancing fluxes within an assumed network stoichiometry, and methods that use

isotopic tracers (e.g. ^{13}C) to obtain additional information for flux analysis. Stoichiometric MFA relies on intracellular metabolite balances and measured extracellular rates to estimate intracellular fluxes. In general, fluxes are estimated under the assumption of metabolic steady state (i.e. time-invariant fluxes), although novel methods for dynamic metabolic flux analysis (DMFA) at metabolic non-steady state have been developed (Leighty and Antoniewicz, 2011). A key limitation of the classical MFA method is that it cannot elucidate fluxes of parallel pathways (e.g. glycolysis vs. pentose phosphate pathway), reversible reactions, and cyclic pathways (e.g. pyruvate cycling). To address this shortcoming, isotopic tracer-driven methods have been developed that can estimate metabolic fluxes via model-based regression of isotopomer measurements obtained by mass spectrometry (MS), tandem MS, and nuclear magnetic resonance (NMR) (Choi and Antoniewicz, 2011; Choi et al., 2012; Jeffrey et al., 2002; Szyperski, 1995; Wittmann, 2007).

Both stoichiometric MFA and ^{13}C-MFA methods have been applied to study CHO cell metabolism. MFA was used, for example, to validate metabolism of peptide-derived amino acids (Nyberg et al., 1999b), study metabolic changes during feeding of co-substrates (Altamirano et al., 2006), and evaluate error propagation of measurement errors (Goudar et al., 2009). MFA was also integrated with kinetic models to predict fed-batch culture profiles (Naderi et al., 2011; Nolan and Lee, 2011). Isotopic tracer methods are not as widely used yet to study CHO cell metabolism, as was recently reviewed (Ahn and Antoniewicz, 2012). A key challenge for applying ^{13}C-MFA in CHO cell cultures is the slow ^{13}C-labeling accumulation in intracellular metabolites (Ahn and Antoniewicz, 2011; Ahn and Antoniewicz, 2012; Deshpande et al., 2009; Goudar et al., 2010; Sengupta et al., 2011). Previously, we reported that isotopic non-

stationary ^{13}C-MFA can be applied to determine fluxes in CHO cells (Ahn and Antoniewicz, 2011). However, long isotopic labeling times (up to 24 h) were needed to accumulate enough ^{13}C-labeling for flux modeling. Two main concerns with long labeling times are: i) poor temporal resolution of fluxes, i.e. we can at best measure average snapshots of metabolism once every 24 h; and ii) the metabolic steady state assumption may be invalid for long labeling times, e.g. during the transition from growth phase to non-growth phase.

In the present work, it was applied a new flux analysis strategy using parallel labeling experiments and combined data regression to study CHO cell metabolism in culture. First, it was selected ^{13}C-tracers for the CHO cell model and validated that isotopic steady state was reached for all relevant intracellular metabolites within a short time (<3 h). Metabolic fluxes were then estimated by integrating complementary data from multiple labeling experiments. Finally, this method enabled detailed flux maps at two key metabolic phases, the exponential growth phase and early stationary phase. Flux results revealed significant rewiring of intracellular metabolic fluxes in the transition from growth to non-growth, including changes in oxidative pentose phosphate pathway, anaplerosis, amino acid metabolism, and fatty acid biosynthesis. Overall, the flux results were in good agreement with previous studies, with two exceptions. First, it was identified, for the first time, that fatty acid biosynthesis is active during the stationary phase (not predicted in any previous study). Second, the shows that TCA cycle flux is likely overestimated using traditional stoichiometric flux balancing approach due to unaccounted losses of carbon in the glycolysis pathway. This was confirmed in this study using follow-up experiments with [U-^{13}C]glucose.

4.2 Materials and Methods

4.2.1 Materials

Culture materials were purchased from Cellgro (Mediatech, Manassas, VA). [1,2-^{13}C]Glucose (99%), [U-^{13}C]glucose (98%), [U-^{13}C]glutamine (98%), [2,2,4,4-^{2}H]citric acid (98%), [2,2,3,3-^{2}H]succinic anhydride (98%), [2,3-^{2}H]fumaric acid (98%) and [U-^{13}C]algal amino acids (97~99%) were purchased from Cambridge Isotope Laboratories (Andover, MA). Free amino acids and amino acid standard H were purchased from Pierce Sci. (Rockford, IL). Norvaline and dimethylglutaric acid were purchased from Sigma-Aldrich (St. Louis, MO). A stock solution of [U-^{13}C]glutamine at 60 mM was prepared in ionized water. [U-^{13}C]Algal hydrolysate was solubilized in 0.1 N HCl at 10 mg/mL. Stock solutions of amino acids and [U-^{13}C]algal hydrolysate were kept at -85°C, to be used for quantification of amino acids. Glucose and glutamine stock solutions were prepared at 250 g/L and 100 mM, respectively, in phosphate buffer saline (PBS) and stored in 4°C, to be used as feed in the CHO cell culture experiments.

4.2.2 Cell Culture

CHO-K1 cells (ATCC Cat. No. CCL-61) were grown as a monolayer culture in T-25 flasks (Corning, NY, Cat. No. 430639) at 5 mL working volume in a humidified 5% CO_2 incubator at 37°C. Cells were sub-cultured every three days at a split ratio of 1:10 before the tracer experiment. The medium was Dulbecco's modified Eagle medium (DMEM, Cat. No. 10-013-CV) supplemented with 10% fetal bovine serum (FBS, Cat. No. 35-011-CV) and 1% penicillin-streptomycin solution (PS, Cat No. 30-004-CI).

4.2.3 Parallel Labeling Experiments

For the isotopic tracer studies with [1,2-^{13}C]glucose and [U-^{13}C]glutamine (and follow-up experiments with [U-^{13}C]glucose), CHO cells were grown over a period of six days with glucose and glutamine feeding on day 2 (exponential growth phase) and day 5 (stationary phase). Figure 4.1 shows schematic overview of parallel labeling experiments for flux analysis at exponential and stationary phase using [1,2-^{13}C]glucose and [U-^{13}C]glutamine tracers. First, cells were grown to confluency to be used as the seed. Cells were detached with trypsin EDTA (0.25% trypsin, Cat. No. 25-053-CI) and washed once with fresh growth medium. After centrifugation, the cells were re-suspended in growth medium at 6×10^5 cells/mL. 1 mL of the seed was inoculated in each T-25 flask together with 4 mL of fresh medium (5 mL/flask total). The initial growth medium was DMEM base (1 g/L glucose and no glutamine, Cat. No. 11054-020, Invitrogen, Carlsbad, CA) with 10% FBS, 1% PS and supplemented with glucose (6.9 mM initial glucose) and glutamine (1.54 mM initial glutamine). In total, thirty T-25 flasks were prepared for the parallel labeling experiments: fifteen flasks were used for analysis of the exponential growth phase and fifteen flasks for the stationary phase. An additional eighteen flasks were prepared and over the six days triplicate flasks were harvested every day for cell counting and measuring concentration profiles of amino acids and organic acids in the culture medium. On days 2 and 5, 47.5 μmol of glucose (9.5 mM increase) and 8.2 μmol of glutamine (1.64 mM increase) were added to all cultures from the 250 g/L glucose and 100 mM glutamine stock solutions. For the tracer experiment at the growth phase (on day 2), five flasks were supplemented with [1,2-^{13}C]glucose and natural glutamine; five flasks were supplemented with natural glucose and [U-^{13}C]glutamine; and five flasks were supplemented with natural glucose and glutamine, to validate natural isotope

abundances by GC-MS. The flasks were harvested one-by-one after 1.5, 3, 6, 9 and 12 h (i.e. fifteen flaks total). The flasks harvested at 12 h were only used for analysis of fatty acids. For the tracer experiments at the stationary phase, natural glucose and glutamine were added on day 2. On day 5, five flasks were supplemented with [1,2-^{13}C]glucose and natural glutamine; five flasks were supplemented with natural glucose and [U-^{13}C]glutamine; and five flasks were supplemented with natural glucose and glutamine. The flasks were then harvested one-by-one after 1.5, 3, 6, 9 and 12 h (i.e. fifteen flaks total). Cells were extracted as described below to obtain intracellular metabolites for analysis of ^{13}C-labeling by GC-MS, including organic acids, amino acids, and fatty acids. Supernatants were collected by centrifugation at 1,000 rpm for 3 min. All samples were stored at -85°C.

4.2.4 Viable Cell Number, Glucose, Lactate and Ammonium Analysis

Cell numbers were measured using a hemocytometer and viability was determined by trypan blue exclusion method. Cell numbers were measured three times per sample. Concentrations of glucose and lactate were measured by YSI 2700 biochemistry analyzer (YSI, Yellow Springs, OH), and ammonium concentration was measured by Bioprofile 100^{plus} analyzer (Nova biomedical, Waltham, MA).

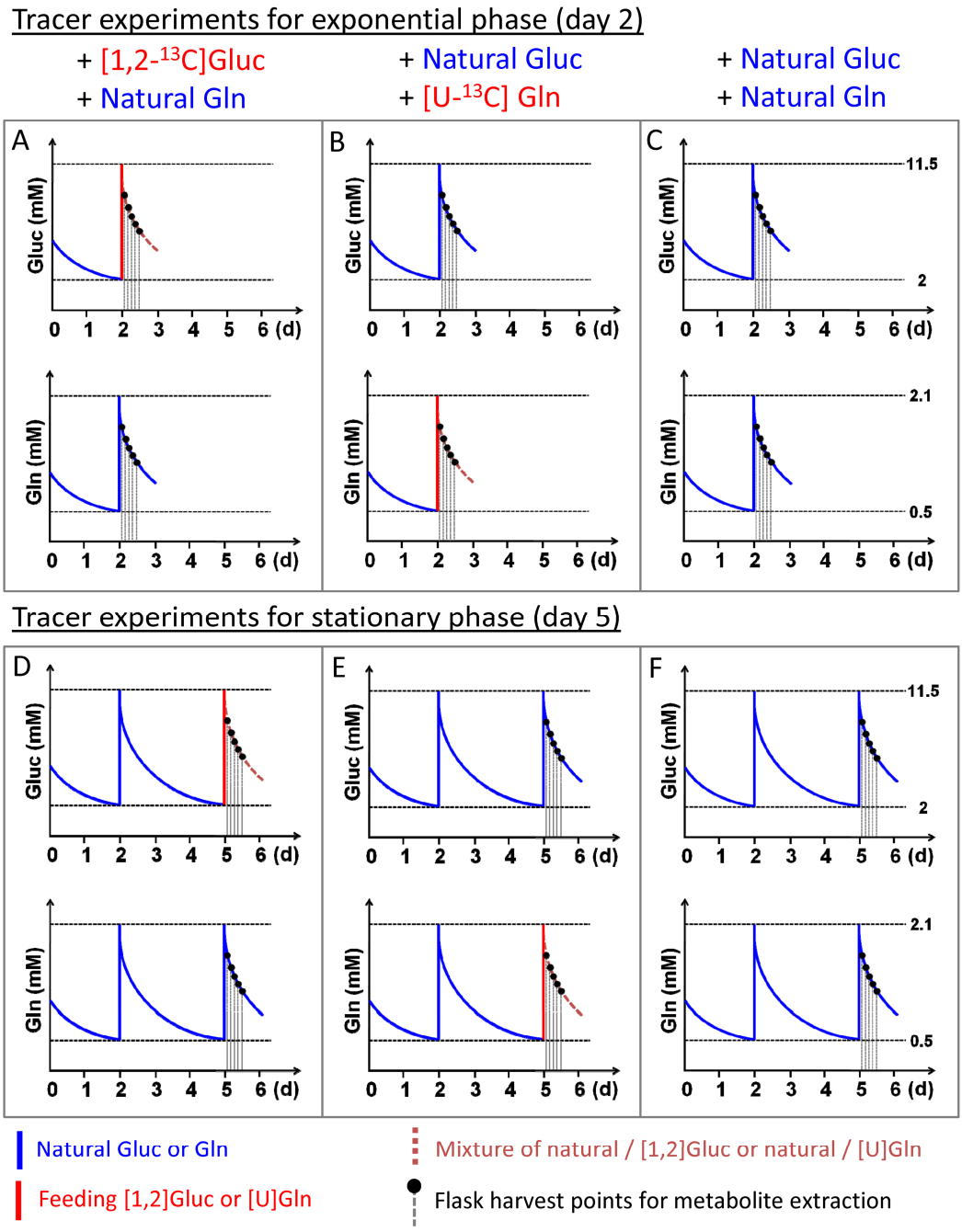

Figure 4.1 Schematic overview of parallel labeling experiments for flux analysis at exponential and stationary phase. [1,2-^{13}C]glucose and [U-^{13}C]glutamine tracers were used. A and D for [1,2-^{13}C]glucose and natural glutamine feeding, B and E for natural glucose and [U-^{13}C]glutamine, and C and F for natural glucose and glutamine.

4.2.5 GC-MS Analysis

GC-MS analysis was performed using an Agilent 7890A GC equipped with a DB-5ms (30 m × 0.25 mm i.d. × 0.25 μm; Agilent J&W Scientific) capillary column, interfaced with a Waters Quattro Micro GC-MS/MS (Milford, MA) operating under ionization by electron impact at 70 eV and 200°C ion source temperature. The injection port and interface temperatures were both 250°C. Helium flow was maintained at 1 mL/min. Mass spectra were recorded in selected ion recording (SIR) mode with 30 ms dwell time. Mass isotopomer distributions were obtained by integration of ion chromatograms (Antoniewicz et al., 2007a), and corrected for natural isotope abundances using Metran software (Fernandez et al., 1996).

4.2.6 Extraction of Intracellular Metabolites

At the sampling times, culture medium was collected from the T-25 flasks and centrifuged to remove detached cells and debris. The attached cells were washed twice with 5 mL of cold saline water (9 g/L NaCl, 4°C). Metabolism was quenched by addition of 1.5 mL of cold methanol (-20°C). After incubation on ice for 5 min, cells were collected with a cell scraper and the cell suspension was transferred into glass tubes with Teflon-sealed caps. 1.5 mL of chloroform was added and the tubes were vortexed vigorously for 10 sec. Next, 1.5 mL of water was added and the tubes were vortexed vigorously for 1 min. All tubes were stored overnight at 4°C. The next day, the tubes were centrifuged at 2,000 rpm and 4°C for 20 min, which resulted in a clear phase separation. The upper aqueous phase (methanol and water) contained polar metabolites and lower organic phase (chloroform) contained non-polar metabolites. 3 mL of the aqueous phase was carefully transferred into two 1.5 mL microcentrifuge tubes using a glass pipette and evaporated to dryness at 37°C under nitrogen gas using

an evaporator (Reacti-Vap/Reacti-Therm III; Fierce, Rockford, IL). During the drying process, the contents of the two tubes were combined. The dried samples were kept at -85°C prior to derivatization and GC-MS analysis. For analysis of fatty acids, 1.5 mL of the organic phase was transferred into a glass tube with a Teflon-sealed cab using a glass pipette and stored at -85°C without drying.

4.2.7 Derivatization and GC-MS Analysis of Intracellular Metabolites

The extracted polar metabolites were dissolved in 50 µL of 2wt% methoxylamine hydrochloride in pyridine and incubated at 37°C for 90 min on a heating block. Next, 80 µL of N-methyl-N-(tert-butyldimethylsilyl)-trifluoroacetamide (MTBSTFA) + 1% tert-butyldimetheylchlorosilane (TBDMCS) (Thermo Scientific, Bellefonte, PA) was added and the samples were incubated for 30 min at 60°C. After an overnight incubation at room temperature, the derivatized samples were centrifuged for 2 min at 14,000×g and the clear liquid was transferred into GC vials for GC-MS analysis. The injection volume was 1-3 µL and samples were injected in splitless or split mode depending on the peak intensities. GC oven temperature was held at 70°C for 2 min, increased to 140°C at 3°C/min, increased to 150°C at 1°C/min, increased to 280°C at 3°C/min and held for 6.33 min. The total run time was 85 min. Mass spectra of selected metabolite fragments (Table 4.1 and 4.2) were collected in SIR mode.

4.2.8 Derivatization and GC-MS Analysis of Fatty Acids

The organic phase from cell extraction was evaporated to dryness at room temperature with nitrogen gas. Next, 1 mL of chloroform, 1 mL of methanol and 40 µL of sulfuric acid were added to the dried samples, and the tubes were incubated on a heating block at 100°C for 2 h. The samples were then allowed to cool down to room

temperature. 0.5 mL of water was added and the samples were vortexed vigorously. The tubes were then centrifuged at 3,000 rpm for 10 min, which resulted in a clear phase separation. The bottom organic phase was transferred into glass vials and dried under nitrogen gas at room temperature. The fatty acid methyl esters (FAME) were re-suspended in 100 μL of hexane and centrifuged for 2 min at 14,000×g. The clear liquid was then transferred into GC vials with glass inserts for GC-MS analysis. The injection volume was 1 μL and samples were injected in splitless or split mode depending on the peak intensities. GC oven temperature was held at 180°C for 2 min, increased to 200°C at 8°C/min, held for 8 min, increased to 280°C at 10°C/min and held for 7.5 min. The total run time was 28 min. The identity of metabolite fragments was confirmed against an analytical standard, fatty acid methyl ester mixture (FAME mix C8-24, Supelco, Bellefonte, PA). Labeling of palmitate was determined from the mass isotopomer distribution of the fragment at *m/z* 270 ($C_{17}H_{34}O_2$), which contains all 16 carbon atoms of palmitate.

Table 4.1 Metabolite fragments of intracellular metabolites measured by GC-MS analysis

Metabolite	Mass (*m/z*)	Carbon atoms	Fragment formula
Organic acids			
Pyruvate	174	1-2-3	$C_6H_{12}O_3NSi$
Lactate	233	2-3	$C_{10}H_{25}O_2Si_2$
Lactate	261	1-2-3	$C_{11}H_{25}O_3Si_2$
Succinate	289	1-2-3-4	$C_{12}H_{25}O_4Si_2$
Fumarate	287	1-2-3-4	$C_{12}H_{23}O_4Si_2$
AKG	346	1-2-3-4-5	$C_{14}H_{28}O_5NSi_2$
Malate	391	2-3-4	$C_{17}H_{39}O_4Si_3$
Malate	419	1-2-3-4	$C_{18}H_{39}O_5Si_3$
PEP	453	1-2-3	$C_{17}H_{38}O_6Si_3P$
DHAP	484	1-2-3	$C_{18}H_{43}O_6NSi_3P$
GLP	571	1-2-3	$C_{23}H_{56}O_6Si_4P$
Citrate	431	1-2-3-4-5	$C_{19}H_{39}O_5Si_3$
Citrate	459	1-2-3-4-5-6	$C_{20}H_{39}O_6Si_3$
3PG	585	1-2-3	$C_{23}H_{54}O_7Si_4P$
Palmitate	270	C1-C16	$C_{17}H_{34}O_2$
Amino acids			
Alanine	232	2-3	$C_{10}H_{26}ONSi_2$
Alanine	260	1-2-3	$C_{11}H_{26}O_2NSi_2$
Aspartate	418	1-2-3-4	$C_{18}H_{40}O_4NSi_3$
Proline	258	2-3-4-5	$C_{12}H_{28}ONSi_2$
Glutamate	330	2-3-4-5	$C_{16}H_{36}O_2NSi_2$
Glutamate	432	1-2-3-4-5	$C_{19}H_{42}O_4NSi_3$
Glutamine	431	1-2-3-4-5	$C_{19}H_{43}O_3N_2Si_3$

Table 4.2 Metabolite fragments of extracellular metabolites measured by GC-MS analysis

Metabolite	Mass (*m/z*)	Carbon atoms	Fragment formula	Internal standard
Organic acids				
Pyruvate	174	1-2-3	$C_6H_{12}O_3NSi$	Norvaline, Dimethylglutarate [2.0 mM]
Succinate	289	1-2-3-4	$C_{12}H_{25}O_4Si_2$	[2,2,3,3-^{2}H]Succinate anhydride [2.0 mM]
Fumarate	287	1-2-3-4	$C_{12}H_{23}O_4Si_2$	[2,3-^{2}H]Fumarate [2.0 mM]
Malate	419	1-2-3-4	$C_{18}H_{39}O_5Si_3$	Norvaline, Dimethylglutarate [2.0 mM]
Citrate	459	1-2-3-4-5-6	$C_{20}H_{39}O_6Si_3$	[2,2,4,4-^{2}H]Citrate [2.0 mM]
Amino acids				[U-^{13}C]amino acids in algal soln.
Alanine	260	1-2-3	$C_{11}H_{26}O_2NSi_2$	8.1 mM of [U-^{13}C]Ala
Glycine	246	1-2	$C_{10}H_{24}O_2NSi_2$	6.1 mM of [U-^{13}C]Gly
Valine	288	1-2-3-4-5	$C_{13}H_{30}O_2NSi_2$	4.0 mM of [U-^{13}C]Val
Leucine	274	2-3-4-5-6	$C_{13}H_{32}ONSi_2$	5.9 mM of [U-^{13}C]Leu
Isoleucine	274	2-3-4-5-6	$C_{13}H_{32}ONSi_2$	2.9 mM of [U-^{13}C]Ile
Proline	258	2-3-4-5	$C_{12}H_{28}ONSi_2$	3.0 mM of [U-^{13}C]Pro
Methionine	320	1-2-3-4-5	$C_{13}H_{30}O_2NSi_2S$	0.8 mM of [U-^{13}C]Met
Serine	390	1-2-3	$C_{17}H_{40}O_3NSi_3$	2.8 mM of [U-^{13}C]Ser
Threonine	404	1-2-3-4	$C_{18}H_{42}O_3NSi_3$	3.3 mM of [U-^{13}C]Thr
Phenylalanine	302	1-2	$C_{14}H_{32}O_2NSi_2$	2.0 mM of [U-^{13}C]Phe
Aspartate	418	1-2-3-4	$C_{18}H_{40}O_4NSi_3$	6.0 mM of [U-^{13}C]Asp
Glutamate	432	1-2-3-4-5	$C_{19}H_{42}O_4NSi_3$	8.1 mM of [U-^{13}C]Glu
Tyrosine	302	1-2	$C_{14}H_{32}O_2NSi_2$	1.8 mM of [U-^{13}C]Tyr
Glutamine	431	1-2-3-4-5	$C_{19}H_{43}O_3N_2Si_3$	Pure [U-^{13}C]Gln soln. 60 mM of [U-^{13}C]Gln

Two internal standards for mass analysis (mass, carbon atoms, fragment formula); Norvaline (*m/z* 288, 1-2-3-4-5, $C_{13}H_{30}O_2NSi_2$), Dimethylglutarate (*m/z* 331, 1-2-3-4-5-6-7, $C_{15}H_{40}O_4Si_2$)

4.2.9 Derivatization and GC-MS Analysis of Glucose

Labeling of glucose in the medium was determined by GC-MS analysis of the aldonitrile pentapropionate derivative of glucose (Antoniewicz et al., 2011). In short, 100 µL of medium was deproteinized with cold acetone (-20°C) and the samples were evaporated to dryness under air flow. Next, 50 µL of hydroxylamine hydrochloride solution (20 mg/mL in pyridine) was added to the samples. The samples were heated at 90°C for 60 min, followed by addition of 100 µL of propionic anhydride. After 30 min incubation at 60°C, the samples were evaporated to dryness, dissolved in 100 µL of ethyl acetate and transferred into GC vials for GC-MS analysis. The injection volume was 1 µL and samples were injected at 1:40 split ratio. GC oven temperature was held at 80 °C for 1 min, increased to 280 °C at 15 °C/min, and held for 6 min. Labeling of glucose was determined from the mass isotopomer distribution of the fragment at *m/z* 370 ($C_{17}H_{24}O_8N_1$), which contains carbon atoms C1-C5 of glucose (Antoniewicz et al., 2011).

4.2.10 Quantification of Extracellular Metabolites

For quantification of extracellular metabolites, 200 µL of culture medium was supplemented with internal standards: 15 µL of 10 mg/mL of [U-^{13}C]algal hydrolysate; 10 µL of 60 mM [U-^{13}C]glutamine; 15 µL of 0.1 N NaOH; 25 µL of 2 mM norvaline and 2 mM dimethylglutarate; 25 µL of 2 mM [2,2,4,4-^{2}H]citric acid, 2 mM [2,2,3,3-^{2}H]succinic anhydride, and 2 mM [2,3-^{2}H]fumaric acid. Additionally, 200 µL of culture medium was prepared without internal standards for analysis of isotopic labeling of extracellular metabolites. Medium samples were deproteinized with 600 µL of cold acetone (-20°C). After centrifugation at 14,000×g for 5 min, the samples were evaporated to dryness under nitrogen gas flow at 37°C. The dried

samples were kept at -85°C before derivatization and GC-MS analysis. Concentrations of extracellular metabolites were determined by regression analysis of mass isotopomer distributions of samples with and without internal standards, i.e. given the known concentrations of metabolites in the internal standards (Hofmann et al., 2008; Mashego et al., 2004; Noguchi et al., 2009). The results for the quantification of amino acids as well as cell number, glucose, lactate and ammonium were described in Table 4.3.

4.2.11 Determination of Biomass Specific Rates

Specific growth rate (μ), specific glutamine uptake rate (q_{Gln}), and specific ammonium production rate (q_{Amm}) were calculated using the method by Glacken et al (Glacken et al., 1988). The glutamine decomposition rate constant (k) was determined to be 0.0023 h^{-1} in control experiments without cells to account for spontaneous degradation of glutamine to pyroglutamate and ammonium in the culture medium (Ozturk and Palsson, 1990). In addition, we accounted for the apparent accumulation of amino acids in the medium due to evaporation effects (Ahn and Antoniewicz, 2011). The biomass specific consumption and production rates of amino acids were calculated from the time course data, after correction for evaporation effects. For the stationary phase, an average cell number of $2.24 \pm 0.25 \times 10^6$ cells/mL (days 4-6) was used for calculating biomass specific rates.

Table 4.3 Measurements of viable cell number (10^6 cells/mL) and concentrations of extracellular metabolites (mM).

	Time (day)						
	0	1	2	3	4	5	6
Cell number ($\times 10^6$)	n/a	0.24	0.59	1.57	1.99	2.47	2.27
Glucose*	6.10	4.74	2.56	7.32	4.87	2.63	9.86
Lactate	0.80	4.28	7.67	14.64	16.38	15.76	15.23
NH_3	0.22	0.58	1.00	2.21	3.19	3.79	4.78
Alanine	0.09	0.17	0.19	0.36	0.54	0.64	0.91
Glycine	0.37	0.50	0.55	0.65	0.64	0.64	0.70
Valine	0.63	0.73	0.69	0.62	0.58	0.56	n/a
Leucine	0.70	0.82	0.76	0.68	0.63	0.60	0.63
Isoleucine	0.71	0.81	0.76	0.68	0.64	0.62	0.65
Proline	0.03	0.06	0.07	0.10	0.14	0.18	0.24
Methionine	0.15	0.17	0.15	0.12	0.11	0.10	0.09
Serine	0.35	0.37	0.26	0.08	0.03	0.02	0.02
Threonine	0.61	0.73	0.66	0.60	0.58	0.59	0.59
Phenylalanine	0.32	0.38	0.36	0.33	0.31	0.30	n/a
Aspartate	0.02	0.05	0.06	0.07	0.07	0.07	0.06
Glutamate	0.07	0.17	0.26	0.36	0.38	0.38	0.37
Tyrosine	0.30	0.34	0.32	0.30	0.28	0.27	n/a
Glutamine*	1.55	1.36	0.87	1.55	0.62	0.18	1.17
Pyruvate	0.98	0.52	0.36	0.68	0.79	0.78	0.79
Succinate	0.05	0.05	0.05	0.05	0.06	0.06	0.06
Fumarate	0.00	0.01	0.01	0.01	0.01	0.01	0.01
Malate	0.04	0.04	0.04	0.05	0.05	0.05	0.06
Citrate	0.22	0.25	0.28	0.39	0.52	0.69	0.81

* Glucose and glutamine were added on days 2 and 5 (see Figure 4.1). The concentration of glucose after the addition on day 2 was 12.06 mM (and 12.13mM on day 5). The concentration of glutamine after the addition on day 2 was 2.51 mM (and 1.82 mM on day 5).

4.2.12 Metabolic Network Model

A compartmentalized metabolic network model of CHO cell metabolism was constructed for ^{13}C-metabolic flux analysis, which was based on a previous model (Ahn and Antoniewicz, 2011). The complete model is given in Table 4.5 at the end of this chapter. A lumped biomass equation (v_{79}) was used to describe cell growth, accounting for anabolic requirements for proteins, lipids, RNA, DNA, and carbohydrates (Ahn and Antoniewicz, 2011; Sheikh et al., 2005). For the conversion of measured growth rate to the flux of the biomass reaction, a dry weight for CHO cells of 0.315 mg/10^6cells was assumed (Altamirano et al., 2001). As an example, a growth rate of 0.033 h^{-1} corresponded to a flux value of 99.6 nmol/10^6cells/h for the biomass reaction (Ahn and Antoniewicz, 2011). Cofactor balances were not included in the model to avoid biases resulting from uncertainties regarding cofactor metabolism. In the model, CO_2 was treated as an unbalanced metabolite that was unlabeled.

4.2.13 Combined ^{13}C-Metabolic Flux Analysis

^{13}C-Metabolic flux analysis at isotopic steady state was performed using Metran (Yoo et al., 2008), a flux analysis software based on the elementary metabolite units (EMU) framework (Antoniewicz et al., 2007b; Young et al., 2008). Metabolic fluxes were estimated by minimizing the variance-weighted sum of squared residuals (SSR) between the experimentally measured and model predicted extracellular uptake and production rates and mass isotopomer distributions of intracellular metabolites (Antoniewicz et al., 2006a; Antoniewicz et al., 2007b). For combined analysis of parallel labeling experiments, data sets from ^{13}C-glucose and ^{13}C-glutamine experiments were fit simultaneously to one flux model. This was achieved as follows.

At each iteration, mass isotopomer distributions were simulated for each tracer using the same fluxes. Next, the Hessian matrix and Jacobian vector from each individual simulation were combined and used to update the search direction for the fluxes at the next iteration. ^{13}C-MFA was continued until a predefined convergence criterion was satisfied, as described before (Antoniewicz et al., 2006a; Antoniewicz et al., 2007b). Flux estimation was repeated at least 10 times starting with random initial values for all fluxes to find a global solution. In ^{13}C-MFA, Metran accounted for potential dilution effects of intracellular metabolite labeling due to influx of unlabeled metabolites by determining the percent isotopic labeling for each measured metabolite, i.e. the so-called G-value (Yoo et al., 2008). As an example, a G-value of 90% denotes that the measured metabolite pool was diluted by 10% from unlabeled sources. At convergence, the fitting results were subjected to a χ^2 statistical test to assess the goodness-of-fit, and accurate 95% confidence intervals were computed for all estimated parameters by evaluating the sensitivity of SSR to flux variations (Antoniewicz et al., 2006a). All computations were performed with Matlab R2008b (Mathworks Inc.).

4.2.14 Isotopomer Spectral Analysis (ISA) of Palmitate

For analysis of lipid metabolism, the isotopomer spectral analysis (ISA) method was applied (Kharroubi et al., 1992; Yoo et al., 2008; Yoo et al., 2004). The ISA method determines two parameters from regression of mass isotopomer distributions of fatty acids: i) the fractional ^{13}C-labeling of lipogenic acetyl-CoA pool, the D-value; and ii) the fraction of newly synthesized fatty acids during labeling time t, the g(t)-value. To estimate the D- and g(t)-parameters for palmitate, an ISA model

was constructed and solved in Metran (Table 4.6). The estimated g(t)-values from ISA analysis were compared to theoretical g(t)-values based on measured growth rate (μ):

$$g(t)^{theoretical} = \frac{palmitate(t) - palmitate(0)}{palmitate(t)} = \frac{\exp(\mu \cdot t) - 1}{\exp(\mu \cdot t)} \quad (4.1)$$

The theoretical g(t)-values from Eq. 4.1 were calculated under the assumption that fatty acids were only produced during cell growth and used for lipids. As such, these g(t)-values provide a lower-bound estimate of the true biosynthesis flux of fatty acids, e.g. since turnover of fatty acids and secretion of fatty acids are not considered in this equation. We used Eq.4.1 also to calculate apparent specific growth rates at both phases from the ISA-estimated g(t)-values, and based on these values we determined a net fatty acid biosynthesis flux, assuming typical lipid content for CHO cells (see biomass reaction in Table 4.5) (Sheikh et al., 2005).

4.3 Results

4.3.1 Cell Growth

CHO cells were grown over a period of six days with glucose and glutamine feeding on days 2 and 5. Figure 4.2 shows the time profiles of viable cell density, glucose, lactate, glutamine, and ammonium concentrations. The viable cell density increased exponentially from 0.2×10^6 cells/mL on day 1 to 1.6×10^6 cells/mL on day 3, and reached a maximum cell density of 2.5×10^6 cells/mL on day 5. On day 6, the cell density decreased slightly to 2.3×10^6 cells/mL. Cell viability was >95% during the entire culture (data not shown). The specific cell growth rate at the exponential phase was 0.038 h^{-1}, between days 1 and 3, and the average cell density during the stationary phase was 2.2×10^6 cells/mL between days 4 and 6.

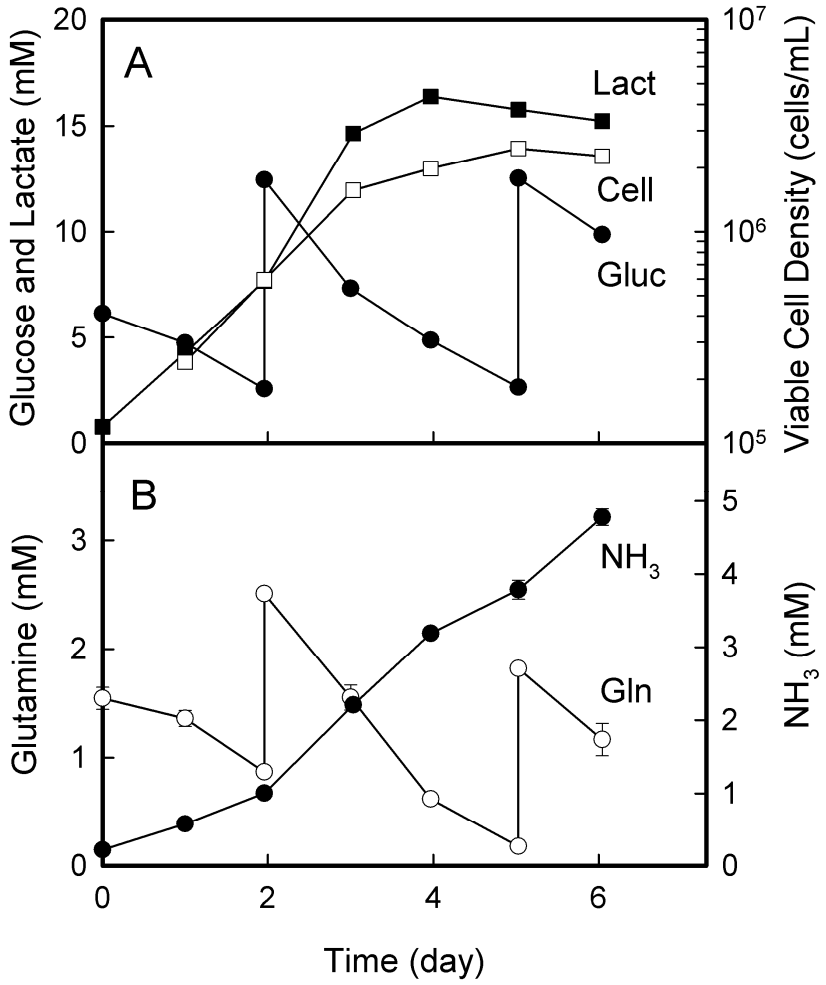

Figure 4.2 (A) Time profiles of viable cell density and glucose and lactate concentrations in the medium (lactate, ■; viable cell density, □; glucose, ●). (B) Time profiles of ammonium and glutamine concentrations (ammonium, ●; glutamine, ○) (Mean ± SD, *n*=3, biological replicates).

4.3.2 Glucose, Glutamine and Lactate Metabolism

The experiment was designed such that glucose and glutamine would be fed twice, first at the exponential growth phase (day 2), and second at the stationary phase (day 5) to introduce ^{13}C-tracers at these times for ^{13}C-MFA. Between days 0 and 2, glucose concentration decreased from 6.1 mM to 2.6 mM, and glutamine concentration decreased from 1.5 mM to 0.9 mM. On day 2, a bolus of glucose and glutamine was added to final concentrations of 12.4 mM and 2.5 mM, respectively. Between days 2 and 5, glucose and glutamine concentrations decreased to 2.6 mM and 0.2 mM, respectively. On day 5, a second bolus of glucose and glutamine was added to final concentrations of 12.5 mM and 1.8 mM, respectively in Figure 4.2A and B. Lactate concentration increased rapidly during the exponential growth phase from 0.8 mM on day 0 to a maximum concentration of 16.4 mM on day 4, after which it decreased to 15.2 mM on day 6 in Figure 4.2A. Figure 4.3A shows the plot of cumulative glucose and lactate concentrations. Between days 1 and 3, the amount of lactate produced per glucose consumed was constant at about 1.4 mol/mol. The theoretical maximum yield of lactate from glucose is 2 mol/mol. Thus, about 70% of glucose consumed was converted to lactate during the exponential growth phase. At the stationary phase, between days 4 to 6, lactate was net consumed by the CHO cells. Figure 4.3B shows the plot of cumulative glucose and cumulative glutamine concentrations; there was no significant change in the ratio of glucose to glutamine consumption during the culture. Figure 4.3C shows the plot of cumulative glutamine and ammonium concentrations; the amount of ammonium produced per glutamine consumed was also relatively constant during the culture. The biomass specific glutamine consumption rate (corrected for glutamine decomposition) was 27.4 nmol/10^6cells/h at the exponential phase (days 1-3) and 7.5 nmol/10^6cells/h at the

stationary phase (days 4-6). The biomass specific ammonium production rate was 45.2 nmol/10^6cells/h at the exponential growth phase and 13.5 nmol/10^6cells/h at the stationary phase. Thus, the amount of ammonium produced per glutamine consumed was relatively constant, i.e. 1.7 mol/mol at the exponential growth phase and 1.8 mol/mol at the stationary phase. The time profiles of all measured extracellular metabolites are given in Table 4.3. Table 4.4 shows the calculated biomass specific uptake and production rates for all measured metabolites at both metabolic phases.

Table 4.4 Biomass specific uptake and production rates of extracellular metabolites (nmol/10^6cells/h).

	Exponential Phase	Stationary Phase
Glucose	– 204.4	– 42.1
Lactate	291.9	– 10.4
NH_3	45.2	13.5
L-Alanine	4.2	1.9
L-Glycine	3.1	0.1
L-Valine	– 4.1	– 0.1
L-Leucine	– 5.1	– 0.3
L-Ileucine	– 4.3	– 0.3
L-Proline	0.4	0.4
L-Methionine	– 1.4	– 0.2
L-Serine	– 8.5	– 0.1
L-Threonine	– 4.7	– 0.1
L-Phenylalanine	– 1.9	– 0.1
L-Aspartate	– 0.1	– 0.4
L-Glutamate	4.0	– 0.9
L-Tyrosine	– 1.6	– 0.2
L-Glutamine*	– 27.4	– 7.5
Pyruvate	12.0	– 0.1
Succinate	0.2	0.1
Fumarate	0.0	0.0
Malate	0.2	0.1
Citrate	3.8	2.8

* Glutamine uptake rate after correction for spontaneous decomposition.

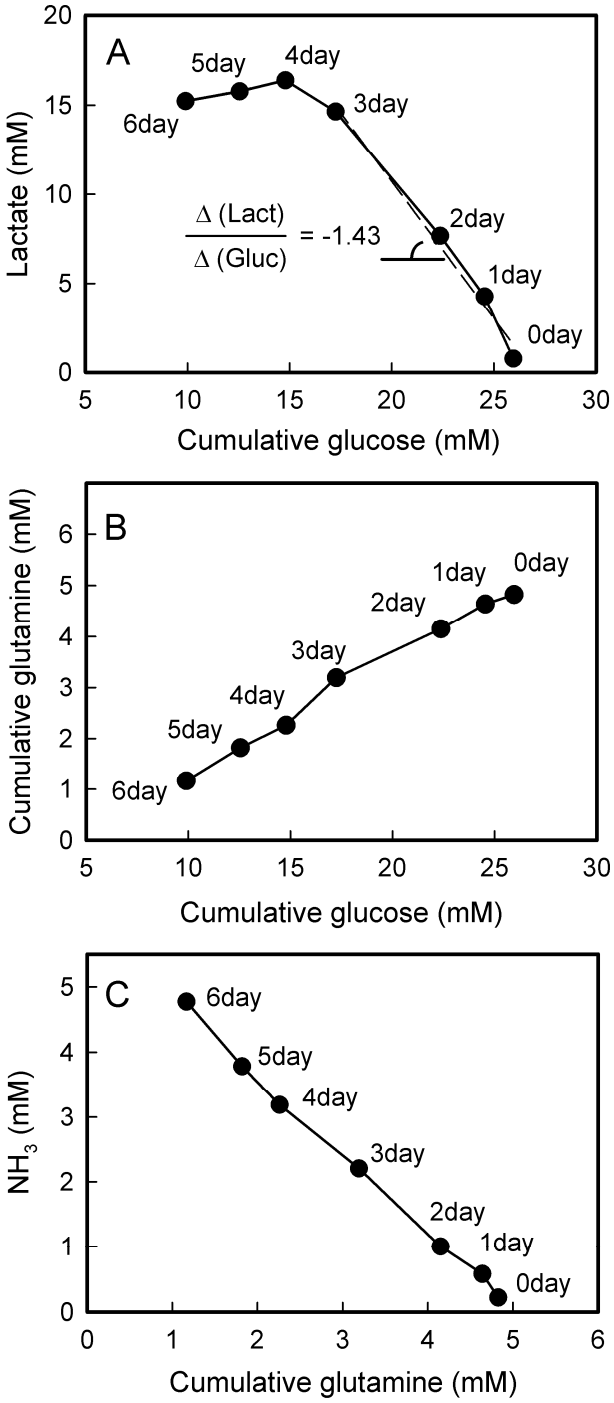

Figure 4.3 (A) Plot of cumulative glucose consumed and lactate produced during the culture. (B) Plot of cumulative glucose consumed and cumulative glutamine. (C) Plot of cumulative glutamine consumed and ammonium produced.

4.3.3 ^{13}C-Labeling Dynamics of Intracellular Metabolites from [U-^{13}C]Glutamine Tracer

Two isotopic tracers were used in this study to investigate CHO cell metabolism in further detail, i.e. [1,2-^{13}C]glucose and [U-^{13}C]glutamine. [U-^{13}C]Glutamine tracer was previously identified as an optimal tracer to study metabolism of immortalized mammalian cells; specifically, it was determined to be a good tracer for analysis of TCA cycle fluxes, given the high consumption of glutamine by mammalian cells and rapid incorporation of glutamine carbon atoms into TCA cycle metabolites (Metallo et al., 2009; Yoo et al., 2008). Figure 4.4 shows the time profiles of ^{13}C-labeling of intracellular metabolites after the addition of [U-^{13}C]glutamine on day 2 (exponential phase) and day 5 (stationary phase). The percentage of labeled isotopomers for each metabolite (100%-M0) was determined from the measured mass isotopomer distributions (MIDs) after correction for natural isotope abundances (Fernandez et al., 1996). The composition of extracellular glutamine was 66% [U-^{13}C]glutamine and 34% natural glutamine on day 2, and 89% [U-^{13}C]glutamine and 11% natural glutamine on day 5. As shown in Figure 4.4, TCA cycle intermediates and related metabolites, glutamine (Gln), glutamate (Glu), α-ketoglutarate (AKG), citrate (Cit), malate (Mal), aspartate (Asp), and fumarate (Fum), reached isotopic steady state within 3 h at both phases. The steady-state labeling percentages of intracellular Gln, Glu, AKG and Cit were 67%, 50%, 47% and 42% at the exponential phase, and 88%, 52%, 50% and 39% at the stationary phase, respectively. Since the ^{13}C-enrichment of [U-^{13}C]glutamine in the medium was different at both phases, the percentages were normalized to the labeling of Gln to compare both phases. The normalized labeling percentages of intracellular Gln, Glu, AKG and Cit were 100%, 74%, 71% and 63% at the exponential phase, and 100%,

59%, 57% and 45% at the stationary phase. Thus, Glu, AKG and Cit were relatively more labeled at the exponential phase than at the stationary phase. This suggested that the influx of [U-^{13}C]glutamine into the TCA cycle decreased slightly, relative to influx of glucose and other unlabeled sources, in the transition from growth to non-growth. Intracellular pyruvate (Pyr), phosphoenolpyruvate (PEP), and other metabolites from the glycolysis pathway did not acquire significant labeling within 9 h. The glycolytic metabolites, Pyr and PEP showed less than 1% labeling at both phases in Figure 4.4C and D. It was indicated that the catabolic enzyme, phosphoenolpyruvate carboxykinase (PEPCK) was inactive in CHO cell metabolism.

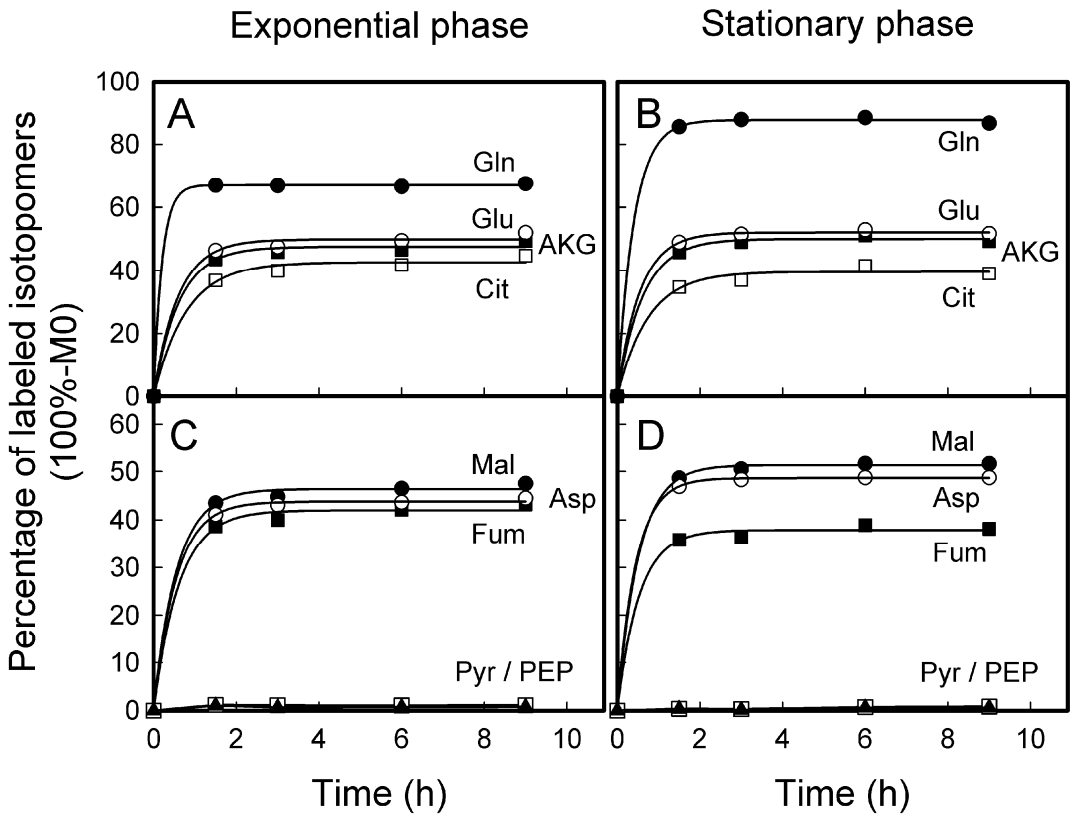

Figure 4.4 Time profiles of isotopic labeling of intracellular metabolites. After the introduction of [U-^{13}C]glutamine, they were analyzed at 1.5, 3, 6 and 9 h at the exponential phase (day 2) and stationary phase (day 5). Percentages of ^{13}C-labeled mass isotopomers (100%-M0) of intracellular metabolites were determined from measured mass isotopomer distributions, after correction for natural isotope abundances. (A, B) metabolites related to glutaminolysis at exponential and stationary phases, respectively (Gln, ●; Glu, ○; AKG, ■; Cit, □); (C, D) metabolites related to pyruvate cycling (Mal, ●; Asp, ○; Fum, ■; Pyr, □; PEP, ▲).

4.3.4 MIDs of Intracellular Metabolites from [U-^{13}C]Glutamine Tracer

In addition to determining the level of enrichment of intracellular metabolites, GC-MS analysis provides information on the distribution of mass isotopomers. Figures. 4.5 and 4.6 show the distributions of ^{13}C-labeled mass isotopomers at both phases for the measured metabolites after correction for natural isotope abundances. The uncorrected GC-MS data for all measured metabolites are given in Appendix B (see Tables B.3-B.6). Figure 4.5 shows the MIDs of three representative metabolites in the TCA cycle, Glu, Suc, and Mal, at four sampling times, 1.5, 3, 6 and 9 h after the addition of [U-^{13}C]glutamine at both phases. Even though the labeling percentages of TCA metabolites were relatively constant after 1.5 h in Figure 4.4, the ratios of ^{13}C-labeled mass isotopomers changed slightly between 1.5 h and 3 h in Figure 4.5. Thus, at least 3 h were needed to reach true isotopic steady state for TCA cycle metabolites using [U-^{13}C]glutamine tracer.

Figure 4.6 shows the MIDs of TCA metabolites at 9 h. Intracellular Gln was mainly M5 (95%) and M4 labeled (5%) at both phases. The M4 mass isotopomer resulted from incomplete labeling of the [U-^{13}C]glutamine tracer. Labeling of intracellular Gln was identical to the labeling of extracellular Gln, suggesting that after Gln was taken up by CHO cells it was irreversibly metabolized to Glu via glutaminase (GLS) and that there was no glutamine synthetase activity (GS). The most striking differences between the exponential phase and stationary phase mass isotopomers were the reduced abundances of M5 mass isotopomers for AKG and Glu, and reduced abundances of M4 mass isotopomers for Suc, Fum, Mal, Asp and Cit in Figure 4.6. For example, the fractional abundance of M5 of AKG dropped from 74% at the exponential phase to 45% at the stationary phase. The lower abundance of M5 of AKG corresponded well with the presumed reduced influx of [U-^{13}C]glutamine into the

TCA cycle (see previous section), as influx of [U-^{13}C]glutamine into the TCA cycle via GDH (or AT) produces M5 labeled AKG, while flux of Cit to AKG via IDH produces M1-M4 mass isotopomers of AKG (see Figure 4.6, labeling of Cit5). Thus, the ratio of M5 to M1-M4 mass isotopomers for AKG corresponds roughly to the flux ratio of GDH to IDH. The MIDs of Glu and AKG were similar, suggesting that reactions between Glu and AKG were highly reversible at both metabolic phases.

As expected, the MID of Suc was identical to that of Glu4 (*m/z* 330, C1-C4), confirming that AKG was the main source for Suc via α-ketoglutarate dehydrogenase in the TCA cycle. The MIDs of Fum, Mal and Asp were similar, but differed from the MID of Suc in that the M3 mass isotopomer was significantly higher in Fum, Mal and Asp (14% at exponential phase, and 8% at stationary phase) compared to M3 of Suc (4% at exponential phase, and 2% at stationary phase). In mammalian cells, there are two pathways that can produce M3 labeled oxaloacetate (OAC) from [U-^{13}C]glutamine (Metallo et al., 2012; Yoo et al., 2008), namely: 1) reductive carboxylation of AKG to Cit via isocitrate dehydrogenase (IDH) followed by ATP citrate lyase (ACL), i.e. AKG(M5) → Cit(M5) → AcCoA(M2) + OAC(M3); and 2) pyruvate cycling via malic enzyme (ME) and pyruvate carboxylase (PC), i.e. AKG(M5) → Mal(M4) → Pyr(M3) → OAC(M3). Considering that intracellular citrate displayed relatively low M5 labeling (~6%) at both metabolic phases (Figure 4.6) suggested that pyruvate cycling via ME was active in CHO cells, especially at the exponential phase.

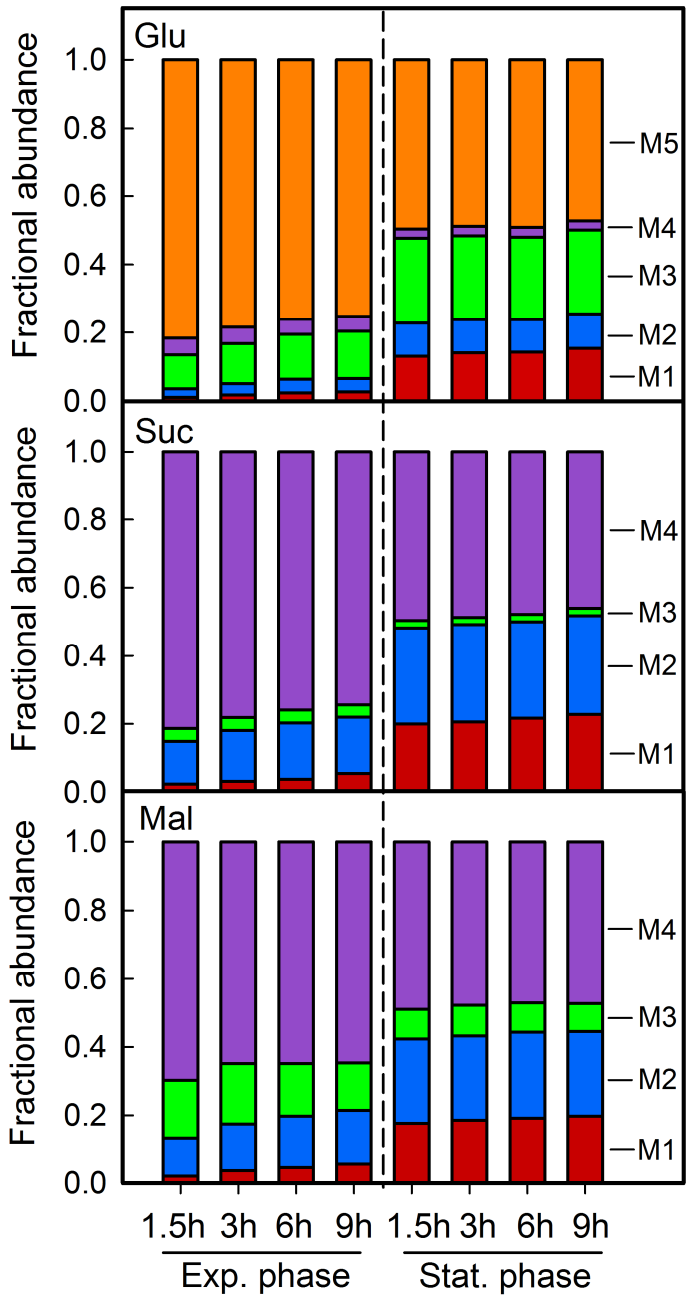

Figure 4.5 Fractional abundances of labeled mass isotopomers at 1.5, 3, 6 and 9 h after the addition of [U-^{13}C]glutamine tracers at the exponential and stationary phase. Three representative metabolites in the TCA cycle as follows: glutamate (*m/z* 432), succinate (*m/z* 289), and malate (*m/z* 419).

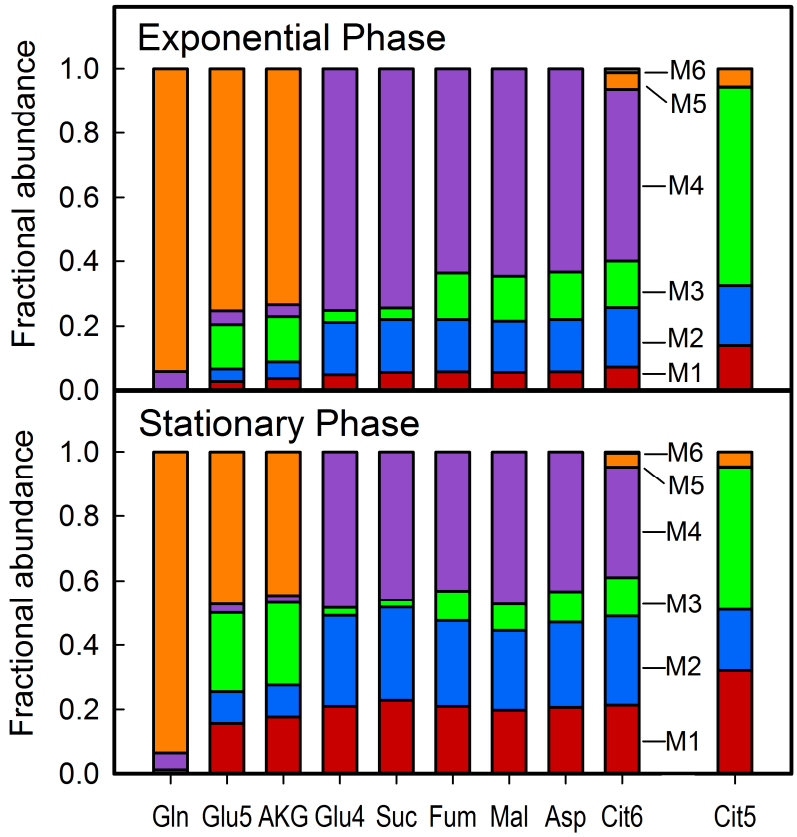

Figure 4.6 Fractional abundances of labeled mass isotopomers at 9 h after the addition of [U-^{13}C]glutamine at the exponential phase (A) and stationary phase (B). The following metabolite fragments: glutamine (*m/z* 431), glutamate (*m/z* 432, C1-C5), AKG (*m/z* 346), glutamate (*m/z* 330, C1-C4), succinate (*m/z* 289), fumarate (*m/z* 287), malate (*m/z* 419), aspartate (*m/z* 418), citrate (*m/z* 459, C1-C6), and citrate (*m/z* 431, C1-C5).

4.3.5 Lipid Metabolism

To our knowledge, lipid metabolism has not been studied in CHO cells before using isotopic tracers. Given that lipid metabolism can have a significant impact on central carbon metabolism to satisfy the needs for cytosolic AcCoA and reducing power NADPH, we investigated lipogenic fluxes in CHO cells using [U-^{13}C]glutamine tracer. *De novo* biosynthesis of palmitate, the most abundant fatty acid in lipids, was analyzed by measuring the incorporation of ^{13}C-atoms into palmitate by GC-MS and estimating fluxes using the isotopomer spectral analysis (ISA) method. Figure 4.7 shows MIDs of palmitate at both phases at 3, 6, 9 and 12 h following the introduction of [U-^{13}C]glutamine tracer on days 2 and 5. Palmitate incorporated ^{13}C-labeling from [U-^{13}C]glutamine at both metabolic phases as evidenced by the increasing abundances of even numbered mass isotopomers, M2, M4 and M6 in Figure 4.7. Figure 4.8 shows results of ISA analysis, which estimates two parameters: 1) D(Gln)-value, the fractional ^{13}C-labeling of lipogenic AcCoA from [U-^{13}C]glutamine; and 2) g(t)-value, the fraction of newly synthesized palmitate after labeling time t. The D-values were relatively constant during both phases, about 7% at the exponential phase and 5% at the stationary phase (Figure 4.8A and B), confirming that isotopic steady state was reached for lipogenic AcCoA pool from [U-^{13}C]glutamine. The relatively low D-values, however, also suggested that [U-^{13}C]glutamine did not contribute significantly to the production of lipogenic AcCoA. The majority of fatty acids were therefore derived from other carbon sources, presumably from glucose at the exponential phase and glucose and lactate at the stationary phase.

The fraction of newly synthesized palmitate at 3, 6, 9 and 12 h after tracer addition was 11%, 19%, 25% and 32% at the exponential phase and 7%, 13%, 18% and 23% at the stationary phase in Figure 4.8C and D. At the exponential phase, the

estimated g(t)-values correlated well with the predicted g(t)-values based on the measured growth rate as described with solid lines in Figure 4.8C. This indicated that the fatty acid biosynthesis flux matched well with the lipid needs for cell growth at the exponential phase. However, surprisingly, at the stationary phase, the fatty acid biosynthesis flux remained high even though no fatty acids were needed for growth in Figure 4.8D. Using Eq. 4.1 we estimated a net lipogenic flux of AcCoA to lipids of 24 nmol/10^6cells/h at the exponential phase and 17 nmol/10^6cells/h at the stationary phase.

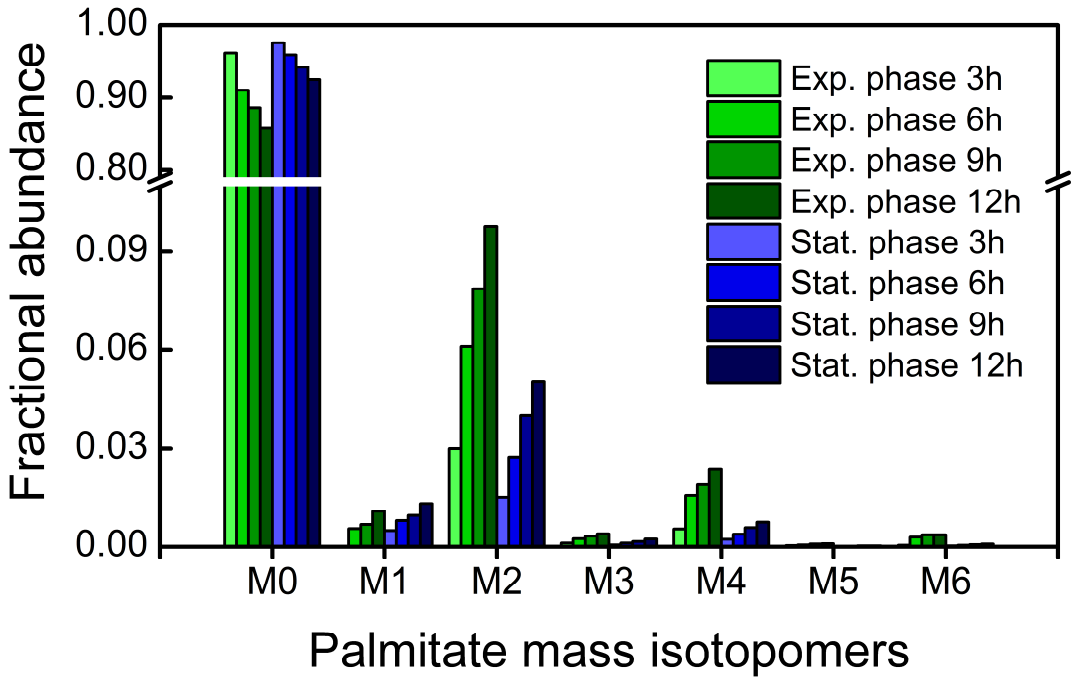

Figure 4.7 Mass isotopomer distributions of palmitate at 3, 6, 9 and 12 h after the introduction of [U-^{13}C]glutamine at the exponential phase (day 2) and stationary phase (day 5). The mass isotopomer distributions were corrected for natural isotope abundances.

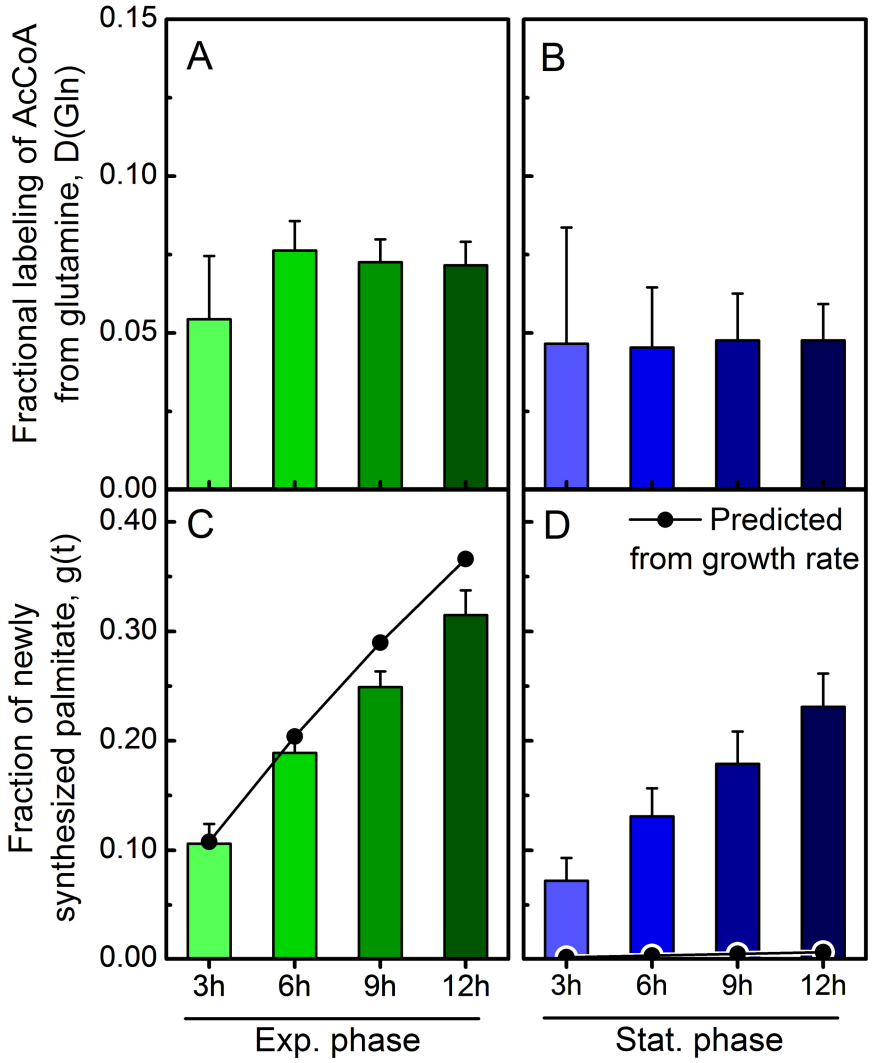

Figure 4.8 Isotopomer spectral analysis (ISA) of palmitate labeling at the exponential phase (day 2) and stationary phase (day 5). (A, B) Fractional ^{13}C-labeling of lipogenic AcCoA from [U-^{13}C]glutamine, D(Gln)-value. (C, D) Fraction of newly synthesized palmitate after labeling time t, g(t)-value. Lines with filled circles show the theoretical g(t)-values assuming lipids are only needed for cell growth, calculated using Eq. 4.1.

4.3.6 ^{13}C-Labeling Dynamics of Intracellular Metabolites from [1,2-^{13}C]Glucose Tracer

A second isotopic tracer, [1,2-^{13}C]glucose, was applied in parallel experiments to complement the results obtained from [U-^{13}C]glutamine tracer. Recently, it was reported that [1,2-^{13}C]glucose can be used to estimate fluxes in CHO cells using isotopic non-stationary ^{13}C-MFA (Ahn and Antoniewicz, 2011). This study focused on short labeling times and ^{13}C-MFA at isotopic steady state. Figure 4.9 shows the dynamic profiles of ^{13}C-labeling of intracellular metabolites after the addition of [1,2-^{13}C]glucose tracer on days 2 and 5. The measured labeling profiles corresponded well with the results in the previous study. Isotopic steady state was reached quickly within 1.5 h for glycolytic intermediates dihydroxyacetone phosphate (DHAP), 3-phosphoglycerate (3PG) and phosphoenolpyruvate (PEP), whereas most other metabolites did not approach isotopic steady state within 9 h, including glycerol-3-phosphate (GLP), lactate (Lact), pyruvate (Pyr), and TCA cycle metabolites in Figure 4.9.

The composition of glucose in the medium was 81% [1,2-^{13}C]glucose and 19% natural glucose on day 2 (exponential phase), and 77% [1,2-^{13}C]glucose and 23% natural glucose on day 5 (stationary phase). The steady-state labeling percentages (100%-M0) of intracellular DHAP, 3PG and PEP were 42%, 33% and 32% at the exponential phase, and 35%, 28% and 27% at the stationary phase in Figure 4.9. The maximum expected labeling of glycolytic intermediates was 40.5% (=81%/2) at the exponential phase and 38.5% (=77%/2) at the stationary phase. This corresponded well with the measured labeling for DHAP. However, the reduced labeling of metabolites 3PG and PEP at both phases indicated that other unlabeled sources contributed to the production of these metabolites; or alternatively, the lower labeling

could be due to compartmentalization effects (Ahn and Antoniewicz, 2011). For example, presence of unlabeled metabolite pools in compartments that do not directly participate in metabolism can dilute isotopic labeling of intracellular metabolites obtained from cell extracts (Ahn and Antoniewicz, 2012; Wahrheit et al., 2011). We estimated that GLP, lactate and pyruvate reached ~80-90% of isotopic steady state labeling at 9 h, which was 21%, 16%, and 15% ^{13}C-labeling at the exponential phase, and 6%, 4%, and 4% at the stationary phase, respectively. The 3-fold lower labeling of GLP at the stationary phase compared to exponential phase suggested that other pathways contributed to GLP formation from unlabeled sources. The 4-fold lower labeling of lactate and pyruvate was consistent with the metabolic shift from net lactate production at exponential phase to net lactate consumption at stationary phase (Ahn and Antoniewicz, 2011).

Figure 4.9E and F show the labeling dynamics of two representative TCA intermediates, Cit and AKG. Neither metabolite approached isotopic steady state within 9 h; the percentages of labeled isotopomers of Cit and AKG at 9 h were 10% and 3% at the exponential phase, and 5% and 3% at the stationary phase, respectively. The 3-fold drop in ^{13}C-labeling from AKG to Cit at the exponential phase, and 2-fold drop at the stationary phase, corresponded well with the presumed reduced influx of glutamine into the TCA cycle that we determined from the experiments with [U-^{13}C]glutamine tracer, where we found that AKG was 74% M5 labeled at the exponential phase (i.e. about 74% contribution from [U-^{13}C]glutamine vs. 26% from citrate), and 45% M5 labeled at the stationary phase, i.e. about 45% contribution from [U-^{13}C]glutamine vs. 55% from citrate in Figure 4.6.

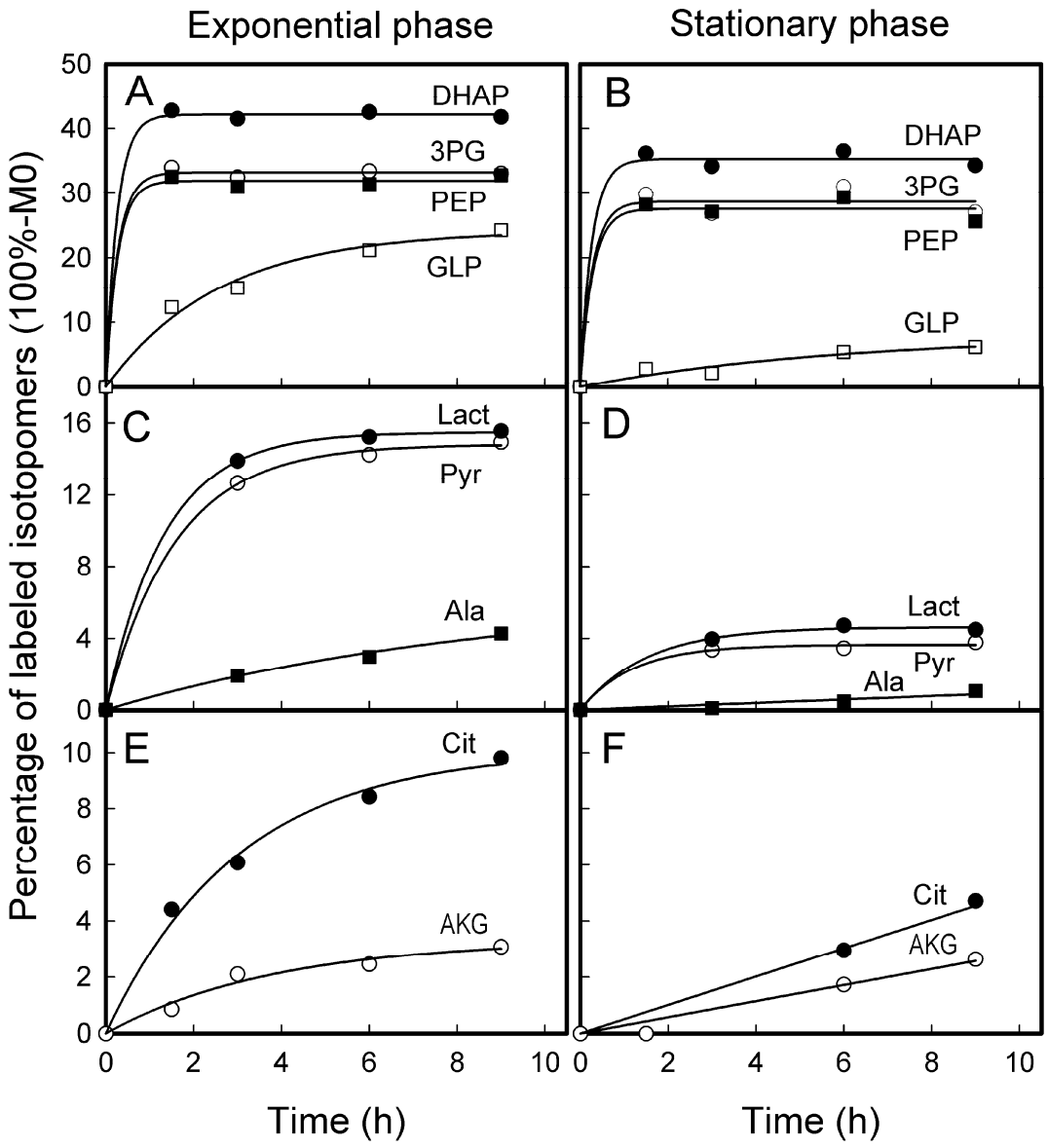

Figure 4.9 Time profiles of isotopic labeling of intracellular metabolites after the introduction of [1,2-^{13}C]glucose at the exponential phase (day 2) and stationary phase (day 5). Percentages of ^{13}C-labeled mass isotopomers (100%-M0) of intracellular metabolites were determined from measured mass isotopomer distributions, after correction for natural isotope abundances. (A, B) metabolites related to glycolysis at exponential and stationary phases, respectively (DHAP, ●; 3PG, ○; PEP, ■; GLP, □); (C, D) metabolites related to pyruvate metabolism (Lact, ●; Pyr, ○; Ala, ■); (E, F) metabolites in the TCA cycle (Cit, ●; AKG, ○).

4.3.7 MIDs of Intracellular Metabolites from [1,2-^{13}C]Glucose Tracer

Figure 4.10 shows the fractional abundances of labeled mass isotopomers for glycolytic intermediates 3PG and PEP. The MIDs at both phases were relatively constant at 1.5, 3, 6 and 9 h, confirming that metabolic and isotopic steady state were reached quickly (<1.5 h). At the exponential phase, 3PG and PEP were predominantly M2 labeled (~97%) with less than 3% of M1 and M3 mass isotopomers. The low abundance of M1 mass isotopomer indicated that the oxidative pentose phosphate pathway (oxPPP) was inactive at the exponential phase, i.e. no loss of ^{13}C-atoms from [1,2-^{13}C]glucose (Ahn and Antoniewicz, 2011). At the stationary phase, the distribution of M1, M2 and M3 mass isotopomers was 23%, 71% and 6%. Thus, the presence of M1 and M3 mass isotopomers suggested that pentose phosphate pathway was active at the stationary phase, since M1 is formed in the oxidative branch of PPP and M3 is formed in the non-oxidative branch of PPP via transketolase (TK) and transaldolase (TA) (Ahn and Antoniewicz, 2011). The MIDs of 3PG and PEP at isotopic steady state after 3 h were correlated well with other triose-phosphate metabolites, DHAP and GLP as shown in Figure 4.11.

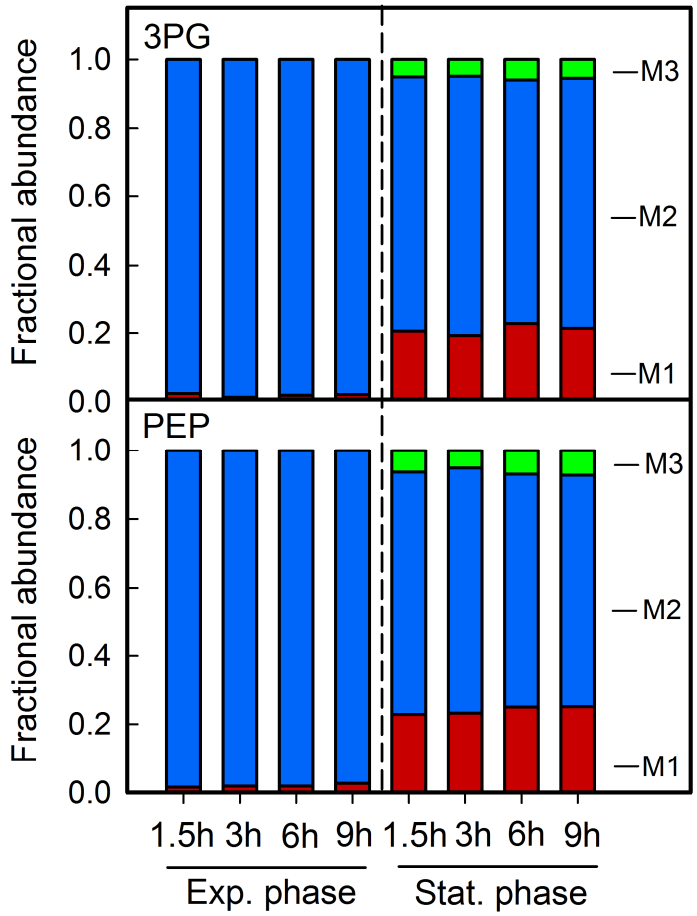

Figure 4.10 Fractional abundances of labeled mass isotopomers at 1.5, 3, 6 and 9 h after the addition of [1,2-^{13}C]glucose. Two representative metabolites in the glycolysis pathway: 3PG (*m/z* 585) and PEP (*m/z* 453).

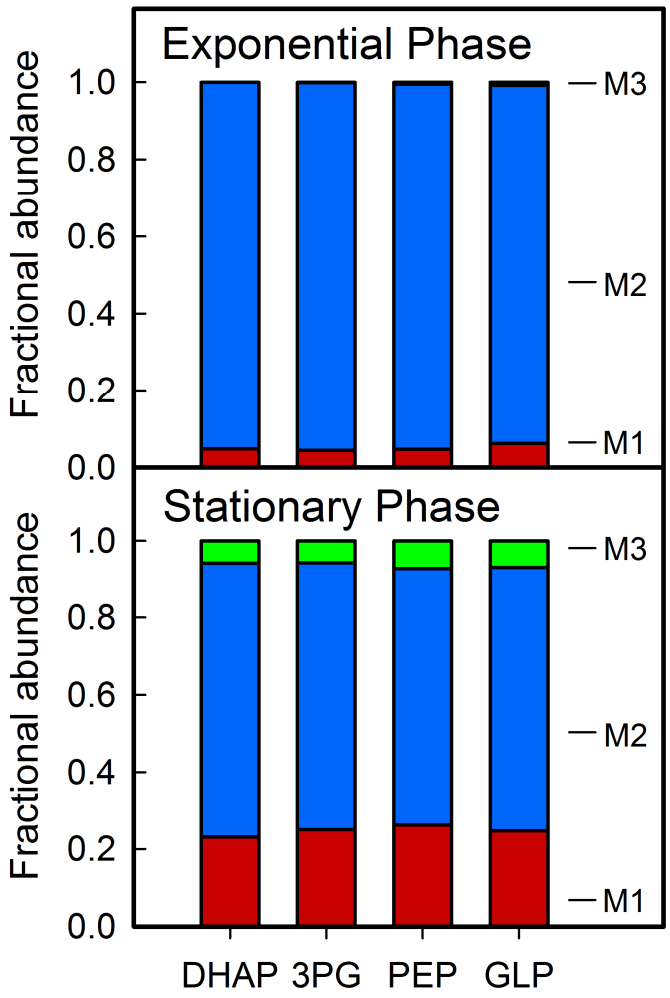

Figure 4.11 Fractional abundances of labeled mass isotopomers at 9 h after the addition of [1,2-^{13}C]glucose, at the exponential phase (A) and stationary phase (B). The following metabolite fragments: DHAP (*m/z* 484), 3PG (*m/z* 585), PEP (*m/z* 453), and GLP (*m/z* 571).

4.3.8 Carbon Flow from Main Substrates: Glucose and Glutamine

Glucose and glutamine are main substrates for carbon and energy sources to immortalized cell lines such as CHO cells and carcinoma cell lines. Thus, chasing carbon flows within cells from the nutrients has key meanings to understand cell physiology of mammalian cells. In this study, it was used for validation of metabolic model before MFA. As ^{13}C-MFA is a model-based technique, good model that can express real metabolism is a critical and indispensible factor to acquire right solution by ^{13}C-MFA. For the study of carbon flow, I devised the ^{13}C-fractional enrichment map of intracellular metabolites after tracer experiments as shown in Figure 4.12. For this study, two tracer sets, [1,2-^{13}C]glucose and [U-^{13}C]glutamine were applied at the conditions of the exponential phase and 9 h after addition of isotopic tracers.

In Figure 4.12A, ^{13}C-atoms from [1,2-^{13}C]glucose (80%, ^{13}C-fractional enrichment) labeled intracellular metabolites related to glycolysis pathway, i.e. DHAP, 3PG and PEP, which were 42%, 34% and 34% of ^{13}C-fractional enrichments. It was indicated that the related reactions in glycolysis pathway were very active. The pyruvate cycling-related metabolites, Pyr, Lact and Ala have 18%, 17% and 6% of ^{13}C-fractional enrichments (100%-M0), respectively (Ala is not suggested in Figure 4.12). Interestingly, it was shown almost 2-times reduction of the enrichments of Pyr and Lact and 5-times reduction of Ala. It has two key points; first, a lot of unlabeled carbon sources from media lactate diluted intracellular lactate. Extracellular lactate has 7% of ^{13}C-fractional enrichments. It suggests the free exchange between intracellular lactate pool and big extracellular lactate pool without atom transition. Considering high yield of lactate to glucose, ca. 1.5 mol/mol, the flow between two pools was very reversible transportation even if the net flux from intracellular lactate to extracellular lactate had high values. Also it gave us why TCA cycle-related metabolites show

isotopic non-stationarity of labeled metabolites by glucose tracers as discussed in Chapter 2. Second, Lact (17%) and Ala (6%) had different labeling percentage. Most of Lact was related to intracellular Pyr and extracellular Lact and also Ala was linked with intracellular Pyr and extracellular Ala. Furthermore, Ala can be connected with other pathways, Ala transaminotransferase. Thus, it may be that unlabeled Ala can dilute labeled Ala pool by TCA cycle-related carbon sources. In TCA cycle, Cit, AKG, Mal and Suc have 11%, 4%, 4% and 4% of ^{13}C-fractional enrichments. It was indicated that pyruvate dehydrogenase (PDH) was main linker between glycolysis and TCA cycle from 2-times higher labeling of Cit than other metabolites.

Figure 4.12B shows labeling map by [U-^{13}C]glutamine tracers (68%, ^{13}C-fractional enrichment). ^{13}C-labeling of Glu, AKG, Suc, Mal and Cit were 52%, 52%, 48%, 48% and 42%, respectively. But, pyruvate cycling-related metabolites, Pyr, Lact and Ala had 2%, 1% and 1%, respectively. Thus, relatively small amount of carbon source from glutamine labeled pyruvate cycling-related metabolites. In addition, glycolysis-related metabolites, DHAP, 3PG and PEP showed no labeling, almost 0%. The responsible reaction for the labeling is phosphoenolpyruvate carboxykinase (PEPCK), one of gluconeogenic enzyme. Therefore, PEPCK activity was very low in CHO metabolism.

In case of lipid metabolism, ^{13}C-labeling of palmitate (lipid) was 17% at [1,2-^{13}C]glucose set and 14% at [U-^{13}C]glutamine. Thus, lipid can be built from two carbon sources at the same time and at the similar contributions. This information was used for building metabolic model for CHO cells in this study.

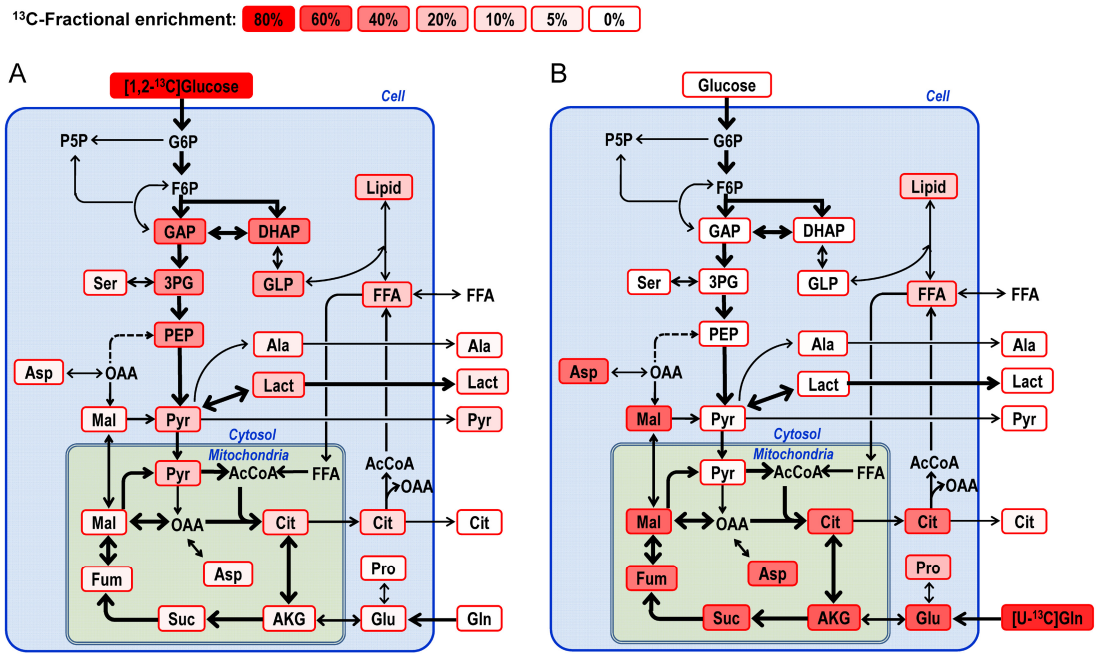

Figure 4.12 ^{13}C-Fractional enrichments of intracellular and extracellular metabolites using [1,2-^{13}C]glucose (A) and [U-^{13}C]glutamine (B). Tracers were used as substrates at the exponential phase. The samples were analyzed at 9 h after addition of isotopic tracers.

4.3.9 Combined ^{13}C-MFA at Isotopic Steady State

Detailed metabolic fluxes in CHO cells were determined using a new combined flux analysis approach that we developed, where multiple parallel labeling experiments, in this case with [1,2-^{13}C]glucose and [U-^{13}C]glutamine tracers, were fitted simultaneous to a single flux model. For ^{13}C-MFA, we fitted the averaged MIDs at 3, 6 and 9 h for DHAP (*m/z* 484), 3PG (*m/z* 585), and PEP (*m/z* 453) from [1,2-^{13}C]glucose tracer experiments; and Suc (*m/z* 289), AKG (*m/z* 346), Mal.m (*m/z* 391, 419), Asp (*m/z* 418), PEP (*m/z* 453), Glu (*m/z* 330, 432), Cit.m (*m/z* 431, 459), Pyr.c (*m/z* 174), Gln (*m/z* 431) and Pro (*m/z* 258) from [U-^{13}C]glutamine tracer experiments; together with extracellular uptake/production rates in Table 4.4, the measured cell

growth rates (corresponding to flux values of 116.0 and 0.5 nmol/10^6/cells/h for reaction v_{79} at the exponential and stationary phase, respectively), and the estimated lipogenic fluxes from ISA analysis. To obtain statistically acceptable fits, we included two mitochondrial pyruvate pools to consider possible pyruvate channeling in CHO cells; one pool was connected to TCA cycle via PC and the other via PDH. Compartmentalization of pyruvate pools was previously reported by Lu et al. based on analysis of ^{13}C-NMR spectra (Lu et al., 2002). ^{13}C-MFA analysis was performed independently for the exponential phase and stationary phase. We obtained statistically acceptable fits for both phases, with minimized variance-weighted sum of squared residuals (SSR) values of 44.7 and 53.2 at the exponential and stationary phases, respectively. The lower and upper bounds for the 95% confidence region of SSR were 38.8 and 80.9, respectively, assuming a χ^2-distribution for SSR with 58 redundant measurements. The complete flux results at both phases are given in Appendix B (see Tables B.1 and B.2), including 95% confidence intervals for all estimated fluxes. The two flux maps are shown schematically in Figure 4.13.

At the exponential phase, the most active metabolic pathway was glycolysis (397 ± 10 nmol/10^6/cells/h), and the majority of pyruvate that was produced via glycolysis was secreted as lactate (292 ± 5 nmol/10^6/cells/h). At the stationary phase, the glycolysis flux was reduced 5-fold (80 ± 4 nmol/10^6/cells/h), and lactate metabolism was rewired from net lactate production to net lactate consumption (10 ± 1 nmol/10^6/cells/h). The oxPPP flux was insignificant at the exponential phase (0.3 ± 0.2 nmol/10^6/cells/h), but became active at the stationary phase (13 ± 2 nmol/10^6/cells/h). The relative oxPPP flux, i.e. normalized to glucose uptake rate, was 0.1% at the exponential phase and 31% at the stationary phase. These values corresponded well

with the ratio of M1/M2 mass isotopomers for DHAP, PEP and 3PG, which were 2.5 ± 0.3 at the exponential phase and 32.2 ± 0.3 at the stationary phase in Figure 4.10. At the exponential phase, most of the mitochondrial pyruvate was converted to AcCoA via PDH (35 ± 2 nmol/10^6/cells/h), while a smaller fraction entered the TCA cycle via PC (12 ± 5 nmol/10^6/cells/h). At the stationary phase, the PDH flux was similar to exponential phase (27 ± 2 nmol/10^6/cells/h), however, no anaplerosis via PC was detected (0.0 ± 0.1 nmol/10^6/cells/h). At both phases, a large fraction of the citrate produced by citrate synthase was transported to the cytosol where it was converted to oxaloacetate and AcCoA via ATP citrate lyase (ACL) for *de novo* fatty acid synthesis. The ACL flux was similar at the exponential phase (23 ± 1 nmol/10^6/cells/h) and stationary phase (17 ± 2 nmol/10^6/cells/h). The net direction of the isocitrate dehydrogenase (IDH) flux was in the forward direction, i.e. from citrate to AKG, and was similar at both phases (9 ± 2 nmol/10^6/cells/h). The reverse IDH flux, i.e. from AKG to citrate, was very small at both phases (2.1 ± 0.3 nmol/10^6/cells/h), indicating that the IDH reaction was not very reversible in CHO cells. The net anaplerotic flux from glutamate to AKG was 2-fold higher at the exponential phase (15 ± 2 nmol/10^6/cells/h) than at the stationary phase (7 ± 1 nmol/10^6/cells/h). As a result, the α-ketoglutarate dehydrogenase flux from AKG to Suc was 50% higher at the exponential phase (24 ± 2 nmol/10^6/cells/h) compared to stationary phase (16 ± 2 nmol/10^6/cells/h). The cytosolic malic enzyme (ME.c) flux was 6-fold higher at the exponential phase (12 ± 4 nmol/10^6/cells/h) than at the stationary phase (2 ± 1 nmol/10^6/cells/h); however, mitochondrial malic enzyme (ME.m) flux was relatively small at both phases, i.e. 4 ± 1 and 2 ± 1 nmol/10^6/cells/h at the exponential and stationary phases, respectively.

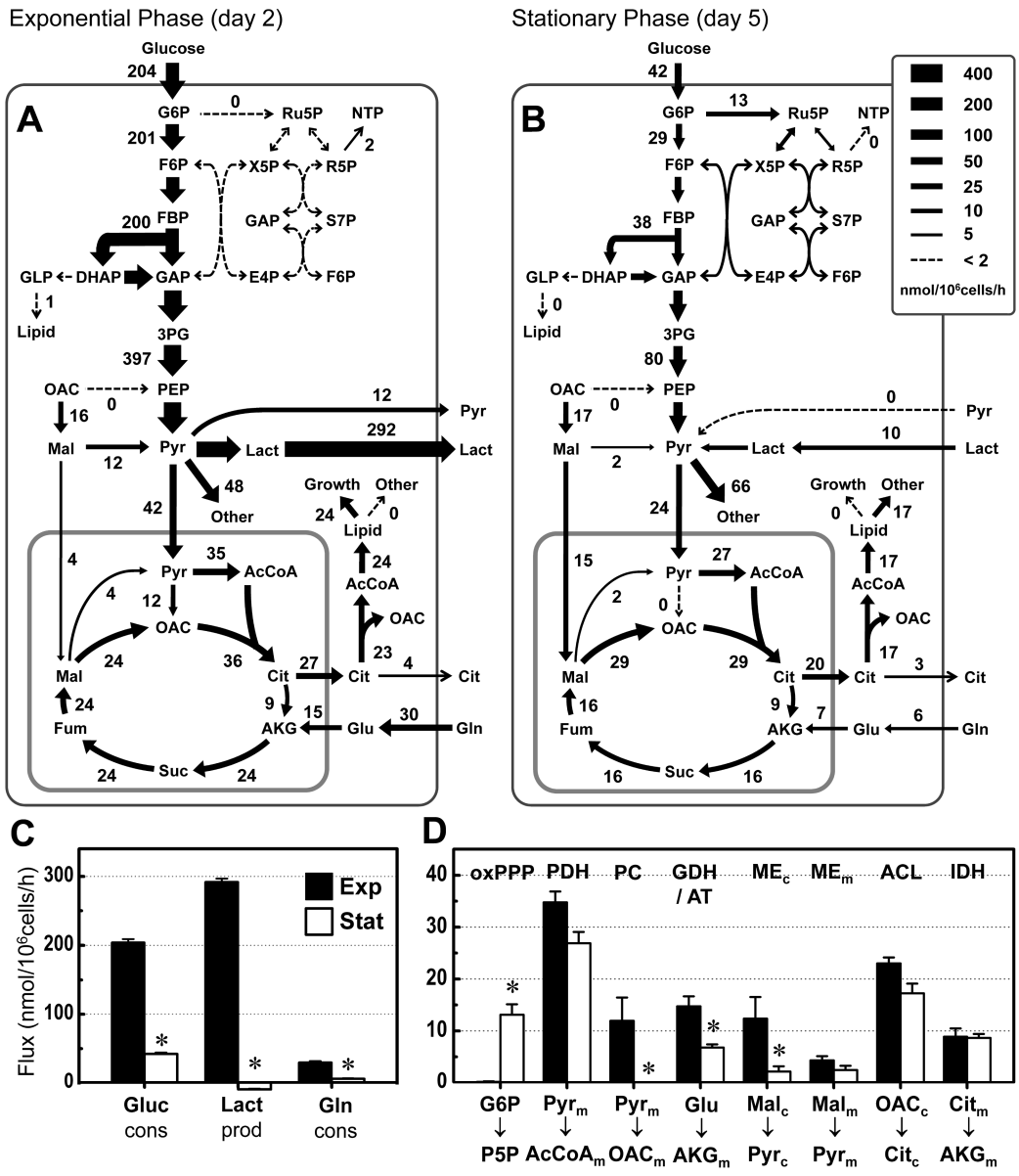

Figure 4.13 Metabolic flux maps for CHO cells at the exponential phase (A) and stationary phase (B) from combined ^{13}C-MFA. (C) Comparison of key extracellular uptake and excretion rates. (D) Comparison of key intracellular metabolic fluxes. Asterisk (*) denotes statistically significant difference ($P < 0.01$). Abbreviations: oxPPP, oxidative pentose phosphate pathway; PDH, pyruvate dehydrogenase; PC, pyruvate carboxylase; GDH/AT, glutamate dehydrogenase or aminotransferase; ME, malic enzyme; ACL, ATP citrate lyase; IDH, isocitrate dehydrogenase.

4.4 Discussion

In this study, the metabolism of CHO-K1 cells was investigated using a new method for flux analysis based on parallel labeling experiments and combined ^{13}C-MFA at isotopic steady state. CHO cells were grown over a period of six days in parallel cultures. On days 2 (growth phase) and 5 (stationary phase), ^{13}C-glucose and ^{13}C-glutamine tracers were introduced, followed by comprehensive analysis of intracellular and extracellular ^{13}C-labeling by mass spectrometry. In this study, we used [1,2-^{13}C]glucose and [U-^{13}C]glutamine as tracers, as these were previously determined to be optimal for measuring fluxes in glycolysis pathway and TCA cycle, although other optimal tracers have been suggested as well (Crown et al., 2012; Crown and Antoniewicz, 2012; Metallo et al., 2009; Walther et al., 2012). For flux analysis, we used a detailed metabolic network model of CHO cell metabolism, consisting of all major central carbon metabolic pathways, amino acid metabolism, fatty acid metabolism, and a lumped reaction for cell growth.

At the exponential growth phase, the flux map was characterized by a high glycolysis flux that resulted in the conversion of 70% of glucose to lactate. The pentose phosphate pathway was inactive at the exponential phase, consistent with previous reports for CHO cells (Ahn and Antoniewicz, 2011). At the stationary phase, the glycolysis flux was reduced 5-fold and the pentose phosphate pathway became activated. We estimated that about 30% of glucose was metabolized via oxPPP and 70% via glycolysis at the stationary phase. In a similar study, we recently estimated that ~20% of glucose was metabolized via oxPPP at the early stationary phase (day 4) (Ahn and Antoniewicz, 2011), while others have reported 41% oxPPP flux in a perfusion culture with CHO cells (Goudar et al., 2010), and even as high as 111% oxPPP flux at the late stationary phase (Sengupta et al., 2011) using ^{13}C-MFA. The

increased oxPPP activity at the stationary phase suggests that CHO cells require additional NADPH at the non-growth phase, perhaps to combat oxidative stress as was suggested by Sengupta et al (Sengupta et al., 2011).

The glutamine consumption rate was significantly reduced (>5-fold) at the stationary phase compared to exponential phase. This not only reflected reduced requirement of amino acids for cell growth, but also resulted in a net reduction of glutamine influx into the TCA cycle. As a result, the activity of the TCA cycle was slightly lower at the stationary phase compared to exponential phase. These results are consistent with a previous study, where we observed slight reduction in TCA fluxes in the transition from growth to non-growth (Ahn and Antoniewicz, 2011). Glutamine metabolism was elucidated in detail in this study using [U-^{13}C]glutamine tracer. In general, mammalian cells can metabolize glutamine by two main pathways: 1) glutaminolysis, which is defined as the conversion of glutamine to pyruvate (i.e. via TCA cycle, malate-aspartate shuttle, and malic enzyme); and 2) reductive carboxylation, which is defined as the conversion of glutamine to citrate via reverse IDH reaction (i.e. from AKG to citrate), that can then be transported to the cytosol to contribute to fatty acid biosynthesis via ACL (Yoo et al., 2008). At both metabolic phases, the majority of glutamine was metabolized via glutaminolysis in CHO cells. The reductive carboxylation flux (i.e. AKG $\rightarrow$ Cit) was relatively low at both phases.

For the first time, we also quantified fatty acid biosynthesis fluxes in CHO cells using ^{13}C-tracers. At the exponential phase, the measured fatty acid biosynthesis flux matched well with the predicted lipid requirements for cell growth. However, surprisingly, fatty acid biosynthesis remained high at the stationary phase when no cell growth was observed. Based on our flux results, it is still unclear what the exact fate is

of these newly synthesized fatty acids. Two possibilities are: 1) fatty acids can be recycled via β-oxidation resulting in a futile cycle; or 2) fatty acids can be secreted into the medium. We did not observe any accumulation of fatty acids in the medium at either the exponential phase or stationary phase (data not shown), nor could we confirm that β-oxidation was occurring. In future studies, fatty acid metabolism will be investigated in more detail to answer this question.

To obtain statistically acceptable fits in this study, it was necessary to include a reaction in the model to account for possible losses of metabolites in the glycolysis pathway. We lumped all such losses into one reaction (v_{18}, outflux of pyruvate). At both phases, the estimated flux value for this reaction was significant, 48 ± 11 and 66 ± 5 nmol/10^6/cells/h at the exponential and stationary phases, respectively. The flux results therefore suggested that CHO cells produced additional metabolites from glucose that were not measured and accounted in the model. To confirm this prediction, we performed follow-up experiments with [U-^{13}C]glucose under the same experimental conditions, followed by full-scan GC-MS analysis of medium samples using three derivatization methods to identify metabolites that accumulated ^{13}C-labeling. We identified seven previously unidentified metabolites in the medium that became M+3 and M+6 labeled from [U-^{13}C]glucose (Appendix B), thus suggesting that these metabolites were produced from glucose. The significance of this finding is that without accounting for these losses in the glycolysis pathway, the TCA cycle flux would be drastically overestimated (2- to 4-fold) using traditional stoichiometric flux balancing. This is the same conclusion that Altamirano et al. reached to explain a similar discrepancy in their data (Altamirano et al., 2006). Altamirano et al. estimated metabolic fluxes in a batch culture of t-PA producing CHO cells using traditional

MFA. Altamirano et al. found that the measured oxygen uptake rate was significantly lower than the estimated oxidative TCA cycle flux based on metabolite balancing. To resolve this discrepancy Altamirano et al. added a reaction to their model for the production of acetoin from intracellular pyruvate. By adding this additional sink of pyruvate they were able reduce the influx of pyruvate into the TCA cycle and match the measured oxygen uptake rate.

4.5 Conclusion

Metabolism of CHO cells in cell culture is still poorly understood. Given the importance of CHO cells in the biopharmaceutical industry, it is expected that research on CHO cell metabolism will be intensified in the coming years (Ahn and Antoniewicz, 2012). Most of studies on CHO cell metabolism have been using metabolite balancing to estimate fluxes, which has well-known limitations to estimate accurate metabolic fluxes due to the underdetermined nature of the problem. For example, important pathways such as the oxidative pentose phosphate pathway and pyruvate carboxylase cannot be estimated without isotopic tracers (Goudar et al., 2010). This is especially concerning given that these pathways appear to be active in CHO cells at different stages in a culture (Ahn and Antoniewicz, 2012). In this study, and in work by others (Altamirano et al., 2006), it was also demonstrated that the metabolite balancing approach can significantly overestimate TCA cycle activity if not all metabolic products are measured and accounted for in the model. This mass balancing problem was identified and quantified here using a new parallel labeling experiments technique that we developed. ^{13}C-MFA studies using parallel labeling experiments can provide a reliable approach for validating modeling assumptions and elucidating detailed metabolic fluxes.

Table 4.5 Metabolic network model for stationary ^{13}C-MFA of CHO metabolism.

Glycolysis			
v1	Gluc.ext (abcdef)	→	G6P (abcdef)
v2	G6P (abcdef)	↔	F6P (abcdef)
v3	F6P (abcdef)	→	FBP (abcdef)
v4	FBP (abcdef)	↔	DHAP (cba) + GAP (def)
v5	DHAP (abc)	↔	GAP (abc)
v6	GAP (abc)	↔	3PG (abc)
v7	3PG (abc)	↔	PEP (abc)
v8	PEP (abc)	→	Pyr.c (abc)
Pentose Phosphate Pathway			
v9	G6P (abcdef)	→	Ru5P (bcdef) + CO2 (a)
v10	Ru5P (abcde)	↔	X5P (abcde)
v11	Ru5P (abcde)	↔	R5P (abcde)
v12	X5P (abcde)	↔	EC2 (ab) + GAP (cde)
v13	F6P (abcdef)	↔	EC2 (ab) + E4P (cdef)
v14	S7P (abcdefg)	↔	EC2 (ab) + R5P (cdefg)
v15	F6P (abcdef)	↔	EC3 (abc) + GAP (def)
v16	S7P (abcdefg)	↔	EC3 (abc) + E4P (defg)
Pyruvate Metabolism			
v17	Pyr.c (abc)	↔	Lact (abc)
v18	Pyr.c (abc)	→	Pyr.snk (abc)
v19	Pyr.c (abc)	→	Pyr.m (abc)
v20	Pyr.m (abc)	→	AcCoA.m (bc) + CO2 (a)
TCA Cycle			
v21	AcCoA.m (ab) + OAC.m (cdef)	→	Cit.m (fedbac)
v22	Cit.m (abcdef)	↔	AKG.m (abcde) + CO2 (f)
v23	½ AKG.m (abcde) + ½ AKG.m (fghij)	→	½ Suc.m (bcde) + ½ Suc.m (jihg) + ½ CO2 (a) + ½ CO2 (f)
v24	½ Suc.m (abcd) + ½ Suc.m (efgh)	↔	½ Fum.m (abcd) + ½ Fum.m (hgfe)
v25	½ Fum.m (abcd) + ½ Fum.m (efgh)	↔	½ Mal.m (abcd) + ½ Mal.m (hgfe)
v26	Mal.m (abcd)	↔	OAC.m (abcd)

Table 4.5 continued

Anaplerosis and Gluconeogenesis			
v27	Mal.m (abcd)	→	Pyr.mII (abc) + CO2 (d)
v28	Pyr.mII (abc) + CO2 (d)	→	OAC.m (abcd)
v29	Pyr.m (abc)	↔	Pyr.mII (abc)
v30	Mal.c (abcd)	→	Pyr.c (abc) + CO2 (d)
v31	Mal.m (abcd)	↔	Mal.c (abcd)
v32	Mal.c (abcd)	↔	OAC.c (abcd)
v33	OAC.c (abcd)	→	PEP (abc) + CO2 (d)
Fatty Acid Metabolism			
v34	Cit.m (abcdef)	↔	Cit.c (abcdef)
v35	Cit.c (abcdef)	→	AcCoA.c (ab) + OAC.c (cdef)
v36	AcCoA.c (ab)	→	FA (ab)
v37	FA (ab)	→	FA.snk (ab)
v38	DHAP (abc)	→	GLP (abc)
Amino Acid Metabolism			
v39	Gln (abcde)	→	Glu (abcde)
v40	Glu (abcde)	↔	AKG.m (abcde)
v41	Glu (abcde)	↔	Pro (abcde)
v42	Asp (abcd)	↔	OAC.c (abcd)
v43	Asp (abcd)	→	Asn (abcd)
v44	Pyr.c (abc)	↔	Ala (abc)
v45	Ser (abc)	↔	Pyr.c (abc)
v46	Ser (abc)	→	Gly (ab) + C1 (c)
v47	Thr (abcd)	→	AcCoA.c (cd) + Gly (ab)
v48	Met (abcde) + CO2 (f)	→	Suc.m (bcdf) + CO2 (a) + C1 (e)
v49	Val (abcde) + CO2 (f)	→	Suc.m (dcef) + CO2 (a) + CO2 (b)
v50	Ile (abcdef) + CO2 (g)	→	Suc.m (bcdg) + AcCoA.m (ef) + CO2(a)
v51	Phe (abcdefghi)	→	Fum.m (defg) + AcCoA.m (bc) + AcCoA.m (hi) + CO2 (a)
v52	Tyr (abcdefghi)	→	Fum.m (defg) + AcCoA.m (bc) + AcCoA.m (hi) + CO2 (a)
v53	Leu (abcdef) + CO2 (g)	→	AcCoA.m (bc) + AcCoA.m (de) + AcCoA.m (gf) + CO2 (a)

Table 4.5 continued

Extracellular transport			
v54	Gln.ext (abcde)	→	Gln (abcde)
v55	Asp.ext (abcd)	→	Asp (abcd)
v56	Ile.ext (abcdef)	→	Ile (abcdef)
v57	Leu.ext (abcdef)	→	Leu (abcdef)
v58	Met.ext (abcde)	→	Met (abcde)
v59	Phe.ext (abcdefghi)	→	Phe (abcdefghi)
v60	Ser.ext (abc)	→	Ser (abc)
v61	Tyr.ext (abcdefghi)	→	Tyr (abcdefghi)
v62	Val.ext (abcde)	→	Val (abcde)
v63	Thr.ext (abcd)	→	Thr (abcd)
v64	Arg.ext (abcdef)	→	Arg (abcdef)
v65	Cys.ext (abc)	→	Cys (abc)
v66	His.ext (abcdef)	→	His (abcdef)
v67	Lys.ext (abcdef)	→	Lys (abcdef)
v68	Trp.ext (abcdefghijk)	→	Trp (abcdefghijk)
v69	Ala (abc)	→	Ala.ext (abc)
v70	Gly (ab)	→	Gly.ext (ab)
v71	Pro (abcde)	→	Pro.ext (abcde)
v72	Glu (abcde)	⇔	Glu.ext (abcde)
v73	Lact (abc)	⇔	Lact.ext (abc)
v74	Pyr.c (abc)	⇔	Pyr.ext (abc)
v75	Suc.m (abcd)	→	Suc.ext (abcd)
v76	Fum.m (abcd)	→	Fum.ext (abcd)
v77	Mal.m (abcd)	→	Mal.ext (abcd)
v78	Cit.c (abcdef)	→	Cit.ext (abcdef)
Biomass reaction			
v79	0.0624 Ala + 0.0392 Arg + 0.0374 Asp + 0.0300 Asn + 0.0151 Cys + 0.0335 Glu + 0.0402 Gln + 0.0560 Gly + 0.0149 His + 0.0337 Ile + 0.0587 Leu + 0.0593 Lys + 0.0144 Met + 0.0228 Phe + 0.0326 Pro + 0.0447 Ser +	→	Biomass

Table 4.5 continued

	0.0402 Thr + 0.0046 Trp + 0.0189 Tyr + 0.0433 Val + 0.0290 G6P + 0.0242 Ru5P + 0.2335 FA + 0.0113 GLP

Metabolic network model was used for ^{13}C-metabolic flux analysis of CHO cells, along with the carbon atom transitions. For each metabolite carbon atoms are identified using letters to represent successive carbon atoms.. The network model includes two mitochondrial pyruvate pools to describe possible pyruvate channeling; one pyruvate pool is connected to TCA cycle via PC and the other via PDH. The pyruvate sink reaction (v_{18}) accounts for potential losses of metabolites in the glycolysis pathway. The fatty acid sink reaction (v_{37}) accounts for all processes that consume FAs, other than cell growth. The net direction of reactions v_{72}, v_{73}, and v_{74} was different at exponential phase and stationary phase.

Table 4.6 Metabolic network model for isotopomer spectral analysis (ISA)

Palmitate synthesis			
v1	AcCoA.m0 (ab)	→	AcCoA.c (ab)
v2	AcCoA.m1 (ab)	→	AcCoA.c (ab)
v3	AcCoA.m2 (ab)	→	AcCoA.c (ab)
v4	AcCoA.c (ab) + AcCoA.c (cd) + AcCoA.c (ef) + AcCoA.c (gh) + AcCoA.c (ij) + AcCoA.c (kl) + AcCoA.c (mn) + AcCoA.c (op)	→	Palm.c (abcdefghijklmnop)
v5	Palm.c (abcdefghijklmnop)	→	Palm.ext (abcdefghijklmnop)

Chapter 5

QUANTIFYING METABOLIC FLUXES OF PENTOSE PHOSPHATE PATHWAY IN CHO CELLS USING MULTIPLE ISOTOPIC TRACERS AND MASS SPECTROMETRY

The pentose phosphate pathway (PPP) plays an important role in cellular metabolism for biosynthesis of RNA and DNA ribose moieties and production of NADPH cofactors. However, due to the complexity of the pathway, cycling and reversible reactions, the quantification of PPP is still challenging using ^{13}C-metabolic flux analysis (^{13}C-MFA). In this work, oxidative and non-oxidative PPP metabolism of Chinese hamster ovary (CHO) cells was studied using isotopic tracers and mass spectrometry. CHO cells were cultured in fed-batch mode with glucose feeding on days 2 and 5. Isotopic tracers were added on day 5 and labeling of intracellular metabolites was analyzed with GC-MS. To quantify oxidative PPP, we designed a mixture of tracers, [1-^{13}C]glucose+[4,5,6-^{13}C]glucose, and compared the results with a more traditional tracer, [1,2-^{13}C]glucose. The measured activity by mass isotopomer distribution (MID) analysis matched well. The biochemical network model for PPP was additionally validated with [2-^{13}C]glucose+[4,5,6-^{13}C]glucose and [3-^{13}C]glucose+[4,5,6-^{13}C]glucose tracers. We found that C_3 carbon fragment (dihydroxyacetone moiety) was lost in the non-oxidative PPP. Furthermore, the PPP model without considering the loss of C_3 fragments showed different flux values of oxidative PPP according to different tracers. By introducing a corrected network model, we achieved consistent solutions for oxidative PPP flux regardless of different tracer usage. Finally, by addition of MS data for new fragments of F6P, we acquired

narrow confidence intervals for the estimated oxidative PPP and good flux observability of transaldolase and transketolase reactions in non-oxidative PPP. Thus, we realized quantification of metabolic fluxes for oxidative and non-oxidative PPP by validation of metabolic model and introduction of new key measurements.

5.1 Introduction

Oxidative and non-oxidative pentose phosphate pathway (PPP) plays a key role in cellular metabolism. PPP consists of oxidative and non-oxidative branches. The two branches are controlled by several key enzymes, e.g. glucose 6-phosphate dehydrogenase (G6PDH), transketolase (TK) and transaldolase (TA) (Furuta et al., 2010; Vander Heiden et al., 2009), and both branches are linked to ribose 5-phosphate (R5P), a precursor for nucleotide synthesis. Oxidative PPP generates one CO_2 and two NADPH from one glucose-6-phosphate (G6P) conversion to R5P. NADPH is a cofactor for biosynthesis of macromolecules and also used to reduce oxidative stress (Tian et al., 1999; Vander Heiden et al., 2009). Non-oxidative PPP is also used for *de novo* synthesis of RNA ribose (Boros et al., 1997; Furuta et al., 2010). The two branches, oxidative and non-oxidative PPP, are connected between glycolysis pathway and pentose 5-phosphate molecules.

^{13}C-Metabolic flux analysis (^{13}C-MFA) is a powerful technique to obtain quantitative information about intracellular metabolic fluxes. After addition of isotopic tracers, labeled atoms (generally ^{13}C-atoms) are incorporated into intracellular metabolites, which are then analyzed by NMR, GC-MS and LC-MS (Choi and Antoniewicz, 2011; Goudar et al., 2010; Rühl et al., 2012; Szyperski, 1995). The mass isotopomer distributions (MIDs) of metabolites from mass spectrometry are converted into metabolic fluxes using nonlinear least square regression and isotopomer balancing

equations (Antoniewicz et al., 2007b; Schmidt et al., 1997; Wiechert et al., 1999). As MIDs of metabolites conserve information about atom transitions in the biochemical reactions, ^{13}C-MFA is also used for validation of cellular pathways (Boghigian et al., 2010; Crown et al., 2011; Metallo et al., 2012; Moxley et al., 2009; Munger et al., 2008). In this study, we applied ^{13}C-MFA to quantify oxidative PPP and validate the biochemical network model for PPP.

The PP pathway consists of largely reversible (bidirectional) reactions that allow cycling between glycolysis, oxidative, and non-oxidative PPP. Due to the metabolic complexity of the pathway, the estimated flux distributions are significantly influenced by the reversibility of PPP reactions, such as TK and TA (Follstad and Stephanopoulos, 1998; Wittmann and Heinzle, 1999). However, relatively small flux value compared to glucose consumption rate gave the importance of PPP fluxes to be underestimated in metabolic flux analysis field despite key role in cellular metabolism (Wiechert and de Graaf, 1997). Van Winden and Heijnen reported that traditional PPP models containing two TK and one TA reactions for non-oxidative PPP had two possible errors: incomplete reactions in PPP and metabolic channeling, and suggested a more realistic metabolic model with six TK and three TA reactions (van Winden et al., 2001). By introducing of one pool of glycolaldehyde moiety (C_2) and dihydroxyacetone moiety (C_3) fragments in non-oxidative PPP reactions, Kleijn et al. proposed the use of half reactions in the model with three TK and two TA reactions for non-oxidative PPP in glycolysis and PPP network model (Kleijn et al., 2005). Recently, metabolic models containing the traditional PPP model were applied for ^{13}C-MFA of Chinese hamster ovary (CHO) metabolism using isotopic tracers (Ahn and Antoniewicz, 2012). Using a mixture of [1-^{13}C]glucose and [U-^{13}C]glucose tracers

and NMR spectroscopy, Goudar et al. estimated 41% oxidative PP flux, relative to glucose consumption rate, during perfusion culture of CHO cells (Goudar et al., 2010). Sengupta et al. measured ^{13}C-labeling of intracellular metabolites in PPP using LC-MS and using the same tracer mixture and estimated high oxidative PPP fluxes in CHO cells at the late non-growth phase of a fed-batch culture (Sengupta et al., 2011). Based on the half-reactions model for PPP metabolic network (Kleijn et al., 2005), Ahn and Antoniewicz estimated 1% oxidative PPP flux at the exponential phase in CHO culture, and 21% at the stationary phase using [1,2-^{13}C]glucose tracers and GC-MS by applying ^{13}C-MFA (Ahn and Antoniewicz, 2011).

In this study, we investigated oxidative and non-oxidative PPP metabolism of CHO cells at the early stationary growth phase using ^{13}C-MFA and validated the PPP network model using mixtures of ^{13}C-glucose tracers. This is the first time that loss of TA-C_3 (dihydroxyacetone moiety, C_3) fragments in non-oxidative PPP was shown by MID analysis. In addition, we validated the PPP model using ^{13}C-MFA and found a discrepancy between the estimated oxidative flux values according to different isotopic tracers. By proposing a corrected network model, we eventually achieved consistent flux values of oxidative PPP regardless of isotopic tracers. Furthermore, we introduced two new GC-MS fragments of F6P. This is also the first time that the two F6P fragments narrowed the confidence intervals of oxidative fluxes and enhanced flux observability of TA and TK reversibilities in the non-oxidative PPP. In conclusion, we found TA-C_3 metabolite loss in PPP by validation of PPP model using designed isotopic tracers, and proposed good tracers and required measurements for estimation of oxidative and non-oxidative PPP fluxes.

5.2 Materials and Methods

5.2.1 Materials

Culture materials were purchased from Cellgro (Mediatech, Manassas, VA). [1,2-^{13}C]Glucose (99%), [1-^{13}C]glucose (99%), [2-^{13}C]glucose (99%), [3-^{13}C]glucose (99%) and [4,5,6-^{13}C]glucose (98%) were purchased from Cambridge Isotope Laboratories (Andover, MA). All glucose stock solutions were prepared at 1.39 M in phosphate buffer saline (PBS) and stored in 4°C, to be used as feed in the CHO cell culture experiments.

5.2.2 Cell Culture

CHO-K1 cells (ATCC Cat. No. CCL-61) were grown in T-25 flasks (Corning, NY, Cat. No. 430639) at 5 mL working volume in a humidified 5% CO_2 incubator at 37°C. Cells from frozen vials in liquid nitrogen storage tank were inoculated into T25 flask after media replacement. Cells were sub-cultured every three days at a split ratio of 1:10. Cells at the fourth subculture were used for the tracer experiment. The growth medium was Dulbecco's modified Eagle medium (DMEM, Cat. No. 10-013-CV) supplemented with 10% fetal bovine serum (FBS, Cat. No. 35-011-CV) and 1% penicillin-streptomycin solution (PS, Cat No. 30-004-CI).

5.2.3 Viable Cell Number, Glucose and Lactate Analysis

Cell numbers were measured using a hemocytometer and viability was determined by trypan blue exclusion method. Cell numbers were measured three times per sample. Concentrations of glucose and lactate were measured by YSI 2700 biochemistry analyzer (YSI, Yellow Springs, OH).

5.2.4 Isotopic Tracer Experiment

For the tracer experiment, CHO cells were grown in fed-batch culture with glucose feeding. First, cells were grown to confluency to be used as the seed. Cells were detached with trypsin EDTA (0.25% trypsin, Cat. No. 25-053-CV) and washed once with fresh growth medium and re-suspended in growth medium at 0.60×10^6 cells/mL and seeded in T-25 flasks (5 mL/flask). The growth medium was DMEM base (1 g/L glucose and 4 mM glutamine, Cat. No. 10-014-CV) supplemented with 10% FBS, 1% PS; glucose concentration was adjusted to 6.7 mM initial concentration using unlabeled glucose stock solution. In total, twenty two T-25 flasks were prepared with CHO cells: twelve flasks were used for glucose and lactate measurements and ten flasks were used for the tracer experiments at the stationary growth phase (day 5). During the six day cultivation, a bolus of glucose was added twice, on days 2 and 5, to a final glucose concentration of ~10 mM. For the tracer experiment, 27 μL of glucose stock solutions (1.39 M) was added to flasks on day 5 to increase the medium glucose concentration from 2.5 mM to 10 mM. The glucose stock solutions were prepared with five different compositions and 1.39 M concentrations of glucose: (1) natural (unlabeled) glucose solution; (2) a mixture of [1-^{13}C]glucose and [4,5,6-^{13}C]glucose (1:1 mol %); (3) a mixture of [2-^{13}C]glucose and [4,5,6-^{13}C]glucose (1:1 mol %); (4) a mixture of [3-^{13}C]glucose and [4,5,6-^{13}C]glucose (1:1 mol %); and (5) [1,2-^{13}C]glucose solution. The five different solutions were added on day 5 into each two flasks, as duplicate experiments. All ten flasks were harvested at 9 h after the addition of isotopic tracers. Cells were extracted as described below to obtain intracellular metabolites for analysis of ^{13}C-labeling. Supernatants were collected by centrifugation at 1,000 rpm for 3 min. All samples were stored at -85°C prior to further analysis.

5.2.5 Extraction of Intracellular Metabolites

At 9 h after the addition of tracers on day 5, culture medium was collected from the T-25 flasks and centrifuged to remove detached cells and debris. The supernatants were used to determine ^{13}C-labeling composition of glucose tracers by GC-MS. The attached cells in T-25 flasks were washed twice with 5 mL of cold saline water (9 g/L NaCl, 4°C). Next, 1.5 mL of cold methanol (-20°C) was quickly added into the flasks to quench cell metabolism. After incubation on ice for 5 min, cells were collected with a cell scraper (BD, NJ, Cat. No. 353086) and the cell suspension was transferred into glass tubes (13×100 mm, Corning, NY, Cat. No. 99447-13) with Teflon-sealed caps. 1.5 mL of chloroform was added and the tubes were vortexed briefly. Next, 1.5 mL of water was added and the tubes were vortexed vigorously for 1 min. All tubes were kept overnight at 4°C. To separate clear two phases, the tubes were centrifuged at 3,000 rpm and 4°C for 20 min. The upper aqueous phase (methanol and water) containing the polar metabolites was transferred into two 1.5 mL microcentrifuge tubes using a glass pipette and evaporated to dryness at 37°C with nitrogen gas and an evaporator (Reacti-Vap/Reacti-Therm III; Fierce, Rockford, IL). For GC-MS analysis, one of tubes was used for methyloxime and tertbutyldimethylsilyl (MOX-TBDMS) derivatization of intracellular metabolites, dihydroxyacetone phosphate (DHAP), glycerol 3-phosphate (GLP), 3-phosphoglycerate (3PG) and phosphoenolpyruvate (PEP); and the other tube was used for methyloxime and trimethylsilyl (MOX-TMS) derivatization of the intracellular metabolite fructose 6-phosphate (F6P) with *in vitro* dephosphorylation. The dried samples were stored at -85°C prior to derivatization and GC-MS analysis.

5.2.6 Derivatization and GC-MS Analysis of Intracellular Metabolites

The dried intracellular metabolites were dissolved in 35 µL of 2wt% methoxylamine hydrochloride in pyridine and incubated at 37°C for 90 min on a heating block. Next, 70 µL of N-methyl-N-(tert-butyldimethylsilyl)-trifluoroacetamide (MTBSTFA) + 1% tert-butyldimetheylchlorosilane (TBDMCS) (Thermo Scientific, Bellefonte, PA, Cat. No. TS-48927) was added and the samples were incubated at 60°C for 30 min. After an overnight incubation at room temperature, the derivatized samples were centrifuged at 14,000×g for 2 min and the clear liquid was transferred into GC vials for GC-MS analysis. The GC-MS system consisted of an Agilent 7890A GC with a DB-5ms (30 m × 0.25 mm i.d. × 0.25 µm; Agilent J&W Scientific) capillary column and Waters Quattro Micro GC-MS/MS (Milford, MA) operating under ionization by electron impact at 70 eV. The interface temperature with GC and ion source temperature were 250°C and 220°C, respectively. Helium flow was maintained at 1 mL/min. The injection volume was 1 µL to 3 µL and samples were injected in splitless or split mode depending on the peak intensities. GC oven temperature was held at 70°C for 2 min, increased to 140°C at 3°C/min, increased to 150°C at 1°C/min, increased to 280°C at 3°C/min and held for 6.33 min. The total run time was 85 min. Mass spectra of selected metabolite fragments (Table 5.1) were collected in SIR mode with 30 ms dwell time. Mass isotopomer distributions were obtained by integration of ion chromatograms (Antoniewicz et al., 2007a), and corrected for natural isotope abundances (Fernandez et al., 1996).

Table 5.1 Metabolite fragments measured by GC-MS for analysis of intracellular metabolites

Metabolite	Mass	Carbon atoms	Fragment formula
DHAP	484	1-2-3	$C_{18}H_{43}O_6NSi_3P$
3PG	585	1-2-3	$C_{23}H_{54}O_7Si_4P$
PEP	453	1-2-3	$C_{17}H_{38}O_6Si_3P$
GLP	571	1-2-3	$C_{23}H_{56}O_6Si_4P$
F6P*	307	4-5-6	$C_{12}H_{31}O_3Si_3$
F6P*	364	1-2-3-4	$C_{14}H_{34}O_4N_1Si_3$

* Fructose was analyzed by GC-MS, which was derived from intracellular F6P after dephophorylation.

5.2.7 Derivatization and GC-MS Analysis of Intracellular F6P

MS fragments of F6P were measured by GC-MS after dephosphorylation with alkaline phosphatase, and MOX-TMS derivatization. The protocol for the enzymatic reaction was modified for this study using White's method (White, 2004). 100 μL of water and 50 μL of glycine buffer (0.1 M of glycine in pH 10.4, 1 mM of Zn acetate, and 1 mM of $MgCl_2$) were added to the dried intracellular metabolites in a microcentrifuge tube. Next, 5 μL (ca. 0.3 IU) of alkaline phosphatase from *Escherichia coli* (Sigma, MO, Cat. No. P4377-100UN) was added and briefly vortexed. After incubation at 37°C for 1 h, the tubes were dried under nitrogen gas at 37°C. The dephosphorylated metabolites were dissolved in 33 μL of 2wt% methoxylamine hydrochloride in pyridine and incubated at 37°C for 90 min. This was combined with 67 μL of N-methyl-N-(trimethylsilyl)trifluoroacetamide (MSTFA) + 1% chlorotrimethylsilane (TMCS) (Thermo Scientific, Bellefonte, PA, Cat. No. TS-48915) and incubated at 60°C for 30 min. After an overnight incubation at room temperature, the derivatized samples were centrifuged at 14,000×g for 2 min and the

clear liquid was transferred into GC vials for GC-MS analysis. The injection volume was 1 to 3 μL, and samples were injected in splitless or split mode depending on the peak intensities. GC oven temperature was held at 80°C for 2 min, increased to 280°C at 7°C/min and held for 4.43 min. The total run time was 35 min. Mass spectra of selected metabolite fragments were collected in SIR mode with 30 ms dwell time. Two GC-MS fragments of fructose derived from F6P were measured, at *m/z* 307 ($C_{12}H_{31}O_3Si_3$) containing carbon atoms C4-C6 of F6P, and at *m/z* 364 ($C_{14}H_{34}O_4N_1Si_3$) containing carbon atoms C1-C4 of F6P, to acquire mass isotopomer distributions in Table 5.1 and Appendix C.

5.2.8 Derivatization and GC-MS Analysis of Glucose in Media

Labeling of glucose in the harvested medium was determined by GC-MS analysis of the aldonitrile pentapropionate derivative and di-o-isopropylidene propionate derivative of glucose (Antoniewicz et al., 2011). Proteins in 200 μL of media samples were precipitated by addition of 600 μL cold acetone (-20°C) and vortexing. The clear liquids were transferred to new microcentrifuge tubes for aldonitrile pentapropionate derivative of glucose or glass tubes for o-isopropylidene propionate derivative of glucose. The samples were dried under nitrogen gas flow. First, for aldonitrile pentapropionate derivative of glucose, the dried samples were mixed with 50 μL of hydroxylamine hydrochloride solution (20 mg/mL in pyridine). The samples were incubated at 90°C for 60 min, followed by addition of 100 μL of propionic anhydride. After 30 min incubation at 60°C, the samples were evaporated to dryness, dissolved in 100 μL of ethyl acetate and transferred into GC vials for GC-MS analysis. Second, for di-o-isopropylidene propionate derivative of glucose, fresh stock of 0.38 M sulfuric acid in acetone was prepared. 500 μL of the sulfuric acid solution

was added to the dried sample tubes and vortexed. The tube was incubated at room temperature for 60 min, and 400 µL of 0.44 M sodium carbonate solution in water was added to stop the reaction. 1 mL of saturated sodium chloride solution in water and 1 mL of ethyl acetate were added to the tubes and vortexed for 15 sec. After centrifugation at 3,000 rpm for 10 min, the top organic phase was transferred to microcentrifuge tubes and dried under nitrogen gas at room temperature. 50 µL of pyridine and 100 µL of propionic anhydride were added and incubated at 60°C for 30 min. After centrifugation for 1 min at 14,000 rpm, the tubes were dried under nitrogen gas at 60°C. The tubes were dissolved in 100 µL ethyl acetate and transferred to GC vials with a glass insert. For both derivatives, the injection volume was 1 µL and samples were injected at 1:40 split ratio. GC oven temperature was held at 80 °C for 1 min, increased to 280 °C at 8 °C/min, and held for 6 min. Labeling of glucose was determined from the mass isotopomer distributions of the fragments at *m/z* 370 ($C_{17}H_{24}O_8N_1$), which contains carbon atoms C1-C5 of glucose for the aldonitrile pentapropionate derivative; and at *m/z* 301 ($C_{14}H_{21}O_7$), which contains carbon atoms C1-C6 of glucose for di-o-isopropylidene propionate derivative (Antoniewicz et al., 2011).

5.2.9 Metabolic Network Model

A PPP metabolic network model was constructed for ^{13}C-metabolic flux analysis, based on a previous network model for CHO cells (Ahn and Antoniewicz, 2011). Two models for PPP were used for metabolic flux analysis. First, the original model of PPP consists of 17 reactions and 15 balanced metabolites (Figure 5.2 and Table 5.2). Second, an extended model of PPP contains an additional reaction (EC3.c to EC3.ext) (Table 5.2). The model consisted of 18 reactions and 15 balanced

metabolites. We assumed that the biosynthesis fluxes to build proteins, lipids, RNA, DNA and carbohydrates were negligible at the stationary phase (day 5) of the CHO cell culture (Ahn and Antoniewicz, 2011). Cofactor balances were not included in the models to avoid biases resulting from uncertainties cofactor metabolism.

5.2.10 Metabolic Flux Analysis

metabolic flux analysis (^{13}C-MFA) based on the elementary metabolite units (EMU) framework (Antoniewicz et al., 2007b; Young et al., 2008). For flux analysis, we used the measured data and a computational tool, Metran software (Yoo et al., 2008). The measured data were mass isotopomer distribution (MID) of mass fragments from intracellular metabolites and biomass specific uptake and production rates. For flux analysis, MID data provide relative flux ratios at branch points of reaction network and biomass specific uptake and production rates provide absolute flux values. In this study, MIDs of intracellular metabolites, DHAP, 3PG, PEP and F6P were used for measured parameters in Appendix C. In addition, 76.4 nmol/10^6cells/h of glucose consumption rate was used as biomass specific uptake rate. The values were estimated using extracellular glucose concentration and viable cell number profiles between days 4 and 6 at the stationary growth phase. Second, metabolic fluxes were estimated by minimizing the variance-weighted sum of squared residuals (SSR) between the experimentally measured and predicted values from model; extracellular uptake and production rates, and mass isotopomer distributions of intracellular metabolites. The conversion between predicted MIDs and estimated flux values were performed by non-linear least-squares regression (Antoniewicz et al., 2006a; Antoniewicz et al., 2007b). The Metran software also accounted for potential dilution effects of intracellular labeling, for example due to influx of unlabeled

metabolites that were not directly measured, by determining the percent isotopic labeling for each measured metabolite (Yoo et al., 2008). As an example, an estimated value of 90% indicates that the measured metabolite pool was diluted 10% from unknown sources. The estimated percentages of isotopic labeling are reported together with the estimated fluxes in Appendix C. In all cases, flux estimation was repeated at least 10 times starting with random initial values for all fluxes to find a global solution. The fitting results were subjected to a χ^2 statistical test to assess the goodness-of-fit, and accurate 95% confidence intervals were computed for all estimated parameters by evaluating the sensitivity of SSR to flux variations (Antoniewicz et al., 2006a). In addition, we performed combined ^{13}C-MFA regression analysis, as was described in Chapter 3. The combined analysis fitted simultaneously multiple data sets from different tracer experiments. All computations were performed with Matlab R2008b (Mathworks Inc.).

Table 5.2 Metabolic network model for ^{13}C-MFA of pentose phosphate pathway

Glycolysis			
v1	Gluc.ext (abcdef)	→	G6P (abcdef)
v2	G6P (abcdef)	↔	F6P (abcdef)
v3	F6P (abcdef)	→	FBP (abcdef)
v4	FBP (abcdef)	↔	DHAP (cba) + GAP (def)
v5	DHAP (abc)	↔	GAP (abc)
v6	GAP (abc)	↔	3PG (abc)
v7	3PG (abc)	↔	PEP (abc)
v8	PEP (abc)	→	Pyr (abc).snk
Pentose Phosphate Pathway			
v9	G6P (abcdef)	→	Ru5P (bcdef) + CO_2 (a)
v10	Ru5P (abcde)	↔	X5P (abcde)
v11	Ru5P (abcde)	↔	R5P (abcde)
v12	X5P (abcde)	↔	EC2 (ab) + GAP (cde)
v13	F6P (abcdef)	↔	EC2 (ab) + E4P (cdef)
v14	S7P (abcdefg)	↔	EC2 (ab) + R5P (cdefg)
v15	F6P (abcdef)	↔	EC3 (abc) + GAP (def)
v16	S7P (abcdefg)	↔	EC3 (abc) + E4P (defg)
Glycerol-3-phosphate Metabolism			
v17	DHAP (abc)	↔	GLP (abc)
EC3 molecules lost			
v18*	EC3.c (abc)	→	EC3.ext (abc)

Original PPP model, v1-v17 reactions; extended PPP model v1-v18 reaction

5.3 Results

5.3.1 Cell Culture and Tracer Experiments

As shown in Figure 5.1, CHO cells were cultured in fed-batch mode over a period of six days. A bolus of glucose was given at the exponential growth phase (day 2), and a second bolus at the stationary growth (non-growth) phase (day 5). The characteristic profiles for culture parameters were shown in previous study (Ahn and Antoniewicz, 2011). In this study, we focused on PPP metabolism of CHO cells at the non-growth phase. Thus, ^{13}C-labeled glucose tracers were added on day 5 and intracellular metabolites were extracted at 9 h after the introduction of isotopic tracers. In the previous study (Ahn and Antoniewicz, 2011; Maier et al., 2008; Sengupta et al., 2011), we confirmed that ^{13}C-labeling of intracellular metabolites related to glycolysis and pentose phosphate pathway (PPP) reached isotopic steady state within 3 h after the addition of isotopic glucose tracers. For this study, at the separate batch, we estimated viable cell density and glucose consumption profiles (data not shown). During days 4 to 6, it showed non-growth phase from viable cell density profile. The averaged viable cell density was $1.65 \pm 0.05 \times 10^6$ cells/mL at the stationary phase. The specific glucose consumption rate was 76.4 nmol/10^6 cells/mL estimated with the averaged cell density and glucose concentration profile, and was used for one of parameters in flux estimation for this study.

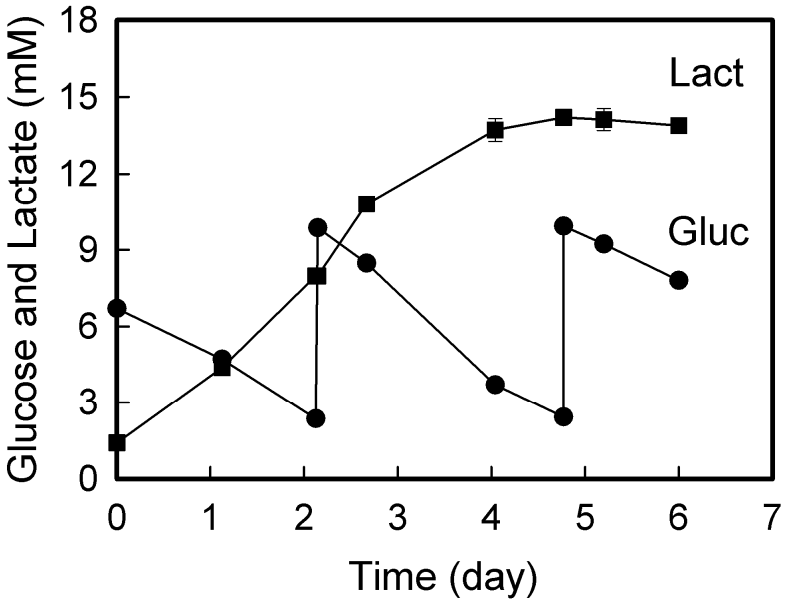

Figure 5.1 Time profiles of glucose and lactate concentrations in the medium (lactate, ■; glucose, ●). Standard deviations of glucose and lactate measurements were within 3.3% by duplicate flasks and each three times measurement.

5.3.2 Metabolic Model for Pentose Phosphate Pathway (PPP)

We constructed a detailed metabolic network model for ^{13}C-MFA to study oxidative PPP in CHO metabolism. In Figure 5.2, the model shows that all glucose consumed is converted to pyruvate by stoichiometric balance, i.e. assuming that other biosynthesis fluxes such as DNA/RNA, glycogen, amino acids and lipid production fluxes are negligible at non-growth condition. The metabolic model for PPP contains oxidative PPP (v9) and non-oxidative PPP with transketolase (TK) (v12-v14) and transaldolase (TA) reactions (v15, v16). Two pools of C_2 and C_3 fragments in TK and TA reactions were used for the model; TK-C_2 is glycolaldehyde moiety with two carbon atoms bound to TK, and TA-C_3 is dihydroxyacetone moiety with three carbon atoms bound to TA (Kleijn et al., 2005; van Winden et al., 2001).

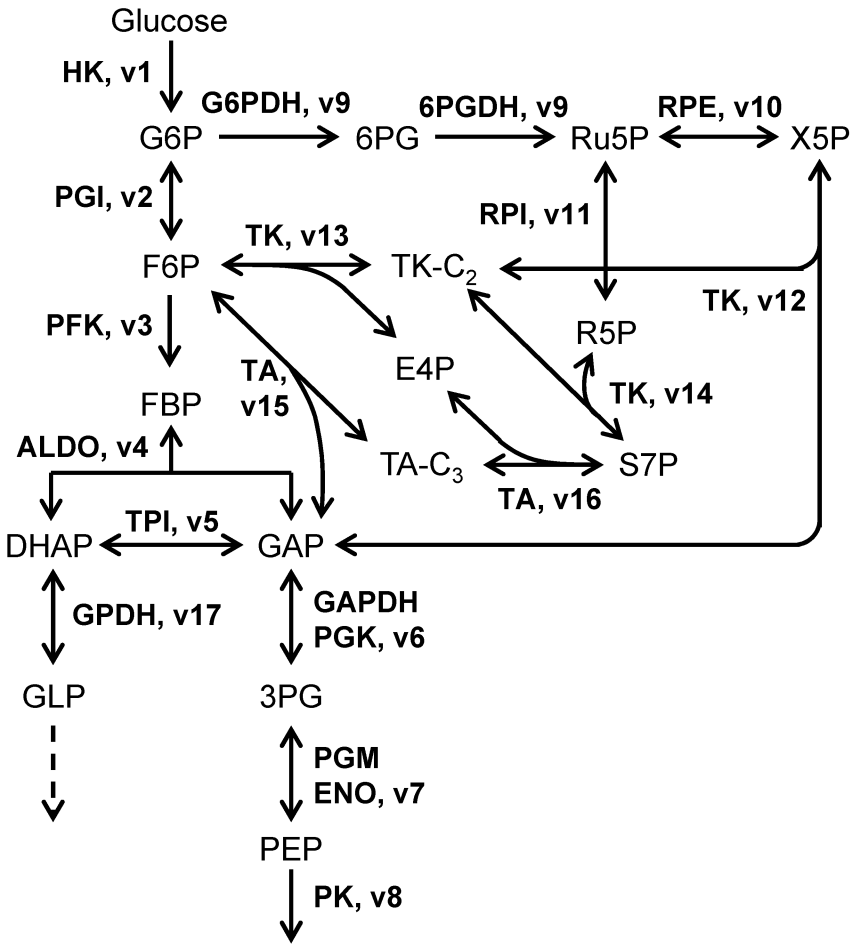

Figure 5.2 Metabolic network model for CHO PPP metabolism. The model consists of 17 reactions containing irreversible and reversible reactions. HK, hexokinase; PGI, phosphoglucose isomerase; PFK, phosphofructokinase-1; ALDO, aldolase; TPI, triose phosphate isomerase; GAPDH, glyceraldehyde 3-phosphate dehydrogenase; PGK, phosphoglycerate kinase; PGM, phosphoglycerate mutase; ENO, enolase; PK, pyruvate kinase; G6PDH, glucose 6-phosphate dehydrogenase; 6PGDH, 6-phosphogluconate dehydrogenase; RPI, ribose 5-phosphate isomerase; TK, transketolase; TA, transaldolase; GPDH, glycerol 3-phosphate dehydrogenase

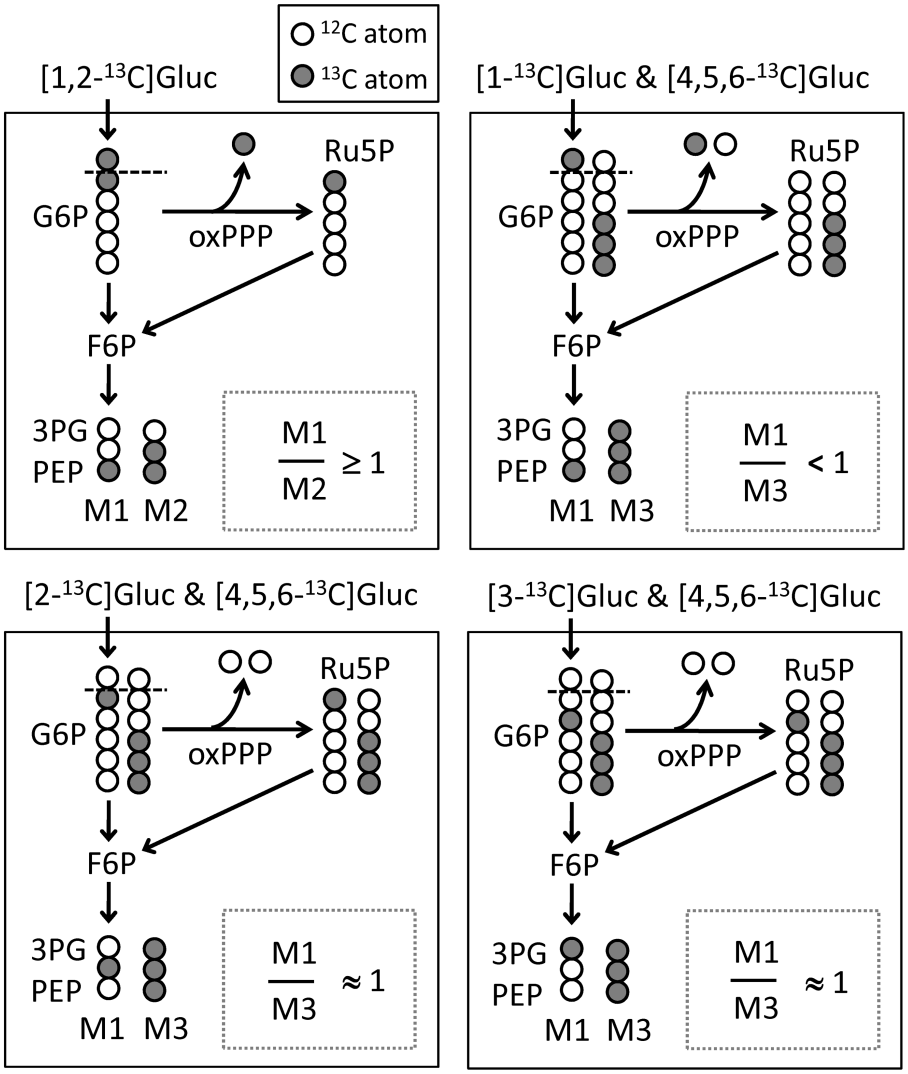

Figure 5.3 Schematic diagram of ^{13}C-atom transitions in oxidative pentose phosphate pathways. The carbon transitions were designed for [1,2-^{13}C]glucose, a mixture of [1-^{13}C]glucose and [4,5,6-^{13}C]glucose, a mixture of [2-^{13}C]glucose and [4,5,6-^{13}C]glucose, a mixture of [3-^{13}C]glucose and [4,5,6-^{13}C]glucose tracers. According to oxidative PPP activity, M1 to M2 ratio is more than 1 at [1,2-^{13}C]glucose tracer, M1 to M3 ratio is less than 1 at a mixture of [1-^{13}C]glucose and [4,5,6-^{13}C]glucose, and M1 to M3 ratio is equal to 1 at a mixture of [2-^{13}C]glucose (or [3-^{13}C]glucose) and [4,5,6-^{13}C]glucose.

5.3.3 Design of Isotopic Glucose Tracers for Oxidative PPP Metabolism

We selected isotopic glucose tracers to estimate oxidative PPP by ^{13}C-MFA. Based on the atom transitions in PPP, we used three glucose tracer sets; a mixture of [1-^{13}C]glucose+[4,5,6-^{13}C]glucose tracer ([1]+[4,5,6]Gluc) for oxidative PPP; and [2-^{13}C]glucose+[4,5,6-^{13}C]glucose tracer ([2]+[4,5,6]Gluc) and [3-^{13}C]glucose+[4,5,6-^{13}C]glucose tracer ([3]+[4,5,6]Gluc) to validate [1]+[4,5,6]Gluc tracer mixture. The results were compared with the traditional glucose tracer for oxidative PPP, [1,2-^{13}C]glucose ([1,2]Gluc). [1,2]Gluc tracer was widely used for flux estimation of PPP and glycolysis pathway (Ahn and Antoniewicz, 2011; Lee et al., 1998; Metallo et al., 2009) and selected as best tracer for the pathway (Metallo et al., 2009). The three tracer mixtures were designed considering four cleavage points in carbon atoms from glucose; first cleavage of carbon atoms from glucose is losing the first carbon atoms by CO_2 production in 6PGDH reaction (C1 and C2-C6) of oxidative PPP (v9). Second, F6P was cleaved between C1-C2 and C3-C6 carbon atoms by TK (v13) in non-oxidative PPP. Third, F6P was cleaved between C1-C3 and C4-C6 by TA (v15) in non-oxidative PPP. In addition, F6P is split to DHAP (C3-C1) and GAP (C4-C6) (v5). Finally, the measurable metabolites by GC-MS, 3PG and PEP are mixture from DHAP and GAP. The M1 mass isotopomer (i.e. one ^{13}C atom) in 3PG and PEP is derived from [1-^{13}C]glucose ([1]Gluc), [2-^{13}C]glucose ([2]Gluc) or [3-^{13}C]glucose ([3]Gluc), and M3 mass isotopomer from [4,5,6-^{13}C]glucose ([4,5,6]Gluc).

Figure 5.3 shows the schematic map of ^{13}C atom transitions in oxidative PPP using four different isotopic tracer sets. Based on the network model and atom transition (Figure 5.2 and Table 5.2), M1 or M3 mass isotopomers from [2]Gluc, [3]Gluc and [4,5,6]Gluc are conserved, but M1 mass isotopomer from [1]Gluc is not conserved due to CO_2 lost in oxidative PPP. Thus, to check metabolic activity of

oxidative PPP, M1 to M3 ratio of 3PG or PEP by addition of [1]+[4,5,6]Gluc tracer mixture (1:1 mol%) would be less than or equal to 100% according to oxidative PPP activity, while [2]+[4,5,6]Gluc tracer mixture (1:1 mol/mol) and [3]+[4,5,6]Gluc tracer (1:1 mol/mol) mixture would show 100% of M1 to M3 ratio in the mass isotopomer distribution (MID) of 3PG and PEP. In case of the tradition tracer, [1,2]Gluc, M1 isotopomers of 3PG or PEP by [1,2]Gluc can be generated by loss of carbons via oxidative PPP activity and the number of M2 isotopomers would decrease. Thus, the M1:M2 ratio would increase by increase of oxidative PPP activity as shown in Figure 5.3.

5.3.4 Loss of C_3 Carbon Atoms of Glucose in PPP

The selected tracers were added to CHO culture and analyzed by GC-MS to study MID of 3PG, PEP and GLP. Figure 5.4 shows that MIDs of extracellular glucose (Gluc.ext), intracellular 3PG, PEP and GLP for [1]+[4,5,6]Gluc, [2]+[4,5,6]Gluc and [3]+[4,5,6]Gluc tracer experiments. For glucose in medium, the percentage of ^{13}C-labeled isotopomers (100-M0%) of Gluc.ext for [1]+[4,5,6]Gluc, [2]+[4,5,6]Gluc and [3]+[4,5,6]Gluc tracer experiments was 74%, 74% and 76%, respectively. Fractional abundances (%) of M1 and M3 isotopomers were 36% and 37% for [1]+[4,5,6]Gluc, 37% and 36% for [2]+[4,5,6]Gluc and 39% and 36% for [3]+[4,5,6]Gluc tracer experiment. 75% of initial glucose tracer concentration (7.5 mM glucose tracers and 2.5 mM natural glucose on day 5) was well matched with the measured data of 100-M0% values at Gluc.ext and the 1:1 mol/mol of the glucose tracer mixtures were similar with the measured ratios of M1 and M3 isotopomer enrichments for the three tracer experiments. For intracellular metabolite of 3PG, the fractional abundances (%) of M1 and M3 isotopomers were 10% and 17% for

[1]+[4,5,6]Gluc, 13% and 16% for [2]+[4,5,6]Gluc and 12% and 17% for [3]+[4,5,6]Gluc tracer experiments. In PEP, fractional abundances (%) of M1 and M3 isotopomers were 8% and 16% for [1]+[4,5,6]Gluc, 11% and 15% for [2]+[4,5,6]Gluc and 10% and 12% for [3]+[4,5,6]Gluc tracer experiments. The MID data for these metabolites suggested two points: (1) M1 isotopomer abundance for [1]+[4,5,6]Gluc was less than [2]+[4,5,6]Gluc, or [3]+[4,5,6]Gluc tracer; and (2) M1 isotopomer abundance was less than M3 isotopomer for all tracer sets. GLP data also showed the same patterns, but the total labeling of ^{13}C isotopomers (100-M0%) was three times lower than for 3PG and PEP because GLP did not reach isotopic steady state (Ahn and Antoniewicz, 2011). In addition, it was shown that the small amount of labeling at M2 isotopomer was less than 2%. One possibility was that two M1 isotopomers were combined and produce M2 isotopomer by TK and TA reaction in non-oxidative PPP.

As shown in Figure 5.5, the ratio of (M1+M2×2)/M3 mass isotopomers was proposed to estimate the contribution of oxidative PPP activity and validate the pathway of metabolic model and carbon atom transition in oxidative PPP, by three mixtures of glucose tracers in Figure 5.2 and 5.3. Two times of M2 (= M2×2) in the ratio was considered to count the contribution of two M1 isotopomers building one M2 isotopomer. The ratio for external Gluc.ext was 98%, 105% and 108% for [1]+[4,5,6]Gluc, [2]+[4,5,6]Gluc and [3]+[4,5,6]Gluc tracer experiments, respectively. The values were close to the expected 100% value. For intracellular metabolites, the mass isotopomers ratio was 66%, 90% and 87% for 3PG, and the ratio for PEP was 58%, 84% and 84% for the same sequence of tracers. As shown in the results, the M1 abundances for [1]+[4,5,6]Gluc experiment was less than [2]+[4,5,6]Gluc, or [3]+[4,5,6]Gluc experiments. The difference between [1]+[4,5,6]Gluc and

[2]+[4,5,6]Gluc, or between [1]+[4,5,6]Gluc and [3]+[4,5,6]Gluc was 24% or 21% for 3PG, respectively; and 26% or 26% for PEP, respectively. GLP showed also 24% and 24% difference, respectively. This suggested carbon loss via oxidative PPP as explained previously. Interestingly, the (M1+M2×2)/M3 isotopomer ratio of [2]+[4,5,6]Gluc and [3]+[4,5,6]Gluc set did not reach 100%. Except loss of ^{13}C atoms via oxidative PPP for [1]Gluc tracer, labeled carbon atoms of the other tracers were expected to be conserved during the biological reactions from glucose to pyruvate through glycolysis and PP pathways. The difference of the ratios between Gluc.ext and [2]+[4,5,6]Gluc, or between Gluc.ext and [3]+[4,5,6]Gluc sets was 8% or 11% for 3PG, respectively; 21% or 21% for PEP, respectively; and 48% or 48% for GLP, respectively. Thus, the differences showed that TA-C_3 fragments were lost in PPP because the lost carbon atoms were related to [1]Gluc, [2]Gluc and [3]Gluc. Therefore, the result suggested that the commonly used PPP model in Figure 5.2 and 5.3 cannot explain the additional carbon loss in PPP, except oxidative PPP activity.

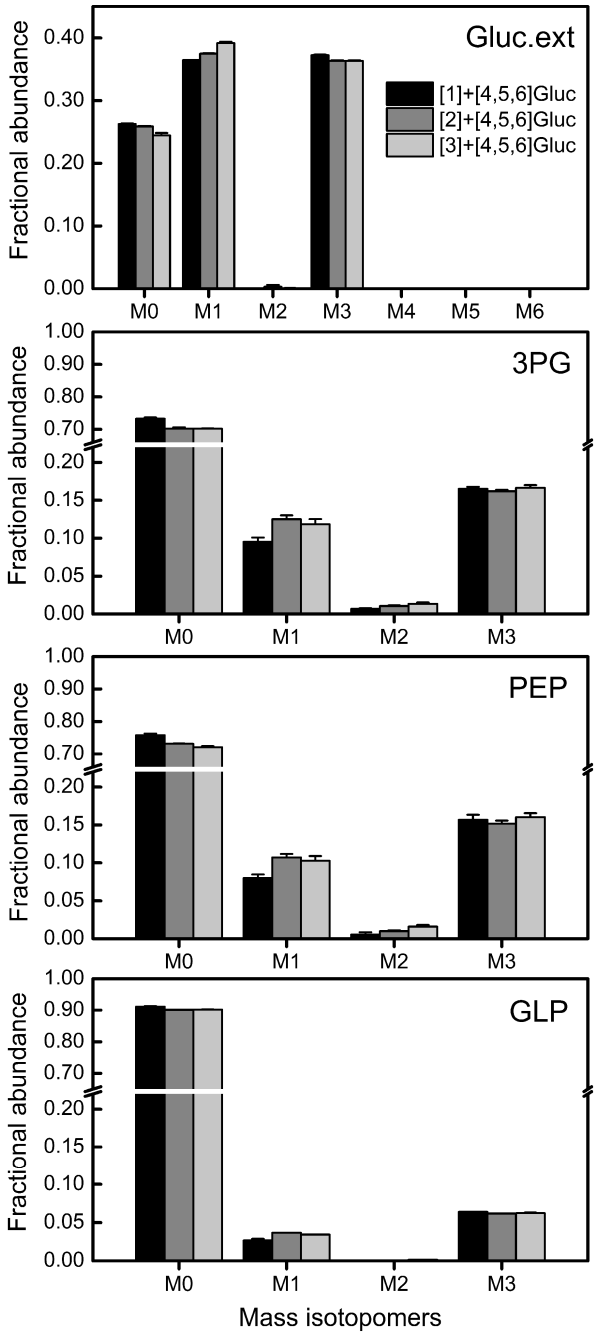

Figure 5.4 Fractional abundances of labeled mass isotopomers at 9 h after the addition of [1-^{13}C]glucose + [4,5,6-^{13}C]glucose tracer ([1]+[4,5,6]Gluc), [2-^{13}C]glucose + [4,5,6-^{13}C]glucose tracer ([2]+[4,5,6]Gluc) and [3-^{13}C]glucose + [4,5,6-^{13}C]glucose tracer mixture ([3]+[4,5,6]Gluc) on day 5. Extracellular glucose and three intracellular metabolites; glucose (*m/z* 301), 3PG (*m/z* 585), PEP (*m/z* 453), and GLP (*m/z* 571).

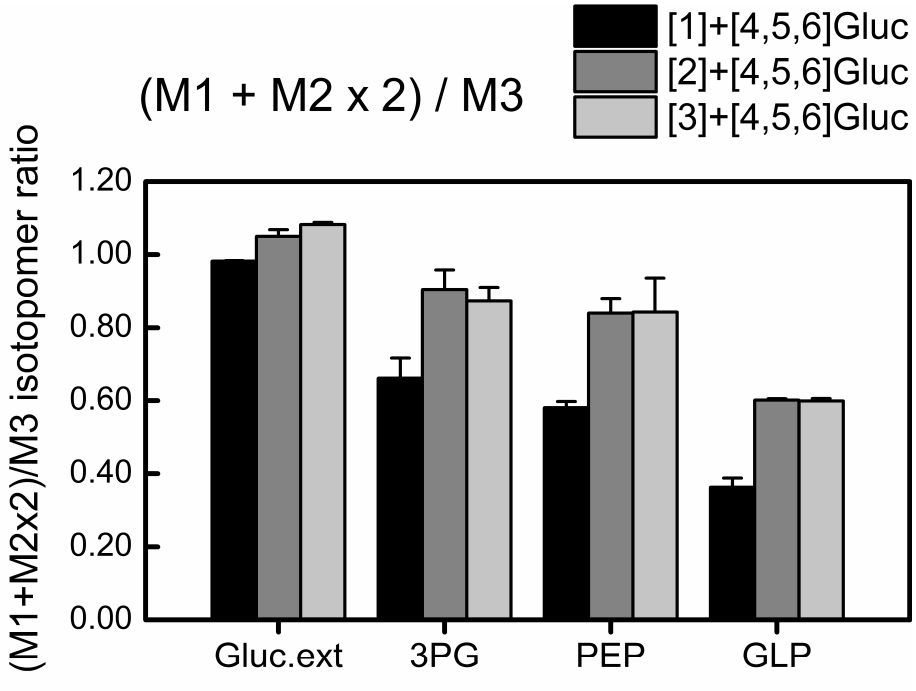

Figure 5.5 The ratio, (M1+M2×2)/M3 of mass isotopomers of extracellular glucose (Gluc.ext), intracellular 3PG, PEP and GLP metabolites at 9 h samples after addition of three different mixture tracers on day 5. The ratios were calculated from the data of Figure 5.4. Extracellular glucose and three intracellular metabolites; glucose (*m/z* 301), 3PG (*m/z* 585), PEP (*m/z* 453), and GLP (*m/z* 571).

5.3.5 Validation of (M1+M2×2)/M3 Isotopomer Ratio to Estimate Oxidative PPP

The TA-C_3 fragments can only come from C1-C3 atoms of six carbon metabolites, F6P, G6P or media glucose (Gluc.ext) based on the suggested metabolic model (Figure 5.2). In the previous section, we suggested loss of TA-C_3 fragments using the ratios, (M1+M2×2)/M3 of mass isotopomers from MID data for 3PG and PEP. However, two assumptions should be validated; first, one ^{13}C-atom in C1-C3 fragment cannot be converted to three ^{13}C-atoms in C1-C3 fragments by atom transition via non-oxidative PPP. Figure 5.6 shows fractional abundances of MID at 9 h after the addition of [1]Gluc on day 5 for extracellular glucose, 3PG, PEP and GLP. The MID of Gluc.ext (*m/z* 370) indicated 78% composition of [1]Gluc from the ratio of M1 isotopomer. Furthermore, the M1 isotopomer ratios of 3PG (*m/z* 585), PEP (*m/z* 453), and GLP (*m/z* 571) were 21%, 18% and 7%, respectively. The M2 ratios of the three fragments were less than 1.3%, and M3 ratios were almost zero. Therefore, there is no possibility for conversion of M1 to M3 by atom transitions via reversible reactions in non-oxidative PPP. This suggests that the atom transition from one ^{13}C atom to three ^{13}C atoms in C1-C3 fragment was not significant. Second, three ^{13}C atoms in C4-C6 fragment of six carbon metabolites should not be changed to one or two ^{13}C atoms in C4-C6 fragment. This can be ascertained using MIDs of 3PG, PEP and GLP labeled by [4,5,6]Gluc tracer. Figure 5.7 shows fractional abundances of MID at 9 h after the addition of [4,5,6]Gluc on day 5 for Gluc.ext, 3PG, PEP and GLP. The M2 isotopomer ratio of Gluc.ext fragment at *m/z* 370 indicated 78% composition of [4,5,6]Gluc in media. The M3 isotopomer ratios of 3PG (*m/z* 585), PEP (*m/z* 453), and GLP (*m/z* 571) were 34%, 30% and 15%, respectively. In addition, there were no

significant values of M1 and M2 mass isotopomers. Thus, the M3 isotopomer from C4-C6 fragments of F6P was not converted to M1 or M2 isotopomers.

Therefore, the rearrangement from one ^{13}C atom to three ^{13}C atoms in C1-C3 fragment of F6P was not significant by atom transition and there was no atom transition from three ^{13}C atoms to one or two ^{13}C atoms in C4-C6 fragment of F6P. Thus, the ratio (M1+M2×2)/M3 indicated that the numerator term only represents C1-C3 fragment from six carbon metabolite (F6P, G6P or Gluc.ext) and the denominator term, M3, was only related to C4-C6 fragment. In other words, M3 isotopomer cannot be built by M1 in the numerator, and M3 isotopomer can only come from C4-C6.

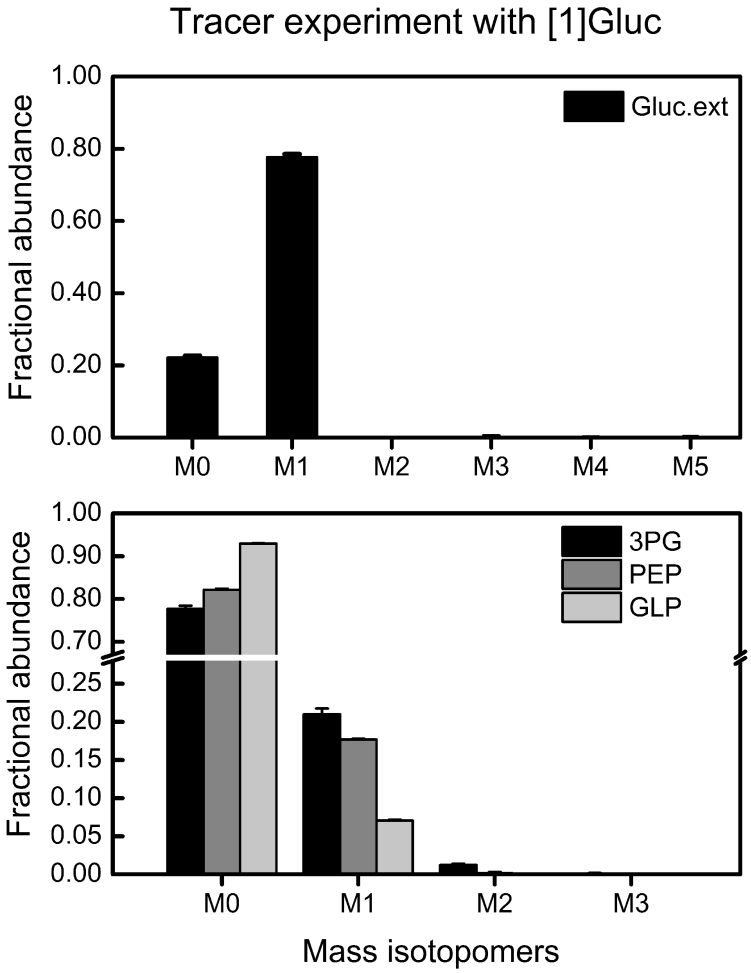

Figure 5.6 Fractional abundances of labeled mass isotopomers at 9 h after the addition of [1-^{13}C]glucose ([1]Gluc) on day 5. The MIDs were analyzed for extracellular glucose (Gluc.ext) and three representative metabolites in the PPP cycle: glucose (*m/z* 370), 3PG (*m/z* 585), PEP (*m/z* 453), and GLP (*m/z* 571). MID of glucose fragments (Gluc.ext) at *m/z* 370 fragments contains carbon atoms of C1-C5 glucose. MIDs of 3PG, PEP and GLP fragments contain three carbon atoms of C1-C3.

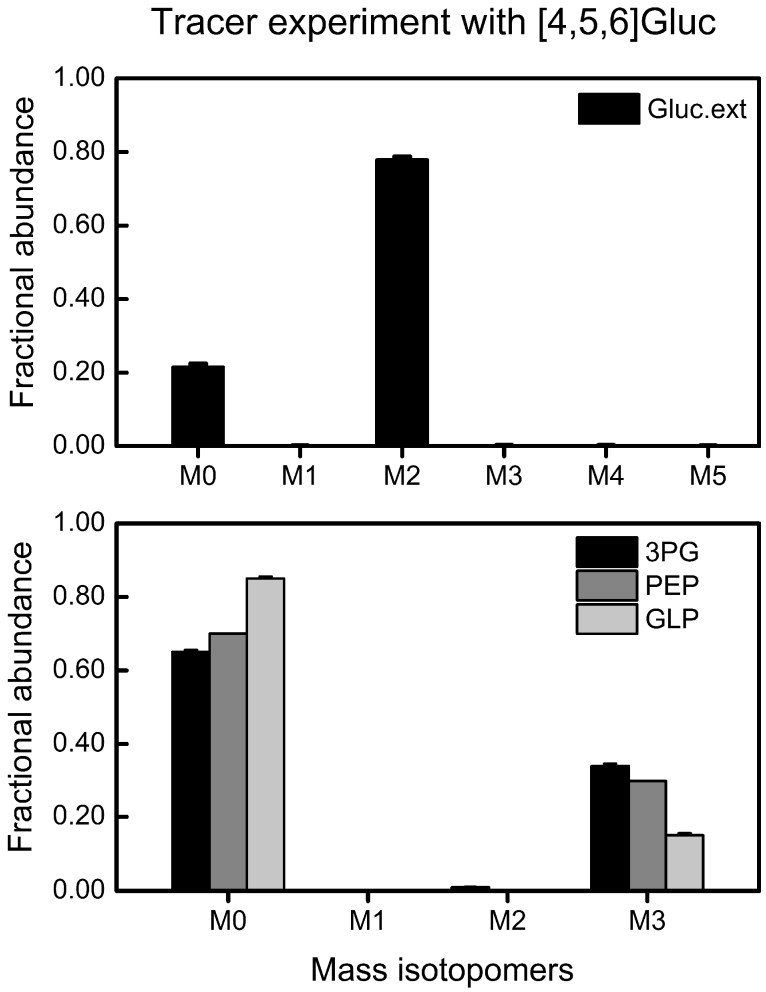

Figure 5.7 Fractional abundances of labeled mass isotopomers at 9 h after the addition of [4,5,6-^{13}C]glucose ([4,5,6]Gluc) on day 5. The MIDs were analyzed for extracellular glucose (Gluc.ext) and three representative metabolites in the PPP cycl*e:* glucose (*m/z 37*0), 3PG (*m/z 585*), PEP (*m/z* 453*),* and GLP (*m/z* 571). MID of glucose fragments (G*luc*.ext) at *m/z* 370 fragments contains carbon atoms of C1-C5 glucose. Thus, C4 and C5 atoms labeled by ^{13}C-atoms from [4,5,6]Gluc shifted mass ions from M0 to M2 of glucose fragments at *m/z* 370. MIDs of 3PG, PEP and GLP fragments contain three carbon atoms of C1-C3.

5.3.6 Metabolic Activity of Oxidative PPP with [1,2-^{13}C]Glucose Tracer

The [1,2]Gluc tracer is a general tracer used to evaluate PPP (Ahn and Antoniewicz, 2011) and was selected as the best tracer for ^{13}C-MFA (Metallo et al., 2009; Walther et al., 2012). Therefore, we compared MIDs and flux results with [1,2]Gluc and the glucose mixture tracers. Figure 5.8 shows the fractional abundance of Gluc.ext and intracellular metabolites, 3PG, PEP and GLP. The composition of [1,2]Gluc was 74% (i.e. fraction of M2 isotopomer) in medium and the other, 26% is natural glucose (i.e. fraction of M0 isotopomer). In Figure 5.8, there is no M1 isotopomer in the MID of extracellular glucose (Gluc.ext). However, in case of intracellular metabolites, M1 isotopomer abundances for 3PG, PEP and GLP were 4%, 4% and 1%, respectively and M2 isotopomer abundances were 20%, 18% and 6%, respectively. In addition, M3 isotopomers were less than 1%, which could be produced by TK and TA reversible reactions. As M1 can be produced from M2 isotopomer by oxidative PPP activity (i.e. loss of $^{13}CO_2$), the M1:M2 ratio corresponds roughly to oxidative PPP activity (Figure 5.3). The M1:M2 ratio for 3PG, PEP and GLP was 21%, 22% and 14%, respectively as shown in Figure 5.6. The M1:M2 ratios for 3PG and PEP from [1,2]Gluc was close to the difference of (M1+M2×2)/M3 values (21% ~ 26%) between [1]+[4,5,6]Gluc and [2]+[4,5,6]Gluc, or between [1]+[4,5,6]Gluc and [3]+[4,5,6]Gluc set. This provides evidence for oxidative PPP activity from two kinds of tracer sets. Interestingly, M1:M2 ratio of GLP had a lower value (14%) than 3PG (21%) and PEP (22%). Based on the metabolic model (Figure 5.2), the ratios should be similar for 3PG, PEP and GLP. Thus, this indicated that GLP metabolites might be used by additional pathway such as micro-channeling by enzyme clusters.

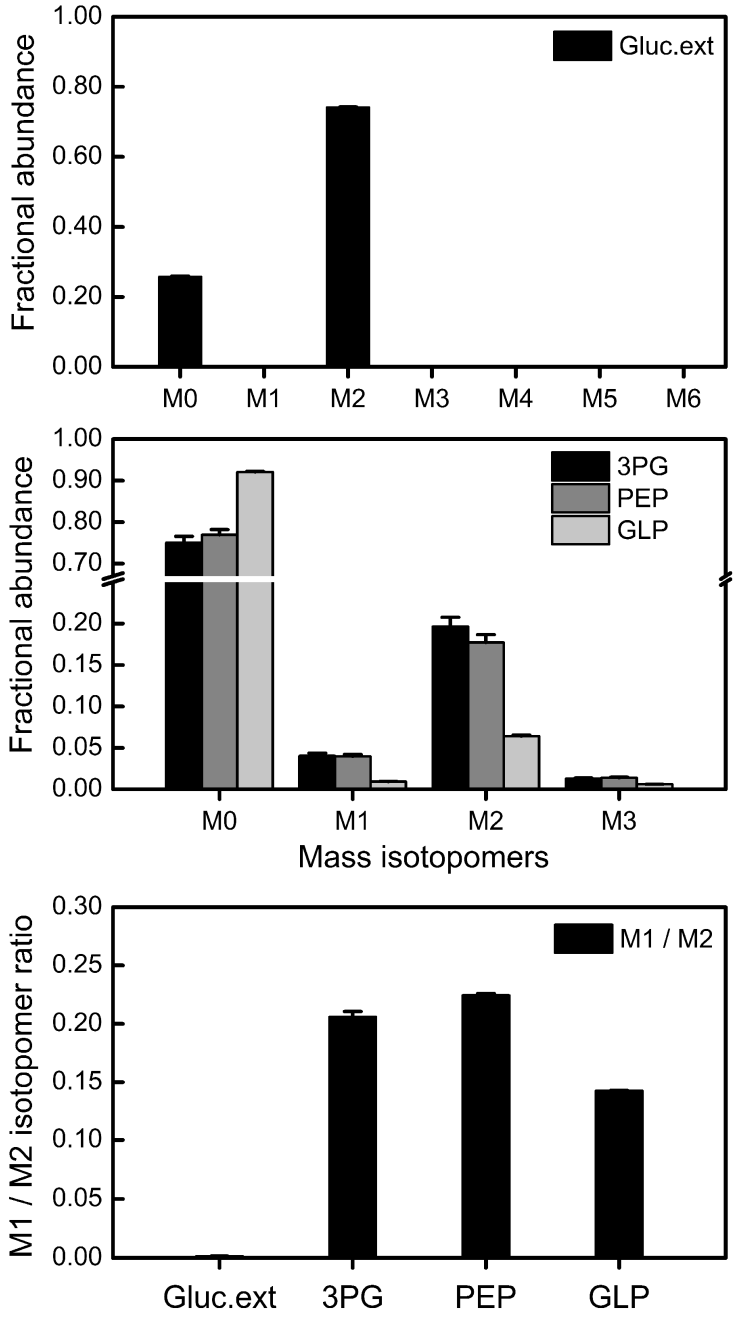

Figure 5.8 Fractional abundances and M1 to M2 ratios of labeled mass isotopomers at 9 h after the addition of [1,2-^{13}C]glucose ([1,2]Gluc). The MIDs were analyzed for extracellular glucose (Gluc.ext) and three representative metabolites in the PPP cycle: glucose (*m/z* 301), 3PG (*m/z* 585), PEP (*m/z* 453), and GLP (*m/z* 571).

5.3.7 Additional Measurements of PPP Metabolites by Dephosphorylation

GC-MS analysis with EI source and quadrupole mass analyzer can measure small volatile metabolites up to *m/z* 600 for MID analysis. Therefore, most of PPP metabolites with C_4, C_5 and C_6 atoms cannot be measured since they have a lot of hydroxyl and carboxyl groups and eventually the derivatized molecular weights are higher than *m/z* 600 after derivatization. Thus, we evaluated new possibilities for analyzing MIDs of PPP metabolites using GC-MS. Recently, White introduced dephosphorylation steps of PPP metabolites with *E.coli* alkaline phosphatase to study *Methanocaldococcus jannaschii* metabolism (White, 2004). Based on this method, we introduced dephosphorylation steps for G6P, F6P and ribose-5-phosphate (R5P) and obtained MS fragments less than *m/z* 600 after conversion to glucose, fructose and ribose and using four different derivatization methods.

Figure 5.9A shows two F6P fragments at *m/z* 307 and *m/z* 364 derived by dephosphorylation of F6P with *E.coli* alkaline phosphatase and methyloxime trimethylsilyl (MOX-TMS) derivatization of the resulting fructose. These fragments were measured by GC-MS for MID analysis and used as additional inputs for ^{13}C-MFA. This is the first time that the two fragments were applied for MID analysis and for ^{13}C-MFA to quantify intracellular fluxes. Especially, the important thing for flux analysis is that the two fragments at *m/z* 307 and *m/z* 364 from F6P contain information on the reversibility of TK and TA in non-oxidative PPP, that have been very challenging to estimate. In this study, we solved this challenge as described in this section using new MS fragments.

We expanded this idea to other metabolites, glucose and ribose and different derivatization methods to acquire more information for flux analysis of PPP in the future, as shown in Table 5.3. The aldehyde and ketone groups of metabolites were

derivatized by 1st reactions by methyloxime, isopropylidene, oxime (or aldonitrile) and methyloxime and the hydroxyl and carboxylic groups were derivatized 2nd reactions by trimethylsilane and propionate. The MS fragments in bold type were acceptable after testing for natural abundances. The accepted MS fragments were cross-checked with the references in MacLeod et. al. and Antoniewicz et. al.'s studies (Antoniewicz et al., 2011; MacLeod et al., 2001). Finally, in Figure 5.9B, we suggested possible MS fragments of fructose, glucose and ribose using four derivatization methods; MOX-TMS, isopropylidene propionate, oxime propionate, methyloxime propionate for MID analysis and ^{13}C-MFA. In future work, these fragments should be validated more rigorously.

Table 5.3 Mass fragments of glucose, fructose and ribose after derivatization by two step reactions for GC-MS analysis

	Mass fragments (*m/z*)			
1st reaction 2nd reaction	Methyloxime Trimethylsilane	Isopropylidene Propionate	Oxime/aldonitrile Propionate	Methyloxime Propionate
Glucose	**103**,117,147,160, 205,217,229,262, **319**,344,364,376, 466,554	101,113,127,141, 157,167,183,199, 215,243,**301**	117,131,155,**173**, 187,215,240,**259**, **284**,314,328,345, **370**,384	112,129,**145**,155, 173,201,215,229, 254,328,345,**387**, 402,416,489
Fructose	**103**,117,147,189, 205,**217**,262,277, **307**,**364**,376,466, 554,**569**	100,109,126,143, 169,183,200,215, 225,243,258,**301**	99,123,141,156, 172,184,197,215, 228,241,254,271, 298,328,401	101,129,155,211, 229,254,259,295, 328,342,384,**387**, 402,416
Ribose	**103**,117,147,160, 189,205,**217**,233, 262,277,**307**,362, 364,452,**467**	97,115,139,153, 171,187,199,215, 229,245,**287**	99,117,129,143, 155,**173**,187,194, 203,**259**,**284**,298	97,112,129,**145**, 168,186,199,242, 259,273,**301**,330, 403

Mass fragments in bold type represent good agreements with natural abundances of theoretical values. Aldonitrile derivatization for aldehyde group of glucose and oxime derivatization for ketone group of fructose and ribose.

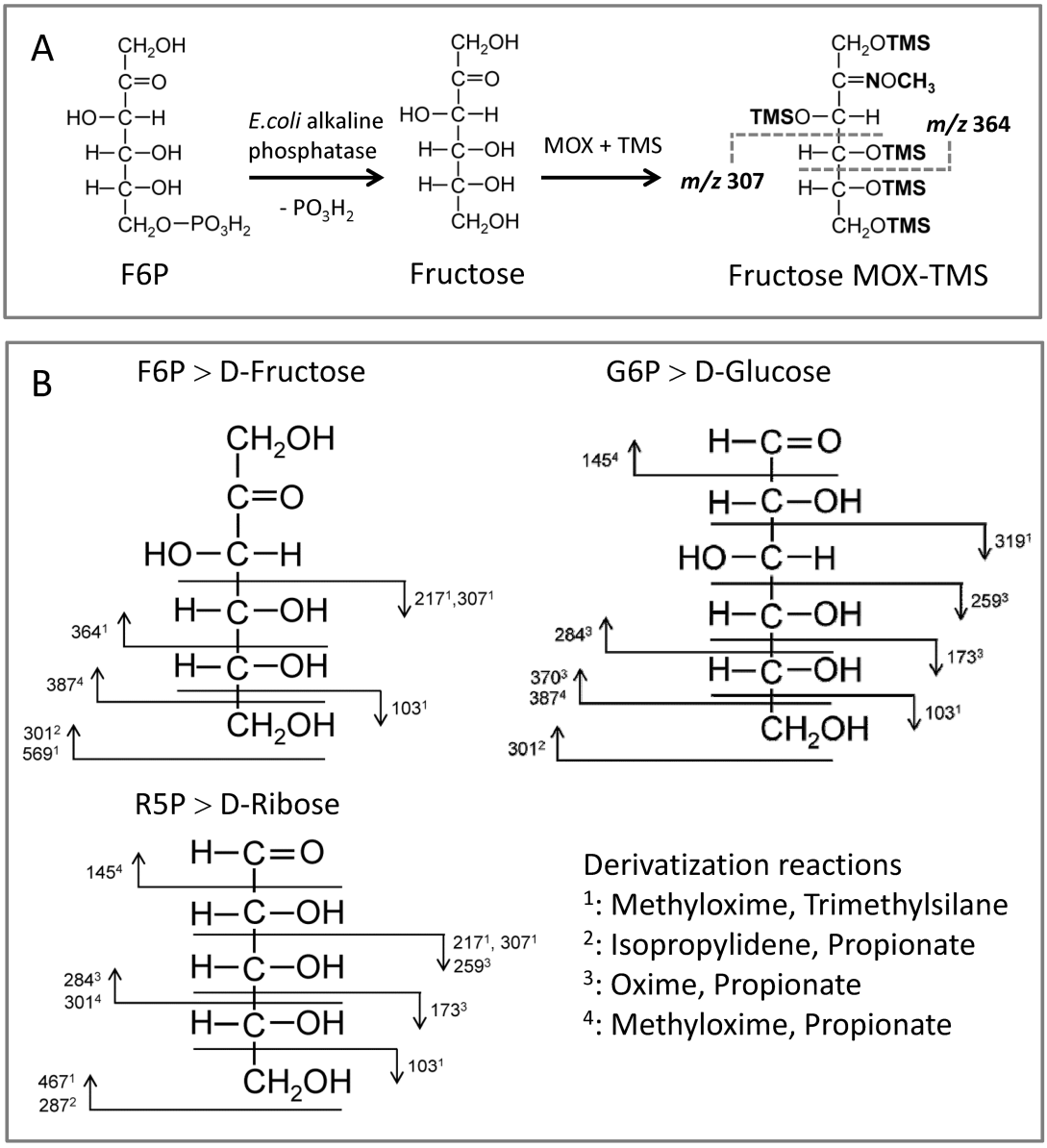

Figure 5.9 (A) Two F6P fragments at *m/z* 307 and *m/z* 364 derived by dephosphorylation of F6P with *E.coli* alkaline phosphatase and methyloxime trimethylsilyl (MOX-TMS) derivatization of fructose. (B) Screening mass fragments of fructose, glucose and ribose using four derivatization methods; MOX-TMS, isopropylidene propionate, oxime propionate, methyloxime propionate.

5.3.8 Flux Estimation of Oxidative PPP

To estimate oxidative PPP flux, we constructed a detailed metabolic network model (Figure 5.2 and Table 5.2). For ^{13}C-MFA, we fitted the MIDs of DHAP (*m/z* 484), 3PG (*m/z* 585) and PEP (*m/z* 453) at 9 h after addition of tracers on day 5, together with glucose uptake rate (76.4 nmol/10^6cells/h). In addition to this basic data set, we measured two fragments of F6P, *m/z* 364, C1-C4; *m/z* 307, C4-C6. Using four data sets from [1,2]Gluc, [1]+[4,5,6]Gluc, [2]+[4,5,6]Gluc and [3]+[4,5,6]Gluc tracer experiments, we obtained statistically acceptable fits with minimized variance-weighted sum of squared residuals (SSR) values and the expected lower and upper bounds for the 95% confidence region of SSR assuming the minimized SSR followed a χ^2-distribution. The complete flux results including 95% confidence intervals for all estimated fluxes, are given in Appendix C (see Tables C.1-C.15).

We performed three kinds of ^{13}C-MFA analyses with two different models and two sets of measurements: (i) the original model (Figure 2) with the basic data; (ii) the extended model with the basic data; and (iii) the extended model with the basic data and additional F6P data. The extended model contained one additional flux compared to the original model, which was an output flux of TA-C_3 in non-oxidative PPP (Table 5.2). In Figure 5.10, ^{13}C-MFA was performed with the three conditions and four data sets. For the original PPP model, the fitted values of oxidative PPP fluxes were 17.5 (lower bound, upper bound of 95% confidence interval; 10, 38.6) nmol/10^6cells/mL at [1,2]Gluc set, 32.3 (29.2, 56.0) nmol/10^6cells/h at [1]+[4,5,6]Gluc, 62.1 (47.8, 73.3) nmol/10^6cells/h at [2]+[4,5,6]Gluc and 67.5 (45.2, 83.4) nmol/10^6cells/h at [3]+[4,5,6]Gluc set. Furthermore, we fitted four data sets by combined analysis of ^{13}C-MFA with the original model simultaneously. However, the total SSR value was not accepted within 95% confidence region of SSR. This suggested that the four data were

not consistent for flux analysis using the original model. Furthermore, as shown in Figure 5.10 (original PPP model), the solution space of oxidative PPP using the original PPP model were not fully overlapping for [1,2]Gluc, [1]+[4,5,6]Gluc and [2]+[4,5,6]Gluc or [3]+[4,5,6]Gluc. Theoretically, the confidence intervals would be overlapping regardless of different tracer sets based on the usage of the same metabolic model.

As shown in Figure 5.5, the (M1+M2×2)/M3 isotopomer ratio, loss of TA-C_3 molecules was not accounted for in the original model. Thus, it was considered the extended model containing output flux of TA-C_3 (TA-C_3 $\rightarrow$ TA-C_3.ext) to the original model. The flux analysis results are shown in Figure 5.7 ("the extended PPP model"). The fitted values of oxidative PPP fluxes were 15.1 (10, 52.3) nmol/10^6cells/h at [1,2]Gluc set, 43.7 (0, 56.7) nmol/10^6cells/h at [1]+[4,5,6]Gluc, 0 (0, 49.8) nmol/10^6cells/h at [2]+[4,5,6]Gluc, 0 (0, 47.6) nmol/10^6cells/h at [3]+[4,5,6]Gluc set and 17.2 (15.3, 26.0) nmol/10^6cells/h at the combined analysis. In this case, most of the solution spaces for the four ^{13}C-MFAs were overlapping. Interestingly, the combined analysis with the extended PPP model achieved narrow confidence interval and was accepted statistically.

Even if the confidence intervals were overlapping for the extended PPP model, the solution spaces were very wide, except for the combined analysis. Normally, this results from low sensitivity of measurement data. Thus, we introduced new data, two fragments of F6P to the extended model and the basic data, and repeated flux analysis. The fitted values of oxidative PPP fluxes were 18.4 (9.6, 48.4) nmol/10^6cells/h at [1,2]Gluc set, 19.5 (9.0, 39.8) nmol/10^6cells/h at [1]+[4,5,6]Gluc, 14.1 (0, 58.4) nmol/10^6cells/h at [2]+[4,5,6]Gluc, 6.9 (0, 21.0) nmol/10^6cells/h at [3]+[4,5,6]Gluc set

and 21.1 (15.0, 33.4) nmol/10^6cells/h at the combined analysis. By introduction of F6P measurements, the confidence interval of [1]+[4,5,6]Gluc set was narrowed. Furthermore, other flux observability for TK and TA was greatly improved for most data sets (Appendix C). Interestingly, [1,2]Gluc set gave consistent solution space regardless of model change and additional data.

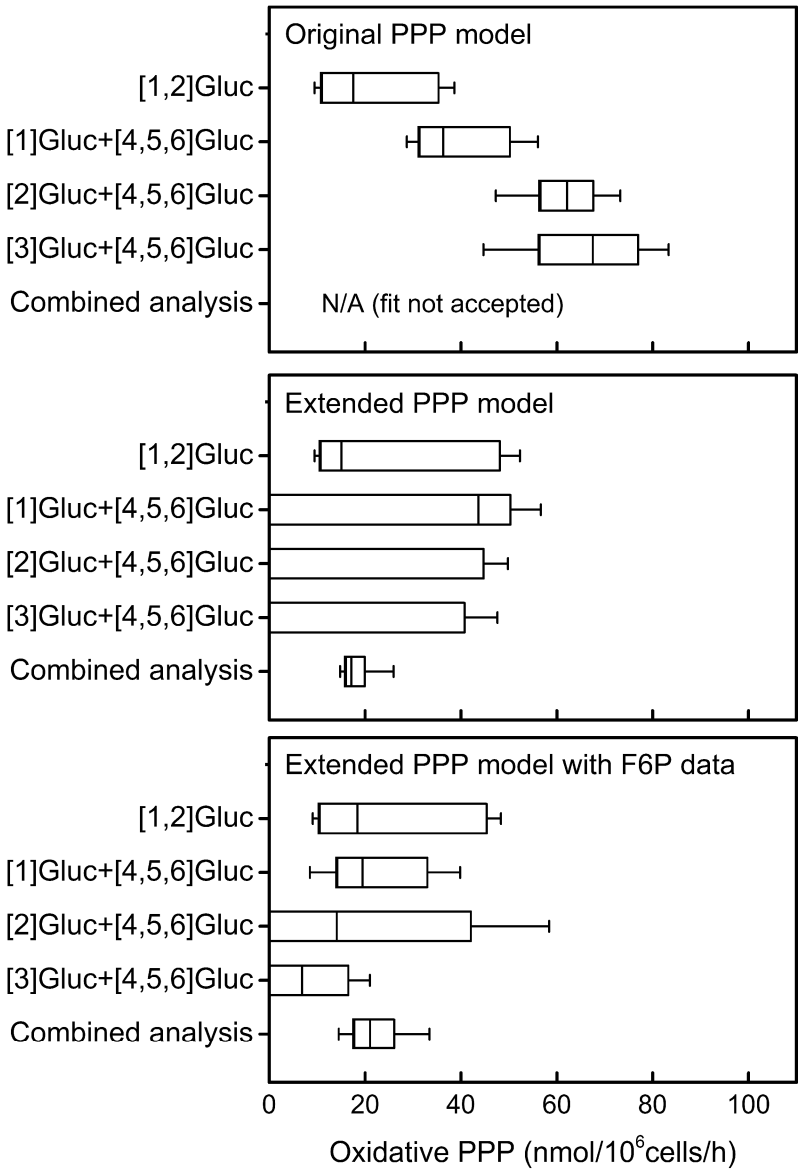

Figure 5.10 Estimated values of oxidative PPP flux (v9) using three ^{13}C-MFA. (A) The original PPP model (Figure 5.2) with the basic data (B) the extended PPP model and with the basic data and F6P data, and (C) the extended PPP model with F6P data. The basic data was DHAP (*m/z* 484), 3PG (*m/z* 585) and PEP (*m/z* 453). Two F6P fragments were *m/z* 307 and *m/z* 364. The extended model contains output flux of TA-C_3 to the original model. In box plot, whisker showed lower and upper bound of 95% confidence interval, inner box showed lower and upper bound of 68% confidence interval and media was used with best fit values.

5.3.9 Two Fragments of F6P related to TA and TK Reversibility

The intracellular metabolite F6P is at a key junction in glycolysis and non-oxidative PP pathway. Thus, appropriate measurement of F6P fragments by GC-MS enables ^{13}C-MFA to achieve good flux observability of the two pathways. Especially, reversibility of non-oxidative PPP is challenging to estimate. Net fluxes of non-oxidative PPP can be determined by oxidative PPP flux, which one end-point of non-oxidative PPP was linked with oxidative PPP at Ru5P metabolite pool and the other with glycolysis pathway at F6P metabolite pool. However, it is challenging to estimate exchange fluxes of transaldolase (TA) and transketolase (TK) reactions in non-oxidative PPP due to limitation of measurements related to PPP metabolites. Here, we proposed a method to measure two new fragments of F6P using dephosphorylation of F6P by *E.coli* alkaline phosphatase as shown in materials and methods section. By conversion of F6P to fructose *in vitro*, two fragments, at *m/z* 307 and *m/z* 364, were measured by MOX-TMS derivatization and GC-MS analysis. The F6P fragment at *m/z* 307 contains C4-C6 carbon atoms of F6P, and F6P fragment at *m/z* 364 contains C1-C4 carbon atoms of F6P as shown in Figure 5.11. In Figure 5.11A, without TA and TK reactions, only M0 and M3 at F6P fragment (*m/z* 307) can be measured by GC-MS and M0 and M1 at F6P fragment (*m/z* 364) can be analyzed. However, the measured data in Figure 5.12 show the additional isotopomers (M1 peak at F6P fragment, *m/z* 307 and M2 peak at F6P fragment, *m/z* 364) due to atom transitions of TA and TK.

First, TA reversibility resulted in M1 isotopomer peak in MID of F6P at *m/z* 307. In Figure 5.12, M1 isotopomer ratios of F6P fragment at *m/z* 307 were 3%, 4% and 4% by addition of [1]+[4,5,6]Gluc, [2]+[4,5,6]Gluc and [3]+[4,5,6]Gluc tracers, respectively. As explained in Figure 5.11B, one ^{13}C-atom from C1-C3 position of F6P from [1]Gluc (the same case with [2]Gluc or [3]Gluc) was transferred to GAP via

triose phosphate isomerase (TPI) and incorporated into C4-C6 fragment of F6P via transaldolase (TA). Thus, M1 peak at F6P fragment *m/z* 307 can provide information on the TA reversibility (or forward and backward fluxes).

Second, TK reversibility resulted in M2 isotopomer peak in MID of F6P at *m/z* 364. In Figure 5.12, M2 isotopomer ratios of F6P fragment at *m/z* 364 were 2%, 4% and 5% by addition of [1]+[4,5,6]Gluc, [2]+[4,5,6]Gluc and [3]+[4,5,6]Gluc tracers, respectively. Other peaks, M3 and M4 ratios, were less than 1.0% and the levels of M3 and M4 isotopomers were close to baseline level. However, M2 isotopomer ratios were significant, i.e. higher than 2%. As explained in Figure 5.11C, two carbon atoms at C1-C2 position of F6P was continuously exchanged with the two carbon units of TK-C_2 pool via the reversibility of TK. Thus, M2 isotopomer was shown in MID of F6P fragment at *m/z* 364 and the levels of M2 ratio were dependent on TK reversibility.

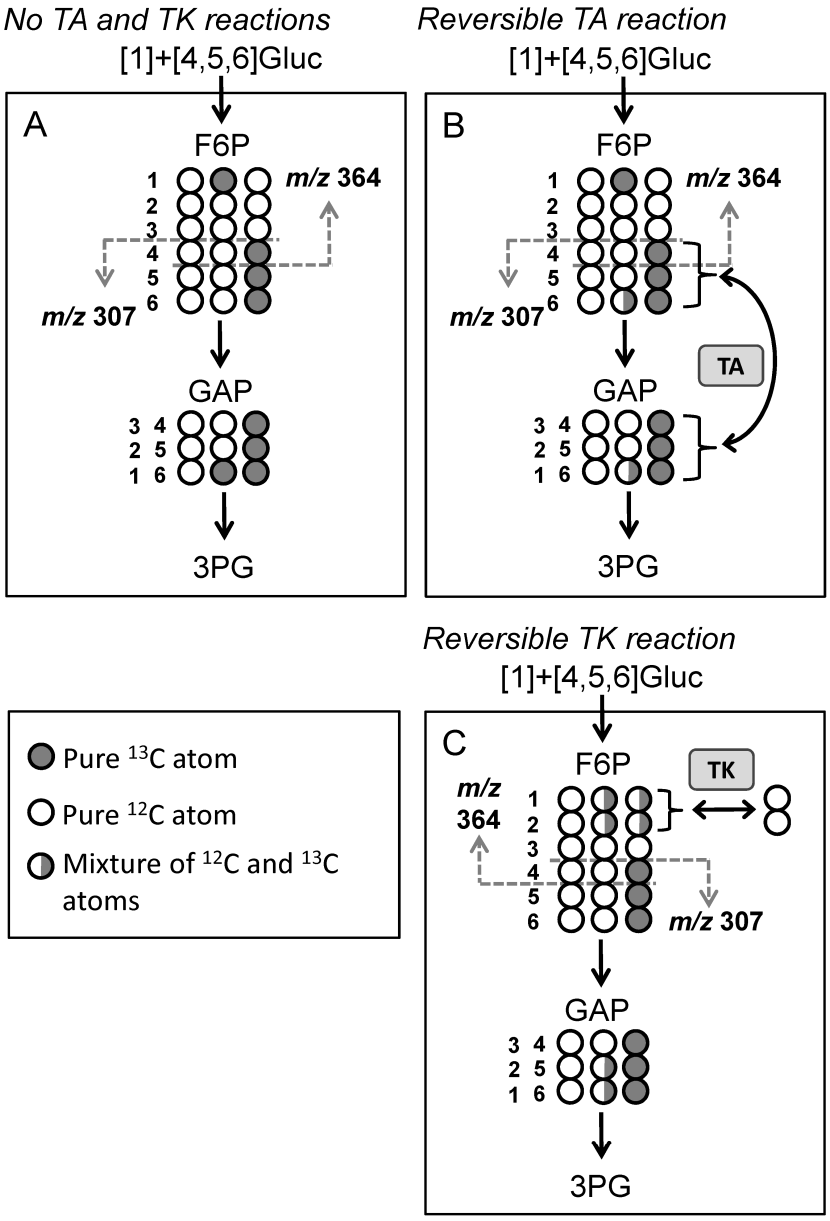

Figure 5.11 Schematic diagram of atom transitions related to transaldolase (TA) and transketolase (TK) in non-oxidative PPP for [1]+[4,5,6]Gluc tracer. (A) Glycolysis pathway without link with TA and TK reactions. (B) Glycolysis pathway with TA reaction. (C) Glycolysis pathway with TK reaction. Two MIDs of F6P fragments at *m/z* 364 (C1-C4) and *m/z* 307 (C4-C6) contain information on the reversibility of TA and TK reactions in which TA exchange carbon atoms of F6P (C4-C6) and GAP (C1-C3), and TK exchange carbon atoms of F6P (C1-C2) and TK-C_2 (C1-C2).

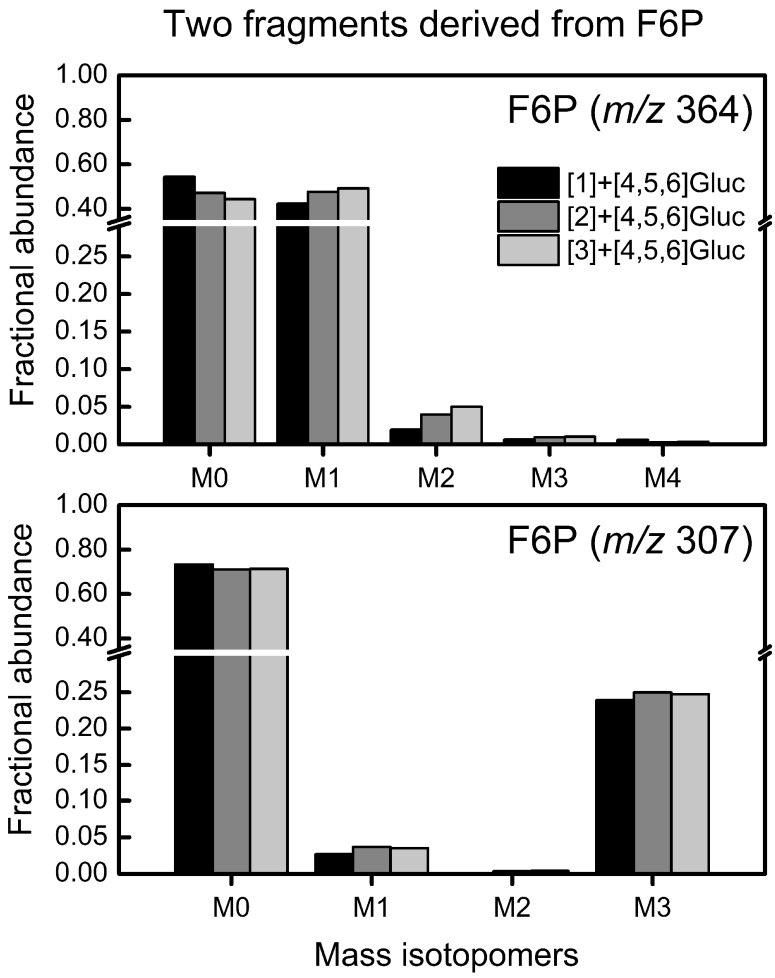

Figure 5.12 Fractional abundances of labeled mass isotopomers at 9 h after the addition of three mixture tracers. The tracers, [1]+[4,5,6]Gluc, [2]+[4,5,6]Gluc and [3]+[4,5,6]Gluc tracers were applied on day 5 and the two fragments of F6P at *m/z* 364 and *m/z* 307 were analyzed by GC-MS.

5.3.10 Flux Estimation of Non-oxidative PPP

In section 5.3.7, oxidative-PPP activity was estimated by ^{13}C-MFA for three different cases; original PPP model, extended model, and extended model with F6P data. At the estimation, the exchange fluxes of TA (v15) and TK (v13) related to non-oxidative PPP were shown in Figure 5.13. Without F6P data, all TA and TK exchange fluxes with [1,2]Gluc, [1]+[4,5,6]Gluc, [2]+[4,5,6]Gluc and [3]+[4,5,6]Gluc were non-observable. In contrast, the extended model containing two MID data of F6P fragments show good flux observability for most of the tracer experiments, except TK exchange flux with [3]+[4,5,6]Gluc tracer. Furthermore, the solution spaces were overlapping. In particular, combined analysis gave narrow confidence intervals. As a result, the two fragments of F6P at *m/z* 307 and *m/z* 364 can guide flux estimation to acquire TA and TK exchange fluxes in the non-oxidative PPP.

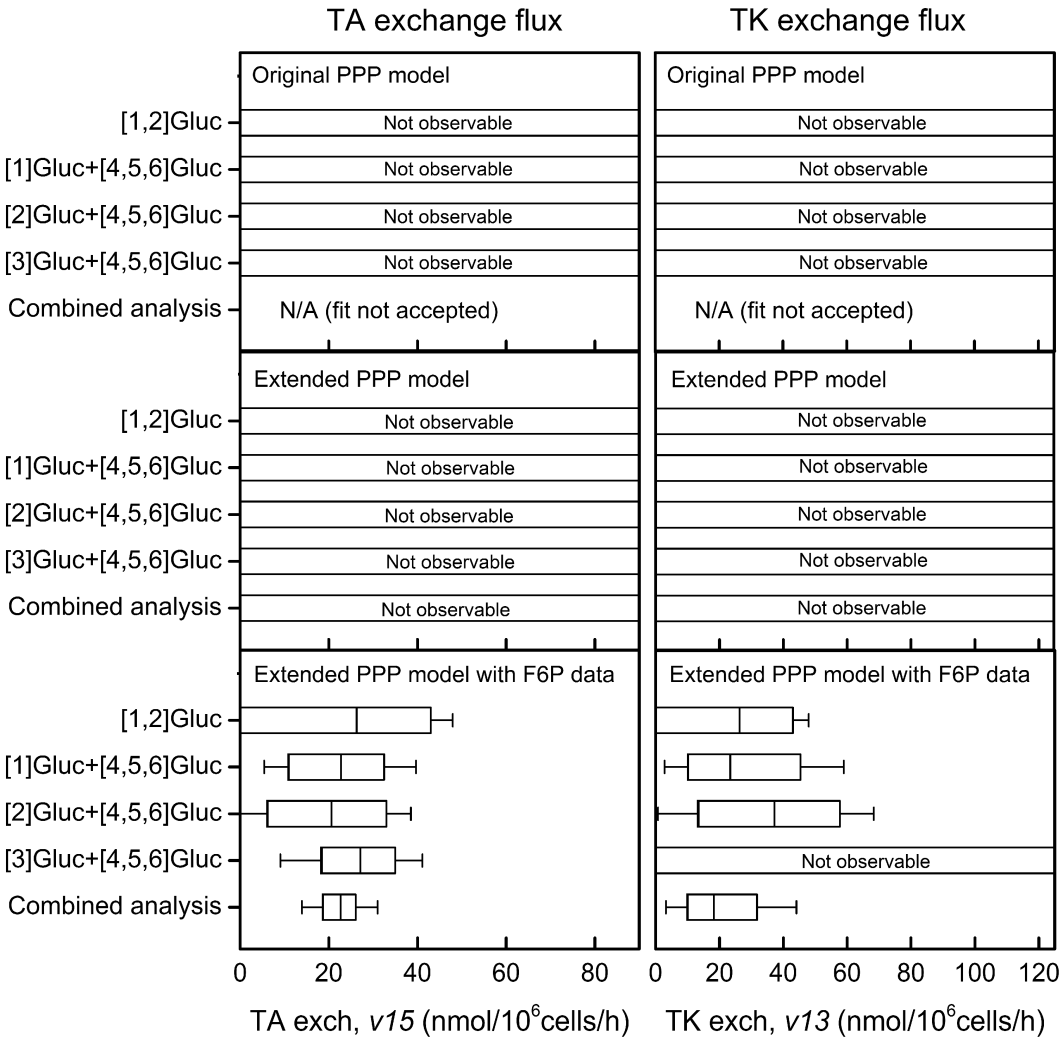

Figure 5.13 Estimated values of non-oxidative PPP fluxes, TA exchange flux (v15) and TK exchange flux (v13) using three ^{13}C-MFA; with the basic data, (A) the original PPP model (Figure 5.2) (B) the extended PPP model and with the basic data and F6P data, (C) the extended PPP model with F6P data. The basic data was DHAP (*m/z* 484), 3PG (*m/z* 585) and PEP (*m/z* 453). Two F6P fragments were *m/z* 307 and *m/z* 364. The extended model contains output flux of TA-C_3 to the original model. In box plot, whisker showed lower and upper bound of 95% confidence interval, inner box showed lower and upper bound of 68% confidence interval and media was used with best fit values.

5.4 Discussion

In this study, we applied ^{13}C-MFA to elucidate PPP metabolism in CHO cells. The PPP model was validated using multiple isotopic tracers and oxidative PPP flux was quantified with ^{13}C-MFA. To validate PPP model (Figure 5.2), we designed several tracer mixture sets: [1]+[4,5,6]Gluc, [2]+[4,5,6]Gluc and [3]+[4,*5,*6]Gluc considering oxidative PPP activity and atom transitions by TK and TA as shown in Figure 5.3. We compared several tracer mixtures and the traditional tracer for oxidative PPP, [1,2]Gluc. The oxidative contribution by estimating MIDs matched well for the mixture tracers and the traditional tracer, as shown in Figure 5.4 and 5.6. However, the mixture tracer for model validation showed significant discrepancy of (M1+M2×2)/M3 isotopomer ratio between intracellular metabolites and Gluc.ext (media glucose) for [2]+[4,5,6]Gluc and [3]+[4,5,6]Gluc sets as shown in Figure 5.5. The ratio of [1]+[4,5,6]Gluc contained the discrepancy between Gluc.ext and [2]+[4,5,6]Gluc (or [3]+[4,5,6]Gluc) as well as oxidative PPP activity. This indicated two possibilities: (i) C1-C3 fragments from glucose carbons were lost in PPP; (ii) the isotopomer ratio, (M1+M2×2)/M3, were underestimated by limitation of measured metabolites. First, by non-specific reactions of TA and TK, unknown reaction in PPP may be activated. Winden et al. reported that the PPP model considering all possibilities of non-specific reactions in TA and TK (six TK and three TA reactions) should be used for ^{13}C-MFA, rather than the traditional model with two TK reactions and one TA reaction (van Winden et al., 2001). Kleijn et al. suggested that two pools of glycolaldehyde (TK-C_2) and dihydroxyacetone moiety (TA-C_3) should be used as intermediates at reversible reactions of three TK and two TA reactions in non-oxidative PPP, and validated the model with ^{13}C-MFA for *Saccharomyces cerevisiae* metabolism (Kleijn et al., 2005). The two studies suggested non-specific reactions of

TA and TK and also free pools of C_2 and C_3 moieties in PP metabolic pathway. In this study, the MID data in Figure 5.5 showed that TA-C_3 fragment were lost regardless of oxidative PPP activity and this indicated that TA-C_3 fragments were linked to other unknown pool(s) by other pathway activation under the specific CHO culture condition. Second possible explanation is that limitation of measured data may result in under-estimation of the ratio (M1+M2×2)/M3 at the labeling of 3PG and PEP. We already counted the contribution of M1 to M2 isotopomer conversion by two times M2 in (M1+M2×2)/M3. M2 isotopomers in ^{13}C-labeling isotopomers were less than 6% at the metabolites, 3PG and PEP. Also, M3 isotopomer could be produced from M1 isotopomer. We checked M3 isotopomer in ^{13}C-labeling isotopomers of 3PG and PEP in the single tracer experiment with [1]Gluc under the same culture condition (Figure 5.6). In the study, M2 isotopomer in ^{13}C-labeling isotopomers were less than 1.3% (matched with this study) and the M3 isotopomer intensity was almost at baseline level. Thus, the conversion from M1 to M3 isotopomer in non-oxidative PPP was negligible. Second validation was performed with [4,5,6]Gluc tracer. Figure 5.7 shows that there were no M1 and M2 intensities at the MIDs of triose-phosphates. This indicates that M3 isotopomer cannot mixed with M1 or M2 isotopomers in MIDs of triose-phosphate using the mixture tracers, [1]Gluc+[4,5,6]Gluc, [2]Gluc+[4,5,6]Gluc and [3]Gluc+[4,5,6]Gluc. After all, using the suggested PPP model (Figure 5.2) was not correlated with the MID data of triose 3-phosphates labeled by the mixture tracers at this CHO culture condition.

In practice, it is possible that this discrepancy between model and measurement data could cause serious distortion of the estimated flux values from ^{13}C-MFA. Recently, metabolic scientists published studies about sensitivity analysis of

metabolic fluxes to screen good isotopic tracers using ^{13}C-MFA simulation (Crown and Antoniewicz, 2012; Metallo et al., 2009; Schellenberger et al., 2012; Walther et al., 2012). Isotopic tracers were selected that narrowed confidence intervals based on the fixed parameters of flux values, network model, measured or artificial data and errors. However, it cannot explain the flux analysis result for the original PPP model in Figure 5.10. Four results from four different tracer sets had similar extents of confidence intervals, but showed different solution space. Therefore, the metabolic network model with model error could result in the poor flux estimation regardless of good fitness of metabolic fluxes and measured data (van Winden et al., 2001). This indicates that model validation is a pre-requisite procedure to acquire real solution by flux analysis as well as precise measurement, since ^{13}C-MFA is a model-driven method. In this study, the model error by TA-C_3 loss should be considered to acquire global solution for PPP fluxes.

As shown in Figure 5.10, to estimate oxidative PPP fluxes, [1,2]Gluc and [1]+[4,5,6]Gluc tracers can be applied selectively according to PPP model, measurement data and confidence intervals (sensitivity) of fluxes. In case of [1,2]Gluc, the best fit values and confidence intervals of oxidative PPP fluxes were independent on the two types of models and additional F6P measurement data (Figure 5.10). The reason is that the ^{13}C-labeling information on C1 and C2 atoms of glucose carbons was not deviated by TA-C_3 loss in PPP. The information of oxidative PPP activity (i.e. the M1/M2 ratio) was kept at the measurable metabolites, 3PG and PEP. However, [1]+[4,5,6]Gluc tracer required the extended model and additional measurement data (F6P) to estimate oxidative PPP. Since M1 isotopomer was located in TA-C_3, the underestimated M1 isotopomer from [1]Gluc was misguided by M3

isotopomer from [4,5,6]Gluc during the computation by ^{13}C-MFA. This kind of error was possible with other isotopic tracers, e.g. [1]Gluc and [U-^{13}C]glucose ([U]Gluc). The mixture tracer is popular and traditional tracer for ^{13}C-MFA (Antoniewicz et al., 2007c; Goudar et al., 2010; Hofmann et al., 2008; Sengupta et al., 2011). If loss of TA-C_3 exists in specific conditions, then the mixture tracer would generate similar errors like [1]+[4,5,6]Gluc experiment in this study.

The additional measurements of F6P fragments enabled ^{13}C-MFA to estimate the reversible fluxes of non-oxidative PPP. As described in Figure 5.13, the exchange fluxes of TA and TK showed good flux observability when the two F6P fragments were applied. The reason for successful flux observability is that the two fragments of F6P, C1-C4 (*m/z* 364) and C4-C6 (*m/z* 307), contained information about reversibility of TA and TK in non-oxidative PPP. As a result, the information could guide TA-C_3 output fluxes with narrow confidence intervals (Appendix C). For example, C4-C6 (*m/z* 307) fragment of F6P had 90% of M3 isotopomer and 10% of M1 isotopomer of labeled isotopomers for [1]+[4,5,6]Gluc experiment (other tracer sets were similar). As shown in Figure 5.11B, the M1 isotopomer could be labeled in F6P by reversible reaction of TA (F6P $\leftrightarrow$ TA-C_3 + GAP) after passing ^{13}C-labeling from DHAP to GAP. If TA reversibility is very high, theoretically, M3 and M1 ratio would reach 100% (1:1 mol/mol) for C4-C6 (*m/z* 307) fragment of F6P. In addition, the achievement of the flux observability in non-oxidative PPP narrowed the confidence intervals of oxidative PPP flux in [1]+[4,5,6]Gluc set. As shown in Figure 5.11, the confidence interval of oxidative PPP flux for the extended model and F6P data were greatly improved compared to the extended model without F6P data. This suggests that the flux with the good precision (e.g. TA and TK) can improve the precision of

the neighbor flux (e.g. oxidative PPP). This is an important lesson for why we should consider the introduction of key measurements, as well as better approaches for tracer design.

5.5 Conclusion

In conclusion, the loss of TA-C_3 fragment in the PP pathway has not been described previously. This finding should be further investigated. It will be important to identify possible reactions that can explain this loss of carbon atoms, and the finding should be further validated with additional measurable data and with other isotopic tracers. In addition, since uncertain metabolic network models can produce poor flux estimation results, the fate of ^{13}C-atoms in isotopic labeling experiments should be better understood before flux analysis is attempted. Strategically, we provide several guidelines for successful ^{13}C-MFA: good tracer design to achieve good sensitivity (e.g. [1]+[4,5,6]Gluc tracer mixture in this study); key measurement data to achieve improved flux observability (e.g. two F6P fragments in this study); parallel labeling experiment coupled with state-of-the-art ^{13}C-MFA analysis techniques to overcome the limitation of single tracer experiments; and most importantly, model validation to acquire accurate and reliable flux solutions.

Chapter 6

METABOLIC FLUX ANALYSIS OF FAO RAT HEPATOMA CELL IN A GLUCONEOGENESIS SYSTEM

Type II diabetes is a growing concern in the world. Hyperglycemia caused by hepatic glucose production is one of the symptoms caused by abnormal regulation of liver metabolism. Here, we investigated fluxes of gluconeogenesis (GNG) in a liver cell line using stable isotope tracers and gas chromatography/mass spectrometry (GC-MS) and elucidated the effects of representative regulators (cAMP, dexamethasone, insulin) on GNG flux and other fluxes in central metabolism. To stimulate glucose production, Fao rat hepatoma cells were cultured in glucose-free medium in the presence of gluconeogenic precursors (glycerol, glutamine, lactate and pyruvate) and isotopic tracers ([U-^{13}C]glycerol, [U-^{13}C]glutamine and [U-^{13}C]lactate). We measured labeled mass isotopomer distributions (MIDs) of intracellular metabolites by isotopic tracers and performed combined ^{13}C-metabolic flux analysis (MFA) with the MID data from [U-^{13}C]glycerol and [U-^{13}C]glutamine. For the study of gluconeogenesis metabolism and for quantification of metabolic fluxes with ^{13}C-MFA, we developed a metabolic model that consisted of gluconeogenesis, glycolysis, pentose phosphate pathway, pyruvate and TCA cycles, amino acid metabolism, ketone body and albumin production, and fatty acid metabolism. Using MID analysis of intracellular metabolites and extracellular glucose secreted from the cells, and using rigorous ^{13}C-MFA analysis, we showed that GNG flux was enhanced by 8-bromo-cAMP, dibutyryl-cAMP and dexamethasone, while insulin significantly suppressed hepatic GNG. Interestingly, the

two cAMP analogues showed differential stimulation of the GNG pathway. In addition, by measuring MS data for F6P, we discovered that the hepatoma cells utilized non-oxidative pentose phosphate pathway in GNG and we quantified the reversible fluxes of transketolase and transaldolase. Finally, we found that dexamethasone showed parallel activation of glycolytic enzymes (e.g. pyruvate kinase) and gluconeogenic enzymes (e.g.phosphoenolpyruvate carboxykinase), as well as other enzymes. In conclusion, in this study we investigated perturbations of GNG pathway to better understand the pathological state of cells observed in Type II diabetes. Our results provide valuable information regarding the metabolic disease phenotype and could be used as a platform for drug screening.

6.1 Introduction

Liver metabolism plays a key role in glucose homeostasis in humans. After food consumption, to reduce glucose levels, liver tissue takes up glucose and stores it as glycogen. Additionally, glucose and amino acids are converted to lipids in the adipose tissue. During fasting, to maintain constant blood glucose level, glucose is liberated by degradation of glycogen stores and synthesized from gluconeogenic precursors such as lactate, amino acids, and glycerol. Mitochondrial AcCoA can also produce ketone bodies. Type II diabetes is characterized by insulin resistance and hyperglycemia (Saltiel, 2001). Uncontrolled glucose production through gluconeogenesis (GNG) in liver tissue contributes to this phenotype. The relevant enzymes for GNG are pyruvate carboxylase (PC, Pyr.m $\rightarrow$ OAC.m), malate dehydrogenase (MDH, OAC.m $\rightarrow$ Mal.m), phosphoenolpyruvate carboxykinase (PEPCK, OAC.c $\rightarrow$ PEP.c), fructose-1,6-bisphophatase (FBPase, FBP $\rightarrow$ F6P) and glucose-6-phosphatase (G6Pase, G6P $\rightarrow$ glucose). The key enzymes for GNG

regulation are PEPCK, FBPase and G6Pase, while the enzymes for the opposite pathway, glycolysis, are pyruvate kinase (PK, PEP $\rightarrow$ Pyr), phosphofructokinase (PFK, F6P $\rightarrow$ FBP) and glucokinase (GK, glucose $\rightarrow$ G6P) (Barthel and Schmoll, 2003). GNG enzymes, PEPCK and G6Pase, are regulated by transcriptional factors for up-regulation by cAMP and dexamethasone and down-regulation by insulin (Vidal-Puig and O'Rahilly, 2001).

As Type II diabetes can be characterized as a metabolic disease, i.e. due to high glucose production, gluconeogenesis metabolism has been studied extensively using isotopic tracers to quantify the underlying metabolic fluxes. Deuterium water was a popular tracer by analyzing labeled glucose secreted *in vivo* and *in vitro* using GC-MS (Antoniewicz et al., 2011; Arnoldi et al., 1998; Guo et al., 1992), or NMR (Jones et al., 2000). By combination of deuterium water and other tracers, TCA cycle was included with gluconeogenesis metabolism, e.g. [U-^{13}C]propionate tracer (Burgess et al., 2004; Jones et al., 2001; Weis et al., 2004). Also, gluconeogenesis and TCA cycle metabolism were studied by several other tracers: ^{13}C-lactate and pyruvate tracers (Des Rosiers et al., 1995; Di Donato et al., 1993; Fernandez and Des Rosiers, 1995), ^{13}C-glucose tracers (Jin et al., 2004; Jones et al., 1998), and $NaH^{13}CO_3$ tracers (Yang et al., 2008). Most previous studies only covered a limited metabolic model with short-cut pathways for gluconeogenesis and simple TCA cycle. The limitation is due to the fact that most techniques utilized only isotopomer ratios to quantify metabolic fluxes, e.g. methods like mass isotopomer distribution analysis (MIDA) (Hellerstein and Neese, 1999). In those cases, flux estimation was confined to simplified network models to describe gluconeogenesis metabolism.

Metabolic flux analysis (MFA) is a more powerful technique for quantifying metabolic fluxes in living cells. The classical MFA technique was based on stoichiometric balances and uptake and production rates of extracellular metabolites as input parameters. It can be easily applicable to biological models for optimization, but the severely under-determined systems resulted often in poor flux observability. For example, Chan et. al. performed classical MFA for estimation of gluconeogenic flux with hepatocytes, however pentose phosphate pathway (PPP) and pyruvate dehydrogenase (PDH) were neglected to avoid mathematical singularities in the model (Chan et al., 2003).

In the past decade, ^{13}C-MFA techniques have been developed to estimate intracellular fluxes using isotopic tracers and mass spectrometry. The measured and simulated MIDs of intracellular metabolites (or extracellular end-products) are fitted by least-square regression to estimate fluxes. Using an iterative solution scheme, the method produces statistically accepted flux maps. The labeled MIDs allow estimation of fluxes in complex models, such as parallel reactions, branches fluxes, and reversible fluxes (Antoniewicz et al., 2007b; Wiechert, 2001). Recently, hepatoma cell lines have been characterized by ^{13}C-MFA (Hofmann et al., 2008; Maier et al., 2008; Noguchi et al., 2009). However, the culture systems were not relevant to gluconeogenesis metabolism.

In this study, we applied ^{13}C-MFA to investigate gluconeogenesis metabolism. Fao rat hepatoma cells were used as *in vitro* gluconeogenic system to evaluate metabolic perturbation during glucose production by using transcriptional activators (8-bromo-cAMP, dibutyryl-cAMP and dexamethasone) and an inhibitor (insulin). Here, we developed a metabolic network model for gluconeogenesis study containing

gluconeogenesis, glycolysis, PPP, glycogen metabolism, pyruvate and TCA cycle, lipid and ketone body metabolism, amino acid metabolism and albumin production. Rigorous analysis of intracellular metabolites with multiple isotopic tracers and GC-MS analysis enabled us to reveal metabolic regulations from metabolic perturbation experiments.

6.2 Materials and Methods

6.2.1 Materials

Culture materials were purchased from Cellgro (Mediatech, Manassas, VA). [U-$^{13}C_3$]glycerol (98%), [U-$^{13}C_5$]glutamine (98%) and [U-^{13}C]algal amino acids (97~99%) were purchased from Cambridge Isotope Laboratories (Andover, MA) and [U-$^{13}C_3$]lactate (99%) was purchased from Sigma-Aldrich (St.Louis, MO). Free amino acids and amino acid standard H were purchased from Pierce Sci. (Rockford, IL). [U-^{13}C]Algal hydrolysate was solubilized in 0.1 N HCl solution at 10 mg/mL and kept at -85°C, to be used for quantification of amino acids.

6.2.2 Cell Culture

Fao rat hepatoma cell lines (ECACC 89042701; Sigma-Aldrich, St.Louis, MO) (Wiebel et al., 1984) were cultured in T-25 flasks (Corning Inc., Corning, NY) in 5% CO_2 incubator at 37°C. Maintenance medium was RPMI 1640 (Cat. No. 10-040) supplemented with 10% fetal bovine serum (FBS, Cat. No. 35-011-CV) and 1% penicillin-streptomycin solution (PS, Cat No. 30-004-CI). 5 mL of culture medium was replaced every two days. At more than 70% confluency, the cells were detached by trypsinization and sub-cultured at 1:6 split ratio.

6.2.3 Tracer Experiments

Figure 6.1 shows the cell culture procedure for gluconeogenesis experiments with isotopic tracers. The maintenance medium was removed when the cells were grown to more than 70% confluency. The attached cells in T-25 flasks were washed twice with 5 mL of Dulbecco's phosphate-buffered saline (DPBS) with calcium and magnesium and pre-incubated for 12 h after addition of 5 mL of RPMI 1640 medium without FBS. After washing twice with DPBS, the culture medium was added with 4.5 mL of RPMI 1640 without FBS and without glucose (Cat No. 10-043-CV), plus 0.5 mL of gluconeogenesis (GNG) precursor stock solution (10 mM glycerol, 100 mM lactate, 10 mM pyruvate and 40 mM glutamine, pH 7.2).

For isotope labeling experiments, three GNG precursor stock solutions were prepared; natural glycerol, glutamine, or lactate in the solutions was replaced with [U-^{13}C]glycerol, [U-^{13}C]glutamine, or [U-^{13}C]lactate, respectively. In order to perturb metabolic fluxes in the GNG pathways, we added dexamethasone (MP Biomedicals, Solon, OH), insulin (Sigma-Aldrich, St.Louis, MO), 8-bromo-cAMP (Tocris bioscience, Ellisville, MO) and N6, 2'-O-dibutyryladenosine 3',5'-cyclic monophosphate sodium salt (dibutyryl-cAMP) (Sigma-Aldrich, St.Louis, MO) at final concentration of 0.5 μM, 100 nM, 0.5 mM and 0.5 mM, respectively. After introduction of GNG precursors and the perturbation agents, cells were cultured for various times (4, 8 and 12 h) or a fixed time, 12 h. For dynamic experiments, nine flasks were used; each three flasks for 4, 8 and 12 h sampling were prepared using three different GNG precursor stocks with different isotopic tracers. In addition, dexamethasone was supplemented to 0.5 μM final concentration to activate the GNG pathway. For the experiment with 12 h fixed time point, four reagents to perturb GNG fluxes, dexamethasone, 8-bromo-cAMP, dibutyryl-cAMP and insulin were added into

the flasks, respectively, and control flasks without the reagent were prepared. The flasks for one condition were prepared in triplicate. Thus, for one kind of tracer experiment, fifteen flasks were cultured at five conditions of four reagents and one control (no addition). The three sets from three kinds of isotopic tracers were performed at the different batch. In total, forty five flasks were used for the labeling experiments at the fixed sampling time, 12 h.

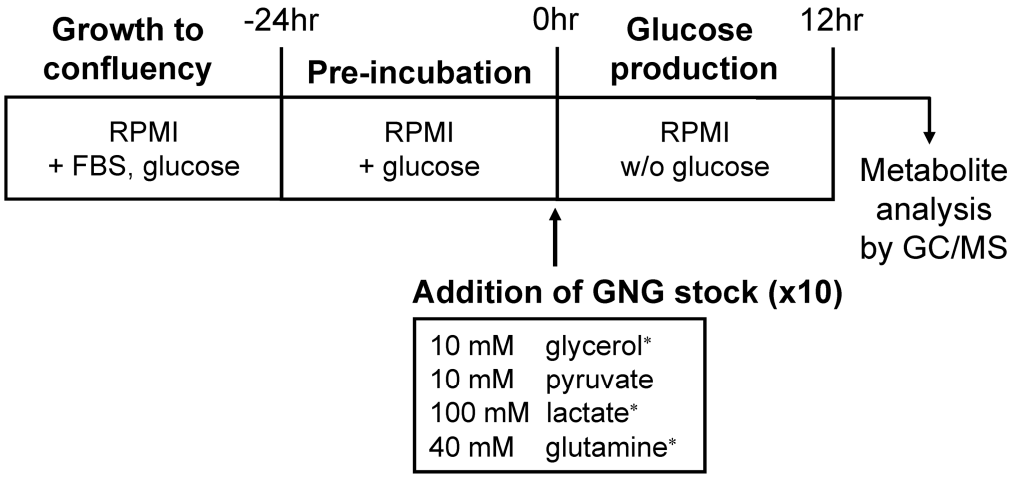

Figure 6.1 Cell culture procedure for gluconeogenesis experiments with Fao rat hepatoma cells. For tracer experiment, gluconeogenesis stock containing an isotopic tracer, [U-^{13}C]glycerol, [U-^{13}C]lactate, or [U-^{13}C]glutamine, instead natural substrate (*), were prepared and added into RPMI 1640 medium without glucose.

6.2.4 Extraction of Intracellular Metabolites

At sampling time, the culture medium was collected from the flasks and after removal of cell debris by centrifugation (1,000 rpm and 5 min) the medium was stored at -85°C for the further analysis. The attached cells in flasks were washed twice with 5 mL of cold saline water (0.9% NaCl, 4°C). Next, 1.5 mL of cold methanol (-20°C) was added to flasks and incubated on ice for 5 min. Cells were detached with a cell scraper and transferred into glass tubes with Teflon-sealed caps. 1.5 mL of chloroform was added and the tubes were vortexed for 10 sec. 1.5 mL of water was added and the tubes were vortexed vigorously for 1 min. The tubes were stored overnight at 4°C and were then centrifuged at 2,000 rpm and 4°C for 20 min. The upper aqueous phase (methanol and water) containing polar metabolites was carefully transferred into two 1.5 mL microcentrifuge tubes using a glass pipette and evaporated to dryness at 37°C with nitrogen gas using an evaporator (Reacti-Vap/Reacti-Therm III; Fierce, Rockford, IL). During the drying process, the contents of the two tubes were combined. The dried samples were stored at -85°C prior to derivatization and GC-MS analysis.

6.2.5 Derivatization of Intracellular Metabolites

Methyloxime tert-butyldimethylsilylation (MOX-TBDMS) was used for derivatization of intracellular metabolites. Dried polar metabolites in the eppendorf tubes were dissolved with 50 µL of 2% methoxylamine hydrochloride (Acros, Moris Plains, NJ) in pyridine. The tubes were incubated on 37°C heating block for 90 min, after mixing by pipetting. 80 µL of N-methyl-N-(tert-butyldimethylsilyl) trifluoroacetamide (MTBSTFA) plus 1% tert-butyldimetheylchlorosilane (TBDMCS) (Thermo Scientific, Bellefonte, PA) was added and the solution was reacted on 60°C

heating block for 30 min. After overnight incubation at room temperature, the derivatized samples were centrifuged for 2 min and the liquid was used for GC-MS analysis.

6.2.6 GC-MS Analysis

Waters micromass Quattro micro GC mass spectrometer (Milford, MA) composed of Agilent 7890A GC and tandem mass spectrometer with electron impact (EI) source and two quadrupoles. GC was equipped with capillary column, DB-5ms 30 m × 0.25 mm × 0.25 μm (Agilent Technologies, Wilmington, DE). Injection port and interface temperature of GC were 250°C. Helium carrier gas was used at the constant flow rate of 1 mL/min. For MS analysis, EI source temperature and electron energy were 200°C and 70 eV, respectively.

6.2.7 GC-MS Analysis of Intracellular Metabolites

For separation of intracellular metabolites, GC oven temperature was held at 70°C at 2 min and increased at 3°C/min to 140°C. 1°C/min ramping temperature was maintained from 140°C to 150°C. At 150°C, the ramping temperature was changed to 3°C/min and the temperature was increased to 280°C and held for 6.33 min. The total run time was 85 min. For MS analysis, mass spectra from specific molecular ions of metabolites were collected by selected ion recording (SIR) (see Table 6.1). 1 to 3 μL of sample containing derivatized polar metabolites was injected into GC in split or splitless mode, considering optimal ion intensity (total ion currents, $10^6 \sim 10^8$).

6.2.8 GC-MS Analysis of Intracellular F6P

Two fragments of fructose-6-phosphate (F6P) were measured by GC-MS after dephosphorylation with alkaline phosphatase and methyloxime-trimethylsilylation (MOX-TMS) derivatization. The protocol for dephosphorylation of F6P was modified using White's method (White, 2004). 100 µL of water and 50 µL of glycine buffer (0.1 M of glycine in pH 10.4, 1 mM of Zn acetate and 1 mM of $MgCl_2$) were added to the dried intracellular metabolites in a microcentrifuge tube. 5 µL (ca. 0.3 IU) of alkaline phosphatase from *Escherichia coli* (Sigma, MO, Cat. No. P4377-100UN) was added and briefly vortexed. After incubation at 37°C for 1 h, the tubes were dried under nitrogen gas at 37°C. The dephosphorylated metabolites were dissolved in 33 µL of 2wt% methoxylamine hydrochloride in pyridine and incubated at 37°C for 90 min. It was combined with 67 µL of N-methyl-N-(trimethylsilyl)trifluoroacetamide (MSTFA) + 1% chlorotrimethylsilane (TMCS) (Thermo Scientific, Bellefonte, PA, Cat. No. TS-48915) and incubated at 60°C for 30 min. After an overnight incubation at room temperature, the derivatized samples were centrifuged at 14,000×g for 2 min and the clear liquid was transferred into GC vials for GC-MS analysis. The injection volume was 1 µL to 3 µL and samples were injected in split or splitless mode depending on the peak intensities. GC oven temperature was held at 80°C for 2 min, increased to 280°C at 7°C/min and held for 4.43 min. The total run time was 35 min. Mass spectra of selected metabolite fragments were collected in SIR mode with 30 ms dwell time. Two fragments of fructose derived from F6P were measured at *m/z* 307 ($C_{12}H_{31}O_3Si_3$) containing carbon atoms C4-C6 of F6P, and at *m/z* 364 ($C_{14}H_{34}O_4N_1Si_3$) containing carbon atoms C1-C4 of F6P (Table 6.1). Before the dephosphorylation reaction, it was validated that there was no meaningful amount of fructose in the medium and in intracellular metabolite samples. In contrast, for analysis of G6P via

dephosphorylation, large amounts of glucose in the medium and inside the cells existed before dephosphorylation. Thus, the measured fragments for intracellular G6P were a mixture of intracellular glucose and G6P. In Table 6.1, the fragments are *m/z* 205, *m/z* 217 and *m/z* 307 of glucose/G6P.

Table 6.1 Metabolite fragments measured by GC-MS for analysis of intracellular and extracellular metabolites.

Metabolite	Mass (*m/z*)	Carbon atoms	Fragment formula
Organic acids			
Pyruvate[1]	174	1-2-3	$C_6H_{12}O_3NSi$
Lactate[1]	233	2-3	$C_{10}H_{25}O_2Si_2$
Lactate[1]	261	1-2-3	$C_{11}H_{25}O_3Si_2$
Succinate[1]	289	1-2-3-4	$C_{12}H_{25}O_4Si_2$
Fumarate[1]	287	1-2-3-4	$C_{12}H_{23}O_4Si_2$
AKG[1]	346	1-2-3-4-5	$C_{14}H_{28}O_5NSi_2$
Malate[1]	419	1-2-3-4	$C_{18}H_{39}O_5Si_3$
PEP[1]	453	1-2-3	$C_{17}H_{38}O_6Si_3P$
DHAP[1]	484	1-2-3	$C_{18}H_{43}O_6NSi_3P$
GLP[1]	571	1-2-3	$C_{23}H_{56}O_6Si_4P$
Citrate[1]	431	1-2-3-4-5	$C_{19}H_{39}O_5Si_3$
Citrate[1]	459	1-2-3-4-5-6	$C_{20}H_{39}O_6Si_3$
3PG[1]	585	1-2-3	$C_{23}H_{54}O_7Si_4P$
GLP[1]	571	1-2-3	$C_{23}H_{56}O_6Si_4P$
F6P[2]*	307	4-5-6	$C_{12}H_{31}O_3Si_3$
F6P[2]*	364	1-2-3-4	$C_{14}H_{34}O_4N_1Si_3$
Glucose/G6P[2]*	205	4-5	$C_8H_{21}O_2Si_2$
Glucose/G6P[2]*	217	3-4-5	$C_9H_{21}O_2Si_2$
Glucose/G6P[2]*	307	3-4-5	$C_{12}H_{31}O_3Si_3$
Glucose[3]	173	5-6	$C_8H_{13}O$
Glucose[3]	259	4-5-6	$C_{12}H_{19}O_6$
Glucose[3]	284	1-2-3-4	$C_{13}H_{18}O_6N$
Glucose[3]	370	1-2-3-4-5	$C_{17}H_{24}O_8N$
Glucose[4]	301	1-2-3-4-5-6	$C_{14}H_{21}O_7$
Amino acids			
Alanine[1]	232	2-3	$C_{10}H_{26}ONSi_2$
Alanine[1]	260	1-2-3	$C_{11}H_{26}O_2NSi_2$
Aspartate[1]	390	2-3-4	$C_{17}H_{40}O_3NSi_3$
Aspartate[1]	418	1-2-3-4	$C_{18}H_{40}O_4NSi_3$
Glutamate[1]	330	2-3-4-5	$C_{16}H_{36}O_2NSi_2$
Glutamate[1]	432	1-2-3-4-5	$C_{19}H_{42}O_4NSi_3$
Glutamine[1]	431	1-2-3-4-5	$C_{19}H_{43}O_3N_2Si_3$

[1]: MOX-TBDMS Derivatization

Table 6.1 continued

[2]: MOX-TMS derivatization
[3]: Aldonitrile pentapropionate derivatization
[4]: Di-O-isopropylidene propionate derivatization
*: Fructose derived from intracellular F6P by dephosphorylation and glucose derived from intracellular Glucose/G6P mixture by dephosphorylation was analyzed by GC-MS

6.2.9 GC-MS Analysis of Extracellular Glucose

The mass isotopomer distribution (MID) of glucose was determined by GC-MS analysis using two derivatization methods, aldonitrile pentapropionate and di-o-isopropylidene propionate derivatization of glucose (Antoniewicz et al., 2011). First, 600 μL cold acetone (-20°C) was added to 200 μL of media samples to precipitate proteins. After vortexing and centrifugation, the clear liquids were transferred to new microcentrifuge tubes for aldonitrile pentapropionate derivatization of glucose, or glass tubes for o-isopropylidene propionate derivatization of glucose. The samples were dried under nitrogen gas flow. First, for aldonitrile pentapropionate derivative of glucose, the dried samples were mixed with 50 μL of hydroxylamine hydrochloride solution (20 mg/mL in pyridine) and incubated at 90°C for 60 min. After brief centrifugation, 100 μL of propionic anhydride was added and mixed. After 30 min incubation at 60°C, the samples were evaporated to dryness under nitrogen gas at 50°C. They were dissolved in 100 μL of ethyl acetate and transferred into GC vials for GC-MS analysis. Second, for di-o-isopropylidene propionate derivative of glucose, fresh 0.38 M sulfuric acid in acetone solution was prepared. 500 μL of the sulfuric acid solution was added to the dried sample in glass tubes and vortexed. The tubes were incubated at room temperature for 60 min. 400 μL of 0.44 M sodium carbonate

solution in water was added to the tubes to stop the reaction. 1 mL of saturated sodium chloride solution in water and 1 mL of ethyl acetate were added to the tubes and vortexed for 15 sec. After centrifugation at 3,000 rpm for 10 min, the top organic phase was transferred to microcentrifuge tubes and dried under nitrogen gas at room temperature. 50 µL of pyridine and 100 µL of propionic anhydride were added and the samples were incubated at 60°C for 30 min. After centrifugation for 1 min at 14,000 rpm, the tubes were dried under nitrogen gas at 60°C. The glucose derivative was dissolved in 100 µL ethyl acetate and the sample transferred to GC vials with a glass insert. For both derivatives, the injection volume was 1 µL and samples were injected at 1:40 split ratio. GC oven temperature was held at 80 °C for 1 min, increased to 280 °C at 8 °C/min, and held for 6 min. As shown in Table 6.1, the labeling of glucose was determined from the mass isotopomer distribution of the fragments at *m/z* 173 ($C_8H_{13}O$), *m/z* 259 ($C_{12}H_{19}O_6$), *m/z* 284 ($C_{13}H_{18}O_6N$) and *m/z* 370 ($C_{17}H_{24}O_8N_1$) for the aldonitrile pentapropionate derivative, and *m/z* 301 ($C_{14}H_{21}O_7$) for di-o-isopropylidene propionate derivative (Antoniewicz et al., 2011).

6.2.10 Quantification of Extracellular Metabolites

To quantify extracellular amino acids, 200 µL of culture medium was supplemented with internal standards: 15 µL of 10 mg/mL of [U-^{13}C]algal hydrolysate. In addition, for analysis of isotopic labeling of extracellular metabolites, 200 µL of culture medium was prepared without internal standards. Media proteins were precipitated by addition of 3-fold volume of cold acetone (-20°C). After vortexing and then centrifugation at 14,000×g for 5 min, the clear liquids were transferred into new microcentrifuge tubes and evaporated to dryness under nitrogen gas flow at 37°C. For derivatization, 35 µL of 2wt% methoxylamine hydrochloride in

pyridine was added to the samples and mixed by pipetting. Next, 60 µL of MTBSTFA + 1% TBDMCS was added and the samples were derivatized at 60°C for 30 min. After an overnight incubation at room temperature, the derivatized samples were centrifuged for 2 min at 14,000×g. The clear liquid was transferred into GC vials for GC-MS analysis. The injection volume was 1 µL and samples were injected in split mode with split ratio ranging from 1:5 to 1:20. The GC oven temperature was held at 80°C for 2 min, increased to 280°C at 7°C/min and held for 9.43 min. The total run time was 40 min. Mass spectra of selected metabolite fragments (Table 6.2) were collected in SIR mode. The concentrations of extracellular metabolites were determined by regression analysis of mass isotopomer distributions of samples with and without internal standards, and given the known concentrations of metabolites in the internal standards (Hofmann et al., 2008; Mashego et al., 2004; Noguchi et al., 2009).

For the quantification of glycerol in media, 200 µL of culture medium was supplemented with 100 µL of 2 mM [U-^{13}C]glycerol solution as internal standard. As discussed in the previous protocol, protein was removed by cold acetone and the samples were dried under air. Glycerol was analyzed by the previous method, using aldonitrile propionate derivatization. The same GC-MS conditions as for glucose were used for glycerol analysis by GC-MS. The glycerol concentrations were determined by comparing the unlabeled M0 ion and M2 ion from the internal standard. The MS fragment at *m/z* 173 ($C_8H_{13}O$) was measured by GC-MS for aldonitrile propionate derivative of glycerol (Table 6.2).

Table 6.2 Metabolite fragments measured by GC-MS for quantification of extracellular amino acids and glycerol.

Metabolite	Mass (*m/z*)	Carbon atoms	Fragment formula	Internal standard
Amino acids				
Alanine[1]	260	1-2-3	$C_{11}H_{26}O_2NSi_2$	[U-^{13}C]Algal soln. [8.1 mM]
Glycine[1]	246	1-2	$C_{10}H_{24}O_2NSi_2$	[U-^{13}C]Algal soln. [6.1 mM]
Valine[1]	288	1-2-3-4-5	$C_{13}H_{30}O_2NSi_2$	[U-^{13}C]Algal soln. [4.0 mM]
Leucine[1]	274	2-3-4-5-6	$C_{13}H_{32}ONSi_2$	[U-^{13}C]Algal soln. [5.9 mM]
Isoleucine[1]	274	2-3-4-5-6	$C_{13}H_{32}ONSi_2$	[U-^{13}C]Algal soln. [2.9 mM]
Proline[1]	258	2-3-4-5	$C_{12}H_{28}ONSi_2$	[U-^{13}C]Algal soln. [3.0 mM]
Methionine[1]	320	1-2-3-4-5	$C_{13}H_{30}O_2NSi_2S$	[U-^{13}C]Algal soln. [0.8 mM]
Serine[1]	390	1-2-3	$C_{17}H_{40}O_3NSi_3$	[U-^{13}C]Algal soln. [2.8 mM]
Threonine[1]	404	1-2-3-4	$C_{18}H_{42}O_3NSi_3$	[U-^{13}C]Algal soln. [3.3 mM]
Phenylalanine[1]	302	1-2	$C_{14}H_{32}O_2NSi_2$	[U-^{13}C]Algal soln. [2.0 mM]
Aspartate[1]	418	1-2-3-4	$C_{18}H_{40}O_4NSi_3$	[U-^{13}C]Algal soln. [6.0 mM]
Glutamate[1]	432	1-2-3-4-5	$C_{19}H_{42}O_4NSi_3$	[U-^{13}C]Algal soln. [8.1 mM]
Glutamine[1]	431	1-2-3-4-5	$C_{19}H_{43}O_3N_2Si_3$	[U-^{13}C]Glutamine [60 mM]
Tyrosine[1]	302	1-2	$C_{14}H_{32}O_2NSi_2$	[U-^{13}C]Algal soln. [1.8 mM]
Organic acids				
Glycerol[2]	173	1-2 or 2-3	$C_8H_{13}O$	[U-^{13}C]Glycerol [2.0 mM]

[1]: MOX-TBDMS derivatization
[2]: Aldonitrile pentapropionate derivatization

6.2.11 Analysis of Cell Number, Glucose and Lactate

Cell numbers were measured using a hemocytometer and viability was determined by trypan blue exclusion method. Cell numbers were measured three times per sample. Concentrations of glucose and lactate were measured by YSI 2700 biochemistry analyzer (YSI, Yellow Springs, OH). Glucose and lactate concentrations were measured three times per sample and averaged.

6.2.12 Analysis of Lactate Dehydrogenase Activity

Lactate dehydrogenase (LDH) activity in culture media was measured by a commercial assay kit (TOX7, Sigma-Aldrich) to show relative cell viability (Legrand et al., 1992). Triplicate samples with 50 μL were aliquated into a 96-well microplate. The assay procedure was performed as suggested by the manufacturer. In short, NADH cofactor, pyruvate, and tetrazolium (dye for colorimetric detection) were added into microplate wells. The plate was incubated at room temperature for 30 min and the LDH reaction was terminated by addition of 1/10 volume of 1N HCl. Using microplate reader, the sample absorbance was measured at a wavelength of 490 nm and the background absorbance of an empty microplate was also measured at 690 nm. Finally, the primary wavelength measurement (490 nm) was subtracted from the background measurement (690 nm).

To acquire maximum values of absorbance (490 nm – 690 nm) at full cell lysis, triton X-100 (TX-100) was used as an agent for cell lysis. Cells in T-25 flasks were cultured to confluency using maintenance medium and incubated with RPMI 1640 media with glucose for 24 h. Eight different GNG media containing 4.5 mL of RPMI 1640 without glucose and 0.5 mL of GNG precursor stock solution were prepared according to TX-100 concentrations in the medium: 10, 1, 10^{-1}, 10^{-2}, 5×10^{-3},

2.5×10^{-3} and 10^{-3} g/L of TX-100, and no addition of TX-100 as control. Eight T-25 flasks with cells were replaced with the media and incubated for 12 h in an CO_2 incubator at 37°C. LDH activity was assayed with the culture medium. The maximum value of absorbance was estimated based on the curve of absorbance (490 nm – 690 nm) versus TX-100 concentration. To measure cytotoxicity of culture sample from tracer experiment, the cytotoxicity was estimated as follows:

$$\text{Cytotoxicity} = \frac{\text{LDH activity (sample)} - \text{LDH activity (initial media)}}{\text{LDH activity (max.value)} - \text{LDH activity (initial media)}} \quad (6.1)$$

Culture media was as sample at 12 h GNG experiment and maximum value of absorbance was acquired from the previous TX-100 cytotoxicity experiment.

6.2.13 Principal Component Analysis (PCA)

PCA was performed using PLS toolbox ver. 1.3 and Matlab R2008b (Mathworks Inc.). The production and consumption rates of extracellular metabolites measured from the [U-^{13}C]glutamine experiment were used as input data for PCA analysis. The data were composed of eighteen variables (extracellular metabolites) and fifteen samples (triplicate experiment with five conditions) as shown in Table 6.3.

Table 6.3 Production and consumption rate of extracellular metabolites during gluconeogenesis experiment with Fao rat hepatoma cells. Data was obtained for experiments with [U-^{13}C]glutamine (SD, n = 3).

	Production and consumption rate (μmol/L/h)				
	Con	Dex	Dib	8Br	Ins
Gluc	23.6 ± 0.9	30.7 ± 1.7	25.7 ± 2.5	26.1 ± 1.2	6.6 ± 0.6
Lact	-214.1 ± 10.3	-250.6 ± 42.5	-271.5 ± 32.0	-247.4 ± 23.9	-233.9 ± 42.1
Glyc	-34.0 ± 3.0	-30.8 ± 2.2	-31.8 ± 1.8	-13.9 ± 0.9	-33.5 ± 1.2
Ala	53.7 ± 1.5	57.5 ± 3.4	59.8 ± 1.4	58.8 ± 1.7	55.5 ± 1.8
Gly	11.7 ± 0.6	16.4 ± 1.6	14.5 ± 0.7	14.2 ± 0.2	8.2 ± 0.6
Val	-3.3 ± 0.3	-3.4 ± 0.5	-3.8 ± 0.3	-4.4 ± 0.4	-5.8 ± 0.3
Leu	-4.1 ± 0.7	-4.5 ± 1.2	-4.7 ± 0.8	-6.0 ± 0.4	-7.2 ± 0.8
Ile	-1.4 ± 0.8	-1.8 ± 1.4	-1.7 ± 1.0	-2.9 ± 0.2	-3.2 ± 0.8
Pro	2.3 ± 0.5	2.3 ± 0.8	2.7 ± 0.6	2.2 ± 0.4	1.8 ± 0.5
Met	-1.9 ± 0.2	-2.2 ± 0.2	-2.2 ± 0.1	-2.4 ± 0.2	-3.0 ± 0.2
Ser	-7.3 ± 0.5	-6.9 ± 0.6	-7.3 ± 0.5	-7.8 ± 0.1	-10.6 ± 0.3
Thr	-2.5 ± 0.3	-2.7 ± 0.5	-3.0 ± 0.3	-3.4 ± 0.3	-4.5 ± 0.3
Phe	-3.2 ± 0.1	-3.5 ± 0.2	-3.7 ± 0.1	-4.0 ± 0.3	-4.2 ± 0.2
Asp	-9.8 ± 0.0	-9.8 ± 0.0	-9.8 ± 0.0	-9.8 ± 0.1	-9.8 ± 0.0
Glu	-9.1 ± 0.0	-9.5 ± 0.0	-9.4 ± 0.0	-9.4 ± 0.0	-9.4 ± 0.0
His	-0.8 ± 0.2	-0.8 ± 0.3	-0.8 ± 0.2	-1.1 ± 0.1	-1.5 ± 0.2
Tyr	-1.2 ± 0.2	-1.1 ± 0.3	-1.4 ± 0.2	-1.8 ± 0.2	-2.9 ± 0.2
Gln	-25.7 ± 14.6	-34.3 ± 19.8	-36.6 ± 15.7	-40.0 ± 5.6	-29.7 ± 13.2

Con, control (no addition); Dex, dexamethasone; Dib, dibutyryl-cAMP; 8Br, 8-bromo-cAMP; Ins, insulin.

6.2.14 Metabolic Network Model

A detailed metabolic network model for Fao rat hepatoma cells was constructed for ^{13}C-metabolic flux analysis. Using one metabolic model, the flux map was estimated by combined analysis with measurement data from [U-^{13}C]glycerol and [U-^{13}C]glutamine tracer experiments. The biochemical reactions and carbon atom transition for each reaction in the model were given in Table 6.4 at the end of this chapter. The model consisted of 82 reactions and 55 balanced metabolites and included reactions for gluconeogenesis, glycolysis, pentose phosphate pathway, glycerol, glycogen, pyruvate, lactate metabolism, tricarboxylic acid (TCA) cycle and amino acid metabolism, ketone body (KB) and albumin metabolism. Cofactor balances were not included in the models to avoid biases resulting from uncertainties regarding fluxes of isoenzymes with alternative cofactor requirements.

6.2.15 Metabolic Flux Analysis

Intracellular metabolic fluxes were estimated using ^{13}C-metabolic flux analysis technique (Yoo et al., 2008). For flux analysis, we used measurement data consisting of MIDs of intracellular metabolites, obtained by mass spectrometry, and external uptake and production rates. The flux map was estimated using the Metran software (Yoo et al., 2008), which is based on the elementary metabolite units (EMU) framework (Antoniewicz et al., 2007b; Young et al., 2008). Using the metabolic network model, optimized metabolic fluxes were estimated by minimizing the variance-weighted sum of squared residuals (SSR) between the predicted and the measured data (Antoniewicz et al., 2006a; Antoniewicz et al., 2007b).

For combined analysis of parallel labeling experiments, data sets from ^{13}C-glycerol and ^{13}C-glutamine experiments were fitted simultaneously to a single flux

model. At each iteration, mass isotopomer distributions were simulated for each tracer using the same fluxes. Next, the Hessian matrix and Jacobian vector from each individual simulation were combined and used to update the search direction for the fluxes at the next iteration. ^{13}C-MFA was continued until a predefined convergence criterion was satisfied, as described before (Antoniewicz et al., 2006a; Antoniewicz et al., 2007b).

6.3 Results

6.3.1 Labeling Dynamics of Intracellular Metabolites

We designed two sets of GNG experiments. First, we measured time course labeling data, consisting of mass isotopomer distributions (MIDs). Fao cells were cultured in GNG culture medium containing three different tracers, [U-^{13}C]lactate, [U-^{13}C]glutamine, and [U-^{13}C]glycerol. ^{13}C-labeling dynamics of intracellular metabolites were determined to evaluate isotopic and metabolic steady state, and to identify carbon flow from GNG precursors to glucose. We fixed appropriate sampling times for flux analysis and acquired information on the fluxes in the GNG system, e.g. low activity of pyruvate kinase (PK) and high activity of transaldolase (TA) and transketolase (TK). The second set of GNG experiments was performed using a fixed time point (12 h), and perturbation of GNG pathway by transcriptional factors described in section 6.3.2.

6.3.1.1 Culture Profiles of Fao Rat Hepatoma Cells

Fao rat hepatoma cells can produce glucose in glucose-free media. As such, this is a good cell model for studying GNG metabolism. As shown in Figure 6.1, the cells were grown to 70% confluency in serum-based medium in T-25 flasks. We applied a pre-incubation step by replacing the medium with serum-free medium with glucose for one day. For the GNG experiment, we cultured Fao cells in serum-free RPMI 1640 medium without glucose to induce glucose production and secretion. As GNG precursors glycerol, pyruvate, lactate and glutamine were supplemented to final concentrations of 1 mM, 1 mM, 10 mM and 4 mM, respectively, as shown in Figure 6.1. After replacing the GNG medium with isotopic tracers, intracellular metabolites were extracted at 4, 8 and 12 h. In addition, a 24 h data point was used only for measurement of medium metabolites. Using GC-MS analysis, ^{13}C-labeling dynamics of intracellular metabolites were measured to determine isotopic and metabolic steady state.

Figure 6.2 shows the measured profiles of extracellular metabolite concentrations for glucose, glycerol and lactate for the tracer experiments of [U-^{13}C]glycerol and [U-^{13}C]glutamine. The concentrations of glycerol and lactate decreased linearly from 0.92 mM glycerol at 0 h to 0.12 mM at 24 h, and from 9.0 mM lactate at 0 h to 4.3 mM at 24 h, during the culture. At the same time, glucose accumulated in the medium from 0 mM at 0 h to 0.71 mM at 24 h after replacing with glucose-free medium. Thus, we demonstrated that Fao rat hepatoma cells could produce glucose from GNG precursors, including glycerol and lactate. Two interesting points were shown here; first, metabolite concentrations increased linearly with culture time, indicating constant external consumption and production rates; and second,

glucose production rate was relatively small compared to the large consumption of glycerol and lactate.

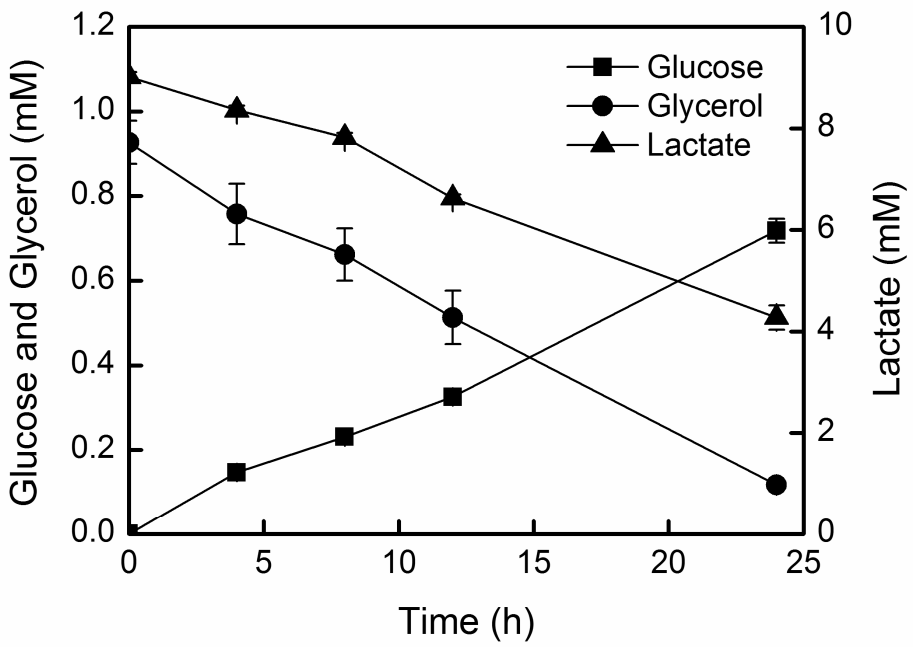

Figure 6.2 Profiles of glucose, glycerol and lactate concentrations during Fao cell culture. Concentrations were measured at 0, 4, 8, 12 and 24 h after replacement with glucose-free medium containing isotopic tracers in Fao hepatoma cell culture, [U-^{13}C]glycerol and [U-^{13}C]glutamine (SD, n = 6).

6.3.1.2 Labeling Dynamics of Intracellular Metabolites with [U-^{13}C]Lactate, [U-^{13}C]Glutamine and [U-^{13}C]Glycerol Tracers

After replacing the GNG medium containing isotopic tracers, [U-^{13}C]lactate, [U-^{13}C]glutamine, or [U-^{13}C]glycerol tracers, intracellular metabolites of Fao cells were extracted at 4, 8 and 12 h at each flask, and extracellular metabolite concentrations were measured (Figure 6.2). As shown in Figure 6.3, the total percentage of labeled isotopomers (100% - M0) of intracellular metabolites was determined by GC-MS. The percentage labeling indicated the proportion of ^{13}C atoms derived from the isotopic tracer relative to ^{12}C carbons from natural metabolites (non tracer-derived carbon sources) in each metabolite.

The labeling dynamic from [U-^{13}C]lactate tracer shown in Figure 6.3 demonstrate overall high ^{13}C-enrichments of intracellular metabolites related to GNG (or glycolysis) pathway, pyruvate, and TCA cycle. The GNG medium for the lactate tracer experiment contained 99% [U-^{13}C]lactate, which was transported into intracellular lactate (Lact) and converted to pyruvate (Pyr) and alanine (Ala). These metabolites reached isotopic steady state after 4 h. The averaged labeling (at 4, 8 and 12 h) for intracellular Lact (*m/z* 261), Pyr (*m/z* 174), and Ala (*m/z* 260) was 83%, 90%, and 91%, respectively. The labeling of TCA cycle-related metabolites, citrate (Cit, *m/z* 459), aspartate (Asp, *m/z* 418), malate (Mal, *m/z* 419), glutamate (Glu, *m/z* 432), succinate (Suc, *m/z* 289) and glutamine (Gln, *m/z* 431) was 75%, 48%, 61%, 57%, 53% and 2%, respectively. The highest labeling of Cit indicated major carbon flow via pyruvate dehydrogenase (PDH) reaction from Lact into the TCA cycle. In addition, the low labeling of intracellular Gln suggested low activity of glutamine synthetase (GS), i.e. low flux from Glu to Gln. In the gluconeogenesis pathway, 3-phosphoglycerate (3PG, *m/z* 585) and phosphoenolpyruvate (PEP, *m/z* 453) reached

isotopic steady state within 4 h, and the averaged labeling percentages were 42% and 41%, respectively. However, dihydroxyacetone phosphate (DHAP, *m/z* 484) approached a maximum value of only 33% at 8 h, and slightly decreased after that. The labeling dynamic of glycerol-3-phosphate (GLP, *m/z* 571) showed non isotopic steady state.

As shown in Figure 6.3, [U-^{13}C]glutamine was incorporated into intracellular Gln pool. Most of TCA cycle-related metabolites reached isotopic steady state within 4 h. The averaged labeling (at 4, 8 and 12 h) of Cit (*m/z* 459), Asp (*m/z* 418), Mal (*m/z* 419), Glu (*m/z* 432), Suc (*m/z* 289) and Gln (*m/z* 431) was 28%, 15%, 22%, 35%, 32% and 74%, respectively. Interestingly, the labeling from Gln to other TCA-related metabolites was significantly reduced, i.e. by more than 2-fold compared to intracellular glutamine. This suggested large dilution flux into the TCA cycle from other carbon sources, for example, extracellular lactate and other amino acids. Glycolysis-related metabolites, Pyr, Lact and Ala incorporated less than 2% labeling during the culture. However, GNG-related metabolites, DHAP, 3PG and PEP reached isotopic steady state within 4 h and showed 16%, 15% and 15% of average labeling, respectively. Therefore, Gln carbon atoms were readily incorporated into the TCA cycle and gluconeogenesis pathway, but did not significantly contribute to pyruvate labeling, thus indicating low activity of pyruvate cycling.

As shown in Figure 6.3, [U-^{13}C]glycerol tracer was 99% labeled in the medium and was incorporated into GLP and gluconeogenesis metabolites. DHAP, 3PG and PEP reached 35%, 29% and 27% average labeling, respectively; however, GLP labeling was at non isotopic steady state. These results suggest the following. First, the labeling dynamic of GLP was non-isotopic steady state and the level was less than

other glycolysis metabolites. In addition, labeling from ^{13}C-glycerol tracer to intracellular GLP was drastically reduced. This suggests that GLP pool was linked to other metabolism as well as gluconeogenesis metabolism. Second, the high labeling of 3PG and PEP indicated that the reactions of gluconeogenesis and glycolysis, e.g. GAP↔3PG and 3PG↔PEP, were very high reversible. The GNG-related metabolites were highly labeled by [U-^{13}C]glycerol, but pyruvate cycling and TCA cycle-related metabolites were labeled less than 2%. This indicated that the carbon source from extracellular glycerol did not reach pyruvate cycling and TCA cycle.

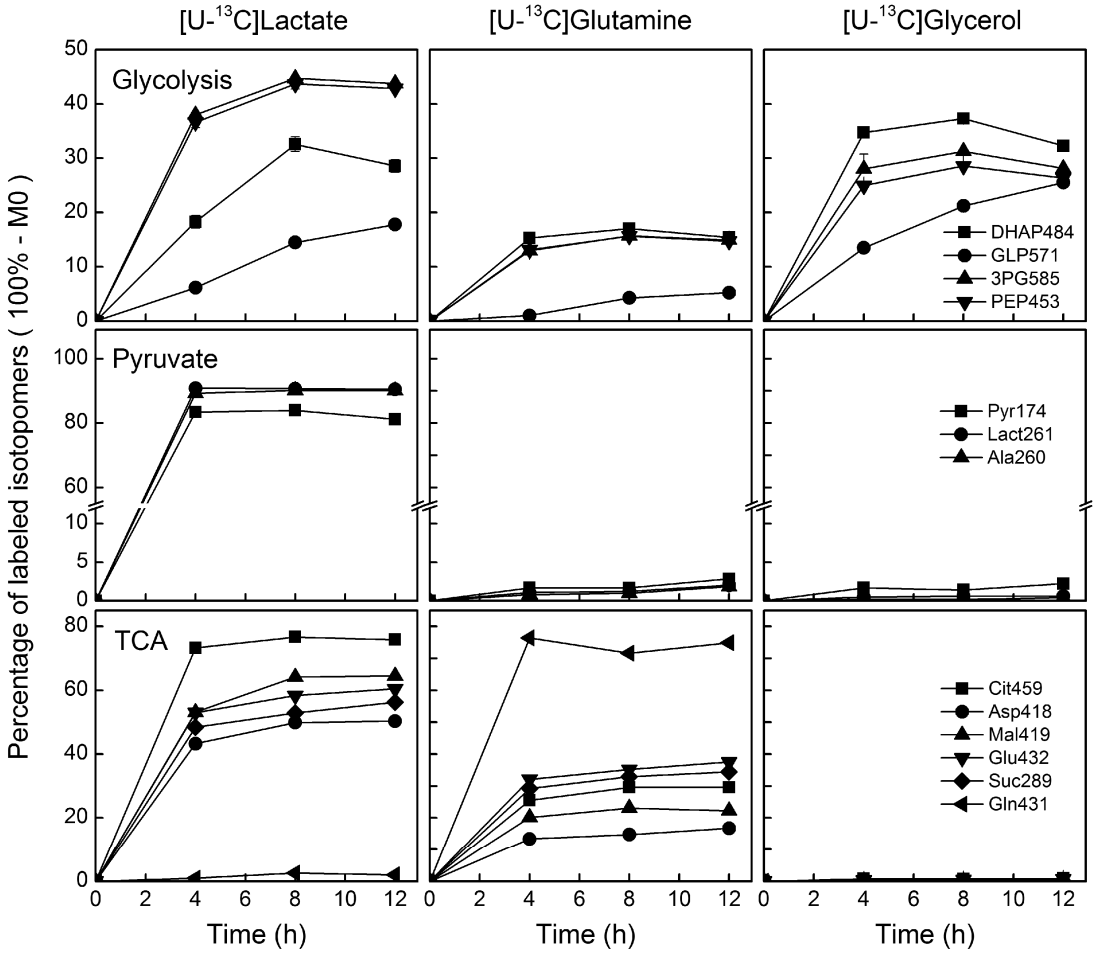

Figure 6.3 ^{13}C-Labeling enrichments of intracellular metabolites at 4, 8 and 12 h after introduction of [U-^{13}C]glycerol, [U-^{13}C]lactate and [U-^{13}C]glutamine (n = 1). Gluconeogenesis-related metabolites, DHAP (*m/z* 484), GLP (*m/z* 571), 3PG (*m/z* 585), PEP (*m/z* 453); Pyruvate cycling-related metabolites, Pyr (*m/z* 174), Lact (*m/z* 261), Ala (*m/z* 260); TCA cycle-related metabolites, Cit (*m/z* 459), Asp (*m/z* 418), Mal (*m/z* 419), Glu (*m/z* 432), Suc (*m/z* 289) and Gln (*m/z* 431)

6.3.1.3 MIDs of Intracellular Metabolites with [U-^{13}C]Lactate, [U-^{13}C]Glutamine and [U-^{13}C]Glycerol Tracers

Figure 6.4 shows the distributions of ^{13}C-labeled mass isotopomers from [U-^{13}C]lactate, [U-^{13}C]glutamine, and [U-^{13}C]glycerol tracer experiments. The MIDs were determined for intracellular metabolites after correction for natural isotope abundances (Fernandez et al., 1996). The MIDs of three representative metabolites, Lact, PEP and Cit at three sampling time (4, 8, and 12 h) were measured after replacing of GNG medium with medium containing [U-^{13}C]lactate. The MID of Lact (*m/z* 261) consists of 97% M3 isotopomer and 3% M1 and M2 isotopomers. The 3% M1 and M2 isotopomers were the result of impurities from the [U-^{13}C]lactate tracer. Even though the labeling percentages of gluconeogenesis, pyruvate cycle and TCA metabolites were relatively constant after 4 h (Figure 6.3), the ratios of ^{13}C-labeled mass isotopomers changed slightly between 4 h and 8 h (Figure 6.4). Thus, technically, at least 8 h was required to reach true isotopic steady state for [U-^{13}C]lactate tracer. MIDs of intracellular metabolites from [U-^{13}C]glutamine and [U-^{13}C]glycerol tracers showed similar patterns as with [U-^{13}C]lactate tracer, regarding labeling dynamics. For the case of [U-^{13}C]glutamine, the MID of Gln (*m/z* 431) contains 93% M5 isotopomer and 7% M1-M4 isotopomers. The 7% isotopomers were also derived from impurities of the [U-^{13}C]glutamine tracer. TCA metabolites, Mal and AKG reached isotopic steady state between 4 h and 8 h. Thus, [U-^{13}C]glutamine tracer also needed at least 8 h for true isotopic steady state. For [U-^{13}C]glycerol experiment, GLP and gluconeogenesis metabolites, DHAP and 3PG, show isotopic steady state after 8 h. In summary, at least 8 h was necessary to reach isotopic steady states for all three tracers. Therefore, for following fixed-time-point experiments we chose 12 h as the sampling time.

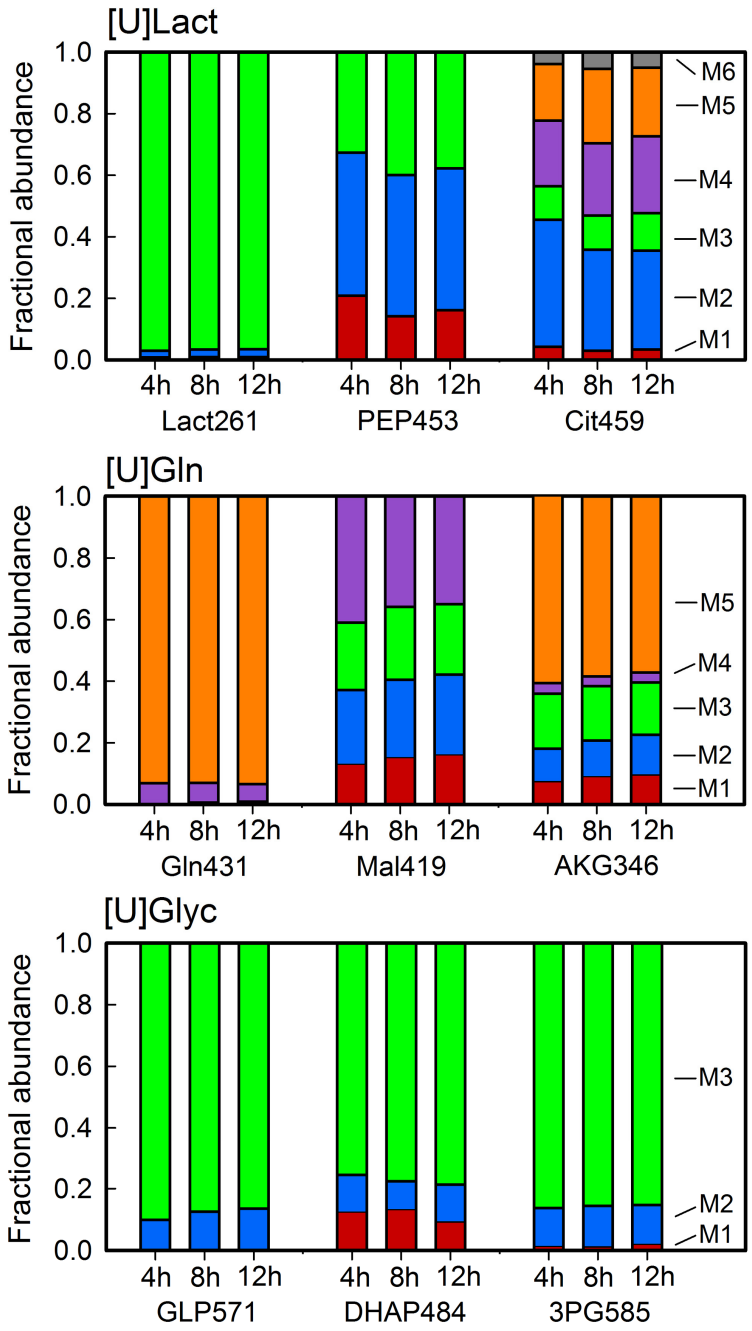

Figure 6.4 Time profiles of fractional abundances of labeled mass isotopomers for intracellular metabolites. Labeling was measured by GC-MS at 4, 8 and 12 h after addition of [U-^{13}C]lactate ([U]Lact), [U-^{13}C]glutamine ([U]Gln) and [U-^{13}C]glycerol ([U]Glyc) tracers (n = 1). Lact261 denoted the fragment at *m/z* 261 of lactate (intracellular metabolite). The data were corrected for natural abundances.

Figure 6.5 shows fractional abundances of labeled mass isotopomers for intracellular metabolites at 12 h, using [U-^{13}C]lactate ([U]Lact), [U-^{13}C]glutamine ([U]Gln) and [U-^{13}C]glycerol ([U]Glyc) tracers. More detailed discussion of the MS data is provided in the next section 6.3.2.

In Figure 6.5([U]Lact), the M3 mass isotopomer of Pyr (*m/z* 174), Lact (*m/z* 261) and Ala (*m/z* 260) was almost 96% of total labeled isotopomers for each metabolite, as [U-^{13}C]lactate tracer was quickly equilibrated with intracellular Pyr. The carbon atoms in Pyr were incorporated into TCA cycle-related metabolites, Asp (*m/z* 418), Mal (*m/z* 419), Fum (*m/z* 287) and Suc (*m/z* 289), which contained broad spectrum of isotopomers from M1 to M4 isotopomers. The M1 and M2 mass isotopomers could be produced by oxidation and atom scrambling in the TCA cycle. The abundance of M4 isotopomer for Asp (*m/z* 418), Mal (*m/z* 419), Fum (*m/z* 287) and Suc (*m/z* 289) was 16%, 18%, 18% and 45%, respectively. The M4 isotopomer could be produced as follows; Pyr (M3) $\rightarrow$ OAC (M3) (by PC), and AcCoA (M2) by PDH $\rightarrow$ Cit (M5) $\rightarrow$ Fum, Mal, Suc and Asp (M4). Thus, these results suggested that high abundance M4 isotopomers were related to high PC and PDH activity. Interestingly, the M3 isotopomer for Asp (*m/z* 418), Mal (*m/z* 419), Fum (*m/z* 287) and Suc (*m/z* 289) was 39%, 39%, 41% and 17%, respectively. The M3 and M4 isotopomers showed very different pattern for Suc and the other C_4 metabolites (Asp, Mal and Fum). The M3 isotopomer ratio of Suc (*m/z* 289) was lower than other C_4 metabolites and the M4 isotopomer was much higher. One possible reason is that Asp, Mal and Fum were involved in reductive carboxylation in the cytosol and oxidation in the TCA cycle in mitochondria at the same time, but Suc was only metabolized in the TCA cycle. As our extracted metabolites were mixtures from two compartments, it

showed two different patterns. Thus, this result provides strong evidence for compartmentalization in mammalian metabolism. Next, C_4 metabolites in TCA cycle flowed into gluconeogenesis pathways by PEPCK. The GNG-related metabolites, DHAP (*m/z* 484), 3PG (*m/z* 585) and PEP (*m/z* 453) had similar MIDs. Thus, this suggested that the biochemical reactions between DHAP and PEP were highly reversible. Furthermore, the C_3 fragment of Asp (*m/z* 390) in the TCA cycle had a similar MID compared to GNG-related fragments (DHAP, *m/z* 484; 3PG, *m/z* 585; PEP, *m/z* 453). This indicated that TCA metabolites were indeed incorporated into the gluconeogenesis pathway. The PEPCK reaction transferred carbon atoms to PEP for gluconeogenesis. However, interestingly, the MID of Asp (*m/z* 390) was different from Pyr metabolism-related fragments (Pyr, *m/z* 174; Lact, *m/z* 261; Ala, *m/z* 260). If PK (PEP $\rightarrow$ Pyr) flux was absolutely trivial, or relatively smaller than LDH (Lact $\rightarrow$ Pyr), the MIDs of the two groups would show different pattern. This became obvious in the next tracer experiment.

In Figure 6.5 ([U]Gln), intracellular Gln (*m/z* 431) had 93% M5 isotopomer and 7% other isotopomers. Thus, [U]Gln in the medium was very quickly equilibrated with intracellular Gln. Interestingly, the MID of Gln (*m/z* 431) was different from Glu (*m/z* 432) and otherwise, AKG (*m/z* 346) had almost same MID as Glu (*m/z* 432). This suggested that there was no glutamine synthetase activity (GS, Glu $\rightarrow$ Gln) and high reversible conversion between AKG and Glu existed by glutamate dehydrogenase (GDH) and/or aminotransferase (AT). In addition, the M5 isotopomer of Cit (*m/z* 459) reached almost 31% abundance. Since the M5 isotopomer from Gln (*m/z* 431) labeled Cit, this suggested high backward flux through isocitrate dehydrogenase (IDH, AKG $\rightarrow$ ICit/Cit). This is related to reductive carboxylation and fatty acid metabolism via

ATP citrate lyase (ACL). The MID patterns of M3 and M4 isotopomers for Suc and other C_4 metabolites (Asp, Mal, Fum) at [U]Gln corresponded to [U]Lact. This was further validation of compartmentalized metabolites and two different metabolisms involved for reductive carboxylation and oxidative metabolism in the TCA cycle. The MIDs of C_3 fragments for [U]Gln experiment showed that the C_3 fragment of Asp (*m/z* 390) in the TCA cycle had the similar MID as GNG-related fragments (DHAP, *m/z* 484; 3PG, *m/z* 585; PEP, *m/z* 453). This was the same result as with [U]Lact experiment. However, the MID of Asp (*m/z* 390) was also similar to Pyr metabolism-related fragments (Pyr, *m/z* 174; Lact, *m/z* 261; Ala, *m/z* 260). Thus, we can propose two possibilities; (i) there is no PK activity; and (ii) relatively smaller PK flux compared to LDH according to dilution contribution on Pyr pools. From the different patterns of Pyr, Lact and Ala for two tracer experiments, we can conclude that PK flux was relatively small compared to LDH flux.

Figure 6.5 ([U]Glyc) shows high M3 isotopomers for GLP (*m/z* 571), DHAP (*m/z* 484), 3PG (*m/z* 585), PEP (*m/z* 453), and Pyr (*m/z* 174), which were 86%, 79%, 85%, 90% and 90%, respectively. The 10-20% of M1 and M2 isotopomer came from atom transitions at F6P fragments, as well as impurity of [U]Glyc. More detailed analysis will be provided in section 6.3.2. Another interesting finding was the fact that no labeling of TCA cycle-related metabolites was observed, except for Pyr. The main reason is that a relatively small PK flux was too weak to label TCA cycle-related metabolites. In addition, even though this was glucose production system by GNG metabolism, PK of glycolytic enzymes was activated at this culture condition. This was a specific finding for the dexamethasone condition. We used dexamethasone for all dynamic experiments. This is also discussed in section 6.3.2.

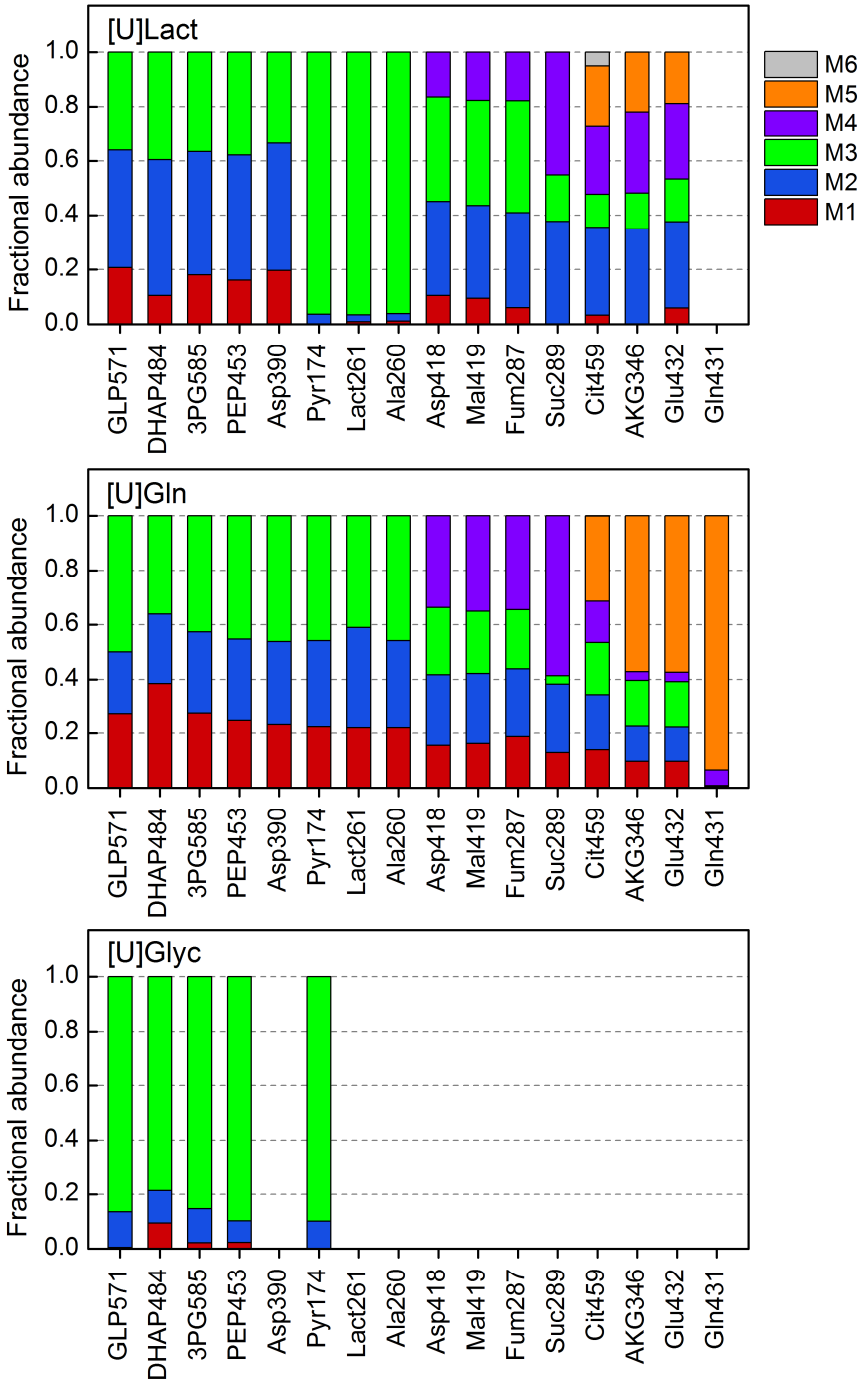

Figure 6.5 Fractional abundances of labeled mass isotopomers for intracellular metabolites at 12 h by [U-^{13}C]lactate ([U]Lact), [U-^{13}C]glutamine ([U]Gln) and [U-^{13}C]glycerol ([U]Glyc) tracers (n = 1).

6.3.1.4 Labeling Dynamics and MIDs of Extracellular Glucose

Figure 6.6 shows the time profiles of total percentage of labeled isotopomers and the fractional abundances of labeled mass isotopomers for extracellular glucose fragments from [U-^{13}C]lactate, [U-^{13}C]glutamine, and [U-^{13}]glycerol tracer experiments. Since Fao cells were cultured in glucose-free medium, all of the glucose was produced by the cells, and the glucose fragments contained information about GNG metabolism.

In Figure 6.6A, the ^{13}C-enrichments from [U-^{13}C]lactate tracer reached isotopic steady state after 8 h, as shown for four glucose fragments at *m/z* 173, *m/z* 259, *m/z* 284, and *m/z* 370. In contrast, the ^{13}C-enrichments from [U-^{13}C]glutamine tracer and [U-^{13}]glycerol tracer reached isotopic steady state before 4 h and slightly increased from 4 h to 12 h. Therefore, to achieve isotopic steady state, more than 8 h was required to satisfy the basic assumption of isotopic stationarity for ^{13}C-MFA. Interestingly, the ^{13}C-labeling profiles show almost 2-fold differences between Gluc370 (or Gluc 284) and Gluc173 (or Gluc 259) in Figure 6.6A. As shown in Table 6.1, the labeling positions of carbon atoms are C1-C5 for Gluc370, C1-C4 for Gluc284, C5-C6 for Gluc173 and C4-C6 for Gluc259. By considering the labeling position and measured data of ^{13}C-enrichments, it can be deduced that the C4-C6 fragment of glucose contained higher portion of M3 isotopomers than the C1-C3 fragment. Additional evidence is provided in Figure 6.6C.

As shown in Figure 6.6B, the dynamics of fractional abundance shows similar pattern with the percentage of labeled isotopomers (Figure 6.6A). The fractional abundance of labeled isotopomers for [U-^{13}C]lactate tracer changed between 4 h and 8 h, and slightly increased between 8 h to 12 h. In case of [U-^{13}C]glutamine, the dynamics was almost constant. The fractional abundance for [U-^{13}C]glycerol tracer

slightly changed in time. Thus, an appropriate time point for sampling can be determined at 8 h after addition of isotopic tracers.

Figure 6.6C shows fractional abundances of Gluc370, Gluc284, Gluc173, Gluc259 and 3PG585 fragments. The intracellular fragment 3PG585 was introduced to compare with medium glucose fragments. Gluc370 and Gluc284 contained C1-C5 and C1-C4 fragment, respectively; and Gluc173 and Gluc259 had C5-C6 and C4-C6 fragments. In addition, Gluc259 fragment matched with 3PG585. Therefore, MIDs of Gluc259 and 3PG585 showed the same distribution since C4-C6 fragment of glucose came from GAP and 3PG regardless of tracer types in Figure 6.6C. Gluc173 and Gluc259 had higher proportions of M2 and M3 isotopomers. However, Gluc370 and Gluc284 contained less M2 and M3 isotopomers and higher M1 and M2 isotopomers than Gluc173 and Gluc259. This suggested that C1-C3 fragment of glucose did not match with C4-C6 fragments. In short, C1-C3 fragment consisted of smaller isotopomer, M1 and M2 than C4-C6 fragment. This result can explain why the labeling of Gluc284 and 370 was higher than for Gluc173 and 259. For example, the number of ^{13}C atoms of M3 isotopomer corresponded to three M1 isotopomers. Thus, the difference in labeling between the two groups was deviated due to isotopomer distributions. Additional evidence is provided in the next section with [U]Glyc tracer and 12 h fixed time points. The different MIDs for C1-C3 and C4-C6 fragments resulted from transaldolase (TA) and transketolase (TK) activity.

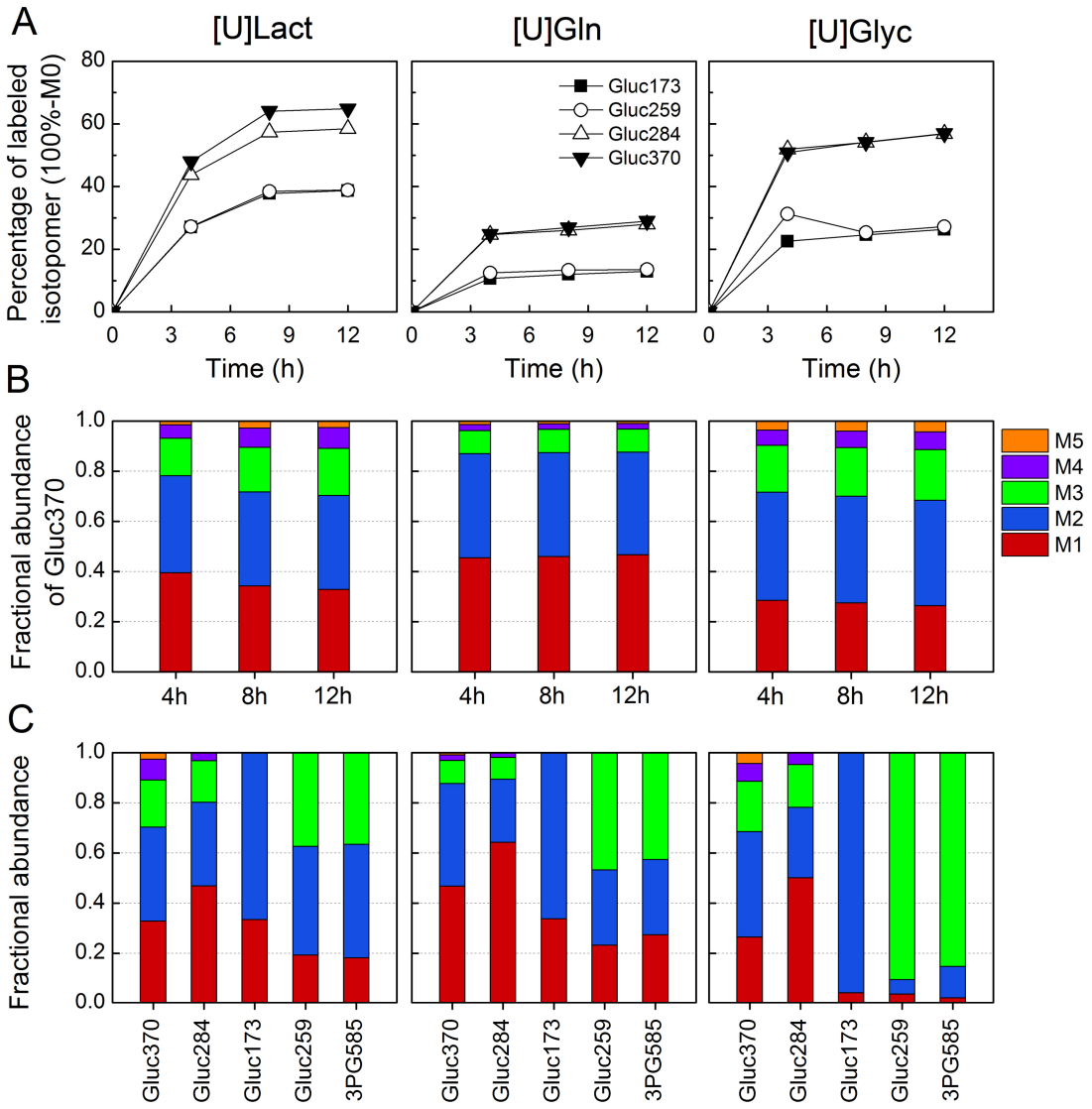

Figure 6.6 (A) Time profiles of percentages labeled isotopomers (100%-M0) for Gluc173 (glucose, *m/z* 173), Gluc259 (glucose, *m/z* 259), Gluc284 (glucose, *m/z* 284) and Gluc370 (glucose, *m/z* 370). (B) Time profiles of fractional abundances for labeled Gluc370 isotopomers from [U-^{13}C]lactate ([U]Lact), [U-^{13}C]glutamine ([U]Gln) and [U-^{13}C]glycerol ([U]Glyc) tracers. (C) Fractional abundances for Gluc370, Gluc284, Gluc173, Gluc259 and 3PG585. Produced glucose in medium was analyzed by aldonitrile pentapropionate derivatization method and GC-MS. Intracellular metabolite 3PG585 data were taken from Figure 6.4 to compare to medium glucose.

6.3.2 Perturbation of GNG Pathway with Transcriptional Activators and Inhibitor

At a fixed sampling time point, 12 h for GNG experiment, Fao cell metabolism was perturbed by GNG-related reagents: two cAMP analogues (8Br, 8-brom-cAMP; Dib, dibutyryl-cAMP), dexamethasone (Dex) and insulin (Ins). Phosphoenolpyruvate carboxykinase (PEPCK), a key enzyme in GNG metabolism, converts oxaloacetate (OAC) to phosphoenolpyruvate (PEP), which is known to be activated by 8Br, Dib and Dex and inhibited by Ins (Vidal-Puig and O'Rahilly, 2001). We designed ^{13}C-tracer and culture experiments based on metabolic perturbation by transcriptional regulation of GNG pathway, and investigated the modulation of intracellular fluxes by applying the four reagents.

6.3.2.1 Cytotoxicity of Fao Cells in Glucose-free Media for GNG Experiment

Cytotoxicity of Fao cells was measured in order to validate no cross-contamination between intra- and extracellular metabolites, and also to confirm that cells were not in apoptotic state. First, in Figure 6.7A, Fao cells at the condition of 12 h culture with GNG media (glucose-free media) were tested to acquire killing curve by analyzing lactate dehydrogenase (LDH) level in medium after addition of triton X-100 (TX-100). LDH activity was measured by a colorimetric method (absorbance at 490 nm – 690 nm) using tetrazolium dye. The absorbance increased to steady state values at 10^{-2} g/L TX-100 and was maintained at relatively constant level despite more addition of TX-100. From this curve, we acquired the values for LDH activity of maximum value and initial medium, which they were used for calculation of cytotoxicity with Eq. (6.1).

Figure 6.7B shows cytotoxicity of Fao cells according to incubation time for GNG experiments with addition of regulatory agents, i.e. Dex, Dib, 8Br and Ins, and

no addition as control, Con. The levels of cytotoxicity increased slowly with time and reached 0.8%, 0.6%, 0.7%, 1.1% and 0.7% at 12 h, respectively. Thus, this indicated that cell death rates were less than 1%. Thus, cell cytotoxicity for GNG culture conditions in this study was not a significant factor during 12 h culture time.

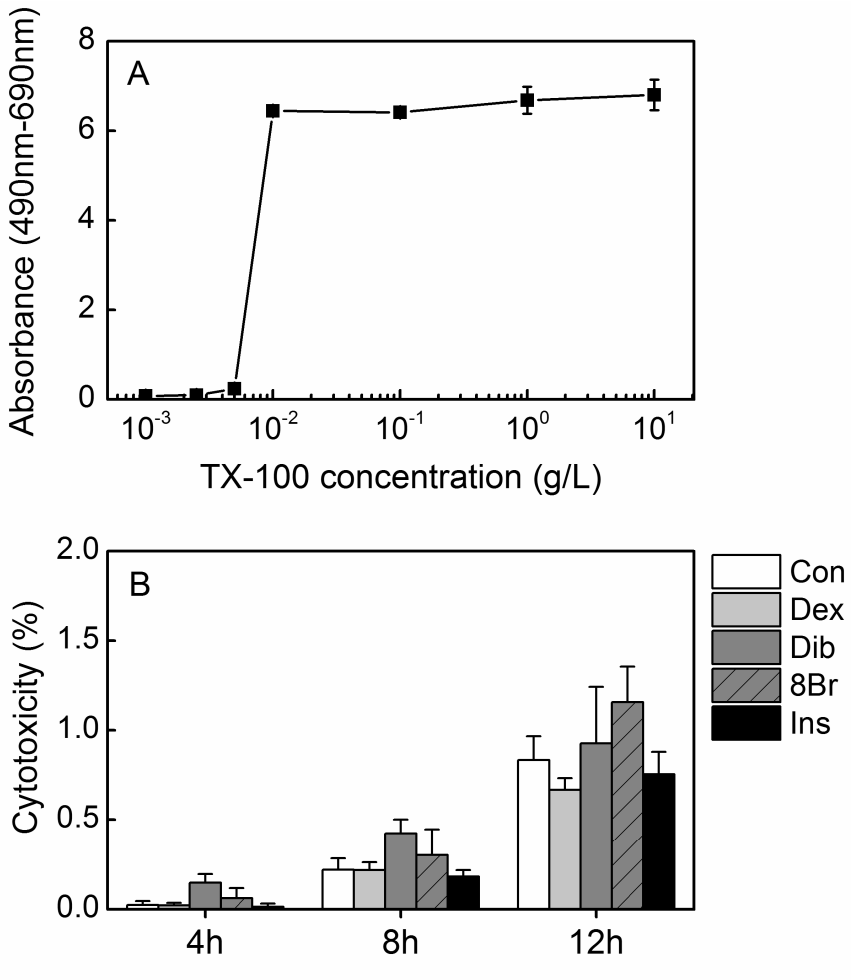

Figure 6.7 (A) Lactate dehydrogenase activity in media after addition of triton X-100 (TX-100). (B) Cell cytotoxicity test according to incubation time during glucose production experiment after addition of regulatory agents, i.e. control (Con), dexamethasone (Dex), dibutyryl-cAMP (Dib), 8-bromo-cAMP (8Br) and insulin (Ins) (SD, n = 3).

6.3.2.2 Cell Culture for Perturbation of GNG Pathways

Fao cells were cultured by replacing GNG medium with medium containing a specific isotopic tracer; [U-^{13}C]lactate, [U-^{13}C]glutamine, or [U-^{13}C]glycerol. Each experiment was performed at five different conditions according to addition of regulatory agents as follow: Dex, Dib, 8Br and Ins, and no addition (Con). During 12 h culture, the cells produced glucose and secreted it into glucose-free medium (GNG medium).

Figure 6.8 shows the production rates of glucose and consumption rates of lactate and glycerol during 12 h culture in three GNG experiments. The data contained three different batches by different tracers and consisted of triplicate flasks for each condition of one batch. In Figure 6.8A, glucose production rates of Con, Dex, Dib, 8Br and Ins were 25.4 ± 1.2, 31.4 ± 1.5, 29.5 ± 1.7, 28.5 ± 1.3and 6.7 ± 1.0 μmol/L/h, respectively. The rates by introduction of GNG enhancers, Dex, Dib and 8Br were slightly higher than the rates for control experiment. It seems that the effects on GNG by Dex, Dib and 8Br were not very significant compared to control set, if only the output flux of glucose was considered. Later, we will discuss in detail the changes in metabolism inside the cell. In case of Ins set, glucose production rate decreased almost 5-fold compared than other sets. Thus, insulin was a strong inhibitor of glucose production.

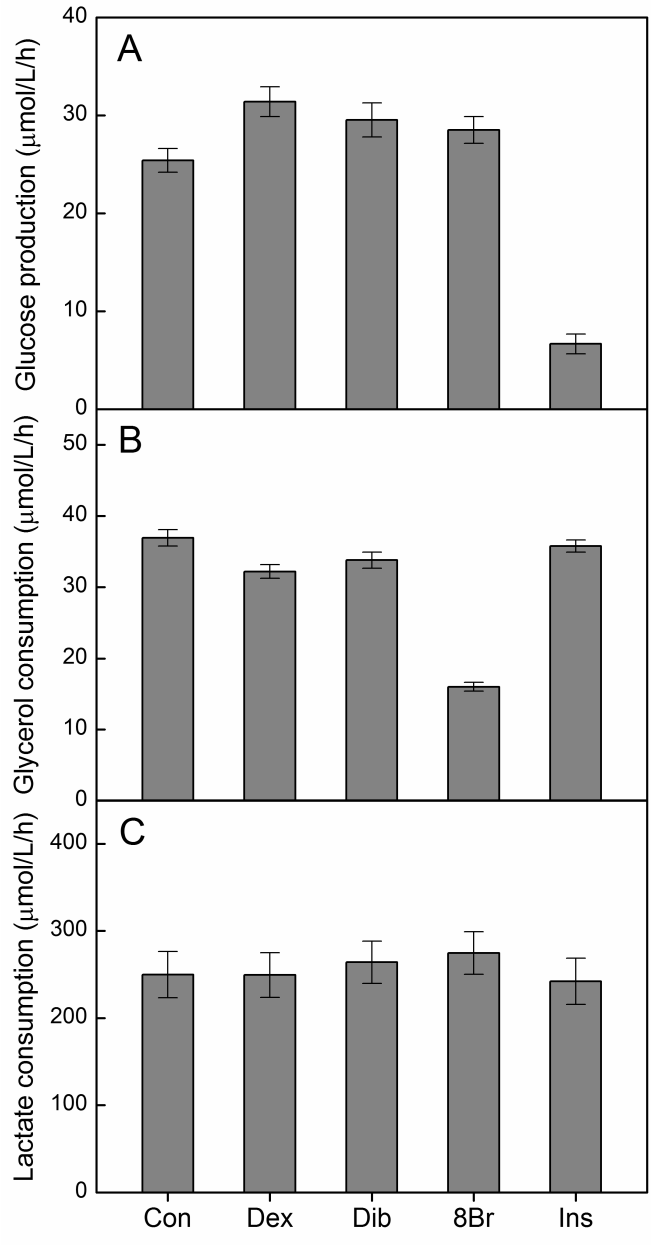

Figure 6.8 The production rates of glucose (A), consumption rates of glycerol (B) and lactate (C). Rates were measured from three experiment sets with [U-^{13}C]glycerol, [U-^{13}C]glutamine, and [U-^{13}C]lactate) as tracers, at a fixed sampling time, 12 h (SE, n = 9).

Figure 6.8B shows the consumption rates of glycerol, which the rates at Con, Dex, Dib, 8Br and Ins were 36.9 ± 1.1, 32.2 ± 0.9, 33.8 ± 1.1, 15.9 ± 0.6, and 35.7 ± 0.8 μmol/L/h. Interestingly, the rates at 8Br set decreased 2-fold compared to other sets. Thus, 8-bromo-cAMP (8Br) effected the consumption of glycerol significantly. Suprisingly, even if two analogues, dibutyryl-cAMP (Dib) and 8Br, were used for cAMP molecules as transcriptional enhancers of PEPCK gene, they showed different glycerol metabolism in Figure 6.7B

Figure 6.8C shows the consumption rates of lactate, which the rates at Con, Dex, Dib, 8Br and Ins were 249 ± 26, 249 ± 25, 264 ± 24, 274 ± 24, and 242 ± 26 μmol/L/h. The levels of lactate consumption rates at all experiments were not significantly different each other. In addition, compared to glucose production or glycerol consumption rates, lactate in media was consumed one order higher than other sets. This suggests several questions as follow; (i) GNG metabolism related to glucose and glycerol were relatively dislocated with TCA cycle metabolism linked to lactate metabolism. Despite introduction of regulatory agents for GNG pathway, lactate metabolism did not change. (ii) Large amount of consumed lactate were used for other cellular metabolism or secreted as different types of metabolites. It was indicated that most of consumed lactate was converted to other cellular metabolism or secreted metabolites.

6.3.2.3 Principal Component Analysis of Cellular Response by Perturbation of GNG

Production and consumption rates of eighteen extracellular metabolites were measured for the GNG experiment with [U-^{13}C]glutamine as shown in Table 6.3. The triplicate data sets for five conditions, Con, Dex, Dib, 8Br and Ins, with the eighteen parameters were utilized as inputs data for principal component analysis (PCA). Two principal component (PC) vectors (i.e. eigen vectors) were selected as 1st PC and 2nd PC, which carried 57% and 18% variance, respectively. Fifteen data with five conditions and triplicate flasks were plotted on two independent axes.

Figure 6.9 shows the score plot of 1st PC (PC1) versus 2nd PC (PC2) by PCA using measurement data of extracellular fluxes for the [U-^{13}C]glutamine experiment. The two vectors, PC1 and PC2, separated and isolated the data points to three groups as follows: group 1, consisting of only data for Con experiment (3 flasks); group 2, for Ins (3 flasks); and group 3, for Dex, Dib and 8Br (9 flasks). PC1 categorized the groups on the left side for group 1 and 3 and the right side for group 2. PC1 vector has large negative values for the vector components related to amino acids consumption rates. This correlated well with the pattern of measured data in Table 6.3. Thus, Ins set shows higher amino acids consumption than other groups. Furthermore, PC2 vector separated the groups on the upper side for group 3 and the bottom side for group 1 and 2. PC2 vector has large positive value for the vector component of glucose produced and large negative value for lactate produced. Table 6.3 data, about production rates of glucose and consumption rates of lactate, indicated that group 3 (Dex, Dib and 8Br) showed higher rates of glucose consumption and lactate production.

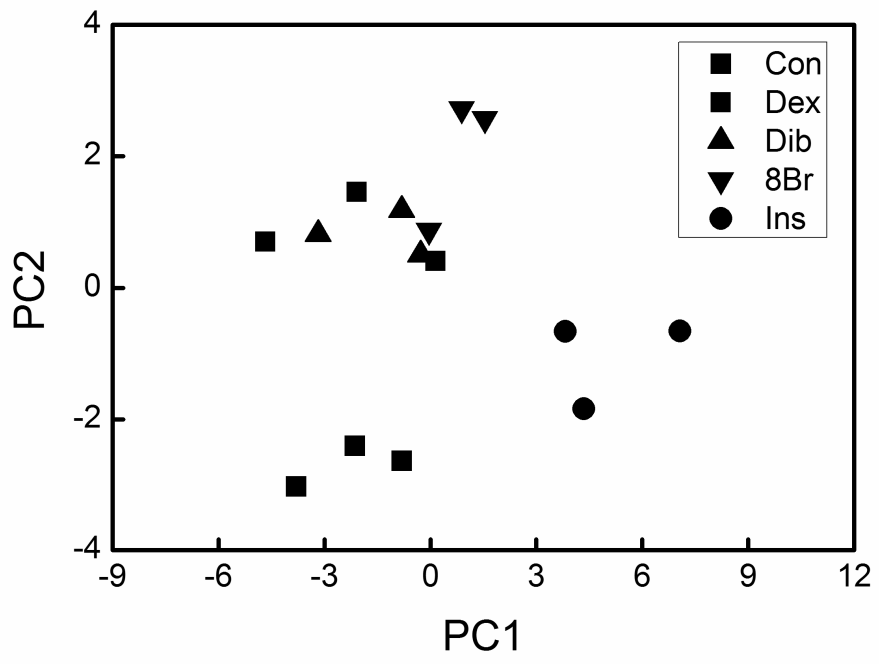

Figure 6.9 Score plot of 1st principal component (PC1) versus 2nd principal component (PC2) by principal component analysis (PCA). 18 variables of extracellular production and consumption rates measured at 15 samples with 5 conditions and triplicates were used for PCA ([U-^{13}C]glutamine experiment)

6.3.2.4 ^{13}C-Labeling Profiles of Intracellular Metabolites for [U-^{13}C]Lactate Tracer

Using GNG medium containing [U-^{13}C]lactate as tracer, Fao cells were culture for 12 h and then intracellular metabolites were extracted and derivatized in order to measure ^{13}C-labeling by GC-MS. Lactate was incorporated into TCA cycle and finally reached gluconeogenesis pathway to produce glucose.

To validate these assumptions about carbon flow from lactate to glucose inside the cells, we designed a new strategy to show the fate of carbon flow using isotopic tracers. First, the total percentages of labeled isotopomers (100% - M0) of intracellular metabolites are measured by GC-MS. Next, the intracellular metabolites were arranged by the level of ^{13}C-enrichments in order from the highest to the lowest. Thus, as the enrichment decreased from left to right direction according to the sequence of metabolite fragments, it indicated that ^{13}C-atoms from the isotopic tracer flowed through the respective metabolite pools and related pathways.

Figure 6.10 shows ^{13}C-labeling profiles of intracellular metabolites according to the sequence of the enrichments from the highest to the lowest levels for [U-^{13}C]lactate experiment using five different conditions: additions of Dex, Dib, 8Br and Ins, and Con, i.e. no addition. ^{13}C-labeling of lactate fragment at *m/z* 261 in the medium was 91% at 12 h after addition of [U-^{13}C]lactate. The extracellular lactate was transported into intracellular lactate pool which was starting point to attend intracellular metabolism. The ^{13}C-labeling profiles can be classified by three groups as follows: (i) the metabolites that were related to lactate metabolism, which were Lact (*m/z* 261) and Ala (*m/z* 260). The labeling percentage of Lact and Ala were around 89% regardless of five conditions, Con, Dex, Dib, 8Br and Ins. These were the highest values in the intracellular metabolites. (ii) TCA cycle metabolites that were in 2nd

labeling group. The ^{13}C-labeling of Cit (*m/z* 459), Pyr (*m/z* 174), Mal (*m/z* 419), Fum (*m/z* 287), AKG (*m/z* 346), Glu (*m/z* 432) and Suc (*m/z* 289) decreased in that order. The sequence from highest to lowest labeling for most data points was Con, Ins, Dib/8Br and Dex in that order. The difference between the highest and the lowest value was at most 11%, between the values for Con and Dex conditions. Interestingly, even though Pyr is metabolically linked to Lact and Ala, the labeling of Pyr was less than that of Lact and Ala. This suggests that multiple Pyr pools were compartmentalized. Since we measured only mixed pools of cytosolic and mitochondrial Pyr, the ^{13}C-labeling of the mixed Pyr pool decreased by combination of the cytosolic pool with high labeling and the mitochondrial pool with low labeling. (iii) GNG-related metabolites were in the 3nd labeling group. The ^{13}C-labeling of PEP (*m/z* 453), 3PG (*m/z* 585), DHAP (*m/z* 484), Ser (*m/z* 390), Gly (*m/z* 246) and GLP (*m/z* 571) decreased in that order. Surprisingly, the sequence of ^{13}C-labeling according to the five GNG conditions were switched and re-arranged as shown in Figure 6.10. The sequence from the highest to the lowest enrichment was for the conditions 8Br, Dib, Dex, Con, and Ins in that order. The difference between the highest and lowest values showed significant gaps, e.g. 18% between the values of metabolites for 8Br and Ins conditions. Moreover, the ^{13}C-labeling for the 8Br experiment showed a plateau line from Fum (*m/z* 287) to DHAP (*m/z* 484). This suggests that there was no dilution during switching carbon flow from TCA cycle to gluconeogenesis pathway, or there was a large exchange flux between the two pathways. However, ^{13}C-labeling for the other four experiments decreased significantly from Suc (*m/z* 289), or Mal (*m/z* 419), to PEP (*m/z* 453). This indicated that metabolites labeled with ^{13}C atoms were

diluted significantly by other natural carbon sources (i.e. ^{12}C atoms), or that relatively small exchange flux between TCA cycle and gluconeogenesis pathway was present.

The most likely reaction to modulate the metabolic flux between gluconeogenesis and TCA cycle is PEPCK for gluconeogenesis pathway. PEPCK links OAC to PEP. Because of this, carbon atoms from TCA cycle can flow to the gluconeogenesis pathway and eventually produce glucose. As a result, the ^{13}C-labeling profiles of intracellular metabolites in Figure 6.10 provided strong evidence that PEPCK reaction was highly activated by 8Br and suppressed by Ins.

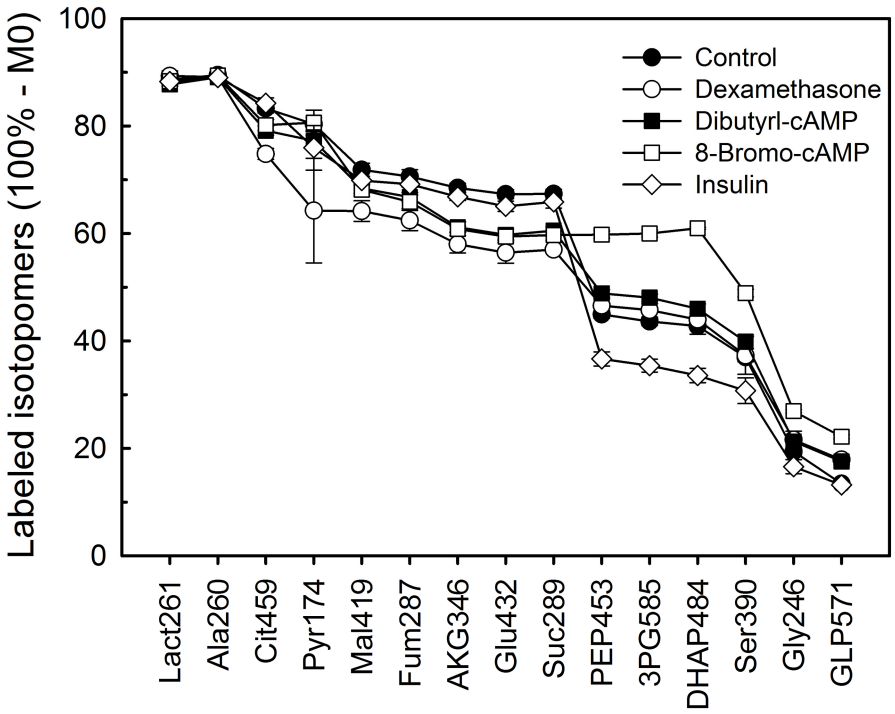

Figure 6.10 ^{13}C-Labeling profiles of intracellular metabolites for [U-^{13}C]lactate experiment. The metabolites were arranged according to the sequences of the enrichment from the highest (Lact at *m/z* 261) to the lowest level (GLP at *m/z* 571) for [U-^{13}C]lactate set using five different conditions: the addition of dexamethasone (Dex), dibutyryl-cAMP (Dib), 8-bromo-cAMP (8Br) and insulin (Ins) and no addition for control (Con) (SD, n = 3).

6.3.2.5 Labeled Mass Isotopomer Distributions for [U-^{13}C]Lactate Tracer

In addition to determining ^{13}C-labeling profiles of intracellular metabolites, mass isotopomer distribution (MID) can be measured by GC-MS. ^{13}C-labeling of metabolites provides information on the carbon flow, and in addition MIDs retain information about fluxes, such as the ratios at branch points and reversibility of biochemical reactions.

Figure 6.11 shows fractional abundances of labeled mass isotopomers for intracellular metabolites at 12 h after the addition of [U-^{13}C]lactate and regulatory agents, Dex, Dib, 8Br and Ins and no addition condition as a control (Con). Interestingly, the MID patterns for the five conditions were very similar. In order to show the similarity of MIDs, we compared the labeled MIDs between conditions for four key metabolite fragments, Asp (*m/z* 418), Cit (*m/z* 459), Mal (*m/z* 419) and AKG (*m/z* 346) in Figure 6.12. As can be seen, MIDs were only slightly different from each other. This result makes is difficult to make statements about significant differences in cellular metabolism between five conditions: Con, Dex, Dib, 8Br and Ins using the MIDs data alone. The similar MID patterns matched with the similar consumption rates of lactate regardless of the introduction of the regulatory agents in Figure 6.8C. ^{13}C-atoms from lactate tracer were directly incorporated into the TCA cycle and the labeling information via TCA cycle was similar for intracellular metabolites. As a result, GNG-related metabolites also had similar MID patterns, e.g. for GLP (*m/z* 571), DHAP (*m/z* 484), 3PG (*m/z* 585) and PEP (*m/z* 453). This suggests that TCA cycle metabolism was not significantly different for the different conditions and the flux distributions would be more dependent on the overall metabolic activities, e.g. consumption rates of lactate, glutamine and amino acids, lipid and ketone body

metabolism and production rates of albumin, rather than measurement data of MIDs for ^{13}C-MFA.

As the MIDs for the five different conditions were similar, we only focused on the control experiment in Figure 6.11(Con) for MID analysis. Initial GNG medium before starting the culture contained 98% composition of [U-^{13}C]lactate. During the culture, it labeled intracellular Lact (*m/z* 261), Ala (*m/z* 260) and Pyr (*m/z* 174). Lact (*m/z* 261) and Ala (*m/z* 260) had 96% and 95% of M3 isotopomers, but Pyr (*m/z* 174) only contained 90% M3. Even if Pyr was junction pool between Lact and Ala, the M3 isotopomer ratio of Pyr decreased and M1 and M2 isotopomers portions were elevated. This difference corresponded to the result of the difference in ^{13}C-labeling between Lact (or Ala) and Pyr in Figure 6.10. Therefore, this suggests that cytosolic Pyr with high M3 isotopomer, ca. 96% was mixed with mitochondrial Pyr containing lower M3 abundance due to atom transitions in TCA cycle.

Next, the M3 isotopomers from Pyr, Lact and Ala were incorporated into the TCA cycle-related metabolites. The C_4 molecules, e.g. Asp (*m/z* 418), Mal (*m/z* 419) and Fum (*m/z* 287), consisted of 7% of M1, 30% of M2, 42% of M3 and 21% of M4 isotopomers. The M1 and M2 isotopomers were built by atom rearrangements in the TCA cycle. It was interesting to observe a high abundance of the M4 isotopomers. This was likely related to high pyruvate carboxylase (PC) and pyruvate dehydrogenase (PDH) fluxes from Pyr. The carbon flow is as follows: Pyr (M3) $\rightarrow$ OAC (M3) by PC; and Pyr (M3) $\rightarrow$ AcCoA (M2) by PDH; OAC (M3) + AcCoA (M2) $\rightarrow$ Cit (M5) by citrate synthase (CS); and Cit (M5) $\rightarrow$ Asp, Fum and Mal (M4) + CO_2 (M1) by oxidation in TCA cycle. Therefore, due to PC, PDH and CS activities, AKG (*m/z* 346), Glu (*m/z* 432) and Cit (*m/z* 431 or *m/z* 459) were M5 labeled. Furthermore, 8% M6

isotopomer of Cit (m/z 459) could result from OAC (M4) by a second turn of the TCA cycle and AcCoA (M2).

Interestingly, MIDs of C_4 molecules, Asp (*m/z* 418), Mal (*m/z* 419) and Fum (*m/z* 287), were different from Suc (*m/z* 289) in the same series of reactions in the TCA cycle. Asp (*m/z* 418), Mal (*m/z* 419) and Fum (*m/z* 287) had 42% of M3 isotopomers, but Suc (*m/z* 289) only had 18%, which was a 2-fold decrease. This can be explained by two different pathways related TCA cycle: (i) reductive carboxylation flux can make more M3 isotopomer on Mal, Asp and Fum. For example, Cit (M5) → OAC (M3) + AcCoA (M2) by ATP citrate lyase (ACL); OAC (M3) ↔ Asp (M3) ↔ Fum (M3) ↔ Mal (M3) ↔ OAC (M3) by reactions between C_4 molecules. (ii) Oxidative metabolism in TCA cycle also can produce M3 isotopomer. For example, Cit (M5) → AKG (M4) + CO2 (M1), AKG (M4) + CO2 (M1) → Suc (M3), Fum (M3), Mal (M3) and Fum (M3). Therefore, the M3 isotopomer of Suc (m/z 289) was only involved in oxidative metabolism and Asp (*m/z* 418), Mal (*m/z* 419) and Fum (*m/z* 287) had mixed M3 isotopomers of oxidative metabolism in TCA cycle and reductive carboxylation from Cit.

The C_3 fragments of TCA cycle metabolites, e.g. Asp (*m/z* 390, C2-C4) and Mal (*m/z* 391, C2-C4) were derived from fragmentization of C_4 fragments Asp (*m/z* 419) and Mal (*m/z* 419) in the mass spectrometer. MIDs of Asp (m/z 390) and Mal (m/z 391) matched well with the measured C_3 fragments of GNG-related metabolites, GLP (*m/z* 571), DHAP (*m/z* 484), 3PG (*m/z* 585) and PEP (*m/z* 453). This provided strong evidence that carbons of metabolites in TCA cycle were transferred to GNG-related metabolites without significant atom transitions. This also indicated that the key junction between gluconeogenesis and TCA cycle was PEPCK reaction.

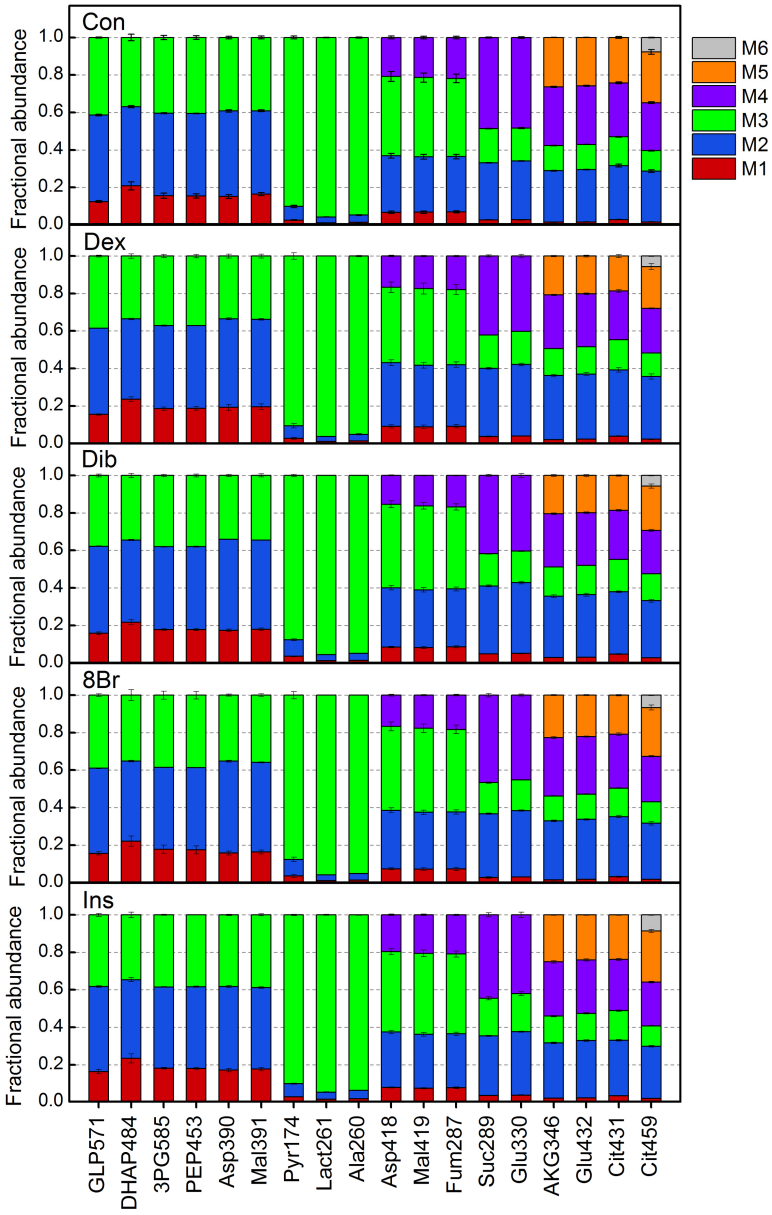

Figure 6.11 Fractional abundances of labeled mass isotopomers at 12 h after the addition of [U-^{13}C]lactate and regulatory agents, dexamethasone (Dex), dibutyryl-cAMP (Dib), 8-bromo-cAMP (8Br) and insulin (Ins) and no addition as a control (Con) for the following metabolite fragments: GLP (*m/z* 571), DHAP (*m/z* 484), 3PG (*m/z* 585), PEP (*m/z* 453), Asp (*m/z* 390), Mal (*m/z* 391), Pyr (*m/z* 174), Lact (*m/z* 261), Ala (*m/z* 260), Asp (*m/z* 418), Mal (*m/z* 419), Fum (*m/z* 287), Suc (*m/z* 289), Glu (*m/z* 330), AKG (*m/z* 346), Glu (*m/z* 432), Cit (*m/z* 431) and Cit (*m/z* 459). MIDs were corrected for natural abundance (SD, n = 3).

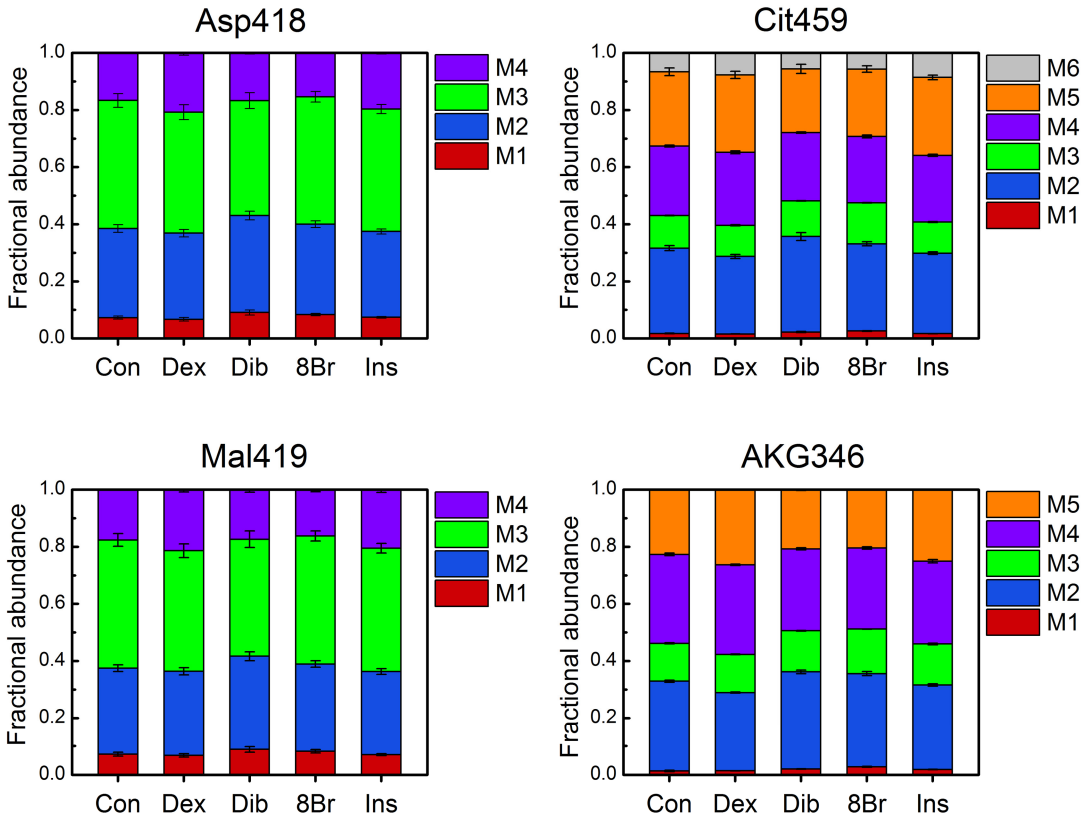

Figure 6.12 Fractional abundance of labeled mass isotopomers for Asp418, Cit459, Mal419 and AKG346 MS fragments labeled by [U-^{13}C]lactate at five conditions; Con, Dex, Dib, 8Br and Ins. The metabolites for GC-MS analysis were extracted at 12 h after addition of isotopic tracers. MIDs were corrected for natural abundance (SD, n = 3).

6.3.2.6 ^{13}C-Labeling Profiles of Intracellular Metabolites for [U-^{13}C]Glutamine Tracer

Using GNG medium containing [U-^{13}C]glutamine tracers, Fao cells were cultured for 12 h, and then the intracellular metabolites were analyzed by GC-MS. Glutamine in medium was transported into the cells and the carbon atoms were incorporated into TCA cycle metabolites. Eventually the carbon atoms from glutamine tracer reached the gluconeogenesis pathway to produce glucose via GNG pathway. To validate these assumptions about carbon flow from glutamine to glucose, we analyzed the levels of ^{13}C-enrichment in intracellular metabolites and arranged them orderly.

Figure 6.13 shows ^{13}C-labeling profiles of intracellular metabolites in terms of the sequence of ^{13}C-enrichments from the highest to the lowest level for [U-^{13}C]glutamine experiment, for five different experimental conditions: additions of Dex, Dib, 8Br and Ins and no addition, Con. ^{13}C-labeling (100% - M0) of Gln fragment at *m/z* 431 in the medium was 76% at 12 h after addition of [U-^{13}C]glutamine tracers. The extracellular glutamine was transported inside the cells and then labeled other intracellular metabolites. In Figure 6.13, the ^{13}C-labeling profiles can be classified by four groups as follows: (i) intracellular Gln (m/z 431) was labeled to 75% of ^{13}C-enrichments at all five experimental conditions. This was the highest values in all intracellular metabolites, and almost at the same levels as extracellular Gln. This indicated that glutamine synthetase (GS) activity was very minimal in Fao rat hepatoma cells. If GS were active, unlabeled Gln produced from Glu would have diluted Gln and decreased ^{13}C-labeling of Gln. (ii) TCA cycle metabolites were in 2nd labeling group. The ^{13}C-labeling of Glu (*m/z* 432), AKG (*m/z* 346), Suc (*m/z* 289), Cit (*m/z* 459), Fum (*m/z* 287), and Mal (*m/z* 419) decreased in that order as sown in Figure 6.13. The sequence from the highest to the lowest labeling by conditions was Dex/8Br,

Ins, Dib and Con. The difference of the highest and the lowest labeling was at most 6% and most trend lines overlapped each other. This suggests that TCA cycle metabolism was not significantly different after the addition of Dex, Dib, 8Br and Ins. (iii) GNG-related metabolites were in 3nd labeling group. The ^{13}C-labeling of PEP (*m/z* 453), 3PG (*m/z* 585) and DHAP (*m/z* 484) decreased in that order. Surprisingly, the sequence of ^{13}C-labeling according to the five GNG conditions were also switched and re-arranged as shown in Figure 6.13. The sequence from the highest to the lowest labeling by conditions was: 8Br, Dex, Dib, Con and Ins. The difference of the largest and the lowest labeling values shows significant gaps, 10% between the values of the GNG-related metabolites at 8Br and Ins. This trend about the highest labeling at 8Br and the lowest at Ins condition by [U-^{13}C]glutamine tracers matched with the experiment with [U-^{13}C]lactate in Figure 6.10. (iv) The final group contained Pyr (*m/z* 174), Lact (*m/z* 261) and Ala (*m/z* 260), related to pyruvate cycle and lactate metabolism. Most labeling percentages were less than 3%. A possible reaction that can label Pyr, Lact and Ala from TCA cycle and gluconeogenesis pathway is pyruvate kinase (PK). Therefore, our results indicated possible low carbon flow from PEP to Pyr via PK.

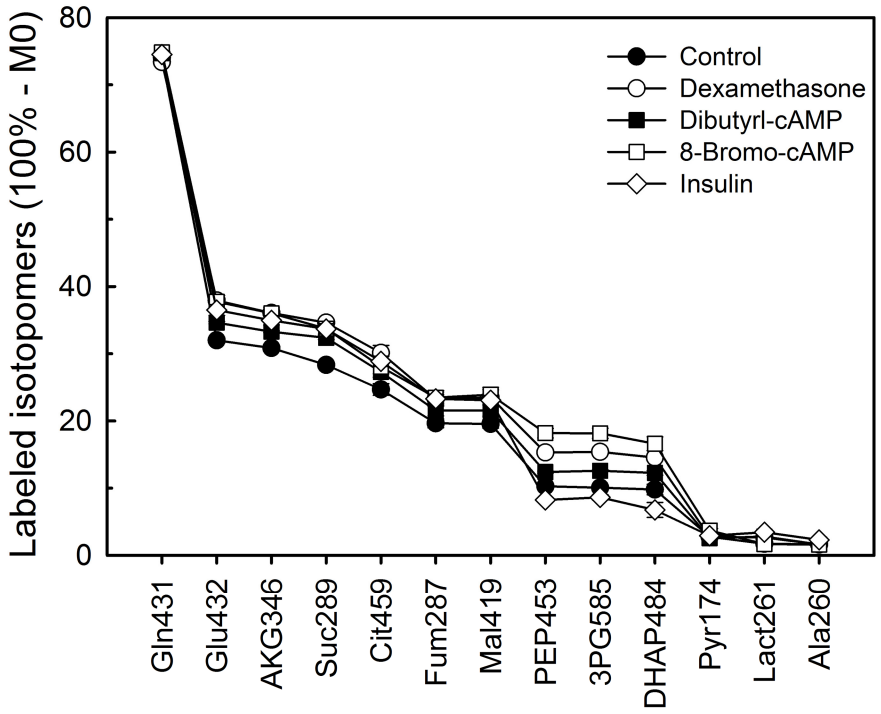

Figure 6.13 ^{13}C-Labeling profiles of intracellular metabolites with [U-^{13}C]glutamine. The metabolites were arranged according to the sequences of the enrichment from the highest (Gln at *m/z* 431) to the lowest level (Ala at *m/z* 260) at [U-^{13}C]glutamine set using five different conditions; the addition of dexamethasone (Dex), dibutyryl-cAMP (Dib), 8-bromo-cAMP (8Br) and insulin (Ins) and no addition for control (Con) (SD, n = 3).

6.3.2.7 Labeled Mass Isotopomer Distributions for [U-^{13}C]Glutamine Tracer

Figure 6.14 shows fractional abundances of labeled mass isotopomers for intracellular metabolites at 12 h after the addition of [U-^{13}C]glutamine and agents for metabolic perturbation, Dex, Dib, 8Br and Ins and no addition as a control (Con). Interestingly, the MID patterns for the five conditions were very similar. This is also the same trend as observed for [U-^{13}C]lactate in Figure 6.11. Figure 6.15 shows very small differences in MIDs between the five conditions for at four representative metabolite fragments, Asp (*m/z* 418), Cit (*m/z* 459), Mal (*m/z* 419) and AKG (*m/z* 346). Thus, it is difficult to extract information about significant differences in cellular metabolism for the five conditions from the MIDs data. ^{13}C-atoms from glutamine tracer were directly incorporated into TCA cycle and the labeling information inscribed into intracellular metabolites via TCA cycle became similar due to limited perturbation by the agents. Eventually, GNG-related metabolites originated from TCA cycle also had the same MID patterns at GLP (*m/z* 571), DHAP (*m/z* 484), 3PG (*m/z* 585) and PEP (*m/z* 453). Thus, this suggests that TCA cycle metabolism was not significantly different for the different experiments by addition of the agents and the similarity of MIDs between conditions was also found at [U-^{13}C]lactate experiment in Figure 6.11 and 6.12.

In this study, we analyzed the MID pattern at Con condition as a representative for all five conditions as shown in Figure 6.14(Con). Composition of [U-^{13}C]lactate in medium was 72%. Labeled isotopomers of Lact at m/z 261 in medium consisted of 94% of M5 isotopomer and 6% of M1 to M4 isotopomers. In Figure 6.14, intracellular Gln fragments also showed same distributions of labeled isotopomers with extracellular Gln. Thus, labeling information of Gln only flowed into Glu irreversibly. If the metabolic reactions between Glu and Gln were reversible, e.g. by glutaminase (GLS)

and glutamine synthetase (GS), the MIDs of intracellular Gln fragments would be similar as Glu fragments. However, the measured MIDs of Glu and Gln were totally different. Thus, we could conclude that Fao cell has no (or very low) activity of GS enzyme.

By glutamate dehydrogenase (GDH), carbon atoms of Glu entered into the TCA cycle through AKG. Interestingly, Glu fragment at *m/z* 432 and AKG at *m/z* 346 had very similar MIDs. This indicated highly reversible reactions between Glu and AKG by GDH or aminotransferase (AT). Furthermore, the MIDs contained information regarding the flux ratio of the branch points between IDH (Cit/ICit → AKG) and GDH (Glu → AKG). The M5 in labeled isotopomers of AKG (*m/z* 346) was 53%, and M1-M4 isotopomers were 47%. Thus, the flux ratio of IDH to GDH was about 1.1 (=53%/47%). This means that the M5 isotopomer of AKG originated from Glu via GDH and M1-M4 isotopomers originated from TCA cycle via IDH.

The M5 isotopomer of Cit at *m/z* 431 and *m/z* 459 reached 27% in total labeled isotopomers (M1 to M5). The M5 isotopomer could be only labeled via backward flux through IDH reaction (AKG → Cit). Thus, the ratio was related to estimation for exchange flux of IDH. Moreover, it was connected to reductive metabolism via ACL (Cit → OAC + AcCoA) for lipid metabolism.

The percentage of M3 isotopomer for Asp (*m/z* 418), Mal (*m/z* 419) and Fum (*m/z* 287) was around 20% in total labeled isotopomers at the C_4 metabolites with four carbon atoms (C_4). However, Suc (*m/z* 289) contained only 3% M3. Therefore, Asp (*m/z* 418), Mal (*m/z* 419) and Fum (*m/z* 287) had 7-fold higher M3 isotopomers than Suc (*m/z* 289). As explained in the previous section 6.3.2.5, the M3 isotopomer of Suc (m/z 289) was only involved in oxidative metabolism and Asp (*m/z* 418), Mal (*m/z*

419) and Fum (*m/z* 287) had mixed M3 isotopomers from oxidative metabolism in the TCA cycle and reductive carboxylation from Cit. As a result, higher M3 isotopomer of Asp, Mal and Fum suggested much higher reductive carboxylation metabolism than oxidative metabolism through the TCA cycle.

As explained in section 6.3.2.5, C_3 fragments with three active carbons, Asp (m/z 390) and Mal (m/z 391) corresponded to C_3 GNG-related metabolites, GLP (*m/z* 571), 3PG (*m/z* 585) and PEP (*m/z* 453). However, DHAP (*m/z* 484) showed different MID pattern compared to the other GNG-related metabolites. The reason is that measurement errors of DHAP (*m/z* 484) were relatively high as shown in Figure 6.13. The matching MIDs between gluconeogenesis and TCA cycle metabolites suggests that carbon atoms from TCA cycle were transferred to GNG-related metabolites without significant atom transitions. The relevant enzyme was PEPCK, which was the key junction flux from TCA cycle to gluconeogenesis (or glycolysis) pathway.

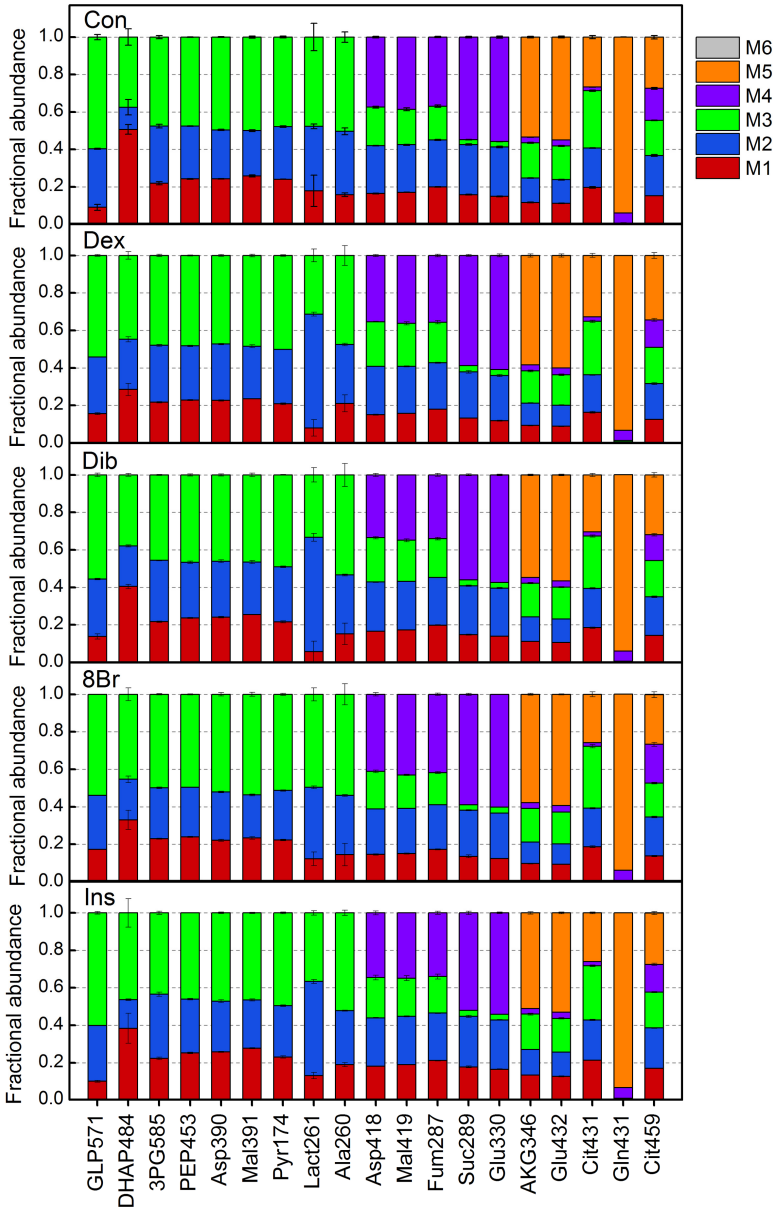

Figure 6.14 Fractional abundances of labeled mass isotopomers at 12 h after the addition of [U-^{13}C]glutamine and regulatory agents. The agents were control (Con), dexamethasone (Dex), dibutyryl-cAMP (Dib), 8-bromo-cAMP (8Br) and insulin (Ins) for the following metabolite fragments: GLP (*m/z* 571), DHAP (*m/z* 484), 3PG (*m/z* 585), PEP (*m/z* 453), Asp (*m/z* 390), Mal (*m/z* 391), Pyr (*m/z* 174), Lact (*m/z* 261), Ala (*m/z* 260), Asp (*m/z* 418), Mal (*m/z* 419), Fum (*m/z* 287), Suc (*m/z* 289), Glu (*m/z* 330), AKG (*m/z* 346), Glu (*m/z* 432), Cit (*m/z* 431), Gln (*m/z* 431) and Cit (*m/z* 459)

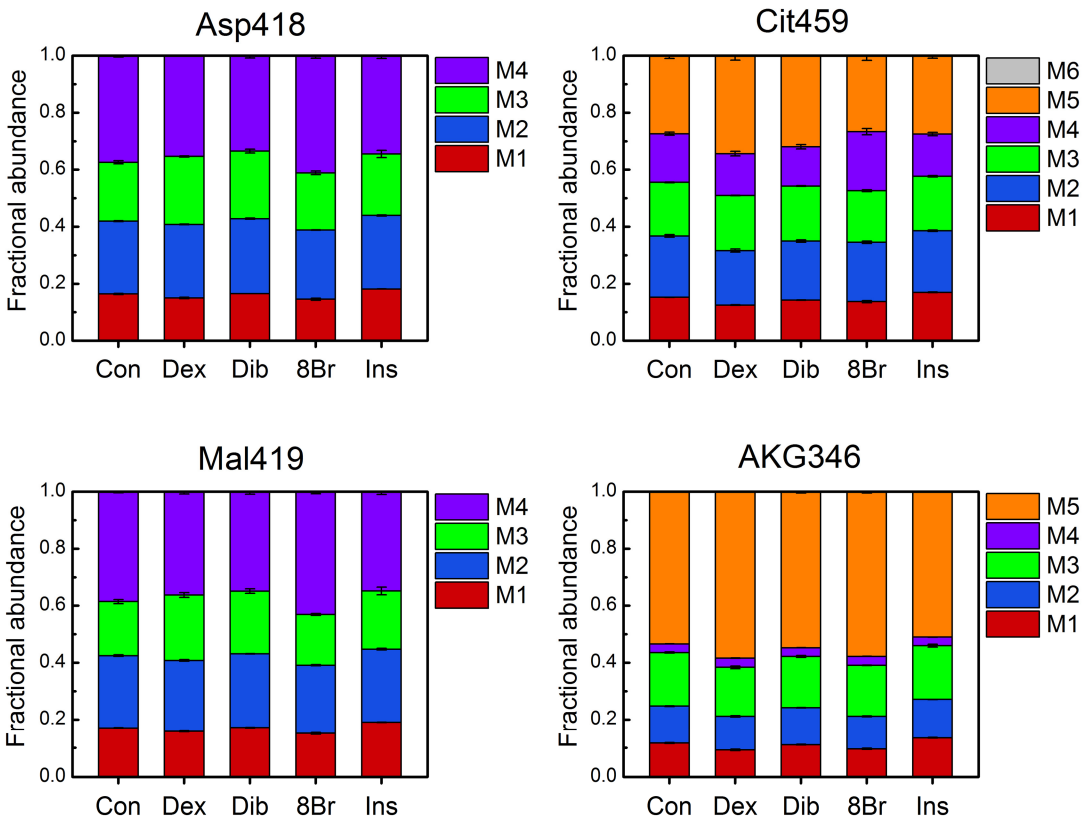

Figure 6.15 Fractional abundance of labeled mass isotopomers of Asp418, Cit459, Mal419 and AKG346. The mass fragments were labeled by [U-^{13}C]glutamine tracers at five conditions; Con, Dex, Dib, 8br and Ins. The metabolites for GC-MS analysis were extracted at 12h after addition of isotopic tracers (SD, n = 3).

6.3.2.8 ^{13}C-Labeling Profiles of Intracellular Metabolites for [U-^{13}C]Glycerol Tracer

Fao cells were cultured for 12 h after replacement with GNG medium containing [U-^{13}C]glycerol as tracer, and then the intracellular metabolites were extracted and analyzed by GC-MS. Glycerol in medium was transported into the cells and incorporated into the gluconeogenesis pathway, and finally carbon atoms from ^{13}C-glycerol tracer reached extracellular glucose.

Figure 6.16 shows ^{13}C-labeling profiles of intracellular metabolites according to the sequence of ^{13}C-enrichments from the highest to the lowest enrichment for [U-^{13}C]glycerol experiment using five different experimental conditions: additions of Dex, Dib, 8Br and Ins and no addition, Con. The percentage of labeled isotopomers at glycerol (m/z 174) in medium was 90% (100% - M0). ^{13}C atoms from [U-^{13}C]glycerol were incorporated into several GNG-related metabolites. The ^{13}C-labeling of DHAP (*m/z* 484), 3PG (*m/z* 585), PEP (*m/z* 453), Ser (*m/z* 390), GLP (*m/z* 571) and Gly (*m/z* 246) decreased in order as shown in Figure 6.16. The ^{13}C-labeling at Ins condition reached the highest level and 8Br experiment showed the lowest level of the five conditions. The labeling of DHAP (*m/z* 484) at Ins was 6-fold higher than at 8Br condition. This suggests that the gluconeogenesis metabolism at Ins condition was significantly dependent on the carbon source from media glycerol and 8Br sets has the lowest dependency on glycerol substrate.

Pyr (*m/z* 174), Asp (*m/z* 418) and AKG (*m/z* 346) had less than 3% labeling, ^{13}C-enrichments of labeled isotopomers (100% - M0). However, only Pyr (*m/z* 174) at Dex condition showed 9% labeling of labeled isotopomers. Possible pathway for labeling of Pyr was via PK (PEP $\rightarrow$ Pyr), one of the key glycolysis enzymes. It

implied that dexamethasone (Dex) slightly activated the glycolysis pathway via PK enzyme as well as PEPCK activation for gluconeogenesis pathway.

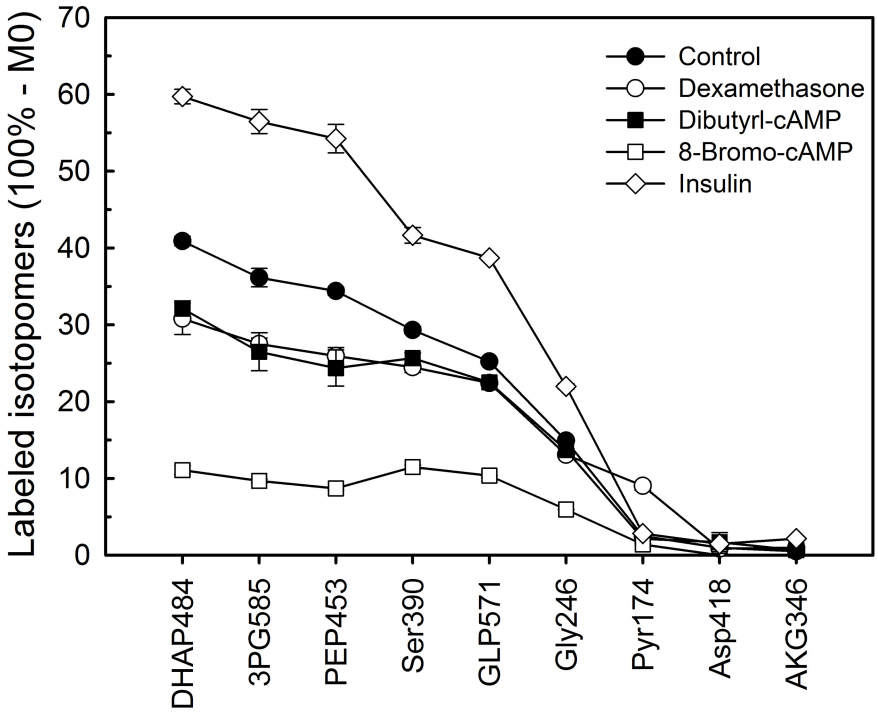

Figure 6.16 ^{13}C-Labeling profiles of intracellular metabolites with [U-^{13}C]glycerol. The metabolites were arranged according to the sequences of the enrichment from the highest (DHAP) to the lowest level (AKG) at [U-^{13}C]glycerol set using five different conditions; control (no addition), dexamethasone, dibutyryl-cAMP, 8-bromo-cAMP and insulin (Span/2, n = 2).

6.3.2.9 Labeled Mass Isotopomer Distributions for [U-^{13}C]Glycerol Tracer

In addition to determining the percentage of labeled isotopomers (100% - M0), fractional abundance of labeled isotopomers for intracellular metabolites and extracellular glucose were measured by GC-MS at 12 h after introduction of [U-^{13}C]glycerol. The fractional abundance was only considered for labeled isotopomers that did not contain ^{12}C atoms (M0 isotopomers).

Figure 6.17 shows fractional abundances of labeled mass isotopomers of F6P fragment at *m/z* 364 and Gluc.ext at *m/z* 284, 370, 301, 259 and 173 from glucose in medium, which were labeled by [U-^{13}C]glycerol as tracer at five conditions; Con, Dex, Dib, 8br and Ins. As shown in Figure 6.17, carbon positions of F6P (*m/z* 364), Gluc.ext (*m/z* 284), Gluc.ext (*m/z* 370), Gluc.ext (*m/z* 301), Gluc.ext (*m/z* 259) Gluc.ext (*m/z* 173) were C1-C4, C1-C4, C1-C5, C1-C6, C4-C6 and C5-C6, respectively. Figure 6.19A shows only the simple gluconeogenesis pathway to produce glucose from glycerol ([U-^{13}C]glycerol) and TCA cycle source (OAC) without transketolase (TK) activity in non-oxidative pentose phosphate pathway (PPP) and the reversibility of fructose-bisphosphate aldolase (ALD) for glycolysis. The possible mass isotopomers for the four fragments can be explained as follows: (i) F6P (*m/z* 364) contains M0, M1, M3 and M4. (ii) Gluc.ext (*m/z* 284) contains M0, M1, M3 and M4. (iii) Gluc.ext (*m/z* 370) contains M0, M2, M3 and M5. (iv) Gluc.ext (*m/z* 301) contains M0, M3 and M6. In addition, Gluc.ext (*m/z* 259) contains only M3 and Gluc.ext (*m/z* 173) has only M2 isotopomer, which was not shown in Figure 6.19A. Interestingly, the measured data in Figure 6.17 showed that F6P (*m/z* 364) and Gluc.ext (*m/z* 284) had an additional M2 isotopomer, Gluc.ext (*m/z* 370) had M1 and M4 isotopomers, and Gluc.ext (*m/z* 301) had M1 and M4 isotopomers. Only Gluc.ext fragments at *m/z* 259 and 173 corresponded well with the anticipated isotopomer in

Figure 6.19A. To explain the atom transitions in measured data, TK reversibility was introduced to the metabolic model. TK in non-oxidative PPP exchanges a two-carbon unit at C1-C2 position in F6P with C1-C2 molecules in the pool of non-oxidative PPP. Thus, C1 and C2 atoms in F6P became a mixture of ^{12}C and ^{13}C atoms as shown in Figure 6.19B. By considering TK reversibility, the broad spectrum of labeled isotopomers in Figure 6.16 can be explained. In addition, this suggests that high reversibility of TK can increase the proportion of M1 isotopomers as explained in Figure 6.19B. The fractional abundances of M1 isotopomers in labeled isotopomers at Con, Dex, Dib, 8Br and Ins conditions were 40%, 47%, 46%, 63% and 31% at F6P fragment at *m/z* 364, respectively. For all fragments, 8Br condition showed the highest M1 ratios and Ins condition had the lowest M1 ratios. Therefore, this indicated that TK reversibility was higher at 8Br condition and lower at Ins condition.

Figure 6.18 shows fractional abundances of labeled mass isotopomers for F6P (*m/z* 307), DHAP (*m/z* 484), 3PG (*m/z* 585) and PEP (*m/z* 453) fragments from intracellular metabolites labeled by [U-^{13}C]glycerol tracer at five conditions: Con, Dex, Dib, 8br and Ins. As shown in Figure 6.19, carbon positions of F6P (*m/z* 307) were C4-C6 and triose phosphate fragments, DHAP (*m/z* 484), 3PG (*m/z* 585) and PEP (*m/z* 453) have the active carbon position of C1-C3. Figure 6.19A shows possible labeling of F6P (*m/z* 307), DHAP (*m/z* 484), 3PG (*m/z* 585) and PEP (*m/z* 453) fragments in case of simple gluconeogenesis pathway. The possible mass isotopomers based on Figure 6.19A are only M0 and M3 isotopomers at the four fragments. However, Figure 6.18 shows M1 and M2 isotopomers as well as large abundance of M3 isotopomers. The purity of [U-^{13}C]glycerol in the medium was measured as 98% purity and 2% impurity. Thus, the 2% impurity could have influenced the M1 and M2

isotopomers of intracellular metabolites. As shown in Figure 6.18, the fractional abundances of M1 and M2 isotopomers at four condition, Con, Dib, 8Br and Ins were less than 8% and interestingly, the abundances at Dex condition reached 14%-20% of M1 and M2 isotopomers. Even if the impurity of ^{13}C-glycerol tracers was counted for M1 and M2 contamination of intracellular metabolites, M1 and M2 proportion was high for all five conditions, and surprisingly, Dex condition showed significantly increased values. This can be explained as shown in Figure 6.19B. By TK reversibility, partial labeled F6P at C1 and C2 atom positions was transferred to triose 3-phosphate metabolites, DHAP, GAP, 3PG and PEP by activation of glycolysis enzyme, phosphofructokinase (PFK) and the reversibility of fructose-bisphosphate aldolase (ALD). Thus, M1 and M2 isotopomers originated from F6P reached the triose 3-phosphate molecules. Furthermore, the level of M1 and M2 isotopomers correlated with the extent of PFK activity and ALD reversibility.

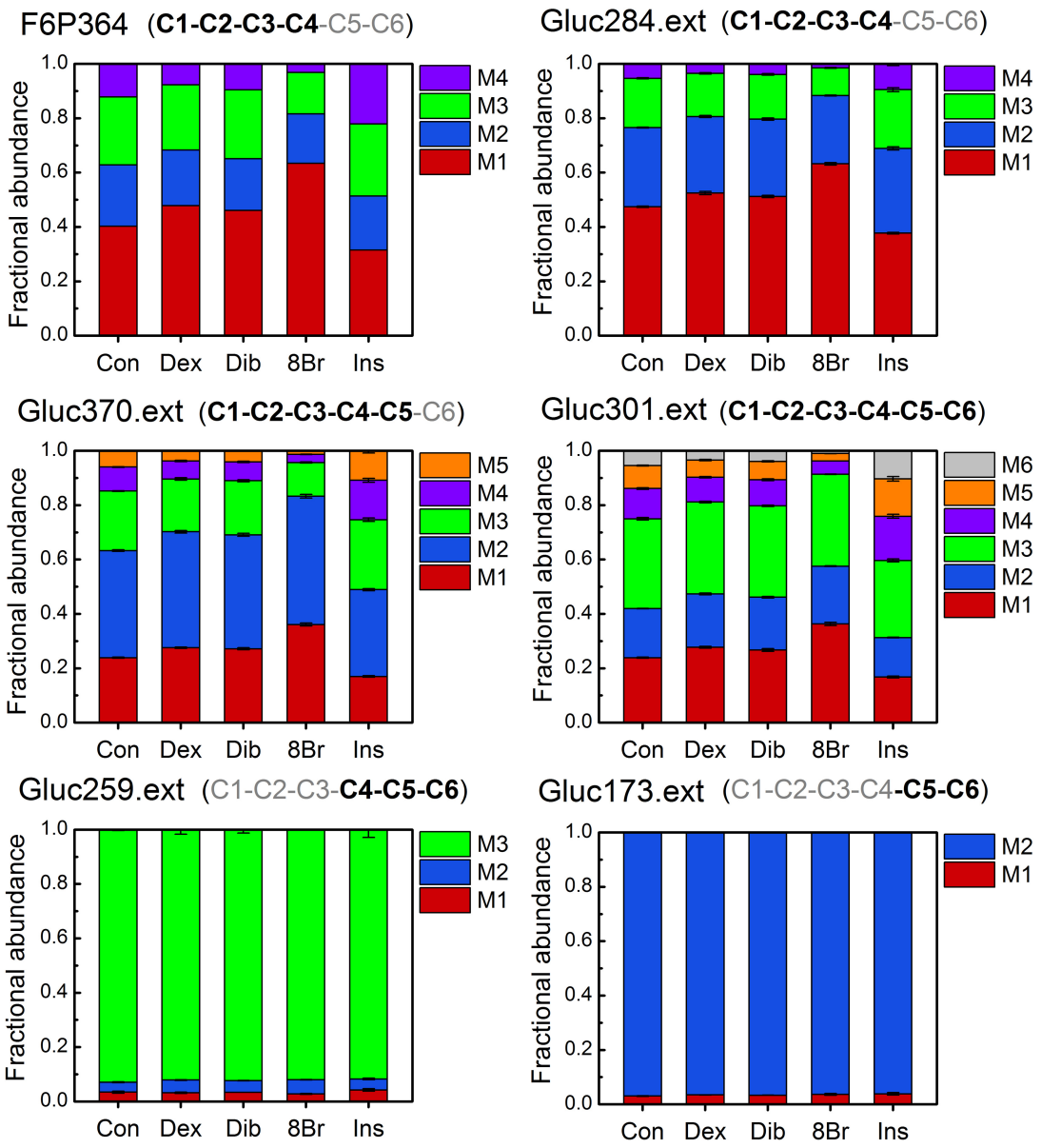

Figure 6.17 Fractional abundances of labeled mass isotopomers of F6P (*m/z* 364) fragment from intracellular metabolite and Gluc (*m/z* 284), Gluc *(m/z* 370), Gluc (*m/z* 301), Gluc (*m/z* 259) and Gluc (*m/z* 173).ext fragments from media glucose labeled by [U-^{13}C]glycerol tracers at five conditions; Con, Dex, Dib, 8br and Ins. The metabolites for GC-MS analysis were extracted at 12h after addition of isotopic tracers (Span/2, n = 2; F6P364 data from one flask sample). Gluc.ext means extracellular glucose.

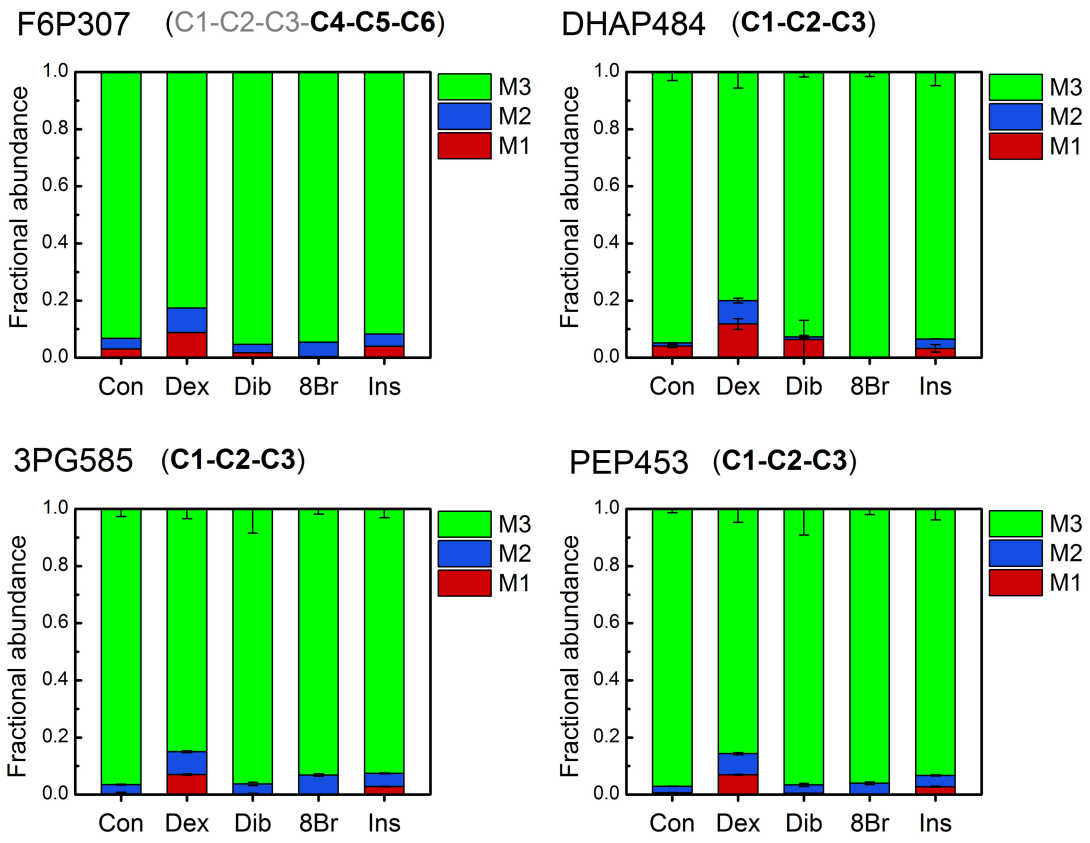

Figure 6.18 Fractional abundances of labeled mass isotopomers of F6P (*m/z* 364), DHAP (*m/z* 484), 3PG (*m/z* 585) and PEP (*m/z* 453) fragments from intracellular metabolites labeled by [U-^{13}C]glycerol tracer at five conditions; Con, Dex, Dib, 8Br and Ins. The metabolites for GC-MS analysis were extracted at 12 h after addition of isotopic tracers (Span/2, n = 2; F6P307 from one flask sample).

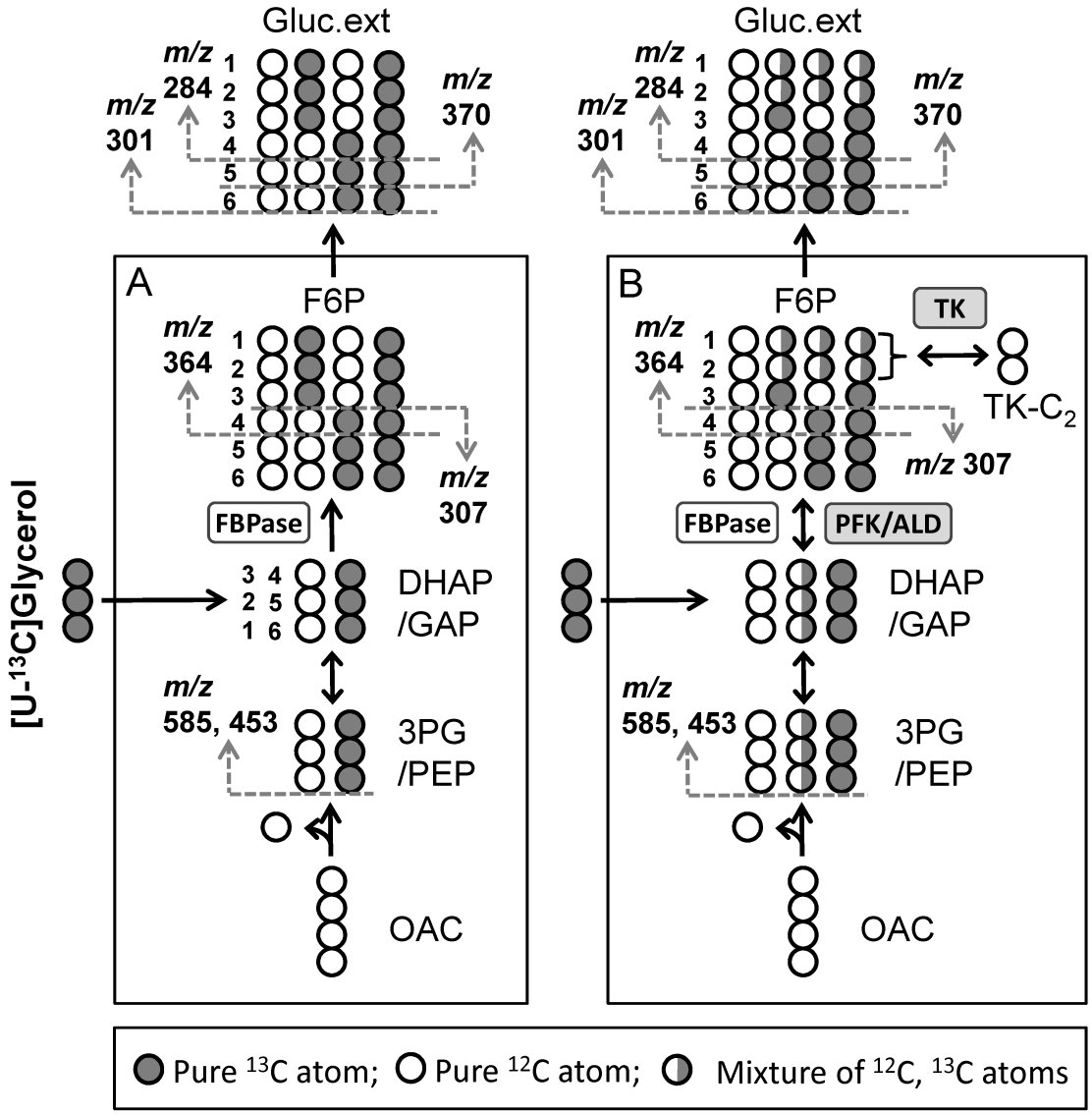

Figure 6.19 Schematic diagram of atom transitions related to transketolase (TK), phosphofructokinase (PFK) and fructose-bisphosphate aldolase (ALD) in non-oxidative PP and gluconeogenesis pathways for [U-^{13}C]glycerol tracer. (A) Gluconeogenesis pathway without reversibility of TK and ALD and (B) with reversibility of TK and ALD. Mass fragments as follow; F6P at *m/z* 364 (C1-C4) and *m/z* 307 (C4-C6), DHAP at *m/z* 484 (C1-C3), GAP at *m/z* 585 (C1-C3), PEP at *m/z* 453 (C1-C3), and Gluc.ext at *m/z* 284 (C1-C4), *m/z* 370 (C1-C5) and *m/z* 301 (C1-C6).

6.3.3 Metabolic Model of Gluconeogenesis

A detailed metabolic network models was constructed for Fao rat hepatoma cells for ^{13}C-metabolic flux analysis. The model consisted of 82 reactions and 55 balanced metabolites and included reactions for gluconeogenesis, glycolysis, oxidative and non-oxidative PPP, glycerol, glycogen, pyruvate, lactate metabolism, tricarboxylic acid (TCA) cycle and amino acid metabolism, ketone body (KB) and albumin metabolism as described in Table 6.4 (at the end of this chapter). In order to evaluate amino acid metabolism, production and consumption rates of amino acids in the medium were added as input and output fluxes as shown in Table 6.3. The reaction for albumin production was built based on amino acid composition of *Rattus norvegicus* albumin (GenBank: AAH8539.1). In addition, KB production was considered to account for large consumption of lactate from medium as shown in Figure 6.8C. PP pathways were introduced to the model based on the measured MIDs data in Figure 6.17 and 6.18. Representative glycolysis reactions, PFK and PK were introduced to the network model as one reversible flux (v4) considering the results in Figure 6.19 for PFK activity and Figure 6.16 for PK activity. In the model, PEPCK was a key flux of gluconeogenesis metabolism to explain ^{13}C-labeling profiles in Figure 6.10, 6.13 and 6.16. In the TCA cycle and pyruvate cycle, malic enzyme (ME) was separated into a cytosolic ME (MEc) and mitochondrial ME (MEm) to evaluate differential activity. Glycerol metabolism was linked to lipid metabolism via GLP metabolite as well as gluconeogenesis and glycolysis pathways. The input flux of fatty acids from medium and β-oxidation of fatty acids were also introduced in the network model.

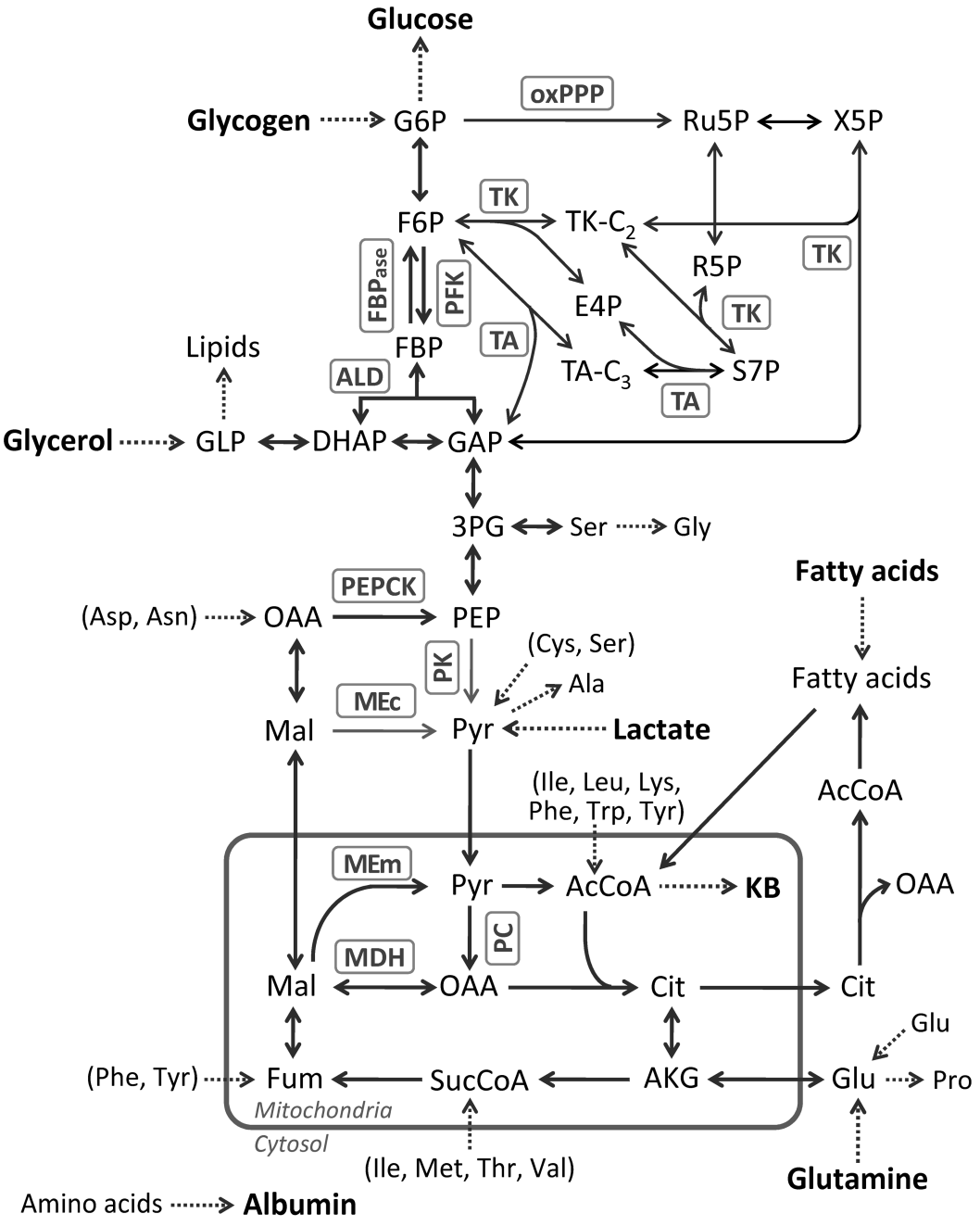

Figure 6.20 Biochemical network of gluconeogenesis pathway. ^{13}C-Metabolic flux analysis was performed by combined analysis with two data sets from [U-^{13}C]glycerol and [U-^{13}C]glutamine. The dotted lines show fluxes with extracellular metabolites (amino acids, albumin, ketone body (KB), glycerol, fatty acids, and glucose) and with intracellular storage (glycogen).

6.3.4 Metabolic Flux Analysis

Metabolic fluxes in Fao rat hepatoma cells were determined using combined flux analysis. The fluxes were estimated with multiple tracer data from [U-^{13}C]glycerol and [U-^{13}C]glutamine tracers that were fitted simultaneously to a single flux model, shown schematically in Figure 6.20. For ^{13}C-MFA, we fitted the MIDs for Gluc.ext (*m/z* 173, 259, 284, 370, 301), F6P (*m/z* 307), DHAP (*m/z* 484), 3PG (*m/z* 585), PEP (*m/z* 453), GLP (*m/z* 571) and Pyr.c (*m/z* 174) for [U-^{13}C]glycerol tracer experiments; and Lact (*m/z* 233, 261), Ala (*m/z* 232, 260), GLP (*m/z* 571), 3PG (*m/z* 585), PEP (*m/z* 453), Pyr.c (*m/z* 174), Cit.m (*m/z* 431, 459), AKG (*m/z* 346), Glu (*m/z* 330, 432), Mal.m (*m/z* 419), Asp (*m/z* 390, 418), Pro (*m/z* 258, 286), and Gln (*m/z* 431) for [U-^{13}C]glutamine tracer experiments. Extracellular uptake/production rates are shown in Table 6.3. We obtained five fitted results by combined ^{13}C-MFA. The minimized variance-weighted sum of squared residuals (SSR) values were 83.7 for Con, 102.1 for Dex, 56.7 for Dib, 69.5 for 8Br and 118.4 for Ins conditions. The lower and upper bounds for the 95% confidence region of SSR were 92.4 and 156.7, respectively, assuming χ^2-distribution for SSR with 58 redundant measurements. Con, Dex and Dib conditions showed slightly over-determined fits. The complete flux results are given in Appendix D (see Tables D.1-D.5), including 95% confidence intervals for all estimated fluxes.

Figure 6.21 shows the input and output fluxes in the gluconeogenesis pathways after estimation with combined ^{13}C-MFA. Input fluxes to gluconeogenesis pathways were glycogen degradation, glycerol consumption, and PEP to 3PG fluxes; and output fluxes from gluconeogenesis metabolism were glucose production, glycerol (GLP) to lipid, and CO_2 generation flux via oxidative PPP. As shown in Figure 6.21A, the total input flux to gluconeogenesis (GNG) flux at 8Br condition (96.9 $\pm$ 7.8 μmol/L/h)

increased 2.6-fold compared to Ins (37.8 ± 7.3 μmol/L/h). Furthermore, Con, Dex and Dib conditions showed similar fluxes, 62.7 ± 6.5, 56.6 ± 5.7 and 65.9 ± 7.2 μmol/L/h, respectively. The PEP to 3PG flux was involved in enolase (ENO, PEP → 2PG) and phosphoglycerate mutase (PGM, 2PG → 3PG). The ENO/PGM flux changed drastically in the flux distribution of the input fluxes. Surprisingly, the ENO/PGM flux at 8Br condition (83.0 ± 6.2 μmol/L/h) increased 3.8-fold higher compared to Con (21.6 ± 2.8 μmol/L/h), but the ENO/PGM flux at Ins (1.5 ± 3.4 μmol/L/h) decreased 14.0-fold compared to Con condition. In addition, the consumption flux of glycerol at 8Br (13.9 ± 1.1 μmol/L/h) decreased 2.5-fold compared to Con (34.4 ± 3.1 μmol/L/h). Except 8Br condition, there were no significant differences for the fluxes of Con, Dex (33.4 ± 2.0 μmol/L/h), Dib (30.8 ± 3.2 μmol/L/h) and Ins (33.6 ± 3.3 μmol/L/h). Thus, 8-bromo-cAMP (8Br) significantly rewired ENO/PGM flux and glycerol metabolism and insulin (Ins) suppressed ENO/PGM flux.

As shown in Figure 6.21B, most of the carbon sources for gluconeogenesis pathway were utilized for glucose production at Dex condition (30.3 ± 2.1 μmol/L/h) and were less dependent on glucose production at Ins (6.6 ± 0.5 μmol/L/h), as the flux ratios of glucose production to total output at Con, Dex, Dib, 8Br and Ins were 0.4, 0.8, 0.5, 0.4 and 0.2, respectively. 8Br condition showed three interesting results: (i) the flux of glycerol to lipid pool at 8Br (44.7 ± 7.8 μmol/L/h) increased 2.5-fold compared to Con (17.7 ± 4.8 μmol/L/h) and there was no flux at Dex condition. (ii) The flux ratios of glucose production to ENO/PGM flux at Con, Dex, Dib, 8Br and Ins were 1.1, 1.7, 0.9, 0.3 and 4.4, respectively. (iii) The flux ratios of glycerol consumption to ENO/PGM flux at Con, Dex, Dib, 8Br and Ins were 1.6, 1.9, 1.0, 0.2 and 22.4,

respectively. Therefore, our results suggest that large influx through ENO/PGM flux flowed into lipid pool via GLP at 8Br condition, based on the three results.

Figure 6.22 shows intracellular fluxes of gluconeogenesis pathway, i.e. glucose-6-phosphate isomerase (GPI), aldolase (ALD, net and exchange fluxes), oxidative PPP and TK (net and exchange fluxes). Overall, the metabolic activities of GPI were similar at Con (29.8 ± 3.2 μmol/L/h), Dex, (30.1 ± 7.6 μmol/L/h), Dib (33.2 ± 4.3 μmol/L/h) and 8Br (26.1 ± 9.5 μmol/L/h), but the fluxes at Ins condition (5.8 ± 4.7 μmol/L/h) reduced 6-fold. Furthermore, ALD showed similar trends as GPI. Interestingly, the exchange flux of ALD at Dex condition showed significantly high values, 5.1 μmol/L/h compared to other conditions, i.e. Con (0.0 ± 0.7 μmol/L/h), Dib (0.0 ± 0.8 μmol/L/h) and 8Br (0.0 ± 1.1 μmol/L/h). Using Eq. 1.4, exchange flux was defined as the minimum flux of forward and backward fluxes, and net flux is defined as the difference of the forward and backward fluxes. Thus, the exchange flux at Dex correlated with the backward flux (i.e. min) of ALD, i.e. (FBP $\rightarrow$ DHAP + GAP), which was related to metabolic activity for glycolysis. Thus, ^{13}C-MFA quantified glycolysis activity as well as gluconeogenesis activity at the Dex condition. In addition, we estimated oxidative PPP (oxPPP) fluxes at Con (12.7 ± 3.1 μmol/L/h), Dex (5.6 ± 7.5 μmol/L/h), Dib (13.2 ± 3.4 μmol/L/h), 8Br (0 ± 8.6 μmol/L/h) and Ins (1.8 ± 5.2 μmol/L/h); however, it was difficult to compare them due to low flux observability. Surprisingly, the exchange fluxes of TK were estimated to almost one order higher values at Con (98.5 ± 12.3 μmol/L/h), Dex (122.6 ± 17.7 μmol/L/h), Dib (127.9 ± 18.9 μmol/L/h), 8Br (148.9 ± 42.05 μmol/L/h) and Ins (29.7 ± 4.7 μmol/L/h) than other fluxes as well as net flux of TK. In the exchange flux, 8Br condition has the highest

values, and the results correlated well with the previous MID analysis in Figure 6.17 and 6.19.

Figure 6.23 shows intracellular fluxes related to pyruvate cycling for PEPCK, PK, PDH, PC, pyruvate transportation (PyrTP), malate dehydrogenase (MDH), cytosolic ME (ME.c) and mitochondrial ME (ME.m). At the center of PEP, three key fluxes were combined and controlled by ENO/PGM flux (PEP $\rightarrow$ 3PG), PEPCK (OAC $\rightarrow$ PEP), and PK (PEP $\rightarrow$ Pyr). In Figure 6.21A, only ENO/PGM flux at 8Br was most activated than Con, Dex, Dib and Ins conditions for gluconeogenesis. However, two PEPCK fluxes at Dex (81.4 ± 9.0 μmol/L/h) and 8Br (89.4 ± 14.1 μmol/L/h) were 2 to 3-fold higher than Con (31.7 ± 5.0 μmol/L/h), Dib (40.2 ± 7.1 μmol/L/h) and Ins (14.6 ± 3.3 μmol/L/h) in Figure 6.23. Thus, the high PEPCK flux at Dex was by-passed to another flux, i.e. PK. The estimated flux of PK at Dex (64.0 ± 11.6 μmol/L/h) increased significantly, 6 to 10-fold higher than at other conditions. This provides strong evidence that Dex up-regulated glycolysis pathway as well as gluconeogenesis pathway. This result matched with the previous analysis in Figure 6.13. The ratios of PDH to PC at Con, Dex, Dib, 8Br and Con were 2.3, 2.5, 2.2, 1.3 and 3.3, respectively. This suggests that insulin (Ins) elevated oxidative metabolism in TCA cycle and that the anabolic reaction by PC was the highest at 8Br condition. In Figure 6.23, most of ME.c fluxes were inactivated, except 8Br condition, and ME.m fluxes were highly activated instead ME.c flux at all conditions. This is also a new finding of this study.

Intracellular fluxes related to TCA cycle were shown in Figure 6.24. Overall, most of the fluxes were in the same order of magnitude and 8Br condition had slightly higher values than other conditions. Albumin flux at Ins (61.0 ± 7.4 μmol/L/h)

condition increased 2-fold compared to Con (32.6 ± 3.0 μmol/L/h), Dex (32.0 ± 2.3 μmol/L/h) and Dib (32.1 ± 4.2 μmol/L/h) conditions. Thus, this provides one possible explanation regarding high consumption rates of amino acids in Table 6.3 and Figure 6.9.

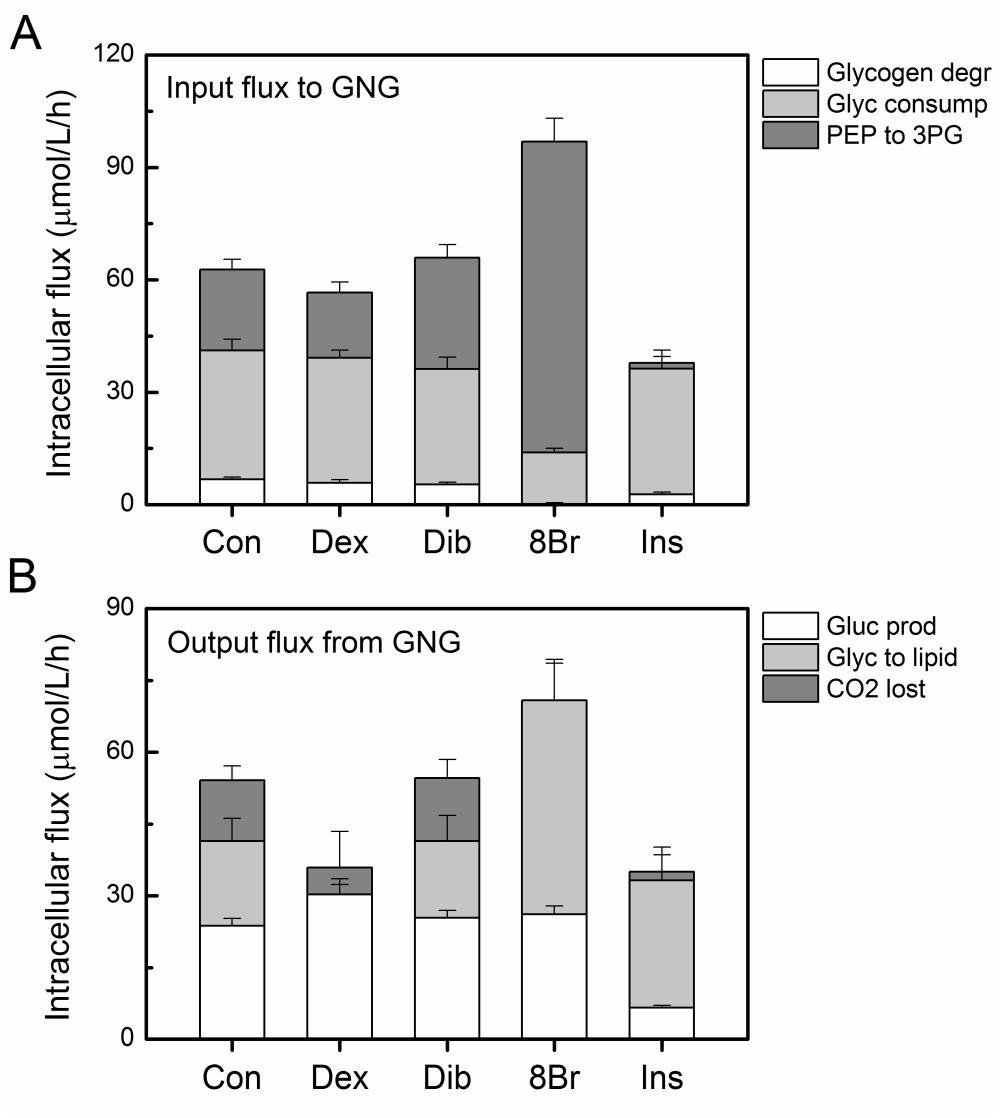

Figure 6.21 Input (A) and output (B) fluxes of gluconeogenesis pathways. Input fluxes consisted of glycogen degradation, glycerol consumption and PEPCK flux and output fluxes had glucose production, glycerol to lipid flux, CO_2 losing via oxidative PPP.

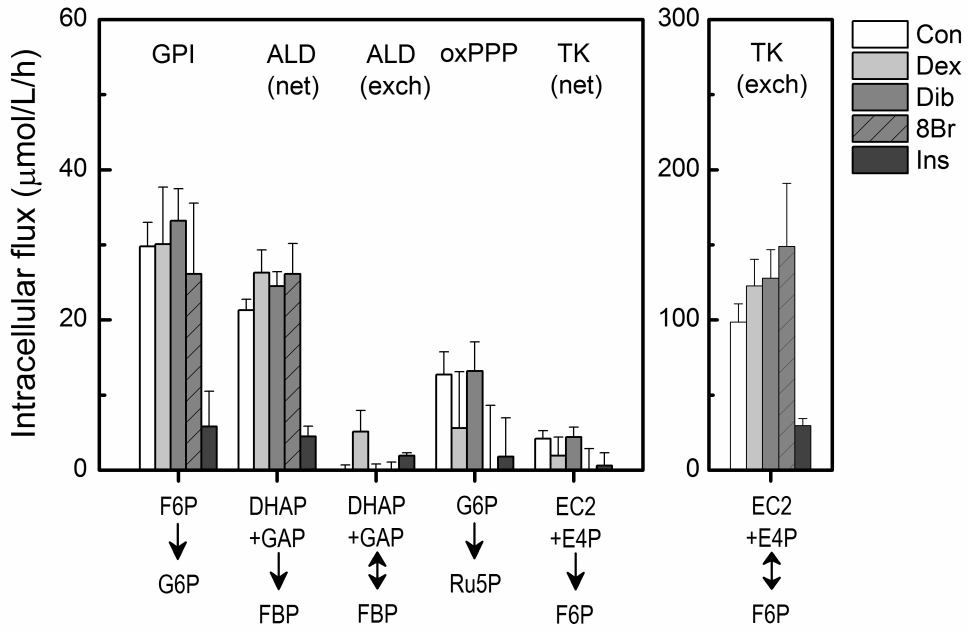

Figure 6.22 Intracellular fluxes related to gluconeogenesis pathway.

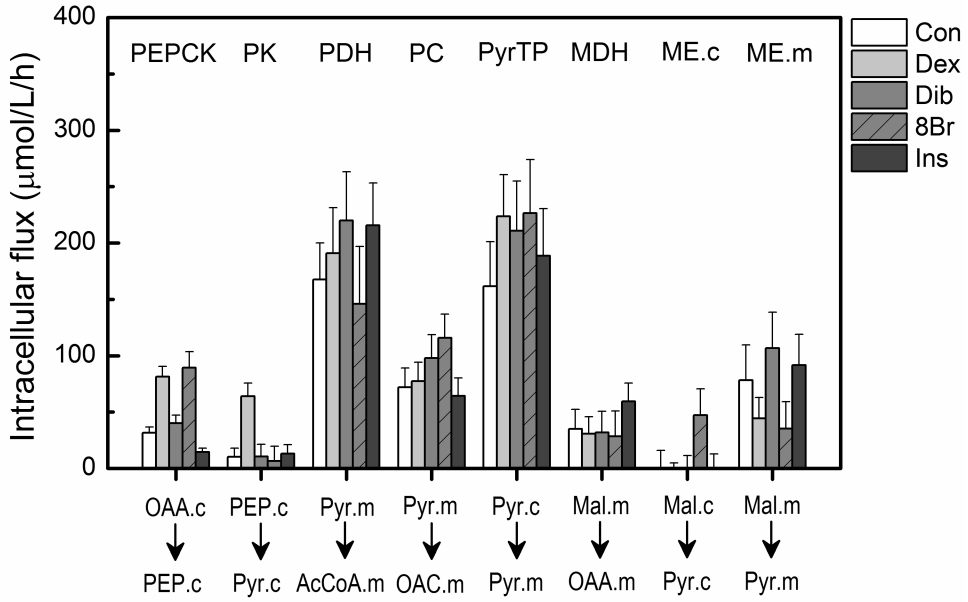

Figure 6.23 Intracellular fluxes related to pyruvate cycling.

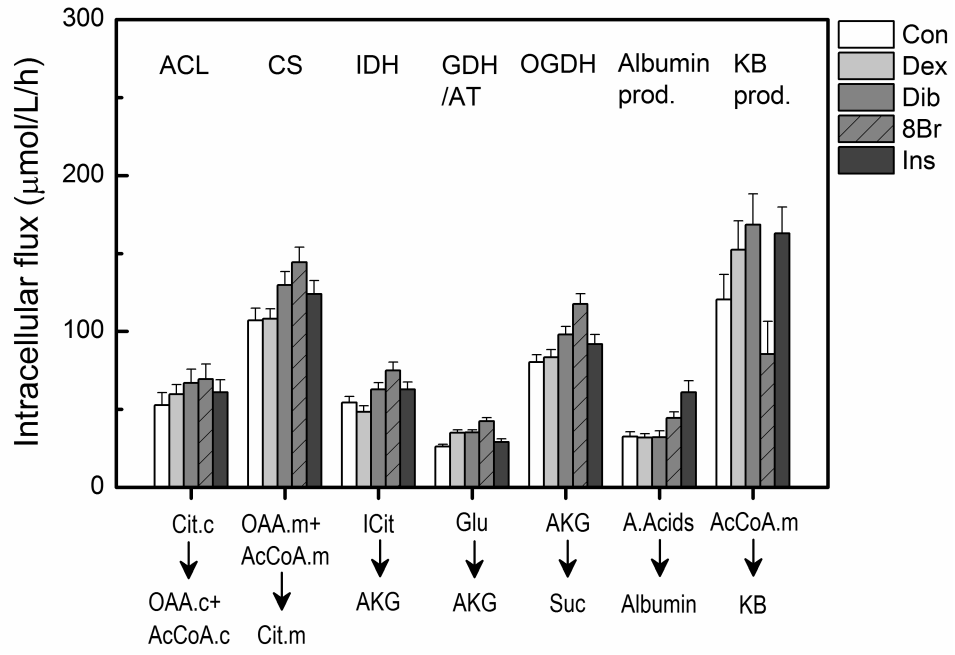

Figure 6.24 Intracellular fluxes in the TCA cycle and related pathways.

6.4 Discussion

In this study, we quantified for the first time metabolic fluxes of Fao rat hepatoma cells using isotopic tracers and GC-MS analysis in order to investigate the regulation of gluconeogenesis metabolism. Fao cells were cultured in glucose-free medium containing one of three different isotopic tracers, [U-^{13}C]glycerol, [U-^{13}C]lactate, or [U-^{13}C]glutamine. After intracellular metabolites were extracted and analyzed by GC-MS, we evaluated ^{13}C-labeling information of intracellular and extracellular metabolites and constructed a detailed metabolic model for gluconeogenesis metabolism. The metabolic model covered most of central metabolism, including: gluconeogenesis and glycolysis metabolism, glycogenolysis,

oxidative and non-oxidative pentose phosphate pathways, fatty acid metabolism with β-oxidation and biosynthesis through ACL, pyruvate metabolism containing anabolic and catabolic reactions, lactate metabolism, amino acid metabolism, metabolism for production of ketone body and albumin. This is the first comprehensible model to study gluconeogenesis and related metabolism. Until now, gluconeogenesis had been studied only using very simplified metabolic model. For examples, gluconeogenesis metabolism was investigated with various tracers: deuterium water (Antoniewicz et al., 2011; Arnoldi et al., 1998; Guo et al., 1992), [U-^{13}C]propionate tracer (Burgess et al., 2004; Jones et al., 2001; Weis et al., 2004) and ^{13}C-glucose tracers (Jin et al., 2004; Jones et al., 1998). However, most of the previous studies only contained limited metabolic reactions, e.g. short cut pathways of gluconeogenesis and simple TCA cycle models. In this study, we proposed a detailed metabolic model covering most of central metabolisms and estimated intracellular fluxes in this model. Significantly, this is the first time that amino acids and pentose phosphate metabolism were quantified. In addition, the estimated flux maps covered key branch point fluxes, parallel fluxes and exchange fluxes, as well as irreversible fluxes using a novel methodology for ^{13}C-MFA.

In this study, the gluconeogenesis experiment at dexamethasone (Dex) condition showed parallel activation of PK for glycolysis, and PEPCK for gluconeogenesis. ^{13}C-Labeling of metabolites in gluconeogenesis pathways at Dex was higher than at Con and Ins conditions for experiments with [U-^{13}C]lactate tracer (Figure 6.10) and [U-^{13}C]glutamine (Figure 6.13). This indicates that ^{13}C-atom flow through PEPCK at Dex condition was more activated than at Con and Ins conditions. In addition, using [U-^{13}C]glycerol tracers (Figure 6.15), ^{13}C-enrichments of GNG-

related metabolites at Dex condition were lower than at Con and Ins conditions. In other words, dilution flux via PEPCK at Dex was higher than at Con and Ins conditions. Thus, PEPCK at Dex condition was activated more than at Con and Ins conditions. Through combined ^{13}C-MFA, we determined that PEPCK flux at Dex increased 2.6-fold compared to Con and 5.6-fold compared to Ins condition. Surprisingly, PK, a representative glycolysis enzyme, was activated by glucocorticoid, Dex. In Figure 6.16, only Dex condition showed ^{13}C-labeling in Pyr from [U-^{13}C]glycerol tracer, while other conditions did not show any labeling in Pyr. This could only be explained by activation of PK. As a result of ^{13}C-MFA in Figure 6.23, PK flux at Dex conditions increased 6-fold higher compared to any other conditions in this study. It corresponded well with the previous report that PK and PEPCK fluxes were elevated simultaneously by Dex addition in primary hepatocytes (Jones et al., 1993). A novel observation in this study is that we observed higher glycolytic fluxes via other glycolysis enzymes as well as PK. Figure 6.18 showed higher proportion of M1 and M2 isotopomers in F6P (*m/z* 307), DHAP (*m/z* 484), 3PG (*m/z* 585) and PEP (*m/z* 453), especially at Dex. This is also strong evidence that Dex activated other glycolytic fluxes, i.e. backward fluxes of gluconeogenesis from F6P to PEP through phosphofructokinase (PFK, F6P $\rightarrow$ FBP) and aldolase (ALD, FBP $\rightarrow$ DHAP + GAP), as well as PK. In Figure 6.22, the exchange flux of ALD showed activity of the backward flux of ALD at Dex, but Con, Dib and 8Br had no glycolytic activities.

For the first time, pentose phosphate pathway (PPP) was estimated by ^{13}C-MFA in hepatic gluconeogenesis metabolism in this study. Importantly, Fao rat hepatoma cells showed high non-oxidative PPP activity by the reversibility of TK in Figure 6.17 and 6.19. Classic MFA based using stoichiometric balances, or traditional

MIDA technique cannot estimate this branch point and reversibility of enzymes. For example, Chan et. al. assumed that oxidative PPP was estimated by lumped reaction by NADPH balance and pyruvate dehydrogenase (PDH) was removed (Chan et al., 2003). However, in reality, as NADPH and NADH were freely exchanged within cells and PDH was the main flux for oxidation in TCA cycle, this could not be ignored. Recently, ^{13}C-MFA was developed as powerful technique for quantifying intracellular fluxes using labeled MIDs of intracellular metabolites. However, without key measurements of MIDs for intracellular metabolites, good flux observability (precision) cannot be achieved. For example, the estimation of non-oxidative PPP has been challenging in this field. In this study, after introduction of new analytical method for analyzing F6P by dephosphorylation, we measured two mass fragments of F6P at *m/z* 307 and 364 and achieved good flux observability of TK and TA in non-oxidative PPP. As a result, we found that Fao rat hepatoma cells showed high exchange flux of TK. The highest TK activity (exchange flux) at 8Br condition was shown in Figure 6.17 and estimated by ^{13}C-MFA in Figure 6.22.

As shown at labeled MIDs of TCA-related metabolites in Figure 6.11 and 6.14, TCA cycle metabolism was not significantly perturbed by introduction of glucocorticoid, transcription activators and inhibitors for gluconeogenesis. This suggested that TCA cycle metabolism may be independently regulated from gluconeogenesis metabolism. Previously, Des Rosiers et. al. estimated the flux of ACL and the exchange flux of IDH (Des Rosiers et al., 1995). To compare with this study, the flux of ACL and the exchange flux of IDH were normalized with citrate synthase (CS) flux. The ratio of ACL to CS flux in Des Rosiers et. al.'s and this study showed the same values, 49%. However, the ratio of IDH exchange flux to CS flux in Des

Rosiers et. al.'s and this study were 81% and 137%, respectively. The difference between two studies was likely due to the specific model cell lines, i.e. Fao rat hepatoma cells in this study, and primary hepatocytes in Des Rosiers et. al. study. Recently, Metallo et. al. reported that high exchange flux (backward flux, AKG → Cit) through IDH was estimated in lung cancerous cells, A549 (Metallo et al., 2012). In Figure 6.14, Cit fragment at *m/z* 459 contained 27% M5 isotopomers, which came from [U-^{13}C]glutamine tracer through the exchange flux of IDH. The level was the similar to Metallo et. al.'s study for cancer cells, and very high level compared to only 5% M5 isotopomers of Cit (*m/z* 459) in CHO cells, in Chapter 4. Therefore, our results suggest that high IDH exchange flux would be related to cancer cell metabolism.

TCA cycle metabolism is linked with ketone body (KB) metabolism, β-oxidation of fatty acids, amino acid metabolism, and albumin production, which were also characterized for liver metabolism. Thus, we added these four pathways into this network model as described in Figure 6.20. Figure 6.8 showed very large lactate consumption, relatively compared to glucose production level. This suggested that lactate carbon flowed to other metabolites. KB is a major end-product in liver tissue. KB originates from AcCoA precursor in mitochondria and the AcCoA can be built by PDH and β-oxidation of fatty acids. Thus, in order to explain the metabolism, we introduced this pathway into the model. In future, the rates of KB production in media and the level of AcCoA from fatty acids should be quantified in order to acquire more concrete results. In addition, amino acid metabolism was up-regulated by insulin. By PCA in Figure 6.9 and quantification of metabolites in Table 6.3, insulin elevated the consumption of amino acids. ^{13}C-MFA results in Figure 6.24 showed that albumin production by addition of insulin increased almost 2-fold compared to the control

experiment. This suggested that insulin activated protein biosynthesis, as well as inhibited gluconeogenesis. The signaling pathway of insulin receptor is connected with protein synthesis and down-regulation of gluconeogenesis (Taniguchi et al., 2006). The estimated value of albumin production rate for the Con condition in this study was 22 μg/10^6cells/24h, which was calculated using the parameters of 33 μmol/L/h albumin production, 5 mL culture volume and 2×10^7 viable cell density in one flask. It has been reported that albumin production rates were measured to 2.5-6 μg/10^6cells/24h with rat hepatoma cells (Bouhnik et al., 1983; Cassio et al., 1981), 6.8-20 μg/10^6cells/24h with primary rat hepatocytes (East et al., 1973), and 10 μg/10^6cells/24h with mouse hepatoma cells (Kanno et al., 2011). The previous reported production levels matched well with the estimated value in this study.

6.5 Conclusion

In order to study gluconeogenesis metabolism, we constructed a comprehensive network model for application with ^{13}C-MFA. The model contained all key metabolic pathways linked to gluconeogenesis. Furthermore, the model was validated by tracing carbon flow from representative carbon sources as isotopic tracers: [U-^{13}C]lactate, [U-^{13}C]glutamine, and [U-^{13}C]glycerol. By introduction of important measurements for intracellular metabolites, we achieved good flux observability, including for difficult to resolve fluxes such as pentose phosphate pathway. As such, this the first comprehensible model and flux estimation covering gluconeogenesis, glycolysis, oxidative and non-oxidative PPP, pyruvate cycle, TCA cycle, amino acid metabolism, fatty acid metabolism and KB and albumin production. Using state-of-the-art methodology for ^{13}C-MFA and rigorous analysis using additional new measurements of intracellular metabolites, we obtained interesting and novel findings

in this study: (i) Dexamethasone activated PK and other glycolysis fluxes, as well as PEPCK, gluconeogenesis flux. (ii). The two cAMP analogues, 8-bromo-cAMP and dibutyryl-cAMP showed differential regulation of metabolism. (iii). During gluconeogenesis, Fao hepatoma cells displayed active non-oxidative PPP, including high exchange flux of TK. In the future, our methodology from this study can be used for drug screening and evaluating other mammalian cell lines.

Table 6.4 Metabolic network model for combined ^{13}C-MFA using [U-^{13}C]glycerol and [U-^{13}C]glutamine experiments

Gluconeogenesis and Glycolysis			
v1	Gluc (abcdef)	→	Gluc.ext (abcdef)
v2	G6P (abcdef)	→	Gluc (abcdef)
v3	G6P (abcdef)	↔	F6P (abcdef)
v4	FBP (abcdef)	↔	F6P (abcdef)
v5	FBP (abcdef)	↔	DHAP (cba) + GAP (def)
v6	DHAP (abc)	↔	GAP (abc)
v7	GAP (abc)	↔	3PG (abc)
v8	3PG (abc)	↔	PEP (abc)
v9	OAC.c (abcd)	→	PEP (abc) + CO2 (d)
v10	PEP (abc)	→	Pyr.c (abc)
Pentose Phosphate Pathway			
v11	G6P (abcdef)	→	Ru5P (bcdef) + CO2 (a)
v12	Ru5P (abcde)	↔	X5P (abcde)
v13	Ru5P (abcde)	↔	R5P (abcde)
v14	X5P (abcde)	↔	EC2 (ab) + GAP (cde)
v15	F6P (abcdef)	↔	EC2 (ab) + E4P (cdef)
v16	S7P (abcdefg)	↔	EC2 (ab) + R5P (cdefg)
v17	F6P (abcdef)	↔	EC3 (abc) + GAP (def)
v18	S7P (abcdefg)	↔	EC3 (abc) + E4P (defg)
Glycerol Metabolism			
v19	DHAP (abc)	↔	GLP (abc)
v20	Glyc (abc)	→	GLP (abc)
v21	GLP (abc)	→	GLP.src (abc)
Glycogen Metabolism			
v22	G6P (abcdef)	↔	G1P (abcdef)
v23	Glycogen.src (abcdef)	→	G1P (abcdef)
Pyruvate and Lactate Metabolism			
v24	Pyr.c (abc)	↔	Pyr.m (abc)
v25	Pyr.c (abc)	↔	Lact (abc)
TCA Cycle			
v26	Pyr.m (abc)	→	AcCoA.m (bc) + CO2 (a)
v27	AcCoA.m (ab) + OAC.m (cdef)	→	Cit.m (fedbac)
v28	Cit.m (abcdef)	↔	ICit.m (abcdef)

Table 6.4 continued

v29	ICit.m (abcdef)	↔	AKG.m (abcde) + CO2 (f)
v30	½ AKG.m (abcde) + ½ AKG.m (fghij)	→	½ Suc.m (bcde) + ½ Suc.m (jihg) + ½ CO2 (a) + ½ CO2 (f)
v31	½ Suc.m (abcd) + ½ Suc.m (efgh)	→	½ Fum.m (abcd) + ½ Fum.m (hgfe)
v32	½ Fum.m (abcd) + ½ Fum.m (efgh)	↔	½ Mal.m (abcd) + ½ Mal.m (hgfe)
v33	Mal.m (abcd)	↔	OAC.m (abcd)
Anaplerosis and Gluconeogenesis			
v34	Mal.m (abcd)	→	Pyr.m (abc) + CO2 (d)
v35	Mal.c (abcd)	→	Pyr.c (abc) + CO2 (d)
v36	Pyr.m (abc) + CO2 (d)	→	OAC.m (abcd)
v37	Mal.c (abcd)	↔	Mal.m (abcd)
v38	Mal.c (abcd)	↔	OAC.c (abcd)
Fatty Acid Metabolism			
v39	Cit.m (abcdef)	↔	Cit.c (abcdef)
v40	Cit.c (abcdef)	→	AcCoA.c (ab) + OAC.c (cdef)
v41	AcCoA.c (ab)	→	FA.c (ab)
v42	FA.c (ab) + FA.src (cd)	→	FA.snk (ab) + FA.m (cd)
v43	FA.m (ab)	→	AcCoA.m (ab)
Amino Acid Metabolism			
v44	Pyr.c (abc)	↔	Ala (abc)
v45	Gln (abcde)	→	Glu (abcde)
v46	Glu (abcde)	↔	AKG.m (abcde)
v47	Glu (abcde)	↔	Pro (abcde)
v48	Asp (abcd)	↔	OAC.c (abcd)
v49	Asp (abcd)	→	Asn (abcd)
v50	Ser (abc)	↔	Pyr.c (abc)
v51	Ser (abc)	↔	Gly (ab) + C1 (c)
v52	Thr (abcd)	→	AcCoA.c (cd) + Gly (ab)
v53	Met (abcde) + CO2 (f)	→	Suc.m (bcdf) + CO2 (a) + C1 (e)
v54	Val (abcde) + CO2 (f)	→	Suc.m (dcef) + CO2 (a) + CO2 (b)
v55	Ile (abcdef) + CO2 (g)	→	Suc.m (bcdg) + AcCoA.m (ef) + CO2(a)
v56	Phe (abcdefghi)	→	Fum.m (defg) + AcCoA.m (bc) + AcCoA.m (hi) + CO2 (a)
v57	Tyr (abcdefghi)	→	Fum.m (defg) + AcCoA.m (bc) + AcCoA.m (hi) + CO2 (a)

Table 6.4 continued

v58	Leu (abcdef) + CO2 (g)	→	AcCoA.m (bc) + AcCoA.m (de) + AcCoA.m (gf) + CO2 (a)
Extracellular Transport			
v59	Gln.ext (abcde)	→	Gln (abcde)
v60	Asp.ext (abcd)	→	Asp (abcd)
v61	Ile.ext (abcdef)	→	Ile (abcdef)
v62	Leu.ext (abcdef)	→	Leu (abcdef)
v63	Met.ext (abcde)	→	Met (abcde)
v64	Phe.ext (abcdefghi)	→	Phe (abcdefghi)
v65	Ser.ext (abc)	→	Ser (abc)
v66	Tyr.ext (abcdefghi)	→	Tyr (abcdefghi)
v67	Val.ext (abcde)	→	Val (abcde)
v68	Thr.ext (abcd)	→	Thr (abcd)
v69	Arg.ext (abcdef)	→	Arg (abcdef)
v70	Cys.ext (abc)	→	Cys (abc)
v71	His.ext (abcdef)	→	His (abcdef)
v72	Lys.ext (abcdef)	→	Lys (abcdef)
v73	Trp.ext (abcdefghijk)	→	Trp (abcdefghijk)
v74	Lact.ext (abc)	→	Lact (abc)
v75	Glu.ext (abcde)	→	Glu (abcde)
v76	Glyc.ext (abc)	→	Glyc (abc)
v77	FA.ext (ab)	→	FA.c (ab)
v78	Pro (abcde)	→	Pro.ext (abcde)
v79	Ala (abc)	→	Ala.ext (abc)
v80	Gly (ab)	→	Gly.ext (ab)
Ketone Body Metabolism			
v81	AcCoA.m (ab)	→	KB.ext (ab)
Albumin Production			
v82	0.1020 Ala + 0.0444 Arg + 0.0526 Asp + 0.0329 Asn + 0.0576 Cys + 0.0938 Glu + 0.0411 Gln + 0.0313 Gly + 0.0247 His + 0.0263 Ile + 0.1003 Leu + 0.0888 Lys + 0.0115 Met + 0.0493 Phe + 0.0493 Pro + 0.0444 Ser + 0.0543 Thr + 0.0033 Trp + 0.0345 Tyr + 0.0576 Val	→	Albumin

Chapter 7

CONCLUSIONS AND FUTURE RESEARCH

In this thesis, we studied the metabolism of two mammalian systems using state-of-the-art ^{13}C-MFA techniques. First, CHO cell metabolism was studied as an example glycolysis system; and second, Fao rat hepatoma cells were studied as an example gluconeogenesis system. Our research results on CHO cell metabolism can be applied to improve medium formulations and also to evaluate engineered cell lines for recombinant protein production. Moreover, the ^{13}C-MFA techniques that we developed for analysis of Fao cell metabolism can be applied for drug screening, e.g. in the pharmaceutical industry. In this Chapter, we summarize overall conclusions from the thesis research and suggest future research on both topics.

7.1 Conclusions of CHO Cell Metabolism in Chapter 3 to 5

Flux analysis with non-stationary ^{13}C-MFA. – This is the first time that non-stationary ^{13}C-MFA was applied to characterize CHO cell metabolism. When glucose was used as isotopic tracer, glycolysis-related metabolites reached isotopic steady state quickly (<3 h), but TCA cycle-related metabolites displayed non-isotopic steady state behavior. Thus, with non-stationary ^{13}C-MFA, we estimated metabolic fluxes that covered most of central metabolic pathways. As a key result, we observed significant metabolic rewiring from growth to non-growth phase during fed-batch culture of CHO cells. Anabolic fluxes and lactate production increased at the exponential phase and oxidative pentose phosphate pathway was activated at the stationary phase.

Flux analysis with stationary ^{13}C-MFA using combined data of [1,2-^{13}C]glucose and [U-^{13}C]glutamine experiments. – Non-stationary ^{13}C-MFA requires measuring MID data at multiple time points and additional measurements of intracellular metabolite pool sizes. Moreover, non-stationary ^{13}C-MFA is demanding in terms of computational time. To resolve these issues we introduced, for the first time, stationary ^{13}C-MFA using combined analysis of [1,2-^{13}C]glucose data for glycolysis pathway and [U-^{13}C]glutamine data for TCA cycle. Using this new approach, we obtained flux results that corresponded well with non-stationary ^{13}C-MFA results. In addition, we quantified, for the first time, lipid metabolism in CHO cell cultures. We found high metabolic activity of lipid metabolism all throughout the culture, even when CHO cells were in stationary phase.

Quantification of pentose phosphate pathway – We also solved a critical problem in MFA related to the estimation of oxidative PPP flux. We initially observed that the solution space for the estimated flux of oxidative PPP was not consistent for different isotopic tracers. Through detailed analysis of mass isotopomers from parallel labeling experiments, we identified that carbon atoms were lost in the non-oxidative PPP, specifically carbon atoms C1-C3 of glucose. Using a corrected metabolic network model we then obtained consistent flux results. Furthermore, by introducing new measurements of F6P fragments, we achieved for the first time good flux observability of fluxes in the non-oxidative PPP pathway.

7.2 Future Research for CHO Cell Metabolism

Carbon loss in glycolysis and PPP pathways – We observed significant carbon loss in the glycolysis and PPP pathways as discussed in Chapters 4 and 5. To further

validate these unexpected findings, the unknown metabolic products should be identified by metabolic profiling and additional ^{13}C-tracer experiments.

Lipid metabolism at non-growth phase – We also observed active lipid synthesis in CHO cells, even when no net cell growth was observed. To better understand the fate of these newly synthesized lipids, the flow of ^{13}C-atoms from lipids to intracellular metabolites should be investigated in detail. This can be achieved, for example, by first growing cells with small amounts of ^{13}C-lipids in the medium and then follow the incorporation of ^{13}C-labeling into intracellular metabolites.

Compartmentalized metabolism – Currently, intracellular metabolites at different compartments cannot be separated without contamination. Thus, the MID data analyzed from mixture metabolites reflected averaged metabolism, e.g. the oxidative metabolism of TCA cycle and reductive carboxylation metabolism by labeled metabolites: malate and fumarate.

Advanced cell culture techniques – We used serum-based media for tracer experiments. But, modern techniques of mammalian cell for industrial purpose provide serum-free media and suspension culture. Thus, the tracer experiments need to be applied using the current techniques.

7.3 Conclusions of Fao Cell Metabolism in Chapter 6

Construction of gluconeogenesis (GNG) model and observation of metabolic regulation of GNG fluxes by metabolic regulations. – In this thesis, we established a comprehensive network model for liver cells and estimated detailed flux maps by combined analysis of multiple isotopic tracer experiments. This is the first time that multiple parallel experiments were combined to determine detailed fluxes in mammalian cells. By using our new approach, we reported several novel findings

regarding metabolic regulation of hepatocyte metabolism by transcriptional factors. We found that dexamethasone activated glycolytic enzymes, e.g. pyruvate kinase, as well as gluconeogenic enzymes, e.g. phosphoenolpyruvate carboxykinase. Furthermore, we found that other glycolytic enzymes were also altered by dexamethasone. In addition, we found that the two cAMP analogues, 8-bromo-cAMP and dibutyryl-cAMP, showed differential regulation of intracellular metabolism. This is the first time that differential regulation was reported for these two transcription activators of gluconeogenesis pathway. Finally, we found that insulin strongly down-regulated gluconeogenesis flux, and as expected, enhanced amino acid metabolism towards albumin production.

7.4 Future Research for Fao Cell Metabolism

Quantification of glycogen, albumin, ketone body and fatty acids – To estimate a more complete metabolic map for hepatocytes, the following additional measurements are suggested: to measure directly the flux of glycogenolysis; to measure directly the albumin production rate; and to quantify ketone body production. These additional measurements would allow improved estimation of intracellular metabolism and could serve as further validation of our modeling predictions.

Glycerol metabolism – In our studies, 8-Bromo-cAMP significantly inhibited glycerol consumption (Figure 6.8) and increased the flux from GLP to lipids (Figure 6.21B). To validate these predictions, the related enzymes should be characterized at the transcriptional level and the related flux between GLP and lipids should be quantified using complementary methods, e.g. using ^{14}C-tracers or ^{2}H-tracers.

REFERENCES

Ahn, W. S., Antoniewicz, M. R., 2011. Metabolic flux analysis of CHO cells at growth and non-growth phases using isotopic tracers and mass spectrometry. Metabolic Engineering. 13**,** 598-609.

Ahn, W. S., Antoniewicz, M. R., 2012. Towards dynamic metabolic flux analysis in CHO cell cultures. Biotechnology Journal. 7**,** 61-74.

Ahn, W. S., Jeon, J.-J., Jeong, Y.-R., Lee, S. J., Yoon, S. K., 2008. Effect of culture temperature on erythropoietin production and glycosylation in a perfusion culture of recombinant CHO cells. Biotechnology and Bioengineering. 101**,** 1234-1244.

Altamirano, C., Illanes, A., Becerra, S., Cairó, J. J., Gòdia, F., 2006. Considerations on the lactate consumption by CHO cells in the presence of galactose. Journal of Biotechnology. 125**,** 547-556.

Altamirano, C., Illanes, A., Casablancas, A., Gamez, X., Cairo, J. J., Godia, C., 2001. Analysis of CHO cells metabolic redistribution in a glutamate-based defined medium in continuous culture. Biotechnology Progress. 17**,** 1032-1041.

Altamirano, C., Paredes, C., Cairó, J. J., Gòdia, F., 2000. Improvement of CHO cell culture medium formulation: simultaneous substitution of glucose and glutamine. Biotechnology Progress. 16**,** 69-75.

Altamirano, C., Paredes, C., Illanes, A., Cairó, J. J., Gòdia, F., 2004. Strategies for fed-batch cultivation of t-PA producing CHO cells: substitution of glucose and glutamine and rational design of culture medium. Journal of Biotechnology. 110**,** 171-179.

Andersen, D. C., Goochee, C. F., 1995. The effect of ammonia on the O-linked glycosylation of granulocyte colony-stimulating factor produced by chinese hamster ovary cells. Biotechnology and Bioengineering. 47**,** 96-105.

Antoniewicz, M. R., Kelleher, J. K., Stephanopoulos, G., 2006a. Determination of confidence intervals of metabolic fluxes estimated from stable isotope measurements. Metabolic Engineering. 8**,** 324-337.

Antoniewicz, M. R., Kelleher, J. K., Stephanopoulos, G., 2007a. Accurate assessment of amino acid mass isotopomer distributions for metabolic flux analysis. Analytical Chemistry. 79**,** 7554-7559.

Antoniewicz, M. R., Kelleher, J. K., Stephanopoulos, G., 2007b. Elementary metabolite units (EMU): A novel framework for modeling isotopic distributions. Metabolic Engineering. 9**,** 68-86.

Antoniewicz, M. R., Kelleher, J. K., Stephanopoulos, G., 2011. Measuring deuterium enrichment of glucose hydrogen atoms by gas chromatography/mass spectrometry. Analytical Chemistry. 83**,** 3211-3216.

Antoniewicz, M. R., Kraynie, D. F., Laffend, L. A., Gonzalez-Lergier, J., Kelleher, J. K., Stephanopoulos, G., 2007c. Metabolic flux analysis in a nonstationary system: Fed-batch fermentation of a high yielding strain of E. coli producing 1,3-propanediol. Metabolic Engineering. 9**,** 277-292.

Antoniewicz, M. R., Stephanopoulos, G., Kelleher, J. K., 2006b. Evaluation of regression models in metabolic physiology: predicting fluxes from isotopic data without knowledge of the pathway. Metabolomics. 2**,** 41-52.

Arnoldi, L., Valsecchi, G., Magni, F., Monti, L. D., Piatti, P. M., Costa, S., Kienle, M. G., 1998. Gluconeogenesis in isolated rat hepatocytes evaluated by gas chromatography/mass spectrometry using deuterated water. Journal of mass spectrometry: JMS. 33**,** 444-452.

Barthel, A., Schmoll, D., 2003. Novel concepts in insulin regulation of hepatic gluconeogenesis. American journal of physiology. Endocrinology and metabolism. 285**,** E685-692.

Bebbington, C. R., Renner, G., Thomson, S., King, D., Abrams, D., Yarranton, G. T., 1992. High-level expression of a recombinant antibody from myeloma cells using a glutamine synthetase gene as an amplifiable selectable marker. Bio/Technology (Nature Publishing Company). 10**,** 169-175.

Bensaad, K., Tsuruta, A., Selak, M. A., Vidal, M. N. C., Nakano, K., Bartrons, R., Gottlieb, E., Vousden, K. H., 2006. TIGAR, a p53-inducible regulator of glycolysis and apoptosis. Cell. 126**,** 107-120.

Beste, D. J. V., Bonde, B., Hawkins, N., Ward, J. L., Beale, M. H., Noack, S., Nöh, K., Kruger, N. J., Ratcliffe, R. G., McFadden, J., 2011. 13C Metabolic flux Analysis identifies an unusual route for pyruvate dissimilation in Mycobacteria which requires isocitrate lyase and carbon dioxide fixation. PLoS Pathog. 7**,** e1002091-e1002091.

Birch, J. R., Racher, A. J., 2006. Antibody production. Advanced Drug Delivery Reviews. 58**,** 671-685.

Boghigian, B. A., Seth, G., Kiss, R., Pfeifer, B. A., 2010. Metabolic flux analysis and pharmaceutical production. Metabolic Engineering. 12**,** 81-95.

Bonarius, H. P., Hatzimanikatis, V., Meesters, K. P., de Gooijer, C. D., Schmid, G., Tramper, J., 1996. Metabolic flux analysis of hybridoma cells in different culture media using mass balances. Biotechnology and Bioengineering. 50**,** 299-318.

Bonarius, H. P., Timmerarends, B., de Gooijer, C. D., Tramper, J., 1998a. Metabolite-balancing techniques vs. 13C tracer experiments to determine metabolic fluxes in hybridoma cells. Biotechnology and Bioengineering. 58**,** 258-262.

Bonarius, H. P. J., Houtman, J. H. M., de Gooijer, C. D., Tramper, J., Schmid, G., 1998b. Activity of glutamate dehydrogenase is increased in ammonia-stressed hybridoma cells. Biotechnology and Bioengineering. 57**,** 447-453.

Bonarius, H. P. J., Schmid, G., Tramper, J., 1997. Flux analysis of underdetermined metabolic networks: the quest for the missing constraints. Trends in Biotechnology. 15**,** 308-314.

Boros, L. G., Puigjaner, J., Cascante, M., Lee, W. N. P., Brandes, J. L., Bassilian, S., Yusuf, F. I., Williams, R. D., Muscarella, P., Melvin, W. S., Schirmer, W. J., 1997. Oxythiamine and dehydroepiandrosterone inhibit the nonoxidative synthesis of ribose and tumor cell proliferation. Cancer Research. 57**,** 4242-4248.

Borys, M. C., Linzer, D. I., Papoutsakis, E. T., 1994. Ammonia affects the glycosylation patterns of recombinant mouse placental lactogen-I by chinese hamster ovary cells in a pH-dependent manner. Biotechnology and Bioengineering. 43**,** 505-514.

Bouhnik, J., Cassio, D., Coezy, E., Corvol, P., Weiss, M. C., 1983. Angiotensinogen production by rat hepatoma cells in culture and analysis of its regulation by techniques of somatic cell genetics. The Journal of cell biology. 97**,** 549-555.

Bray, H. G., James, S. P., Raffan, I. M., Thorpe, W. V., 1949. The enzymic hydrolysis of glutamine and its spontaneous decomposition in buffer solutions. The Biochemical Journal. 44**,** 625-627.

Brin, M., 1962. Effects of thiamine deficiency and of oxythiamine on rat tissue transketolase. The Journal of Nutrition. 78**,** 179-183.

Burgess, S. C., Hausler, N., Merritt, M., Jeffrey, F. M. H., Storey, C., Milde, A., Koshy, S., Lindner, J., Magnuson, M. A., Malloy, C. R., Sherry, A. D., 2004. Impaired tricarboxylic acid cycle activity in mouse livers lacking cytosolic phosphoenolpyruvate carboxykinase. The Journal of biological chemistry. 279**,** 48941-48949.

Cassio, D., Weiss, M. C., Ott, M. O., Sala-Trepat, J. M., Friès, J., Erdos, T., 1981. Expression of the albumin gene in rat hepatoma cells and their dedifferentiated variants. Cell. 27**,** 351-358.

Chan, C., Berthiaume, F., Lee, K., Yarmush, M. L., 2003. Metabolic flux analysis of hepatocyte function in hormone- and amino acid-supplemented plasma. Metabolic Engineering. 5**,** 1-15.

Chee Furng Wong, D., Tin Kam Wong, K., Tang Goh, L., Kiat Heng, C., Gek Sim Yap, M., 2005. Impact of dynamic online fed-batch strategies on metabolism, productivity and N-glycosylation quality in CHO cell cultures. Biotechnology and Bioengineering. 89**,** 164-177.

Chen, H., Yue, J.-X., Yang, S.-H., Ding, H., Zhao, R.-W., Zhang, S., 2009. Overexpression of transketolase-like gene 1 is associated with cell proliferation in uterine cervix cancer. Journal of Experimental & Clinical Cancer Research: CR. 28**,** 43-43.

Chen, K., Liu, Q., Xie, L., Sharp, P. A., Wang, D. I., 2001. Engineering of a mammalian cell line for reduction of lactate formation and high monoclonal antibody production. Biotechnology and Bioengineering. 72**,** 55-61.

Chen, P., Harcum, S. W., 2005. Effects of amino acid additions on ammonium stressed CHO cells. Journal of Biotechnology. 117**,** 277-286.

Chen, X., Alonso, A. P., Allen, D. K., Reed, J. L., Shachar-Hill, Y., 2011. Synergy between (13)C-metabolic flux analysis and flux balance analysis for understanding metabolic adaptation to anaerobiosis in E. coli. Metabolic Engineering. 13**,** 38-48.

Choi, J., Antoniewicz, M. R., 2011. Tandem mass spectrometry: a novel approach for metabolic flux analysis. Metabolic Engineering. 13**,** 225-233.

Choi, J., Grossbach, M. T., Antoniewicz, M. R., 2012. Measuring complete isotopomer distribution of aspartate using gas chromatography/tandem mass spectrometry. Analytical chemistry. 84**,** 4628-4632.

Christensen, B., Nielsen, J., 2000. Metabolic network analysis of Penicillium chrysogenum using (13)C-labeled glucose. Biotechnology and Bioengineering. 68**,** 652-659.

Christofk, H. R., Vander Heiden, M. G., Harris, M. H., Ramanathan, A., Gerszten, R. E., Wei, R., Fleming, M. D., Schreiber, S. L., Cantley, L. C., 2008. The M2 splice isoform of pyruvate kinase is important for cancer metabolism and tumour growth. Nature. 452**,** 230-233.

Clark, K. J. R., Chaplin, F. W. R., Harcum, S. W., 2004. Temperature effects on product-quality-related enzymes in batch CHO cell cultures producing recombinant tPA. Biotechnology Progress. 20**,** 1888-1892.

Cockett, M. I., Bebbington, C. R., Yarranton, G. T., 1990. High level expression of tissue inhibitor of metalloproteinases in Chinese hamster ovary cells using glutamine synthetase gene amplification. Bio/Technology (Nature Publishing Company). 8**,** 662-667.

Covert, M. W., Schilling, C. H., Famili, I., Edwards, J. S., Goryanin, II, Selkov, E., Palsson, B. O., 2001. Metabolic modeling of microbial strains in silico. Trends in Biochemical Sciences. 26**,** 179-186.

Crown, S. B., Ahn, W. S., Antoniewicz, M. R., 2012. Rational design of 13C-labeling experiments for metabolic flux analysis in mammalian cells. BMC Systems Biology. 6**,** 43-43.

Crown, S. B., Antoniewicz, M. R., 2012. Selection of tracers for 13C-metabolic flux analysis using elementary metabolite units (EMU) basis vector methodology. Metabolic engineering. 14**,** 150-161.

Crown, S. B., Indurthi, D. C., Ahn, W. S., Choi, J., Papoutsakis, E. T., Antoniewicz, M. R., 2011. Resolving the TCA cycle and pentose-phosphate pathway of Clostridium acetobutylicum ATCC 824: Isotopomer analysis, in vitro activities and expression analysis. Biotechnology Journal. 6**,** 300-305.

Cruz, H. J., Freitas, C. M., Alves, P. M., Moreira, J. L., Carrondo, M. J. T., 2000. Effects of ammonia and lactate on growth, metabolism, and productivity of BHK cells. Enzyme and Microbial Technology. 27**,** 43-52.

Cruz, H. J., Moreira, J. L., Carrondo, M. J., 1999. Metabolic shifts by nutrient manipulation in continuous cultures of BHK cells. Biotechnology and Bioengineering. 66**,** 104-113.

Curthoys, N. P., Watford, M., 1995. Regulation of glutaminase activity and glutamine metabolism. Annual Review of Nutrition. 15**,** 133-159.

Dauner, M., Sauer, U., 2000. GC-MS analysis of amino acids rapidly provides rich information for isotopomer balancing. Biotechnology Progress. 16**,** 642-649.

Des Rosiers, C., Di Donato, L., Comte, B., Laplante, A., Marcoux, C., David, F., Fernandez, C. A., Brunengraber, H., 1995. Isotopomer analysis of citric acid cycle and gluconeogenesis in rat liver. Reversibility of isocitrate dehydrogenase and involvement of ATP-citrate lyase in gluconeogenesis. The Journal of biological chemistry. 270**,** 10027-10036.

Deshpande, R., Yang, T. H., Heinzle, E., 2009. Towards a metabolic and isotopic steady state in CHO batch cultures for reliable isotope-based metabolic profiling. Biotechnology Journal. 4**,** 247-263.

Di Donato, L., Des Rosiers, C., Montgomery, J. A., David, F., Garneau, M., Brunengraber, H., 1993. Rates of gluconeogenesis and citric acid cycle in perfused livers, assessed from the mass spectrometric assay of the 13C labeling pattern of glutamate. The Journal of Biological Chemistry. 268**,** 4170-4180.

Dinnis, D. M., James, D. C., 2005. Engineering mammalian cell factories for improved recombinant monoclonal antibody production: lessons from nature? Biotechnology and Bioengineering. 91**,** 180-189.

Dorai, H., Kyung, Y. S., Ellis, D., Kinney, C., Lin, C., Jan, D., Moore, G., Betenbaugh, M. J., 2009. Expression of anti-apoptosis genes alters lactate metabolism of Chinese Hamster Ovary cells in culture. Biotechnology and Bioengineering. 103**,** 592-608.

East, A. G., Louis, L. N., Hoffenberg, R., 1973. Albumin synthesis by isolated rat liver cells. Experimental cell research. 76**,** 41-46.

Elias, C. B., Carpentier, E., Durocher, Y., Bisson, L., Wagner, R., Kamen, A., 2003. Improving glucose and glutamine metabolism of human HEK 293 and Trichoplusia ni insect cells engineered to express a cytosolic pyruvate carboxylase enzyme. Biotechnology Progress. 19**,** 90-97.

Europa, A. F., Gambhir, A., Fu, P. C., Hu, W. S., 2000. Multiple steady states with distinct cellular metabolism in continuous culture of mammalian cells. Biotechnology and Bioengineering. 67**,** 25-34.

Fernandez, C. A., Des Rosiers, C., 1995. Modeling of liver citric acid cycle and gluconeogenesis based on 13C mass isotopomer distribution analysis of intermediates. The Journal of biological chemistry. 270**,** 10037-10042.

Fernandez, C. A., DesRosiers, C., Previs, S. F., David, F., Brunengraber, H., 1996. Correction of C-13 mass isotopomer distributions for natural stable isotope abundance. Journal of Mass Spectrometry. 31**,** 255-262.

Fico, A., Paglialunga, F., Cigliano, L., Abrescia, P., Verde, P., Martini, G., Iaccarino, I., Filosa, S., 2004. Glucose-6-phosphate dehydrogenase plays a crucial role in protection from redox-stress-induced apoptosis. Cell Death and Differentiation. 11**,** 823-831.

Fitzpatrick, L., Jenkins, H. A., Butler, M., 1993. Glucose and glutamine metabolism of a murine B-lymphocyte hybridoma grown in batch culture. Applied Biochemistry and Biotechnology. 43**,** 93-116.

Fogolín, M. B., Wagner, R., Etcheverrigaray, M., Kratje, R., 2004. Impact of temperature reduction and expression of yeast pyruvate carboxylase on hGM-CSF-producing CHO cells. Journal of Biotechnology. 109**,** 179-191.

Follstad, B. D., Balcarcel, R. R., Stephanopoulos, G., Wang, D. I., 1999. Metabolic flux analysis of hybridoma continuous culture steady state multiplicity. Biotechnology and Bioengineering. 63**,** 675-683.

Follstad, B. D., Stephanopoulos, G., 1998. Effect of reversible reactions on isotope label redistribution--analysis of the pentose phosphate pathway. European Journal of Biochemistry / FEBS. 252**,** 360-371.

Furuta, E., Okuda, H., Kobayashi, A., Watabe, K., 2010. Metabolic genes in cancer: Their roles in tumor progression and clinical implications. Biochimica et Biophysica Acta (BBA) - Reviews on Cancer. 1805**,** 141-152.

Gambhir, A., Korke, R., Lee, J., Fu, P.-C., Europa, A., Hu, W.-S., 2003. Analysis of cellular metabolism of hybridoma cells at distinct physiological states. Journal of Bioscience and Bioengineering. 95**,** 317-327.

Glacken, M. W., Adema, E., Sinskey, A. J., 1988. Mathematical descriptions of hybridoma culture kinetics: I. Initial metabolic rates. Biotechnology and Bioengineering. 32**,** 491-506.

Goudar, C., Biener, R., Boisart, C., Heidemann, R., Piret, J., de Graaf, A., Konstantinov, K., 2010. Metabolic flux analysis of CHO cells in perfusion

culture by metabolite balancing and 2D C-13, H-1 COSY NMR spectroscopy. Metabolic Engineering. 12**,** 138-149.

Goudar, C., Biener, R., Zhang, C., Michaels, J., Piret, J., Konstantinov, K., 2006. Towards industrial application of quasi real-time metabolic flux analysis for mammalian cell culture. Cell Culture Engineering. vol. 101, pp. 99-118.

Goudar, C. T., Biener, R., Konstantinov, K. B., Piret, J. M., 2009. Error propagation from prime variables into specific rates and metabolic fluxes for mammalian cells in perfusion culture. Biotechnology Progress. 25**,** 986-998.

Grillberger, L., Kreil, T. R., Nasr, S., Reiter, M., 2009. Emerging trends in plasma-free manufacturing of recombinant protein therapeutics expressed in mammalian cells. Biotechnol J. 4**,** 186-201.

Guo, Z. K., Lee, W. N., Katz, J., Bergner, A. E., 1992. Quantitation of positional isomers of deuterium-labeled glucose by gas chromatography/mass spectrometry. Analytical Biochemistry. 204**,** 273-282.

Hansen, H. A., Emborg, C., 1994. Influence of ammonium on growth, metabolism, and productivity of a continuous suspension Chinese hamster ovary cell culture. Biotechnology Progress. 10**,** 121-124.

Hassell, T., Gleave, S., Butler, M., 1991. Growth inhibition in animal cell culture. The effect of lactate and ammonia. Applied Biochemistry and Biotechnology. 30**,** 29-41.

Hellerstein, M. K., Neese, R. A., 1999. Mass isotopomer distribution analysis at eight years: theoretical, analytic, and experimental considerations. The American journal of physiology. 276**,** E1146-1170.

Henry, O., Durocher, Y., 2011. Enhanced glycoprotein production in HEK-293 cells expressing pyruvate carboxylase. Metabolic engineering. 13**,** 499-507.

Henry, O., Perrier, M., Kamen, A., 2005. Metabolic flux analysis of HEK-293 cells in perfusion cultures for the production of adenoviral vectors. Metabolic Engineering. 7**,** 467-476.

Hofmann, U., Maier, K., Nicbel, A., Vacun, G., Reuss, M., Mauch, K., 2008. Identification of metabolic fluxes in hepatic cells from transient C-13-labeling experiments: Part I. Experimental observations. Biotechnology and Bioengineering. 100**,** 344-354.

Hossler, P., Khattak, S. F., Li, Z. J., 2009. Optimal and consistent protein glycosylation in mammalian cell culture. Glycobiology. 19**,** 936-949.

Irani, N., Beccaria, A. J., Wagner, R., 2002. Expression of recombinant cytoplasmic yeast pyruvate carboxylase for the improvement of the production of human erythropoietin by recombinant BHK-21 cells. Journal of Biotechnology. 93**,** 269-282.

Irani, N., Wirth, M., van Den Heuvel, J., Wagner, R., 1999. Improvement of the primary metabolism of cell cultures by introducing a new cytoplasmic pyruvate carboxylase reaction. Biotechnology and Bioengineering. 66**,** 238-246.

Jeffrey, F. M. H., Roach, J. S., Storey, C. J., Sherry, A. D., Malloy, C. R., 2002. C-13 isotopomer analysis of glutamate by tandem mass spectrometry. Analytical Biochemistry. 300**,** 192-205.

Jenkins, H. A., Butler, M., Dickson, A. J., 1992. Characterization of glutamine metabolism in two related murine hybridomas. Journal of Biotechnology. 23**,** 167-182.

Jensen, M. V., Joseph, J. W., Ronnebaum, S. M., Burgess, S. C., Sherry, A. D., Newgard, C. B., 2008. Metabolic cycling in control of glucose-stimulated insulin secretion. American Journal of Physiology. Endocrinology and Metabolism. 295**,** E1287-1297.

Jeong, D. W., Cho, I. T., Kim, T. S., Bae, G. W., Kim, I. H., Kim, I. Y., 2006. Effects of lactate dehydrogenase suppression and glycerol-3-phosphate dehydrogenase overexpression on cellular metabolism. Molecular and Cellular Biochemistry. 284**,** 1-8.

Jin, E. S., Jones, J. G., Merritt, M., Burgess, S. C., Malloy, C. R., Sherry, A. D., 2004. Glucose production, gluconeogenesis, and hepatic tricarboxylic acid cycle fluxes measured by nuclear magnetic resonance analysis of a single glucose derivative. Analytical Biochemistry. 327**,** 149-155.

Jones, C. G., Hothi, S. K., Titheradge, M. A., 1993. Effect of dexamethasone on gluconeogenesis, pyruvate kinase, pyruvate carboxylase and pyruvate dehydrogenase flux in isolated hepatocytes. The Biochemical journal. 289 (Pt 3)**,** 821-828.

Jones, J. G., Carvalho, R. A., Franco, B., Sherry, A. D., Malloy, C. R., 1998. Measurement of hepatic glucose output, Krebs cycle, and gluconeogenic fluxes

by NMR analysis of a single plasma glucose sample. Analytical Biochemistry. 263**,** 39-45.

Jones, J. G., Carvalho, R. A., Sherry, A. D., Malloy, C. R., 2000. Quantitation of Gluconeogenesis by 2H Nuclear Magnetic Resonance Analysis of Plasma Glucose Following Ingestion of 2H2O. Analytical Biochemistry. 277**,** 121-126.

Jones, J. G., Solomon, M. A., Cole, S. M., Sherry, A. D., Malloy, C. R., 2001. An integrated (2)H and (13)C NMR study of gluconeogenesis and TCA cycle flux in humans. American journal of physiology. Endocrinology and metabolism. 281**,** E848-856.

Kanno, S.-i., Kurauchi, K., Tomizawa, A., Yomogida, S., Ishikawa, M., 2011. Albumin modulates docosahexaenoic acid-induced cytotoxicity in human hepatocellular carcinoma cell lines. Toxicology Letters. 200**,** 154-161.

Kelleher, J. K., Masterson, T. M., 1992. Model equations for condensation biosynthesis using stable isotopes and radioisotopes. The American Journal of Physiology. 262**,** E118-125.

Kharroubi, A. T., Masterson, T. M., Aldaghlas, T. A., Kennedy, K. A., Kelleher, J. K., 1992. Isotopomer spectral analysis of triglyceride fatty acid synthesis in 3T3-L1 cells. The American Journal of Physiology. 263**,** E667-675.

Khattak, S. F., Xing, Z., Kenty, B., Koyrakh, I., Li, Z. J., 2010. Feed development for fed-batch CHO production process by semisteady state analysis. Biotechnology Progress. 26**,** 797-804.

Kiefer, P., Nicolas, C., Letisse, F., Portais, J.-C., 2007. Determination of carbon labeling distribution of intracellular metabolites from single fragment ions by ion chromatography tandem mass spectrometry. Analytical Biochemistry. 360**,** 182-188.

Kim, S. H., Lee, G. M., 2007a. Down-regulation of lactate dehydrogenase-A by siRNAs for reduced lactic acid formation of Chinese hamster ovary cells producing thrombopoietin. Applied Microbiology and Biotechnology. 74**,** 152-159.

Kim, S. H., Lee, G. M., 2007b. Functional expression of human pyruvate carboxylase for reduced lactic acid formation of Chinese hamster ovary cells (DG44). Applied Microbiology and Biotechnology. 76**,** 659-665.

Kingston, R. E., Kaufman, R. J., Bebbington, C. R., Rolfe, M. R., 2002. Amplification using CHO cell expression vectors. Current protocols in molecular biology / edited by Frederick M. Ausubel ... [et al.]. Chapter 16**,** Unit 16.23-Unit 16.23.

Klamt, S., Schuster, S., Gilles, E. D., 2002. Calculability analysis in underdetermined metabolic networks illustrated by a model of the central metabolism in purple nonsulfur bacteria. Biotechnology and Bioengineering. 77**,** 734-751.

Klapa, M. I., Aon, J.-C., Stephanopoulos, G., 2003. Systematic quantification of complex metabolic flux networks using stable isotopes and mass spectrometry. European Journal of Biochemistry / FEBS. 270**,** 3525-3542.

Kleijn, R. J., van Winden, W. A., van Gulik, W. M., Heijnen, J. J., 2005. Revisiting the 13C-label distribution of the non-oxidative branch of the pentose phosphate pathway based upon kinetic and genetic evidence. The FEBS Journal. 272**,** 4970-4982.

Korke, R., Gatti, M. D., Lau, A. L. Y., Lim, J. W. E., Seow, T. K., Chung, M. C. M., Hu, W. S., 2004. Large scale gene expression profiling of metabolic shift of mammalian cells in culture. Journal of Biotechnology. 107**,** 1-17.

Kurokawa, H., Park, Y. S., Iijima, S., Kobayashi, T., 1994. Growth characteristics in fed-batch culture of hybridoma cells with control of glucose and glutamine concentrations. Biotechnology and Bioengineering. 44**,** 95-103.

Lao, M. S., Toth, D., 1997. Effects of ammonium and lactate on growth and metabolism of a recombinant Chinese hamster ovary cell culture. Biotechnology Progress. 13**,** 688-691.

Lee, W. N., Boros, L. G., Puigjaner, J., Bassilian, S., Lim, S., Cascante, M., 1998. Mass isotopomer study of the nonoxidative pathways of the pentose cycle with [1,2-13C2]glucose. The American Journal of Physiology. 274**,** E843-851.

Legrand, C., Bour, J. M., Jacob, C., Capiaumont, J., Martial, A., Marc, A., Wudtke, M., Kretzmer, G., Demangel, C., Duval, D., Hache, J., 1992. Lactate dehydrogenase (LDH) activity of the number of dead cells in the medium of cultured eukaryotic cells as marker. Journal of Biotechnology. 25**,** 231-243.

Leighty, R. W., Antoniewicz, M. R., 2011. Dynamic metabolic flux analysis (DMFA): A framework for determining fluxes at metabolic non-steady state. Metabolic Engineering. 13**,** 745-755.

Lequeux, G., Beauprez, J., Maertens, J., Van Horen, E., Soetaert, W., Vandamme, E., Vanrolleghem, P. A., 2010. Dynamic metabolic flux analysis demonstrated on

cultures where the limiting substrate is changed from carbon to nitrogen and vice versa. Journal of Biomedicine & Biotechnology. 2010.

Lin, A., Agrawal, P., 1988. Glutamine decomposition in DMEM: Effect of pH and serum concentration. Biotechnology Letters. 10**,** 695-698.

Ljunggren, J., Häggström, L., 1994. Catabolic control of hybridoma cells by glucose and glutamine limited fed batch cultures. Biotechnology and Bioengineering. 44**,** 808-818.

Llaneras, F., Picó, J., 2007. A procedure for the estimation over time of metabolic fluxes in scenarios where measurements are uncertain and/or insufficient. BMC Bioinformatics. 8**,** 421-421.

Lu, D., Mulder, H., Zhao, P., Burgess, S. C., Jensen, M. V., Kamzolova, S., Newgard, C. B., Sherry, A. D., 2002. 13C NMR isotopomer analysis reveals a connection between pyruvate cycling and glucose-stimulated insulin secretion (GSIS). Proceedings of the National Academy of Sciences of the United States of America. 99**,** 2708-2713.

MacLeod, J. K., Flanigan, I. L., Williams, J. F., Collins, J. G., 2001. Mass spectrometric studies of the path of carbon in photosynthesis: positional isotopic analysis of 13C-labelled C4 to C7 sugar phosphates. Journal of Mass Spectrometry. 36**,** 500-508.

Maier, K., Hofmann, U., Reuss, M., Mauch, K., 2008. Identification of metabolic fluxes in hepatic cells from transient C-13-labeling experiments: Part II. Flux estimation. Biotechnology and Bioengineering. 100**,** 355-370.

Maranga, L., Goochee, C. F., 2006. Metabolism of PER.C6 cells cultivated under fed-batch conditions at low glucose and glutamine levels. Biotechnology and Bioengineering. 94**,** 139-150.

Martens, D. E., 2007. Metabolic Flux Analysis of Mammalian Cells. In: Al-Rubeai, M., Fussenegger, M., Eds.), Systems Biology. vol. 5. Springer Netherlands, Dordrecht, pp. 275-299.

Martinelle, K., Doverskog, M., Jacobsson, U., Chapman, B. E., Kuchel, P. W., Häggström, L., 1998. Elevated glutamate dehydrogenase flux in glucose-deprived hybridoma and myeloma cells: evidence from 1H/15N NMR. Biotechnology and Bioengineering. 60**,** 508-517.

Marx, A., Eikmanns, B. J., Sahm, H., de Graaf, A. A., Eggeling, L., 1999. Response of the central metabolism in Corynebacterium glutamicum to the use of an NADH-dependent glutamate dehydrogenase. Metabolic Engineering. 1**,** 35-48.

Mashego, M. R., Wu, L., Van Dam, J. C., Ras, C., Vinke, J. L., Van Winden, W. A., Van Gulik, W. M., Heijnen, J. J., 2004. MIRACLE: mass isotopomer ratio analysis of U-13C-labeled extracts. A new method for accurate quantification of changes in concentrations of intracellular metabolites. Biotechnology and Bioengineering. 85**,** 620-628.

Mastrangelo, A. J., Hardwick, J. M., Zou, S., Betenbaugh, M. J., 2000. Part II. Overexpression of bcl-2 family members enhances survival of mammalian cells in response to various culture insults. Biotechnology and Bioengineering. 67**,** 555-564.

McQueen, A., Bailey, J. E., 1990. Growth inhibition of hybridoma cells by ammonium ion: correlation with effects on intracellular pH. Bioprocess Engineering. 6**,** 49-61.

Metallo, C. M., Gameiro, P. A., Bell, E. L., Mattaini, K. R., Yang, J., Hiller, K., Jewell, C. M., Johnson, Z. R., Irvine, D. J., Guarente, L., Kelleher, J. K., Vander Heiden, M. G., Iliopoulos, O., Stephanopoulos, G., 2012. Reductive glutamine metabolism by IDH1 mediates lipogenesis under hypoxia. Nature. 481**,** 380-384.

Metallo, C. M., Walther, J. L., Stephanopoulos, G., 2009. Evaluation of 13C isotopic tracers for metabolic flux analysis in mammalian cells. Journal of Biotechnology. 144**,** 167-174.

Moxley, J. F., Jewett, M. C., Antoniewicz, M. R., Villas-Boas, S. G., Alper, H., Wheeler, R. T., Tong, L., Hinnebusch, A. G., Ideker, T., Nielsen, J., Stephanopoulos, G., 2009. Linking high-resolution metabolic flux phenotypes and transcriptional regulation in yeast modulated by the global regulator Gcn4p. Proceedings of the National Academy of Sciences of the United States of America. 106**,** 6477-6482.

Munger, J., Bennett, B. D., Parikh, A., Feng, X.-J., McArdle, J., Rabitz, H. A., Shenk, T., Rabinowitz, J. D., 2008. Systems-level metabolic flux profiling identifies fatty acid synthesis as a target for antiviral therapy. Nature Biotechnology. 26**,** 1179-1186.

Nadeau, I., Jacob, D., Perrier, M., Kamen, A., 2000. 293SF metabolic flux analysis during cell growth and infection with an adenoviral vector. Biotechnology Progress. 16**,** 872-884.

Naderi, S., Meshram, M., Wei, C., McConkey, B., Ingalls, B., Budman, H., Scharer, J., 2011. Development of a mathematical model for evaluating the dynamics of normal and apoptotic Chinese hamster ovary cells. Biotechnology progress. 27**,** 1197-1205.

Neermann, J., Wagner, R., 1996. Comparative analysis of glucose and glutamine metabolism in transformed mammalian cell lines, insect and primary liver cells. Journal of Cellular Physiology. 166**,** 152-169.

Niklas, J., Heinzle, E., 2012. Metabolic flux analysis in systems biology of mammalian cells. Advances in biochemical engineering/biotechnology. 127**,** 109-132.

Niklas, J., Sandig, V., Heinzle, E., 2011a. Metabolite channeling and compartmentation in the human cell line AGE1.HN determined by (13)C labeling experiments and (13)C metabolic flux analysis. Journal of Bioscience and Bioengineering.

Niklas, J., Schneider, K., Heinzle, E., 2010. Metabolic flux analysis in eukaryotes. Current Opinion in Biotechnology. 21**,** 63-69.

Niklas, J., Schräder, E., Sandig, V., Noll, T., Heinzle, E., 2011b. Quantitative characterization of metabolism and metabolic shifts during growth of the new human cell line AGE1.HN using time resolved metabolic flux analysis. Bioprocess and Biosystems Engineering. 34**,** 533-545.

Noack, S., Nöh, K., Moch, M., Oldiges, M., Wiechert, W., 2011. Stationary versus non-stationary (13)C-MFA: A comparison using a consistent dataset. Journal of Biotechnology. 154**,** 179-190.

Noguchi, Y., Young, J. D., Aleman, J. O., Hansen, M. E., Kelleher, J. K., Stephanopoulos, G., 2009. Effect of Anaplerotic Fluxes and Amino Acid Availability on Hepatic Lipoapoptosis. Journal of Biological Chemistry. 284**,** 33425-33436.

Nolan, R. P., Lee, K., 2011. Dynamic model of CHO cell metabolism. Metabolic Engineering. 13**,** 108-124.

Nyberg, G. B., Balcarcel, R. R., Follstad, B. D., Stephanopoulos, G., Wang, D. I., 1999a. Metabolic effects on recombinant interferon-gamma glycosylation in continuous culture of Chinese hamster ovary cells. Biotechnology and Bioengineering. 62**,** 336-347.

Nyberg, G. B., Balcarcel, R. R., Follstad, B. D., Stephanopoulos, G., Wang, D. I. C., 1999b. Metabolism of peptide amino acids by Chinese hamster ovary cells grown in a complex medium. Biotechnology and Bioengineering. 62**,** 324-335.

Omasa, T., Higashiyama, K. I., Shioya, S., Suga, K. i., 1992. Effects of lactate concentration on hybridoma culture in lactate-controlled fed-batch operation. Biotechnology and Bioengineering. 39**,** 556-564.

Ozturk, S. S., Palsson, B. O., 1990. Chemical decomposition of glutamine in cell culture media: effect of media type, pH, and serum concentration. Biotechnology Progress. 6**,** 121-128.

Ozturk, S. S., Palsson, B. O., 1991. Growth, metabolic, and antibody production kinetics of hybridoma cell culture: 1. Analysis of data from controlled batch reactors. Biotechnology Progress. 7**,** 471-480.

Ozturk, S. S., Riley, M. R., Palsson, B. O., 1992. Effects of ammonia and lactate on hybridoma growth, metabolism, and antibody production. Biotechnology and Bioengineering. 39**,** 418-431.

Paredes, C., Sanfeliu, A., Cardenas, F., Cairo, J. J., Godia, F., 1998. Estimation of the intracellular fluxes for a hybridoma cell line by material balances. Enzyme and Microbial Technology. 23**,** 187-198.

Petch, D., Butler, M., 1994. Profile of energy metabolism in a murine hybridoma: glucose and glutamine utilization. Journal of Cellular Physiology. 161**,** 71-76.

Provost, A., Bastin, G., 2004. Dynamic metabolic modelling under the balanced growth condition. Journal of Process Control. 14**,** 717-728.

Provost, A., Bastin, G., Agathos, S. N., Schneider, Y. J., 2006. Metabolic design of macroscopic bioreaction models: application to Chinese hamster ovary cells. Bioprocess and Biosystems Engineering. 29**,** 349-366.

Quek, L.-E., Wittmann, C., Nielsen, L., Kromer, J., 2009. OpenFLUX: efficient modelling software for 13C-based metabolic flux analysis. Microbial Cell Factories. 8**,** 25-25.

Quek, L. E., Dietmair, S., Kromer, J. O., Nielsen, L. K., 2010. Metabolic flux analysis in mammalian cell culture. Metabolic Engineering. 12**,** 161-171.

Rühl, M., Rupp, B., Nöh, K., Wiechert, W., Sauer, U., Zamboni, N., 2012. Collisional fragmentation of central carbon metabolites in LC-MS/MS increases precision

of 13C metabolic flux analysis. Biotechnology and Bioengineering. 109**,** 763-771.

Saltiel, A. R., 2001. New perspectives into the molecular pathogenesis and treatment of Type 2 diabetes. Cell. 104**,** 517-529.

Schaub, J., Mauch, K., Reuss, M., 2008. Metabolic flux analysis in Escherichia coli by integrating isotopic dynamic and isotopic stationary 13C labeling data. Biotechnology and Bioengineering. 99**,** 1170-1185.

Schellenberger, J., Zielinski, D. C., Choi, W., Madireddi, S., Portnoy, V., Scott, D. A., Reed, J. L., Osterman, A. L., Palsson, B. O., 2012. Predicting outcomes of steady-state 13C isotope tracing experiments with Monte Carlo sampling. BMC Systems Biology. 6**,** 9-9.

Schmidt, K., Carlsen, M., Nielsen, J., Villadsen, J., 1997. Modeling isotopomer distributions in biochemical networks using isotopomer mapping matrices. Biotechnology and Bioengineering. 55**,** 831-840.

Schmidt, K., Marx, A., de Graaf, A. A., Wiechert, W., Sahm, H., Nielsen, J., Villadsen, J., 1998. 13C tracer experiments and metabolite balancing for metabolic flux analysis: Comparing two approaches. Biotechnology and Bioengineering. 58**,** 254-257.

Schneider, M., Marison, I. W., vonStockar, U., 1996. The importance of ammonia in mammalian cell culture. Journal of Biotechnology. 46**,** 161-185.

Sengupta, N., Rose, S. T., Morgan, J. A., 2011. Metabolic flux analysis of CHO cell metabolism in the late non-growth phase. Biotechnology and Bioengineering. 108**,** 82-92.

Seow, T. K., Korke, R., Liang, R. C., Ong, S. E., Ou, K., Wong, K., Hu, W. S., Chung, M. C., 2001. Proteomic investigation of metabolic shift in mammalian cell culture. Biotechnology Progress. 17**,** 1137-1144.

Sheikh, K., Forster, J., Nielsen, L. K., 2005. Modeling hybridoma cell metabolism using a generic genome-scale metabolic model of Mus musculus. Biotechnology Progress. 21**,** 112-121.

Singh, R. P., Al-Rubeai, M., Gregory, C. D., Emery, A. N., 1994. Cell death in bioreactors: a role for apoptosis. Biotechnology and Bioengineering. 44**,** 720-726.

Stephanopoulos, G., Aristidou, A. A., Nielsen, J. H., Nielsen, J., 1998. Metabolic engineering: principles and methodologies. Academic Press.

Street, J. C., Delort, A. M., Braddock, P. S., Brindle, K. M., 1993. A 1H/15N n.m.r. study of nitrogen metabolism in cultured mammalian cells. Biochemical Journal. 291**,** 485-492.

Szyperski, T., 1995. Biosynthetically directed fractional 13C-labeling of proteinogenic amino acids. An efficient analytical tool to investigate intermediary metabolism. European Journal of Biochemistry / FEBS. 232**,** 433-448.

Taniguchi, C. M., Emanuelli, B., Kahn, C. R., 2006. Critical nodes in signalling pathways: insights into insulin action. Nature Reviews Molecular Cell Biology. 7**,** 85-96.

Thorens, B., Vassalli, P., 1986. Chloroquine and ammonium chloride prevent terminal glycosylation of immunoglobulins in plasma cells without affecting secretion. Nature. 321**,** 618-620.

Tian, W. N., Braunstein, L. D., Apse, K., Pang, J., Rose, M., Tian, X., Stanton, R. C., 1999. Importance of glucose-6-phosphate dehydrogenase activity in cell death. The American Journal of Physiology. 276**,** C1121-1131.

Tian, W. N., Braunstein, L. D., Pang, J., Stuhlmeier, K. M., Xi, Q. C., Tian, X., Stanton, R. C., 1998. Importance of glucose-6-phosphate dehydrogenase activity for cell growth. The Journal of Biological Chemistry. 273**,** 10609-10617.

Tritsch, G. L., Moore, G. E., 1962. Spontaneous decomposition of glutamine in cell culture media. Experimental Cell Research. 28**,** 360-364.

Trummer, E., Fauland, K., Seidinger, S., Schriebl, K., Lattenmayer, C., Kunert, R., Vorauer-Uhl, K., Weik, R., Borth, N., Katinger, H., Müller, D., 2006. Process parameter shifting: Part I. Effect of DOT, pH, and temperature on the performance of Epo-Fc expressing CHO cells cultivated in controlled batch bioreactors. Biotechnology and Bioengineering. 94**,** 1033-1044.

Tuttle, S., Stamato, T., Perez, M. L., Biaglow, J., 2000. Glucose-6-phosphate dehydrogenase and the oxidative pentose phosphate cycle protect cells against apoptosis induced by low doses of ionizing radiation. Radiation Research. 153**,** 781-787.

Vallino, J. J., Stephanopoulos, G., 1993. Metabolic flux distributions in Corynebacterium glutamicum during growth and lysine overproduction. Biotechnology and Bioengineering. 41**,** 633-646.

van Winden, W., Verheijen, P., Heijnen, S., 2001. Possible pitfalls of flux calculations based on (13)C-labeling. Metabolic Engineering. 3**,** 151-162.

van Winden, W. A., Heijnen, J. J., Verheijen, P. J. T., 2002. Cumulative bondomers: a new concept in flux analysis from 2D [13C,1H] COSY NMR data. Biotechnology and Bioengineering. 80**,** 731-745.

Vander Heiden, M. G., Cantley, L. C., Thompson, C. B., 2009. Understanding the Warburg effect: the metabolic requirements of cell proliferation. Science (New York, N.Y.). 324**,** 1029-1033.

Vidal-Puig, A., O'Rahilly, S., 2001. Metabolism - Controlling the glucose factory. Nature. 413**,** 125-126.

Vriezen, N., van Dijken, J. P., 1998. Fluxes and enzyme activities in central metabolism of myeloma cells grown in chemostat culture. Biotechnology and Bioengineering. 59**,** 28-39.

Wahl, S. A., Nöh, K., Wiechert, W., 2008. 13C labeling experiments at metabolic nonstationary conditions: an exploratory study. BMC Bioinformatics. 9**,** 152-152.

Wahrheit, J., Nicolae, A., Heinzle, E., 2011. Eukaryotic metabolism: Measuring compartment fluxes. Biotechnology Journal. 6**,** 1071-1085.

Walsh, G., 2010. Biopharmaceutical benchmarks 2010. Nature Biotechnology. 28**,** 917-924.

Walther, J. L., Metallo, C. M., Zhang, J., Stephanopoulos, G., 2012. Optimization of 13C isotopic tracers for metabolic flux analysis in mammalian cells. Metabolic engineering. 14**,** 162-171.

Warburg, O., 1956. On the origin of cancer cells. Science (New York, N.Y.). 123**,** 309-314.

Weis, B. C., Margolis, D., Burgess, S. C., Merritt, M. E., Wise, H., Sherry, A. D., Malloy, C. R., 2004. Glucose production pathways by 2H and 13C NMR in patients with HIV-associated lipoatrophy. Magnetic Resonance in Medicine: Official Journal of the Society of Magnetic Resonance in Medicine / Society of Magnetic Resonance in Medicine. 51**,** 649-654.

Wheeler, T. J., Hinkle, P. C., 1985. The glucose transporter of mammalian cells. Annual Review of Physiology. 47**,** 503-517.

White, R. H., 2004. L-aspartate semialdehyde and a 6-deoxy-5-ketohexose 1-phosphate are the precursors to the aromatic amino acids in Methanocaldococcus jannaschii. Biochemistry. 43**,** 7618-7627.

Wiebel, F. J., Park, S. S., Kiefer, F., Gelboin, H. V., 1984. Expression of cytochromes P-450 in rat hepatoma cells. Analysis by monoclonal antibodies specific for cytochromes P-450 from rat liver induced by 3-methylcholanthrene or phenobarbital. European journal of biochemistry / FEBS. 145**,** 455-462.

Wiechert, W., 2001. 13C metabolic flux analysis. Metabolic Engineering. 3**,** 195-206.

Wiechert, W., de Graaf, A. A., 1997. Bidirectional reaction steps in metabolic networks: I. Modeling and simulation of carbon isotope labeling experiments. Biotechnology and Bioengineering. 55**,** 101-117.

Wiechert, W., Mollney, M., Isermann, N., Wurzel, W., de Graaf, A. A., 1999. Bidirectional reaction steps in metabolic networks: III. Explicit solution and analysis of isotopomer labeling systems. Biotechnology and Bioengineering. 66**,** 69-85.

Wiechert, W., Nöh, K., 2005. From stationary to instationary metabolic flux analysis. Advances in Biochemical Engineering/Biotechnology. 92**,** 145-172.

Wilson, J. E., 2003. Isozymes of mammalian hexokinase: structure, subcellular localization and metabolic function. J Exp Biol. 206**,** 2049-2057.

Wittmann, C., 2002. Metabolic flux analysis using mass spectrometry. Advances in Biochemical Engineering/Biotechnology. 74**,** 39-64.

Wittmann, C., 2007. Fluxome analysis using GC-MS. Microbial Cell Factories. 6.

Wittmann, C., Heinzle, E., 1999. Mass spectrometry for metabolic flux analysis. Biotechnology and Bioengineering. 62**,** 739-750.

Wolf, A., Agnihotri, S., Micallef, J., Mukherjee, J., Sabha, N., Cairns, R., Hawkins, C., Guha, A., 2011. Hexokinase 2 is a key mediator of aerobic glycolysis and promotes tumor growth in human glioblastoma multiforme. The Journal of Experimental Medicine. 208**,** 313-326.

Wurm, F. M., 2004. Production of recombinant protein therapeutics in cultivated mammalian cells. Nature Biotechnology. 22**,** 1393-1398.

Xie, L., Zhou, W., Robinson, D., 2003. Protein production by large-scale mammalian cell culture. In: Makrides, S. C., (Ed.), Gene Transfer and Expression in Mammalian Cells. vol. Volume 38. Elsevier, pp. 605-623.

Xing, Z., Kenty, B., Koyrakh, I., Borys, M., Pan, S.-H., Li, Z. J., 2011. Optimizing amino acid composition of CHO cell culture media for a fusion protein production. Process Biochemistry. 46**,** 1423-1429.

Yallop, C. A., Norby, P. L., Jensen, R., Reinbach, H., Svendsen, I., 2003. Characterisation of G418-induced metabolic load in recombinant CHO and BHK cells: effect on the activity and expression of central metabolic enzymes. Cytotechnology. 42**,** 87-99.

Yang, J., Wongsa, S., Kadirkamanathan, V., Billings, S. A., Wright, P. C., 2005. Metabolic flux distribution analysis by 13C-tracer experiments using the Markov chain-Monte Carlo method. Biochemical Society Transactions. 33**,** 1421-1422.

Yang, L. L., Kombu, R. S., Kasumov, T., Zhu, S. H., Cendrowski, A. V., David, F., Anderson, V. E., Kelleher, J. K., Brunengraber, H., 2008. Metabolomic and mass isotopomer analysis of liver gluconeogenesis and citric acid cycle - I. Interrelation between gluconeogenesis and cataplerosis; Formation of methoxamates from aminooxyacetate and ketoacids. Journal of Biological Chemistry. 283**,** 21978-21987.

Yang, M., Butler, M., 2000a. Effect of ammonia on the glycosylation of human recombinant erythropoietin in culture. Biotechnology Progress. 16**,** 751-759.

Yang, M., Butler, M., 2000b. Effects of ammonia on CHO cell growth, erythropoietin production, and glycosylation. Biotechnology and Bioengineering. 68**,** 370-380.

Yang, M., Butler, M., 2002. Effects of ammonia and glucosamine on the heterogeneity of erythropoietin glycoforms. Biotechnology Progress. 18**,** 129-138.

Yoo, H., Antoniewicz, M. R., Stephanopoulos, G., Kelleher, J. K., 2008. Quantifying reductive carboxylation flux of glutamine to lipid in a brown adipocyte cell line. Journal of Biological Chemistry. 283**,** 20621-20627.

Yoo, H., Stephanopoulos, G., Kelleher, J. K., 2004. Quantifying carbon sources for de novo lipogenesis in wild-type and IRS-1 knockout brown adipocytes. Journal of Lipid Research. 45**,** 1324-1332.

Yoon, S. K., Choi, S. L., Song, J. Y., Lee, G. M., 2005. Effect of culture pH on erythropoietin production by chinese hamster ovary cells grown in suspension at 32.5 and 37.0 degrees C. Biotechnology and Bioengineering. 89**,** 345-356.

Yoon, S. K., Song, J. Y., Lee, G. M., 2003. Effect of low culture temperature on specific productivity, transcription level, and heterogeneity of erythropoietin in chinese hamster ovary cells. Biotechnology and Bioengineering. 82**,** 289-298.

Young, J. D., Walther, J. L., Antoniewicz, M. R., Yoo, H., Stephanopoulos, G., 2008. An Elementary Metabolite Unit (EMU) based method of isotopically nonstationary flux analysis. Biotechnology and Bioengineering. 99**,** 686-699.

Zamboni, N., 2011. 13C metabolic flux analysis in complex systems. Current Opinion in Biotechnology. 22**,** 103-108.

Zamorano, F., Wouwer, A. V., Bastin, G., 2010. A detailed metabolic flux analysis of an underdetermined network of CHO cells. Journal of Biotechnology. 150**,** 497-508.

Zhou, J. X., Tressel, T., Yang, X., Seewoester, T., 2008. Implementation of advanced technologies in commercial monoclonal antibody production. Biotechnology Journal. 3**,** 1185-1200.

Zhou, W., Rehm, J., Hu, W. S., 1995. High viable cell concentration fed-batch cultures of hybridoma cells through on-line nutrient feeding. Biotechnology and Bioengineering. 46**,** 579-587.

Zhu, M. M., Goyal, A., Rank, D. L., Gupta, S. K., Vanden Boom, T., Lee, S. S., 2005. Effects of elevated pCO2 and osmolality on growth of CHO cells and production of antibody-fusion protein B1: a case study. Biotechnology Progress. 21**,** 70-77.

Zupke, C., Stephanopoulos, G., 1994. Modeling of isotope distributions and intracellular fluxes in metabolic networks using atom mapping matrices. Biotechnology Progress. 10**,** 489-498.

Zupke, C., Stephanopoulos, G., 1995. Intracellular flux analysis in hybridomas using mass balances and in vitro13C nmr. Biotechnology and Bioengineering. 45**,** 292-303.

Appendix A

SUPPLEMENTARY DATA OF CHAPTER 3

Table A.1 Results of non-stationary ^{13}C-MFA. Shown are the estimated net and exchange fluxes (nmol/10^{6}cell/h) at the exponential phases with 95% confidence intervals.

			Exponential Phase				
Reaction			Flux	95% Confidence interval			
Gluc.ext → G6P	v1		207.0	[	172.6	,	240.8]
G6P ↔ F6P	v2	net	203.2	[	168.4	,	236.4]
		exch	0.0	[	0.0	,	Inf]
F6P → DHAP + GAP	v3		203.2	[	168.6	,	237.2]
DHAP ↔ GAP	v4	net	202.8	[	168.2	,	237.2]
		exch	0.0	[	0.0	,	255.1]
GAP ↔ 3PG	v5	net	406.0	[	338.1	,	475.0]
		exch	442.4	[	0.0	,	>1000]
3PG ↔ PEP	v6	net	406.0	[	338.1	,	475.0]
		exch	128.6	[	0.0	,	Inf]
PEP → Pyr	v7		406.0	[	338.1	,	475.0]
G6P → P5P + CO2	v8		1.8	[	1.5	,	2.2]
P5P ↔ X5P	v9	net	0.1	[	-0.2	,	0.2]
		exch	6.4	[	0.0	,	Inf]
P5P ↔ R5P	v10	net	0.0	[	-0.1	,	0.1]
		exch	>1000	[	0.0	,	Inf]
X5P ↔ EC2 + GAP	v11	net	0.1	[	-0.2	,	0.2]
		exch	3.8	[	0.0	,	Inf]
F6P ↔ EC2 + E4P	v12	net	0.0	[	-0.1	,	0.1]
		exch	3.4	[	0.0	,	Inf]

Table A.1 continued

S7P ↔ EC2 + R5P	v13	net	0.0	[	-0.1	,	0.1	]
		exch	>1000	[	0.0	,	Inf	]
F6P ↔ EC3 + GAP	v14	net	0.0	[	-0.1	,	0.1	]
		exch	2.2	[	0.0	,	>1000	]
S7P ↔ EC3 + E4P	v15	net	0.0	[	-0.1	,	0.1	]
		exch	>1000	[	0.0	,	Inf	]
Pyr ↔ Lact	v16	net	289.8	[	240.4	,	347.5	]
		exch	>1000	[	>1000	,	>1000	]
Lact ↔ Lact.snk	v17	net	0.0	[	0.0	,	0.0	]
		exch	>1000	[	>1000	,	>1000	]
Lact → Lact.ext	v18		289.8	[	240.4	,	347.5	]
Pyr ↔ Pyr.m	v19	net	109.7	[	36.9	,	182.1	]
		exch	>1000	[	392.8	,	Inf	]
Pyr.m → AcCoA.m + CO2	v20		138.3	[	67.9	,	207.2	]
AcCoA.m + OAC.m →Cit.m	v21		154.4	[	81.7	,	248.2	]
Cit.m ↔ AKG.m + CO2	v22	net	154.4	[	80.6	,	238.4	]
		exch	40.4	[	0.0	,	166.6	]
AKG.m → Suc.m + CO2	v23		178.6	[	106.3	,	259.3	]
Suc.m ↔ Fum.m	v24	net	185.3	[	111.8	,	270.1	]
		exch	91.6	[	0.0	,	Inf	]
Fum.m ↔ Mal.m	v25	net	187.4	[	113.8	,	266.5	]
		exch	>1000	[	0.0	,	Inf	]
Mal.m ↔ OAC.m	v26	net	133.9	[	74.3	,	213.1	]
		exch	336.7	[	0.0	,	>1000	]
Mal.m → Pyr.m + CO2	v27		53.5	[	32.5	,	84.8	]
Pyr.m + CO2 → OAC.m	v28		24.9	[	7.1	,	56.5	]
Mal.m ↔ Mal.c	v29	net	0.0	[	-77.0	,	0.0	]
		exch	133.5	[	32.0	,	259.5	]
Mal.c ↔ OAC.c	v30	net	0.0	[	-77.0	,	0.0	]
		exch	>1000	[	0.0	,	Inf	]
Cit.m ↔ Cit.c	v31	net	0.0	[	0.0	,	77.0	]

Table A.1 continued

		exch	74.9	[	3.9	,	792.1]
Cit.c → AcCoA.c + OAC.c	v32		0.0	[	0.0	,	77.0]
AcCoA.c → FA.c	v33		1.6	[	0.9	,	82.1]
FA.ext → FA.c	v34		15.2	[	0.0	,	53.5]
FA.c ↔ FA.m	v35	net	0.0	[	0.0	,	41.1]
		exch	57.7	[	0.0	,	Inf]
FA.m → AcCoA.m	v36		0.0	[	0.0	,	41.1]
DHAP → GLP	v37		0.4	[	0.3	,	0.5]
GLP.ext → GLP	v38		0.5	[	0.4	,	0.5]
Ala ↔ Pyr	v39	net	-6.6	[	-7.3	,	-6.1]
		exch	0.0	[	0.0	,	197.8]
Ser → Gly + C1	v40		5.2	[	4.5	,	6.1]
Ser → Pyr	v41		0.0	[	0.0	,	0.8]
AKG.m ↔ Glu	v42	net	-24.2	[	-30.5	,	-16.9]
		exch	41.5	[	28.9	,	90.3]
Glu → Pro	v43		2.1	[	1.9	,	2.4]
Gln → Glu	v44		33.8	[	26.9	,	40.5]
Asp ↔ OAC.m	v45	net	-4.4	[	-5.1	,	-4.1]
		exch	0.4	[	0.0	,	19.1]
Asp → Asn	v46		2.2	[	2.0	,	2.5]
Thr → AcCoA.c + Gly	v47		1.6	[	0.9	,	2.1]
Met + CO2 → Suc.m + CO2 + C1	v48		0.7	[	0.3	,	0.9]
Val + CO2 → Suc.m + CO2 + CO2	v49		2.1	[	1.0	,	2.8]
Ile + CO2 → Suc.m + AcCoA.m + CO2	v50		4.0	[	2.7	,	4.8]
Phe → Fum.m + AcCoA.m + AcCoA.m + CO2	v51		1.2	[	0.6	,	1.6]
Tyr → Fum.m + AcCoA.m + AcCoA.m + CO2	v52		0.8	[	0.4	,	1.1]
Leu + CO2 → AcCoA.m + AcCoA.m + AcCoA.m + CO2	v53		2.7	[	1.1	,	3.6]

Table A.1 continued

Ala → Ala.ext	v54	2.1	[	1.7	,	2.5]
Gly → Gly.ext	v55	2.7	[	2.3	,	3.2]
Pro.ext → Pro	v56	0.3	[	0.2	,	0.3]
Glu → Glu.ext	v57	5.2	[	4.2	,	6.2]
Asp.ext → Asp	v58	0.4	[	0.3	,	0.5]
Gln.ext → Gln	v59	36.7	[	29.8	,	43.6]
Ile.ext → Ile	v60	6.4	[	5.2	,	7.5]
Leu.ext → Leu	v61	6.9	[	5.5	,	8.2]
Met.ext → Met	v62	1.7	[	1.4	,	2.0]
Phe.ext → Phe	v63	2.9	[	2.3	,	3.4]
Ser.ext → Ser	v64	8.4	[	7.2	,	9.2]
Tyr.ext → Tyr	v65	2.2	[	1.8	,	2.6]
Val.ext → Val	v66	5.3	[	4.3	,	6.3]
Thr.ext → Thr	v67	4.5	[	3.8	,	5.1]
Arg.ext → Arg	v68	2.8	[	2.6	,	3.2]
Cys.ext → Cys	v69	1.1	[	1.0	,	1.3]
His.ext → His	v70	1.1	[	1.0	,	1.2]
Lys.ext → Lys	v71	4.3	[	3.9	,	4.9]
Trp.ext → Trp	v72	0.3	[	0.3	,	0.4]
Biomass formation	v73	72.1	[	65.9	,	82.7]

Table A.2 Results of non-stationary ^{13}C-MFA. Shown are the estimated net and exchange fluxes (nmol/10^6cell/h) at the stationary phases with 95% confidence intervals.

			Stationary Phase				
Reaction			Flux	95% Confidence interval			
Gluc.ext → G6P	v1		50.3	[	43.6	,	59.9]
G6P ↔ F6P	v2	net	40.2	[	33.9	,	49.3]
		exch	>1000	[	1.6	,	Inf]
F6P → DHAP + GAP	v3		46.9	[	40.4	,	56.3]
DHAP ↔ GAP	v4	net	46.9	[	40.4	,	56.2]
		exch	59.6	[	0.0	,	Inf]
GAP ↔ 3PG	v5	net	97.2	[	84.0	,	116.0]
		exch	4.0	[	0.0	,	>1000]
3PG ↔ PEP	v6	net	97.2	[	84.0	,	116.0]
		exch	86.2	[	0.0	,	Inf]
PEP → Pyr	v7		97.2	[	84.0	,	116.0]
G6P → P5P + CO2	v8		10.1	[	8.6	,	12.0]
P5P ↔ X5P	v9	net	6.7	[	5.7	,	8.0]
		exch	24.3	[	4.9	,	Inf]
P5P ↔ R5P	v10	net	3.4	[	2.8	,	4.0]
		exch	>1000	[	15.5	,	Inf]
X5P ↔ EC2 + GAP	v11	net	6.7	[	5.7	,	8.0]
		exch	21.3	[	4.7	,	Inf]
F6P ↔ EC2 + E4P	v12	net	-3.4	[	-4.0	,	-2.8]
		exch	3.3	[	0.0	,	42.2]
S7P ↔ EC2 + R5P	v13	net	-3.4	[	-4.0	,	-2.8]
		exch	140.5	[	21.1	,	Inf]
F6P ↔ EC3 + GAP	v14	net	-3.4	[	-4.0	,	-2.8]
		exch	761.3	[	26.0	,	>1000]
S7P ↔ EC3 + E4P	v15	net	3.4	[	2.8	,	4.0]
		exch	27.1	[	7.7	,	>1000]
Pyr ↔ Lact	v16	net	-2.5	[	-3.0	,	-2.0]
		exch	>1000	[	252.7	,	Inf]

Table A.2 continued

Lact↔ Lact.snk	v17	net	0.0	[	0.0	,	0.0]
		exch	459.6	[	0.0	,	>1000]
Lact→ Lact.ext	v18		2.5	[	2.0	,	3.0]
Pyr ↔ Pyr.m	v19	net	99.8	[	86.6	,	118.6]
		exch	>1000	[	79.5	,	Inf]
Pyr.m → AcCoA.m + CO2	v20		106.3	[	93.1	’	125.1]
AcCoA.m + OAC.m → Cit.m	v21		109.0	[	95.7	’	131.9]
Cit.m ↔ AKG.m + CO2	v22	net	109.0	[	95.7	,	132.7]
		exch	3.1	[	0.0	,	119.5]
AKG.m → Suc.m + CO2	v23		113.9	[	100.6	,	137.4]
Suc.m ↔ Fum.m	v24	net	114.7	[	101.4	,	139.4]
		exch	116.8	[	0.0	,	Inf]
Fum.m ↔ Mal.m	v25	net	115.0	[	101.7	,	140.2]
		exch	527.5	[	0.0	,	>1000]
Mal.m ↔ OAC.m	v26	net	96.9	[	80.6	,	119.2]
		exch	53.3	[	0.0	,	Inf]
Mal.m → Pyr.m + CO2	v27		18.1	[	7.7	,	43.1]
Pyr.m + CO2 → OAC.m	v28		11.7	[	1.2	,	40.0]
Mal.m ↔ Mal.c	v29	net	0.0	[	-49.7	,	0.0]
		exch	0.1	[	0.0	,	Inf]
Mal.c ↔ OAC.c	v30	net	0.0	[	-49.7	,	0.0]
		exch	0.1	[	0.0	,	Inf]
Cit.m ↔ Cit.c	v31	net	0.0	[	0.0	,	49.7]
		exch	58.1	[	5.1	,	164.8]
Cit.c → AcCoA.c + OAC.c	v32		0.0	[	0.0	’	49.7]
AcCoA.c → FA.c	v33		0.3	[	0.2	,	26.9]
FA.ext → FA.c	v34		0.0	[	0.0	,	19.2]
FA.c ↔ FA.m	v35	net	0.2	[	0.2	,	19.1]
		exch	13.5	[	0.0	,	Inf]
FA.m → AcCoA.m	v36		0.2	[	0.2	,	19.1]

Table A.2 continued

DHAP → GLP	v37		0.0	[	0.0	,	0.0	]
GLP.ext → GLP	v38		0.0	[	0.0	,	0.0	]
Ala ↔ Pyr	v39	net	-0.6	[	-0.7	,	-0.5	]
		exch	746.6	[	0.0	,	>1000	]
Ser → Gly + C1	v40		0.2	[	0.1	,	0.4	]
Ser → Pyr	v41		0.7	[	0.4	,	0.9	]
AKG.m ↔ Glu	v42	net	-4.9	[	-5.7	,	-4.1	]
		exch	>1000	[	133.3	,	Inf	]
Glu → Pro	v43		0.0	[	0.0	,	0.1	]
Gln → Glu	v44		4.2	[	3.3	,	5.0	]
Asp ↔ OAC.m	v45	net	0.5	[	0.4	,	0.6	]
		exch	3.0	[	1.4	,	95.0	]
Asp → Asn	v46		0.0	[	0.0	,	0.0	]
Thr → AcCoA.c + Gly	v47		0.3	[	0.2	,	0.4	]
Val + CO2 → Suc.m + CO2 + CO2	v49		0.3	[	0.2	,	0.4	]
Ile + CO2 → Suc.m + AcCoA.m + CO2	v50		0.4	[	0.3	,	0.4	]
Phe → Fum.m + AcCoA.m + AcCoA.m + CO2	v51		0.2	[	0.1	,	0.2	]
Tyr → Fum.m + AcCoA.m + AcCoA.m + CO2	v52		0.2	[	0.1	,	0.2	]
Leu + CO2 → AcCoA.m + AcCoA.m + AcCoA.m + CO2	v53		0.5	[	0.4	,	0.6	]
Ala → Ala.ext	v54		0.6	[	0.4	,	0.7	]
Gly → Gly.ext	v55		0.5	[	0.4	,	0.6	]
Pro.ext → Pro	v56		-0.0	[	-0.0	,	-0.0	]
Glu → Glu.ext	v57		-0.8	[	-1.0	,	-0.6	]
Asp.ext → Asp	v58		0.5	[	0.4	,	0.6	]
Gln.ext → Gln	v59		4.2	[	3.3	,	5.0	]
Ile.ext → Ile	v60		0.4	[	0.3	,	0.4	]

Table A.2 continued

Leu.ext → Leu	v61	0.5	[	0.4	,	0.6]
Met.ext → Met	v62	0.1	[	0.1	,	0.2]
Phe.ext → Phe	v63	0.2	[	0.1	,	0.2]
Ser.ext → Ser	v64	0.9	[	0.7	,	1.1]
Tyr.ext → Tyr	v65	0.2	[	0.1	,	0.2]
Val.ext → Val	v66	0.3	[	0.3	,	0.4]
Thr.ext → Thr	v67	0.3	[	0.3	,	0.4]
Arg.ext → Arg	v68	0.0	[	0.0	,	0.0]
Cys.ext → Cys	v69	0.0	[	0.0	,	0.0]
His.ext → His	v70	0.0	[	0.0	,	0.0]
Lys.ext → Lys	v71	0.0	[	0.0	,	0.0]
Trp.ext → Trp	v72	0.0	[	0.0	,	0.0]
Biomass formation	v73	0.2	[	0.2	,	0.3]

Table A.3 Mass isotopomer distributions of intracellular metabolites measured by GC-MS. (data not corrected for natural isotope abundances)

	Exponential Phase			Stationary Phase		
Isotopomer	6 h	12 h	24 h	6 h	12 h	24 h
Pyr174 (M0)	0.7426	0.7117	0.6681	0.8131	0.8028	0.7887
Pyr175 (M1)	0.1125	0.1137	0.1025	0.1070	0.1047	0.1037
Pyr176 (M2)	0.1225	0.1473	0.1980	0.0691	0.0795	0.0926
Pyr177 (M3)	0.0160	0.0184	0.0223	0.0082	0.0099	0.0115
Pyr178 (M4)	0.0056	0.0074	0.0084	0.0023	0.0027	0.0030
Pyr179 (M5)	0.0008	0.0015	0.0007	0.0004	0.0003	0.0005
Lact233 (M0)	0.6652	0.6338	0.5888	0.7309	0.7193	0.7060
Lact234 (M1)	0.1464	0.1421	0.1355	0.1596	0.1572	0.1554
Lact235 (M2)	0.1524	0.1802	0.2202	0.0913	0.1021	0.1139
Lact236 (M3)	0.0264	0.0318	0.0398	0.0143	0.0165	0.0188
Lact237 (M4)	0.0095	0.0121	0.0157	0.0038	0.0049	0.0059
Lact261 (M0)	0.6432	0.6156	0.5657	0.7119	0.6986	0.6868
Lact262 (M1)	0.1526	0.1454	0.1382	0.1674	0.1654	0.1622
Lact263 (M2)	0.1607	0.1859	0.2279	0.0970	0.1079	0.1179
Lact264 (M3)	0.0306	0.0361	0.0466	0.0181	0.0210	0.0236
Lact265 (M4)	0.0114	0.0148	0.0189	0.0050	0.0062	0.0082
Lact266 (M5)	0.0016	0.0023	0.0029	0.0008	0.0010	0.0014
Ala232 (M0)	0.7390	0.7184	0.6801	0.7456	0.7365	0.7167
Ala233 (M1)	0.1635	0.1608	0.1544	0.1646	0.1632	0.1612
Ala234 (M2)	0.0821	0.0999	0.1345	0.0760	0.0840	0.1009
Ala235 (M3)	0.0125	0.0164	0.0233	0.0114	0.0131	0.0165
Ala236 (M4)	0.0029	0.0045	0.0077	0.0024	0.0031	0.0046
Ala260 (M0)	0.7287	0.7110	0.6732	0.7370	0.7279	0.7082
Ala261 (M1)	0.1709	0.1658	0.1584	0.1693	0.1679	0.1654
Ala262 (M2)	0.0825	0.0976	0.1329	0.0776	0.0853	0.1014
Ala263 (M3)	0.0144	0.0197	0.0261	0.0130	0.0150	0.0191
Ala264 (M4)	0.0032	0.0051	0.0082	0.0028	0.0036	0.0053
Ala265 (M5)	0.0006	0.0010	0.0013	0.0004	0.0005	0.0008
Suc289 (M0)	0.7070	0.6943	0.6487	0.7131	0.6929	0.6590
Suc290 (M1)	0.1807	0.1754	0.1810	0.1791	0.1838	0.1950
Suc291 (M2)	0.0883	0.0998	0.1267	0.0848	0.0942	0.1111
Suc292 (M3)	0.0161	0.0204	0.0297	0.0160	0.0193	0.0245
Suc293 (M4)	0.0044	0.0068	0.0105	0.0049	0.0054	0.0072

Table A.3 continued

Suc294 (M5)	0.0028	0.0026	0.0027	0.0020	0.0037	0.0029
Suc295 (M6)	0.0006	0.0007	0.0007	0.0003	0.0008	0.0005
Fum287 (M0)	0.7140	0.6943	0.6585	0.7117	0.7095	0.6869
Fum288 (M1)	0.1747	0.1760	0.1784	0.1791	0.1817	0.1866
Fum289 (M2)	0.0874	0.0982	0.1213	0.0832	0.0838	0.0959
Fum290 (M3)	0.0166	0.0213	0.0282	0.0188	0.0169	0.0213
Fum291 (M4)	0.0053	0.0077	0.0106	0.0046	0.0051	0.0075
Fum292 (M5)	0.0012	0.0019	0.0024	0.0015	0.0017	0.0012
Fum293 (M6)	0.0007	0.0006	0.0007	0.0010	0.0012	0.0007
Ser390 (M0)	0.6303	0.6275	0.6134	0.6218	0.6166	0.6218
Ser391 (M1)	0.2202	0.2194	0.2215	0.2174	0.2205	0.2181
Ser392 (M2)	0.1125	0.1140	0.1233	0.1176	0.1201	0.1175
Ser393 (M3)	0.0284	0.0297	0.0312	0.0314	0.0315	0.0317
Ser394 (M4)	0.0073	0.0080	0.0088	0.0095	0.0092	0.0089
Ser395 (M5)	0.0013	0.0015	0.0017	0.0022	0.0021	0.0020
AKG346 (M0)	0.6254	0.5933	0.5682	0.6455	0.6345	0.5809
AKG347 (M1)	0.1704	0.1653	0.1646	0.1835	0.1855	0.1964
AKG348 (M2)	0.1392	0.1761	0.1816	0.1167	0.1230	0.1440
AKG349 (M3)	0.0342	0.0385	0.0479	0.0256	0.0288	0.0370
AKG350 (M4)	0.0156	0.0178	0.0199	0.0055	0.0077	0.0177
AKG351 (M5)	0.0040	0.0032	0.0059	0.0056	0.0052	0.0079
AKG352 (M6)	0.0038	0.0017	0.0034	0.0016	0.0007	0.0002
AKG353 (M7)	0.0077	0.0075	0.0085	0.0161	0.0159	0.0163
Mal391 (M0)	0.6241	0.5995	0.5673	0.6277	0.6090	0.5694
Mal392 (M1)	0.2168	0.2233	0.2306	0.2244	0.2300	0.2372
Mal393 (M2)	0.1172	0.1266	0.1429	0.1092	0.1180	0.1366
Mal394 (M3)	0.0299	0.0348	0.0413	0.0288	0.0319	0.0392
Mal395 (M4)	0.0092	0.0117	0.0148	0.0074	0.0097	0.0127
Mal396 (M5)	0.0028	0.0041	0.0031	0.0025	0.0014	0.0049
Mal419 (M0)	0.6156	0.5945	0.5560	0.6151	0.5984	0.5615
Mal420 (M1)	0.2202	0.2176	0.2164	0.2266	0.2288	0.2345
Mal421 (M2)	0.1221	0.1351	0.1566	0.1179	0.1257	0.1428
Mal422 (M3)	0.0307	0.0367	0.0482	0.0297	0.0340	0.0429
Mal423 (M4)	0.0090	0.0123	0.0173	0.0081	0.0101	0.0136
Mal424 (M5)	0.0018	0.0029	0.0043	0.0018	0.0020	0.0033
Mal425 (M6)	0.0007	0.0010	0.0013	0.0010	0.0012	0.0015

Table A.3 continued

Asp302 (M0)	0.7055	0.7095	0.6724	0.7064	0.6995	0.6785
Asp303 (M1)	0.1916	0.1995	0.2009	0.1924	0.1938	0.2007
Asp304 (M2)	0.0836	0.0910	0.1008	0.0825	0.0861	0.0963
Asp305 (M3)	0.0157	0.0000	0.0206	0.0153	0.0166	0.0196
Asp306 (M4)	0.0035	0.0000	0.0052	0.0034	0.0039	0.0050
Asp390 (M0)	0.6248	0.6081	0.5781	0.6268	0.6170	0.5885
Asp391 (M1)	0.2232	0.2256	0.2317	0.2266	0.2292	0.2395
Asp392 (M2)	0.1146	0.1220	0.1361	0.1107	0.1150	0.1250
Asp393 (M3)	0.0285	0.0330	0.0396	0.0276	0.0296	0.0353
Asp394 (M4)	0.0075	0.0093	0.0120	0.0069	0.0079	0.0096
Asp395 (M5)	0.0014	0.0019	0.0026	0.0015	0.0013	0.0020
Asp418 (M0)	0.6159	0.5999	0.5663	0.6170	0.6030	0.5753
Asp419 (M1)	0.2229	0.2206	0.2191	0.2280	0.2301	0.2331
Asp420 (M2)	0.1194	0.1284	0.1481	0.1145	0.1214	0.1343
Asp421 (M3)	0.0306	0.0356	0.0450	0.0292	0.0326	0.0404
Asp422 (M4)	0.0091	0.0122	0.0166	0.0089	0.0099	0.0129
Asp423 (M5)	0.0018	0.0027	0.0039	0.0019	0.0023	0.0034
Asp424 (M6)	0.0004	0.0007	0.0010	0.0005	0.0008	0.0006
PEP453 (M0)	0.4377	0.4487	0.4178	0.4434	0.4494	0.4599
PEP454 (M1)	0.1540	0.1608	0.1514	0.1780	0.1868	0.1925
PEP455 (M2)	0.2767	0.2675	0.2909	0.2470	0.2344	0.2211
PEP456 (M3)	0.0839	0.0779	0.0895	0.0849	0.0850	0.0843
PEP457 (M4)	0.0379	0.0364	0.0412	0.0357	0.0333	0.0328
PEP458 (M5)	0.0097	0.0087	0.0094	0.0110	0.0112	0.0094
Glu330 (M0)	0.6889	0.6681	0.6272	0.6824	0.6650	0.6244
Glu331 (M1)	0.1979	0.1981	0.1995	0.2046	0.2089	0.2193
Glu332 (M2)	0.0896	0.1022	0.1259	0.0894	0.0979	0.1163
Glu333 (M3)	0.0183	0.0233	0.0335	0.0186	0.0217	0.0299
Glu334 (M4)	0.0044	0.0068	0.0111	0.0042	0.0054	0.0082
Glu335 (M5)	0.0007	0.0013	0.0023	0.0007	0.0009	0.0015
Glu336 (M6)	0.0002	0.0003	0.0005	0.0002	0.0002	0.0003
Glu432 (M0)	0.6102	0.5936	0.5555	0.6046	0.5877	0.5481
Glu433 (M1)	0.2273	0.2236	0.2182	0.2312	0.2321	0.2343
Glu434 (M2)	0.1201	0.1304	0.1526	0.1206	0.1297	0.1493
Glu435 (M3)	0.0311	0.0363	0.0478	0.0321	0.0363	0.0469
Glu436 (M4)	0.0090	0.0123	0.0193	0.0092	0.0112	0.0163

Table A.3 continued

Glu437 (M5)	0.0019	0.0030	0.0051	0.0020	0.0025	0.0040
Glu438 (M6)	0.0004	0.0007	0.0014	0.0004	0.0006	0.0010
Glu439 (M7)	0.0001	0.0002	0.0003	0.0001	0.0001	0.0002
GAP484 (M0)	0.4084	0.4012	0.3822	0.3898	0.4045	0.4019
GAP485 (M1)	0.1485	0.1499	0.1456	0.1728	0.1896	0.1845
GAP486 (M2)	0.2994	0.2988	0.3132	0.2721	0.2541	0.2552
GAP487 (M3)	0.0927	0.0939	0.0992	0.1037	0.0940	0.0999
GAP488 (M4)	0.0419	0.0460	0.0481	0.0520	0.0454	0.0460
GAP489 (M5)	0.0090	0.0100	0.0118	0.0096	0.0123	0.0127
GLP571 (M0)	0.4492	0.4163	0.3776	0.4975	0.4824	0.4622
GLP572 (M1)	0.2113	0.1972	0.1822	0.2373	0.2326	0.2288
GLP573 (M2)	0.2160	0.2421	0.2695	0.1724	0.1819	0.1931
GLP574 (M3)	0.0803	0.0924	0.1074	0.0627	0.0689	0.0765
GLP575 (M4)	0.0341	0.0410	0.0494	0.0237	0.0267	0.0306
GLP576 (M5)	0.0092	0.0111	0.0139	0.0065	0.0075	0.0087
Cit459 (M0)	0.5523	0.5100	0.4467	0.5870	0.5610	0.5242
Cit460 (M1)	0.2123	0.2023	0.1895	0.2288	0.2283	0.2282
Cit461 (M2)	0.1607	0.1872	0.2220	0.1315	0.1456	0.1644
Cit462 (M3)	0.0472	0.0596	0.0789	0.0362	0.0428	0.0533
Cit463 (M4)	0.0185	0.0275	0.0428	0.0110	0.0148	0.0207
Cit464 (M5)	0.0047	0.0072	0.0122	0.0026	0.0036	0.0052
Cit465 (M6)	0.0013	0.0022	0.0043	0.0006	0.0009	0.0016
Cit466 (M7)	0.0011	0.0023	0.0024	0.0009	0.0012	0.0009
Cit467 (M8)	0.0019	0.0017	0.0012	0.0013	0.0018	0.0016
3PG585 (M0)	0.3856	0.3863	0.3579	0.3711	0.3716	0.3773
3PG586 (M1)	0.1821	0.1871	0.1725	0.1978	0.2022	0.2074
3PG587 (M2)	0.2660	0.2705	0.2938	0.2545	0.2606	0.2495
3PG588 (M3)	0.1020	0.1062	0.1188	0.1202	0.1128	0.1110
3PG589 (M4)	0.0490	0.0499	0.0570	0.0565	0.0527	0.0548

Appendix B

SUPPLEMENTARY DATA OF CHAPTER 4

Table B.1 Results of combined ^{13}C-MFA using [1,2-^{13}C]glucose and [U-^{13}C]glutamine parallel labeling experiments at the exponential phase. Shown are the estimated net and exchange fluxes (nmol/10^6cell/h) and G-values with 95% confidence intervals.

Exponential Phase							
Reaction			Flux	95% Conf. interval			
Gluc.ext → G6P	v1		204.1	[	194.4	, 213.9	]
G6P ↔ F6P	v2	net	201.0	[	191.1	, 210.9	]
		exch	(0.0, >1e3)	[	0.0	, >1e4	]
F6P→FBP	v3		199.5	[	189.7	, 209.3	]
FBP ↔ DHAP + GAP	v4	net	199.5	[	189.7	, 209.3	]
		exch	(0.0, >1e4)	[	0.0	, >1e4	]
DHAP ↔ GAP	v5	net	198.3	[	188.5	, 208.2	]
		exch	(0.0, >1e4)	[	0.0	, >1e4	]
GAP ↔ 3PG	v6	net	397.1	[	377.5	, 416.7	]
		exch	(0.0, >1e4)	[	0.0	, >1e4	]
3PG ↔ PEP	v7	net	397.1	[	377.5	, 416.7	]
		exch	(0.0, >1e4)	[	0.0	, >1e4	]
PEP → Pyr.c	v8		397.1	[	377.5	, 417.1	]
G6P → Ru5P + CO2	v9		0.2	[	0.0	, 2.5	]
Ru5P ↔ X5P	v10	net	-1.5	[	-1.8	, 0.0	]
		exch	(115.0, >1e4)	[	0.0	, >1e4	]
Ru5P ↔ R5P	v11	net	-0.8	[	-0.9	, 0.0	]
		exch	0.0	[	0.0	, 0.3	]
X5P ↔ EC2 + GAP	v12	net	-1.5	[	-1.8	, 0.0	]

Table B.1 continued

		exch	(111.9, >1e4)	[	0.0	,	>1e4]
F6P ↔ EC2 + E4P	v13	net	0.8	[	-0.0	,	0.9]
		exch	(0.0, >1e3)	[	0.0	,	>1e4]
S7P ↔ EC2 + R5P	v14	net	0.8	[	-0.0	,	0.9]
		exch	(0.0, >1e4)	[	0.0	,	1e4]
F6P ↔ EC3 + GAP	v15	net	0.8	[	-0.0	,	0.9]
		exch	(0.0, >1e4)	[	0.0	,	>1e4]
S7P ↔ EC3 + E4P	v16	net	-0.8	[	-0.9	,	0.0]
		exch	(0.0, >1e4)	[	0.0	,	>1e4]
Pyr.c ↔ Lact	v17	net	292.0	[	282.3	,	301.8]
		exch	(0.0, >1e4)	[	0.0	,	>1e4]
Pyr.c → Pyr.snk	v18		48.3	[	24.9	,	70.3]
Pyr.c → Pyr.m	v19		42.4	[	30.4	,	48.6]
Pyr.m → AcCoA.m + CO2	v20		34.8	[	30.6	,	39.7]
AcCoA.m + OAC.m → Cit.m	v21		35.7	[	31.7	,	40.5]
Cit.m ↔ AKG.m + CO2	v22	net	8.9	[	5.7	,	10.6]
		exch	2.1	[	1.4	,	2.9]
AKG.m → Suc.m + CO2	v23		23.6	[	18.4	,	29.1]
Suc.m ↔ Fum.m	v24	net	24.4	[	19.1	,	29.9]
		exch	1.3	[	0.0	,	10.2]
Fum.m ↔ Mal.m	v25	net	24.3	[	19.0	,	29.9]
		exch	(55.2, 916.0)	[	0.0	,	>1e4]
Mal.m ↔ OAC.m	v26	net	23.7	[	20.5	,	30.5]
		exch	73.0	[	14.0	,	440.4]
Mal.m → Pyr.mII + CO2	v27		4.3	[	2.7	,	6.6]
Pyr.mII + CO2 → OAC.m	v28		11.9	[	3.0	,	15.5]
Pyr.m ↔ Pyr.mII	v29	net	7.6	[	-0.8	,	9.9]
		exch	0.0	[	0.0	,	6.6]
Mal.c → Pyr.c + CO2	v30		12.4	[	4.1	,	18.3]
Mal.m ↔ Mal.c	v31	net	-3.9	[	-11.5	,	2.5]
		exch	(105.6, 410.7)	[	26.8	,	>1e4]

Table B.1 continued

Mal.c ↔ OAC.c	v32	net	-16.3	[	-20.5	,	-9.4]
		exch	(139.0, >1e4)	[	27.7	,	>1e4]
OAC.c → PEP + CO2	v33		0.0	[	0.0	,	6.7]
Cit.m ↔ Cit.c	v34	net	26.8	[	24.5	,	31.2]
		exch	(0.0, >1e4)	[	0.0	,	>1e4]
Cit.c → AcCoA.c + OAC.c	v35		23.0	[	20.8	,	27.4]
AcCoA.c → FA	v36		23.7	[	21.9	,	27.9]
FA → FA.snk	v37		0.0	[	0.0	,	3.9]
DHAP → GLP	v38		1.1	[	1.1	,	1.2]
Gln → Glu	v39		25.8	[	21.9	,	30.2]
Glu ↔ AKG.m	v40	net	14.7	[	10.8	,	19.1]
		exch	(631.4, >1e3)	[	226.7	,	>1e4]
Glu ↔ Pro	v41	net	3.7	[	3.5	,	4.0]
		exch	(0.0, >1e4)	[	0.0	,	>1e4]
Asp ↔ OAC.c	v42	net	-6.8	[	-7.3	,	-6.3]
		exch	(0.0, >1e4)	[	0.0	,	>1e4]
Asp → Asn	v43		3.0	[	2.8	,	3.3]
Pyr.c ↔ Ala	v44	net	10.5	[	9.6	,	11.4]
		exch	(0.0, >1e4)	[	0.0	,	>1e4]
Ser ↔ Pyr.c	v45	net	-4.2	[	-6.4	,	-2.0]
		exch	(0.0, >1e4)	[	0.0	,	>1e4]
Ser → Gly + C1	v46		8.1	[	6.9	,	9.4]
Thr → AcCoA.c + Gly	v47		0.6	[	0.0	,	1.6]
Met + CO2 → Suc.m + CO2 + C1	v48		0.0	[	0.0	,	0.3]
Val + CO2 → Suc.m + CO2 + CO2	v49		0.0	[	0.0	,	0.6]
Ile + CO2 → Suc.m + AcCoA.m + CO2	v50		0.9	[	0.1	,	1.7]
Phe → Fum.m + AcCoA.m + AcCoA.m + CO2	v51		0.0	[	0.0	,	0.5]
Tyr → Fum.m + AcCoA.m + AcCoA.m + CO2	v52		0.0	[	0.0	,	0.4]

Table B.1 continued

Leu + CO2 → AcCoA.m + AcCoA.m + AcCoA.m + CO2	v53	0.0	[	0.0	,	0.5]
Gln.ext → Gln	v54	29.9	[	25.9	,	34.3]
Asp.ext → Asp	v55	0.1	[	0.0	,	0.1]
Ile.ext → Ile	v56	4.3	[	3.5	,	5.1]
Leu.ext → Leu	v57	5.9	[	5.5	,	6.5]
Met.ext → Met	v58	1.5	[	1.4	,	1.6]
Phe.ext → Phe	v59	2.3	[	2.2	,	2.6]
Ser.ext → Ser	v60	8.5	[	6.8	,	10.2]
Tyr.ext → Tyr	v61	1.9	[	1.8	,	2.2]
Val.ext → Val	v62	4.4	[	4.1	,	4.7]
Thr.ext → Thr	v63	4.7	[	3.9	,	5.6]
Arg.ext → Arg	v64	4.0	[	3.7	,	4.3]
Cys.ext → Cys	v65	1.5	[	1.4	,	1.6]
His.ext → His	v66	1.5	[	1.4	,	1.6]
Lys.ext → Lys	v67	6.0	[	5.6	,	6.4]
Trp.ext → Trp	v68	0.5	[	0.4	,	0.5]
Ala → Ala.ext	v69	4.2	[	3.4	,	5.0]
Gly → Gly.ext	v70	3.1	[	2.5	,	3.7]
Pro → Pro.ext	v71	0.4	[	0.3	,	0.5]
Glu → Glu.ext	v72	4.0	[	3.2	,	4.7]
Lact→ Lact.ext	v73	292.0	[	282.3	,	301.8]
Pyr.c → Pyr.ext	v74	12.0	[	9.7	,	14.3]
Suc.m → Suc.ext	v75	0.2	[	0.0	,	0.5]
Fum.m → Fum.ext	v76	0.0	[	0.0	,	0.0]
Mal.m → Mal.ext	v77	0.2	[	0.1	,	0.2]
Cit.c → Cit.ext	v78	3.7	[	3.0	,	4.5]
Biomass reaction	v79	101.2	[	93.8	,	108.4]

Metabolite	G-value	95% Conf. interval		
DHAP	0.58	[0.50	,	0.94]
3PG	0.80	[0.78	,	0.82]

Table B.1 continued

PEP	0.77	[	0.75 ,	0.78]
Gln	1.00	[	0.99 ,	1.00]
AKG	0.80	[	0.72 ,	0.82]
Suc	0.82	[	0.73 ,	0.87]
Mal.m	1.00	[	0.72 ,	1.00]
Asp	0.96	[	0.69 ,	1.00]
Cit.m	0.98	[	0.67 ,	1.00]
Glu	0.83	[	0.75 ,	0.85]
Pro	0.32	[	0.28 ,	0.33]

G-value, fractional labeling of metabolites

Table B.2 Results of combined ^{13}C-MFA using [1,2-^{13}C]glucose and [U-^{13}C]glutamine parallel labeling experiments at the stationary phase. Shown are the estimated net and exchange fluxes (nmol/10^{6}cell/h) and G-values with 95% confidence intervals.

Stationary Phase							
Reaction			Flux	95% Conf. interval			
Gluc.ext → G6P	v1		42.4	[	38.3	, 46.5	]
G6P ↔ F6P	v2	net	29.2	[	18.4	, 34.9	]
		exch	(0.0, 92.4)	[	0.0	, >1e4	]
F6P→FBP	v3		38.0	[	32.8	, 42.5	]
FBP ↔ DHAP + GAP	v4	net	38.0	[	32.8	, 42.5	]
		exch	(0.0, >1e4)	[	0.0	, >1e4	]
DHAP ↔ GAP	v5	net	38.0	[	32.8	, 42.5	]
		exch	(0.0, >1e4)	[	0.0	, >1e4	]
GAP ↔ 3PG	v6	net	80.3	[	71.5	89.0	]
		exch	(0.0, >1e4)	[	0.0	, >1e4	]
3PG ↔ PEP	v7	net	80.3	[	71.5	89.0	]
		exch	(0.0, >1e4)	[	0.0	, >1e4	]
PEP → Pyr.c	v8		80.3	[	71.5	89.2	]
G6P → Ru5P + CO2	v9		13.1	[	9.1	, 25.1	]
Ru5P ↔ X5P	v10	net	8.7	[	6.1	, 16.7	]
		exch	(0.0, >1e4)	[	0.0	, >1e4	]
Ru5P ↔ R5P	v11	net	4.4	[	3.0	, 8.4	]
		exch	(0.0, >1e4)	[	0.0	, 1e4	]
X5P ↔ EC2 + GAP	v12	net	8.7	[	6.1	, 16.7	]
		exch	(0.0, >1e4)	[	0.0	, >1e4	]
F6P ↔ EC2 + E4P	v13	net	-4.4	[	-8.4	, -3.0	]
		exch	(8.8, 307.6)	[	0.0	, >1e3	]
S7P ↔ EC2 + R5P	v14	net	-4.4	[	-8.4	, -3.0	]
		exch	(0.0, >1e4)	[	0.0	, >1e4	]
F6P ↔ EC3 + GAP	v15	net	-4.4	[	-8.4	, -3.0	]
		exch	(0.0, >1e4)	[	0.0	, >1e4	]
S7P ↔ EC3 + E4P	v16	net	4.4	[	3.0	, 8.4	]

Table B.2 continued

		exch	(0.0, 2.2)	[0.0 ,	>1e4	]
Pyr.c ↔ Lact	v17	net	-10.0	[-12.0 ,	-8.1	]
		exch	(0.0, >1e3)	[0.0 ,	>1e4	]
Pyr.c → Pyr.snk	v18		66.4	[56.3 ,	76.2	]
Pyr.c → Pyr.m	v19		24.4	[20.5 ,	28.9	]
Pyr.m → AcCoA.m + CO2	v20		26.9	[22.5 ,	31.4	]
AcCoA.m + OAC.m → Cit.m	v21		28.9	[24.5 ,	33.3	]
Cit.m ↔ AKG.m + CO2	v22	net	8.7	[7.2 ,	10.6	]
		exch	2.1	[1.5 ,	2.7	]
AKG.m → Suc.m + CO2	v23		15.5	[12.8 ,	18.4	]
Suc.m ↔ Fum.m	v24	net	15.8	[13.1 ,	18.8	]
		exch	0.0	[0.0 ,	11.4	]
Fum.m ↔ Mal.m	v25	net	16.1	[13.4 ,	19.0	]
		exch	(48.1, 200.6)	[3.1 ,	>1e4	]
Mal.m ↔ OAC.m	v26	net	28.9	[24.5 ,	33.3	]
		exch	(0.0, >1e4)	[0.0 ,	>1e4	]
Mal.m → Pyr.mII + CO2	v27		2.5	[0.8 ,	4.3	]
Pyr.mII + CO2 → OAC.m	v28		0.0	[0.0 ,	1.7	]
Pyr.m ↔ Pyr.mII	v29	net	-2.5	[-4.2 ,	-0.4	]
		exch	(0.0, >1e3)	[0.0 ,	>1e4	]
Mal.c → Pyr.c + CO2	v30		2.2	[0.2 ,	3.9	]
Mal.m ↔ Mal.c	v31	net	-15.4	[11.2 ,	19.6	]
		exch	(39.0, 181.6)	[1.4 ,	>1e4	]
Mal.c ↔ OAC.c	v32	net	-17.6	[-21.4 ,	-13.6	]
		exch	(60.5, >1e3)	[1.3 ,	>1e4	]
OAC.c → PEP + CO2	v33		0.1	[0.0 ,	1.5	]
Cit.m ↔ Cit.c	v34	net	20.2	[16.5 ,	24.0	]
		exch	(0.0, >1e4)	[0.0 ,	>1e4	]
Cit.c → AcCoA.c + OAC.c	v35		17.3	[13.5 ,	21.1	]
AcCoA.c → FA	v36		17.3	[13.6 ,	21.1	]
FA → FA.snk	v37		17.2	[13.5 ,	21.0	]

Table B.2 continued

DHAP → GLP	v38		0.0	[	0.0	,	0.0]
Gln → Glu	v39		6.4	[	5.2	,	7.7]
Glu ↔ AKG.m	v40	net	6.8	[	5.6	,	8.1]
		exch	200.4	[	107.6	,	997.3]
Glu ↔ Pro	v41	net	0.4	[	0.4	,	0.5]
		exch	(0.0, >1e4)	[	0.0	,	>1e4]
Asp ↔ OAC.c	v42	net	0.4	[	0.2	,	0.5]
		exch	(1.4, >1e4)	[	0.8	,	>1e4]
Asp → Asn	v43		0.0	[	0.0	,	0.0]
Pyr.c ↔ Ala	v44	net	1.9	[	1.5	,	2.3]
		exch	(0.0, >1e4)	[	0.0	,	>1e4]
Ser ↔ Pyr.c	v45	net	0.0	[	-0.0	,	0.0]
		exch	(0.0, >1e4)	[	0.0	,	>1e4]
Ser → Gly + C1	v46		0.1	[	0.0	,	0.1]
Thr → AcCoA.c + Gly	v47		0.1	[	0.0	,	0.1]
Met + CO2 → Suc.m + CO2 + C1	v48		0.1	[	0.1	,	0.2]
Val + CO2 → Suc.m + CO2 + CO2	v49		0.0	[	0.0	,	0.1]
Ile + CO2 → Suc.m + AcCoA.m + CO2	v50		0.2	[	0.2	,	0.3]
Phe → Fum.m + AcCoA.m + AcCoA.m + CO2	v51		0.0	[	0.0	,	0.1]
Tyr → Fum.m + AcCoA.m + AcCoA.m + CO2	v52		0.2	[	0.1	,	0.3]
Leu + CO2 → AcCoA.m + AcCoA.m + AcCoA.m + CO2	v53		0.4	[	0.3	,	0.5]
Gln.ext → Gln	v54		6.4	[	5.2	,	7.7]
Asp.ext → Asp	v55		0.4	[	0.2	,	0.6]
Ile.ext → Ile	v56		0.3	[	0.2	,	0.3]
Leu.ext → Leu	v57		0.5	[	0.4	,	0.6]
Met.ext → Met	v58		0.2	[	0.1	,	0.2]
Phe.ext → Phe	v59		0.1	[	0.0	,	0.1]
Ser.ext → Ser	v60		0.1	[	0.1	,	0.1]

Table B.2 continued

Tyr.ext → Tyr	v61	0.2	[	0.1 ,	0.3]
Val.ext → Val	v62	0.1	[	0.0 ,	0.1]
Thr.ext → Thr	v63	0.1	[	0.1 ,	0.1]
Arg.ext → Arg	v64	0.0	[	0.0 ,	0.0]
Cys.ext → Cys	v65	0.0	[	0.0 ,	0.0]
His.ext → His	v66	0.0	[	0.0 ,	0.0]
Lys.ext → Lys	v67	0.0	[	0.0 ,	0.0]
Trp.ext → Trp	v68	0.0	[	0.0 ,	0.0]
Ala → Ala.ext	v69	1.9	[	1.5 ,	2.3]
Gly → Gly.ext	v70	0.1	[	0.1 ,	0.1]
Pro → Pro.ext	v71	0.4	[	0.3 ,	0.5]
Glu.ext → Glu	v72	0.9	[	0.7 ,	1.0]
Lact.ext → Lact	v73	10.0	[	8.1 ,	12.0]
Pyr.ext → Pyr.c	v74	0.1	[	0.1 ,	0.1]
Suc.m → Suc.ext	v75	0.1	[	0.1 ,	0.1]
Fum.m → Fum.ext	v76	0.1	[	0.1 ,	0.1]
Mal.m → Mal.ext	v77	0.1	[	0.1 ,	0.1]
Cit.c → Cit.ext	v78	3.0	[	2.4 ,	3.5]
Biomass reaction	v79	0.5	[	0.5 ,	0.6]

Metabolite	G-value	95% Conf. interval	
DHAP	0.56	[0.44 ,	0.98]
3PG	0.79	[0.75 ,	0.86]
PEP	0.75	[0.71 ,	0.82]
Gln	0.99	[0.98 ,	1.00]
AKG	0.74	[0.70 ,	0.83]
Suc	0.71	[0.67 ,	0.79]
Mal.m	0.82	[0.77 ,	0.97]
Asp	0.80	[0.74 ,	1.00]
Cit.m	0.61	[0.57 ,	0.73]
Glu	0.76	[0.72 ,	0.85]
Pro	0.25	[0.23 ,	0.28]

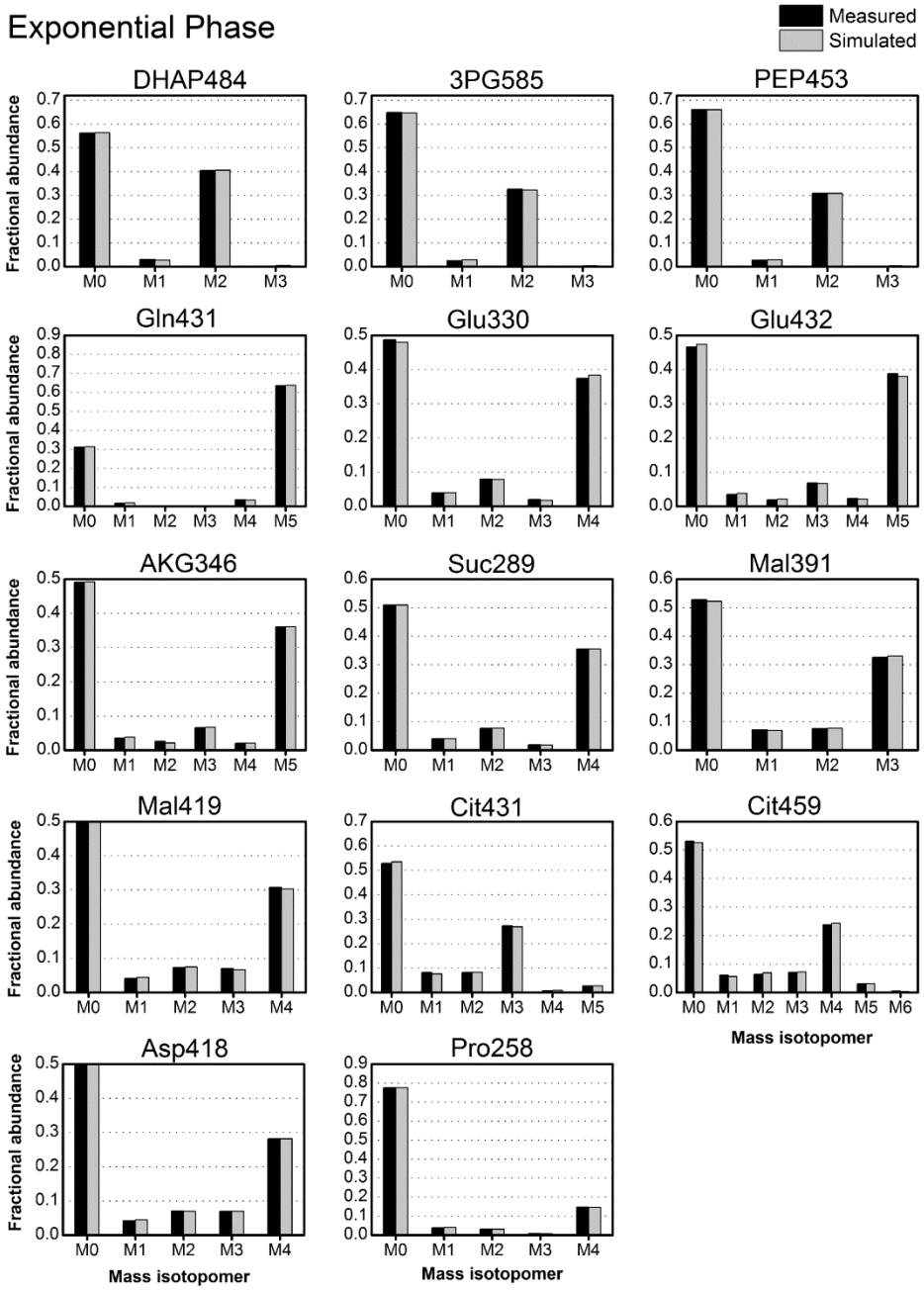

Figure B.1 Measured and fitted mass isotopomer distributions of intracellular metabolites from combined ^{13}C-MFA analysis at the exponential phase. [1,2-^{13}C]Glucose experimental data are DHAP484, 3PG585 and PEP453. [U-^{13}C]Glutamine experimental data are Gln431, Glu330, Glu432, AKG346, Suc289, Mal391, Mal419, Cit431, Cit459, Asp418 and Pro258. (data corrected for natural isotope abundances)

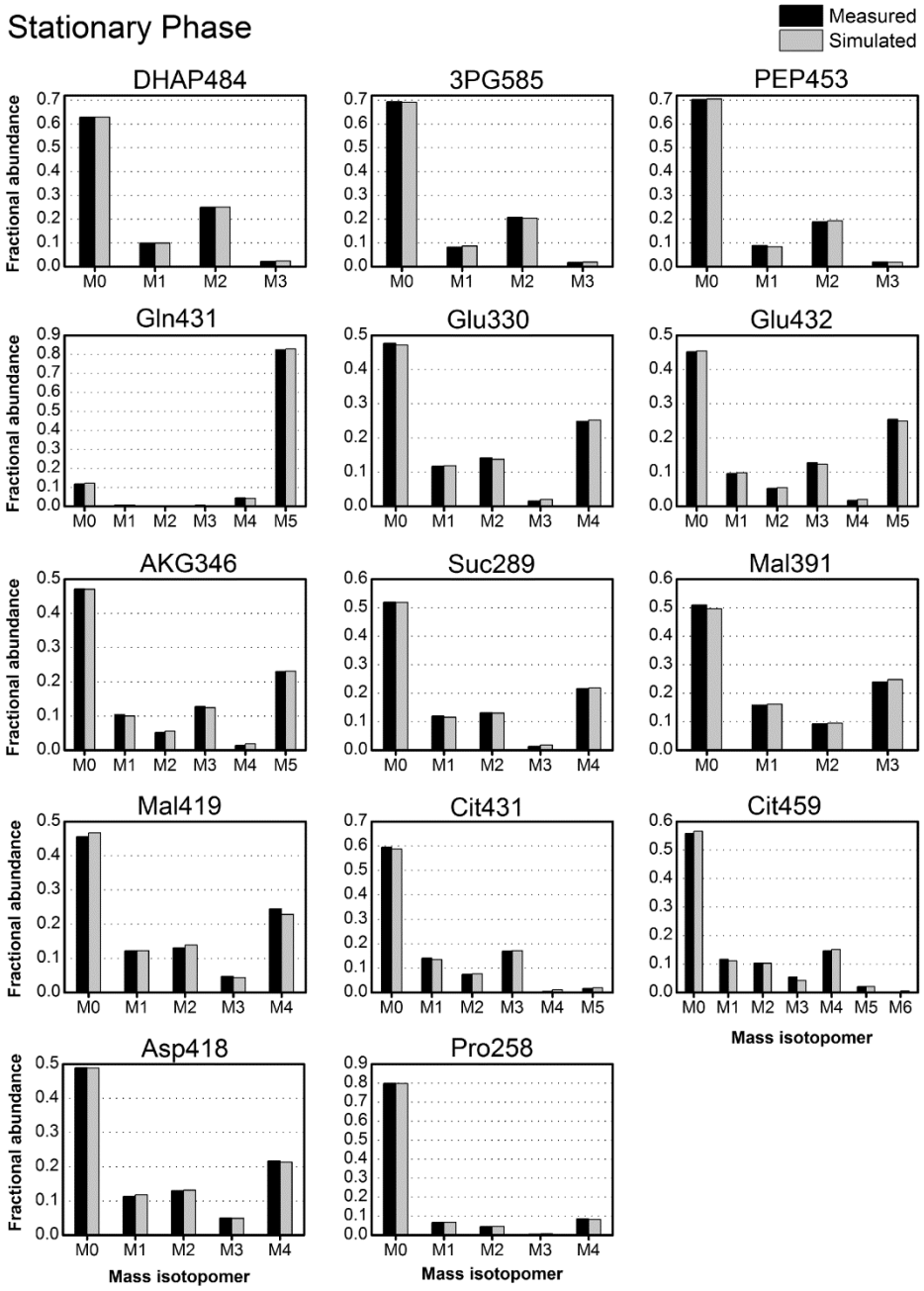

Figure B.2 Measured and fitted mass isotopomer distributions of intracellular metabolites from combined ^{13}C-MFA analysis at the stationary phase. [1,2-^{13}C]Glucose experimental data are DHAP484, 3PG585 and PEP453. [U-^{13}C]Glutamine experimental data are Gln431, Glu330, Glu432, AKG346, Suc289, Mal391, Mal419, Cit431, Cit459, Asp418 and Pro258. (data corrected for natural isotope abundances)

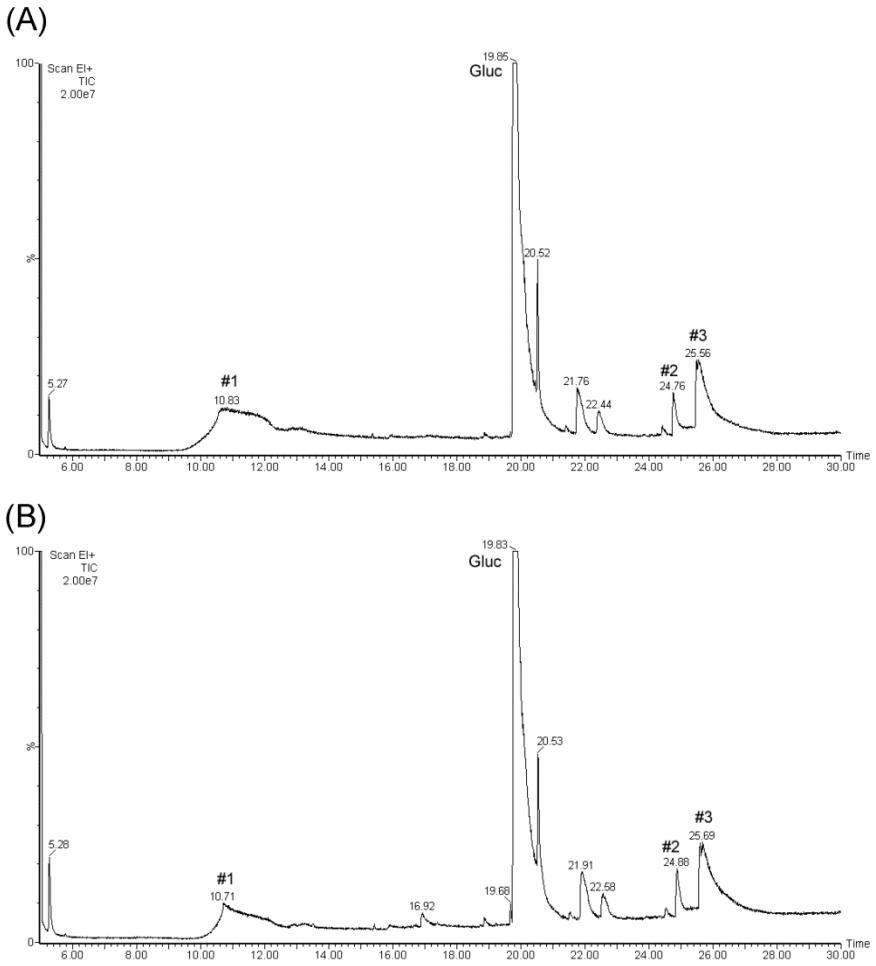

Figure B.3 GC-MS analysis of extracellular metabolites in follow-up experiments with [U-^{13}C]glucose (aldonitrile-acetate derivatization method). Shown are the total ion current (TIC) chromatograms of medium samples prepared at 24 h after addition of natural glucose (A), or [U-^{13}C]glucose (B) on day 2. From careful inspection of MIDs for eluted peaks we identified three metabolites (#1, #2, #3) that became ^{13}C-labeled from [U-^{13}C]glucose (MIDs are shown in Appendix B, Figure B.6). The identity of the three previously unidentified metabolites is still unknown.

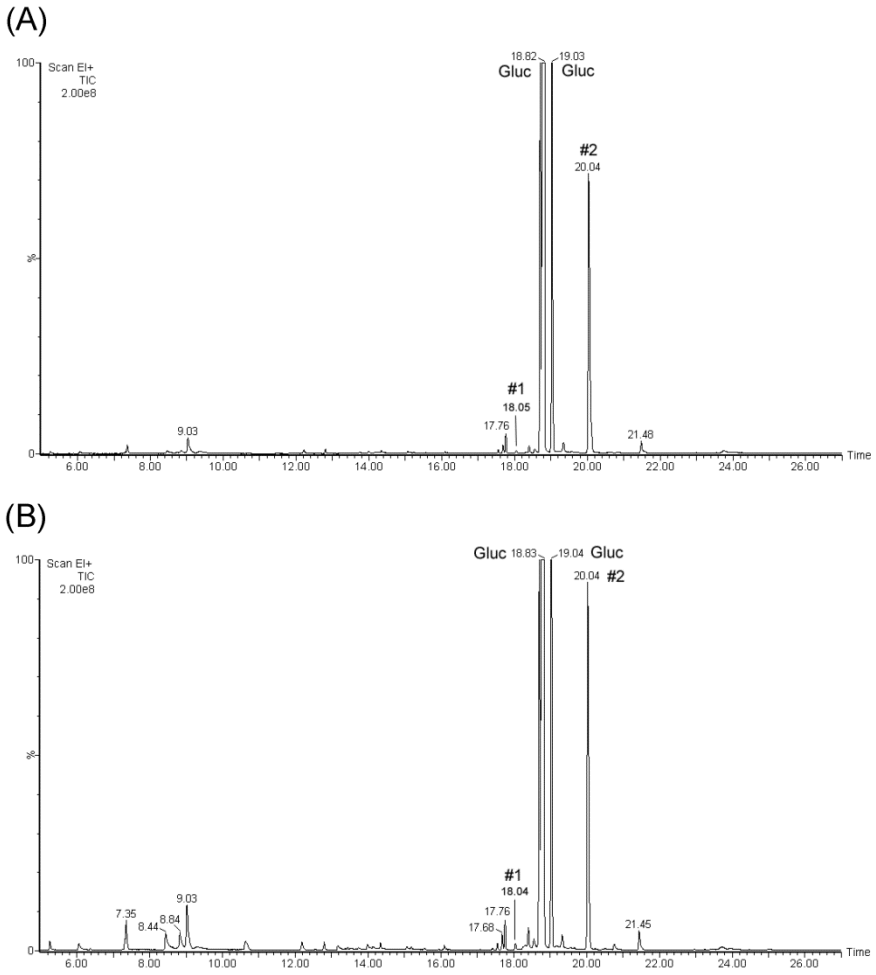

Figure B.4 GC-MS analysis of extracellular metabolites in follow-up experiments with [U-^{13}C]glucose (methyloxime trimethylsilyl MOX-TMS derivatization method). Shown are the total ion current (TIC) chromatograms of medium samples prepared at 24 h after addition of natural glucose (A), or [U-^{13}C]glucose (B) on day 2. From careful inspection of MIDs for eluted peaks we identified two metabolites (#1, #2) that became ^{13}C-labeled from [U-^{13}C]glucose (MIDs are shown in Appendix B, Figure B.6). The identity of the two previously unidentified metabolites #1 and #2 is still unknown.

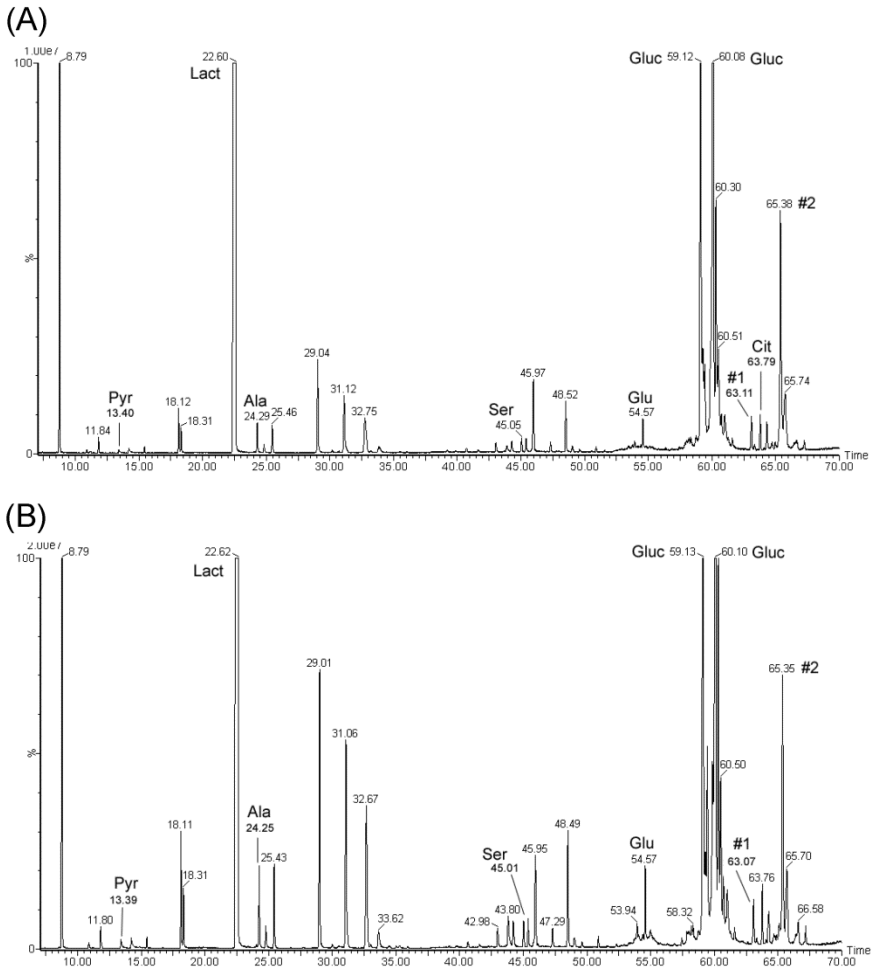

Figure B.5 GC-MS analysis of extracellular metabolites in follow-up experiments with [U-^{13}C]glucose (methyloxime tert-butyldimethylsilyl MOX-TBDMS derivatization method). Shown are the total ion current (TIC) chromatograms of medium samples prepared at 24 h after addition of natural glucose (A), or [U-^{13}C]glucose (B) on day 2. From careful inspection of MIDs for eluted peaks we identified eight metabolites (Pyr, Lact, Ala, Ser, Glu, Cit, #1, #2) that became ^{13}C-labeled from [U-^{13}C]glucose (MIDs are shown in Appendix B, Figure B.6). The identity of the two previously unidentified metabolites #1 and #2 is still unknown.

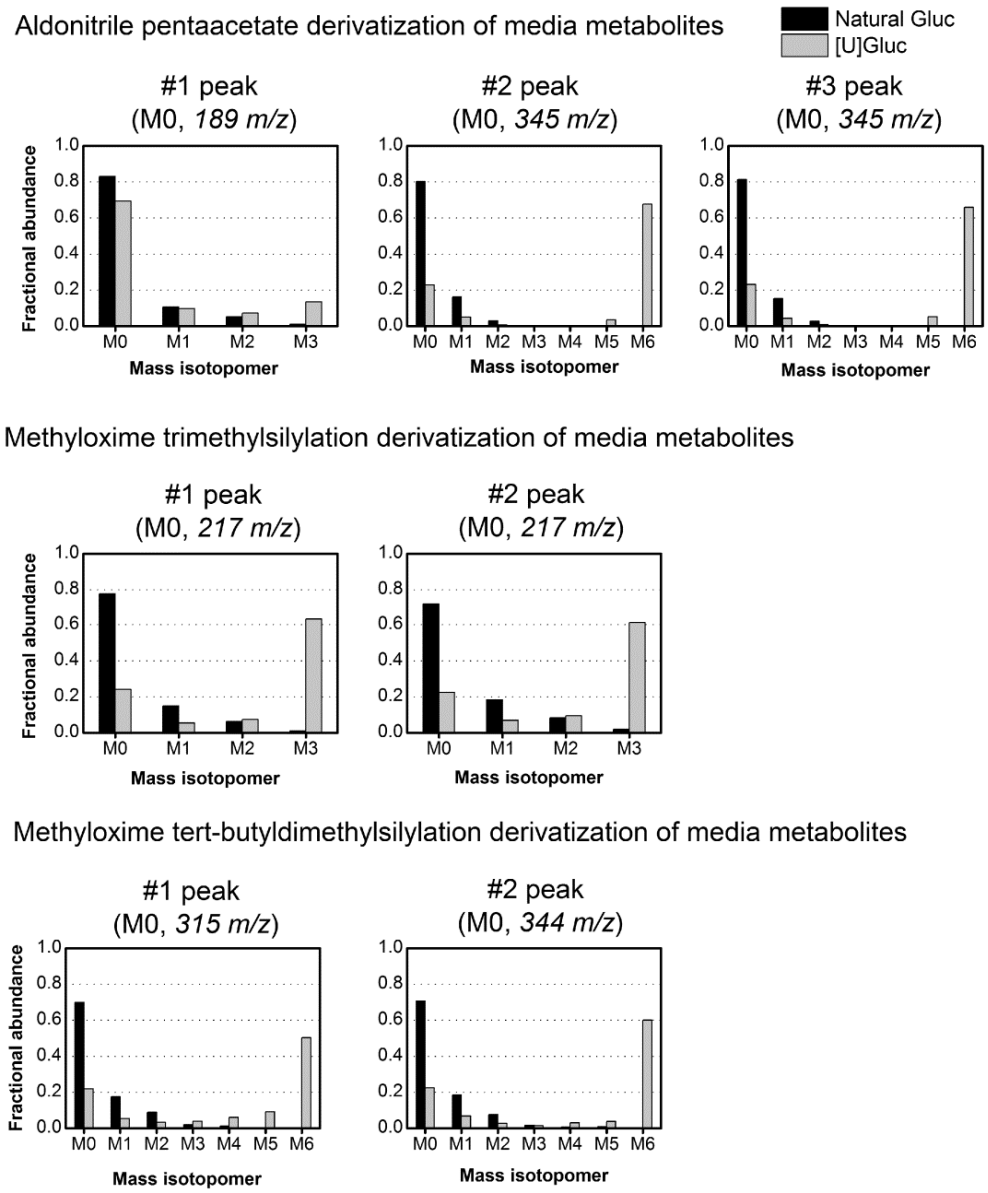

Figure B.6 Comparison of mass isotopomer distributions (MIDs) of previously unidentified metabolites in follow-up experiments with natural glucose (black bars) and [U-^{13}C]glucose (grey bars). The GC-MS chromatograms are shown in Appendix B, Figures B3-B5. For aldonitrile-acetate derivatization method, metabolite #1 became M+3 labeled, and metabolites #2 and #3 became M+6 labeled in experiments with [U-^{13}C]glucose. For MOX-TMS derivatization method, metabolites #1 and #2 became M+3 labeled from [U-^{13}C]glucose. For MOX-TBDMS derivatization method, metabolites #1 and #2 became M+6 labeled from [U-^{13}C]glucose.

Table B.3 Mass isotopomer distributions of intracellular metabolites at the exponential and stationary phases for [U-^{13}C]glutamine experiments measured by GC-MS. (data not corrected for natural isotope abundances)

	Exponential Phase				Stationary Phase			
Isotopomer	1.5 h	3 h	6 h	9 h	1.5 h	3 h	6 h	9 h
Pyr174 (M0)	0.8343	0.8352	0.8356	0.8348	0.8487	0.8488	0.8457	0.8448
Pyr175 (M1)	0.1051	0.1050	0.1048	0.1053	0.1047	0.1027	0.1055	0.1057
Pyr176 (M2)	0.0433	0.0437	0.0445	0.0443	0.0406	0.0416	0.0412	0.0414
Pyr177 (M3)	0.0139	0.0130	0.0122	0.0125	0.0049	0.0053	0.0062	0.0068
Pyr178 (M4)	0.0026	0.0023	0.0021	0.0022	0.0009	0.0013	0.0010	0.0010
Pyr179 (M5)	0.0008	0.0006	0.0008	0.0008	0.0002	0.0004	0.0003	0.0003
Lact233 (M0)	0.7580	0.7574	0.7575	0.7566	0.7585	0.7584	0.7571	0.7559
Lact234 (M1)	0.1619	0.1614	0.1608	0.1609	0.1615	0.1612	0.1614	0.1613
Lact235 (M2)	0.0684	0.0694	0.0698	0.0704	0.0686	0.0688	0.0697	0.0707
Lact236 (M3)	0.0098	0.0100	0.0100	0.0101	0.0097	0.0098	0.0100	0.0101
Lact237 (M4)	0.0019	0.0019	0.0019	0.0019	0.0018	0.0018	0.0019	0.0019
Lact261 (M0)	0.7433	0.7420	0.7431	0.7427	0.7449	0.7446	0.7436	0.7421
Lact262 (M1)	0.1656	0.1686	0.1673	0.1663	0.1687	0.1684	0.1685	0.1687
Lact263 (M2)	0.0713	0.0726	0.0719	0.0713	0.0723	0.0724	0.0722	0.0726
Lact264 (M3)	0.0120	0.0132	0.0128	0.0134	0.0114	0.0118	0.0128	0.0133
Lact265 (M4)	0.0062	0.0031	0.0041	0.0050	0.0024	0.0024	0.0026	0.0027
Lact266 (M5)	0.0015	0.0006	0.0009	0.0012	0.0003	0.0003	0.0004	0.0005
Ala232 (M0)	0.7545	0.7527	0.7492	0.7453	0.7545	0.7527	0.7492	0.7453
Ala233 (M1)	0.1649	0.1642	0.1646	0.1639	0.1649	0.1642	0.1646	0.1639
Ala234 (M2)	0.0689	0.0709	0.0732	0.0768	0.0689	0.0709	0.0732	0.0768
Ala235 (M3)	0.0100	0.0102	0.0108	0.0116	0.0100	0.0102	0.0108	0.0116
Ala236 (M4)	0.0018	0.0019	0.0022	0.0025	0.0018	0.0019	0.0022	0.0025
Ala260 (M0)	0.7430	0.7414	0.7403	0.7394	0.7462	0.7451	0.7444	0.7427
Ala261 (M1)	0.1687	0.1686	0.1683	0.1682	0.1695	0.1697	0.1699	0.1701
Ala262 (M2)	0.0693	0.0698	0.0700	0.0700	0.0700	0.0702	0.0699	0.0704
Ala263 (M3)	0.0156	0.0166	0.0174	0.0182	0.0120	0.0124	0.0132	0.0138
Ala264 (M4)	0.0028	0.0030	0.0032	0.0033	0.0021	0.0022	0.0023	0.0025
Ala265 (M5)	0.0007	0.0007	0.0008	0.0009	0.0003	0.0004	0.0004	0.0005
Pro258 (M0)	0.6318	0.6172	0.6026	0.5974	0.6512	0.6363	0.6176	0.6160
Pro259 (M1)	0.1519	0.1507	0.1481	0.1482	0.1703	0.1709	0.1728	0.1735
Pro260 (M2)	0.0707	0.0753	0.0794	0.0827	0.0888	0.0934	0.0973	0.0984
Pro261 (M3)	0.0163	0.0181	0.0195	0.0202	0.0188	0.0203	0.0222	0.0224
Pro262 (M4)	0.1013	0.1087	0.1181	0.1189	0.0559	0.0625	0.0711	0.0707
Pro263 (M5)	0.0199	0.0212	0.0228	0.0231	0.0106	0.0118	0.0135	0.0135
Pro264 (M6)	0.0081	0.0087	0.0096	0.0095	0.0044	0.0049	0.0056	0.0055
Suc289 (M0)	0.4349	0.4112	0.4024	0.3841	0.4260	0.4183	0.3958	0.4050
Suc290 (M1)	0.1076	0.1057	0.1060	0.1084	0.1630	0.1646	0.1680	0.1719
Suc291 (M2)	0.0838	0.0929	0.0997	0.1025	0.1466	0.1501	0.1554	0.1564
Suc292 (M3)	0.0279	0.0311	0.0330	0.0340	0.0399	0.0405	0.0429	0.0431
Suc293 (M4)	0.2696	0.2792	0.2796	0.2880	0.1753	0.1768	0.1856	0.1747

Table B.3 continued

Suc294 (M5)	0.0528	0.0553	0.0548	0.0575	0.0345	0.0341	0.0367	0.0343
Suc295 (M6)	0.0233	0.0246	0.0245	0.0254	0.0145	0.0156	0.0157	0.0146
Fum287 (M0)	0.4534	0.4434	0.4276	0.4195	0.4733	0.4698	0.4510	0.4567
Fum288 (M1)	0.1145	0.1164	0.1169	0.1185	0.1614	0.1638	0.1652	0.1684
Fum289 (M2)	0.0793	0.0883	0.0954	0.0995	0.1306	0.1304	0.1347	0.1354
Fum290 (M3)	0.0686	0.0709	0.0708	0.0675	0.0549	0.0555	0.0582	0.0573
Fum291 (M4)	0.2194	0.2170	0.2235	0.2282	0.1396	0.1409	0.1481	0.1416
Fum292 (M5)	0.0456	0.0451	0.0463	0.0468	0.0282	0.0279	0.0300	0.0286
Fum293 (M6)	0.0193	0.0189	0.0195	0.0201	0.0119	0.0118	0.0126	0.0120
AKG346 (M0)	0.4067	0.3902	0.3853	0.3651	0.3890	0.3654	0.3510	0.3645
AKG347 (M1)	0.1087	0.1059	0.1055	0.1066	0.1447	0.1471	0.1512	0.1571
AKG348 (M2)	0.0548	0.0614	0.0616	0.0621	0.0863	0.0906	0.0900	0.0909
AKG349 (M3)	0.0448	0.0549	0.0583	0.0659	0.1105	0.1162	0.1189	0.1170
AKG350 (M4)	0.0245	0.0269	0.0283	0.0301	0.0351	0.0385	0.0381	0.0366
AKG351 (M5)	0.2785	0.2790	0.2800	0.2865	0.1799	0.1862	0.1933	0.1810
AKG352 (M6)	0.0566	0.0553	0.0555	0.0579	0.0364	0.0367	0.0384	0.0357
AKG353 (M7)	0.0253	0.0265	0.0255	0.0259	0.0181	0.0193	0.0190	0.0172
Mal391 (M0)	0.3754	0.3617	0.3599	0.3497	0.3620	0.3519	0.3378	0.3437
Mal392 (M1)	0.1494	0.1533	0.1581	0.1594	0.2065	0.2066	0.2107	0.2154
Mal393 (M2)	0.1119	0.1173	0.1198	0.1202	0.1430	0.1446	0.1473	0.1477
Mal394 (M3)	0.2510	0.2556	0.2522	0.2560	0.2002	0.2061	0.2108	0.2043
Mal395 (M4)	0.0778	0.0774	0.0757	0.0790	0.0613	0.0639	0.0647	0.0617
Mal396 (M5)	0.0345	0.0347	0.0343	0.0356	0.0270	0.0269	0.0287	0.0273
Mal419 (M0)	0.3621	0.3537	0.3431	0.3364	0.3291	0.3167	0.3095	0.3097
Mal420 (M1)	0.1328	0.1346	0.1339	0.1348	0.1700	0.1710	0.1718	0.1740
Mal421 (M2)	0.0933	0.1030	0.1082	0.1119	0.1533	0.1556	0.1591	0.1587
Mal422 (M3)	0.0755	0.0820	0.0793	0.0766	0.0768	0.0803	0.0812	0.0796
Mal423 (M4)	0.2304	0.2242	0.2305	0.2340	0.1887	0.1920	0.1936	0.1936
Mal424 (M5)	0.0723	0.0705	0.0719	0.0727	0.0563	0.0579	0.0580	0.0576
Mal425 (M6)	0.0336	0.0321	0.0330	0.0335	0.0257	0.0266	0.0267	0.0267
Asp418 (M0)	0.3765	0.3641	0.3604	0.3549	0.3455	0.3318	0.3258	0.3268
Asp419 (M1)	0.1390	0.1392	0.1414	0.1420	0.1751	0.1766	0.1774	0.1807
Asp420 (M2)	0.0946	0.1029	0.1093	0.1127	0.1555	0.1586	0.1596	0.1617
Asp421 (M3)	0.0765	0.0803	0.0796	0.0762	0.0800	0.0832	0.0833	0.0832
Asp422 (M4)	0.2144	0.2147	0.2123	0.2157	0.1691	0.1733	0.1762	0.1714
Asp423 (M5)	0.0683	0.0684	0.0672	0.0680	0.0520	0.0531	0.0540	0.0529
Asp424 (M6)	0.0306	0.0306	0.0299	0.0305	0.0228	0.0234	0.0237	0.0232
PEP453 (M0)	0.6394	0.6421	0.6417	0.6416	0.6411	0.6420	0.6394	0.6394
PEP454 (M1)	0.2181	0.2174	0.2171	0.2175	0.2190	0.2178	0.2194	0.2188
PEP455 (M2)	0.1055	0.1044	0.1056	0.1051	0.1060	0.1055	0.1068	0.1064
PEP456 (M3)	0.0276	0.0271	0.0268	0.0271	0.0255	0.0256	0.0260	0.0266
PEP457 (M4)	0.0075	0.0071	0.0071	0.0067	0.0069	0.0069	0.0067	0.0068
PEP458 (M5)	0.0018	0.0020	0.0017	0.0019	0.0016	0.0021	0.0016	0.0019
Glu330 (M0)	0.3756	0.3656	0.3680	0.3535	0.3746	0.3593	0.3486	0.3564
Glu331 (M1)	0.1119	0.1129	0.1172	0.1169	0.1682	0.1700	0.1698	0.1746
Glu332 (M2)	0.0808	0.0900	0.0990	0.1029	0.1554	0.1594	0.1595	0.1610

Table B.3 continued

Glu333 (M3)	0.0323	0.0349	0.0368	0.0384	0.0486	0.0506	0.0511	0.0511
Glu334 (M4)	0.2993	0.2976	0.2843	0.2915	0.1912	0.1968	0.2042	0.1941
Glu335 (M5)	0.0718	0.0711	0.0678	0.0694	0.0445	0.0459	0.0480	0.0451
Glu336 (M6)	0.0283	0.0279	0.0270	0.0275	0.0175	0.0180	0.0188	0.0178
Glu432 (M0)	0.3402	0.3325	0.3203	0.3051	0.3221	0.3062	0.2975	0.3049
Glu433 (M1)	0.1270	0.1263	0.1243	0.1200	0.1586	0.1581	0.1570	0.1623
Glu434 (M2)	0.0657	0.0680	0.0690	0.0674	0.0999	0.1009	0.1003	0.1038
Glu435 (M3)	0.0473	0.0548	0.0618	0.0663	0.1109	0.1149	0.1159	0.1163
Glu436 (M4)	0.0301	0.0328	0.0346	0.0368	0.0461	0.0479	0.0486	0.0483
Glu437 (M5)	0.2675	0.2644	0.2676	0.2795	0.1812	0.1879	0.1939	0.1830
Glu438 (M6)	0.0830	0.0822	0.0831	0.0854	0.0553	0.0572	0.0592	0.0556
Glu439 (M7)	0.0393	0.0389	0.0393	0.0396	0.0258	0.0267	0.0275	0.0260
DHAP484(M0)	0.6314	0.6297	0.6337	0.6329	0.6304	0.6325	0.6303	0.6288
DHAP485(M1)	0.2258	0.2270	0.2259	0.2268	0.2272	0.2245	0.2279	0.2276
DHAP486(M2)	0.1067	0.1069	0.1066	0.1069	0.1072	0.1070	0.1075	0.1075
DHAP487(M3)	0.0252	0.0253	0.0252	0.0254	0.0259	0.0266	0.0259	0.0268
DHAP488(M4)	0.0087	0.0091	0.0072	0.0066	0.0079	0.0077	0.0068	0.0075
DHAP489(M5)	0.0022	0.0019	0.0014	0.0014	0.0013	0.0017	0.0016	0.0018
Gln431 (M0)	0.2113	0.2118	0.2134	0.2079	0.0929	0.0784	0.0743	0.0854
Gln432 (M1)	0.0784	0.0787	0.0792	0.0777	0.0351	0.0293	0.0280	0.0328
Gln433 (M2)	0.0360	0.0358	0.0358	0.0352	0.0160	0.0148	0.0133	0.0158
Gln434 (M3)	0.0097	0.0098	0.0098	0.0097	0.0073	0.0073	0.0068	0.0078
Gln435 (M4)	0.0261	0.0270	0.0259	0.0260	0.0319	0.0316	0.0324	0.0332
Gln436 (M5)	0.4362	0.4348	0.4341	0.4398	0.5591	0.5776	0.5778	0.5639
Gln437 (M6)	0.1380	0.1377	0.1374	0.1393	0.1755	0.1786	0.1830	0.1774
Gln438 (M7)	0.0644	0.0644	0.0644	0.0644	0.0822	0.0825	0.0844	0.0838
GLP571 (M0)	0.5577	0.5576	0.5594	0.5584	0.5605	0.5605	0.5571	0.5582
GLP572 (M1)	0.2541	0.2540	0.2533	0.2541	0.2518	0.2518	0.2537	0.2522
GLP573 (M2)	0.1344	0.1347	0.1340	0.1340	0.1337	0.1345	0.1345	0.1343
GLP574 (M3)	0.0400	0.0400	0.0395	0.0398	0.0396	0.0396	0.0402	0.0408
GLP575 (M4)	0.0113	0.0114	0.0114	0.0112	0.0117	0.0112	0.0118	0.0118
GLP576 (M5)	0.0024	0.0024	0.0024	0.0025	0.0027	0.0025	0.0026	0.0027
Cit431 (M0)	0.3913	0.3545	0.3436	0.3349	0.4061	0.4018	0.3777	0.3967
Cit432 (M1)	0.1631	0.1571	0.1582	0.1597	0.2095	0.2125	0.2108	0.2148
Cit433 (M2)	0.1163	0.1188	0.1215	0.1218	0.1342	0.1371	0.1383	0.1358
Cit434 (M3)	0.1886	0.1980	0.2098	0.2136	0.1455	0.1476	0.1598	0.1450
Cit435 (M4)	0.0654	0.0683	0.0726	0.0728	0.0486	0.0493	0.0534	0.0485
Cit436 (M5)	0.0493	0.0512	0.0494	0.0479	0.0296	0.0311	0.0331	0.0308
Cit437 (M6)	0.0199	0.0365	0.0329	0.0366	0.0195	0.0149	0.0201	0.0197
Cit459 (M0)	0.3887	0.3690	0.3574	0.3399	0.4015	0.3885	0.3600	0.3751
Cit460 (M1)	0.1507	0.1490	0.1504	0.1480	0.1970	0.1961	0.1898	0.1936
Cit461 (M2)	0.1021	0.1053	0.1049	0.1139	0.1375	0.1433	0.1490	0.1511
Cit462 (M3)	0.0722	0.0776	0.0772	0.0780	0.0725	0.0765	0.0821	0.0804
Cit463 (M4)	0.1614	0.1671	0.1770	0.1865	0.1122	0.1141	0.1297	0.1170
Cit464 (M5)	0.0741	0.0777	0.0778	0.0790	0.0483	0.0496	0.0548	0.0505
Cit465 (M6)	0.0342	0.0356	0.0363	0.0371	0.0205	0.0212	0.0233	0.0215

Table B.3 continued

Cit466 (M7)	0.0101	0.0121	0.0126	0.0116	0.0069	0.0073	0.0074	0.0067
Cit467 (M8)	0.0067	0.0067	0.0067	0.0060	0.0037	0.0034	0.0040	0.0041
3PG585 (M0)	0.5535	0.5530	0.5568	0.5536	0.5548	0.5584	0.5526	0.5532
3PG586 (M1)	0.2520	0.2518	0.2508	0.2520	0.2495	0.2488	0.2518	0.2499
3PG587 (M2)	0.1377	0.1380	0.1367	0.1372	0.1372	0.1350	0.1371	0.1375
3PG588 (M3)	0.0412	0.0415	0.0408	0.0419	0.0411	0.0405	0.0415	0.0413
3PG589 (M4)	0.0124	0.0126	0.0119	0.0124	0.0130	0.0130	0.0130	0.0135
3PG590 (M5)	0.0032	0.0031	0.0028	0.0030	0.0044	0.0043	0.0040	0.0045

Table B.4 Mass isotopomer distributions of palmitate at the exponential and stationary phases for [U-^{13}C]glutamine experiments measured by GC-MS. (data not corrected for natural isotope abundances)

	Exponential Phase				Stationary Phase			
Isotopomer	3 h	6 h	9 h	12 h	3 h	6 h	9 h	12 h
Palm 270 (M0)	0.7910	0.7488	0.7293	0.7059	0.8032	0.7889	0.7746	0.7608
Palm 271 (M1)	0.1507	0.1484	0.1457	0.1444	0.1583	0.1581	0.1567	0.1571
Palm 272 (M2)	0.0420	0.0681	0.0827	0.0989	0.0306	0.0411	0.0515	0.0607
Palm 273 (M3)	0.0067	0.0123	0.0155	0.0188	0.0041	0.0064	0.0087	0.0108
Palm 274 (M4)	0.0054	0.0149	0.0181	0.0224	0.0024	0.0040	0.0060	0.0076
Palm 275 (M5)	0.0011	0.0026	0.0033	0.0041	0.0004	0.0007	0.0011	0.0013
Palm 276 (M6)	0.0005	0.0029	0.0036	0.0037	0.0003	0.0005	0.0007	0.0009
Palm 277 (M7)	0.0006	0.0011	0.0010	0.0008	0.0004	0.0001	0.0004	0.0004
Palm 278 (M8)	0.0004	0.0006	0.0006	0.0006	0.0002	0.0001	0.0001	0.0002
Palm 279 (M9)	0.0007	0.0002	0.0001	0.0002	0.0001	0.0000	0.0001	0.0000
Palm 280 (M10)	0.0008	0.0002	0.0001	0.0002	0.0001	0.0001	0.0001	0.0000
Palm 281 (M11)	0.0000	0.0000	0.0000	0.0000	0.0000	0.0000	0.0000	0.0000
Palm 282 (M12)	0.0000	0.0000	0.0000	0.0000	0.0000	0.0000	0.0000	0.0000
Palm 283 (M13)	0.0000	0.0000	0.0000	0.0000	0.0000	0.0000	0.0000	0.0000
Palm 284 (M14)	0.0000	0.0000	0.0000	0.0000	0.0000	0.0000	0.0000	0.0000
Palm 285 (M15)	0.0000	0.0000	0.0000	0.0000	0.0000	0.0000	0.0000	0.0000
Palm 286 (M16)	0.0000	0.0000	0.0000	0.0000	0.0000	0.0000	0.0000	0.0000

Table B.5 Mass isotopomer distributions of intracellular metabolites at the exponential and stationary phases for [1,2-^{13}C]glucose experiments measured by GC-MS. (data not corrected for natural isotope abundances)

	Exponential Phase				Stationary Phase			
Isotopomer	1.5 h	3 h	6 h	9 h	1.5 h	3 h	6 h	9 h
Pyr174 (M0)	0.7233	0.7330	0.7221	0.7199	0.8212	0.8191	0.8124	0.8146
Pyr175 (M1)	0.0971	0.0971	0.0960	0.0966	0.1073	0.1067	0.1070	0.1052
Pyr176 (M2)	0.1535	0.1466	0.1574	0.1592	0.0616	0.0643	0.0694	0.0699
Pyr177 (M3)	0.0162	0.0156	0.0169	0.0174	0.0075	0.0078	0.0086	0.0079
Pyr178 (M4)	0.0086	0.0067	0.0067	0.0063	0.0019	0.0019	0.0024	0.0022
Pyr179 (M5)	0.0012	0.0011	0.0009	0.0006	0.0003	0.0003	0.0003	0.0002
Lact233 (M0)	0.6728	0.6649	0.6604	0.6503	0.7399	0.7360	0.7340	0.7327
Lact234 (M1)	0.1475	0.1471	0.1464	0.1449	0.1615	0.1610	0.1597	0.1579
Lact235 (M2)	0.1459	0.1523	0.1562	0.1654	0.0828	0.0863	0.0889	0.0914
Lact236 (M3)	0.0251	0.0264	0.0273	0.0289	0.0127	0.0134	0.0139	0.0142
Lact237 (M4)	0.0087	0.0093	0.0097	0.0105	0.0031	0.0034	0.0036	0.0038
Lact261 (M0)	0.6579	0.6512	0.6393	0.6344	0.7247	0.7211	0.7204	0.7180
Lact262 (M1)	0.1526	0.1522	0.1500	0.1501	0.1688	0.1680	0.1662	0.1653
Lact263 (M2)	0.1492	0.1543	0.1647	0.1684	0.0866	0.0899	0.0916	0.0947
Lact264 (M3)	0.0282	0.0293	0.0317	0.0328	0.0154	0.0161	0.0166	0.0167
Lact265 (M4)	0.0105	0.0113	0.0124	0.0124	0.0039	0.0042	0.0045	0.0046
Lact266 (M5)	0.0016	0.0017	0.0019	0.0019	0.0006	0.0006	0.0007	0.0007
Ala232 (M0)	0.7536	0.7534	0.7513	0.7502	0.7497	0.7536	0.7534	0.7513
Ala233 (M1)	0.1659	0.1657	0.1664	0.1666	0.1668	0.1659	0.1657	0.1664
Ala234 (M2)	0.0688	0.0691	0.0702	0.0709	0.0710	0.0688	0.0691	0.0702
Ala235 (M3)	0.0100	0.0100	0.0103	0.0104	0.0106	0.0100	0.0100	0.0103
Ala236 (M4)	0.0018	0.0018	0.0019	0.0019	0.0019	0.0018	0.0018	0.0019
Ala260 (M0)	0.7357	0.7312	0.7232	0.7135	0.7460	0.7446	0.7418	0.7374
Ala261 (M1)	0.1685	0.1674	0.1654	0.1638	0.1696	0.1690	0.1687	0.1683
Ala262 (M2)	0.0797	0.0839	0.0914	0.0998	0.0713	0.0728	0.0750	0.0786
Ala263 (M3)	0.0129	0.0139	0.0155	0.0175	0.0109	0.0112	0.0119	0.0127
Ala264 (M4)	0.0028	0.0031	0.0039	0.0048	0.0020	0.0021	0.0024	0.0027
Ala265 (M5)	0.0004	0.0005	0.0005	0.0007	0.0002	0.0003	0.0003	0.0004
Pro258 (M0)	0.7413	0.7381	0.7342	0.7316	0.7378	0.7367	0.7345	0.7319
Pro259 (M1)	0.1737	0.1755	0.1759	0.1767	0.1786	0.1781	0.1795	0.1803
Pro260 (M2)	0.0696	0.0711	0.0736	0.0753	0.0700	0.0714	0.0718	0.0732
Pro261 (M3)	0.0109	0.0112	0.0119	0.0124	0.0112	0.0114	0.0116	0.0121
Pro262 (M4)	0.0026	0.0033	0.0032	0.0030	0.0021	0.0021	0.0022	0.0023
Pro263 (M5)	0.0015	0.0007	0.0008	0.0009	0.0003	0.0003	0.0003	0.0003
Pro264 (M6)	0.0003	0.0001	0.0004	0.0001	0.0001	0.0000	0.0001	0.0001
Suc289 (M0)	0.7301	0.7260	0.7183	0.7131	0.7306	0.7308	0.7226	0.7138
Suc290 (M1)	0.1739	0.1731	0.1734	0.1730	0.1766	0.1743	0.1783	0.1798
Suc291 (M2)	0.0777	0.0818	0.0870	0.0910	0.0752	0.0768	0.0798	0.0848
Suc292 (M3)	0.0125	0.0134	0.0148	0.0161	0.0126	0.0123	0.0134	0.0150
Suc293 (M4)	0.0025	0.0031	0.0039	0.0042	0.0024	0.0029	0.0027	0.0034

Table B.5 continued

Suc294 (M5)	0.0028	0.0021	0.0023	0.0022	0.0020	0.0021	0.0025	0.0027
Suc295 (M6)	0.0006	0.0005	0.0004	0.0004	0.0006	0.0008	0.0007	0.0005
Fum287 (M0)	0.7250	0.7223	0.7162	0.7112	0.7308	0.7331	0.7216	0.7166
Fum288 (M1)	0.1777	0.1758	0.1755	0.1755	0.1757	0.1726	0.1787	0.1797
Fum289 (M2)	0.0800	0.0819	0.0862	0.0905	0.0759	0.0766	0.0802	0.0834
Fum290 (M3)	0.0138	0.0149	0.0165	0.0169	0.0138	0.0137	0.0146	0.0158
Fum291 (M4)	0.0029	0.0039	0.0044	0.0046	0.0031	0.0030	0.0040	0.0037
Fum292 (M5)	0.0004	0.0008	0.0008	0.0008	0.0005	0.0006	0.0006	0.0006
Fum293 (M6)	0.0001	0.0004	0.0004	0.0004	0.0002	0.0003	0.0002	0.0004
AKG346 (M0)	0.7086	0.6988	0.6974	0.6928	0.7152	0.7161	0.7014	0.6957
AKG347 (M1)	0.1845	0.1802	0.1813	0.1828	0.1847	0.1794	0.1861	0.1869
AKG348 (M2)	0.0840	0.0885	0.0936	0.0970	0.0807	0.0820	0.0878	0.0924
AKG349 (M3)	0.0160	0.0201	0.0186	0.0194	0.0140	0.0153	0.0165	0.0173
AKG350 (M4)	0.0039	0.0055	0.0056	0.0055	0.0029	0.0035	0.0040	0.0043
AKG351 (M5)	0.0010	0.0030	0.0017	0.0007	0.0008	0.0010	0.0010	0.0011
AKG352 (M6)	0.0003	0.0017	0.0009	0.0004	0.0003	0.0010	0.0006	0.0006
AKG353 (M7)	0.0017	0.0023	0.0009	0.0014	0.0014	0.0017	0.0027	0.0016
Mal391 (M0)	0.6413	0.6406	0.6339	0.6293	0.6482	0.6554	0.6398	0.6338
Mal392 (M1)	0.2199	0.2202	0.2215	0.2212	0.2162	0.2099	0.2203	0.2216
Mal393 (M2)	0.1071	0.1064	0.1104	0.1124	0.1030	0.1020	0.1060	0.1087
Mal394 (M3)	0.0241	0.0247	0.0255	0.0267	0.0237	0.0236	0.0240	0.0258
Mal395 (M4)	0.0060	0.0062	0.0071	0.0082	0.0061	0.0064	0.0068	0.0073
Mal396 (M5)	0.0016	0.0020	0.0015	0.0022	0.0027	0.0028	0.0032	0.0028
Mal419 (M0)	0.6308	0.6266	0.6205	0.6151	0.6354	0.6330	0.6262	0.6196
Mal420 (M1)	0.2228	0.2230	0.2227	0.2212	0.2220	0.2212	0.2246	0.2242
Mal421 (M2)	0.1114	0.1140	0.1180	0.1213	0.1079	0.1093	0.1126	0.1159
Mal422 (M3)	0.0269	0.0276	0.0293	0.0308	0.0256	0.0255	0.0270	0.0290
Mal423 (M4)	0.0066	0.0071	0.0078	0.0091	0.0072	0.0084	0.0077	0.0087
Mal424 (M5)	0.0011	0.0013	0.0014	0.0017	0.0012	0.0014	0.0015	0.0016
Mal425 (M6)	0.0003	0.0005	0.0004	0.0007	0.0006	0.0012	0.0006	0.0009
Asp418 (M0)	0.6311	0.6262	0.6194	0.6145	0.6328	0.6310	0.6255	0.6201
Asp419 (M1)	0.2242	0.2244	0.2245	0.2234	0.2253	0.2241	0.2261	0.2268
Asp420 (M2)	0.1098	0.1129	0.1169	0.1205	0.1086	0.1106	0.1123	0.1152
Asp421 (M3)	0.0266	0.0277	0.0294	0.0308	0.0257	0.0264	0.0276	0.0287
Asp422 (M4)	0.0068	0.0073	0.0081	0.0088	0.0062	0.0066	0.0070	0.0075
Asp423 (M5)	0.0012	0.0013	0.0015	0.0017	0.0011	0.0012	0.0012	0.0014
Asp424 (M6)	0.0002	0.0002	0.0003	0.0003	0.0002	0.0002	0.0003	0.0002
PEP453 (M0)	0.4327	0.4423	0.4396	0.4310	0.4600	0.4668	0.4528	0.4764
PEP454 (M1)	0.1536	0.1554	0.1549	0.1559	0.2011	0.2026	0.2046	0.2068
PEP455 (M2)	0.2830	0.2770	0.2787	0.2819	0.2219	0.2191	0.2225	0.2071
PEP456 (M3)	0.0859	0.0817	0.0827	0.0863	0.0792	0.0754	0.0815	0.0746
PEP457 (M4)	0.0370	0.0359	0.0360	0.0367	0.0300	0.0288	0.0307	0.0279
PEP458 (M5)	0.0078	0.0077	0.0080	0.0083	0.0078	0.0073	0.0079	0.0074
Glu330 (M0)	0.7014	0.6971	0.6895	0.6823	0.7041	0.7013	0.6934	0.6865
Glu331 (M1)	0.1988	0.1987	0.1989	0.1988	0.1983	0.1980	0.2012	0.2021
Glu332 (M2)	0.0806	0.0837	0.0886	0.0938	0.0793	0.0816	0.0847	0.0887

Table B.5 continued

Glu333 (M3)	0.0155	0.0164	0.0181	0.0195	0.0149	0.0155	0.0167	0.0180
Glu334 (M4)	0.0032	0.0035	0.0042	0.0047	0.0028	0.0030	0.0034	0.0039
Glu335 (M5)	0.0005	0.0005	0.0007	0.0008	0.0004	0.0004	0.0005	0.0006
Glu336 (M6)	0.0001	0.0001	0.0001	0.0001	0.0001	0.0001	0.0001	0.0001
Glu432 (M0)	0.6251	0.6214	0.6135	0.6178	0.6252	0.6213	0.6164	0.6099
Glu433 (M1)	0.2285	0.2282	0.2275	0.2241	0.2299	0.2300	0.2302	0.2300
Glu434 (M2)	0.1106	0.1130	0.1183	0.1168	0.1101	0.1123	0.1148	0.1188
Glu435 (M3)	0.0273	0.0283	0.0303	0.0302	0.0268	0.0279	0.0292	0.0308
Glu436 (M4)	0.0070	0.0075	0.0085	0.0088	0.0066	0.0071	0.0077	0.0084
Glu437 (M5)	0.0013	0.0014	0.0017	0.0018	0.0011	0.0012	0.0014	0.0016
Glu438 (M6)	0.0002	0.0003	0.0003	0.0004	0.0002	0.0002	0.0002	0.0003
Glu439 (M7)	0.0000	0.0001	0.0001	0.0001	0.0001	0.0001	0.0001	0.0001
DHAP484(M0)	0.3597	0.3687	0.3625	0.3674	0.4030	0.4162	0.3998	0.4142
DHAP485(M1)	0.1377	0.1391	0.1382	0.1446	0.1987	0.1974	0.2008	0.2003
DHAP486(M2)	0.3336	0.3292	0.3334	0.3253	0.2553	0.2520	0.2536	0.2464
DHAP487(M3)	0.1060	0.1039	0.1065	0.1048	0.0957	0.0911	0.0958	0.0924
DHAP488(M4)	0.0518	0.0475	0.0484	0.0467	0.0378	0.0347	0.0395	0.0370
DHAP489(M5)	0.0112	0.0115	0.0110	0.0112	0.0095	0.0087	0.0104	0.0098
Gln431 (M0)	0.6307	0.6295	0.6302	0.6295	0.6304	0.6282	0.6292	0.6288
Gln432 (M1)	0.2317	0.2327	0.2323	0.2335	0.2311	0.2311	0.2327	0.2324
Gln433 (M2)	0.1050	0.1054	0.1050	0.1047	0.1057	0.1074	0.1055	0.1060
Gln434 (M3)	0.0254	0.0254	0.0254	0.0253	0.0254	0.0258	0.0252	0.0254
Gln435 (M4)	0.0060	0.0058	0.0058	0.0058	0.0059	0.0060	0.0058	0.0059
Gln436 (M5)	0.0010	0.0010	0.0011	0.0010	0.0011	0.0011	0.0011	0.0011
Gln437 (M6)	0.0002	0.0002	0.0002	0.0002	0.0003	0.0002	0.0003	0.0002
Gln438 (M7)	0.0000	0.0000	0.0000	0.0000	0.0001	0.0002	0.0002	0.0002
GLP571 (M0)	0.4840	0.4678	0.4358	0.4190	0.5357	0.5368	0.5216	0.5174
GLP572 (M1)	0.2268	0.2180	0.2067	0.1997	0.2460	0.2443	0.2443	0.2437
GLP573 (M2)	0.1887	0.2019	0.2253	0.2375	0.1485	0.1502	0.1566	0.1589
GLP574 (M3)	0.0673	0.0737	0.0853	0.0919	0.0494	0.0486	0.0538	0.0555
GLP575 (M4)	0.0265	0.0305	0.0370	0.0408	0.0162	0.0161	0.0188	0.0193
GLP576 (M5)	0.0068	0.0081	0.0100	0.0112	0.0042	0.0038	0.0049	0.0052
Cit431 (M0)	-	0.5738	0.5541	0.5397	0.6182	0.6150	0.6052	0.5975
Cit432 (M1)	-	0.2150	0.2141	0.2089	0.2246	0.2230	0.2253	0.2250
Cit433 (M2)	-	0.1362	0.1495	0.1587	0.1107	0.1131	0.1172	0.1239
Cit434 (M3)	-	0.0363	0.0422	0.0469	0.0269	0.0279	0.0303	0.0314
Cit435 (M4)	-	0.0122	0.0146	0.0179	0.0074	0.0075	0.0086	0.0097
Cit436 (M5)	-	0.0028	0.0035	0.0041	0.0020	0.0019	0.0021	0.0020
Cit437 (M6)	-	0.0238	0.0219	0.0238	0.0103	0.0115	0.0113	0.0104
Cit459 (M0)	0.5885	0.5780	0.5641	0.5557	0.6198	0.6010	0.5980	0.5869
Cit460 (M1)	0.2239	0.2225	0.2200	0.2186	0.2339	0.2275	0.2298	0.2284
Cit461 (M2)	0.1315	0.1383	0.1474	0.1521	0.1066	0.1251	0.1231	0.1306
Cit462 (M3)	0.0365	0.0391	0.0434	0.0458	0.0275	0.0327	0.0332	0.0360
Cit463 (M4)	0.0120	0.0133	0.0162	0.0182	0.0075	0.0092	0.0098	0.0111
Cit464 (M5)	0.0026	0.0031	0.0038	0.0045	0.0015	0.0019	0.0021	0.0024
Cit465 (M6)	0.0006	0.0008	0.0011	0.0013	0.0003	0.0004	0.0005	0.0006

Table B.5 continued

Cit466 (M7)	0.0017	0.0016	0.0020	0.0021	0.0009	0.0006	0.0012	0.0013
Cit467 (M8)	0.0025	0.0031	0.0020	0.0017	0.0019	0.0016	0.0023	0.0026
3PG585 (M0)	0.3648	0.3732	0.3676	0.3698	0.3870	0.4038	0.3799	0.4012
3PG586 (M1)	0.1733	0.1747	0.1732	0.1757	0.2145	0.2171	0.2164	0.2191
3PG587 (M2)	0.2823	0.2778	0.2813	0.2777	0.2374	0.2289	0.2374	0.2261
3PG588 (M3)	0.1116	0.1088	0.1103	0.1100	0.1020	0.0963	0.1043	0.0963
3PG589 (M4)	0.0529	0.0513	0.0527	0.0520	0.0448	0.0408	0.0470	0.0428
3PG590 (M5)	0.0152	0.0143	0.0149	0.0147	0.0143	0.0132	0.0150	0.0145

Table B.6 Mass isotopomer distributions of palmitate at the exponential and stationary phases for [1,2-^{13}C]glucose experiments measured by GC-MS. (data not corrected for natural isotope abundances)

	Exponential Phase				Stationary Phase			
Isotopomer	3 h	6 h	9 h	12 h	3 h	6 h	9 h	12 h
Palm 270 (M0)	0.7812	0.7570	0.7231	0.6865	0.8159	0.8114	0.8008	0.7882
Palm 271 (M1)	0.1497	0.1487	0.1430	0.1392	0.1602	0.1586	0.1587	0.1585
Palm 272 (M2)	0.0462	0.0654	0.0862	0.1063	0.0211	0.0260	0.0339	0.0435
Palm 273 (M3)	0.0075	0.0113	0.0166	0.0212	0.0020	0.0029	0.0045	0.0064
Palm 274 (M4)	0.0089	0.0117	0.0208	0.0314	0.0003	0.0007	0.0014	0.0026
Palm 275 (M5)	0.0016	0.0021	0.0039	0.0060	0.0000	0.0001	0.0002	0.0004
Palm 276 (M6)	0.0022	0.0019	0.0039	0.0065	0.0001	0.0001	0.0001	0.0002
Palm 277 (M7)	0.0009	0.0011	0.0010	0.0011	0.0001	0.0001	0.0002	0.0002
Palm 278 (M8)	0.0009	0.0005	0.0008	0.0011	0.0001	0.0001	0.0001	0.0001
Palm 279 (M9)	0.0004	0.0002	0.0003	0.0003	0.0001	0.0000	0.0001	0.0000
Palm 280 (M10)	0.0006	0.0002	0.0004	0.0003	0.0000	0.0000	0.0001	0.0000
Palm 281 (M11)	0.0000	0.0000	0.0000	0.0000	0.0000	0.0000	0.0000	0.0000
Palm 282 (M12)	0.0000	0.0000	0.0000	0.0000	0.0000	0.0000	0.0000	0.0000
Palm 283 (M13)	0.0000	0.0000	0.0000	0.0000	0.0000	0.0000	0.0000	0.0000
Palm 284 (M14)	0.0000	0.0000	0.0000	0.0000	0.0000	0.0000	0.0000	0.0000
Palm 285 (M15)	0.0000	0.0000	0.0000	0.0000	0.0000	0.0000	0.0000	0.0000
Palm 286 (M16)	0.0000	0.0000	0.0000	0.0000	0.0000	0.0000	0.0000	0.0000

Table B.7 Molar percentage enrichments (MPE, mol%) of extracellular metabolites for [U-^{13}C]glutamine tracer experiments. (measurement error ±0.3 mol%)

	Exponential Phase					Stationary Phase				
	1.5 h	3 h	6 h	9 h	12 h	1.5 h	3 h	6 h	9 h	12 h
Pyr174	-	0.0%	0.4%	0.4%	0.5%	-	0.0%	0.2%	0.8%	0.8%
Lact261	0.1%	0.2%	0.4%	0.5%	0.7%	0.1%	0.2%	0.4%	0.4%	0.7%
Ala260	-	0.2%	0.6%	0.5%	0.9%	0.1%	0.0%	0.4%	0.3%	0.6%
Cit459	0.3%	1.0%	2.2%	3.6%	5.1%	0.7%	1.7%	3.4%	4.3%	5.9%

Table B.8 Molar percentage enrichments (MPE, mol%) of extracellular metabolites for [1,2-^{13}C]glucose tracer experiments. (measurement error ±0.3 mol%)

	Exponential Phase					Stationary Phase				
	1.5 h	3 h	6 h	9 h	12 h	1.5 h	3 h	6 h	9 h	12 h
Pyr174	4.1%	5.4%	8.8%	12%	14%	0.4%	1.3%	2.2%	3.7%	5.0%
Lact261	2.7%	4.7%	7.9%	11%	13%	0.6%	1.2%	2.3%	3.1%	4.1%
Ala260	0.6%	0.7%	1.4%	2.1%	3.5%	-0.3%	-0.2%	0.3%	0.5%	0.9%
Cit459	0.3%	0.1%	0.3%	0.7%	1.2%	-0.2%	0.0%	0.3%	0.2%	0.2%

Appendix C

SUPPLEMENTARY DATA OF CHAPTER 5

Table C.1 Results of ^{13}C-MFA with [1,2-^{13}C]glucose tracer using original PPP model. Shown are the estimated net and exchange fluxes (nmol/10^6cell/h) with 95% confidence intervals.

[1,2-^{13}C]Glucose tracer experiment						
			Original PPP model			
Reaction			Flux	95% Conf. interval		
Gluc.ext → G6P	v1		76.4	[69.0 ,	83.8]	
G6P ↔ F6P	v2	net	58.9	[37.5 ,	70.8]	
		exch	(0.0, >1e4)	[0.0 ,	>1e4]	
F6P→FBP	v3		70.6	[59.1 ,	79.2]	
FBP ↔ DHAP + GAP	v4	net	70.6	[59.1 ,	79.2]	
		exch	(0.0, >1e4)	[0.0 ,	>1e4]	
DHAP ↔ GAP	v5	net	70.6	[59.1 ,	79.2]	
		exch	(0.0, >1e4)	[0.0 ,	>1e4]	
GAP ↔ 3PG	v6	net	147.0	[128.4 ,	162.9]	
		exch	(0.0, >1e4)	[0.0 ,	>1e4]	
3PG ↔ PEP	v7	net	147.0	[128.4 ,	162.9]	
		exch	(0.0, >1e4)	[0.0 ,	>1e4]	
PEP → Pyr.snk	v8		147.0	[128.4 ,	162.9]	
G6P → Ru5P + CO2	v9		17.5	[10.0 ,	38.6]	
Ru5P ↔ X5P	v10	net	11.7	[6.7 ,	25.8]	
		exch	(0.0, >1e4)	[0.0 ,	>1e4]	
Ru5P ↔ R5P	v11	net	5.8	[3.3 ,	12.9]	
		exch	(0.0, >1e4)	[0.0 ,	>1e4]	
X5P ↔ EC2 + GAP	v12	net	11.7	[6.7 ,	25.8]	

Table C.1 continued

		exch	(0.0, >1e4)	[	0.0	,	>1e4]
F6P ↔ EC2 + E4P	v13	net	-5.8	[	-12.9	,	-3.3]
		exch	(0.0, >1e4)	[	0.0	,	>1e4]
S7P ↔ EC2 + R5P	v14	net	-5.8	[	-12.9	,	-3.3]
		exch	(0.0, >1e4)	[	0.0	,	>1e4]
F6P ↔ EC3 + GAP	v15	net	-5.8	[	-12.9	,	-3.3]
		exch	(0.0, >1e4)	[	0.0	,	>1e4]
S7P ↔ EC3 + E4P	v16	net	5.8	[	3.3	,	12.9]
		exch	(0.0, >1e4)	[	0.0	,	>1e4]
DHAP ↔ GLP	v17	net	0.0	[	-0.0	,	0.0]
		exch	(0.0, >1e4)	[	0.0	,	>1e4]

Metabolites	G-value				
		95% Conf. interval			
DHAP	0.63	[	0.40	,	0.94]
3PG	0.73	[	0.69	,	0.79]
PEP	0.66	[	0.63	,	0.72]

G-value, fractional labeling of metabolites

Table C.2 Results of ^{13}C-MFA with [1-^{13}C]glucose+[4,5,6-^{13}C]glucose tracer using original PPP model. Shown are the estimated net and exchange fluxes (nmol/10^{6}cell/h) with 95% confidence intervals.

[1-^{13}C]Glucose+[4,5,6-^{13}C]glucose tracer experiment							
			Original PPP model				
Reaction			Flux	95% Conf. interval			
Gluc.ext → G6P	v1		76.4	[	69.0	,	83.8]
G6P ↔ F6P	v2	net	40.1	[	21.3	,	48.2]
		exch	(0.0, >1e4)	[	0.0	,	>1e4]
F6P→FBP	v3		64.3	[	54.9	,	71.7]

Table C.2 continued

FBP ↔ DHAP + GAP	v4	net	64.3	[	54.9	,	71.7]
		exch	(0.0, >1e4)	[	0.0	,	>1e4]
DHAP ↔ GAP	v5	net	64.3	[	54.9	,	71.7]
		exch	316.0	[	223.5	,	477.6]
GAP ↔ 3PG	v6	net	140.7	[	124.6	,	155.4]
		exch	(0.0, >1e4)	[	0.0	,	>1e4]
3PG ↔ PEP	v7	net	140.7	[	124.6	,	155.4]
		exch	(0.0, >1e4)	[	0.0	,	>1e4]
PEP → Pyr.snk	v8		140.7	[	124.6	,	155.4]
G6P → Ru5P + CO2	v9		32.3	[	29.2	,	56.04]
Ru5P ↔ X5P	v10	net	24.2	[	19.5	,	37.4]
		exch	(0.0, >1e4)	[	0.0	,	>1e4]
Ru5P ↔ R5P	v11	net	12.1	[	9.7	,	18.7]
		exch	(0.0, >1e4)	[	0.0	,	>1e4]
X5P ↔ EC2 + GAP	v12	net	24.2	[	19.5	,	37.4]
		exch	(0.0, >1e4)	[	0.0	,	>1e4]
F6P ↔ EC2 + E4P	v13	net	-12.1	[	-18.7	,	-9.7]
		exch	(0.0, >1e4)	[	0.0	,	>1e4]
S7P ↔ EC2 + R5P	v14	net	-12.1	[	-18.7	,	-9.7]
		exch	(0.0, >1e4)	[	0.0	,	>1e4]
F6P ↔ EC3 + GAP	v15	net	-12.1	[	-18.7	,	-9.7]
		exch	(0.0, >1e4)	[	0.0	,	>1e4]
S7P ↔ EC3 + E4P	v16	net	12.9	[	9.7	,	18.7]
		exch	(0.0, >1e4)	[	0.0	,	>1e4]
DHAP ↔ GLP	v17	net	0.0	[	-0.0	,	0.0]
		exch	(0.0, >1e4)	[	0.0	,	>1e4]

Metabolites	G-value		95% Conf. interval		
DHAP	0.95	[	0.89	,	1.00]
3PG	0.87	[	0.82	,	0.90]
PEP	0.77	[	0.72	,	0.80]

Table C.3 Results of ^{13}C-MFA with [2-^{13}C]glucose+[4,5,6-^{13}C]glucose tracer using original PPP model. Shown are the estimated net and exchange fluxes (nmol/10^{6}cell/h) with 95% confidence intervals.

[2-^{13}C]Glucose+[4,5,6-^{13}C]glucose tracer experiment							
			Original PPP model				
Reaction			Flux	95% Conf. interval			
Gluc.ext → G6P	v1		76.4	[	69.0	,	83.8]
G6P ↔ F6P	v2	net	14.3	[	5.4	,	28.3]
		exch	(>1e3, >1e4)	[	143.4	,	>1e4]
F6P→FBP	v3		55.7	[	49.6	,	62.0]
FBP ↔ DHAP + GAP	v4	net	55.7	[	49.6	,	62.0]
		exch	(0.0, >1e4)	[	0.0	,	>1e4]
DHAP ↔ GAP	v5	net	55.7	[	49.6	,	62.0]
		exch	296.9	[	217.9	,	428.6]
GAP ↔ 3PG	v6	net	132.1	[	119.0	,	145.3]
		exch	(0.0, >1e4)	[	0.0	,	>1e4]
3PG ↔ PEP	v7	net	132.1	[	119.0	,	145.3]
		exch	(0.0, >1e4)	[	0.0	,	>1e4]
PEP → Pyr.snk	v8		132.1	[	119.0	,	145.3]
G6P → Ru5P + CO2	v9		62.1	[	47.8	,	73.3]
Ru5P ↔ X5P	v10	net	41.4	[	31.9	,	48.8]
		exch	(0.0, >1e4)	[	0.0	,	>1e4]
Ru5P ↔ R5P	v11	net	20.7	[	15.9	,	24.4]
		exch	(0.0, >1e4)	[	0.0	,	>1e4]
X5P ↔ EC2 + GAP	v12	net	41.4	[	31.9	,	48.8]
		exch	(0.0, >1e4)	[	0.0	,	>1e4]
F6P ↔ EC2 + E4P	v13	net	-20.7	[	-24.4	,	-15.9]
		exch	(0.0, 2.84)	[	0.0	,	>1e4]
S7P ↔ EC2 + R5P	v14	net	-20.7	[	-24.4	,	-15.9]
		exch	(0.0, >1e4)	[	0.0	,	>1e4]
F6P ↔ EC3 + GAP	v15	net	-20.7	[	-24.4	,	-15.9]
		exch	(0.0, >1e4)	[	0.0	,	>1e4]
S7P ↔ EC3 + E4P	v16	net	20.7	[	15.9	,	24.4]

Table C.3 continued

		exch	0.0	[	0.0	,	16.1]
DHAP ↔ GLP	v17	net	0.0	[	-0.0	,	0.0]
		exch	(0.0, >1e4)	[	0.0	,	>1e4]

Metabolites	G-value				95% Conf. interval
DHAP	0.84	[	0.82	,	0.86]
3PG	0.79	[	0.77	,	0.81]
PEP	0.70	[	0.69	,	0.72]

Table C.4 Results of ^{13}C-MFA with [3-^{13}C]glucose and [4,5,6-^{13}C]glucose tracer using original PPP model. Shown are the estimated net and exchange fluxes (nmol/10^{6}cell/h) with 95% confidence intervals.

[3-^{13}C]Glucose+[4,5,6-^{13}C]glucose tracer experiment							
			Original PPP model				
Reaction			Flux		95% Conf. interval		
Gluc.ext → G6P	v1		76.4	[	69.0	,	83.8]
G6P ↔ F6P	v2	net	8.9	[	-6.5	,	31.0]
		exch	(>1e4, >1e4)	[	593.6	,	>1e4]
F6P→FBP	v3		53.9	[	48.3	,	61.8]
FBP ↔ DHAP + GAP	v4	net	53.9	[	48.3	,	61.8]
		exch	(0.0, >1e4)	[	0.0	,	>1e4]
DHAP ↔ GAP	v5	net	53.9	[	48.3	,	61.8]
		exch	336.8	[	264.23	,	429.3]
GAP ↔ 3PG	v6	net	130.3	[	122.2	,	140.4]
		exch	(0.0, >1e4)	[	0.0	,	>1e4]
3PG ↔ PEP	v7	net	130.3	[	122.2	,	140.4]
		exch	(0.0, >1e4)	[	0.0	,	>1e4]

Table C.4 continued

PEP → Pyr.snk	v8		130.3	[	122.2	,	140.4]
G6P → Ru5P + CO2	v9		67.5	[	45.2	,	83.4]
Ru5P ↔ X5P	v10	net	45.0	[	30.1	,	55.6]
		exch	(>1e4, >1e4)	[	51.9	,	>1e4]
Ru5P ↔ R5P	v11	net	22.5	[	15.1	,	27.8]
		exch	(>1e4, >1e4)	[	79.7	,	>1e4]
X5P ↔ EC2 + GAP	v12	net	45.0	[	30.1	,	55.6]
		exch	(>1e4, >1e4)	[	51.9	,	>1e4]
F6P ↔ EC2 + E4P	v13	net	-22.5	[	-27.8	,	-15.1]
		exch	0.0	[	0.0	,	37.7]
S7P ↔ EC2 + R5P	v14	net	-22.5	[	-27.8	,	-15.1]
		exch	(282.0, >1e4)	[	13.4	,	>1e4]
F6P ↔ EC3 + GAP	v15	net	-22.5	[	-27.8	,	-15.1]
		exch	(502.2, >1e4)	[	19.2	,	>1e4]
S7P ↔ EC3 + E4P	v16	net	22.5	[	15.1	,	27.8]
		exch	67.5	[	11.3	,	295.8]
DHAP ↔ GLP	v17	net	0.0	[	-0.0	,	0.0]
		exch	(0.0, >1e4)	[	0.0	,	>1e4]

Metabolites	G-value		95% Conf. interval		
DHAP	0.83	[	0.79	,	0.88]
3PG	0.79	[	0.75	,	0.83]
PEP	0.74	[	0.71	,	0.78]

Table C.5 Results of ^{13}C-MFA with combined data* using original PPP model. Shown are the estimated net and exchange fluxes (nmol/10^6cell/h) with 95% confidence intervals.

Combined data*							
			Original PPP model				
Reaction			Flux	95% Conf. interval			
Gluc.ext → G6P	v1		76.4	[	72.7	,	80.11]
G6P ↔ F6P	v2	net	33.3	[	29.3	,	35.1]
		exch	(>1e4, >1e4)	[	0.0	,	>1e4]
F6P→FBP	v3		62.0	[	58.8	,	64.1]
FBP ↔ DHAP + GAP	v4	net	62.0	[	58.8	,	64.1]
		exch	(0.0, >1e4)	[	0.0	,	>1e4]
DHAP ↔ GAP	v5	net	62.0	[	58.8	,	64.1]
		exch	500.3	[	399.6	,	556.1]
GAP ↔ 3PG	v6	net	138.4	[	131.6	,	143.9]
		exch	(0.0, >1e4)	[	0.0	,	>1e4]
3PG ↔ PEP	v7	net	138.4	[	131.6	,	143.9]
		exch	(0.0, >1e4)	[	0.0	,	>1e4]
PEP → Pyr.snk	v8		138.4	[	131.6	,	143.9]
G6P → Ru5P + CO2	v9		43.1	[	41.1	,	47.4]
Ru5P ↔ X5P	v10	net	28.7	[	27.4	,	31.6]
		exch	(0.0, >1e4)	[	0.0	,	>1e4]
Ru5P ↔ R5P	v11	net	14.4	[	13.7	,	15.8]
		exch	(>1e4, >1e4)	[	>1e4	,	>1e4]
X5P ↔ EC2 + GAP	v12	net	28.7	[	27.4	,	31.6]
		exch	(0.0, >1e4)	[	0.0	,	>1e4]
F6P ↔ EC2 + E4P	v13	net	-14.4	[	-15.8	,	-13.7]
		exch	-0.0	[	0.0	,	8.9]
S7P ↔ EC2 + R5P	v14	net	-14.4	[	-15.8	,	-13.7]
		exch	(>1e4, >1e4)	[	>1e4	,	>1e4]
F6P ↔ EC3 + GAP	v15	net	-14.4	[	-15.8	,	-13.7]
		exch	20.8	[	14.1	,	28.9]
S7P ↔ EC3 + E4P	v16	net	14.4	[	13.7	,	15.8]

Table C.5 continued

		exch	(>1e4, >1e4)	[	>1e4	,	>1e4]
DHAP ↔ GLP	v17	net	0.0	[	-0.0	,	0.0]
		exch	(0.0, >1e4)	[	0.0	,	>1e4]

Metabolites	G-value	95% Conf. interval		
[1,2-^{13}C]Glucose set				
DHAP	0.84	[0.83	,	0.87]
3PG	0.80	[0.79	,	0.82]
PEP	0.73	[0.72	,	0.75]
[1-^{13}C]Glucose+[4,5,6-^{13}C]glucose set				
DHAP	0.90	[0.89	,	0.93]
3PG	0.84	[0.82	,	0.86]
PEP	0.74	[0.73	,	0.76]
[2-^{13}C]Glucose+[4,5,6-^{13}C]glucose set				
DHAP	0.84	[0.82	,	0.85]
3PG	0.79	[0.77	,	0.80]
PEP	0.70	[0.69	,	0.72]
[3-^{13}C]Glucose+[4,5,6-^{13}C]glucose set				
DHAP	0.81	[0.80	,	0.83]
3PG	0.78	[0.76	,	0.79]
PEP	0.73	[0.71	,	0.74]

*^{13}C-MFA fitted simultaneously four measurement data from the set of [1,2-^{13}C]glucose, [1-^{13}C]glucose+[4,5,6-^{13}C]glucose mixture, [1,2-^{13}C]glucose, [1-^{13}C]glucose+[4,5,6-^{13}C]glucose mixture, [2-^{13}C]glucose+[4,5,6-^{13}C]glucose mixture and [3-^{13}C]glucose+[4,5,6-^{13}C]glucose mixture.

Table C.6 Results of ^{13}C-MFA with [1,2-^{13}C]glucose tracer using extended PPP model. Shown are the estimated net and exchange fluxes (nmol/10^6cell/h) with 95% confidence intervals.

[1,2-^{13}C]Glucose tracer experiment							
			Extended PPP model				
Reaction			Flux	95% Conf. interval			
Gluc.ext → G6P	v1		76.4	[	69.0	,	83.8]
G6P ↔ F6P	v2	net	61.3	[	25.2	,	71.2]
		exch	(0.0, >1e4)	[	0.0	,	>1e4]
F6P→FBP	v3		40.9	[	36.0	,	79.3]
FBP ↔ DHAP + GAP	v4	net	40.9	[	36.0	,	79.3]
		exch	(0.0, >1e4)	[	0.0	,	>1e4]
DHAP ↔ GAP	v5	net	40.9	[	36.0	,	79.3]
		exch	(0.0, >1e4)	[	0.0	,	>1e4]
GAP ↔ 3PG	v6	net	117.3	[	105.2	,	163.0]
		exch	(0.0, >1e4)	[	0.0	,	>1e4]
3PG ↔ PEP	v7	net	117.3	[	105.2	,	163.0]
		exch	(0.0, >1e4)	[	0.0	,	>1e4]
PEP → Pyr.snk	v8		117.3	[	105.2	,	163.0]
G6P → Ru5P + CO2	v9		15.1	[	10.0	,	52.3]
Ru5P ↔ X5P	v10	net	10.1	[	6.6	,	34.9]
		exch	(0.0, >1e4)	[	0.0	,	>1e4]
Ru5P ↔ R5P	v11	net	5.0	[	3.3	,	17.4]
		exch	(0.0, >1e4)	[	0.0	,	>1e4]
X5P ↔ EC2 + GAP	v12	net	10.1	[	6.6	,	34.9]
		exch	(0.0, >1e4)	[	0.0	,	>1e4]
F6P ↔ EC2 + E4P	v13	net	-5.0	[	-17.4	,	-3.3]
		exch	(0.0, >1e4)	[	0.0	,	>1e4]
S7P ↔ EC2 + R5P	v14	net	-5.0	[	-17.4	,	-3.3]
		exch	(0.0, >1e4)	[	0.0	,	>1e4]
F6P ↔ EC3 + GAP	v15	net	25.5	[	-9.8	,	31.7]
		exch	(0.0, >1e4)	[	0.0	,	>1e4]
S7P ↔ EC3 + E4P	v16	net	5.0	[	3.3	,	17.4]

Table C.6 continued

		exch	(0.0, >1e4)	[	0.0	,	>1e4]
DHAP ↔ GLP	v17	net	0.0	[	-0.0	,	0.0]
		exch	(0.0, >1e4)	[	0.0	,	>1e4]
EC3 → EC3.snk	v18	net	30.5	[	0.0	,	35.8]

Metabolites	G-value				
		95% Conf. interval			
DHAP	0.83	[	0.40	,	1.00]
3PG	1.00	[	0.69	,	1.00]
PEP	0.91	[	0.63	,	0.94]

Table C.7 Results of ^{13}C-MFA with [1-^{13}C]glucose and [4,5,6-^{13}C]glucose tracer using extended PPP model. Shown are the estimated net and exchange fluxes (nmol/10^6cell/h) with 95% confidence intervals.

[1-^{13}C]Glucose and [4,5,6-^{13}C]glucose tracer experiment							
			Extended PPP model				
Reaction			Flux	95% Conf. interval			
Gluc.ext → G6P	v1		76.4	[	69.0	,	83.8]
G6P ↔ F6P	v2	net	32.7	[	20.8	,	83.8]
		exch	(0.0, >1e4)	[	0.0	,	>1e4]
F6P→FBP	v3		61.8	[	61.9	,	71.7]
FBP ↔ DHAP + GAP	v4	net	61.8	[	61.9	,	71.7]
		exch	(0.0, >1e4)	[	0.0	,	>1e4]
DHAP ↔ GAP	v5	net	61.8	[	61.9	,	71.7]
		exch	310.5	[	190.5	,	469.4]
GAP ↔ 3PG	v6	net	138.3	[	107.4	,	155.4]
		exch	(0.0, >1e4)	[	0.0	,	>1e4]
3PG ↔ PEP	v7	net	138.3	[	107.4	,	155.4]

Table C.7 continued

		exch	(0.0, >1e4)	[	0.0	,	>1e4]
PEP → Pyr.snk	v8		138.3	[	107.4	,	155.4]
G6P → Ru5P + CO2	v9		43.7	[	0.0	,	56.7]
Ru5P ↔ X5P	v10	net	29.1	[	29.1	,	37.8]
		exch	(0.0,2.0)	[	0.0	,	>1e4]
Ru5P ↔ R5P	v11	net	14.6	[	14.6	,	18.9]
		exch	(0.0, >1e4)	[	0.0	,	>1e4]
X5P ↔ EC2 + GAP	v12	net	29.1	[	29.1	,	37.8]
		exch	(0.0, >1e4)	[	0.0	,	>1e4]
F6P ↔ EC2 + E4P	v13	net	-14.6	[	-18.9	,	-14.6]
		exch	(0.0, >1e4)	[	0.0	,	>1e4]
S7P ↔ EC2 + R5P	v14	net	-14.6	[	-18.9	,	-14.6]
		exch	(0.0, >1e4)	[	0.0	,	>1e4]
F6P ↔ EC3 + GAP	v15	net	-14.6	[	-18.9	,	38.0]
		exch	(0.0, >1e4)	[	0.0	,	>1e4]
S7P ↔ EC3 + E4P	v16	net	14.6	[	14.6	,	18.9]
		exch	(0.0, >1e4)	[	0.0	,	>1e4]
DHAP ↔ GLP	v17	net	0.0	[	-0.0	,	0.0]
		exch	(0.0, >1e4)	[	0.0	,	>1e4]
EC3 → EC3.snk	v18	net	0.0	[	0.0	,	38.0]

Metabolites	G-value	95% Conf. interval		
DHAP	0.93	[0.76	,	1.00]
3PG	0.85	[0.72	,	0.90]
PEP	0.75	[0.63	,	0.80]

Table C.8 Results of ^{13}C-MFA with [2-^{13}C]glucose and [4,5,6-^{13}C]glucose tracer using extended PPP model. Shown are the estimated net and exchange fluxes (nmol/10^{6}cell/h) with 95% confidence intervals.

[2-^{13}C]Glucose and [4,5,6-^{13}C]glucose tracer experiment						
			Extended PPP model			
Reaction			Flux	95% Conf. interval		
Gluc.ext → G6P	v1		76.4	[69.0	,	83.8]
G6P ↔ F6P	v2	net	76.4	[69.0	,	83.8]
		exch	(0.0, >1e4)	[0.0	,	>1e4]
F6P→FBP	v3		58.2	[48.1	,	65.8]
FBP ↔ DHAP + GAP	v4	net	58.2	[48.1	,	65.8]
		exch	(0.0, >1e4)	[0.0	,	>1e4]
DHAP ↔ GAP	v5	net	58.2	[48.1	,	65.8]
		exch	298.5	[213.4	,	429.2]
GAP ↔ 3PG	v6	net	134.6	[117.6	,	148.7]
		exch	(0.0, >1e4)	[0.0	,	>1e4]
3PG ↔ PEP	v7	net	134.6	[117.6	,	148.7]
		exch	(0.0, >1e4)	[0.0	,	>1e4]
PEP → Pyr.snk	v8		134.6	[117.6	,	148.7]
G6P → Ru5P + CO2	v9		0.0	[0.0	,	49.8]
Ru5P ↔ X5P	v10	net	0.0	[0.0	,	33.2]
		exch	(0.0, >1e4)	[0.0	,	>1e4]
Ru5P ↔ R5P	v11	net	0.0	[0.0	,	16.6]
		exch	(0.0, >1e4)	[0.0	,	>1e4]
X5P ↔ EC2 + GAP	v12	net	0.0	[0.0	,	33.2]
		exch	(0.0, >1e4)	[0.0	,	>1e4]
F6P ↔ EC2 + E4P	v13	net	-0.0	[-16.6	,	-0.0]
		exch	(0.0,499.0)	[0.0	,	>1e4]
S7P ↔ EC2 + R5P	v14	net	-0.0	[-16.6	,	-0.0]
		exch	(113.4,1e4)	[0.0	,	>1e4]
F6P ↔ EC3 + GAP	v15	net	18.2	[-22.7	,	25.6]
		exch	(0.0, >1e4)	[0.0	,	>1e4]
S7P ↔ EC3 + E4P	v16	net	0.0	[0.0	,	16.6]

Table C.8 continued

		exch	(0.0, >1e4)	[	0.0	,	>1e4]
DHAP ↔ GLP	v17	net	0.0	[	-0.0	,	0.0]
		exch	(0.0, >1e4)	[	0.0	,	>1e4]
EC3 → EC3.snk	v18	net	18.2	[	0.0	,	25.6]

Metabolites	G-value				
		95% Conf. interval			
DHAP	0.87	[	0.81	,	0.89]
3PG	0.81	[	0.77	,	0.83]
PEP	0.72	[	0.68	,	0.74]

Table C.9 Results of ^{13}C-MFA with [3-^{13}C]glucose and [4,5,6-^{13}C]glucose tracer using extended PPP model. Shown are the estimated net and exchange fluxes (nmol/10^{6}cell/h) with 95% confidence intervals.

[3-^{13}C]Glucose and [4,5,6-^{13}C]glucose tracer experiment							
			Extended PPP model				
Reaction			Flux	95% Conf. interval			
Gluc.ext → G6P	v1		76.4	[	69.0	,	83.8]
G6P ↔ F6P	v2	net	76.4	[	24.6	,	83.8]
		exch	(0.0, >1e4)	[	0.0	,	>1e4]
F6P→FBP	v3		54.9	[	42.2	,	63.1]
FBP ↔ DHAP + GAP	v4	net	54.9	[	42.2	,	63.1]
		exch	(0.0, >1e4)	[	0.0	,	>1e4]
DHAP ↔ GAP	v5	net	54.9	[	42.2	,	63.1]
		exch	(0.0, >1e4)	[	0.0	,	>1e4]
GAP ↔ 3PG	v6	net	131.3	[	111.5	,	144.7]
		exch	(0.0, >1e4)	[	0.0	,	>1e4]
3PG ↔ PEP	v7	net	131.3	[	111.5	,	144.7]

Table C.9 continued

		exch	(0.0, >1e4)	[	0.0	,	>1e4]
PEP → Pyr.snk	v8		131.3	[	111.5	,	144.7]
G6P → Ru5P + CO2	v9		0.0	[	0.0	,	47.6]
Ru5P ↔ X5P	v10	net	0.0	[	0.0	,	34.8]
		exch	(185.8, >1e4)	[	185.8	,	>1e4]
Ru5P ↔ R5P	v11	net	0.0	[	0.0	,	17.5]
		exch	(272.5, >1e4)	[	272.5	,	>1e4]
X5P ↔ EC2 + GAP	v12	net	0.0	[	0.0	,	34.8]
		exch	(236.1, >1e4)	[	236.1	,	>1e4]
F6P ↔ EC2 + E4P	v13	net	-0.0	[	-17.5	,	-0.0]
		exch	(0.0, >1e4)	[	0.0	,	>1e4]
S7P ↔ EC2 + R5P	v14	net	-0.0	[	-17.5	,	-0.0]
		exch	(0.0, >1e4)	[	0.0	,	>1e4]
F6P ↔ EC3 + GAP	v15	net	21.5	[	-5.8	,	27.3]
		exch	(0.0, >1e4)	[	0.0	,	>1e4]
S7P ↔ EC3 + E4P	v16	net	0.0	[	0.0	,	17.5]
		exch	(0.0, >1e4)	[	0.0	,	>1e4]
DHAP ↔ GLP	v17	net	0.0	[	-0.0	,	0.0]
		exch	(0.0, >1e4)	[	0.0	,	>1e4]
EC3 → EC3.snk	v18	net	21.5	[	10.5	,	27.2]

Metabolites	G-value				95% Conf. interval
DHAP	0.86	[	0.78	,	0.87]
3PG	0.81	[	0.75	,	0.82]
PEP	0.76	[	0.70	,	0.77]

Table C.10 Results of ^{13}C-MFA with combined data using extended PPP model. Shown are the estimated net and exchange fluxes (nmol/10^6cell/h) with 95% confidence intervals.

Combined data							
			Extended PPP model				
Reaction			Flux	95% Conf. interval			
Gluc.ext → G6P	v1		76.4	[	72.7	,	80.1]
G6P ↔ F6P	v2	net	59.2	[	50.4	,	62.8]
		exch	(0.0,3.8)	[	0.0	,	>1e4]
F6P→FBP	v3		52.3	[	49.0	,	55.7]
FBP ↔ DHAP + GAP	v4	net	52.3	[	49.0	,	55.7]
		exch	(0.0, >1e4)	[	0.0	,	>1e4]
DHAP ↔ GAP	v5	net	52.3	[	49.0	,	55.7]
		exch	294.8	[	243.9	,	364.3]
GAP ↔ 3PG	v6	net	128.7	[	122.1	,	135.3]
		exch	(0.0, >1e4)	[	0.0	,	>1e4]
3PG ↔ PEP	v7	net	128.7	[	122.1	,	135.3]
		exch	(0.0, >1e4)	[	0.0	,	>1e4]
PEP → Pyr.snk	v8		128.7	[	122.1	,	135.3]
G6P → Ru5P + CO2	v9		17.2	[	15.3	,	26.0]
Ru5P ↔ X5P	v10	net	11.4	[	10.2	,	17.3]
		exch	(0.0, 0.7)	[	0.0	,	>1e4]
Ru5P ↔ R5P	v11	net	5.7	[	5.1	,	8.7]
		exch	(>1e4, >1e4)	[	0.0	,	>1e4]
X5P ↔ EC2 + GAP	v12	net	11.4	[	10.2	,	17.3]
		exch	(0.0, >1e4)	[	0.0	,	>1e4]
F6P ↔ EC2 + E4P	v13	net	-5.7	[	-8.7	,	-5.1]
		exch	(71.8, >1e4)	[	61.3	,	>1e4]
S7P ↔ EC2 + R5P	v14	net	-5.7	[	-8.7	,	-5.1]
		exch	(>1e4, >1e4)	[	0.0	,	>1e4]
F6P ↔ EC3 + GAP	v15	net	12.7	[	5.8	,	15.5]
		exch	(>1e4, >1e4)	[	>1e4	,	>1e4]
S7P ↔ EC3 + E4P	v16	net	5.7	[	5.1	,	8.7]

Table C.10 continued

		exch	1.2	[	0.0	,	15.2]
DHAP ↔ GLP	v17	net	0.0	[	-0.0	,	0.0]
		exch	(0.0, >1e4)	[	0.0	,	>1e4]
EC3 → EC3.snk	v18	net	18.4	[	14.2	,	20.9]

Metabolites	G-value		95% Conf. interval		
[1,2-^{13}C]Glucose set					
DHAP	0.84	[	0.81	,	0.86]
3PG	0.86	[	0.83	,	0.88]
PEP	0.78	[	0.75	,	0.81]
[1-^{13}C]Glucose+[4,5,6-^{13}C]glucose set					
DHAP	0.85	[	0.82	,	0.88]
3PG	0.79	[	0.77	,	0.81]
PEP	0.70	[	0.68	,	0.72]
[2-^{13}C]Glucose+[4,5,6-^{13}C]glucose set					
DHAP	0.84	[	0.82	,	0.85]
3PG	0.79	[	0.77	,	0.81]
PEP	0.70	[	0.68	,	0.72]
[3-^{13}C]Glucose+[4,5,6-^{13}C]glucose set					
DHAP	0.83	[	0.81	,	0.85]
3PG	0.79	[	0.77	,	0.81]
PEP	0.74	[	0.72	,	0.76]

Table C.11 Results of ^{13}C-MFA with [1,2-^{13}C]glucose tracer using extended PPP model with F6P data. Shown are the estimated net and exchange fluxes (nmol/10^{6}cell/h) with 95% confidence intervals.

[1,2-^{13}C]glucose tracer experiment							
			Extended PPP model with F6P data				
Reaction			Flux	95% Conf. interval			
Gluc.ext → G6P	v1		76.4	[	69.0	,	83.8]
G6P ↔ F6P	v2	net	58.0	[	28.9	,	71.4]
		exch	(0.0, >1e4)	[	0.0	,	>1e4]
F6P→FBP	v3		41.9	[	35.1	,	79.2]
FBP ↔ DHAP + GAP	v4	net	41.9	[	35.1	,	79.2]
		exch	(0.0, >1e4)	[	0.0	,	>1e4]
DHAP ↔ GAP	v5	net	41.9	[	35.1	,	79.2]
		exch	(0.0, >1e4)	[	0.0	,	>1e4]
GAP ↔ 3PG	v6	net	118.3	[	104.6	,	162.7]
		exch	(0.0, >1e4)	[	0.0	,	>1e4]
3PG ↔ PEP	v7	net	118.3	[	104.6	,	162.7]
		exch	(0.0, >1e4)	[	0.0	,	>1e4]
PEP → Pyr.snk	v8		118.3	[	104.6	,	162.7]
G6P → Ru5P + CO2	v9		18.4	[	9.6	,	48.4]
Ru5P ↔ X5P	v10	net	12.3	[	6.4	,	32.2]
		exch	(6.2, >1e4)	[	0.0	,	>1e4]
Ru5P ↔ R5P	v11	net	6.1	[	3.2	,	16.1]
		exch	(9.7, >1e4)	[	0.0	,	>1e4]
X5P ↔ EC2 + GAP	v12	net	12.3	[	6.4	,	32.2]
		exch	(5.4, >1e4)	[	0.0	,	>1e4]
F6P ↔ EC2 + E4P	v13	net	-6.1	[	-16.1	,	-3.2]
		exch	(0.0, 51.0)	[	0.0	,	>1e4]
S7P ↔ EC2 + R5P	v14	net	-6.1	[	-16.1	,	-3.2]
		exch	(7.5, >1e4)	[	0.0	,	>1e4]
F6P ↔ EC3 + GAP	v15	net	22.3	[	-12.2	,	31.1]
		exch	26.3	[	0.0	,	47.9]
S7P ↔ EC3 + E4P	v16	net	6.1	[	3.2	,	16.1]

Table C.11 continued

		exch	(9.9, >1e4)	[	0.0	,	>1e4]
DHAP ↔ GLP	v17	net	0.0	[	-0.0	,	0.0]
		exch	(0.0, >1e4)	[	0.0	,	>1e4]
EC3 → EC3.snk	v18	net	28.4	[	0.0	,	35.0]

Metabolites	G-value				95% Conf. interval
DHAP	0.75	[	0.39	,	1.00
3PG	1.00	[	0.69	,	1.00
PEP	0.91	[	0.63	,	0.94
F6P	0.80	[	0.74	,	0.84

Table C.12 Results of ^{13}C-MFA with [1-^{13}C]glucose and [4,5,6-^{13}C]glucose tracer using extended PPP model with F6P data. Shown are the estimated net and exchange fluxes (nmol/10^{6}cell/h) with 95% confidence intervals.

[1-^{13}C]Glucose and [4,5,6-^{13}C]glucose tracer experiment							
			Extended PPP model with F6P data				
Reaction			Flux		95% Conf. interval		
Gluc.ext → G6P	v1		76.4	[	69.0	,	83.8]
G6P ↔ F6P	v2	net	56.9	[	36.5	,	69.4]
		exch	(0.0, >1e4)	[	0.0	,	>1e4]
F6P→FBP	v3		51.6	[	44.4	,	60.2]
FBP ↔ DHAP + GAP	v4	net	51.6	[	44.4	,	60.2]
		exch	(0.0, >1e4)	[	0.0	,	>1e4]
DHAP ↔ GAP	v5	net	51.6	[	44.4	,	60.2]
		exch	287.5	[	203.6	,	438.8]
GAP ↔ 3PG	v6	net	128.0	[	114.5	,	142.2]
		exch	(0.0, >1e4)	[	0.0	,	>1e4]

Table C.12 continued

3PG ↔ PEP	v7	net	128.0	[	114.5	,	142.2]
		exch	(0.0, >1e4)	[	0.0	,	>1e4]
PEP → Pyr.snk	v8		128.0	[	114.5	,	142.2]
G6P → Ru5P + CO2	v9		19.5	[	9.0	,	39.8]
Ru5P ↔ X5P	v10	net	13.0	[	6.0	,	26.6]
		exch	(0.0, >1e4)	[	0.0	,	>1e4]
Ru5P ↔ R5P	v11	net	6.5	[	3.0	,	13.3]
		exch	(0.0, >1e4)	[	0.0	,	>1e4]
X5P ↔ EC2 + GAP	v12	net	13.0	[	6.0	,	26.6]
		exch	(0.0, >1e4)	[	0.0	,	>1e4]
F6P ↔ EC2 + E4P	v13	net	-6.5	[	-13.3	,	-3.0]
		exch	23.4	[	3.3	,	59.0]
S7P ↔ EC2 + R5P	v14	net	-6.5	[	-13.3	,	-3.0]
		exch	(0.0, >1e4)	[	0.0	,	>1e4]
F6P ↔ EC3 + GAP	v15	net	11.8	[	-7.1	,	23.4]
		exch	22.7	[	5.8	,	39.6]
S7P ↔ EC3 + E4P	v16	net	6.5	[	3.0	,	13.3]
		exch	(0.0, >1e4)	[	0.0	,	>1e4]
DHAP ↔ GLP	v17	net	0.0	[	-0.0	,	0.0]
		exch	(0.0, >1e4)	[	0.0	,	>1e4]
EC3 → EC3.snk	v18	net	18.3	[	5.7	,	28.9]

Metabolites	G-value		95% Conf. interval		
DHAP	0.85	[	0.81	,	0.90]
3PG	0.79	[	0.76	,	0.83]
PEP	0.70	[	0.67	,	0.73]
F6P	0.75	[	0.72	,	0.78]

Table C.13 Results of ^{13}C-MFA with [2-^{13}C]glucose and [4,5,6-^{13}C]glucose tracer using extended PPP model with F6P data. Shown are the estimated net and exchange fluxes (nmol/10^{6}cell/h) with 95% confidence intervals.

[2-^{13}C]Glucose and [4,5,6-^{13}C]glucose tracer experiment							
			Extended PPP model with F6P data				
Reaction			Flux	95% Conf. interval			
Gluc.ext → G6P	v1		76.4	[	69.0	,	83.8]
G6P ↔ F6P	v2	net	62.3	[	18.6	,	83.7]
		exch	(0.0, >1e4)	[	0.0	,	>1e4]
F6P→FBP	v3		56.9	[	49.5	,	64.6]
FBP ↔ DHAP + GAP	v4	net	56.9	[	49.5	,	64.6]
		exch	(0.0, >1e4)	[	0.0	,	>1e4]
DHAP ↔ GAP	v5	net	56.9	[	49.5	,	64.6]
		exch	295.0	[	216.6	,	423.6]
GAP ↔ 3PG	v6	net	133.3	[	119.2	,	147.6]
		exch	(0.0, >1e4)	[	0.0	,	>1e4]
3PG ↔ PEP	v7	net	133.3	[	119.2	,	147.6]
		exch	(0.0, >1e4)	[	0.0	,	>1e4]
PEP → Pyr.snk	v8		133.3	[	119.2	,	147.6]
G6P → Ru5P + CO2	v9		14.1	[	0.0	,	58.4]
Ru5P ↔ X5P	v10	net	9.4	[	0.0	,	38.9]
		exch	(0.0, >1e4)	[	0.0	,	>1e4]
Ru5P ↔ R5P	v11	net	4.7	[	0.0	,	19.5]
		exch	(472.2, >1e4)	[	472.2	,	>1e4]
X5P ↔ EC2 + GAP	v12	net	9.4	[	0.0	,	38.9]
		exch	(0.0, >1e4)	[	0.0	,	>1e4]
F6P ↔ EC2 + E4P	v13	net	-4.7	[	-19.5	,	-0.0]
		exch	37.2	[	1.4	,	68.4]
S7P ↔ EC2 + R5P	v14	net	-4.7	[	-19.5	,	-0.0]
		exch	(5.2, >1e4)	[	0.0	,	>1e4]
F6P ↔ EC3 + GAP	v15	net	10.1	[	-17.3	,	23.1]
		exch	20.6	[	0.0	,	38.5]
S7P ↔ EC3 + E4P	v16	net	4.7	[	0.0	,	19.5]

Table C.13 continued

		exch	(6.3, >1e4)	[	0.0	,	>1e4]
DHAP ↔ GLP	v17	net	0.0	[	-0.0	,	0.0]
		exch	(0.0, >1e4)	[	0.0	,	>1e4]
EC3 → EC3.snk	v18	net	14.8	[	1.8	,	23.1]

Metabolites	G-value				
DHAP	0.85	[	0.82	,	0.88]
3PG	0.80	[	0.77	,	0.83]
PEP	0.72	[	0.69	,	0.74]
F6P	0.79	[	0.77	,	0.81]

Table C.14 Results of ^{13}C-MFA with [3-^{13}C]glucose and [4,5,6-^{13}C]glucose tracer using extended PPP model with F6P data. Shown are the estimated net and exchange fluxes (nmol/10^{6}cell/h) with 95% confidence intervals.

[3-^{13}C]Glucose and [4,5,6-^{13}C]glucose tracer experiment							
			Extended PPP model with F6P data				
Reaction			Flux		95% Conf. interval		
Gluc.ext → G6P	v1		76.4	[	69.0	,	83.8]
G6P ↔ F6P	v2	net	69.5	[	54.0	,	83.0]
		exch	(0.0, >1e4)	[	0.0	,	>1e4]
F6P→FBP	v3		53.4	[	46.2	,	61.5]
FBP ↔ DHAP + GAP	v4	net	53.4	[	46.2	,	61.5]
		exch	(0.0, >1e4)	[	0.0	,	>1e4]
DHAP ↔ GAP	v5	net	53.4	[	46.2	,	61.5]
		exch	304.3	[	220.3	,	448.3]
GAP ↔ 3PG	v6	net	129.8	[	116.2	,	143.9]
		exch	(0.0, >1e4)	[	0.0	,	>1e4]

Table C.14 continued

3PG ↔ PEP	v7	net	129.8	[	116.2	,	143.9]
		exch	(0.0, >1e4)	[	0.0	,	>1e4]
PEP → Pyr.snk	v8		129.8	[	116.2	,	143.9]
G6P → Ru5P + CO2	v9		6.9	[	0.0	,	21.0]
Ru5P ↔ X5P	v10	net	4.6	[	0.0	,	14.0]
		exch	(3.25, >1e4)	[	0.0	,	>1e4]
Ru5P ↔ R5P	v11	net	2.3	[	0.0	,	7.0]
		exch	(>1e4, >1e4)	[	>1e4	,	>1e4]
X5P ↔ EC2 + GAP	v12	net	4.6	[	0.0	,	14.0]
		exch	(0.0, >1e4)	[	0.0	,	>1e4]
F6P ↔ EC2 + E4P	v13	net	-2.3	[	-7.0	,	-0.0]
		exch	(>1e4, >1e4)	[	0.0	,	>1e4]
S7P ↔ EC2 + R5P	v14	net	-2.3	[	-7.0	,	-0.0]
		exch	(35.77, >1e4)	[	0.0	,	>1e4]
F6P ↔ EC3 + GAP	v15	net	18.4	[	9.2	,	24.9]
		exch	27.1	[	9.5	,	41.1]
S7P ↔ EC3 + E4P	v16	net	2.3	[	0.0	,	7.0]
		exch	(>1e4, >1e4)	[	>1e4	,	>1e4]
DHAP ↔ GLP	v17	net	0.0	[	-0.0	,	0.0]
		exch	(0.0, >1e4)	[	0.0	,	>1e4]
EC3 → EC3.snk	v18	net	20.7	[	15.4	,	25.2]

Metabolites	G-value		95% Conf. interval		
DHAP	0.84	[	0.81	,	0.87]
3PG	0.80	[	0.77	,	0.83]
PEP	0.75	[	0.72	,	0.78]
F6P	0.79	[	0.76	,	0.81]

Table C.15 Results of ^{13}C-MFA with combined data using extended PPP model with F6P data. Shown are the estimated net and exchange fluxes (nmol/10^{6}cell/h) with 95% confidence intervals.

Combined data							
			Extended PPP model with F6P data				
Reaction			Flux	95% Conf. interval			
Gluc.ext → G6P	v1		76.4	[	72.7	,	80.1]
G6P ↔ F6P	v2	net	55.3	[	43.0	,	62.4]
		exch	(0.0, 9.7)	[	0.0	,	>1e4]
F6P→FBP	v3		53.0	[	49.7	,	56.4]
FBP ↔ DHAP + GAP	v4	net	53.0	[	49.7	,	56.4]
		exch	(0.0, >1e4)	[	0.0	,	>1e4]
DHAP ↔ GAP	v5	net	53.0	[	49.7	,	56.4]
		exch	292.8	[	242.4	,	361.4]
GAP ↔ 3PG	v6	net	129.4	[	122.8	,	136.0]
		exch	(0.0, >1e4)	[	0.0	,	>1e4]
3PG ↔ PEP	v7	net	129.4	[	122.8	,	136.0]
		exch	(0.0, >1e4)	[	0.0	,	>1e4]
PEP → Pyr.snk	v8		129.4	[	122.8	,	136.0]
G6P → Ru5P + CO2	v9		21.1	[	15.0	,	33.4]
Ru5P ↔ X5P	v10	net	14.0	[	10.0	,	22.3]
		exch	(18.0, >1e4)	[	0.0	,	>1e4]
Ru5P ↔ R5P	v11	net	7.0	[	5.0	,	11.1]
		exch	(12.3, 20.3)	[	0.0	,	175.0]
X5P ↔ EC2 + GAP	v12	net	14.0	[	10.0	,	22.3]
		exch	(8.2, 12.4)	[	0.0	,	>1e4]
F6P ↔ EC2 + E4P	v13	net	-7.0	[	-11.1	,	-5.0]
		exch	18.2	[	3.7	,	44.1]
S7P ↔ EC2 + R5P	v14	net	-7.0	[	-11.1	,	-5.0]
		exch	(973.6, >1e4)	[	6.7	,	>1e4]
F6P ↔ EC3 + GAP	v15	net	9.4	[	0.2	,	14.6]
		exch	22.7	[	14.3	,	31.0]
S7P ↔ EC3 + E4P	v16	net	7.0	[	5.0	,	11.1]

Table C.15 continued

		exch	(>1e4, >1e4)	[	>1e4	,	>1e4]
DHAP ↔ GLP	v17	net	0.0	[	-0.0	,	0.0]
		exch	(0.0, >1e4)	[	0.0	,	>1e4]
EC3 → EC3.snk	v18	net	16.4	[	11.1	,	20.1]

Metabolites	G-value		95% Conf. interval		
[1,2-^{13}C]Glucose set					
DHAP	0.84	[	0.82	,	0.87]
3PG	0.86	[	0.83	,	0.89]
PEP	0.79	[	0.76	,	0.81]
F6P	0.80	[	0.77	,	0.82]
[1-^{13}C]Glucose+[4,5,6-^{13}C]glucose set					
DHAP	0.85	[	0.83	,	0.88]
3PG	0.79	[	0.77	,	0.81]
PEP	0.70	[	0.68	,	0.72]
F6P	0.76	[	0.74	,	0.77]
[2-^{13}C]Glucose+[4,5,6-^{13}C]glucose set					
DHAP	0.85	[	0.83	,	0.86]
3PG	0.80	[	0.78	,	0.81]
PEP	0.71	[	0.69	,	0.73]
F6P	0.79	[	0.78	,	0.80]
[3-^{13}C]Glucose+[4,5,6-^{13}C]glucose set					
DHAP	0.83	[	0.81	,	0.84]
3PG	0.79	[	0.77	,	0.80]
PEP	0.74	[	0.72	,	0.76]
F6P	0.78	[	0.76	,	0.79]

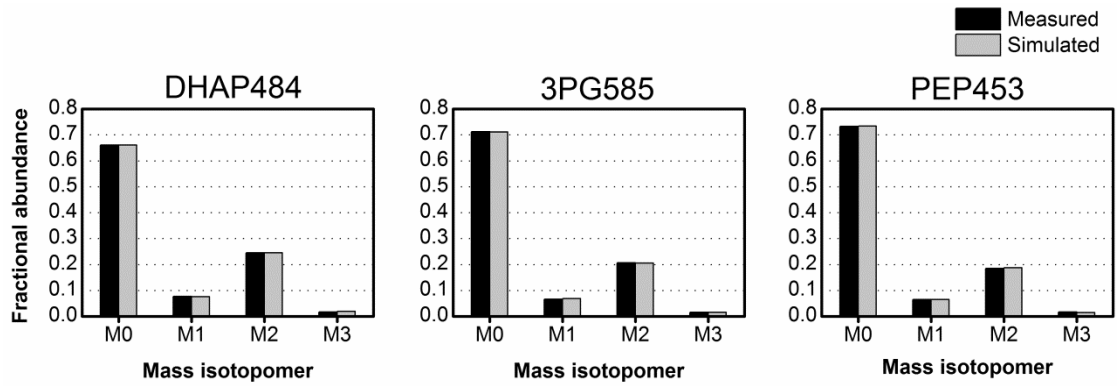

Figure C.1 Measured and fitted mass isotopomer distributions for the experiment with [1,2-^{13}C]glucose and original PPP model (shown MIDs were corrected for natural isotope abundances).

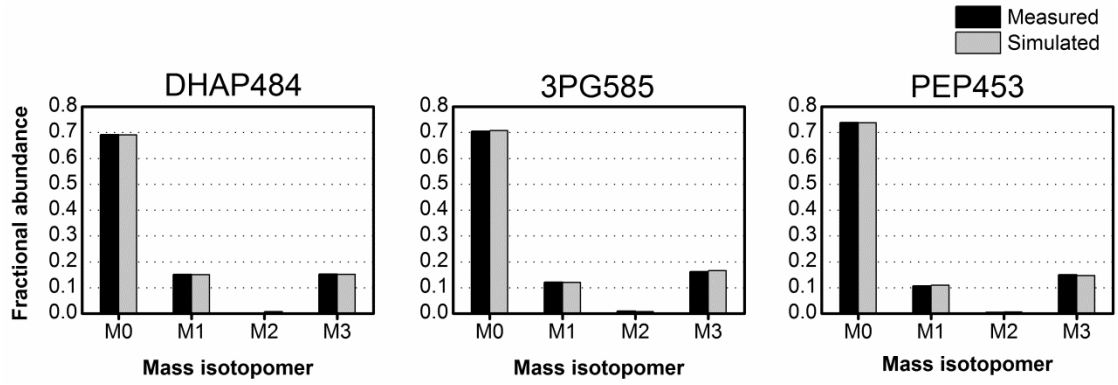

Figure C.2 Measured and fitted mass isotopomer distributions for the experiment with [1-^{13}C]glucose+[4,5,6-^{13}C]glucose and original PPP model (shown MIDs were corrected for natural isotope abundances).

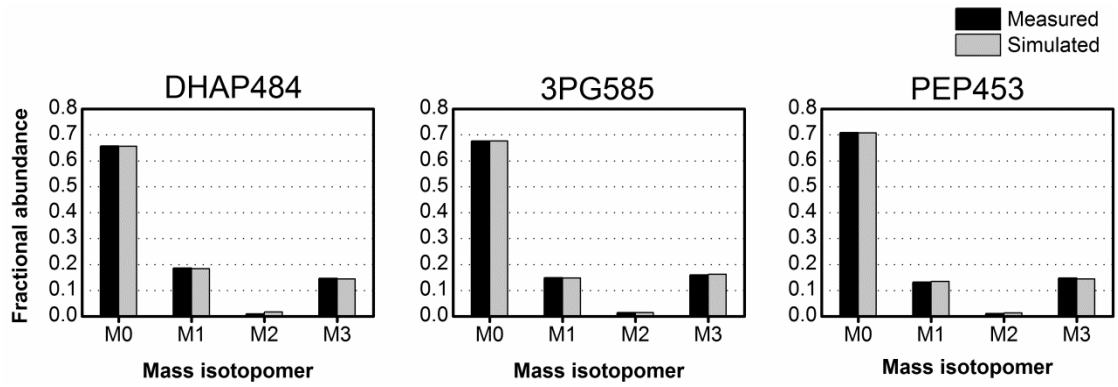

Figure C.3 Measured and fitted mass isotopomer distributions for the experiment with [2-^{13}C]glucose+[4,5,6-^{13}C]glucose and original PPP model (shown MIDs were corrected for natural isotope abundances).

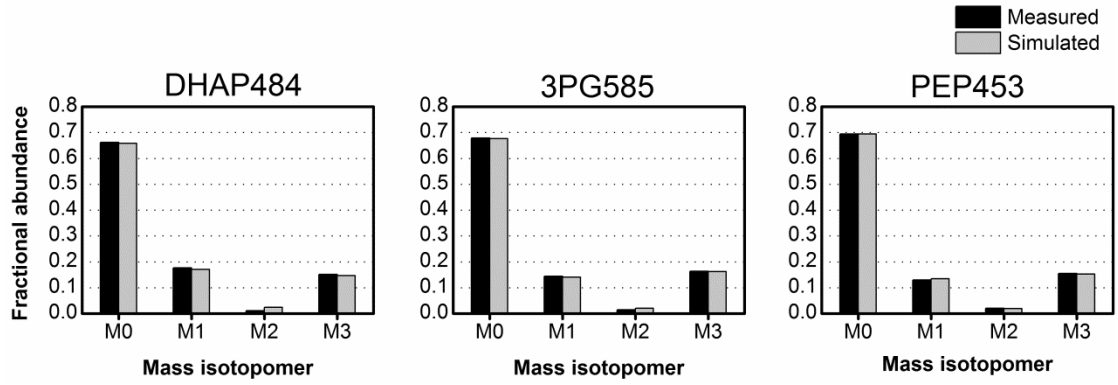

Figure C.4 Measured and fitted mass isotopomer distributions for the experiment with [3-^{13}C]glucose+[4,5,6-^{13}C]glucose and original PPP model (shown MIDs were corrected for natural isotope abundances).

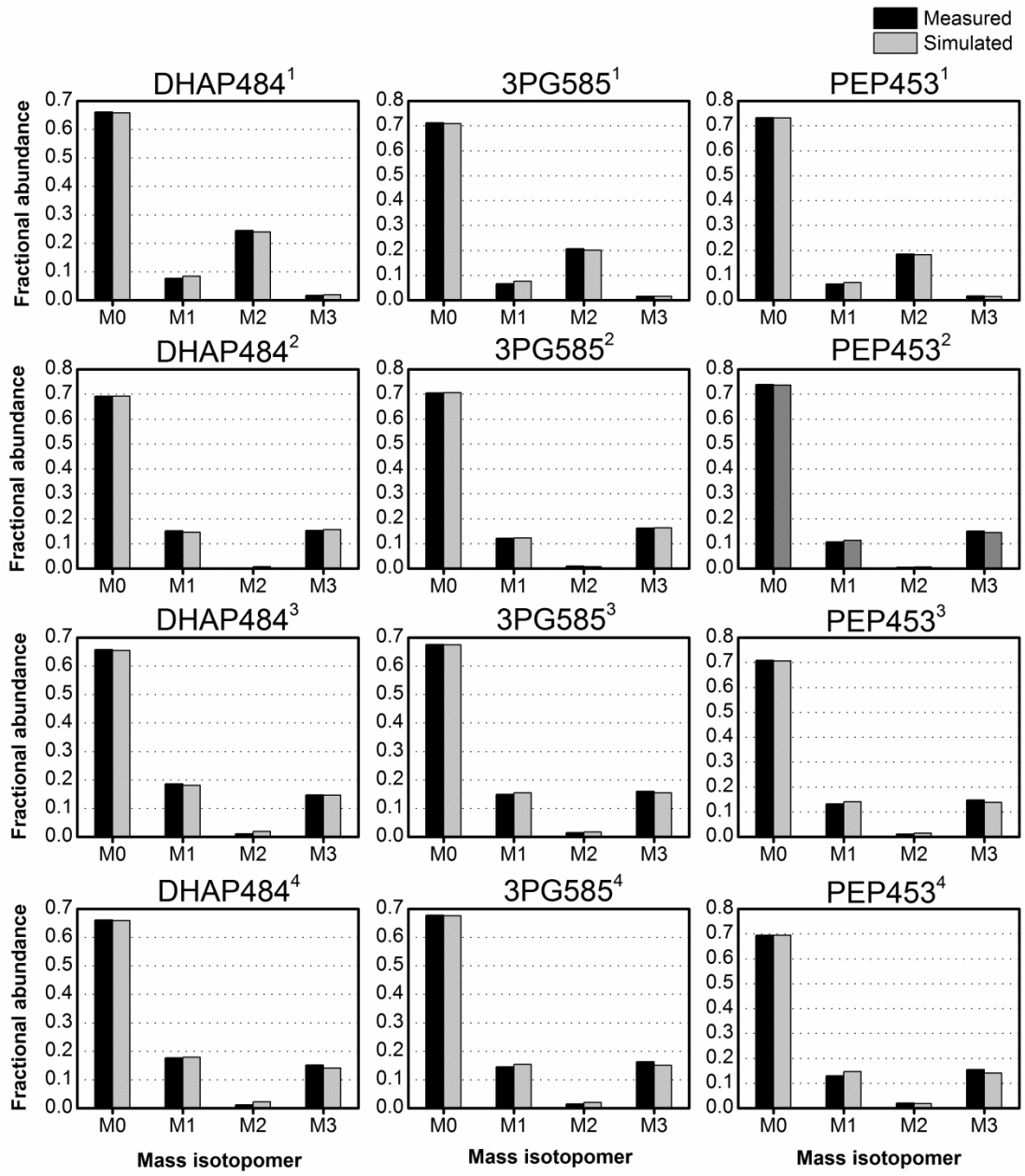

Figure C.5 Measured and fitted mass isotopomer distributions for the experiment with combined data and original PPP model (shown MIDs were corrected for natural isotope abundances). This result cannot be accepted due to large sum of squared residual error. (superscript 1, [1,2-^{13}C]glucose data; superscript 2, [1-^{13}C]glucose+[4,5,6-^{13}C]glucose data; superscript 3, [2-^{13}C]glucose+[4,5,6-^{13}C]glucose data; superscript 3, [3-^{13}C]glucose+[4,5,6-^{13}C]glucose data)

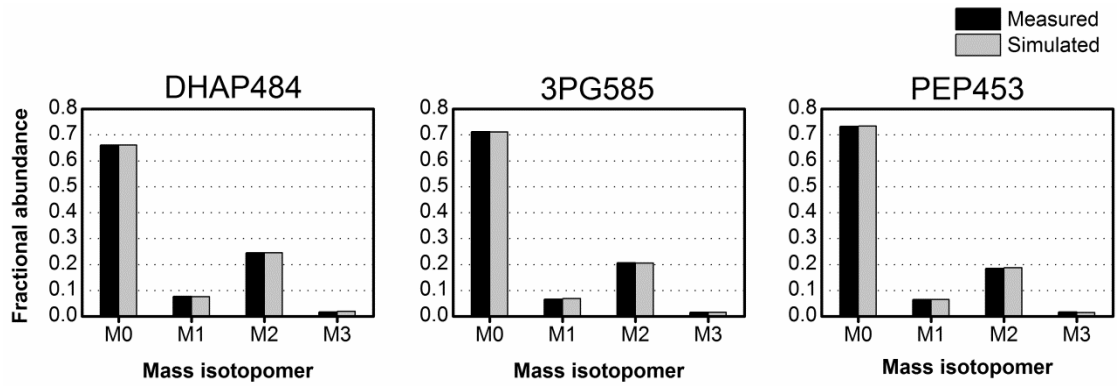

Figure C.6 Measured and fitted mass isotopomer distributions for the experiment with [1,2-^{13}C]glucose and extended PPP model (shown MIDs were corrected for natural isotope abundances).

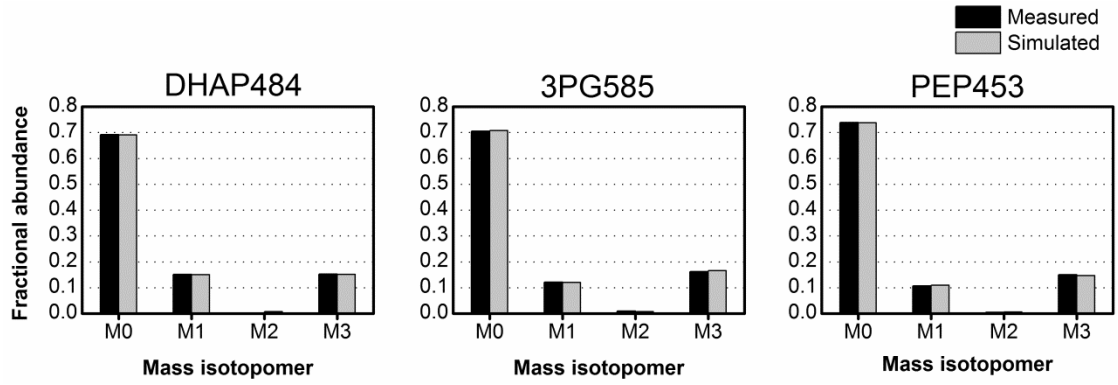

Figure C.7 Measured and fitted mass isotopomer distributions for the experiment with [1-^{13}C]glucose+[4,5,6-^{13}C]glucose and extended PPP model (shown MIDs were corrected for natural isotope abundances).

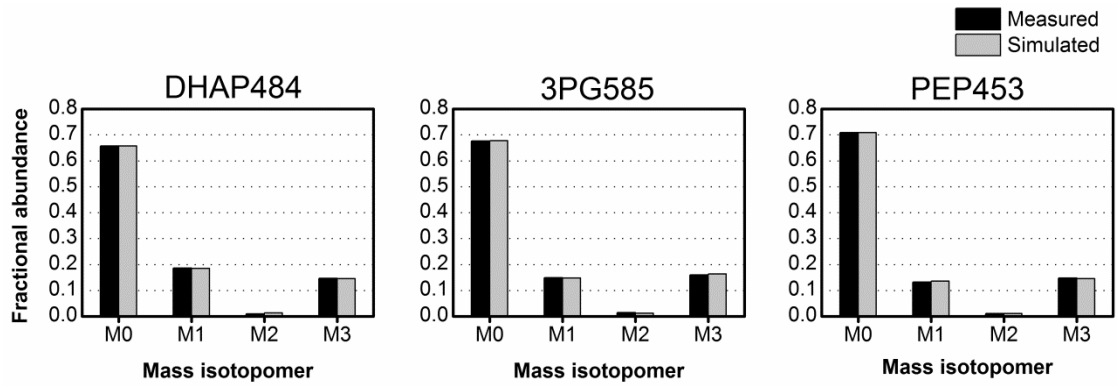

Figure C.8 Measured and fitted mass isotopomer distributions for the experiment with [2-^{13}C]glucose+[4,5,6-^{13}C]glucose and extended PPP model (shown MIDs were corrected for natural isotope abundances).

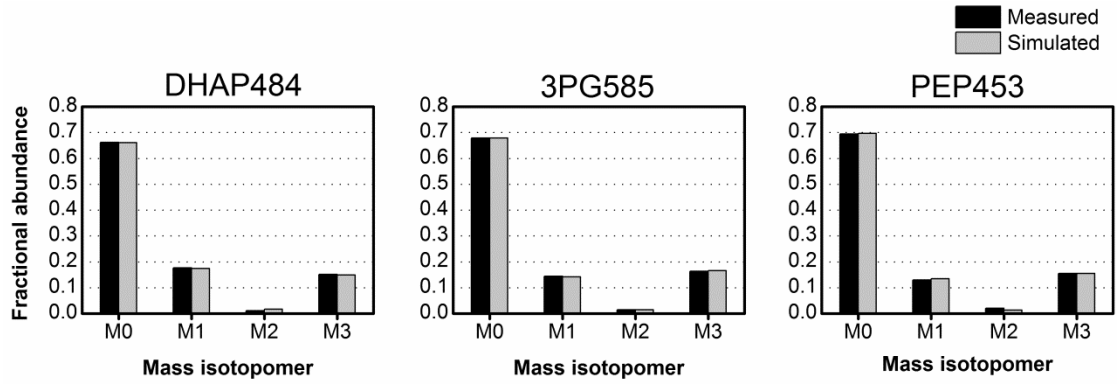

Figure C.9 Measured and fitted mass isotopomer distributions for the experiment with [3-^{13}C]glucose+[4,5,6-^{13}C]glucose and extended PPP model (shown MIDs were corrected for natural isotope abundances).

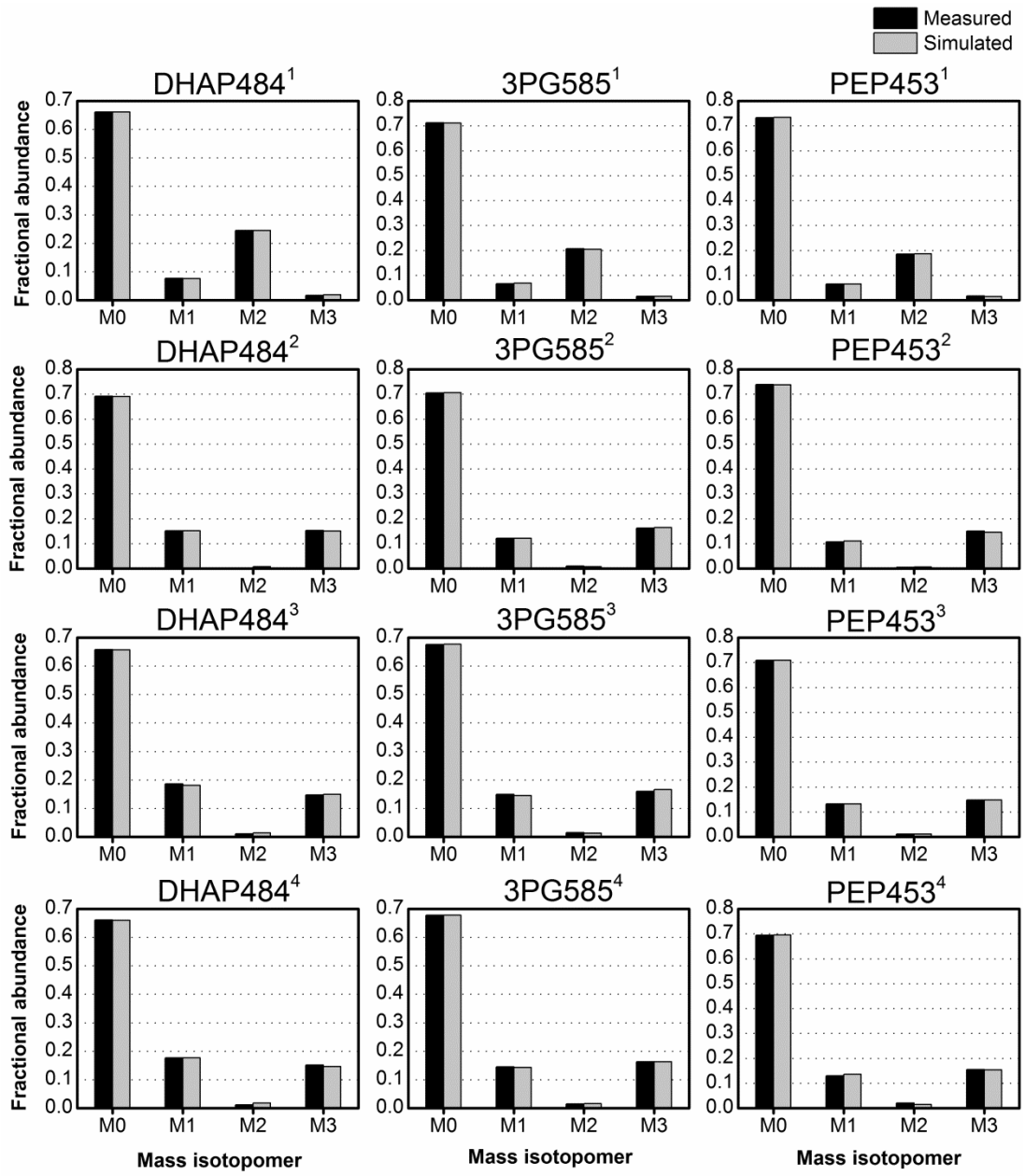

Figure C.10 Measured and fitted mass isotopomer distributions for the experiment with combined data and extended PPP model (shown MIDs were corrected for natural isotope abundances). (superscript 1, [1,2-^{13}C]glucose data; superscript 2, [1-^{13}C]glucose+[4,5,6-^{13}C]glucose data; superscript 3, [2-^{13}C]glucose+[4,5,6-^{13}C]glucose data; superscript 3, [3-^{13}C]glucose+[4,5,6-^{13}C]glucose data)

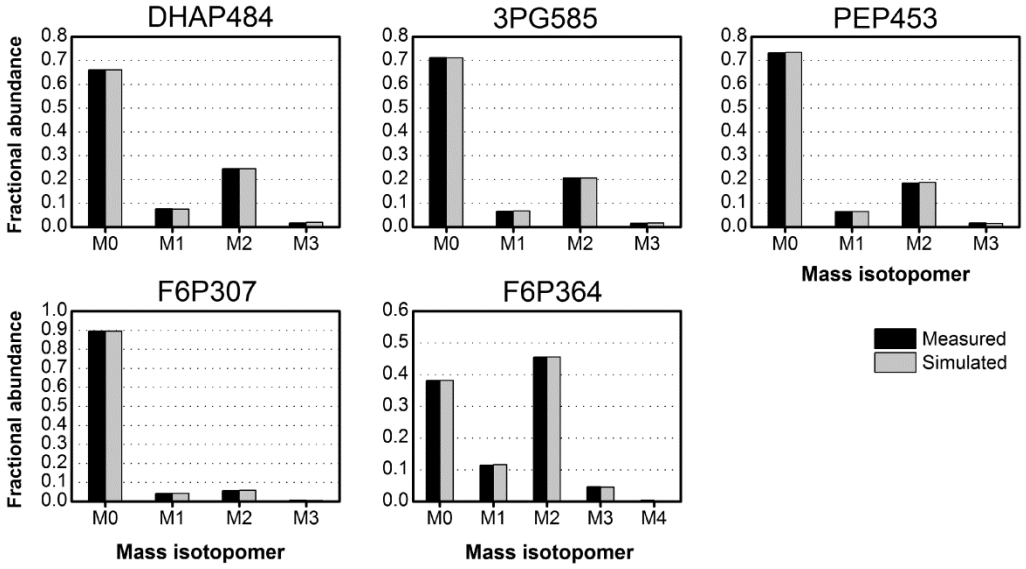

Figure C.11 Measured and fitted mass isotopomer distributions for the experiment with [1,2-^{13}C]glucose and extended PPP model with F6P data (shown MIDs were corrected for natural isotope abundances).

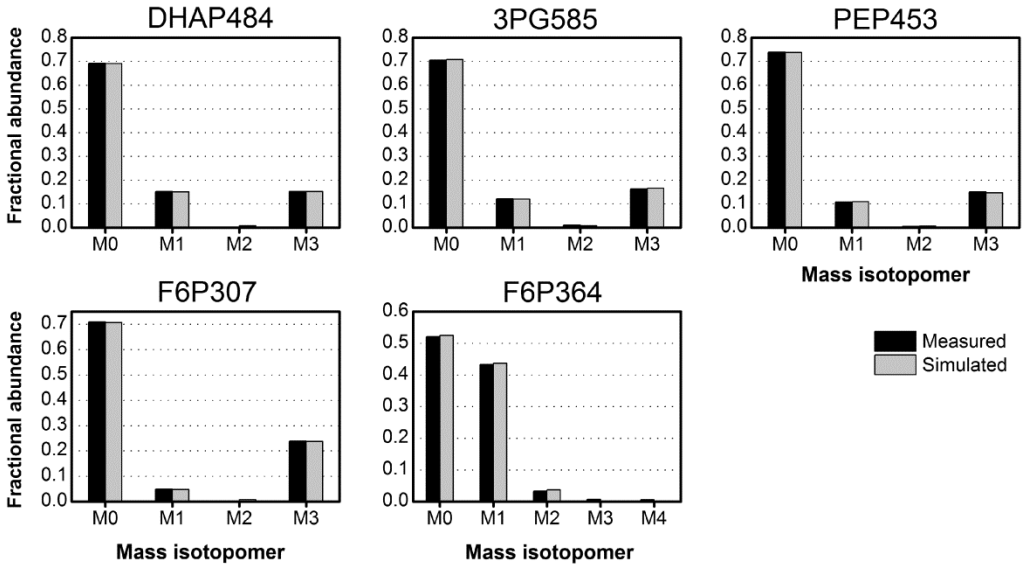

Figure C.12 Measured and fitted mass isotopomer distributions for the experiment with [1-^{13}C]glucose+[4,5,6-^{13}C]glucose and extended PPP model with F6P data (shown MIDs were corrected for natural isotope abundances).

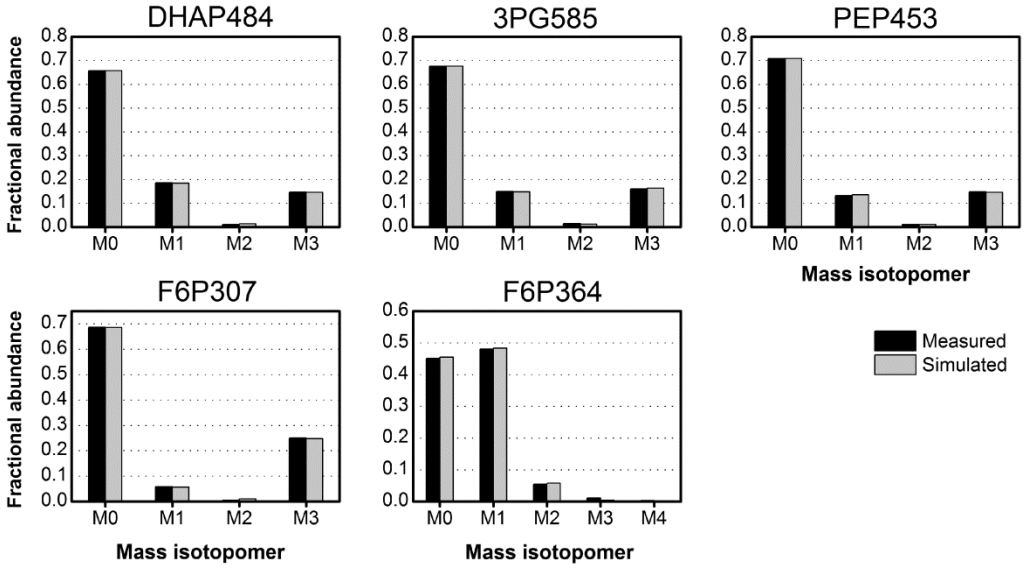

Figure C.13 Measured and fitted mass isotopomer distributions for the experiment with [2-^{13}C]glucose+[4,5,6-^{13}C]glucose and extended PPP model with F6P data (shown MIDs were corrected for natural isotope abundances).

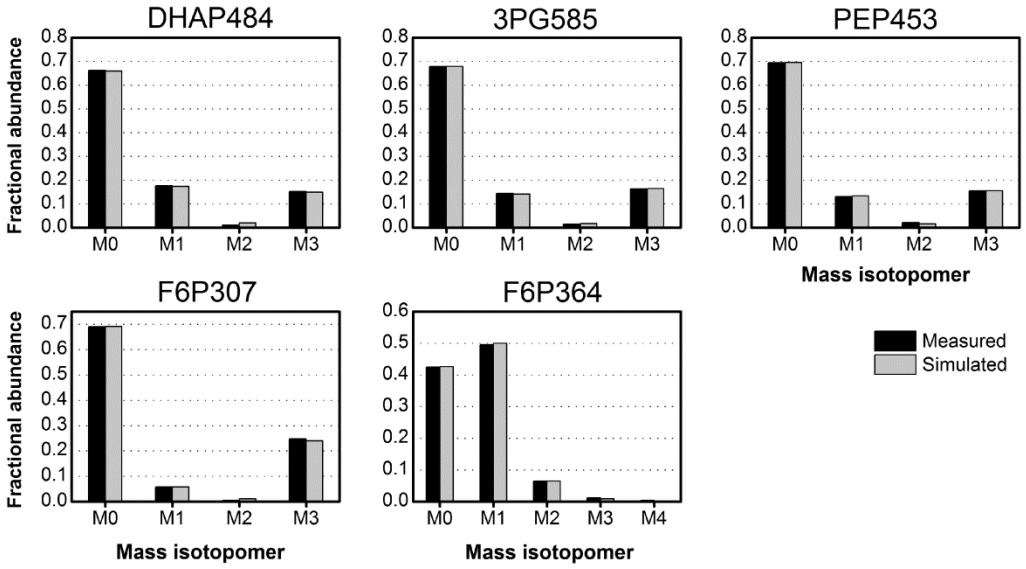

Figure C.14 Measured and fitted mass isotopomer distributions for the experiment with [3-^{13}C]glucose+[4,5,6-^{13}C]glucose and extended PPP model with F6P data (shown MIDs were corrected for natural isotope abundances).

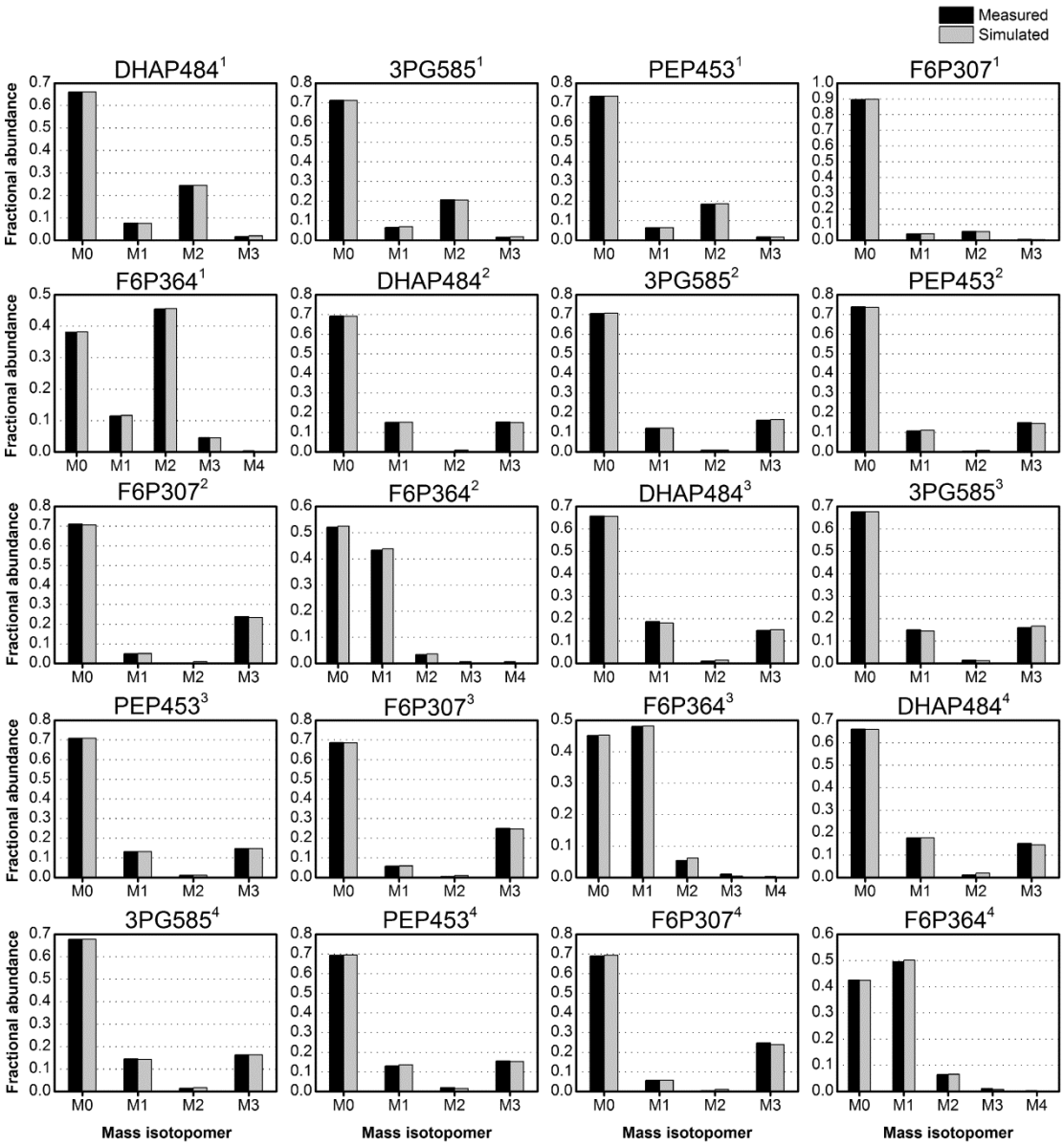

Figure C.15 Measured and fitted mass isotopomer distributions for the experiment with combined data and extended PPP model with F6P data (shown MIDs were corrected for natural isotope abundances). (superscript 1, [1,2-^{13}C]glucose data; superscript 2, [1-^{13}C]glucose+[4,5,6-^{13}C]glucose data; superscript 3, [2-^{13}C]glucose+[4,5,6-^{13}C]glucose data; superscript 3, [3-^{13}C]glucose+[4,5,6-^{13}C]glucose data)

Table C.17 Mass isotopomer distributions of media glucose measured by GC-MS. (data not corrected for natural isotope abundances)

Isotopomer	[1,2-^{13}C]Gluc		[1-^{13}C]Gluc + [4,5,6-^{13}C]Gluc		[2-^{13}C]Gluc + [4,5,6-^{13}C]Gluc		[3-^{13}C]Gluc + [4,5,6-^{13}C]Gluc	
	Flask #1	Flask #2	Flask #1	Flask #2	Flask #1	Flask #2	Flask #1	Flask #2
Gluc301 (M0)	0.2168	0.2140	0.2207	0.2182	0.2152	0.2185	0.1996	0.2064
Gluc302 (M1)	0.0353	0.0350	0.3447	0.3445	0.3524	0.3543	0.3656	0.3629
Gluc303 (M2)	0.6432	0.6457	0.0521	0.0524	0.0579	0.0533	0.0560	0.0549
Gluc304 (M3)	0.0880	0.0884	0.3329	0.3351	0.3270	0.3258	0.3298	0.3269
Gluc305 (M4)	0.0150	0.0152	0.0415	0.0418	0.0398	0.0404	0.0412	0.0410
Gluc306 (M5)	0.0015	0.0015	0.0072	0.0072	0.0067	0.0069	0.0070	0.0071
Gluc307 (M6)	0.0002	0.0002	0.0007	0.0007	0.0008	0.0007	0.0007	0.0007
Gluc308 (M7)	0.0000	0.0000	0.0001	0.0001	0.0002	0.0001	0.0001	0.0001
Gluc309 (M8)	0.0000	0.0000	0.0000	0.0000	0.0001	0.0000	0.0000	0.0000

Table C.18 Mass isotopomer distributions of intracellular metabolites measured by GC-MS. (data not corrected for natural isotope abundances)

Isotopomer	[1,2-^{13}C]Gluc		[1-^{13}C]Gluc + [4,5,6-^{13}C]Gluc		[2-^{13}C]Gluc + [4,5,6-^{13}C]Gluc		[3-^{13}C]Gluc + [4,5,6-^{13}C]Gluc	
	Flask #1	Flask #2	Flask #1	Flask #2	Flask #1	Flask #2	Flask #1	Flask #2
DHAP484(M0)	0.4310	0.4514	0.4523	0.4553	0.4297	0.4390	0.4325	0.4335
DHAP485(M1)	0.1922	0.1923	0.2481	0.2443	0.2628	0.2574	0.2575	0.2530
DHAP486(M2)	0.2460	0.2335	0.1079	0.1061	0.1162	0.1130	0.1155	0.1119
DHAP487(M3)	0.0877	0.0818	0.1333	0.1347	0.1334	0.1327	0.1356	0.1401
DHAP488(M4)	0.0343	0.0330	0.0412	0.0421	0.0405	0.0410	0.0411	0.0428
DHAP489(M5)	0.0088	0.0081	0.0173	0.0175	0.0174	0.0169	0.0178	0.0187
3PG585 (M0)	0.4050	0.4210	0.4040	0.4090	0.3874	0.3923	0.3888	0.3906
3PG586 (M1)	0.2130	0.2168	0.2448	0.2407	0.2535	0.2501	0.2513	0.2445
3PG587 (M2)	0.2292	0.2187	0.1312	0.1286	0.1367	0.1343	0.1357	0.1349
3PG588 (M3)	0.0964	0.0901	0.1396	0.1414	0.1421	0.1428	0.1430	0.1466
3PG589 (M4)	0.0428	0.0400	0.0546	0.0545	0.0549	0.0548	0.0557	0.0569
3PG590 (M5)	0.0136	0.0133	0.0259	0.0258	0.0255	0.0258	0.0256	0.0264
PEP453 (M0)	0.4847	0.5008	0.4901	0.4840	0.4704	0.4697	0.4613	0.4658
PEP454 (M1)	0.1952	0.1977	0.2248	0.2166	0.2356	0.2294	0.2307	0.2240
PEP455 (M2)	0.2125	0.2019	0.1023	0.1032	0.1092	0.1084	0.1131	0.1083
PEP456 (M3)	0.0728	0.0678	0.1284	0.1375	0.1302	0.1352	0.1367	0.1416
PEP457 (M4)	0.0279	0.0253	0.0376	0.0403	0.0379	0.0397	0.0402	0.0415
PEP458 (M5)	0.0069	0.0064	0.0168	0.0183	0.0168	0.0178	0.0180	0.0188
GLP571 (M0)	0.5070	0.5086	0.5028	0.5049	0.4986	0.4981	0.4992	0.4983
GLP572 (M1)	0.2413	0.2419	0.2502	0.2488	0.2528	0.2524	0.2515	0.2514
GLP573 (M2)	0.1650	0.1639	0.1309	0.1307	0.1330	0.1332	0.1334	0.1332
GLP574 (M3)	0.0592	0.0586	0.0778	0.0775	0.0776	0.0781	0.0778	0.0785
GLP575 (M4)	0.0217	0.0213	0.0273	0.0272	0.0272	0.0274	0.0273	0.0277
GLP576 (M5)	0.0059	0.0057	0.0109	0.0109	0.0108	0.0108	0.0108	0.0109
F6P307 (M0)	0.6288	-	0.5019	-	0.4862	-	0.4884	-
F6P308 (M1)	0.1912	-	0.1639	-	0.1661	-	0.1657	-
F6P309 (M2)	0.1327	-	0.0781	-	0.0795	-	0.0799	-
F6P310 (M3)	0.0336	-	0.1864	-	0.1948	-	0.1931	-
F6P311 (M4)	0.0113	-	0.0466	-	0.0492	-	0.0488	-
F6P369 (M5)	0.0262	-	0.0233	-	0.0187	-	0.0175	-
F6P370 (M6)	0.0081	-	0.0102	-	0.0064	-	0.0060	-
F6P371 (M7)	0.2589	-	0.3499	-	0.3060	-	0.2884	-

Table C.19 Mass isotopomer distributions of intracellular and extracellular metabolites measured by GC-MS to test natural abundance. The metabolites were derived from the culture with natural glucose as control to test measurement errors of GC-MS. (data not corrected for natural isotope abundances)

	Injection						
Isotopomer	1	2	3	Avg.	Std.	Theo.*	Abs. % Err.**
Gluc301 (M0)	0.8409	0.8409	0.8409	0.8409	0.0000	0.8418	0.09
Gluc302 (M1)	0.1338	0.1338	0.1339	0.1338	0.0000	0.1339	0.01
Gluc303 (M2)	0.0224	0.0225	0.0223	0.0224	0.0001	0.0218	0.06
Gluc304 (M3)	0.0025	0.0026	0.0026	0.0025	0.0000	0.0023	0.02
Gluc305 (M4)	0.0003	0.0003	0.0003	0.0003	0.0000	0.0002	0.01
Gluc306 (M5)	0.0000	0.0000	0.0000	0.0000	0.0000	0.0000	0.00
Gluc307 (M6)	0.0000	0.0000	0.0000	0.0000	0.0000	0.0000	0.00
DHAP484 (M0)	0.6364	0.6363	0.6369	0.6366	0.0003	0.6341	0.24
DHAP485 (M1)	0.2290	0.2282	0.2287	0.2286	0.0004	0.2295	0.09
DHAP486 (M2)	0.1089	0.1086	0.1087	0.1088	0.0002	0.1098	0.10
DHAP487 (M3)	0.0256	0.0269	0.0256	0.0261	0.0007	0.0266	0.05
3PG585 (M0)	0.5606	0.5601	0.5606	0.5604	0.0003	0.5580	0.24
3PG586 (M1)	0.2577	0.2565	0.2567	0.2570	0.0006	0.2600	0.30
3PG587 (M2)	0.1395	0.1401	0.1402	0.1399	0.0003	0.1396	0.03
3PG588 (M3)	0.0422	0.0434	0.0425	0.0427	0.0006	0.0425	0.02
PEP453 (M0)	0.6447	0.6464	0.6451	0.6454	0.0009	0.6437	0.17
PEP454 (M1)	0.2192	0.2180	0.2188	0.2187	0.0006	0.2231	0.44
PEP455 (M2)	0.1103	0.1096	0.1106	0.1102	0.0005	0.1080	0.22
PEP456 (M3)	0.0258	0.0260	0.0255	0.0257	0.0003	0.0253	0.05
GLP571 (M0)	0.5656	0.5647	0.5650	0.5651	0.0005	0.5590	0.62
GLP572 (M1)	0.2571	0.2581	0.2575	0.2575	0.0005	0.2604	0.28
GLP573 (M2)	0.1365	0.1364	0.1368	0.1366	0.0002	0.1386	0.20
GLP574 (M3)	0.0408	0.0408	0.0407	0.0407	0.0000	0.0420	0.13
F6P307 (M0)	0.6873	0.6882	0.6878	0.6878	0.0005	0.6839	0.39
F6P308 (M1)	0.1958	0.1950	0.1955	0.1954	0.0004	0.1981	0.26
F6P309 (M2)	0.0978	0.0976	0.0975	0.0976	0.0001	0.0984	0.08
F6P310 (M3)	0.0191	0.0192	0.0192	0.0192	0.0000	0.0196	0.04
F6P364 (M0)	0.6625	0.6654	0.6654	0.6644	0.0017	0.6619	0.25
F6P365 (M1)	0.2071	0.2042	0.2050	0.2054	0.0015	0.2091	0.37
F6P366 (M2)	0.1017	0.1006	0.1000	0.1007	0.0009	0.1018	0.11
F6P367 (M3)	0.0226	0.0226	0.0230	0.0227	0.0002	0.0219	0.08
F6P368 (M4)	0.0062	0.0073	0.0067	0.0067	0.0005	0.0053	0.14

Gluc301 was from media metabolite and the others were all from intracellular metabolites.

* Theoretical mass isotopomer distribution calculated by natural abundance of isotopes in nature.

** Absolute % error between theoretical values and measured values by GC-MS.

Table C.20 Mass isotopomer distributions of pure fructose, glucose and ribose fragments measured by MOX-TMS derivatization and GC-MS. (data not corrected for natural isotope abundances)

	Injection						
Isotopomer	1	2	3	Avg.	Std.	Theo.	Abs. % Err.
Fructose							
Fruc103 (M0)	0.9133	0.9133	0.9133	0.9133	0.0000	0.9119	0.14%
Fruc104 (M1)	0.0867	0.0867	0.0867	0.0867	0.0000	0.0881	0.14%
Fruc217 (M0)	0.7640	0.7641	0.7635	0.7639	0.0003	0.7664	0.25%
Fruc218 (M1)	0.1563	0.1563	0.1564	0.1564	0.0001	0.1564	0.00%
Fruc219 (M2)	0.0695	0.0694	0.0697	0.0695	0.0002	0.0680	0.15%
Fruc220 (M3)	0.0102	0.0102	0.0103	0.0103	0.0001	0.0092	0.11%
Fruc307 (M0)	0.6870	0.6874	0.6866	0.6870	0.0004	0.6839	0.31%
Fruc308 (M1)	0.1959	0.1955	0.1958	0.1957	0.0002	0.1981	0.23%
Fruc309 (M2)	0.0978	0.0979	0.0983	0.0980	0.0002	0.0984	0.04%
Fruc310 (M3)	0.0193	0.0192	0.0193	0.0193	0.0000	0.0196	0.03%
Fruc364 (M0)	0.6623	0.6626	0.6623	0.6624	0.0002	0.6619	0.05%
Fruc365 (M1)	0.2092	0.2091	0.2095	0.2092	0.0002	0.2091	0.01%
Fruc366 (M2)	0.1009	0.1008	0.1007	0.1008	0.0001	0.1018	0.10%
Fruc367 (M3)	0.0222	0.0221	0.0222	0.0222	0.0000	0.0219	0.02%
Fruc368 (M4)	0.0054	0.0054	0.0054	0.0054	0.0000	0.0053	0.01%
Fruc569 (M0)	0.5179	0.5168	0.5184	0.5177	0.0008	0.5115	0.63%
Fruc570 (M1)	0.2592	0.2597	0.2593	0.2594	0.0002	0.2604	0.10%
Fruc571 (M2)	0.1516	0.1520	0.1511	0.1516	0.0004	0.1542	0.27%
Fruc572 (M3)	0.0502	0.0503	0.0501	0.0502	0.0001	0.0518	0.16%
Fruc573 (M4)	0.0163	0.0164	0.0163	0.0163	0.0001	0.0170	0.07%
Fruc574 (M5)	0.0039	0.0040	0.0039	0.0039	0.0000	0.0042	0.03%
Fruc575 (M6)	0.0009	0.0009	0.0009	0.0009	0.0000	0.0009	0.00%
Glucose							
Gluc103 (M0)	0.9113	0.9116	0.9119	0.9116	0.0003	0.9119	0.02%
Gluc104 (M1)	0.0887	0.0884	0.0881	0.0884	0.0003	0.0881	0.02%
Gluc319 (M0)	0.6771	0.6765	0.6763	0.6766	0.0004	0.6733	0.33%
Gluc320 (M1)	0.2009	0.2019	0.2019	0.2016	0.0006	0.2024	0.08%
Gluc321 (M2)	0.0975	0.0971	0.0972	0.0973	0.0002	0.0991	0.18%
Gluc322 (M3)	0.0198	0.0198	0.0199	0.0198	0.0000	0.0203	0.05%
Gluc323 (M4)	0.0047	0.0047	0.0047	0.0047	0.0000	0.0049	0.02%
Gluc554 (M0)	0.5210	0.5199	0.5226	0.5212	0.0014	0.5174	0.38%
Gluc555 (M1)	0.2573	0.2573	0.2571	0.2573	0.0001	0.2575	0.02%

Table C.20 continued

Gluc556 (M2)	0.1514	0.1518	0.1502	0.1511	0.0009	0.1530	0.19%
Gluc557 (M3)	0.0496	0.0499	0.0493	0.0496	0.0003	0.0506	0.10%
Gluc558 (M4)	0.0161	0.0163	0.0161	0.0162	0.0001	0.0166	0.04%
Gluc559 (M5)	0.0038	0.0038	0.0038	0.0038	0.0000	0.0040	0.02%
Gluc560 (M6)	0.0008	0.0009	0.0008	0.0009	0.0000	0.0009	0.00%
Ribose							
Rib103 (M0)	0.9131	0.9132	0.9133	0.9132	0.0001	0.9119	0.13%
Rib104 (M1)	0.0869	0.0868	0.0867	0.0868	0.0001	0.0881	0.13%
Rib217 (M0)	0.7632	0.7635	0.7635	0.7634	0.0002	0.7664	0.30%
Rib218 (M1)	0.1565	0.1563	0.1563	0.1564	0.0001	0.1564	0.00%
Rib219 (M2)	0.0703	0.0702	0.0702	0.0702	0.0000	0.0680	0.22%
Rib220 (M3)	0.0100	0.0100	0.0100	0.0100	0.0000	0.0092	0.08%
Rib307 (M0)	0.6881	0.6883	0.6883	0.6882	0.0001	0.6839	0.43%
Rib308 (M1)	0.1963	0.1961	0.1961	0.1962	0.0001	0.1981	0.19%
Rib309 (M2)	0.0965	0.0966	0.0966	0.0966	0.0000	0.0984	0.19%
Rib310 (M3)	0.0191	0.0190	0.0190	0.0190	0.0001	0.0196	0.06%
Rib467 (M0)	0.5861	0.5877	0.5859	0.5866	0.0010	0.5818	0.48%
Rib468 (M1)	0.2386	0.2387	0.2392	0.2388	0.0003	0.2400	0.12%
Rib469 (M2)	0.1281	0.1268	0.1277	0.1275	0.0007	0.1298	0.22%
Rib470 (M3)	0.0351	0.0349	0.0352	0.0350	0.0002	0.0360	0.10%
Rib471 (M4)	0.0100	0.0099	0.0100	0.0100	0.0001	0.0103	0.03%
Rib472 (M5)	0.0020	0.0020	0.0020	0.0020	0.0000	0.0021	0.01%

Table C.21 Mass isotopomer distributions of pure fructose, glucose and ribose fragments measured by isopropylidene propionate derivatization and GC-MS. (data not corrected for natural isotope abundances)

	Injection						
Isotopomer	1	2	3	Avg.	Std.	Theo.	Abs. % Err.
Fructose							
Fruc301 (M0)	0.8426	0.8425	0.8426	0.8426	0.0001	0.8418	0.08%
Fruc302 (M1)	0.1328	0.1328	0.1328	0.1328	0.0000	0.1339	0.11%
Fruc303 (M2)	0.0219	0.0220	0.0219	0.0219	0.0000	0.0218	0.01%
Fruc304 (M3)	0.0024	0.0024	0.0024	0.0024	0.0000	0.0023	0.01%
Fruc305 (M4)	0.0003	0.0002	0.0002	0.0002	0.0000	0.0002	0.00%
Fruc306 (M5)	0.0000	0.0000	0.0000	0.0000	0.0000	0.0000	0.00%
Fruc307 (M6)	0.0000	0.0000	0.0000	0.0000	0.0000	0.0000	0.00%
Glucose							
Gluc301 (M0)	0.8433	0.8434	0.8434	0.8433	0.0001	0.8418	0.15%
Gluc302 (M1)	0.1325	0.1324	0.1324	0.1324	0.0001	0.1339	0.15%
Gluc303 (M2)	0.0218	0.0218	0.0217	0.0217	0.0000	0.0218	0.01%
Gluc304 (M3)	0.0023	0.0023	0.0023	0.0023	0.0000	0.0023	0.00%
Gluc305 (M4)	0.0002	0.0002	0.0002	0.0002	0.0000	0.0002	0.00%
Gluc306 (M5)	0.0000	0.0000	0.0000	0.0000	0.0000	0.0000	0.00%
Gluc307 (M6)	0.0000	0.0000	0.0000	0.0000	0.0000	0.0000	0.00%
Ribose							
Rib287 (M0)	0.8529	0.8527	0.8523	0.8526	0.0003	0.8513	0.13%
Rib288 (M1)	0.1240	0.1242	0.1247	0.1243	0.0004	0.1258	0.15%
Rib289 (M2)	0.0205	0.0208	0.0207	0.0206	0.0001	0.0206	0.00%
Rib290 (M3)	0.0022	0.0021	0.0021	0.0021	0.0001	0.0021	0.00%
Rib291 (M4)	0.0003	0.0002	0.0002	0.0003	0.0000	0.0002	0.01%
Rib292 (M5)	0.0002	0.0000	0.0000	0.0001	0.0001	0.0000	0.01%

Table C.22 Mass isotopomer distributions of pure glucose and ribose fragments measured by oxime (or aldonitrile) propionate derivatization and GC-MS. (data not corrected for natural isotope abundances)

	Injection						
Isotopomer	1	2	3	Avg.	Std.	Theo.	Abs. % Err.
Glucose							
Gluc173 (M0)	0.9080	0.9081	0.9084	0.9082	0.0002	0.9068	0.14%
Gluc174 (M1)	0.0811	0.0809	0.0808	0.0810	0.0002	0.0826	0.16%
Gluc175 (M2)	0.0109	0.0109	0.0108	0.0109	0.0001	0.0106	0.03%
Gluc259 (M0)	0.8646	0.8635	0.8638	0.8639	0.0006	0.8628	0.12%
Gluc260 (M1)	0.1157	0.1164	0.1164	0.1162	0.0004	0.1177	0.15%
Gluc261 (M2)	0.0178	0.0182	0.0180	0.0180	0.0002	0.0178	0.02%
Gluc262 (M3)	0.0018	0.0019	0.0018	0.0018	0.0001	0.0017	0.01%
Gluc284 (M0)	0.8509	0.8606	0.8540	0.8552	0.0050	0.8504	0.48%
Gluc285 (M1)	0.1262	0.1179	0.1237	0.1226	0.0042	0.1283	0.57%
Gluc286 (M2)	0.0194	0.0181	0.0189	0.0188	0.0007	0.0192	0.04%
Gluc287 (M3)	0.0022	0.0021	0.0022	0.0022	0.0001	0.0019	0.03%
Gluc288 (M4)	0.0013	0.0012	0.0012	0.0012	0.0000	0.0002	0.10%
Gluc370 (M0)	0.8100	0.8101	0.8106	0.8102	0.0003	0.8095	0.07%
Gluc371 (M1)	0.1570	0.1566	0.1564	0.1566	0.0003	0.1589	0.23%
Gluc372 (M2)	0.0289	0.0290	0.0288	0.0289	0.0001	0.0278	0.11%
Gluc373 (M3)	0.0037	0.0038	0.0036	0.0037	0.0001	0.0034	0.03%
Gluc374 (M4)	0.0004	0.0005	0.0004	0.0004	0.0000	0.0004	0.00%
Gluc375 (M5)	0.0001	0.0001	0.0001	0.0001	0.0000	0.0000	0.01%
Ribose							
Rib173 (M0)	0.9079	0.9084	0.9085	0.9083	0.0003	0.9068	0.14%
Rib174 (M1)	0.0813	0.0809	0.0808	0.0810	0.0003	0.0826	0.16%
Rib175 (M2)	0.0108	0.0108	0.0107	0.0108	0.0001	0.0106	0.01%
Rib284 (M0)	0.8491	0.8557	0.8501	0.8516	0.0036	0.8504	0.13%
Rib285 (M1)	0.1240	0.1184	0.1232	0.1219	0.0030	0.1283	0.65%
Rib286 (M2)	0.0236	0.0227	0.0234	0.0233	0.0005	0.0192	0.41%
Rib287 (M3)	0.0027	0.0026	0.0027	0.0027	0.0001	0.0019	0.08%
Rib288 (M4)	0.0006	0.0006	0.0006	0.0006	0.0000	0.0002	0.04%
Rib259 (M0)	0.8582	0.8580	0.8574	0.8578	0.0004	0.8628	0.49%
Rib260 (M1)	0.1216	0.1217	0.1222	0.1218	0.0003	0.1177	0.41%
Rib261 (M2)	0.0185	0.0185	0.0186	0.0185	0.0001	0.0178	0.07%
Rib262 (M3)	0.0018	0.0019	0.0019	0.0018	0.0000	0.0017	0.01%

Table C.23 Mass isotopomer distributions of pure fructose, glucose and ribose fragments measured by methyloxime (MOX) propionate derivatization and GC-MS. (data not corrected for natural isotope abundances)

	Injection						
Isotopomer	1	2	3	Avg.	Std.	Theo.	Abs. % Err.
Fructose							
Fruc387 (M0)	0.8009	0.8004	0.8010	0.8008	0.0003	0.8075	0.67%
Fruc388 (M1)	0.1633	0.1637	0.1629	0.1633	0.0004	0.1590	0.43%
Fruc389 (M2)	0.0308	0.0308	0.0310	0.0309	0.0001	0.0294	0.15%
Fruc390 (M3)	0.0044	0.0044	0.0044	0.0044	0.0000	0.0037	0.07%
Fruc391 (M4)	0.0005	0.0006	0.0005	0.0005	0.0000	0.0004	0.01%
Fruc392 (M5)	0.0001	0.0001	0.0001	0.0001	0.0000	0.0000	0.01%
Glucose							
Gluc145 (M0)	0.9238	0.9239	0.9240	0.9239	0.0001	0.9257	0.18%
Gluc146 (M1)	0.0671	0.0671	0.0669	0.0670	0.0001	0.0667	0.03%
Gluc147 (M2)	0.0091	0.0091	0.0091	0.0091	0.0000	0.0076	0.15%
Gluc387 (M0)	0.8024	0.8022	0.8016	0.8021	0.0004	0.8075	0.54%
Gluc388 (M1)	0.1625	0.1625	0.1631	0.1627	0.0004	0.1590	0.37%
Gluc389 (M2)	0.0305	0.0306	0.0306	0.0306	0.0001	0.0294	0.12%
Gluc390 (M3)	0.0041	0.0041	0.0041	0.0041	0.0000	0.0037	0.04%
Gluc391 (M4)	0.0005	0.0005	0.0005	0.0005	0.0000	0.0004	0.01%
Gluc392 (M5)	0.0001	0.0001	0.0001	0.0001	0.0000	0.0000	0.01%
Ribose							
Rib145 (M0)	0.9219	0.9224	0.9222	0.9222	0.0002	0.9257	0.35%
Rib146 (M1)	0.0679	0.0677	0.0676	0.0677	0.0002	0.0667	0.10%
Rib147 (M2)	0.0101	0.0100	0.0102	0.0101	0.0001	0.0076	0.25%
Rib301 (M0)	0.8431	0.8436	0.8428	0.8432	0.0004	0.8481	0.50%
Rib302 (M1)	0.1323	0.1318	0.1326	0.1322	0.0004	0.1285	0.37%
Rib303 (M2)	0.0219	0.0219	0.0219	0.0219	0.0000	0.0210	0.09%
Rib304 (M3)	0.0024	0.0025	0.0025	0.0025	0.0000	0.0022	0.03%
Rib305 (M4)	0.0003	0.0003	0.0003	0.0003	0.0000	0.0002	0.01%

Appendix D

SUPPLEMENTARY DATA OF CHAPTER 6

Table D.1 Results of combined ^{13}C-MFA by parallel labeling experiments of [U-^{13}C]glycerol and [U-^{13}C]glutamine at the control condition. Shown are the estimated net and exchange fluxes (nmol/10^6cell/h) and G-values with 95% confidence intervals.

Control condition							
Reaction			Flux	95% Conf. interval			
Gluc → Gluc.ext	v1		23.7	[	20.5	,	26.8]
G6P → Gluc	v2		23.7	[	20.5	,	26.8]
G6P ↔ F6P	v3	net	-29.8	[	-36.2	,	-16.6]
		exch	>1e3	[	>1e3	,	>1e3]
FBP ↔ F6P	v4	net	21.3	[	16.5	,	24.2]
		exch	(0, >1e4)	[	0	,	>1e4]
FBP ↔ DHAP + GAP	v5	net	-21.3	[	-24.2	,	-16.5]
		exch	0.0	[	0.0	,	1.4]
DHAP ↔ GAP	v6	net	-4.6	[	-10.4	,	0.9]
		exch	452.7	[	316.2	,	641.1]
GAP ↔ 3PG	v7	net	-21.6	[	-27.1	,	-15.7]
		exch	>1e3	[	>1e3	,	>1e3]
3PG ↔ PEP	v8	net	-21.6	[	-27.1	,	-15.7]
		exch	819.7	[	685.2	,	>1e3]
OAC.c → PEP + CO2	v9		31.7	[	27.6	,	37.5]
PEP → Pyr.c	v10		10.1	[	3.7	,	19.2]
G6P → Ru5P + CO2	v11		12.7	[	0.0	,	18.8]
Ru5P ↔ X5P	v12	net	8.5	[	0.0	,	12.5]
		exch	(12.0, >1e4)	[	0.0	,	>1e4]

Table D.1 continued

Ru5P ↔ R5P	v13	net	4.2	[	0.0	,	6.3	]
		exch	0.0	[	0.0	,	11.5	]
X5P ↔ EC2 + GAP	v14	net	8.5	[	0.0	,	12.5	]
		exch	(11.6, >1e4)	[	0.0	,	>1e4	]
F6P ↔ EC2 + E4P	v15	net	-4.2	[	-6.3	,	-0.0	]
		exch	98.5	[	74.6	,	123.1	]
S7P ↔ EC2 + R5P	v16	net	-4.2	[	-6.3	,	-0.0	]
		exch	477.7	[	20.2	,	>1e3	]
F6P ↔ EC3 + GAP	v17	net	-4.2	[	-6.3	,	-0.0	]
		exch	14.1	[	7.8	,	25.0	]
S7P ↔ EC3 + E4P	v18	net	4.3	[	0.0	,	6.3	]
		exch	(513.2, >1e4)	[	0.0	,	>1e4	]
GLP ↔ DHAP	v19	net	16.7	[	9.5	,	22.3	]
		exch	19.7	[	10.5	,	141.2	]
Glyc → GLP	v20		34.4	[	27.4	,	40.5	]
GLP → GLP.src	v21		17.7	[	6.8	,	27.2	]
G6P ↔ G1P	v22	net	-6.7	[	-8.0	,	-5.1	]
		exch	(0.0, 154.7)	[	0.0	,	>1e3	]
Glycogen.src → G1P	v23		6.7	[	5.1	,	8.0	]
Pyr.c ↔ Pyr.m	v24	net	161.5	[	133.8	,	212.9	]
		exch	368.1	[	68.3	,	>1e3	]
Pyr.c ↔ Lact	v25	net	-213.8	[	-242.3	,	-187.5	]
		exch	123.5	[	77.1	,	198.8	]
Pyr.m → AcCoA.m + CO2	v26		167.6	[	137.4	,	202.0	]
AcCoA.m + OAC.m → Cit.m	v27		107.0	[	91.6	,	122.7	]
Cit.m ↔ ICit.m	v28	net	54.4	[	45.2	,	62.1	]
		exch	146.6	[	101.6	,	202.6	]
ICit.m ↔ AKG.m + CO2	v29	net	54.4	[	45.2	,	62.1	]
		exch	146.3	[	102.0	,	204.1	]
AKG.m → Suc.m + CO2	v30		80.4	[	68.8	,	89.8	]
Suc.m → Fum.m	v31		83.9	[	72.2	,	93.4	]

Table D.1 continued

Fum.m ↔ Mal.m	v32	net	85.6	[	73.8	,	95.3]
		exch	477.3	[	380.6	,	616.3]
Mal.m ↔ OAC.m	v33	net	34.9	[	17.6	,	52.5]
		exch	654.5	[	260.4	,	>1e3]
Mal.m → Pyr.m + CO2	v34		78.2	[	33.8	,	96.6]
Mal.c → Pyr.c + CO2	v35		0.6	[	0.0	,	30.4]
Pyr.m + CO2 → OAC.m	v36		72.1	[	54.2	,	87.9]
Mal.c ↔ Mal.m	v37	net	27.5	[	-0.8	,	44.4]
		exch	689.1	[	627.3	,	756.3]
Mal.c ↔ OAC.c	v38	net	-28.1	[	-44.4	,	-12.0]
		exch	854.5	[	787.5	,	935.1]
Cit.m ↔ Cit.c	v39	net	52.7	[	37.7	,	68.9]
		exch	(0.0, >1e4)	[	0.0	,	>1e4]
Cit.c → AcCoA.c + OAC.c	v40		52.7	[	37.7	,	68.9]
AcCoA.c → FA.c	v41		53.4	[	38.4	,	69.7]
FA.c+FA.src→FA.snk +FA.m	v42		53.4	[	38.4	,	69.7]
FA.m → AcCoA.m	v43		53.4	[	38.4	,	69.7]
Pyr.c ↔ Ala	v44	net	56.8	[	46.4	,	67.4]
		exch	31.1	[	0.0	,	14.0]
Gln → Glu	v45		24.2	[	21.5	,	26.3]
Glu ↔ AKG.m	v46	net	26.1	[	22.4	,	29.0]
		exch	(902.0, >1e3)	[	543.5	,	>1e4]
Glu ↔ Pro	v47	net	3.9	[	3.4	,	4.4]
		exch	(0.0, >1e4)	[	0.0	,	>1e4]
OAC.c ↔ Asp	v48	net	-7.1	[	-9.1	,	-5.0]
		exch	28.5	[	20.3	,	39.4]
Asp → Asn	v49		1.1	[	0.8	,	1.3]
Ser ↔ Pyr.c	v50	net	-6.1	[	-9.1	,	-3.2]
		exch	215.0	[	0.0	,	530.0]
Ser ↔ Gly + C1	v51	net	12.0	[	9.5	,	14.5]
		exch	41.7	[	0.0	,	275.3]

Table D.1 continued

Thr → AcCoA.c + Gly	v52	0.7	[	0.0	,	1.5]
Met+CO2 →Suc.m+CO2 +C1	v53	1.5	[	1.1	,	1.9]
Val+CO2→Suc.m+CO2+CO2	v54	1.4	[	0.7	,	2.2]
Ile + CO2 → Suc.m + AcCoA.m + CO2	v55	0.5	[	0.3	,	0.8]
Phe → Fum.m + AcCoA.m + AcCoA.m + CO2	v56	1.6	[	0.9	,	2.3]
Tyr → Fum.m + AcCoA.m + AcCoA.m + CO2	v57	0.1	[	0.0	,	0.4]
Leu+CO2→AcCoAm +AcCoA.m+AcCoA.m+CO2	v58	0.8	[	0.0	,	2.0]
Gln.ext → Gln	v59	25.5	[	22.8	,	27.6]
Asp.ext → Asp	v60	9.9	[	7.9	,	11.8]
Ile.ext → Ile	v61	1.4	[	1.2	,	1.6]
Leu.ext → Leu	v62	4.1	[	3.3	,	4.9]
Met.ext → Met	v63	1.9	[	1.5	,	2.3]
Phe.ext → Phe	v64	3.2	[	2.6	,	3.8]
Ser.ext → Ser	v65	7.3	[	5.9	,	8.7]
Tyr.ext → Tyr	v66	1.2	[	1.0	,	1.4]
Val.ext → Val	v67	3.3	[	2.7	,	3.9]
Thr.ext → Thr	v68	2.5	[	1.9	,	3.1]
Arg.ext → Arg	v69	1.4	[	1.1	,	1.7]
Cys.ext → Cys	v70	1.9	[	1.4	,	2.2]
His.ext → His	v71	0.8	[	0.6	,	1.0]
Lys.ext → Lys	v72	2.9	[	2.2	,	3.4]
Trp.ext → Trp	v73	0.1	[	0.1	,	0.1]
Lact.ext → Lact	v74	213.8	[	187.5	,	242.3]
Glu.ext → Glu	v75	8.8	[	7.1	,	10.5]
Glyc.ext → Glyc	v76	34.4	[	27.4	,	40.5]
FA.ext → FA.c	v77	0.0	[	0.0	,	0.0]
Pro → Pro.ext	v78	2.3	[	1.9	,	2.7]
Ala → Ala.ext	v79	53.5	[	43.1	,	64.1]
Gly → Gly.ext	v80	11.7	[	9.4	,	14.0]

Table D.1 continued

AcCoA.m → KB.ext	v81	120.4	[	93.8	,	152.8]
Albumin production	v82	32.6	[	24.6	,	38.5]

Metabolite	G-value	95% Conf. interval			
GLP	0.35	[	0.32	,	0.48]
Lact	1.00	[	0.63	,	1.00]
Ala	0.51	[	0.31	,	0.77]
Pro	0.41	[	0.39	,	0.44]
GLP	1.00	[	0.44	,	1.00]

G-value, fractional labeling of metabolites

Table D.2 Results of combined ^{13}C-MFA by parallel labeling experiments of [U-^{13}C]glycerol and [U-^{13}C]glutamine at the dexamethasone condition. Shown are the estimated net and exchange fluxes (nmol/10^{6}cell/h) and G-values with 95% confidence intervals.

Dexamethasone condition							
Reaction			Flux	95% Conf. interval			
Gluc → Gluc.ext	v1		30.3	[	26.5	,	34.4]
G6P → Gluc	v2		30.3	[	26.5	,	34.4]
G6P ↔ F6P	v3	net	-30.1	[	-45.3	,	-22.1]
		exch	919.5	[	784.2	,	>1e3]
FBP ↔ F6P	v4	net	23.3	[	22.1	,	32.3]
		exch	(9.9, >1e4)	[	1.5	,	>1e4]
FBP ↔ DHAP + GAP	v5	net	-26.3	[	-32.3	,	-22.1]
		exch	5.1	[	1.1	,	10.8]
DHAP ↔ GAP	v6	net	7.0	[	2.1	,	11.7]
		exch	>1e3	[	>1e3	,	>1e3]
GAP ↔ 3PG	v7	net	-17.4	[	-23.0	,	-10.8]
		exch	>1e3	[	>1e3	,	>1e3]
3PG ↔ PEP	v8	net	-17.4	[	-23.0	,	-10.8]
		exch	>1e3	[	>1e3	,	>1e3]
OAC.c → PEP + CO2	v9		81.4	[	73.2	,	91.2]
PEP → Pyr.c	v10		64.0	[	53.6	,	76.7]
G6P → Ru5P + CO2	v11		5.6	[	0.0	,	20.6]
Ru5P ↔ X5P	v12	net	3.8	[	0.0	,	13.7]
		exch	(11.9, >1e4)	[	0.0	,	>1e4]
Ru5P ↔ R5P	v13	net	1.9	[	0.0	,	6.9]
		exch	6.8	[	0.0	,	17.7]
X5P ↔ EC2 + GAP	v14	net	3.8	[	0.0	,	13.7]
		exch	(10.4, >1e4)	[	0.0	,	>1e4]
F6P ↔ EC2 + E4P	v15	net	-1.9	[	-6.9	,	-0.0]
		exch	122.6	[	96.0	,	158.0]
S7P ↔ EC2 + R5P	v16	net	-1.9	[	-6.9	,	-0.0]
		exch	(130.4, 176.3)	[	0.0	,	>1e4]

Table D.2 continued

F6P ↔ EC3 + GAP	v17	net	-1.9	[	-6.9	,	-0.0	]
		exch	15.3	[	1.9	,	34.3	]
S7P ↔ EC3 + E4P	v18	net	1.9	[	0.0	,	6.9	]
		exch	(20.7, >1e4)	[	0.0	,	>1e4	]
GLP ↔ DHAP	v19	net	33.3	[	29.3	,	36.8	]
		exch	23.2	[	16.2	,	55.4	]
Glyc → GLP	v20		33.4	[	30.2	,	37.4	]
GLP → GLP.src	v21		0.0	[	0.0	,	6.5	]
G6P ↔ G1P	v22	net	-5.8	[	-7.5	,	-4.7	]
		exch	(0.0, 161.7)	[	0.0	,	>1e3	]
Glycogen.src → G1P	v23		5.8	[	4.7	,	7.5	]
Pyr.c ↔ Pyr.m	v24	net	223.7	[	189.5	,	263.5	]
		exch	0.0	[	0.0	,	67.7	]
Pyr.c ↔ Lact	v25	net	-231.8	[	-263.7	,	-202.6	]
		exch	320.7	[	243.1	,	398.7	]
Pyr.m → AcCoA.m + CO2	v26		190.8	[	152.5	,	233.5	]
AcCoA.m + OAC.m → Cit.m	v27		108.0	[	96.2	,	120.9	]
Cit.m ↔ ICit.m	v28	net	48.3	[	40.9	,	56.1	]
		exch	202.6	[	148.6	,	324.8	]
ICit.m ↔ AKG.m + CO2	v29	net	48.3	[	40.9	,	56.1	]
		exch	202.7	[	148.6	,	325.1	]
AKG.m → Suc.m + CO2	v30		83.3	[	73.5	,	93.5	]
Suc.m → Fum.m	v31		87.6	[	77.8	,	97.9	]
Fum.m ↔ Mal.m	v32	net	89.5	[	79.7	,	100.0	]
		exch	589.2	[	477.9	,	708.3	]
Mal.m ↔ OAC.m	v33	net	30.6	[	14.5	,	44.7	]
		exch	677.9	[	368.6	,	>1e3	]
Mal.m → Pyr.m + CO2	v34		44.4	[	25.7	,	62.8	]
Mal.c → Pyr.c + CO2	v35		0.0	[	0.0	,	9.5	]
Pyr.m + CO2 → OAC.m	v36		77.4	[	61.4	,	95.1	]
Mal.c ↔ Mal.m	v37	net	-14.5	[	-29.4	,	-1.4	]

Table D.2 continued

		exch	>1e3	[	>1e3	,	>1e3	]
Mal.c ↔ OAC.c	v38	net	14.5	[	1.5	,	29.0	]
		exch	(>1e3, >1e4)	[	734.5	,	>1e4	]
Cit.m ↔ Cit.c	v39	net	59.8	[	48.1	,	72.1	]
		exch	(0.0, >1e4)	[	0.0	,	>1e4	]
Cit.c → AcCoA.c + OAC.c	v40		59.8	[	48.1	,	72.1	]
AcCoA.c → FA.c	v41		60.7	[	49.0	,	73.1	]
FA.c+FA.src→FA.snk+FA.m	v42		60.7	[	49.0	,	73.1	]
FA.m → AcCoA.m	v43		60.7	[	49.0	,	73.1	]
Pyr.c ↔ Ala	v44	net	61.1	[	50.3	,	72.4	]
		exch	105.2	[	16.2	,	190.1	]
Gln → Glu	v45		32.5	[	29.8	,	35.3	]
Glu ↔ AKG.m	v46	net	35.0	[	31.2	,	38.8	]
		exch	648.4	[	417.9	,	>1e3	]
Glu ↔ Pro	v47	net	3.9	[	3.3	,	4.3	]
		exch	(0.0, >1e4)	[	0.0	,	>1e4	]
OAC.c ↔ Asp	v48	net	-7.1	[	-9.2	,	-5.1	]
		exch	27.2	[	20.3	,	36.3	]
Asp → Asn	v49		1.1	[	0.8	,	1.2	]
Ser ↔ Pyr.c	v50	net	-11.0	[	-14.5	,	-7.4	]
		exch	(0.0, 69.1)	[	0.0	,	272.5	]
Ser ↔ Gly + C1	v51	net	16.5	[	13.3	,	19.7	]
		exch	(0.0, 65.1)	[	0.0	,	306.9	]
Thr → AcCoA.c + Gly	v52		1.0	[	0.3	,	1.7	]
Met+CO2→Suc.m+CO2+C1	v53		1.8	[	1.4	,	2.2	]
Val+CO2→Suc.m+CO2+CO2	v54		1.6	[	0.9	,	2.3	]
Ile + CO2 → Suc.m + AcCoA.m + CO2	v55		1.0	[	0.6	,	1.4	]
Phe → Fum.m + AcCoA.m + AcCoA.m + CO2	v56		1.9	[	1.1	,	2.8	]
Tyr → Fum.m + AcCoA.m + AcCoA.m + CO2	v57		0.0	[	0.0	,	0.3	]

Table D.2 continued

Leu + CO2 → AcCoA.m + AcCoA.m + AcCoA.m + CO2	v58	1.3	[	0.2	,	2.6]
Gln.ext → Gln	v59	33.9	[	31.1	,	36.6]
Asp.ext → Asp	v60	9.9	[	7.9	,	11.8]
Ile.ext → Ile	v61	1.8	[	1.4	,	2.2]
Leu.ext → Leu	v62	4.5	[	3.6	,	5.5]
Met.ext → Met	v63	2.2	[	1.8	,	2.6]
Phe.ext → Phe	v64	3.5	[	2.7	,	4.3]
Ser.ext → Ser	v65	6.9	[	5.5	,	8.3]
Tyr.ext → Tyr	v66	1.1	[	1.0	,	1.3]
Val.ext → Val	v67	3.4	[	2.8	,	4.0]
Thr.ext → Thr	v68	2.7	[	2.1	,	3.3]
Arg.ext → Arg	v69	1.4	[	1.1	,	1.6]
Cys.ext → Cys	v70	1.8	[	1.4	,	2.1]
His.ext → His	v71	0.8	[	0.6	,	0.9]
Lys.ext → Lys	v72	2.8	[	2.2	,	3.3]
Trp.ext → Trp	v73	0.1	[	0.1	,	0.1]
Lact.ext → Lact	v74	231.8	[	202.6	,	263.7]
Glu.ext → Glu	v75	9.3	[	7.5	,	11.1]
Glyc.ext → Glyc	v76	33.4	[	30.2	,	37.4]
FA.ext → FA.c	v77	0.0	[	0.0	,	0.0]
Pro → Pro.ext	v78	2.3	[	1.9	,	2.7]
Ala → Ala.ext	v79	57.8	[	47.0	,	69.1]
Gly → Gly.ext	v80	16.4	[	13.3	,	19.6]
AcCoA.m → KB.ext	v81	152.3	[	119.6	,	189.3]
Albumin production	v82	32.0	[	24.4	,	36.6]

Metabolite	G-value	95% Conf. interval		
GLP	0.36	[0.33	,	0.44]
Lact	1.00	[0.64	,	1.00]
Ala	0.57	[0.34	,	0.80]
Pro	0.38	[0.36	,	0.40]
GLP	0.98	[0.64	,	1.00]

Table D.3 Results of combined ^{13}C-MFA by parallel labeling experiments of [U-^{13}C]glycerol and [U-^{13}C]glutamine at the dibutyryl-cAMP condition. Shown are the estimated net and exchange fluxes (nmol/10^{6}cell/h) and G-values with 95% confidence intervals.

Dibutyryl-cAMP condition							
Reaction			Flux	95% Conf. interval			
Gluc → Gluc.ext	v1		25.4	[	21.8	,	28.5]
G6P → Gluc	v2		25.4	[	21.8	,	28.5]
G6P ↔ F6P	v3	net	-33.2	[	-41.7	,	-19.1]
		exch	520.0	[	392.8	,	846.5]
FBP ↔ F6P	v4	net	24.5	[	19.1	,	28.3]
		exch	(0.0, >1e4)	[	0.0	,	>1e4]
FBP ↔ DHAP + GAP	v5	net	-24.5	[	-28.3	,	-19.1]
		exch	0.0	[	0.0	,	1.6]
DHAP ↔ GAP	v6	net	-9.6	[	-16.6	,	-3.9]
		exch	760.1	[	623.9	,	954.7]
GAP ↔ 3PG	v7	net	-29.7	[	-36.6	,	-23.2]
		exch	926.5	[	802.0	,	>1e3]
3PG ↔ PEP	v8	net	-29.7	[	-36.6	,	-23.2]
		exch	640.0	[	500.1	,	810.6]
OAC.c → PEP + CO2	v9		40.2	[	33.3	,	47.5]
PEP → Pyr.c	v10		10.5	[	0.0	,	21.9]
G6P → Ru5P + CO2	v11		13.2	[	0.0	,	20.9]
Ru5P ↔ X5P	v12	net	8.8	[	0.0	,	14.0]
		exch	(0.0, >1e4)	[	0.0	,	>1e4]
Ru5P ↔ R5P	v13	net	4.4	[	0.0	,	7.0]
		exch	(0.0, >1e4)	[	0.0	,	>1e4]
X5P ↔ EC2 + GAP	v14	net	8.8	[	0.0	,	14.0]
		exch	1.7	[	0.0	,	13.8]
F6P ↔ EC2 + E4P	v15	net	-4.4	[	-7.0	,	-0.0]
		exch	127.9	[	96.4	,	165.6]
S7P ↔ EC2 + R5P	v16	net	-4.4	[	-7.0	,	-0.0]
		exch	(71.1, 192.2)	[	0.0	,	>1e4]

Table D.3 continued

F6P ↔ EC3 + GAP	v17	net	-4.4	[	-7.0	,	-0.0]
		exch	13.1	[	3.2	,	22.7]
S7P ↔ EC3 + E4P	v18	net	4.4	[	0.0	,	7.0]
		exch	(2.2, >1e4)	[	0.0	,	>1e4]
GLP ↔ DHAP	v19	net	14.8	[	7.2	,	20.5]
		exch	21.7	[	14.9	,	83.0]
Glyc → GLP	v20		30.8	[	24.8	,	37.1]
GLP → GLP.src	v21		16.0	[	5.8	,	26.8]
G6P ↔ G1P	v22	net	-5.4	[	-6.6	,	-4.1]
		exch	(0.0, 217.9)	[	0.0	,	>1e3]
Glycogen.src → G1P	v23		5.4	[	4.1	,	6.6]
Pyr.c ↔ Pyr.m	v24	net	210.9	[	178.1	,	266.1]
		exch	242.9	[	40.4	,	491.6]
Pyr.c ↔ Lact	v25	net	-271.2	[	-310.4	,	-242.0]
		exch	850.6	[	756.3	,	923.0]
Pyr.m → AcCoA.m + CO2	v26		220.0	[	180.1	,	266.7]
AcCoA.m + OAC.m → Cit.m	v27		129.8	[	115.8	,	146.9]
Cit.m ↔ ICit.m	v28	net	62.9	[	52.5	,	71.3]
		exch	228.2	[	165.9	,	350.3]
ICit.m ↔ AKG.m + CO2	v29	net	62.9	[	52.5	,	71.3]
		exch	229.1	[	166.1	,	352.9]
AKG.m → Suc.m + CO2	v30		98.1	[	84.5	,	108.3]
Suc.m → Fum.m	v31		102.7	[	89.0	,	113.0]
Fum.m ↔ Mal.m	v32	net	105.1	[	91.3	,	115.4]
		exch	864.1	[	772.1	,	>1e3]
Mal.m ↔ OAC.m	v33	net	32.0	[	16.0	,	53.4]
		exch	698.0	[	363.8	,	>1e3]
Mal.m → Pyr.m + CO2	v34		106.8	[	62.8	,	126.5]
Mal.c → Pyr.c + CO2	v35		0.0	[	0.0	,	22.6]
Pyr.m + CO2 → OAC.m	v36		97.8	[	74.4	,	115.9]
Mal.c ↔ Mal.m	v37	net	33.8	[	12.1	,	51.6]

Table D.3 continued

		exch	>1e3	[	965.3	,	>1e3]
Mal.c ↔ OAC.c	v38	net	-33.8	[	-51.8	,	-18.9]
		exch	>1e3	[	>1e3	,	>1e3]
Cit.m ↔ Cit.c	v39	net	66.9	[	53.8	,	84.5]
		exch	(0.0, >1e4)	[	0.0	,	>1e4]
Cit.c → AcCoA.c + OAC.c	v40		66.9	[	53.8	,	84.5]
AcCoA.c → FA.c	v41		68.1	[	55.0	,	85.8]
FA.c+FA.src→FA.snk+FA.m	v42		68.1	[	55.0	,	85.8]
FA.m → AcCoA.m	v43		68.1	[	55.0	,	85.8]
Pyr.c ↔ Ala	v44	net	62.5	[	51.6	,	74.9]
		exch	163.2	[	72.2	,	243.2]
Gln → Glu	v45		33.2	[	29.9	,	35.8]
Glu ↔ AKG.m	v46	net	35.2	[	30.9	,	38.5]
		exch	>1e3	[	597.0	,	>1e3]
Glu ↔ Pro	v47	net	4.3	[	3.6	,	5.0]
		exch	(0.0, >1e4)	[	0.0	,	>1e4]
OAC.c ↔ Asp	v48	net	-7.1	[	-9.1	,	-5.0]
		exch	39.3	[	27.3	,	55.2]
Asp → Asn	v49		1.1	[	0.8	,	1.3]
Ser ↔ Pyr.c	v50	net	-8.3	[	-11.9	,	-5.0]
		exch	208.5	[	0.0	,	441.1]
Ser ↔ Gly + C1	v51	net	14.2	[	11.3	,	17.4]
		exch	204.9	[	0.0	,	466.2]
Thr → AcCoA.c + Gly	v52		1.2	[	0.5	,	2.0]
Met+CO2→Suc.m+CO2+C1	v53		1.8	[	1.4	,	2.2]
Val+CO2→Suc.m+CO2+CO2	v54		1.9	[	1.0	,	2.8]
Ile + CO2 → Suc.m + AcCoA.m + CO2	v55		0.9	[	0.4	,	1.3]
Phe → Fum.m + AcCoA.m + AcCoA.m + CO2	v56		2.1	[	1.2	,	3.0]
Tyr → Fum.m + AcCoA.m + AcCoA.m + CO2	v57		0.3	[	0.0	,	0.6]

Table D.3 continued

Leu + CO2 → AcCoA.m + AcCoA.m + AcCoA.m + CO2	v58	1.5	[	0.2	,	2.7]
Gln.ext → Gln	v59	34.5	[	31.3	,	37.2]
Asp.ext → Asp	v60	9.8	[	7.9	,	11.8]
Ile.ext → Ile	v61	1.7	[	1.3	,	2.1]
Leu.ext → Leu	v62	4.7	[	3.7	,	5.7]
Met.ext → Met	v63	2.2	[	1.8	,	2.6]
Phe.ext → Phe	v64	3.7	[	2.9	,	4.5]
Ser.ext → Ser	v65	7.3	[	5.9	,	8.7]
Tyr.ext → Tyr	v66	1.4	[	1.2	,	1.6]
Val.ext → Val	v67	3.8	[	3.0	,	4.6]
Thr.ext → Thr	v68	3.0	[	2.4	,	3.6]
Arg.ext → Arg	v69	1.4	[	1.1	,	1.8]
Cys.ext → Cys	v70	1.9	[	1.4	,	2.3]
His.ext → His	v71	0.8	[	0.6	,	1.0]
Lys.ext → Lys	v72	2.9	[	2.2	,	3.6]
Trp.ext → Trp	v73	0.1	[	0.1	,	0.1]
Lact.ext → Lact	v74	271.2	[	242.0	,	310.4]
Glu.ext → Glu	v75	9.3	[	7.5	,	10.9]
Glyc.ext → Glyc	v76	30.8	[	24.8	,	37.1]
FA.ext → FA.c	v77	0.0	[	0.0	,	0.0]
Pro → Pro.ext	v78	2.7	[	2.1	,	3.3]
Ala → Ala.ext	v79	59.2	[	48.3	,	71.5]
Gly → Gly.ext	v80	14.5	[	11.6	,	17.4]
AcCoA.m → KB.ext	v81	168.5	[	137.6	,	208.0]
Albumin production	v82	32.1	[	24.7	,	40.4]

Metabolite	G-value	95% Conf. interval				
GLP	0.36	[	0.33	,	0.48	]
Lact	0.77	[	0.46	,	1.00	]
Ala	0.55	[	0.29	,	0.82	]
Pro	0.43	[	0.40	,	0.45	]
GLP	1.00	[	0.59	,	1.00	]

Table D.4 Results of combined ^{13}C-MFA by parallel labeling experiments of [U-^{13}C]glycerol and [U-^{13}C]glutamine at the 8-bromo-cAMP condition. Shown are the estimated net and exchange fluxes (nmol/10^{6}cell/h) and G-values with 95% confidence intervals.

8-Bromo-cAMP condition							
Reaction			Flux	95% Conf. interval			
Gluc → Gluc.ext	v1		26.1	[	22.6	, 29.6	]
G6P → Gluc	v2		26.1	[	22.6	, 29.6	]
G6P ↔ F6P	v3	net	-26.1	[	-45.0	, -22.7	]
		exch	>1e3	[	>1e3	, >1e3	]
FBP ↔ F6P	v4	net	26.1	[	22.7	, 34.2	]
		exch	(0.0, >1e4)	[	0.0	, >1e4	]
FBP ↔ DHAP + GAP	v5	net	-26.1	[	-34.2	, -22.7	]
		exch	0.0	[	0.0	, 2.1	]
DHAP ↔ GAP	v6	net	-56.9	[	-69.6	, -42.8	]
		exch	>1e3	[	>1e3	, >1e3	]
GAP ↔ 3PG	v7	net	-83.0	[	-95.4	, -69.1	]
		exch	470.9	[	382.4	, 563.0	]
3PG ↔ PEP	v8	net	-83.0	[	-95.4	, -69.1	]
		exch	919.2	[	803.8	, >1e3	]
OAC.c → PEP + CO2	v9		89.4	[	76.5	, 104.6	]
PEP → Pyr.c	v10		6.5	[	0.0	, 26.5	]
G6P → Ru5P + CO2	v11		0.0	[	0.0	, 17.2	]
Ru5P ↔ X5P	v12	net	0.0	[	0.0	, 11.5	]
		exch	(>1e3, >1e4)	[	>1e3	, >1e4	]
Ru5P ↔ R5P	v13	net	0.0	[	0.0	, 5.7	]
		exch	8.7	[	0.0	, 11.6	]
X5P ↔ EC2 + GAP	v14	net	0.0	[	0.0	, 11.5	]
		exch	(>1e3, >1e4)	[	>1e3	, >1e4	]
F6P ↔ EC2 + E4P	v15	net	-0.0	[	-5.7	, -0.0	]
		exch	148.9	[	104.5	, 233.0	]
S7P ↔ EC2 + R5P	v16	net	-0.0	[	-5.7	, -0.0	]
		exch	(>1e3, >1e4)	[	>1e3	, >1e4	]

Table D.4 continued

F6P ↔ EC3 + GAP	v17	net	-0.0	[	-5.7	,	-0.0	]
		exch	(0.0, 13.3)	[	0.0	,	105.0	]
S7P ↔ EC3 + E4P	v18	net	0.0	[	0.0	,	5.7	]
		exch	(>1e3, >1e4)	[	>1e3	,	>1e4	]
GLP ↔ DHAP	v19	net	-30.8	[	-44.7	,	-14.1	]
		exch	441.0	[	343.5	,	538.7	]
Glyc → GLP	v20		13.9	[	11.9	,	16.1	]
GLP → GLP.src	v21		44.7	[	26.8	,	60.3	]
G6P ↔ G1P	v22	net	-0.0	[	-1.0	,	-0.0	]
		exch	(0.0, >1e4)	[	0.0	,	>1e4	]
Glycogen.src → G1P	v23		0.0	[	0.0	,	1.0	]
Pyr.c ↔ Pyr.m	v24	net	226.5	[	181.0	,	276.2	]
		exch	(0.0, 39.0)	[	0.0	,	591.6	]
Pyr.c ↔ Lact	v25	net	-245.1	[	-280.9	,	-209.5	]
		exch	>1e3	[	>1e3	,	>1e3	]
Pyr.m → AcCoA.m + CO2	v26		146.0	[	95.8	,	197.8	]
AcCoA.m + OAC.m → Cit.m	v27		144.3	[	127.2	,	163.7	]
Cit.m ↔ ICit.m	v28	net	75.0	[	64.9	,	85.5	]
		exch	179.4	[	131.0	,	264.4	]
ICit.m ↔ AKG.m + CO2	v29	net	75.0	[	64.9	,	85.5	]
		exch	188.9	[	135.6	,	289.8	]
AKG.m → Suc.m + CO2	v30		117.5	[	104.4	,	131.0	]
Suc.m → Fum.m	v31		123.0	[	109.8	,	136.5	]
Fum.m ↔ Mal.m	v32	net	125.0	[	111.7	,	138.7	]
		exch	>1e3	[	>1e3	,	>1e3	]
Mal.m ↔ OAC.m	v33	net	28.5	[	5.5	,	50.4	]
		exch	(>1e3, >1e3)	[	616.1	,	>1e3	]
Mal.m → Pyr.m + CO2	v34		35.4	[	11.9	,	59.4	]
Mal.c → Pyr.c + CO2	v35		47.1	[	23.6	,	70.3	]
Pyr.m + CO2 → OAC.m	v36		115.8	[	95.7	,	137.8	]
Mal.c ↔ Mal.m	v37	net	-61.2	[	-87.6	,	-35.6	]

Table D.4 continued

		exch	>1e3	[	>1e3	,	>1e3	]
Mal.c ↔ OAC.c	v38	net	14.1	[	-9.0	,	37.1	]
		exch	(350.1, >1e3)	[	218.9	,	>1e4	]
Cit.m ↔ Cit.c	v39	net	69.3	[	51.9	,	88.8	]
		exch	(0.0, >1e4)	[	0.0	,	>1e4	]
Cit.c → AcCoA.c + OAC.c	v40		69.3	[	51.9	,	88.8	]
AcCoA.c → FA.c	v41		70.2	[	52.9	,	89.9	]
FA.c+FA.src→FA.snk+FA.m	v42		70.2	[	52.9	,	89.9	]
FA.m → AcCoA.m	v43		70.2	[	52.9	,	89.9	]
Pyr.c ↔ Ala	v44	net	63.4	[	52.0	,	74.9	]
		exch	111.6	[	24.9	,	198.2	]
Gln → Glu	v45		41.8	[	38.3	,	45.4	]
Glu ↔ AKG.m	v46	net	42.5	[	38.4	,	46.7	]
		exch	>1e3	[	710.0	,	>1e3	]
Glu ↔ Pro	v47	net	4.4	[	3.8	,	4.9	]
		exch	(0.0, >1e4)	[	0.0	,	>1e4	]
OAC.c ↔ Asp	v48	net	-6.0	[	-8.1	,	-4.0	]
		exch	32.1	[	23.6	,	43.8	]
Asp → Asn	v49		1.5	[	1.2	,	1.7	]
Ser ↔ Pyr.c	v50	net	-8.8	[	-12.1	,	-5.4	]
		exch	>1e3	[	>1e3	,	>1e3	]
Ser ↔ Gly + C1	v51	net	14.6	[	11.8	,	17.5	]
		exch	56.1	[	0.0	,	215.1	]
Thr → AcCoA.c + Gly	v52		1.0	[	0.3	,	1.7	]
Met+CO2→Suc.m+CO2+C1	v53		1.9	[	1.5	,	2.3	]
Val+CO2→Suc.m+CO2+CO2	v54		1.8	[	0.9	,	2.7	]
Ile + CO2 → Suc.m + AcCoA.m + CO2	v55		1.7	[	1.1	,	2.4	]
Phe → Fum.m + AcCoA.m + AcCoA.m + CO2	v56		1.8	[	0.9	,	2.7	]
Tyr → Fum.m + AcCoA.m + AcCoA.m + CO2	v57		0.3	[	0.0	,	0.7	]

Table D.4 continued

Leu + CO2 → AcCoA.m + AcCoA.m + AcCoA.m + CO2	v58	1.5	[	0.1	,	3.0]
Gln.ext → Gln	v59	43.7	[	40.1	,	47.2]
Asp.ext → Asp	v60	9.8	[	7.9	,	11.8]
Ile.ext → Ile	v61	2.9	[	2.3	,	3.5]
Leu.ext → Leu	v62	6.0	[	4.8	,	7.2]
Met.ext → Met	v63	2.4	[	2.0	,	2.8]
Phe.ext → Phe	v64	4.0	[	3.2	,	4.8]
Ser.ext → Ser	v65	7.8	[	6.2	,	9.4]
Tyr.ext → Tyr	v66	1.8	[	1.4	,	2.2]
Val.ext → Val	v67	4.4	[	3.6	,	5.2]
Thr.ext → Thr	v68	3.4	[	2.8	,	4.0]
Arg.ext → Arg	v69	2.0	[	1.6	,	2.3]
Cys.ext → Cys	v70	2.6	[	2.1	,	3.0]
His.ext → His	v71	1.1	[	0.9	,	1.3]
Lys.ext → Lys	v72	4.0	[	3.3	,	4.7]
Trp.ext → Trp	v73	0.1	[	0.1	,	0.2]
Lact.ext → Lact	v74	245.1	[	209.5	,	280.9]
Glu.ext → Glu	v75	9.3	[	7.6	,	10.9]
Glyc.ext → Glyc	v76	13.9	[	11.9	,	16.1]
FA.ext → FA.c	v77	0.0	[	0.0	,	0.0]
Pro → Pro.ext	v78	2.2	[	1.8	,	2.6]
Ala → Ala.ext	v79	58.9	[	47.5	,	70.3]
Gly → Gly.ext	v80	14.2	[	11.5	,	16.9]
AcCoA.m → KB.ext	v81	85.5	[	39.5	,	127.3]
Albumin production	v82	44.5	[	36.6	,	52.4]

Metabolite	G-value	95% Conf. interval				
GLP	0.77	[	0.72	,	0.83]
Lact	0.49	[	0.24	,	0.82]
Ala	0.36	[	0.15	,	0.64]
Pro	0.40	[	0.38	,	0.43]
GLP	0.41	[	0.34	,	0.47]

Table D.5 Results of combined ^{13}C-MFA by parallel labeling experiments of [U-^{13}C]glycerol and [U-^{13}C]glutamine at the insulin condition. Shown are the estimated net and exchange fluxes (nmol/10^{6}cell/h) and G-values with 95% confidence intervals.

Insulin condition							
Reaction			Flux	95% Conf. interval			
Gluc → Gluc.ext	v1		6.6	[	5.6	,	7.6]
G6P → Gluc	v2		6.6	[	5.6	,	7.6]
G6P ↔ F6P	v3	net	-5.8	[	-15.2	,	-3.4]
		exch	684.5	[	440.7	,	>1e3]
FBP ↔ F6P	v4	net	4.5	[	3.4	,	7.2]
		exch	(2.5, >1e4)	[	1.4	,	>1e4]
FBP ↔ DHAP + GAP	v5	net	-4.5	[	-7.2	,	-3.4]
		exch	1.9	[	1.3	,	2.7]
DHAP ↔ GAP	v6	net	2.4	[	-4.3	,	9.1]
		exch	923.5	[	747.8	,	>1e3]
GAP ↔ 3PG	v7	net	-1.5	[	-8.3	,	5.3]
		exch	>1e3	[	>1e3	,	>1e3]
3PG ↔ PEP	v8	net	-1.5	[	-8.3	,	5.3]
		exch	354.4	[	248.0	,	486.3]
OAC.c → PEP + CO2	v9		14.6	[	11.3	,	17.8]
PEP → Pyr.c	v10		13.1	[	5.3	,	21.2]
G6P → Ru5P + CO2	v11		1.8	[	0.0	,	12.1]
Ru5P ↔ X5P	v12	net	1.2	[	0.0	,	8.1]
		exch	(4.8, >1e4)	[	0.0	,	>1e4]
Ru5P ↔ R5P	v13	net	0.6	[	0.0	,	4.0]
		exch	(7.4, >1e4)	[	0.0	,	>1e4]
X5P ↔ EC2 + GAP	v14	net	1.2	[	0.0	,	8.1]
		exch	4.3	[	0.0	,	7.8]
F6P ↔ EC2 + E4P	v15	net	-0.6	[	-4.0	,	-0.0]
		exch	29.7	[	23.2	,	39.1]
S7P ↔ EC2 + R5P	v16	net	-0.6	[	-4.0	,	-0.0]
		exch	(159.5, >1e4)	[	0.0	,	>1e4]

Table D.5 continued

F6P ↔ EC3 + GAP	v17	net	-0.6	[	-4.0	,	-0.0]
		exch	4.7	[	2.1	,	10.1]
S7P ↔ EC3 + E4P	v18	net	0.6	[	0.0	,	4.0]
		exch	(53.5, >1e4)	[	0.0	,	>1e4]
GLP ↔ DHAP	v19	net	7.0	[	-0.4	,	14.5]
		exch	45.6	[	16.8	,	200.5]
Glyc → GLP	v20		33.6	[	27.2	,	40.1]
GLP → GLP.src	v21		26.6	[	15.8	,	37.3]
G6P ↔ G1P	v22	net	-2.7	[	-3.9	,	-2.1]
		exch	(0.0, 349.8)	[	0.0	,	>1e3]
Glycogen.src → G1P	v23		2.7	[	2.1	,	3.9]
Pyr.c ↔ Pyr.m	v24	net	188.6	[	157.6	,	241.5]
		exch	253.5	[	83.3	,	534.2]
Pyr.c ↔ Lact	v25	net	-238.1	[	-265.9	,	-211.8]
		exch	>1e3	[	>1e3	,	>1e3]
Pyr.m → AcCoA.m + CO2	v26		215.7	[	179.2	,	254.3]
AcCoA.m + OAC.m → Cit.m	v27		123.9	[	109.1	,	141.2]
Cit.m ↔ ICit.m	v28	net	62.9	[	54.2	,	72.2]
		exch	193.2	[	139.8	,	312.9]
ICit.m ↔ AKG.m + CO2	v29	net	62.9	[	54.2	,	72.2]
		exch	194.7	[	140.4	,	317.6]
AKG.m → Suc.m + CO2	v30		91.9	[	80.8	,	104.0]
Suc.m → Fum.m	v31		98.1	[	86.6	,	110.4]
Fum.m ↔ Mal.m	v32	net	100.0	[	88.3	,	112.8]
		exch	>1e3	[	>1e3	,	>1e3]
Mal.m ↔ OAC.m	v33	net	59.4	[	43.3	,	75.6]
		exch	(610,5, 895.0)	[	295.8	,	>1e4]
Mal.m → Pyr.m + CO2	v34		91.6	[	56.5	,	111.1]
Mal.c → Pyr.c + CO2	v35		0.0	[	0.0	,	25.7]
Pyr.m + CO2 → OAC.m	v36		64.4	[	49.5	,	81.3]
Mal.c ↔ Mal.m	v37	net	50.9	[	27.4	,	67.3]

Table D.5 continued

		exch	>1e3	[	>1e3	,	>1e3]
Mal.c ↔ OAC.c	v38	net	-50.9	[	-67.3	,	-36.2]
		exch	>1e3	[	>1e3	,	>1e3]
Cit.m ↔ Cit.c	v39	net	61.0	[	46.9	,	76.9]
		exch	(0.0, >1e4)	[	0.0	,	>1e4]
Cit.c → AcCoA.c + OAC.c	v40		61.0	[	46.9	,	76.9]
AcCoA.c → FA.c	v41		62.2	[	48.0	,	78.2]
FA.c+FA.src→FA.snk+FA.m	v42		62.2	[	48.0	,	78.2]
FA.m → AcCoA.m	v43		62.2	[	48.0	,	78.2]
Pyr.c ↔ Ala	v44	net	61.6	[	50.8	,	72.6]
		exch	166.6	[	75.7	,	257.1]
Gln → Glu	v45		30.9	[	28.0	,	33.8]
Glu ↔ AKG.m	v46	net	29.0	[	25.0	,	33.1]
		exch	730.5	[	460.1	,	>1e3]
Glu ↔ Pro	v47	net	4.8	[	4.0	,	5.7]
		exch	(0.0, >1e4)	[	0.0	,	>1e4]
OAC.c ↔ Asp	v48	net	-4.6	[	-6.9	,	-2.2]
		exch	36.6	[	26.4	,	50.8]
Asp → Asn	v49		2.0	[	1.5	,	2.5]
Ser ↔ Pyr.c	v50	net	-1.0	[	-4.5	,	2.4]
		exch	227.5	[	1.9	,	497.9]
Ser ↔ Gly + C1	v51	net	8.9	[	6.7	,	11.2]
		exch	57.4	[	0.0	,	319.5]
Thr → AcCoA.c + Gly	v52		1.2	[	0.0	,	2.5]
Met+CO2→Suc.m+CO2+C1	v53		2.3	[	1.7	,	2.9]
Val+CO2→Suc.m+CO2+CO2	v54		2.3	[	0.8	,	3.7]
Ile + CO2 → Suc.m + AcCoA.m + CO2	v55		1.6	[	0.9	,	2.3]
Phe → Fum.m + AcCoA.m + AcCoA.m + CO2	v56		1.2	[	0.1	,	2.3]
Tyr → Fum.m + AcCoA.m + AcCoA.m + CO2	v57		0.8	[	0.0	,	1.6]

Table D.5 continued

Leu + CO2 → AcCoA.m + AcCoA.m + AcCoA.m + CO2	v58	1.1	[	0.0	,	3.2]
Gln.ext → Gln	v59	33.4	[	30.5	,	36.4]
Asp.ext → Asp	v60	9.8	[	7.8	,	11.7]
Ile.ext → Ile	v61	3.2	[	2.6	,	3.8]
Leu.ext → Leu	v62	7.2	[	5.9	,	8.6]
Met.ext → Met	v63	3.0	[	2.4	,	3.6]
Phe.ext → Phe	v64	4.2	[	3.4	,	5.0]
Ser.ext → Ser	v65	10.6	[	8.5	,	12.8]
Tyr.ext → Tyr	v66	2.9	[	2.3	,	3.5]
Val.ext → Val	v67	5.8	[	4.6	,	7.0]
Thr.ext → Thr	v68	4.5	[	3.5	,	5.5]
Arg.ext → Arg	v69	2.7	[	2.0	,	3.4]
Cys.ext → Cys	v70	3.5	[	2.6	,	4.4]
His.ext → His	v71	1.5	[	1.1	,	1.9]
Lys.ext → Lys	v72	5.4	[	4.1	,	6.7]
Trp.ext → Trp	v73	0.2	[	0.2	,	0.3]
Lact.ext → Lact	v74	238.1	[	211.8	,	265.9]
Glu.ext → Glu	v75	8.7	[	7.0	,	10.3]
Glyc.ext → Glyc	v76	33.6	[	27.2	,	40.1]
FA.ext → FA.c	v77	0.0	[	0.0	,	0.0]
Pro → Pro.ext	v78	1.8	[	1.4	,	2.2]
Ala → Ala.ext	v79	55.4	[	44.6	,	66.3]
Gly → Gly.ext	v80	8.2	[	6.6	,	9.8]
AcCoA.m → KB.ext	v81	162.9	[	129.7	,	196.8]
Albumin production	v82	61.0	[	45.7	,	75.8]

Metabolite	G-value	95% Conf. interval		
GLP	0.54	[0.48	,	0.60]
Lact	1.00	[0.76	,	1.00]
Ala	0.73	[0.50	,	0.98]
Pro	0.50	[0.48	,	0.53]
GLP	0.75	[0.47	,	1.00]

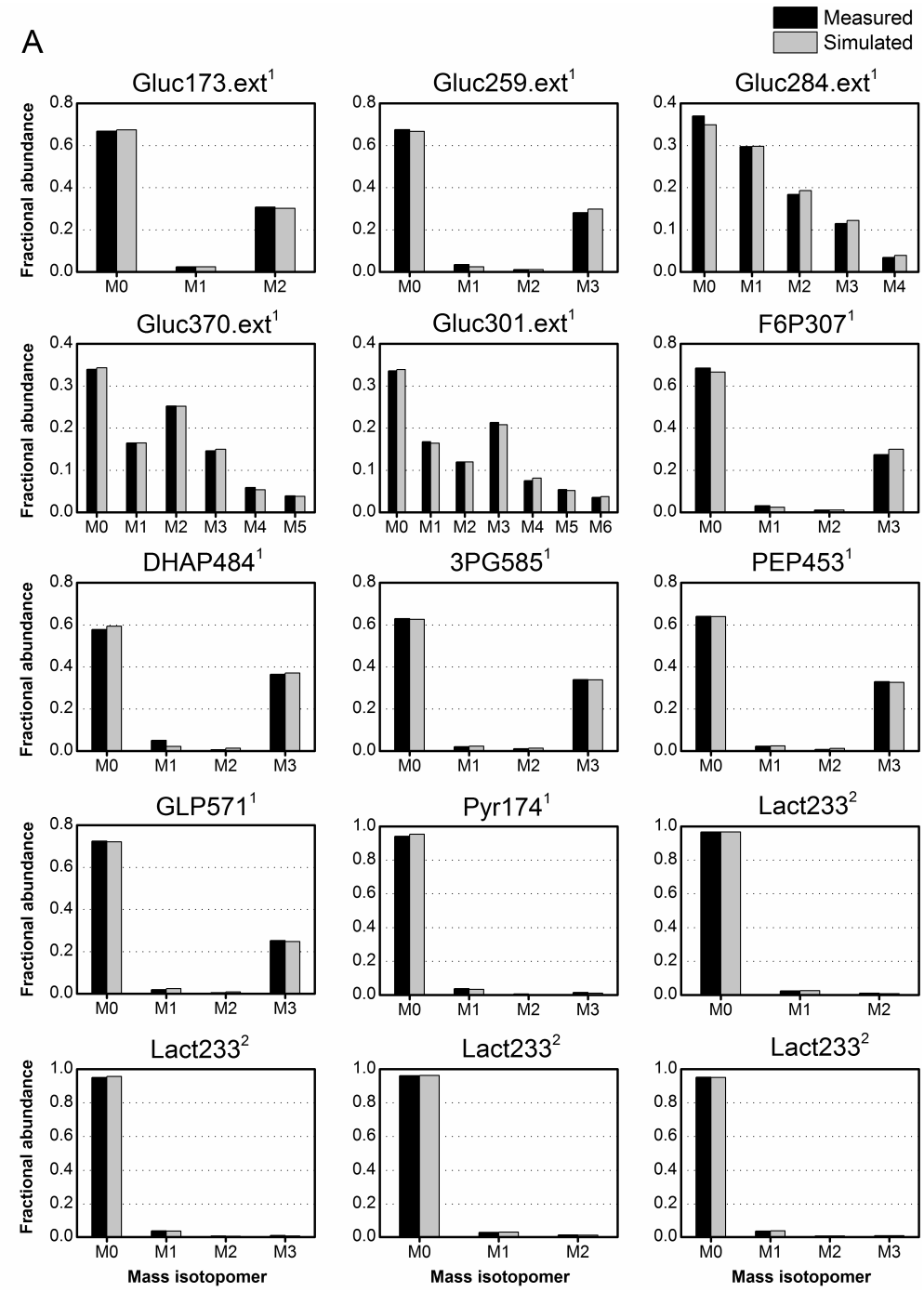
A
Measured
Simulated
Gluc173.ext[1]
Gluc259.ext[1]
Gluc284.ext[1]
Gluc370.ext[1]
Gluc301.ext[1]
F6P307[1]
DHAP484[1]
3PG585[1]
PEP453[1]
GLP571[1]
Pyr174[1]
Lact233[2]
Lact233[2]
Lact233[2]
Fractional abundance
Mass isotopomer

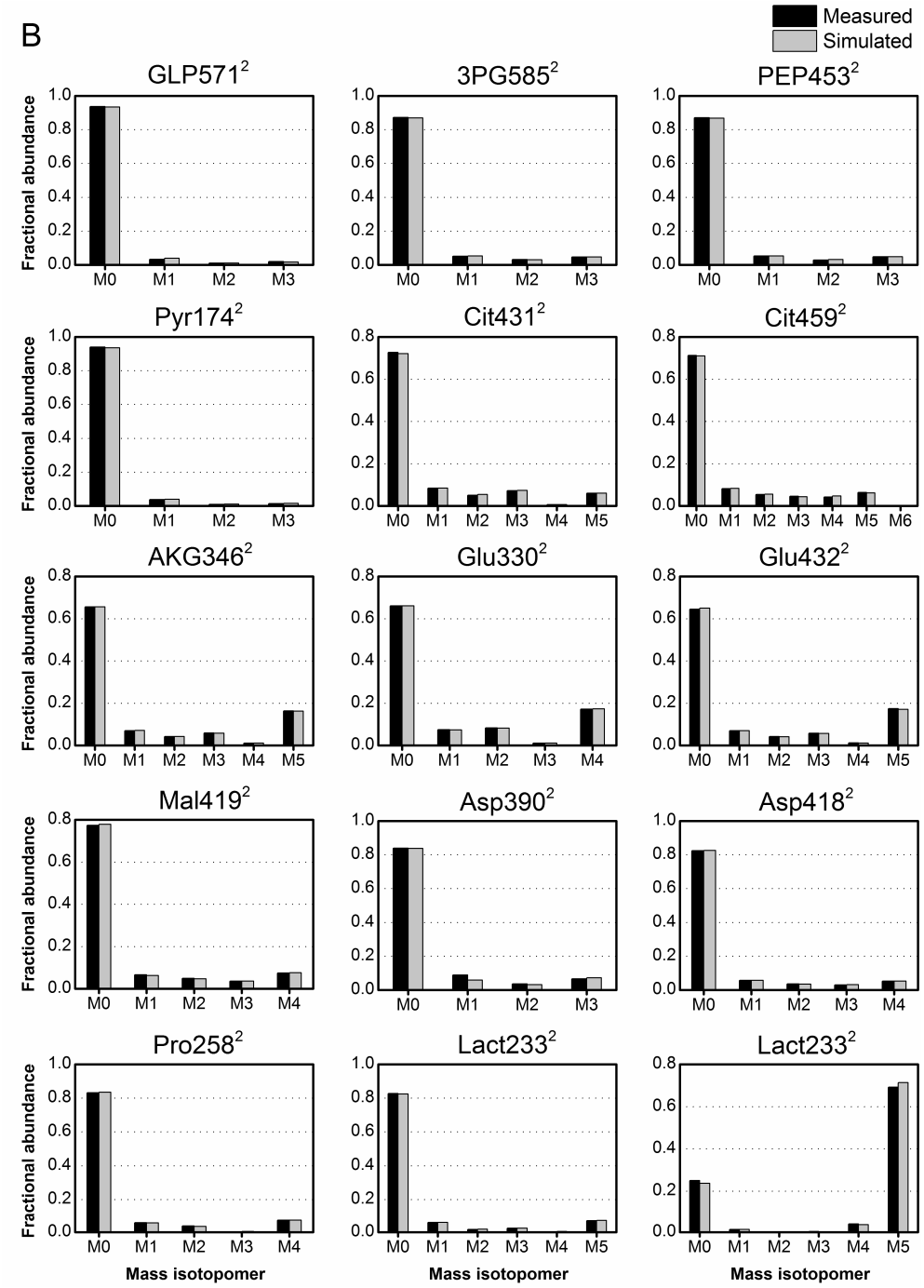

Figure D.1 Measured and fitted mass isotopomer distributions for the experiment with combined data at the control condition (A and B). Superscript 1 indicates the data from [U-^{13}C]glycerol and 2 from [U-^{13}C]glutamine. (MIDs were corrected for natural isotope abundances)

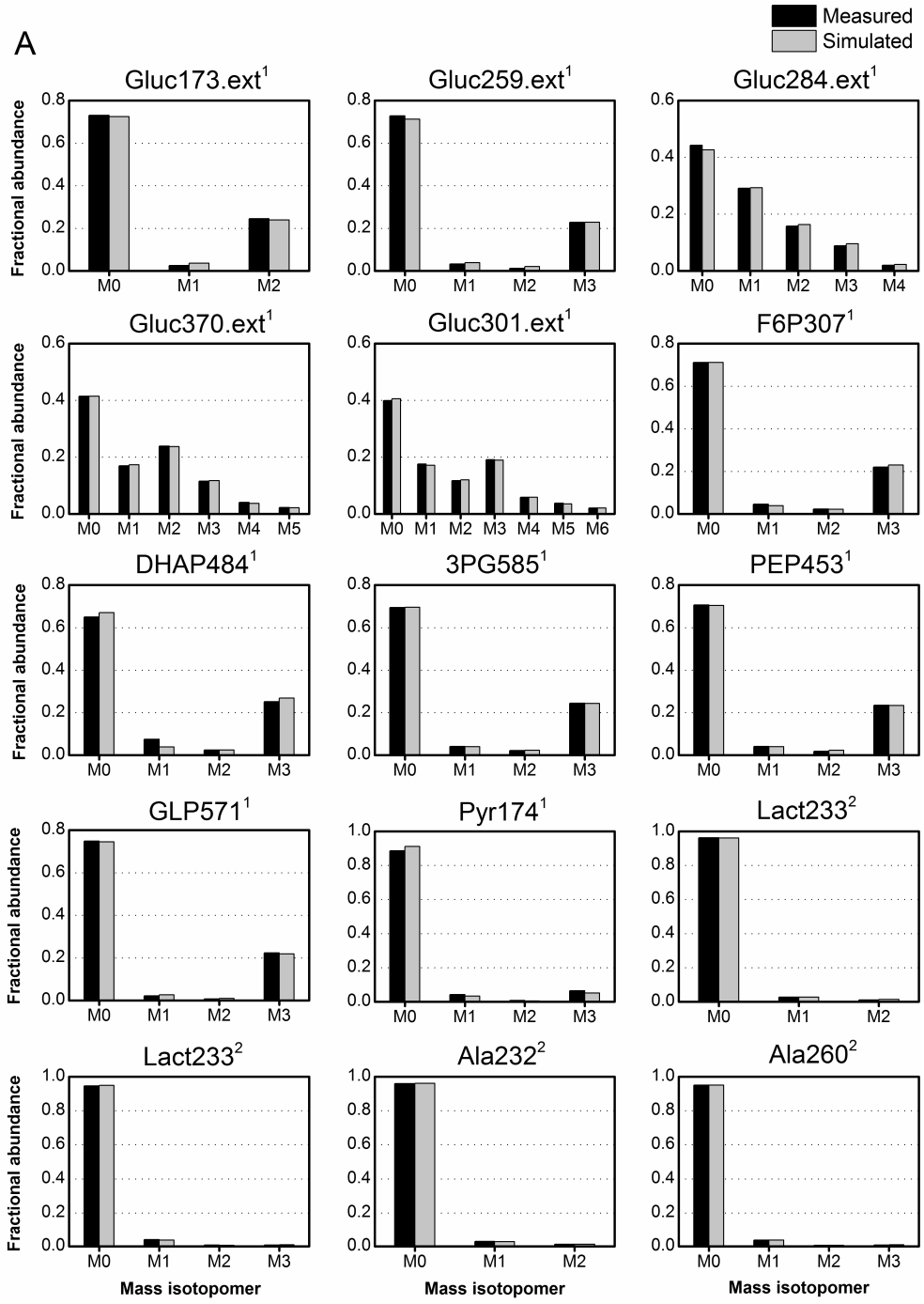
A
Measured
Simulated
Gluc173.ext[1]
Gluc259.ext[1]
Gluc284.ext[1]
Gluc370.ext[1]
Gluc301.ext[1]
F6P307[1]
DHAP484[1]
3PG585[1]
PEP453[1]
GLP571[1]
Pyr174[1]
Lact233[2]
Lact233[2]
Ala232[2]
Ala260[2]
Fractional abundance
Mass isotopomer

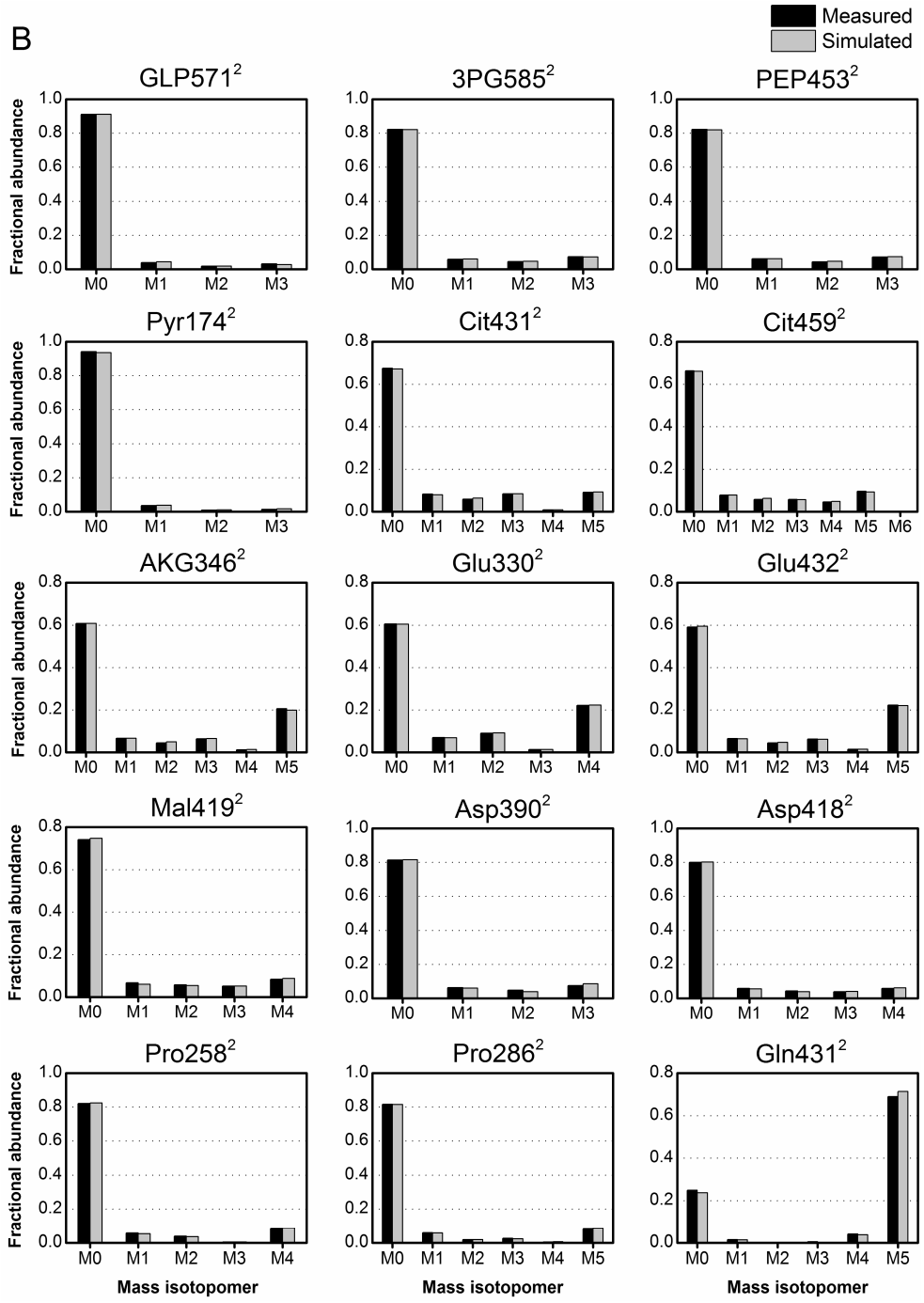

Figure D.2 Measured and fitted mass isotopomer distributions for the experiment with combined data at the dexamethasone condition (A and B). Superscript 1 indicates the data from [U-^{13}C]glycerol and 2 from [U-^{13}C]glutamine. (MIDs were corrected for natural isotope abundances)

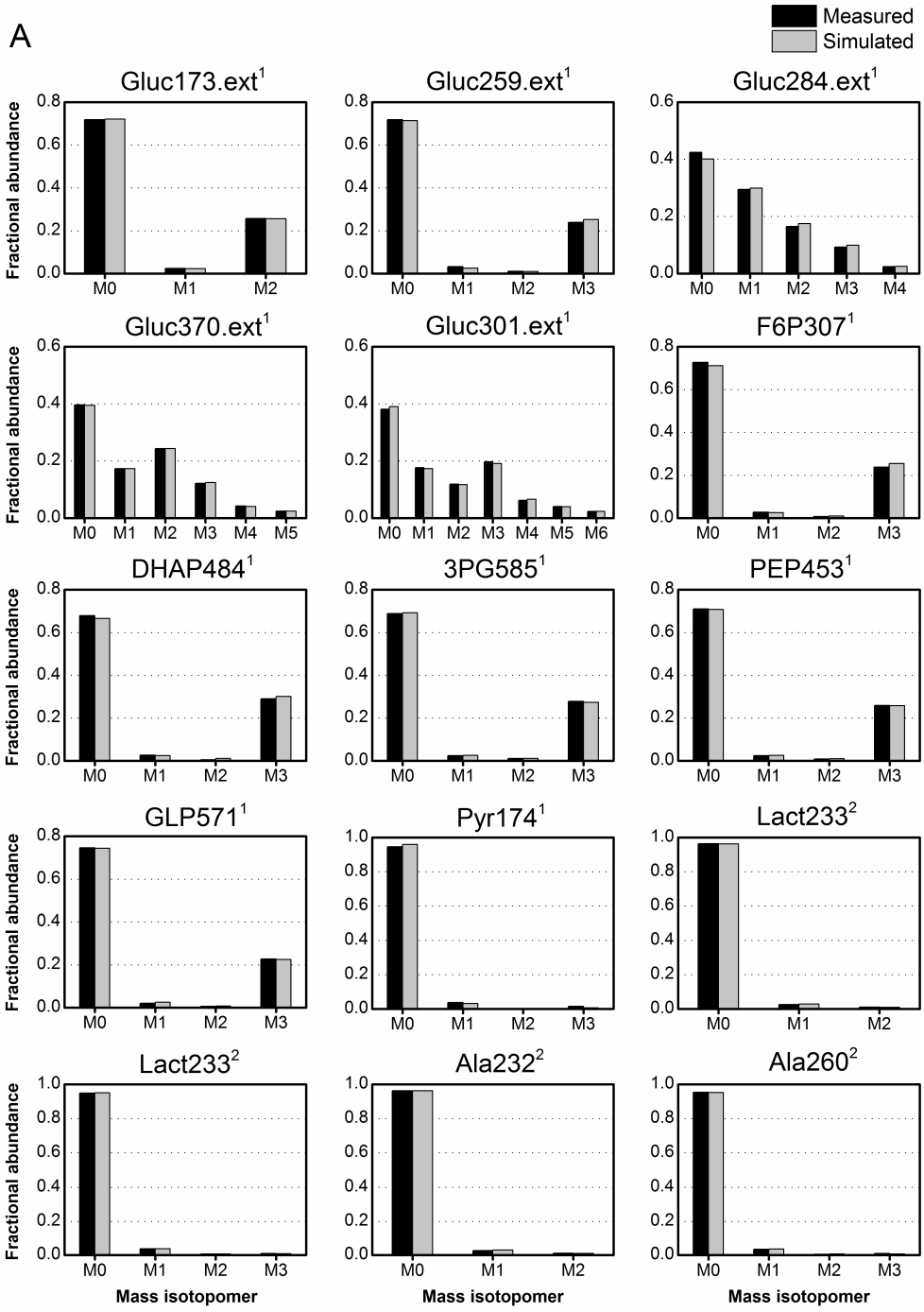
A
Measured
Simulated
Gluc173.ext1
Gluc259.ext1
Gluc284.ext1
Gluc370.ext1
Gluc301.ext1
F6P307 1
DHAP484 1
3PG585 1
PEP453 1
GLP571 1
Pyr174 1
Lact233 2
Lact233 2
Ala232 2
Ala260 2
Fractional abundance
Mass isotopomer
M0
M1
M2
M3
M4
M5
M6

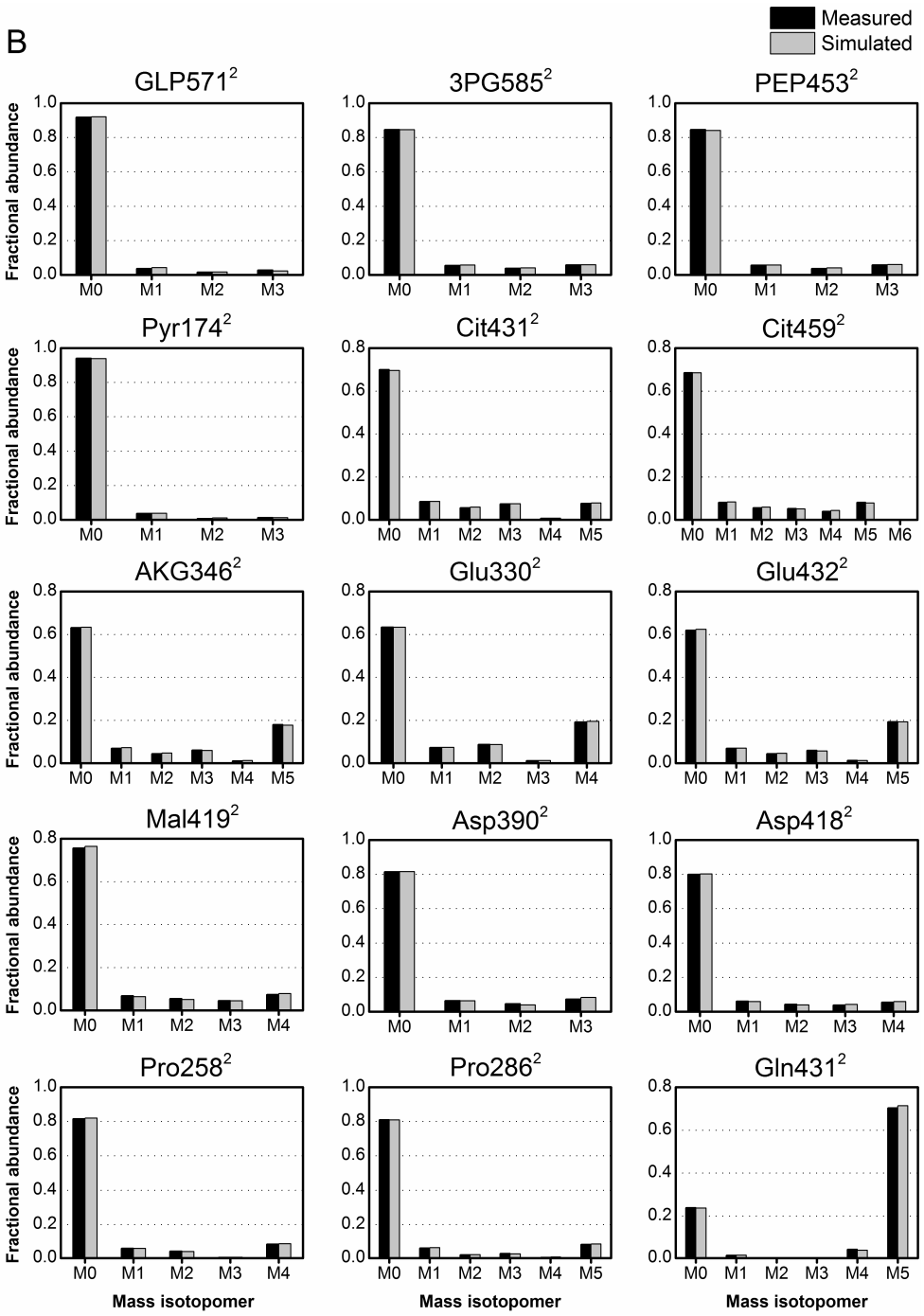

Figure D.3 Measured and fitted mass isotopomer distributions for the experiment with combined data at the dibutyryl-cAMP condition (A and B). Superscript 1 indicates the data from [U-^{13}C]glycerol and 2 from [U-^{13}C]glutamine. (MIDs were corrected for natural isotope abundances)

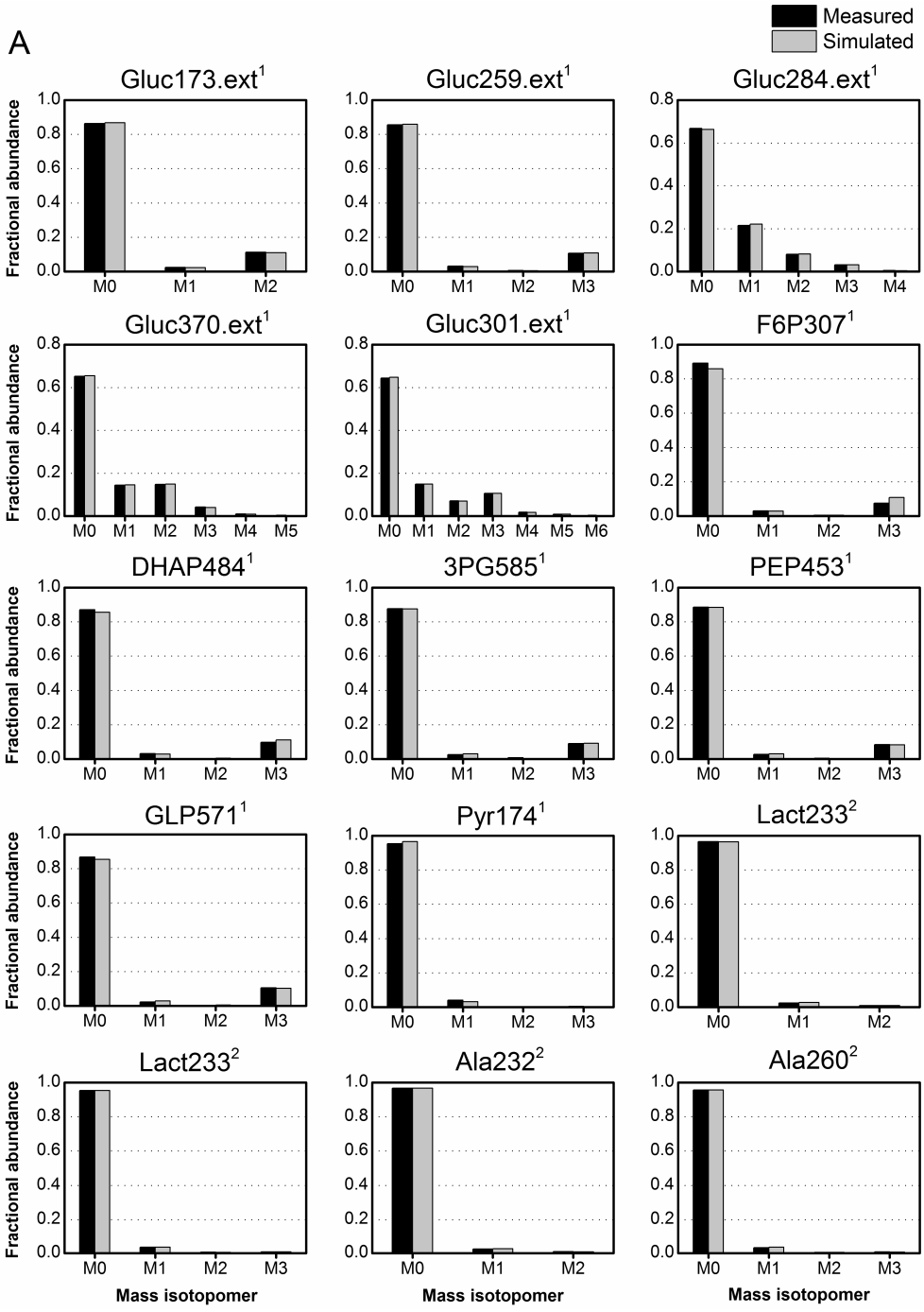
A
Measured
Simulated
Gluc173.ext1
Gluc259.ext1
Gluc284.ext1
Gluc370.ext1
Gluc301.ext1
F6P307 1
DHAP484 1
3PG585 1
PEP453 1
GLP571 1
Pyr174 1
Lact233 2
Lact233 2
Ala232 2
Ala260 2
Fractional abundance
Mass isotopomer

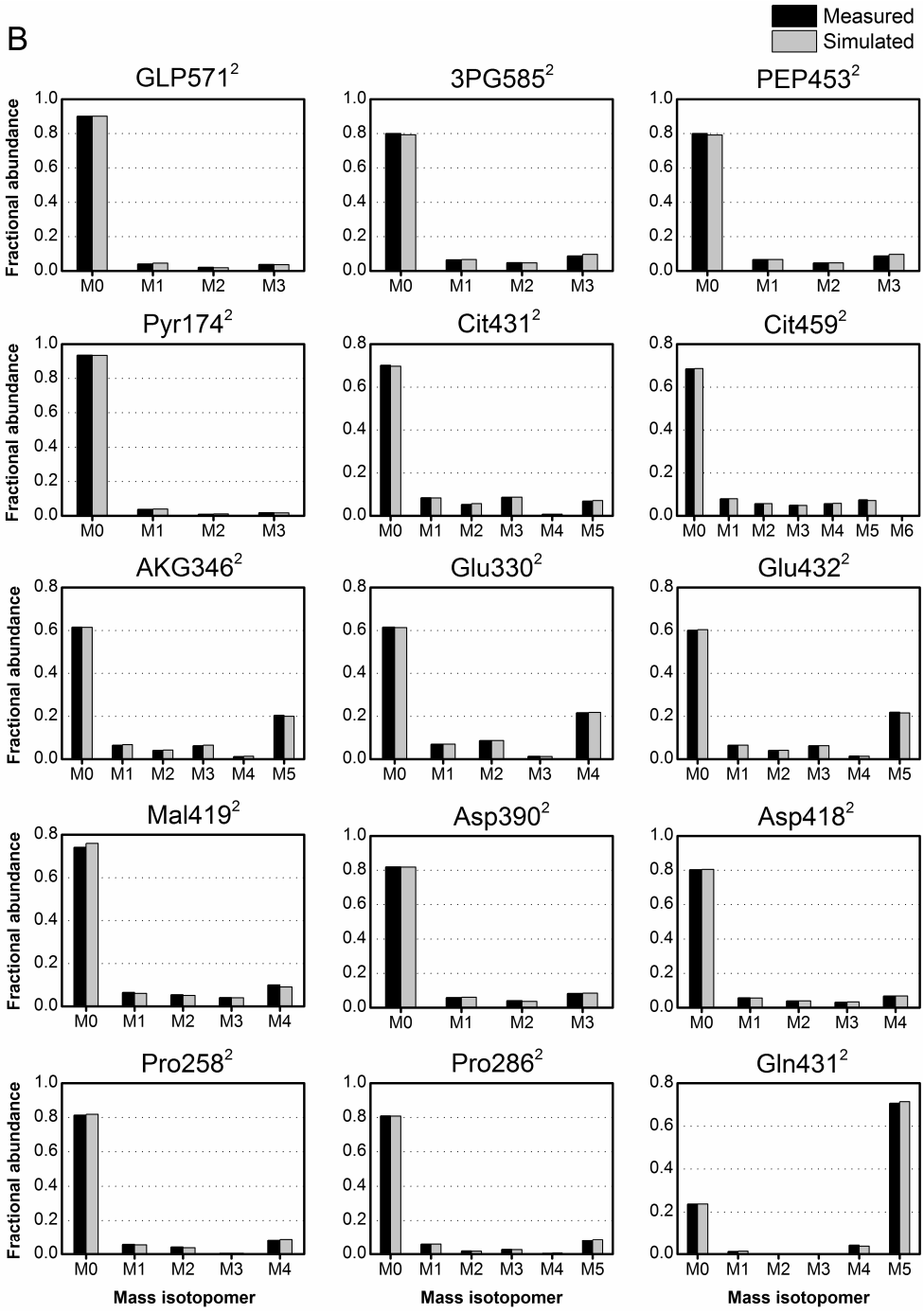

Figure D.4 Measured and fitted mass isotopomer distributions for the experiment with combined data at the 8-bromo-cAMP condition (A and B). Superscript 1 indicates the data from [U-^{13}C]glycerol and 2 from [U-^{13}C]glutamine. (MIDs were corrected for natural isotope abundances)

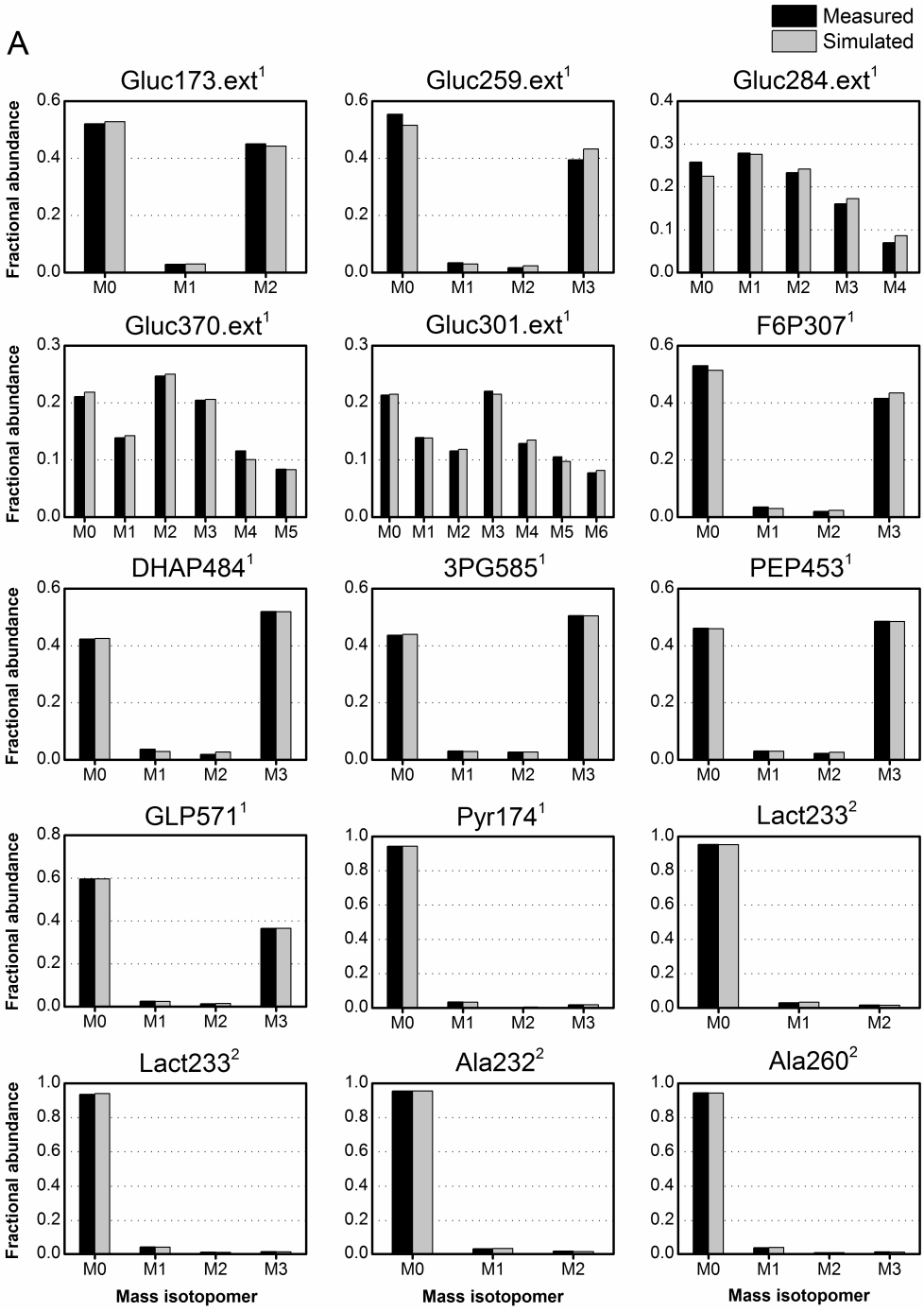
A
Measured
Simulated
Gluc173.ext[1]
Gluc259.ext[1]
Gluc284.ext[1]
Gluc370.ext[1]
Gluc301.ext[1]
F6P307[1]
DHAP484[1]
3PG585[1]
PEP453[1]
GLP571[1]
Pyr174[1]
Lact233[2]
Lact233[2]
Ala232[2]
Ala260[2]
Fractional abundance
Mass isotopomer

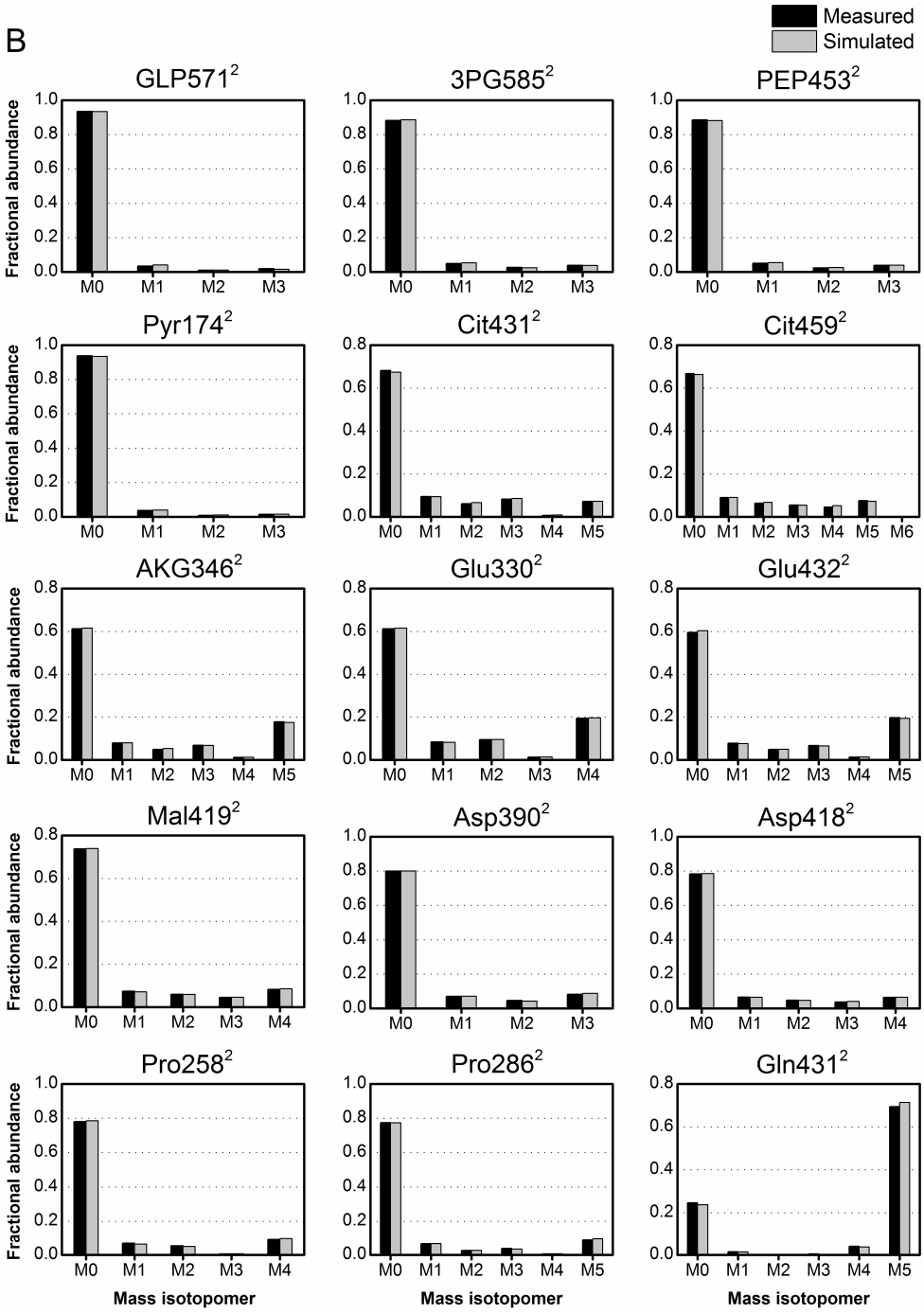

Figure D.5 Measured and fitted mass isotopomer distributions for the experiment with combined data at the insulin condition (A and B). Superscript 1 indicates the data from [U-^{13}C]glycerol and 2 from [U-^{13}C]glutamine. (MIDs were corrected for natural isotope abundances)

Table D.6 Mass isotopomer distributions of intracellular metabolites at 4, 8 and 12 h after addition of [U-^{13}C]lactate, [U-^{13}C]glutamine and [U-^{13}C]glycerol. They were measured by MOX-TBDMS derivatization and GC-MS. (data not corrected for natural isotope abundances)

	[U-^{13}C]lactate			[U-^{13}C]glutamine			[U-^{13}C]glycerol		
Isotopomer	4 h	8 h	12 h	4 h	8 h	12 h	4 h	8 h	12 h
Pyr174 (M0)	0.1567	0.1515	0.1775	0.8399	0.8402	0.8306	0.8405	0.8427	0.8364
Pyr175 (M1)	0.0236	0.0209	0.0230	0.1056	0.1057	0.1078	0.1030	0.1030	0.1029
Pyr176 (M2)	0.0341	0.0380	0.0354	0.0432	0.0432	0.0463	0.0393	0.0399	0.0400
Pyr177 (M3)	0.7857	0.7896	0.7642	0.0113	0.0110	0.0154	0.0173	0.0145	0.0207
Lact233 (M0)	0.0993	0.1011	0.1018	0.7615	0.7602	0.7556	0.7653	0.7646	0.7642
Lact234 (M1)	0.0345	0.0363	0.0371	0.1649	0.1647	0.1657	0.1638	0.1639	0.1641
Lact235 (M2)	0.8662	0.8626	0.8611	0.0736	0.0751	0.0787	0.0709	0.0715	0.0717
Lact261 (M0)	0.0860	0.0872	0.0887	0.7406	0.7398	0.7347	0.7444	0.7439	0.7437
Lact262 (M1)	0.0263	0.0273	0.0280	0.1705	0.1698	0.1701	0.1697	0.1696	0.1697
Lact263 (M2)	0.0288	0.0310	0.0322	0.0749	0.0752	0.0767	0.0739	0.0743	0.0741
Lact264 (M3)	0.8590	0.8545	0.8511	0.0140	0.0152	0.0185	0.0120	0.0122	0.0124
Ala232 (M0)	0.1056	0.0968	0.0972	0.7584	0.7568	0.7525	0.7620	0.7620	0.7611
Ala233 (M1)	0.0376	0.0366	0.0376	0.1689	0.1691	0.1701	0.1684	0.1681	0.1683
Ala234 (M2)	0.8568	0.8666	0.8652	0.0727	0.0741	0.0774	0.0696	0.0699	0.0706
Ala260 (M0)	0.1001	0.0921	0.0924	0.7414	0.7405	0.7348	0.7455	0.7457	0.7439
Ala261 (M1)	0.0315	0.0303	0.0307	0.1719	0.1715	0.1724	0.1716	0.1712	0.1717
Ala262 (M2)	0.0366	0.0328	0.0347	0.0726	0.0728	0.0746	0.0716	0.0716	0.0720
Ala263 (M3)	0.8318	0.8449	0.8423	0.0141	0.0153	0.0183	0.0114	0.0116	0.0123
Gly246 (M0)	0.6900	0.6489	0.6315	0.7364	0.7281	0.7210	0.7012	0.6886	0.6710
Gly247 (M1)	0.1875	0.1977	0.2035	0.1703	0.1705	0.1737	0.1558	0.1542	0.1514
Gly248 (M2)	0.1225	0.1534	0.1650	0.0932	0.1014	0.1053	0.1429	0.1572	0.1775
Pro258 (M0)	0.6223	0.5995	0.6148	0.6515	0.6485	0.6551	0.7362	0.7371	0.7359
Pro259 (M1)	0.1412	0.1390	0.1437	0.1698	0.1713	0.1721	0.1793	0.1790	0.1795
Pro260 (M2)	0.1298	0.1232	0.1152	0.0906	0.0928	0.0912	0.0715	0.0714	0.0711
Pro261 (M3)	0.0431	0.0461	0.0425	0.0193	0.0196	0.0192	0.0111	0.0106	0.0111
Pro262 (M4)	0.0635	0.0923	0.0838	0.0689	0.0677	0.0625	0.0020	0.0020	0.0024
Pro286 (M0)	0.6548	0.6576	0.6629	0.6483	0.6451	0.6504	0.7315	0.7333	0.7309
Pro287 (M1)	0.1370	0.1315	0.1396	0.1702	0.1715	0.1724	0.1816	0.1810	0.1818
Pro288 (M2)	0.1190	0.1053	0.0999	0.0759	0.0774	0.0784	0.0720	0.0714	0.0722
Pro289 (M3)	0.0279	0.0265	0.0250	0.0317	0.0328	0.0314	0.0114	0.0113	0.0114
Pro290 (M4)	0.0386	0.0454	0.0418	0.0099	0.0101	0.0096	0.0029	0.0024	0.0026
Pro291 (M5)	0.0227	0.0336	0.0308	0.0640	0.0630	0.0580	0.0006	0.0006	0.0011

Table D.6 continued

Suc289 (M0)	0.3991	0.3715	0.3462	0.5454	0.5187	0.5075	0.7376	0.7378	0.7371
Suc290 (M1)	0.0927	0.0789	0.0785	0.1536	0.1545	0.1558	0.1739	0.1740	0.1744
Suc291 (M2)	0.2270	0.2073	0.2069	0.1145	0.1238	0.1277	0.0749	0.0747	0.0750
Suc292 (M3)	0.1128	0.1095	0.1222	0.0305	0.0336	0.0351	0.0115	0.0112	0.0111
Suc293 (M4)	0.1683	0.2328	0.2462	0.1561	0.1694	0.1741	0.0023	0.0024	0.0024
Fum287 (M0)	0.3834	0.3111	0.3041	0.6053	0.5845	0.5876	0.7292	0.7311	0.7305
Fum288 (M1)	0.1174	0.0865	0.1012	0.1680	0.1692	0.1712	0.1778	0.1774	0.1777
Fum289 (M2)	0.1913	0.1878	0.2044	0.1013	0.1078	0.1086	0.0753	0.0749	0.0751
Fum290 (M3)	0.2035	0.2677	0.2445	0.0514	0.0608	0.0589	0.0146	0.0138	0.0142
Fum291 (M4)	0.1044	0.1470	0.1458	0.0741	0.0777	0.0736	0.0032	0.0029	0.0026
Ser390 (M0)	0.5225	0.4599	0.4360	0.6017	0.5868	0.5743	0.5457	0.5240	0.4993
Ser391 (M1)	0.2536	0.2677	0.2773	0.2349	0.2395	0.2444	0.2365	0.2409	0.2435
Ser392 (M2)	0.1552	0.1787	0.1877	0.1214	0.1273	0.1326	0.1384	0.1467	0.1554
Ser393 (M3)	0.0687	0.0936	0.0991	0.0420	0.0464	0.0488	0.0794	0.0883	0.1018
AKG346 (M0)	0.3622	0.3233	0.3103	0.5174	0.4928	0.4754	0.7153	0.7148	0.7150
AKG347 (M1)	0.0937	0.0829	0.0813	0.1549	0.1548	0.1535	0.1873	0.1874	0.1874
AKG348 (M2)	0.2157	0.1934	0.1920	0.0861	0.0907	0.0956	0.0795	0.0799	0.0796
AKG349 (M3)	0.0982	0.0991	0.1044	0.0611	0.0673	0.0705	0.0147	0.0146	0.0148
AKG350 (M4)	0.1335	0.1624	0.1701	0.0233	0.0251	0.0270	0.0028	0.0028	0.0028
AKG351 (M5)	0.0968	0.1388	0.1420	0.1572	0.1694	0.1780	0.0005	0.0006	0.0005
Mal419 (M0)	0.3162	0.2479	0.2445	0.5251	0.5067	0.5109	0.6342	0.6343	0.6343
Mal420 (M1)	0.1474	0.1197	0.1298	0.2052	0.2046	0.2065	0.2243	0.2242	0.2244
Mal421 (M2)	0.1992	0.1943	0.2107	0.1274	0.1331	0.1336	0.1075	0.1076	0.1075
Mal422 (M3)	0.2087	0.2620	0.2465	0.0650	0.0746	0.0721	0.0274	0.0273	0.0272
Mal423 (M4)	0.1285	0.1762	0.1686	0.0774	0.0811	0.0768	0.0068	0.0066	0.0066
Asp390 (M0)	0.3998	0.3584	0.3567	0.5774	0.5695	0.5591	0.6470	0.6470	0.6464
Asp391 (M1)	0.2046	0.1859	0.1944	0.2187	0.2197	0.2205	0.2229	0.2231	0.2229
Asp392 (M2)	0.2299	0.2475	0.2488	0.1246	0.1290	0.1331	0.1051	0.1052	0.1052
Asp393 (M3)	0.1658	0.2082	0.2001	0.0793	0.0818	0.0873	0.0250	0.0248	0.0255
Asp418 (M0)	0.3770	0.3383	0.3341	0.5617	0.5530	0.5415	0.6347	0.6343	0.6334
Asp419 (M1)	0.1676	0.1483	0.1564	0.2130	0.2132	0.2124	0.2256	0.2257	0.2257
Asp420 (M2)	0.1818	0.1754	0.1887	0.1199	0.1230	0.1263	0.1064	0.1067	0.1067
Asp421 (M3)	0.1729	0.2072	0.1947	0.0530	0.0579	0.0621	0.0266	0.0266	0.0268
Asp422 (M4)	0.1007	0.1307	0.1261	0.0524	0.0530	0.0578	0.0067	0.0067	0.0074
PEP453 (M0)	0.4357	0.3964	0.4004	0.5747	0.5615	0.5653	0.5236	0.5068	0.5165
PEP454 (M1)	0.2041	0.1816	0.1878	0.2192	0.2174	0.2202	0.1855	0.1770	0.1834
PEP455 (M2)	0.2105	0.2255	0.2249	0.1281	0.1307	0.1330	0.1045	0.0946	0.1029

Table D.6 continued

PEP456 (M3)	0.1497	0.1966	0.1870	0.0780	0.0905	0.0815	0.1864	0.2216	0.1972
Glu330 (M0)	0.3659	0.3303	0.3175	0.5121	0.4905	0.4757	0.7023	0.7012	0.7011
Glu331 (M1)	0.1176	0.1071	0.1046	0.1705	0.1718	0.1714	0.2006	0.2008	0.2012
Glu332 (M2)	0.2206	0.2079	0.2076	0.1192	0.1280	0.1336	0.0791	0.0798	0.0794
Glu333 (M3)	0.1279	0.1316	0.1380	0.0352	0.0385	0.0408	0.0150	0.0152	0.0151
Glu334 (M4)	0.1679	0.2230	0.2323	0.1630	0.1712	0.1784	0.0029	0.0030	0.0031
Glu432 (M0)	0.3085	0.2785	0.2646	0.4573	0.4380	0.4235	0.6232	0.6229	0.6214
Glu433 (M1)	0.1392	0.1243	0.1227	0.1859	0.1843	0.1826	0.2311	0.2309	0.2318
Glu434 (M2)	0.2033	0.1874	0.1856	0.1068	0.1108	0.1148	0.1098	0.1099	0.1104
Glu435 (M3)	0.1190	0.1199	0.1263	0.0678	0.0744	0.0778	0.0277	0.0279	0.0279
Glu436 (M4)	0.1325	0.1570	0.1654	0.0299	0.0328	0.0348	0.0069	0.0070	0.0070
Glu437 (M5)	0.0975	0.1329	0.1353	0.1522	0.1597	0.1665	0.0013	0.0014	0.0015
DHAP484 (M0)	0.5417	0.4565	0.4812	0.5499	0.5429	0.5506	0.4583	0.4444	0.4737
DHAP485 (M1)	0.1921	0.1789	0.1945	0.2464	0.2372	0.2383	0.1969	0.1967	0.1929
DHAP486 (M2)	0.1696	0.2031	0.1887	0.1321	0.1337	0.1351	0.1196	0.1140	0.1171
DHAP487 (M3)	0.0966	0.1615	0.1357	0.0716	0.0862	0.0760	0.2252	0.2451	0.2164
Gln431 (M0)	0.6191	0.6104	0.6136	0.1963	0.2312	0.2075	0.6258	0.6274	0.4838
Gln432 (M1)	0.2352	0.2328	0.2329	0.0733	0.0866	0.0782	0.2340	0.2329	0.4059
Gln433 (M3)	0.1079	0.1098	0.1081	0.0339	0.0402	0.0372	0.1072	0.1067	0.1883
Gln434 (M4)	0.0271	0.0293	0.0286	0.0108	0.0127	0.0128	0.0259	0.0258	0.0461
Gln435 (M5)	0.0080	0.0118	0.0111	0.0455	0.0421	0.0406	0.0061	0.0061	0.0109
Gln436 (M6)	0.0026	0.0060	0.0056	0.6402	0.5873	0.6237	0.0011	0.0011	0.0020
GLP571 (M0)	0.5323	0.4960	0.4797	0.5556	0.5425	0.5371	0.5115	0.4802	0.4621
GLP572 (M1)	0.2551	0.2448	0.2452	0.2594	0.2567	0.2583	0.2369	0.2240	0.2161
GLP573 (M2)	0.1509	0.1676	0.1748	0.1374	0.1405	0.1439	0.1344	0.1355	0.1361
GLP574 (M3)	0.0617	0.0916	0.1004	0.0478	0.0603	0.0608	0.1172	0.1603	0.1857
Cit459 (M0)	0.1712	0.1513	0.1563	0.4665	0.4424	0.4417	0.6136	0.6139	0.6130
Cit460 (M1)	0.0850	0.0723	0.0759	0.1967	0.1928	0.1938	0.2338	0.2324	0.2338
Cit461 (M2)	0.2357	0.1993	0.1950	0.1194	0.1228	0.1269	0.1126	0.1137	0.1132
Cit462 (M3)	0.1349	0.1259	0.1293	0.0670	0.0745	0.0755	0.0300	0.0302	0.0301
Cit463 (M4)	0.1594	0.1722	0.1788	0.0527	0.0542	0.0548	0.0079	0.0079	0.0080
Cit464 (M5)	0.1433	0.1847	0.1757	0.0730	0.0850	0.0803	0.0017	0.0015	0.0016
Cit465 (M6)	0.0704	0.0943	0.0891	0.0247	0.0284	0.0269	0.0003	0.0003	0.0003
3PG585 (M0)	0.3786	0.3477	0.3510	0.5030	0.4910	0.4927	0.4505	0.4361	0.4496
3PG586 (M1)	0.2284	0.2062	0.2136	0.2519	0.2494	0.2534	0.2125	0.2059	0.2133
3PG587 (M2)	0.2256	0.2360	0.2370	0.1556	0.1586	0.1607	0.1358	0.1367	0.1367
3PG588 (M3)	0.1675	0.2100	0.1985	0.0896	0.1010	0.0932	0.2012	0.2212	0.2003

Table D.7 Mass isotopomer distributions of secreted glucose at 4, 8 and 12 h after addition of [U-^{13}C]lactate, [U-^{13}C]glutamine and [U-^{13}C]glycerol. They were measured by aldonitrile pentapropionate derivatization and GC-MS. (data not corrected for natural isotope abundances)

	[U-^{13}C]lactate			[U-^{13}C]glutamine			[U-^{13}C]glycerol		
Isotopomer	4 h	8 h	12 h	4 h	8 h	12 h	4 h	8 h	12 h
Gluc173 (M0)	0.6596	0.5631	0.5546	0.8051	0.7941	0.7868	0.6964	0.6803	0.6646
Gluc174 (M1)	0.1554	0.1713	0.1689	0.1029	0.1081	0.1113	0.0757	0.0733	0.0707
Gluc175 (M2)	0.1690	0.2441	0.2545	0.0802	0.0865	0.0915	0.2038	0.2244	0.2413
Gluc176 (M3)	0.0126	0.0176	0.0183	0.0069	0.0071	0.0071	0.0158	0.0164	0.0176
Gluc177 (M4)	0.0035	0.0039	0.0037	0.0050	0.0042	0.0032	0.0083	0.0056	0.0060
Gluc259 (M0)	0.6239	0.5284	0.5261	0.7454	0.7397	0.7410	0.5212	0.6371	0.6217
Gluc260 (M1)	0.1381	0.1391	0.1368	0.1233	0.1268	0.1283	0.0955	0.0963	0.0935
Gluc261 (M2)	0.1255	0.1648	0.1671	0.0546	0.0546	0.0543	0.0734	0.0285	0.0276
Gluc262 (M3)	0.0944	0.1449	0.1485	0.0567	0.0608	0.0620	0.1680	0.2023	0.2209
Gluc263 (M4)	0.0149	0.0191	0.0179	0.0138	0.0126	0.0105	0.0855	0.0274	0.0285
Gluc264 (M5)	0.0032	0.0038	0.0036	0.0063	0.0055	0.0039	0.0565	0.0083	0.0078
Gluc284 (M0)	0.4750	0.3607	0.3514	0.6350	0.6240	0.6084	0.4039	0.3878	0.3650
Gluc285 (M1)	0.2704	0.2909	0.2870	0.2273	0.2349	0.2453	0.2852	0.2930	0.2984
Gluc286 (M2)	0.1597	0.2039	0.2087	0.0860	0.0901	0.0958	0.1632	0.1712	0.1805
Gluc287 (M3)	0.0676	0.1032	0.1121	0.0317	0.0322	0.0337	0.0972	0.1023	0.1087
Gluc288 (M4)	0.0172	0.0309	0.0307	0.0098	0.0100	0.0089	0.0334	0.0345	0.0370
Gluc289 (M5)	0.0050	0.0062	0.0061	0.0103	0.0089	0.0079	0.0171	0.0111	0.0104
Gluc290 (M6)	0.0051	0.0043	0.0040	0.0000	0.0000	0.0000	0.0000	0.0000	0.0000
Gluc370 (M0)	0.4208	0.2909	0.2847	0.6065	0.5902	0.5740	0.3976	0.3707	0.3479
Gluc371 (M1)	0.2375	0.2364	0.2300	0.2110	0.2169	0.2232	0.1966	0.1944	0.1913
Gluc372 (M2)	0.1963	0.2413	0.2424	0.1227	0.1309	0.1380	0.2166	0.2254	0.2322
Gluc373 (M3)	0.0935	0.1370	0.1438	0.0393	0.0425	0.0453	0.1166	0.1264	0.1357
Gluc374 (M4)	0.0372	0.0636	0.0690	0.0114	0.0121	0.0127	0.0448	0.0507	0.0563
Gluc375 (M5)	0.0119	0.0256	0.0253	0.0047	0.0042	0.0042	0.0227	0.0264	0.0298
Gluc376 (M6)	0.0023	0.0043	0.0041	0.0028	0.0020	0.0017	0.0041	0.0048	0.0053
Gluc377 (M7)	0.0006	0.0009	0.0007	0.0018	0.0012	0.0010	0.0010	0.0013	0.0014

Table D.8 Mass isotopomer distributions of intracellular metabolites at [U-^{13}C]lactate experiments (Flask #1 in triplicates). They were measured by MOX-TBDMS derivatization and GC-MS. (data not corrected for natural isotope abundances)

	Con	Dex	Dib	8Br	Ins
Isotopomer	Flask #1	Flask #1	Flask #1	Flask #1	Flask #1
Pyr174 (M0)	0.1698	0.3672	0.2037	0.1481	0.2476
Pyr175 (M1)	0.0372	0.0578	0.0481	0.0372	0.0457
Pyr176 (M2)	0.0587	0.0519	0.0730	0.0637	0.0551
Pyr177 (M3)	0.6490	0.4621	0.5961	0.6670	0.5785
Pyr178 (M4)	0.0589	0.0420	0.0547	0.0583	0.0502
Pyr179 (M5)	0.0266	0.0191	0.0243	0.0258	0.0228
Lact233 (M0)	0.0954	0.0896	0.1063	0.1014	0.0958
Lact234 (M1)	0.0350	0.0317	0.0371	0.0350	0.0369
Lact235 (M2)	0.6808	0.6874	0.6708	0.6763	0.6808
Lact236 (M3)	0.1306	0.1323	0.1286	0.1295	0.1291
Lact237 (M4)	0.0582	0.0591	0.0572	0.0577	0.0573
Lact261 (M0)	0.0841	0.0777	0.0928	0.0895	0.0826
Lact262 (M1)	0.0265	0.0242	0.0286	0.0274	0.0272
Lact263 (M2)	0.0312	0.0278	0.0323	0.0304	0.0338
Lact264 (M3)	0.6670	0.6749	0.6570	0.6644	0.6639
Lact265 (M4)	0.1315	0.1343	0.1304	0.1295	0.1328
Lact266 (M5)	0.0599	0.0613	0.0591	0.0589	0.0599
Ala232 (M0)	0.0839	0.0875	0.0868	0.0843	0.0853
Ala233 (M1)	0.0336	0.0335	0.0341	0.0326	0.0363
Ala234 (M2)	0.6894	0.6850	0.6851	0.6885	0.6874
Ala235 (M3)	0.1353	0.1357	0.1358	0.1362	0.1337
Ala236 (M4)	0.0578	0.0583	0.0582	0.0584	0.0572
Ala260 (M0)	0.0797	0.0831	0.0824	0.0807	0.0830
Ala261 (M1)	0.0277	0.0279	0.0282	0.0272	0.0299
Ala262 (M2)	0.0383	0.0366	0.0357	0.0324	0.0388
Ala263 (M3)	0.6666	0.6649	0.6661	0.6727	0.6623
Ala264 (M4)	0.1303	0.1303	0.1303	0.1298	0.1292
Ala265 (M5)	0.0575	0.0573	0.0574	0.0572	0.0570
Gly218 (M0)	0.6278	0.6058	0.6079	0.5657	0.6516
Gly219 (M1)	0.2712	0.2888	0.2870	0.3216	0.2520
Gly220 (M2)	0.0817	0.0844	0.0843	0.0887	0.0790
Gly221 (M3)	0.0192	0.0210	0.0208	0.0239	0.0174
Gly246 (M0)	0.6130	0.5911	0.5935	0.5526	0.6350

Table D.8 continued

Gly247 (M1)	0.1933	0.2004	0.2008	0.2090	0.1887
Gly248 (M2)	0.1543	0.1653	0.1632	0.1881	0.1412
Gly249 (M3)	0.0299	0.0328	0.0323	0.0378	0.0268
Gly250 (M4)	0.0095	0.0105	0.0103	0.0124	0.0083
Pro258 (M0)	0.4933	0.5542	0.5257	0.5296	0.4824
Pro259 (M1)	0.1256	0.1412	0.1369	0.1333	0.1201
Pro260 (M2)	0.1275	0.1226	0.1328	0.1263	0.1360
Pro261 (M3)	0.0701	0.0570	0.0636	0.0598	0.0814
Pro262 (M4)	0.1453	0.0986	0.1116	0.1202	0.1434
Pro263 (M5)	0.0279	0.0195	0.0218	0.0225	0.0269
Pro264 (M6)	0.0102	0.0069	0.0076	0.0083	0.0097
Pro286 (M0)	0.4974	0.5536	0.5318	0.5875	0.4777
Pro287 (M1)	0.1255	0.1416	0.1360	0.1422	0.1224
Pro288 (M2)	0.1191	0.1163	0.1225	0.1034	0.1280
Pro289 (M3)	0.0562	0.0493	0.0556	0.0405	0.0635
Pro290 (M4)	0.0921	0.0678	0.0760	0.0611	0.0945
Pro291 (M5)	0.0860	0.0556	0.0613	0.0504	0.0893
Pro292 (M6)	0.0181	0.0122	0.0129	0.0114	0.0187
Pro293 (M7)	0.0057	0.0038	0.0041	0.0035	0.0061
Suc289 (M0)	0.2361	0.3179	0.2884	0.3018	0.2460
Suc290 (M1)	0.0702	0.0909	0.0901	0.0819	0.0743
Suc291 (M2)	0.1852	0.1916	0.2000	0.1865	0.1918
Suc292 (M3)	0.1349	0.1193	0.1244	0.1141	0.1457
Suc293 (M4)	0.2953	0.2226	0.2353	0.2517	0.2705
Suc294 (M5)	0.0566	0.0417	0.0450	0.0461	0.0520
Suc295 (M6)	0.0218	0.0159	0.0169	0.0180	0.0197
Fum287 (M0)	0.2104	0.2634	0.2386	0.2497	0.2250
Fum288 (M1)	0.0839	0.1030	0.0968	0.0911	0.0897
Fum289 (M2)	0.1827	0.1889	0.1863	0.1815	0.1816
Fum290 (M3)	0.2782	0.2503	0.2748	0.2732	0.2716
Fum291 (M4)	0.1845	0.1462	0.1528	0.1550	0.1755
Fum292 (M5)	0.0470	0.0380	0.0402	0.0391	0.0443
Fum293 (M6)	0.0134	0.0102	0.0104	0.0105	0.0124
Ser302 (M0)	0.5668	0.5620	0.5437	0.4989	0.5947
Ser303 (M1)	0.2143	0.2174	0.2219	0.2290	0.2093
Ser304 (M2)	0.1678	0.1683	0.1783	0.2055	0.1523
Ser305 (M3)	0.0390	0.0399	0.0426	0.0507	0.0336
Ser306 (M4)	0.0120	0.0124	0.0134	0.0160	0.0100

Table D.8 continued

Ser362 (M0)	0.4166	0.4169	0.3947	0.3375	0.4641
Ser363 (M1)	0.3120	0.3080	0.3115	0.3217	0.2934
Ser364 (M2)	0.1913	0.1932	0.2054	0.2370	0.1737
Ser365 (M3)	0.0616	0.0626	0.0672	0.0783	0.0537
Ser366 (M4)	0.0185	0.0195	0.0213	0.0255	0.0153
Ser390 (M0)	0.4088	0.4084	0.3861	0.3285	0.4556
Ser391 (M1)	0.2683	0.2658	0.2669	0.2677	0.2583
Ser392 (M2)	0.1822	0.1826	0.1901	0.2079	0.1674
Ser393 (M3)	0.1000	0.1009	0.1109	0.1371	0.0857
Ser394 (M4)	0.0313	0.0323	0.0353	0.0443	0.0257
Ser395 (M5)	0.0093	0.0100	0.0108	0.0145	0.0073
AKG346 (M0)	0.2217	0.2906	0.2727	0.2852	0.2333
AKG347 (M1)	0.0660	0.0859	0.0843	0.0792	0.0705
AKG348 (M2)	0.1657	0.1803	0.1812	0.1730	0.1764
AKG349 (M3)	0.1076	0.1053	0.1143	0.0988	0.1146
AKG350 (M4)	0.1948	0.1611	0.1668	0.1739	0.1792
AKG351 (M5)	0.1843	0.1333	0.1371	0.1454	0.1715
AKG352 (M6)	0.0451	0.0330	0.0333	0.0341	0.0411
AKG353 (M7)	0.0148	0.0104	0.0102	0.0105	0.0134
Mal391 (M0)	0.1809	0.2251	0.2041	0.2080	0.1982
Mal392 (M1)	0.1376	0.1568	0.1488	0.1422	0.1488
Mal393 (M2)	0.2685	0.2687	0.2769	0.2764	0.2613
Mal394 (M3)	0.2833	0.2406	0.2544	0.2595	0.2701
Mal395 (M4)	0.0952	0.0803	0.0854	0.0847	0.0892
Mal396 (M5)	0.0345	0.0284	0.0304	0.0292	0.0323
Mal419 (M0)	0.1734	0.2164	0.1952	0.2012	0.1891
Mal420 (M1)	0.0910	0.1113	0.1036	0.1006	0.0985
Mal421 (M2)	0.1751	0.1839	0.1795	0.1773	0.1742
Mal422 (M3)	0.2694	0.2494	0.2709	0.2685	0.2621
Mal423 (M4)	0.1970	0.1619	0.1696	0.1725	0.1871
Mal424 (M5)	0.0700	0.0581	0.0615	0.0609	0.0666
Mal425 (M6)	0.0241	0.0193	0.0199	0.0190	0.0227
Asp390 (M0)	0.3214	0.3615	0.3362	0.3435	0.2925
Asp391 (M1)	0.1594	0.1771	0.1697	0.1661	0.1636
Asp392 (M2)	0.2202	0.2150	0.2263	0.2241	0.2297
Asp393 (M3)	0.2039	0.1683	0.1826	0.1816	0.2145
Asp394 (M4)	0.0696	0.0576	0.0628	0.0625	0.0728
Asp395 (M5)	0.0256	0.0204	0.0223	0.0222	0.0269

Table D.8 continued

Asp418 (M0)	0.3160	0.3546	0.3300	0.3374	0.2857
Asp419 (M1)	0.1336	0.1516	0.1435	0.1424	0.1286
Asp420 (M2)	0.1550	0.1612	0.1597	0.1569	0.1633
Asp421 (M3)	0.1953	0.1740	0.1958	0.1915	0.2100
Asp422 (M4)	0.1359	0.1082	0.1160	0.1167	0.1443
Asp423 (M5)	0.0481	0.0382	0.0420	0.0420	0.0512
Asp424 (M6)	0.0160	0.0122	0.0130	0.0131	0.0170
PEP453 (M0)	0.3589	0.3353	0.3252	0.2608	0.4163
PEP454 (M1)	0.1661	0.1713	0.1680	0.1502	0.1868
PEP455 (M2)	0.2042	0.2152	0.2177	0.2397	0.1859
PEP456 (M3)	0.1867	0.1896	0.1973	0.2410	0.1476
PEP457 (M4)	0.0618	0.0644	0.0669	0.0792	0.0467
PEP458 (M5)	0.0224	0.0242	0.0249	0.0292	0.0166
Glu330 (M0)	0.2294	0.2962	0.2795	0.2887	0.2426
Glu331 (M1)	0.0789	0.1006	0.1014	0.0952	0.0861
Glu332 (M2)	0.1823	0.1939	0.2001	0.1859	0.1937
Glu333 (M3)	0.1340	0.1242	0.1265	0.1177	0.1511
Glu334 (M4)	0.2810	0.2136	0.2193	0.2344	0.2443
Glu335 (M5)	0.0692	0.0527	0.0540	0.0573	0.0608
Glu336 (M6)	0.0252	0.0188	0.0193	0.0208	0.0215
Glu432 (M0)	0.2010	0.2610	0.2469	0.2554	0.2133
Glu433 (M1)	0.0818	0.1051	0.1032	0.1011	0.0879
Glu434 (M2)	0.1599	0.1753	0.1759	0.1681	0.1718
Glu435 (M3)	0.1124	0.1120	0.1191	0.1059	0.1204
Glu436 (M4)	0.1826	0.1532	0.1578	0.1614	0.1684
Glu437 (M5)	0.1778	0.1312	0.1339	0.1410	0.1619
Glu438 (M6)	0.0614	0.0456	0.0465	0.0491	0.0556
Glu439 (M7)	0.0231	0.0168	0.0170	0.0180	0.0210
DHAP484 (M0)	0.3716	0.3461	0.3398	0.2501	0.4137
DHAP485 (M1)	0.1829	0.1891	0.1830	0.1665	0.2067
DHAP486 (M2)	0.1953	0.2088	0.2131	0.2363	0.1820
DHAP487 (M3)	0.1675	0.1714	0.1776	0.2291	0.1311
DHAP488 (M4)	0.0618	0.0622	0.0638	0.0859	0.0484
DHAP489 (M5)	0.0209	0.0224	0.0227	0.0321	0.0181
Gln431 (M0)	0.6207	0.6171	0.6231	0.6241	0.6224
Gln432 (M1)	0.2296	0.2292	0.2305	0.2300	0.2301
Gln433 (M2)	0.1074	0.1085	0.1073	0.1070	0.1073
Gln434 (M3)	0.0272	0.0281	0.0269	0.0266	0.0269

Table D.8 continued

Gln435 (M4)	0.0092	0.0102	0.0082	0.0081	0.0084
Gln436 (M5)	0.0044	0.0050	0.0030	0.0031	0.0036
Gln437 (M6)	0.0013	0.0015	0.0009	0.0009	0.0011
Gln438 (M7)	0.0004	0.0005	0.0003	0.0003	0.0004
GLP571 (M0)	0.4782	0.4511	0.4533	0.4339	0.4796
GLP572 (M1)	0.2322	0.2258	0.2270	0.2201	0.2359
GLP573 (M2)	0.1584	0.1674	0.1673	0.1727	0.1589
GLP574 (M3)	0.0866	0.1007	0.0990	0.1120	0.0834
GLP575 (M4)	0.0328	0.0399	0.0389	0.0445	0.0313
GLP576 (M5)	0.0117	0.0151	0.0145	0.0168	0.0109
Cit431 (M0)	0.1034	0.1543	0.1313	0.1316	0.1006
Cit432 (M1)	0.0524	0.0746	0.0704	0.0625	0.0532
Cit433 (M2)	0.1752	0.1987	0.1977	0.1907	0.1840
Cit434 (M3)	0.1425	0.1449	0.1554	0.1412	0.1500
Cit435 (M4)	0.2158	0.1889	0.1984	0.2073	0.2100
Cit436 (M5)	0.2099	0.1599	0.1664	0.1803	0.2045
Cit437 (M6)	0.0731	0.0573	0.0587	0.0639	0.0705
Cit438 (M7)	0.0277	0.0214	0.0216	0.0227	0.0272
Cit459 (M0)	0.0994	0.1500	0.1232	0.1247	0.0943
Cit460 (M1)	0.0458	0.0666	0.0592	0.0554	0.0446
Cit461 (M2)	0.1621	0.1845	0.1771	0.1741	0.1696
Cit462 (M3)	0.1144	0.1235	0.1350	0.1188	0.1184
Cit463 (M4)	0.1822	0.1656	0.1718	0.1724	0.1741
Cit464 (M5)	0.2168	0.1741	0.1884	0.1987	0.2137
Cit465 (M6)	0.1203	0.0905	0.0971	0.1044	0.1241
Cit466 (M7)	0.0445	0.0337	0.0361	0.0389	0.0459
Cit467 (M8)	0.0145	0.0115	0.0121	0.0124	0.0152
3PG585 (M0)	0.3288	0.3053	0.2966	0.2352	0.3732
3PG586 (M1)	0.1893	0.1906	0.1872	0.1656	0.2111
3PG587 (M2)	0.2107	0.2220	0.2243	0.2419	0.1978
3PG588 (M3)	0.1899	0.1973	0.2045	0.2495	0.1545
3PG589 (M4)	0.0813	0.0849	0.0875	0.1079	0.0635

The measurement error of mass isotopomer distribution by MS analysis was less than 0.2 mo% and flask-to-flask error of mass isotopomer distributions in triplicates was less than 1.8 mol%.

Table D.9 Mass isotopomer distributions of intracellular metabolites at [U-^{13}C]lactate experiments (Flask #2 and #3 in triplicates). They were measured by MOX-TBDMS derivatization and GC-MS. (data not corrected for natural isotope abundances)

	Con	Dex	Dib	8Br	Ins	Con	Dex	Dib	8Br	Ins
isotopomer	Flask #2	Flask #2	Flask #2	Flask #2	Flask #2	Flask #3	Flask #3	Flask #3	Flask #3	Flask #3
Pyr174 (M0)	0.1778	0.3395	0.2028	0.1873	0.1815	0.1574	0.2112	0.1781	0.1634	0.1900
Pyr175 (M1)	0.0407	0.0531	0.0489	0.0475	0.0400	0.0373	0.0477	0.0444	0.0488	0.0413
Pyr176 (M2)	0.0654	0.0460	0.0727	0.0763	0.0555	0.0580	0.0641	0.0687	0.0788	0.0593
Pyr177 (M3)	0.6325	0.4968	0.5970	0.6086	0.6391	0.6607	0.5981	0.6260	0.6265	0.6270
Pyr178 (M4)	0.0578	0.0446	0.0545	0.0556	0.0578	0.0596	0.0544	0.0572	0.0574	0.0568
Pyr179 (M5)	0.0257	0.0202	0.0242	0.0246	0.0261	0.0269	0.0246	0.0255	0.0253	0.0257
Lact233 (M0)	0.0991	0.0864	0.1037	0.0976	0.1023	0.0975	0.1030	0.1016	0.0994	0.1033
Lact234 (M1)	0.0353	0.0304	0.0359	0.0344	0.0385	0.0345	0.0350	0.0361	0.0347	0.0399
Lact235 (M2)	0.6778	0.6915	0.6733	0.6797	0.6726	0.6799	0.6755	0.6754	0.6774	0.6709
Lact236 (M3)	0.1299	0.1326	0.1293	0.1302	0.1291	0.1301	0.1291	0.1294	0.1302	0.1286
Lact237 (M4)	0.0578	0.0591	0.0576	0.0580	0.0575	0.0579	0.0574	0.0576	0.0583	0.0573
Lact261 (M0)	0.0890	0.0751	0.0942	0.0830	0.0915	0.0847	0.0884	0.0894	0.0901	0.0906
Lact262 (M1)	0.0274	0.0232	0.0285	0.0258	0.0292	0.0262	0.0267	0.0278	0.0273	0.0296
Lact263 (M2)	0.0313	0.0266	0.0315	0.0299	0.0342	0.0302	0.0292	0.0320	0.0304	0.0370
Lact264 (M3)	0.6629	0.6794	0.6558	0.6692	0.6557	0.6674	0.6646	0.6606	0.6618	0.6535
Lact265 (M4)	0.1305	0.1347	0.1309	0.1320	0.1306	0.1318	0.1313	0.1308	0.1308	0.1304
Lact266 (M5)	0.0591	0.0612	0.0594	0.0602	0.0589	0.0599	0.0599	0.0595	0.0596	0.0590
Ala232 (M0)	0.0835	0.0855	0.0865	0.0842	0.0862	0.0831	0.0847	0.0864	0.0831	0.0882
Ala233 (M1)	0.0331	0.0323	0.0335	0.0326	0.0367	0.0325	0.0324	0.0340	0.0322	0.0384
Ala234 (M2)	0.6903	0.6889	0.6861	0.6888	0.6850	0.6907	0.6900	0.6863	0.6905	0.6821
Ala235 (M3)	0.1353	0.1354	0.1358	0.1360	0.1347	0.1357	0.1353	0.1354	0.1360	0.1341
Ala236 (M4)	0.0577	0.0579	0.0581	0.0583	0.0574	0.0581	0.0576	0.0579	0.0582	0.0573
Ala260 (M0)	0.0793	0.0818	0.0823	0.0798	0.0819	0.0794	0.0816	0.0828	0.0799	0.0842
Ala261 (M1)	0.0273	0.0273	0.0278	0.0270	0.0292	0.0270	0.0272	0.0282	0.0269	0.0306
Ala262 (M2)	0.0360	0.0337	0.0343	0.0342	0.0391	0.0347	0.0321	0.0346	0.0330	0.0411
Ala263 (M3)	0.6694	0.6694	0.6675	0.6703	0.6633	0.6708	0.6703	0.6667	0.6714	0.6588
Ala264 (M4)	0.1307	0.1305	0.1305	0.1310	0.1297	0.1307	0.1311	0.1303	0.1311	0.1288
Ala265 (M5)	0.0574	0.0575	0.0575	0.0578	0.0570	0.0576	0.0579	0.0575	0.0579	0.0567
Gly218 (M0)	0.6181	0.6196	0.6158	0.5652	0.6510	0.6235	0.5953	0.6035	0.5697	0.6338
Gly219 (M1)	0.2794	0.2782	0.2808	0.3219	0.2523	0.2747	0.2974	0.2907	0.3183	0.2661
Gly220 (M2)	0.0825	0.0824	0.0833	0.0890	0.0792	0.0822	0.0855	0.0847	0.0883	0.0812
Gly221 (M3)	0.0199	0.0198	0.0202	0.0240	0.0175	0.0195	0.0217	0.0211	0.0237	0.0188
Gly246 (M0)	0.6033	0.6045	0.6011	0.5504	0.6359	0.6094	0.5810	0.5896	0.5549	0.6185

Table D.9 continued

Gly247 (M1)	0.1964	0.1975	0.1995	0.2093	0.1886	0.1947	0.2029	0.2022	0.2087	0.1930
Gly248 (M2)	0.1594	0.1575	0.1583	0.1893	0.1406	0.1560	0.1710	0.1650	0.1864	0.1503
Gly249 (M3)	0.0312	0.0308	0.0312	0.0384	0.0267	0.0304	0.0341	0.0328	0.0377	0.0290
Gly250 (M4)	0.0099	0.0098	0.0099	0.0127	0.0083	0.0097	0.0110	0.0105	0.0125	0.0092
Pro258 (M0)	0.5057	0.5657	0.5337	0.5213	0.4669	0.5019	0.5483	0.5160	0.5201	0.4585
Pro259 (M1)	0.1276	0.1427	0.1373	0.1317	0.1220	0.1261	0.1392	0.1342	0.1318	0.1194
Pro260 (M2)	0.1257	0.1209	0.1323	0.1271	0.1406	0.1258	0.1257	0.1353	0.1285	0.1402
Pro261 (M3)	0.0666	0.0547	0.0621	0.0618	0.0853	0.0683	0.0581	0.0653	0.0622	0.0824
Pro262 (M4)	0.1384	0.0922	0.1074	0.1248	0.1468	0.1414	0.1015	0.1182	0.1248	0.1579
Pro263 (M5)	0.0264	0.0175	0.0201	0.0245	0.0281	0.0267	0.0200	0.0229	0.0239	0.0304
Pro264 (M6)	0.0097	0.0063	0.0071	0.0088	0.0102	0.0098	0.0071	0.0081	0.0086	0.0112
Pro286 (M0)	0.5058	0.5672	0.5363	0.5204	0.4691	0.5067	0.5472	0.5147	0.5208	0.4575
Pro287 (M1)	0.1278	0.1431	0.1369	0.1326	0.1209	0.1263	0.1397	0.1339	0.1327	0.1180
Pro288 (M2)	0.1173	0.1149	0.1227	0.1201	0.1308	0.1173	0.1194	0.1253	0.1211	0.1297
Pro289 (M3)	0.0541	0.0464	0.0555	0.0527	0.0661	0.0543	0.0501	0.0592	0.0529	0.0659
Pro290 (M4)	0.0897	0.0626	0.0736	0.0840	0.0967	0.0889	0.0703	0.0819	0.0834	0.1040
Pro291 (M5)	0.0822	0.0512	0.0586	0.0703	0.0914	0.0832	0.0572	0.0661	0.0696	0.0975
Pro292 (M6)	0.0176	0.0112	0.0127	0.0152	0.0192	0.0178	0.0125	0.0146	0.0151	0.0208
Pro293 (M7)	0.0057	0.0035	0.0039	0.0048	0.0062	0.0057	0.0039	0.0044	0.0047	0.0066
Suc289 (M0)	0.2476	0.3202	0.2979	0.2920	0.2536	0.2464	0.3223	0.2952	0.3067	0.2628
Suc290 (M1)	0.0721	0.0908	0.0929	0.0831	0.0773	0.0721	0.0934	0.0920	0.0859	0.0781
Suc291 (M2)	0.1828	0.1948	0.2017	0.1883	0.1919	0.1839	0.1940	0.2014	0.1876	0.1874
Suc292 (M3)	0.1314	0.1193	0.1229	0.1183	0.1454	0.1333	0.1181	0.1217	0.1159	0.1347
Suc293 (M4)	0.2890	0.2193	0.2253	0.2528	0.2605	0.2874	0.2150	0.2295	0.2409	0.2651
Suc294 (M5)	0.0559	0.0403	0.0429	0.0472	0.0517	0.0555	0.0417	0.0436	0.0457	0.0522
Suc295 (M6)	0.0213	0.0153	0.0164	0.0182	0.0194	0.0213	0.0157	0.0165	0.0173	0.0197
Fum287 (M0)	0.2143	0.2794	0.2500	0.2446	0.2324	0.2282	0.2913	0.2488	0.2631	0.2266
Fum288 (M1)	0.0874	0.1080	0.1016	0.0943	0.0947	0.0929	0.1153	0.1041	0.1016	0.0908
Fum289 (M2)	0.1874	0.1910	0.1888	0.1834	0.1890	0.1929	0.1973	0.1960	0.1901	0.1819
Fum290 (M3)	0.2720	0.2355	0.2644	0.2699	0.2549	0.2491	0.2151	0.2558	0.2456	0.2705
Fum291 (M4)	0.1803	0.1416	0.1467	0.1566	0.1727	0.1797	0.1375	0.1474	0.1517	0.1728
Fum292 (M5)	0.0456	0.0351	0.0385	0.0404	0.0437	0.0442	0.0340	0.0379	0.0377	0.0448
Fum293 (M6)	0.0130	0.0095	0.0100	0.0107	0.0127	0.0130	0.0094	0.0100	0.0103	0.0127
Ser302 (M0)	0.5582	0.5733	0.5521	0.4971	0.5921	0.5654	0.5408	0.5417	0.5046	0.5711
Ser303 (M1)	0.2171	0.2157	0.2211	0.2301	0.2106	0.2147	0.2220	0.2231	0.2287	0.2154
Ser304 (M2)	0.1721	0.1625	0.1731	0.2061	0.1523	0.1684	0.1804	0.1794	0.2015	0.1644
Ser305 (M3)	0.0405	0.0375	0.0413	0.0504	0.0348	0.0396	0.0433	0.0425	0.0494	0.0377
Ser306 (M4)	0.0122	0.0110	0.0124	0.0163	0.0101	0.0119	0.0135	0.0133	0.0158	0.0113

Table D.9 continued

Ser362 (M0)	0.4081	0.4310	0.4040	0.3344	0.4632	0.4175	0.3879	0.3886	0.3422	0.4375
Ser363 (M1)	0.3146	0.3063	0.3106	0.3226	0.2953	0.3136	0.3202	0.3164	0.3257	0.3001
Ser364 (M2)	0.1946	0.1856	0.2001	0.2375	0.1724	0.1892	0.2038	0.2062	0.2302	0.1861
Ser365 (M3)	0.0634	0.0593	0.0649	0.0793	0.0536	0.0612	0.0672	0.0675	0.0769	0.0585
Ser366 (M4)	0.0194	0.0180	0.0204	0.0264	0.0156	0.0186	0.0211	0.0213	0.0251	0.0179
Ser390 (M0)	0.3994	0.4235	0.3961	0.3257	0.4546	0.4094	0.3794	0.3799	0.3344	0.4284
Ser391 (M1)	0.2691	0.2653	0.2673	0.2685	0.2586	0.2688	0.2707	0.2707	0.2717	0.2607
Ser392 (M2)	0.1861	0.1785	0.1869	0.2088	0.1684	0.1829	0.1935	0.1921	0.2070	0.1768
Ser393 (M3)	0.1030	0.0946	0.1057	0.1376	0.0853	0.0988	0.1102	0.1109	0.1309	0.0956
Ser394 (M4)	0.0326	0.0296	0.0337	0.0447	0.0258	0.0310	0.0353	0.0355	0.0425	0.0299
Ser395 (M5)	0.0098	0.0085	0.0103	0.0147	0.0073	0.0091	0.0109	0.0109	0.0136	0.0088
AKG346 (M0)	0.2258	0.3027	0.2867	0.2779	0.2403	0.2338	0.3138	0.2793	0.2857	0.2429
AKG347 (M1)	0.0670	0.0883	0.0888	0.0800	0.0729	0.0688	0.0918	0.0860	0.0825	0.0730
AKG348 (M2)	0.1645	0.1818	0.1831	0.1727	0.1759	0.1650	0.1797	0.1788	0.1747	0.1714
AKG349 (M3)	0.1064	0.1049	0.1130	0.1011	0.1133	0.1066	0.1020	0.1130	0.1014	0.1091
AKG350 (M4)	0.1941	0.1548	0.1592	0.1741	0.1760	0.1890	0.1507	0.1648	0.1690	0.1796
AKG351 (M5)	0.1829	0.1275	0.1284	0.1474	0.1673	0.1794	0.1227	0.1352	0.1421	0.1692
AKG352 (M6)	0.0447	0.0304	0.0311	0.0357	0.0408	0.0434	0.0301	0.0327	0.0341	0.0411
AKG353 (M7)	0.0146	0.0094	0.0096	0.0111	0.0135	0.0140	0.0093	0.0100	0.0103	0.0136
Mal391 (M0)	0.1850	0.2373	0.2159	0.2068	0.2067	0.1960	0.2509	0.2171	0.2221	0.1993
Mal392 (M1)	0.1404	0.1620	0.1537	0.1436	0.1555	0.1480	0.1730	0.1570	0.1531	0.1460
Mal393 (M2)	0.2717	0.2651	0.2753	0.2779	0.2579	0.2658	0.2597	0.2761	0.2715	0.2621
Mal394 (M3)	0.2772	0.2333	0.2460	0.2574	0.2603	0.2700	0.2201	0.2426	0.2453	0.2688
Mal395 (M4)	0.0929	0.0759	0.0812	0.0851	0.0873	0.0884	0.0719	0.0798	0.0799	0.0909
Mal396 (M5)	0.0328	0.0264	0.0279	0.0292	0.0323	0.0319	0.0245	0.0275	0.0282	0.0329
Mal419 (M0)	0.1781	0.2288	0.2039	0.1976	0.1983	0.1885	0.2408	0.2062	0.2127	0.1905
Mal420 (M1)	0.0947	0.1175	0.1088	0.1016	0.1037	0.1008	0.1257	0.1118	0.1100	0.0990
Mal421 (M2)	0.1795	0.1873	0.1829	0.1778	0.1818	0.1863	0.1946	0.1894	0.1858	0.1752
Mal422 (M3)	0.2643	0.2365	0.2624	0.2672	0.2467	0.2451	0.2186	0.2535	0.2468	0.2618
Mal423 (M4)	0.1920	0.1569	0.1638	0.1731	0.1827	0.1902	0.1506	0.1622	0.1666	0.1850
Mal424 (M5)	0.0682	0.0552	0.0593	0.0624	0.0644	0.0661	0.0523	0.0581	0.0587	0.0662
Mal425 (M6)	0.0234	0.0180	0.0192	0.0204	0.0224	0.0233	0.0176	0.0190	0.0195	0.0226
Asp390 (M0)	0.3268	0.3922	0.3543	0.3593	0.2899	0.3424	0.3794	0.3514	0.3786	0.2737
Asp391 (M1)	0.1618	0.1859	0.1750	0.1694	0.1663	0.1696	0.1885	0.1763	0.1781	0.1568
Asp392 (M2)	0.2206	0.2030	0.2200	0.2178	0.2303	0.2128	0.2078	0.2211	0.2093	0.2383
Asp393 (M3)	0.1985	0.1505	0.1710	0.1729	0.2137	0.1883	0.1538	0.1718	0.1602	0.2253
Asp394 (M4)	0.0675	0.0509	0.0590	0.0594	0.0729	0.0637	0.0522	0.0588	0.0546	0.0772
Asp395 (M5)	0.0247	0.0175	0.0208	0.0212	0.0269	0.0232	0.0183	0.0207	0.0192	0.0287

Table D.9 continued

Asp418 (M0)	0.3201	0.3856	0.3465	0.3521	0.2821	0.3362	0.3719	0.3434	0.3722	0.2664
Asp419 (M1)	0.1369	0.1616	0.1495	0.1472	0.1295	0.1436	0.1609	0.1498	0.1553	0.1230
Asp420 (M2)	0.1583	0.1597	0.1600	0.1548	0.1698	0.1613	0.1675	0.1652	0.1582	0.1660
Asp421 (M3)	0.1901	0.1535	0.1834	0.1821	0.2044	0.1722	0.1532	0.1798	0.1627	0.2209
Asp422 (M4)	0.1324	0.0963	0.1091	0.1113	0.1458	0.1277	0.1005	0.1102	0.1036	0.1514
Asp423 (M5)	0.0466	0.0331	0.0393	0.0398	0.0512	0.0440	0.0347	0.0392	0.0364	0.0542
Asp424 (M6)	0.0155	0.0101	0.0122	0.0126	0.0172	0.0149	0.0113	0.0123	0.0116	0.0180
PEP453 (M0)	0.3508	0.3496	0.3327	0.2567	0.4117	0.3589	0.3499	0.3333	0.2651	0.3997
PEP454 (M1)	0.1670	0.1777	0.1722	0.1567	0.1856	0.1727	0.1796	0.1729	0.1678	0.1821
PEP455 (M2)	0.2077	0.2116	0.2162	0.2407	0.1877	0.2055	0.2116	0.2177	0.2407	0.1924
PEP456 (M3)	0.1888	0.1794	0.1907	0.2351	0.1494	0.1815	0.1775	0.1889	0.2226	0.1567
PEP457 (M4)	0.0629	0.0600	0.0644	0.0803	0.0483	0.0599	0.0597	0.0639	0.0758	0.0510
PEP458 (M5)	0.0229	0.0216	0.0239	0.0304	0.0172	0.0215	0.0217	0.0234	0.0281	0.0181
Glu330 (M0)	0.2351	0.3128	0.2957	0.2864	0.2530	0.2411	0.3232	0.2877	0.2950	0.2566
Glu331 (M1)	0.0801	0.1059	0.1067	0.0949	0.0888	0.0819	0.1076	0.1034	0.0975	0.0884
Glu332 (M2)	0.1807	0.1944	0.2007	0.1859	0.1921	0.1804	0.1911	0.1976	0.1866	0.1886
Glu333 (M3)	0.1304	0.1222	0.1240	0.1187	0.1474	0.1316	0.1178	0.1224	0.1181	0.1370
Glu334 (M4)	0.2799	0.1986	0.2047	0.2355	0.2384	0.2733	0.1953	0.2167	0.2272	0.2465
Glu335 (M5)	0.0687	0.0488	0.0503	0.0577	0.0593	0.0672	0.0480	0.0531	0.0556	0.0611
Glu336 (M6)	0.0251	0.0173	0.0179	0.0209	0.0209	0.0245	0.0171	0.0190	0.0201	0.0219
Glu432 (M0)	0.2057	0.2761	0.2601	0.2519	0.2224	0.2116	0.2855	0.2532	0.2595	0.2247
Glu433 (M1)	0.0830	0.1109	0.1084	0.1006	0.0911	0.0852	0.1140	0.1053	0.1035	0.0916
Glu434 (M2)	0.1584	0.1774	0.1781	0.1682	0.1714	0.1588	0.1757	0.1734	0.1696	0.1677
Glu435 (M3)	0.1109	0.1110	0.1181	0.1071	0.1184	0.1107	0.1079	0.1176	0.1071	0.1143
Glu436 (M4)	0.1824	0.1450	0.1508	0.1625	0.1650	0.1777	0.1420	0.1560	0.1581	0.1671
Glu437 (M5)	0.1761	0.1220	0.1255	0.1422	0.1575	0.1735	0.1189	0.1321	0.1372	0.1591
Glu438 (M6)	0.0608	0.0423	0.0435	0.0496	0.0540	0.0600	0.0412	0.0458	0.0477	0.0550
Glu439 (M7)	0.0228	0.0154	0.0158	0.0182	0.0203	0.0227	0.0150	0.0167	0.0175	0.0207
DHAP484 (M0)	0.3502	0.3588	0.3488	0.2469	0.4297	0.3610	0.3575	0.3381	0.2492	0.4148
DHAP485 (M1)	0.1889	0.1962	0.1895	0.1740	0.2015	0.1905	0.1973	0.1905	0.1883	0.1975
DHAP486 (M2)	0.2011	0.2038	0.2097	0.2439	0.1777	0.1999	0.2061	0.2141	0.2471	0.1839
DHAP487 (M3)	0.1699	0.1604	0.1697	0.2251	0.1292	0.1640	0.1594	0.1724	0.2134	0.1375
DHAP488 (M4)	0.0652	0.0595	0.0602	0.0811	0.0462	0.0620	0.0586	0.0615	0.0757	0.0485
DHAP489 (M5)	0.0246	0.0213	0.0221	0.0289	0.0157	0.0226	0.0210	0.0234	0.0264	0.0178
Gln431 (M0)	0.6221	0.6194	0.6231	0.6227	0.6233	0.6227	0.6169	0.6232	0.6245	0.6219
Gln432 (M1)	0.2297	0.2291	0.2308	0.2311	0.2306	0.2298	0.2287	0.2309	0.2307	0.2303
Gln433 (M3)	0.1069	0.1079	0.1074	0.1074	0.1071	0.1070	0.1084	0.1073	0.1070	0.1074

Table D.9 continued

Gln434 (M4)	0.0269	0.0277	0.0270	0.0267	0.0267	0.0268	0.0282	0.0269	0.0266	0.0270
Gln435 (M5)	0.0089	0.0098	0.0080	0.0081	0.0081	0.0087	0.0106	0.0080	0.0078	0.0085
Gln436 (M6)	0.0040	0.0045	0.0028	0.0030	0.0031	0.0037	0.0052	0.0028	0.0026	0.0036
Gln437 (M7)	0.0012	0.0014	0.0008	0.0008	0.0009	0.0011	0.0016	0.0008	0.0007	0.0010
Gln438 (M8)	0.0004	0.0005	0.0003	0.0003	0.0003	0.0004	0.0006	0.0002	0.0002	0.0004
GLP571 (M0)	0.4770	0.4580	0.4572	0.4298	0.4795	0.4836	0.4557	0.4598	0.4336	0.4827
GLP572 (M1)	0.2321	0.2287	0.2291	0.2199	0.2363	0.2337	0.2276	0.2286	0.2221	0.2356
GLP573 (M2)	0.1590	0.1659	0.1669	0.1735	0.1589	0.1573	0.1661	0.1655	0.1731	0.1578
GLP574 (M3)	0.0870	0.0961	0.0957	0.1137	0.0832	0.0833	0.0978	0.0953	0.1103	0.0824
GLP575 (M4)	0.0331	0.0375	0.0374	0.0456	0.0313	0.0312	0.0384	0.0372	0.0441	0.0308
GLP576 (M5)	0.0117	0.0138	0.0137	0.0175	0.0109	0.0109	0.0144	0.0136	0.0168	0.0107
Cit431 (M0)	0.1084	0.1632	0.1391	0.1209	0.1103	0.1164	0.1716	0.1363	0.1338	0.1000
Cit432 (M1)	0.0548	0.0784	0.0742	0.0606	0.0573	0.0573	0.0816	0.0743	0.0659	0.0528
Cit433 (M2)	0.1787	0.2030	0.2010	0.1917	0.1872	0.1810	0.2073	0.2009	0.1955	0.1856
Cit434 (M3)	0.1432	0.1463	0.1556	0.1448	0.1499	0.1438	0.1462	0.1571	0.1453	0.1484
Cit435 (M4)	0.2136	0.1828	0.1931	0.2105	0.2036	0.2071	0.1779	0.1939	0.2016	0.2123
Cit436 (M5)	0.2035	0.1524	0.1600	0.1831	0.1973	0.1988	0.1451	0.1603	0.1739	0.2039
Cit437 (M6)	0.0709	0.0542	0.0563	0.0647	0.0684	0.0693	0.0515	0.0565	0.0616	0.0703
Cit438 (M7)	0.0269	0.0196	0.0207	0.0237	0.0261	0.0264	0.0188	0.0206	0.0225	0.0267
Cit459 (M0)	0.1022	0.1554	0.1331	0.1159	0.1047	0.1096	0.1627	0.1314	0.1283	0.0942
Cit460 (M1)	0.0467	0.0696	0.0635	0.0525	0.0487	0.0500	0.0729	0.0634	0.0580	0.0448
Cit461 (M2)	0.1640	0.1899	0.1823	0.1751	0.1733	0.1684	0.1960	0.1828	0.1818	0.1707
Cit462 (M3)	0.1152	0.1254	0.1353	0.1199	0.1195	0.1172	0.1263	0.1365	0.1215	0.1178
Cit463 (M4)	0.1844	0.1653	0.1694	0.1745	0.1758	0.1856	0.1658	0.1749	0.1754	0.1755
Cit464 (M5)	0.2123	0.1656	0.1787	0.2013	0.2030	0.2013	0.1552	0.1758	0.1860	0.2125
Cit465 (M6)	0.1176	0.0866	0.0922	0.1075	0.1175	0.1131	0.0815	0.0906	0.1000	0.1235
Cit466 (M7)	0.0434	0.0317	0.0341	0.0399	0.0431	0.0413	0.0293	0.0332	0.0367	0.0457
Cit467 (M8)	0.0141	0.0106	0.0115	0.0134	0.0144	0.0136	0.0102	0.0112	0.0125	0.0152
3PG585 (M0)	0.3206	0.3186	0.3028	0.2310	0.3733	0.3267	0.3154	0.3028	0.2377	0.3621
3PG586 (M1)	0.1890	0.1971	0.1909	0.1707	0.2102	0.1954	0.1979	0.1913	0.1811	0.2065
3PG587 (M2)	0.2144	0.2193	0.2227	0.2448	0.1976	0.2130	0.2194	0.2239	0.2461	0.2018
3PG588 (M3)	0.1934	0.1865	0.1987	0.2462	0.1557	0.1861	0.1871	0.1977	0.2337	0.1626
3PG589 (M4)	0.0827	0.0784	0.0849	0.1072	0.0633	0.0789	0.0802	0.0844	0.1014	0.0670

Table D.10 Mass isotopomer distributions of media glucose and glycerol at [U-^{13}C]lactate (Flask #1 in triplicates). They were measured by aldonitrile pentapropionate derivatization and GC-MS. (data not corrected for natural isotope abundances)

	Con	Dex	Dib	8Br	Ins
Isotopomer	Flask #1	Flask #1	Flask #1	Flask #1	Flask #1
Glyc173 (M0)	0.8758	0.8627	0.8625	0.8676	-
Glyc174 (M1)	0.0893	0.0928	0.0933	0.0916	-
Glyc175 (M2)	0.0319	0.0405	0.0403	0.0373	-
Glyc176 (M3)	0.0026	0.0033	0.0033	0.0030	-
Glyc177 (M4)	0.0004	0.0007	0.0005	0.0005	-
Gluc173 (M0)	0.5347	0.5103	0.5094	0.4417	0.5831
Gluc174 (M1)	0.1639	0.1689	0.1693	0.1796	0.1633
Gluc175 (M2)	0.2778	0.2967	0.2967	0.3498	0.2327
Gluc176 (M3)	0.0201	0.0209	0.0212	0.0248	0.0175
Gluc177 (M4)	0.0035	0.0033	0.0034	0.0041	0.0035
Gluc370 (M0)	0.2478	0.2225	0.2228	0.1704	0.2953
Gluc371 (M1)	0.2317	0.2225	0.2249	0.2014	0.2494
Gluc372 (M2)	0.2556	0.2610	0.2631	0.2652	0.2419
Gluc373 (M3)	0.1563	0.1696	0.1679	0.1963	0.1325
Gluc374 (M4)	0.0764	0.0866	0.0849	0.1128	0.0583
Gluc375 (M5)	0.0276	0.0321	0.0310	0.0460	0.0193
Gluc376 (M6)	0.0040	0.0049	0.0046	0.0069	0.0028
Gluc377 (M7)	0.0006	0.0008	0.0007	0.0011	0.0005

Triplicate experiments at each condition were analyzed by aldonitrile pentapropionate derivatization and GC-MS. Only first flak set in triplicates was shown in this table. The measurement error of mass isotopomer distribution by MS analysis was less than 0.2 mo% and flask-to-flask error of mass isotopomer distributions in triplicates was less than 1.4 mol%. (Glyc173, glycerol at *m/z* 173)

Table D.11 Mass isotopomer distributions of media glucose and glycerol at [U-^{13}C]lactate (Flask #2 and #3 in triplicates). They were measured by aldonitrile pentapropionate derivatization and GC-MS and used for MID analysis. (data not corrected for natural isotope abundances)

	Con	Dex	Dib	8Br	Ins	Con	Dex	Dib	8Br	Ins
Isotopomer	Flask #2	Flask #2	Flask #2	Flask #2	Flask #2	Flask #3	Flask #3	Flask #3	Flask #3	Flask #3
Glyc173 (M0)	0.8765	0.8674	0.8639	0.8679	-	0.8784	0.8602	0.8596	0.8701	-
Glyc174 (M1)	0.0887	0.0916	0.0934	0.0914	-	0.0883	0.0937	0.0942	0.0908	-
Glyc175 (M2)	0.0318	0.0373	0.0390	0.0371	-	0.0304	0.0420	0.0423	0.0359	-
Glyc176 (M3)	0.0026	0.0031	0.0032	0.0030	-	0.0025	0.0035	0.0034	0.0028	-
Glyc177 (M4)	0.0004	0.0005	0.0005	0.0005	-	0.0003	0.0006	0.0005	0.0004	-
Gluc173 (M0)	0.5250	0.5193	0.5154	0.4375	0.5877	0.5281	0.5016	0.5026	0.4428	0.5687
Gluc174 (M1)	0.1624	0.1707	0.1714	0.1775	0.1656	0.1640	0.1696	0.1678	0.1790	0.1599
Gluc175 (M2)	0.2884	0.2866	0.2893	0.3556	0.2264	0.2841	0.3038	0.3043	0.3491	0.2491
Gluc176 (M3)	0.0207	0.0202	0.0206	0.0253	0.0169	0.0203	0.0215	0.0218	0.0251	0.0186
Gluc177 (M4)	0.0035	0.0032	0.0033	0.0042	0.0033	0.0035	0.0035	0.0035	0.0041	0.0038
Gluc370 (M0)	0.2396	0.2369	0.2336	0.1668	0.3006	0.2431	0.2181	0.2219	0.1701	0.2749
Gluc371 (M1)	0.2269	0.2268	0.2259	0.1987	0.2516	0.2277	0.2197	0.2242	0.1995	0.2426
Gluc372 (M2)	0.2590	0.2576	0.2604	0.2626	0.2421	0.2579	0.2623	0.2621	0.2634	0.2504
Gluc373 (M3)	0.1613	0.1628	0.1629	0.1993	0.1289	0.1601	0.1721	0.1679	0.1973	0.1426
Gluc374 (M4)	0.0793	0.0812	0.0822	0.1163	0.0558	0.0783	0.0887	0.0863	0.1148	0.0642
Gluc375 (M5)	0.0289	0.0296	0.0298	0.0479	0.0180	0.0283	0.0333	0.0320	0.0469	0.0218
Gluc376 (M6)	0.0041	0.0044	0.0045	0.0072	0.0026	0.0040	0.0049	0.0049	0.0070	0.0031
Gluc377 (M7)	0.0007	0.0007	0.0007	0.0012	0.0004	0.0007	0.0008	0.0008	0.0011	0.0005

Table D.12 Mass isotopomer distributions of intracellular metabolites at [U-^{13}C]glutamine experiments (Flask #1 in triplicates). They were measured by MOX-TBDMS derivatization and GC-MS and used for MID analysis and flux estimation. (data not corrected for natural isotope abundances)

	Con	Dex	Dib	8Br	Ins
Isotopomer	Flask #1	Flask #1	Flask #1	Flask #1	Flask #1
Pyr174 (M0)	0.8283	0.7919	0.7804	0.8243	0.7840
Pyr175 (M1)	0.1083	0.1410	0.1522	0.1082	0.1476
Pyr176 (M2)	0.0454	0.0478	0.0486	0.0457	0.0489
Pyr177 (M3)	0.0156	0.0158	0.0152	0.0190	0.0169
Pyr178 (M4)	0.0017	0.0028	0.0028	0.0022	0.0021
Pyr179 (M5)	0.0006	0.0008	0.0009	0.0008	0.0006
Lact233 (M0)	0.7471	0.7430	0.7433	0.7495	0.7378
Lact234 (M1)	0.1630	0.1638	0.1632	0.1621	0.1643
Lact235 (M2)	0.0760	0.0781	0.0784	0.0747	0.0817
Lact236 (M3)	0.0114	0.0120	0.0121	0.0112	0.0129
Lact237 (M4)	0.0025	0.0031	0.0031	0.0025	0.0033
Lact261 (M0)	0.7306	0.7011	0.7004	0.7326	0.6997
Lact262 (M1)	0.1691	0.1619	0.1595	0.1671	0.1628
Lact263 (M2)	0.0753	0.0808	0.0802	0.0743	0.0810
Lact264 (M3)	0.0183	0.0194	0.0201	0.0172	0.0229
Lact265 (M4)	0.0054	0.0288	0.0311	0.0070	0.0262
Lact266 (M5)	0.0015	0.0082	0.0089	0.0020	0.0075
Ala232 (M0)	0.7422	0.7406	0.7433	0.7464	0.7366
Ala233 (M1)	0.1669	0.1686	0.1667	0.1658	0.1683
Ala234 (M2)	0.0767	0.0766	0.0758	0.0742	0.0798
Ala235 (M3)	0.0118	0.0118	0.0117	0.0113	0.0125
Ala236 (M4)	0.0025	0.0025	0.0025	0.0023	0.0028
Ala260 (M0)	0.7327	0.7319	0.7339	0.7360	0.7276
Ala261 (M1)	0.1710	0.1721	0.1705	0.1703	0.1713
Ala262 (M2)	0.0743	0.0743	0.0732	0.0727	0.0748
Ala263 (M3)	0.0179	0.0176	0.0181	0.0171	0.0212
Ala264 (M4)	0.0035	0.0034	0.0035	0.0033	0.0041
Ala265 (M5)	0.0008	0.0008	0.0008	0.0007	0.0011
Gly218 (M0)	0.7325	0.7163	0.7226	0.7145	0.7335
Gly219 (M1)	0.1854	0.1988	0.1942	0.2009	0.1852
Gly220 (M2)	0.0705	0.0722	0.0710	0.0717	0.0698
Gly221 (M3)	0.0116	0.0127	0.0122	0.0128	0.0115

Table D.12 continued

Gly246 (M0)	0.7238	0.7055	0.7113	0.7022	0.7218
Gly247 (M1)	0.1660	0.1684	0.1674	0.1682	0.1666
Gly248 (M2)	0.0914	0.1035	0.0998	0.1061	0.0924
Gly249 (M3)	0.0150	0.0177	0.0169	0.0183	0.0153
Gly250 (M4)	0.0039	0.0050	0.0047	0.0052	0.0040
Pro258 (M0)	0.6430	0.6248	0.6287	0.6294	0.5941
Pro259 (M1)	0.1709	0.1772	0.1717	0.1679	0.1805
Pro260 (M2)	0.0925	0.0930	0.0945	0.0932	0.1035
Pro261 (M3)	0.0189	0.0208	0.0205	0.0205	0.0244
Pro262 (M4)	0.0602	0.0669	0.0675	0.0706	0.0772
Pro263 (M5)	0.0104	0.0125	0.0123	0.0132	0.0145
Pro264 (M6)	0.0040	0.0050	0.0048	0.0052	0.0057
Pro286 (M0)	0.6393	0.6796	0.6820	0.6245	0.6547
Pro287 (M1)	0.1715	0.1707	0.1713	0.1682	0.1705
Pro288 (M2)	0.0780	0.0702	0.0703	0.0776	0.0741
Pro289 (M3)	0.0326	0.0234	0.0234	0.0349	0.0310
Pro290 (M4)	0.0095	0.0064	0.0060	0.0108	0.0088
Pro291 (M5)	0.0559	0.0396	0.0376	0.0670	0.0486
Pro292 (M6)	0.0095	0.0072	0.0068	0.0123	0.0088
Pro293 (M7)	0.0040	0.0031	0.0029	0.0050	0.0037
Suc289 (M0)	0.5314	0.4866	0.5013	0.4995	0.4877
Suc290 (M1)	0.1602	0.1493	0.1555	0.1505	0.1622
Suc291 (M2)	0.1189	0.1220	0.1227	0.1184	0.1304
Suc292 (M3)	0.0297	0.0339	0.0330	0.0315	0.0357
Suc293 (M4)	0.1282	0.1640	0.1486	0.1598	0.1454
Suc294 (M5)	0.0226	0.0310	0.0271	0.0285	0.0268
Suc295 (M6)	0.0091	0.0132	0.0117	0.0119	0.0118
Fum287 (M0)	0.5970	0.5727	0.5837	0.5739	0.5668
Fum288 (M1)	0.1704	0.1666	0.1701	0.1648	0.1717
Fum289 (M2)	0.1027	0.1065	0.1055	0.1041	0.1098
Fum290 (M3)	0.0460	0.0571	0.0536	0.0489	0.0550
Fum291 (M4)	0.0657	0.0754	0.0679	0.0849	0.0751
Fum292 (M5)	0.0133	0.0159	0.0140	0.0169	0.0157
Fum293 (M6)	0.0048	0.0058	0.0051	0.0065	0.0058
Ser302 (M0)	0.6659	0.6543	0.6570	0.6495	0.6523
Ser303 (M1)	0.1870	0.1888	0.1890	0.1900	0.1847
Ser304 (M2)	0.1170	0.1230	0.1211	0.1255	0.1340
Ser305 (M3)	0.0240	0.0260	0.0257	0.0267	0.0221

Table D.12 continued

Ser306 (M4)	0.0061	0.0079	0.0072	0.0083	0.0068
Ser362 (M0)	0.5978	0.5710	0.5783	0.5624	0.5991
Ser363 (M1)	0.2448	0.2560	0.2536	0.2570	0.2444
Ser364 (M2)	0.1191	0.1284	0.1254	0.1335	0.1183
Ser365 (M3)	0.0307	0.0353	0.0339	0.0371	0.0305
Ser366 (M4)	0.0077	0.0094	0.0089	0.0101	0.0078
Ser390 (M0)	0.5880	0.5616	0.5682	0.5515	0.5885
Ser391 (M1)	0.2350	0.2394	0.2391	0.2399	0.2349
Ser392 (M2)	0.1221	0.1304	0.1284	0.1325	0.1222
Ser393 (M3)	0.0412	0.0502	0.0473	0.0555	0.0408
Ser394 (M4)	0.0112	0.0145	0.0135	0.0162	0.0110
Ser395 (M5)	0.0026	0.0039	0.0035	0.0045	0.0026
AKG346 (M0)	0.4974	0.4625	0.4806	0.4673	0.4659
AKG347 (M1)	0.1577	0.1471	0.1539	0.1476	0.1578
AKG348 (M2)	0.0906	0.0886	0.0912	0.0861	0.0948
AKG349 (M3)	0.0631	0.0661	0.0651	0.0652	0.0718
AKG350 (M4)	0.0224	0.0248	0.0236	0.0242	0.0256
AKG351 (M5)	0.1309	0.1633	0.1440	0.1627	0.1427
AKG352 (M6)	0.0265	0.0329	0.0290	0.0327	0.0288
AKG353 (M7)	0.0115	0.0146	0.0126	0.0142	0.0126
Mal391 (M0)	0.5368	0.5101	0.5212	0.5146	0.5083
Mal392 (M1)	0.2140	0.2090	0.2124	0.2083	0.2147
Mal393 (M2)	0.1241	0.1327	0.1315	0.1248	0.1317
Mal394 (M3)	0.0909	0.1056	0.0965	0.1094	0.1038
Mal395 (M4)	0.0250	0.0310	0.0279	0.0304	0.0302
Mal396 (M5)	0.0092	0.0116	0.0105	0.0125	0.0113
Mal419 (M0)	0.5135	0.4920	0.5024	0.4920	0.4896
Mal420 (M1)	0.2046	0.1984	0.2025	0.1971	0.2030
Mal421 (M2)	0.1264	0.1285	0.1285	0.1261	0.1315
Mal422 (M3)	0.0583	0.0693	0.0657	0.0613	0.0666
Mal423 (M4)	0.0679	0.0774	0.0702	0.0859	0.0759
Mal424 (M5)	0.0208	0.0243	0.0218	0.0263	0.0236
Mal425 (M6)	0.0086	0.0103	0.0090	0.0114	0.0100
Asp390 (M0)	0.5572	0.5410	0.5418	0.5444	0.5323
Asp391 (M1)	0.2159	0.2126	0.2142	0.2117	0.2152
Asp392 (M2)	0.1208	0.1269	0.1270	0.1217	0.1264
Asp393 (M3)	0.0759	0.0838	0.0823	0.0866	0.0886
Asp394 (M4)	0.0226	0.0263	0.0256	0.0262	0.0276

Table D.12 continued

Asp395 (M5)	0.0077	0.0094	0.0091	0.0096	0.0099
Asp418 (M0)	0.5458	0.5309	0.5309	0.5326	0.5203
Asp419 (M1)	0.2113	0.2071	0.2087	0.2067	0.2086
Asp420 (M2)	0.1204	0.1223	0.1233	0.1202	0.1254
Asp421 (M3)	0.0511	0.0586	0.0584	0.0530	0.0588
Asp422 (M4)	0.0504	0.0565	0.0549	0.0613	0.0606
Asp423 (M5)	0.0153	0.0177	0.0172	0.0189	0.0188
Asp424 (M6)	0.0058	0.0072	0.0067	0.0075	0.0076
PEP453 (M0)	0.5762	0.5448	0.5608	0.5299	0.5848
PEP454 (M1)	0.2154	0.2112	0.2132	0.2103	0.2165
PEP455 (M2)	0.1205	0.1271	0.1244	0.1280	0.1183
PEP456 (M3)	0.0629	0.0820	0.0716	0.0923	0.0559
PEP457 (M4)	0.0175	0.0251	0.0211	0.0280	0.0157
PEP458 (M5)	0.0075	0.0099	0.0089	0.0115	0.0088
Glu330 (M0)	0.4880	0.4474	0.4686	0.4542	0.4527
Glu331 (M1)	0.1731	0.1599	0.1682	0.1614	0.1723
Glu332 (M2)	0.1220	0.1226	0.1236	0.1207	0.1296
Glu333 (M3)	0.0356	0.0380	0.0372	0.0371	0.0397
Glu334 (M4)	0.1365	0.1742	0.1522	0.1703	0.1548
Glu335 (M5)	0.0322	0.0415	0.0360	0.0404	0.0366
Glu336 (M6)	0.0126	0.0163	0.0141	0.0159	0.0143
Glu432 (M0)	0.4286	0.3934	0.4124	0.3993	0.3962
Glu433 (M1)	0.1823	0.1681	0.1769	0.1698	0.1773
Glu434 (M2)	0.1085	0.1036	0.1075	0.1023	0.1099
Glu435 (M3)	0.0689	0.0706	0.0701	0.0698	0.0766
Gln435 (M4)	0.0292	0.0319	0.0305	0.0313	0.0333
Gln436 (M5)	0.1258	0.1595	0.1395	0.1564	0.1423
Gln437 (M6)	0.0388	0.0495	0.0431	0.0485	0.0439
Gln438 (M7)	0.0182	0.0234	0.0202	0.0228	0.0206
DHAP484 (M0)	0.5714	0.5378	0.5523	0.5259	0.5783
DHAP485 (M1)	0.2352	0.2249	0.2309	0.2277	0.2336
DHAP486 (M2)	0.1132	0.1283	0.1242	0.1264	0.1164
DHAP487 (M3)	0.0548	0.0771	0.0650	0.0825	0.0507
DHAP488 (M4)	0.0194	0.0241	0.0208	0.0283	0.0166
DHAP489 (M5)	0.0060	0.0079	0.0068	0.0093	0.0046
Gln431 (M0)	0.1683	0.1679	0.1615	0.1595	0.1657
Gln432 (M1)	0.0633	0.0635	0.0604	0.0596	0.0625
Gln433 (M2)	0.0299	0.0307	0.0284	0.0279	0.0300

Table D.12 continued

Gln434 (M3)	0.0100	0.0107	0.0089	0.0088	0.0104
Gln435 (M4)	0.0292	0.0300	0.0298	0.0297	0.0299
Gln436 (M5)	0.4761	0.4730	0.4830	0.4853	0.4766
Gln437 (M6)	0.1515	0.1520	0.1548	0.1555	0.1526
Gln438 (M7)	0.0717	0.0725	0.0734	0.0738	0.0724
GLP571 (M0)	0.5335	0.5197	0.5248	0.5141	0.5342
GLP572 (M1)	0.2502	0.2473	0.2484	0.2461	0.2506
GLP573 (M2)	0.1390	0.1413	0.1404	0.1419	0.1388
GLP574 (M3)	0.0543	0.0627	0.0596	0.0666	0.0538
GLP575 (M4)	0.0177	0.0217	0.0201	0.0233	0.0175
GLP576 (M5)	0.0052	0.0073	0.0065	0.0080	0.0051
Cit431 (M0)	0.4810	0.4479	0.4644	0.4644	0.4530
Cit432 (M1)	0.2065	0.1952	0.2017	0.2012	0.2050
Cit433 (M2)	0.1257	0.1255	0.1267	0.1248	0.1304
Cit434 (M3)	0.0832	0.0908	0.0851	0.0922	0.0920
Cit435 (M4)	0.0300	0.0342	0.0318	0.0335	0.0344
Cit436 (M5)	0.0509	0.0727	0.0623	0.0580	0.0597
Cit437 (M6)	0.0159	0.0234	0.0197	0.0182	0.0177
Cit438 (M7)	0.0068	0.0104	0.0084	0.0077	0.0077
Cit459 (M0)	0.4696	0.4374	0.4527	0.4515	0.4408
Cit460 (M1)	0.2011	0.1891	0.1956	0.1937	0.1979
Cit461 (M2)	0.1261	0.1232	0.1257	0.1242	0.1300
Cit462 (M3)	0.0659	0.0729	0.0703	0.0674	0.0740
Cit463 (M4)	0.0489	0.0533	0.0484	0.0584	0.0537
Cit464 (M5)	0.0580	0.0810	0.0703	0.0678	0.0678
Cit465 (M6)	0.0196	0.0272	0.0235	0.0235	0.0231
Cit466 (M7)	0.0083	0.0119	0.0103	0.0097	0.0098
Cit467 (M8)	0.0025	0.0041	0.0032	0.0038	0.0029
3PG585 (M0)	0.5015	0.4761	0.4877	0.4649	0.5055
3PG586 (M1)	0.2463	0.2402	0.2428	0.2388	0.2472
3PG587 (M2)	0.1487	0.1532	0.1527	0.1534	0.1492
3PG588 (M3)	0.0758	0.0942	0.0851	0.1031	0.0715
3PG589 (M4)	0.0276	0.0363	0.0316	0.0397	0.0266

Triplicate experiments at each condition were analyzed by MOX-TBDMS derivatization and GC-MS. The measurement error of mass isotopomer distribution by MS analysis was less than 0.2 mo% and flask-to-flask error of mass isotopomer distributions in triplicates was less than 0.8 mol%.

Table D.13 Mass isotopomer distributions of intracellular metabolites at [U-^{13}C]glutamine experiments (Flask #2 and #3 in triplicates). They were measured by MOX-TBDMS derivatization and GC-MS. (data not corrected for natural isotope abundances)

	Con	Dex	Dib	8Br	Ins	Con	Dex	Dib	8Br	Ins
isotopomer	Flask #2	Flask #2	Flask #2	Flask #2	Flask #2	Flask #3	Flask #3	Flask #3	Flask #3	Flask #3
Pyr174 (M0)	0.8302	0.8288	0.8324	0.8209	0.8277	0.8299	0.8311	0.8318	0.8194	0.8298
Pyr175 (M1)	0.1077	0.1071	0.1069	0.1083	0.1080	0.1077	0.1068	0.1070	0.1083	0.1075
Pyr176 (M2)	0.0448	0.0454	0.0446	0.0469	0.0453	0.0450	0.0448	0.0448	0.0472	0.0448
Pyr177 (M3)	0.0150	0.0163	0.0141	0.0207	0.0167	0.0151	0.0151	0.0144	0.0220	0.0157
Pyr178 (M4)	0.0016	0.0017	0.0016	0.0023	0.0018	0.0017	0.0016	0.0016	0.0024	0.0017
Pyr179 (M5)	0.0005	0.0006	0.0005	0.0008	0.0006	0.0005	0.0005	0.0005	0.0008	0.0005
Lact233 (M0)	0.7474	0.7440	0.7447	0.7463	0.7385	0.7471	0.7450	0.7430	0.7454	0.7384
Lact234 (M1)	0.1631	0.1632	0.1629	0.1631	0.1646	0.1634	0.1632	0.1636	0.1632	0.1646
Lact235 (M2)	0.0755	0.0778	0.0775	0.0764	0.0809	0.0756	0.0769	0.0784	0.0768	0.0809
Lact236 (M3)	0.0114	0.0120	0.0119	0.0115	0.0127	0.0114	0.0118	0.0121	0.0116	0.0127
Lact237 (M4)	0.0026	0.0031	0.0029	0.0027	0.0033	0.0025	0.0031	0.0030	0.0029	0.0033
Lact261 (M0)	0.7326	0.7047	0.7068	0.7297	0.7010	0.7306	0.7090	0.7002	0.7275	0.7030
Lact262 (M1)	0.1672	0.1614	0.1609	0.1674	0.1622	0.1689	0.1616	0.1616	0.1672	0.1624
Lact263 (M2)	0.0743	0.0797	0.0789	0.0751	0.0805	0.0753	0.0787	0.0810	0.0756	0.0802
Lact264 (M3)	0.0179	0.0190	0.0194	0.0183	0.0222	0.0179	0.0187	0.0199	0.0187	0.0224
Lact265 (M4)	0.0064	0.0275	0.0266	0.0074	0.0267	0.0058	0.0250	0.0291	0.0087	0.0250
Lact266 (M5)	0.0018	0.0078	0.0077	0.0022	0.0076	0.0017	0.0071	0.0083	0.0026	0.0072
Ala232 (M0)	0.7443	0.7415	0.7442	0.7418	0.7384	0.7445	0.7436	0.7419	0.7409	0.7379
Ala233 (M1)	0.1664	0.1682	0.1664	0.1673	0.1680	0.1663	0.1671	0.1676	0.1678	0.1676
Ala234 (M2)	0.0753	0.0762	0.0754	0.0766	0.0786	0.0752	0.0753	0.0763	0.0769	0.0792
Ala235 (M3)	0.0116	0.0117	0.0116	0.0118	0.0123	0.0116	0.0115	0.0117	0.0119	0.0125
Ala236 (M4)	0.0024	0.0025	0.0025	0.0025	0.0027	0.0024	0.0024	0.0025	0.0025	0.0028
Ala260 (M0)	0.7337	0.7335	0.7343	0.7324	0.7294	0.7334	0.7345	0.7320	0.7323	0.7279
Ala261 (M1)	0.1708	0.1715	0.1705	0.1710	0.1710	0.1708	0.1710	0.1716	0.1712	0.1710
Ala262 (M2)	0.0735	0.0736	0.0732	0.0737	0.0742	0.0737	0.0732	0.0741	0.0739	0.0745
Ala263 (M3)	0.0179	0.0173	0.0179	0.0185	0.0205	0.0179	0.0174	0.0181	0.0184	0.0214
Ala264 (M4)	0.0034	0.0033	0.0034	0.0036	0.0040	0.0034	0.0033	0.0035	0.0035	0.0042
Ala265 (M5)	0.0008	0.0008	0.0008	0.0008	0.0010	0.0008	0.0008	0.0008	0.0009	0.0011
Gly218 (M0)	0.7353	0.7162	0.7235	0.7103	0.7365	0.7357	0.7179	0.7214	0.7107	0.7339
Gly219 (M1)	0.1839	0.1991	0.1935	0.2040	0.1830	0.1837	0.1979	0.1949	0.2037	0.1851
Gly220 (M2)	0.0696	0.0720	0.0708	0.0725	0.0692	0.0693	0.0716	0.0714	0.0724	0.0696
Gly221 (M3)	0.0113	0.0128	0.0122	0.0132	0.0113	0.0113	0.0126	0.0123	0.0132	0.0114

Table D.13 continued

Gly246 (M0)	0.7238	0.7051	0.7123	0.6988	0.7237	0.7239	0.7061	0.7101	0.6982	0.7211
Gly247 (M1)	0.1662	0.1679	0.1671	0.1688	0.1665	0.1660	0.1679	0.1680	0.1692	0.1669
Gly248 (M2)	0.0912	0.1041	0.0993	0.1082	0.0912	0.0913	0.1034	0.1002	0.1086	0.0928
Gly249 (M3)	0.0150	0.0178	0.0168	0.0188	0.0149	0.0150	0.0177	0.0170	0.0188	0.0153
Gly250 (M4)	0.0039	0.0051	0.0046	0.0054	0.0038	0.0039	0.0050	0.0047	0.0054	0.0040
Pro258 (M0)	0.6422	0.6318	0.6290	0.6153	0.6107	0.6395	0.6264	0.6252	0.6151	0.5977
Pro259 (M1)	0.1714	0.1728	0.1716	0.1667	0.1710	0.1712	0.1764	0.1714	0.1663	0.1699
Pro260 (M2)	0.0928	0.0918	0.0943	0.0964	0.1007	0.0931	0.0926	0.0951	0.0964	0.1035
Pro261 (M3)	0.0196	0.0202	0.0207	0.0218	0.0231	0.0195	0.0206	0.0211	0.0219	0.0243
Pro262 (M4)	0.0594	0.0658	0.0668	0.0789	0.0749	0.0617	0.0662	0.0692	0.0793	0.0827
Pro263 (M5)	0.0106	0.0125	0.0125	0.0149	0.0140	0.0108	0.0127	0.0130	0.0150	0.0155
Pro264 (M6)	0.0042	0.0050	0.0049	0.0060	0.0056	0.0042	0.0050	0.0051	0.0061	0.0062
Pro286 (M0)	0.6400	0.6624	0.6605	0.6102	0.6507	0.6357	0.6552	0.6663	0.6093	0.6437
Pro287 (M1)	0.1717	0.1700	0.1709	0.1666	0.1712	0.1717	0.1696	0.1708	0.1664	0.1703
Pro288 (M2)	0.0780	0.0727	0.0733	0.0787	0.0751	0.0783	0.0733	0.0727	0.0788	0.0757
Pro289 (M3)	0.0327	0.0268	0.0280	0.0380	0.0317	0.0334	0.0288	0.0267	0.0383	0.0331
Pro290 (M4)	0.0091	0.0075	0.0078	0.0120	0.0091	0.0096	0.0083	0.0074	0.0122	0.0098
Pro291 (M5)	0.0553	0.0482	0.0474	0.0752	0.0494	0.0572	0.0511	0.0446	0.0753	0.0537
Pro292 (M6)	0.0094	0.0089	0.0086	0.0139	0.0091	0.0100	0.0095	0.0082	0.0141	0.0098
Pro293 (M7)	0.0039	0.0038	0.0036	0.0057	0.0038	0.0042	0.0045	0.0034	0.0058	0.0041
Suc289 (M0)	0.5302	0.4846	0.5022	0.4854	0.4975	0.5306	0.4801	0.4985	0.4894	0.4869
Suc290 (M1)	0.1604	0.1495	0.1554	0.1502	0.1628	0.1596	0.1494	0.1540	0.1531	0.1601
Suc291 (M2)	0.1184	0.1203	0.1222	0.1212	0.1267	0.1171	0.1200	0.1212	0.1201	0.1274
Suc292 (M3)	0.0302	0.0338	0.0328	0.0329	0.0345	0.0301	0.0341	0.0333	0.0326	0.0355
Suc293 (M4)	0.1285	0.1673	0.1487	0.1674	0.1416	0.1297	0.1705	0.1526	0.1634	0.1506
Suc294 (M5)	0.0230	0.0313	0.0270	0.0301	0.0259	0.0233	0.0321	0.0284	0.0291	0.0276
Suc295 (M6)	0.0093	0.0133	0.0118	0.0127	0.0110	0.0096	0.0138	0.0120	0.0122	0.0119
Fum287 (M0)	0.5948	0.5689	0.5812	0.5630	0.5708	0.5875	0.5579	0.5724	0.5593	0.5607
Fum288 (M1)	0.1707	0.1660	0.1697	0.1650	0.1718	0.1701	0.1653	0.1691	0.1642	0.1709
Fum289 (M2)	0.1030	0.1065	0.1059	0.1060	0.1086	0.1038	0.1086	0.1080	0.1072	0.1101
Fum290 (M3)	0.0465	0.0584	0.0541	0.0528	0.0550	0.0498	0.0642	0.0588	0.0540	0.0608
Fum291 (M4)	0.0665	0.0778	0.0696	0.0887	0.0730	0.0692	0.0810	0.0714	0.0905	0.0756
Fum292 (M5)	0.0135	0.0165	0.0144	0.0178	0.0152	0.0143	0.0170	0.0150	0.0182	0.0161
Fum293 (M6)	0.0049	0.0060	0.0051	0.0068	0.0056	0.0052	0.0061	0.0053	0.0067	0.0058
Ser302 (M0)	0.6774	0.6506	0.6604	0.6437	0.6639	0.6741	0.6554	0.6619	0.6419	0.6598
Ser303 (M1)	0.1895	0.1885	0.1892	0.1895	0.1853	0.1884	0.1903	0.1894	0.1899	0.1856
Ser304 (M2)	0.1062	0.1255	0.1209	0.1296	0.1223	0.1097	0.1237	0.1186	0.1309	0.1262
Ser305 (M3)	0.0205	0.0269	0.0223	0.0284	0.0224	0.0216	0.0234	0.0226	0.0289	0.0228

Table D.13 continued

Ser306 (M4)	0.0064	0.0085	0.0072	0.0087	0.0060	0.0062	0.0072	0.0075	0.0085	0.0056
Ser362 (M0)	0.5987	0.5695	0.5808	0.5552	0.6053	0.5980	0.5715	0.5790	0.5539	0.6008
Ser363 (M1)	0.2445	0.2566	0.2527	0.2580	0.2416	0.2450	0.2564	0.2541	0.2603	0.2435
Ser364 (M2)	0.1185	0.1290	0.1244	0.1375	0.1160	0.1187	0.1279	0.1246	0.1367	0.1178
Ser365 (M3)	0.0307	0.0355	0.0335	0.0386	0.0295	0.0307	0.0350	0.0337	0.0385	0.0302
Ser366 (M4)	0.0077	0.0095	0.0087	0.0108	0.0076	0.0078	0.0093	0.0088	0.0107	0.0078
Ser390 (M0)	0.5890	0.5596	0.5705	0.5442	0.5958	0.5882	0.5614	0.5694	0.5438	0.5910
Ser391 (M1)	0.2349	0.2397	0.2385	0.2404	0.2333	0.2351	0.2399	0.2394	0.2419	0.2345
Ser392 (M2)	0.1217	0.1311	0.1280	0.1338	0.1197	0.1218	0.1310	0.1284	0.1343	0.1211
Ser393 (M3)	0.0408	0.0508	0.0464	0.0592	0.0386	0.0410	0.0497	0.0463	0.0580	0.0401
Ser394 (M4)	0.0111	0.0148	0.0132	0.0174	0.0102	0.0112	0.0144	0.0131	0.0171	0.0107
Ser395 (M5)	0.0025	0.0040	0.0033	0.0051	0.0023	0.0026	0.0037	0.0033	0.0049	0.0025
AKG346 (M0)	0.4988	0.4592	0.4803	0.4563	0.4731	0.4950	0.4588	0.4788	0.4584	0.4638
AKG347 (M1)	0.1583	0.1454	0.1542	0.1468	0.1589	0.1571	0.1456	0.1533	0.1472	0.1570
AKG348 (M2)	0.0904	0.0872	0.0910	0.0874	0.0942	0.0900	0.0876	0.0909	0.0874	0.0947
AKG349 (M3)	0.0623	0.0654	0.0643	0.0680	0.0692	0.0624	0.0641	0.0638	0.0675	0.0696
AKG350 (M4)	0.0222	0.0248	0.0234	0.0254	0.0246	0.0225	0.0248	0.0235	0.0252	0.0253
AKG351 (M5)	0.1301	0.1689	0.1449	0.1676	0.1395	0.1340	0.1700	0.1472	0.1665	0.1471
AKG352 (M6)	0.0263	0.0341	0.0292	0.0337	0.0281	0.0271	0.0343	0.0296	0.0332	0.0297
AKG353 (M7)	0.0115	0.0150	0.0127	0.0148	0.0123	0.0119	0.0149	0.0129	0.0145	0.0129
Mal391 (M0)	0.5318	0.5067	0.5192	0.5034	0.5108	0.5272	0.4965	0.5107	0.5010	0.5022
Mal392 (M1)	0.2145	0.2086	0.2124	0.2085	0.2148	0.2131	0.2073	0.2117	0.2085	0.2138
Mal393 (M2)	0.1254	0.1335	0.1312	0.1274	0.1318	0.1270	0.1375	0.1353	0.1287	0.1343
Mal394 (M3)	0.0929	0.1080	0.0985	0.1149	0.1019	0.0963	0.1128	0.1016	0.1157	0.1068
Mal395 (M4)	0.0258	0.0313	0.0280	0.0326	0.0298	0.0267	0.0336	0.0296	0.0329	0.0314
Mal396 (M5)	0.0095	0.0119	0.0107	0.0131	0.0109	0.0098	0.0122	0.0112	0.0132	0.0115
Mal419 (M0)	0.5135	0.4886	0.5010	0.4815	0.4928	0.5068	0.4783	0.4927	0.4791	0.4840
Mal420 (M1)	0.2044	0.1977	0.2022	0.1958	0.2036	0.2032	0.1961	0.2010	0.1951	0.2019
Mal421 (M2)	0.1261	0.1284	0.1286	0.1279	0.1305	0.1266	0.1299	0.1301	0.1286	0.1314
Mal422 (M3)	0.0583	0.0704	0.0659	0.0647	0.0665	0.0615	0.0759	0.0706	0.0660	0.0719
Mal423 (M4)	0.0681	0.0795	0.0712	0.0903	0.0740	0.0709	0.0828	0.0735	0.0912	0.0768
Mal424 (M5)	0.0209	0.0250	0.0221	0.0277	0.0230	0.0219	0.0262	0.0230	0.0280	0.0241
Mal425 (M6)	0.0088	0.0105	0.0091	0.0123	0.0097	0.0092	0.0109	0.0094	0.0121	0.0101
Asp390 (M0)	0.5525	0.5376	0.5446	0.5302	0.5369	0.5473	0.5280	0.5371	0.5321	0.5274
Asp391 (M1)	0.2154	0.2112	0.2141	0.2110	0.2151	0.2147	0.2104	0.2130	0.2111	0.2140
Asp392 (M2)	0.1213	0.1273	0.1261	0.1246	0.1257	0.1229	0.1301	0.1293	0.1250	0.1287
Asp393 (M3)	0.0788	0.0858	0.0812	0.0945	0.0858	0.0818	0.0906	0.0849	0.0927	0.0909
Asp394 (M4)	0.0236	0.0282	0.0252	0.0289	0.0270	0.0247	0.0303	0.0264	0.0286	0.0288

Table D.13 continued

Asp395 (M5)	0.0083	0.0100	0.0089	0.0108	0.0096	0.0087	0.0107	0.0093	0.0106	0.0102
Asp418 (M0)	0.5404	0.5283	0.5336	0.5183	0.5256	0.5355	0.5203	0.5260	0.5209	0.5156
Asp419 (M1)	0.2106	0.2064	0.2093	0.2045	0.2095	0.2097	0.2053	0.2078	0.2047	0.2078
Asp420 (M2)	0.1212	0.1224	0.1227	0.1224	0.1242	0.1218	0.1240	0.1244	0.1221	0.1257
Asp421 (M3)	0.0522	0.0592	0.0577	0.0573	0.0582	0.0546	0.0623	0.0614	0.0578	0.0630
Asp422 (M4)	0.0533	0.0584	0.0538	0.0680	0.0577	0.0551	0.0611	0.0562	0.0660	0.0613
Asp423 (M5)	0.0162	0.0182	0.0167	0.0211	0.0179	0.0169	0.0191	0.0175	0.0205	0.0191
Asp424 (M6)	0.0063	0.0075	0.0064	0.0085	0.0071	0.0066	0.0080	0.0068	0.0082	0.0077
PEP453 (M0)	0.5756	0.5421	0.5620	0.5226	0.5873	0.5726	0.5392	0.5602	0.5217	0.5854
PEP454 (M1)	0.2156	0.2103	0.2136	0.2098	0.2166	0.2150	0.2097	0.2133	0.2100	0.2162
PEP455 (M2)	0.1208	0.1272	0.1240	0.1292	0.1178	0.1214	0.1281	0.1254	0.1298	0.1185
PEP456 (M3)	0.0633	0.0834	0.0708	0.0968	0.0542	0.0650	0.0843	0.0715	0.0967	0.0557
PEP457 (M4)	0.0180	0.0254	0.0207	0.0295	0.0152	0.0187	0.0256	0.0210	0.0295	0.0156
PEP458 (M5)	0.0068	0.0118	0.0088	0.0121	0.0089	0.0073	0.0130	0.0086	0.0124	0.0086
Glu330 (M0)	0.4879	0.4449	0.4685	0.4414	0.4622	0.4833	0.4430	0.4658	0.4437	0.4535
Glu331 (M1)	0.1731	0.1586	0.1679	0.1599	0.1737	0.1717	0.1579	0.1670	0.1601	0.1716
Glu332 (M2)	0.1213	0.1215	0.1222	0.1233	0.1280	0.1209	0.1202	0.1226	0.1227	0.1284
Glu333 (M3)	0.0355	0.0378	0.0369	0.0385	0.0388	0.0357	0.0377	0.0371	0.0382	0.0395
Glu334 (M4)	0.1371	0.1782	0.1538	0.1779	0.1485	0.1417	0.1812	0.1560	0.1767	0.1558
Glu335 (M5)	0.0325	0.0423	0.0364	0.0423	0.0351	0.0335	0.0431	0.0369	0.0420	0.0369
Glu336 (M6)	0.0127	0.0167	0.0143	0.0167	0.0137	0.0131	0.0169	0.0146	0.0165	0.0144
Glu432 (M0)	0.4297	0.3908	0.4124	0.3881	0.4056	0.4256	0.3897	0.4104	0.3903	0.3980
Glu433 (M1)	0.1826	0.1667	0.1768	0.1672	0.1801	0.1811	0.1661	0.1759	0.1678	0.1772
Glu434 (M2)	0.1082	0.1025	0.1072	0.1025	0.1105	0.1076	0.1021	0.1074	0.1027	0.1100
Glu435 (M3)	0.0681	0.0700	0.0691	0.0723	0.0745	0.0681	0.0688	0.0690	0.0717	0.0749
Gln435 (M4)	0.0289	0.0319	0.0303	0.0327	0.0321	0.0292	0.0317	0.0304	0.0324	0.0327
Gln436 (M5)	0.1257	0.1635	0.1406	0.1630	0.1359	0.1297	0.1660	0.1424	0.1617	0.1428
Gln437 (M6)	0.0389	0.0508	0.0435	0.0505	0.0419	0.0400	0.0515	0.0440	0.0501	0.0440
Gln438 (M7)	0.0183	0.0240	0.0204	0.0238	0.0196	0.0188	0.0243	0.0207	0.0236	0.0206
DHAP484 (M0)	0.5659	0.5401	0.5552	0.5178	0.5909	0.5640	0.5412	0.5509	0.5309	0.5900
DHAP485 (M1)	0.2389	0.2213	0.2312	0.2280	0.2265	0.2364	0.2192	0.2328	0.2191	0.2272
DHAP486 (M2)	0.1179	0.1274	0.1233	0.1272	0.1126	0.1196	0.1281	0.1243	0.1252	0.1132
DHAP487 (M3)	0.0544	0.0785	0.0638	0.0865	0.0491	0.0570	0.0789	0.0649	0.0851	0.0492
DHAP488 (M4)	0.0175	0.0246	0.0198	0.0302	0.0159	0.0177	0.0245	0.0204	0.0293	0.0155
DHAP489 (M5)	0.0055	0.0081	0.0067	0.0103	0.0050	0.0053	0.0080	0.0067	0.0104	0.0049
Gln431 (M0)	0.1651	0.1698	0.1613	0.1611	0.1629	0.1649	0.1719	0.1619	0.1617	0.1601
Gln432 (M1)	0.0619	0.0643	0.0602	0.0604	0.0612	0.0617	0.0652	0.0603	0.0605	0.0600
Gln433 (M2)	0.0291	0.0311	0.0281	0.0284	0.0294	0.0289	0.0317	0.0284	0.0285	0.0287

Table D.13 continued

Gln434 (M3)	0.0094	0.0112	0.0088	0.0092	0.0098	0.0091	0.0116	0.0088	0.0092	0.0094
Gln435 (M4)	0.0294	0.0298	0.0296	0.0298	0.0300	0.0293	0.0297	0.0298	0.0296	0.0301
Gln436 (M5)	0.4797	0.4714	0.4838	0.4825	0.4815	0.4800	0.4697	0.4824	0.4833	0.4850
Gln437 (M6)	0.1532	0.1510	0.1549	0.1550	0.1531	0.1534	0.1496	0.1549	0.1543	0.1541
Gln438 (M7)	0.0725	0.0716	0.0735	0.0736	0.0724	0.0728	0.0707	0.0737	0.0731	0.0728
GLP571 (M0)	0.5336	0.5194	0.5255	0.5146	0.5349	0.5347	0.5205	0.5271	0.5160	0.5351
GLP572 (M1)	0.2504	0.2469	0.2485	0.2462	0.2507	0.2503	0.2473	0.2485	0.2467	0.2508
GLP573 (M2)	0.1389	0.1412	0.1404	0.1418	0.1386	0.1386	0.1411	0.1401	0.1418	0.1386
GLP574 (M3)	0.0541	0.0632	0.0592	0.0663	0.0534	0.0537	0.0625	0.0584	0.0655	0.0534
GLP575 (M4)	0.0177	0.0218	0.0200	0.0232	0.0172	0.0175	0.0215	0.0196	0.0225	0.0172
GLP576 (M5)	0.0053	0.0074	0.0064	0.0080	0.0051	0.0052	0.0072	0.0062	0.0074	0.0050
Cit431 (M0)	0.4797	0.4445	0.4632	0.4545	0.4555	0.4728	0.4243	0.4553	0.4519	0.4477
Cit432 (M1)	0.2062	0.1940	0.2016	0.2008	0.2047	0.2040	0.1860	0.1989	0.1993	0.2033
Cit433 (M2)	0.1255	0.1249	0.1262	0.1273	0.1294	0.1257	0.1221	0.1273	0.1273	0.1316
Cit434 (M3)	0.0830	0.0910	0.0845	0.0981	0.0895	0.0848	0.0896	0.0859	0.0960	0.0923
Cit435 (M4)	0.0301	0.0346	0.0315	0.0359	0.0334	0.0309	0.0347	0.0325	0.0352	0.0350
Cit436 (M5)	0.0521	0.0760	0.0644	0.0578	0.0603	0.0563	0.0791	0.0682	0.0624	0.0622
Cit437 (M6)	0.0163	0.0243	0.0199	0.0182	0.0189	0.0177	0.0451	0.0222	0.0194	0.0193
Cit438 (M7)	0.0071	0.0108	0.0088	0.0075	0.0083	0.0077	0.0190	0.0097	0.0085	0.0086
Cit459 (M0)	0.4673	0.4334	0.4514	0.4423	0.4438	0.4594	0.4239	0.4439	0.4394	0.4346
Cit460 (M1)	0.2005	0.1877	0.1955	0.1927	0.1983	0.1986	0.1851	0.1933	0.1915	0.1961
Cit461 (M2)	0.1256	0.1224	0.1251	0.1268	0.1290	0.1256	0.1218	0.1250	0.1255	0.1298
Cit462 (M3)	0.0660	0.0730	0.0700	0.0703	0.0730	0.0681	0.0751	0.0721	0.0715	0.0761
Cit463 (M4)	0.0491	0.0535	0.0480	0.0636	0.0516	0.0500	0.0533	0.0478	0.0605	0.0532
Cit464 (M5)	0.0597	0.0848	0.0721	0.0674	0.0685	0.0643	0.0920	0.0774	0.0720	0.0724
Cit465 (M6)	0.0203	0.0282	0.0239	0.0237	0.0230	0.0218	0.0306	0.0255	0.0249	0.0243
Cit466 (M7)	0.0086	0.0126	0.0106	0.0096	0.0099	0.0092	0.0137	0.0114	0.0105	0.0105
Cit467 (M8)	0.0029	0.0043	0.0034	0.0036	0.0028	0.0030	0.0045	0.0035	0.0041	0.0030
3PG585 (M0)	0.5024	0.4741	0.4888	0.4583	0.5094	0.4996	0.4722	0.4885	0.4581	0.5085
3PG586 (M1)	0.2463	0.2394	0.2431	0.2381	0.2474	0.2449	0.2395	0.2426	0.2377	0.2475
3PG587 (M2)	0.1478	0.1538	0.1527	0.1544	0.1488	0.1491	0.1547	0.1526	0.1551	0.1481
3PG588 (M3)	0.0760	0.0956	0.0841	0.1076	0.0692	0.0777	0.0962	0.0846	0.1075	0.0701
3PG589 (M4)	0.0274	0.0371	0.0313	0.0416	0.0253	0.0287	0.0373	0.0317	0.0416	0.0258

Table D.14 Mass isotopomer distributions of media glucose and glycerol at [U-^{13}C]glutamine (Flask #1 in triplicates). They were measured by aldonitrile pentapropionate derivatization and GC-MS and used for MID analysis and flux estimation. (data not corrected for natural isotope abundances)

	Con	Dex	Dib	8Br	Ins
Isotopomer	Flask #1	Flask #1	Flask #1	Flask #1	Flask #1
Glyc173 (M0)	0.8971	0.8922	0.8926	0.8942	0.8985
Glyc174 (M1)	0.0837	0.0841	0.0847	0.0844	0.0832
Glyc175 (M2)	0.0171	0.0201	0.0201	0.0191	0.0162
Glyc176 (M3)	0.0020	0.0029	0.0023	0.0020	0.0017
Glyc177 (M4)	0.0002	0.0007	0.0003	0.0003	0.0003
Gluc173 (M0)	0.8112	0.7870	0.7846	0.7597	0.8209
Gluc174 (M1)	0.1063	0.1116	0.1120	0.1173	0.1034
Gluc175 (M2)	0.0755	0.0933	0.0951	0.1131	0.0674
Gluc176 (M3)	0.0058	0.0068	0.0070	0.0084	0.0060
Gluc177 (M4)	0.0012	0.0013	0.0013	0.0015	0.0023
Gluc259 (M0)	0.7639	0.7440	0.7409	0.7164	0.7644
Gluc260 (M1)	0.1275	0.1310	0.1314	0.1328	0.1268
Gluc261 (M2)	0.0529	0.0530	0.0557	0.0652	0.0551
Gluc262 (M3)	0.0492	0.0637	0.0638	0.0759	0.0454
Gluc263 (M4)	0.0055	0.0070	0.0070	0.0084	0.0064
Gluc264 (M5)	0.0010	0.0013	0.0012	0.0015	0.0019
Gluc284 (M0)	0.6573	0.6156	0.6159	0.5752	0.6670
Gluc285 (M1)	0.2297	0.2449	0.2448	0.2616	0.2247
Gluc286 (M2)	0.0777	0.0924	0.0939	0.1088	0.0747
Gluc287 (M3)	0.0222	0.0301	0.0304	0.0380	0.0200
Gluc288 (M4)	0.0044	0.0059	0.0061	0.0078	0.0040
Gluc289 (M5)	0.0031	0.0053	0.0034	0.0035	0.0036
Gluc290 (M6)	0.0057	0.0057	0.0056	0.0052	0.0060
Gluc370 (M0)	0.6154	0.5760	0.5728	0.5305	0.6292
Gluc371 (M1)	0.2178	0.2231	0.2245	0.2309	0.2164
Gluc372 (M2)	0.1204	0.1392	0.1403	0.1589	0.1121
Gluc373 (M3)	0.0355	0.0457	0.0461	0.0572	0.0320
Gluc374 (M4)	0.0087	0.0123	0.0125	0.0170	0.0079
Gluc375 (M5)	0.0020	0.0031	0.0032	0.0046	0.0019
Gluc376 (M6)	0.0003	0.0005	0.0005	0.0007	0.0003
Gluc377 (M7)	0.0001	0.0002	0.0001	0.0001	0.0001

Measurement error, <0.2 mo%; flask-to-flask error, <0.5 mol%

Table D.15 Mass isotopomer distributions of media glucose and glycerol at [U-^{13}C]glutamine (Flask #2 and #3 in triplicates). They were measured by aldonitrile pentapropionate derivatization and GC-MS and used for MID analysis. (data not corrected for natural isotope abundances)

	Con	Dex	Dib	8Br	Ins	Con	Dex	Dib	8Br	Ins
Isotopomer	Flask #2	Flask #2	Flask #2	Flask #2	Flask #2	Flask #3	Flask #3	Flask #3	Flask #3	Flask #3
Glyc173 (M0)	0.8980	0.8920	0.8935	0.8936	0.8974	0.8973	0.8922	0.8933	0.8936	0.8977
Glyc174 (M1)	0.0834	0.0847	0.0845	0.0845	0.0844	0.0836	0.0847	0.0845	0.0844	0.0838
Glyc175 (M2)	0.0167	0.0207	0.0196	0.0196	0.0164	0.0170	0.0205	0.0197	0.0196	0.0166
Glyc176 (M3)	0.0016	0.0023	0.0022	0.0020	0.0016	0.0019	0.0023	0.0022	0.0020	0.0017
Glyc177 (M4)	0.0002	0.0004	0.0003	0.0003	0.0003	0.0002	0.0003	0.0003	0.0003	0.0003
Gluc173 (M0)	0.8106	0.7832	0.7855	0.7614	0.8146	0.8113	0.7844	0.7845	0.7602	0.8090
Gluc174 (M1)	0.1066	0.1121	0.1116	0.1176	0.1060	0.1067	0.1121	0.1118	0.1177	0.1068
Gluc175 (M2)	0.0759	0.0960	0.0946	0.1113	0.0715	0.0750	0.0951	0.0953	0.1122	0.0756
Gluc176 (M3)	0.0057	0.0073	0.0070	0.0082	0.0059	0.0057	0.0071	0.0071	0.0083	0.0064
Gluc177 (M4)	0.0011	0.0015	0.0013	0.0015	0.0020	0.0012	0.0014	0.0013	0.0015	0.0023
Gluc259 (M0)	0.7699	0.7333	0.7410	0.7166	0.7580	0.7669	0.7294	0.7353	0.7187	0.7547
Gluc260 (M1)	0.1276	0.1285	0.1305	0.1323	0.1271	0.1276	0.1292	0.1317	0.1324	0.1269
Gluc261 (M2)	0.0480	0.0652	0.0567	0.0659	0.0614	0.0518	0.0672	0.0589	0.0644	0.0621
Gluc262 (M3)	0.0481	0.0644	0.0635	0.0753	0.0470	0.0475	0.0655	0.0654	0.0751	0.0499
Gluc263 (M4)	0.0055	0.0072	0.0071	0.0085	0.0056	0.0055	0.0073	0.0073	0.0081	0.0055
Gluc264 (M5)	0.0010	0.0013	0.0012	0.0014	0.0010	0.0008	0.0014	0.0013	0.0014	0.0009
Gluc284 (M0)	0.6553	0.6066	0.6184	0.5790	0.6574	0.6567	0.6158	0.6153	0.5765	0.6465
Gluc285 (M1)	0.2305	0.2480	0.2457	0.2615	0.2301	0.2296	0.2459	0.2458	0.2622	0.2360
Gluc286 (M2)	0.0786	0.0963	0.0917	0.1072	0.0782	0.0782	0.0926	0.0939	0.1079	0.0814
Gluc287 (M3)	0.0222	0.0327	0.0293	0.0366	0.0208	0.0220	0.0303	0.0302	0.0371	0.0223
Gluc288 (M4)	0.0043	0.0066	0.0059	0.0073	0.0043	0.0045	0.0062	0.0060	0.0074	0.0047
Gluc289 (M5)	0.0031	0.0038	0.0035	0.0032	0.0033	0.0031	0.0035	0.0033	0.0034	0.0032
Gluc290 (M6)	0.0059	0.0059	0.0055	0.0053	0.0059	0.0060	0.0057	0.0054	0.0055	0.0058
Gluc370 (M0)	0.6169	0.5707	0.5735	0.5380	0.6171	0.6184	0.5728	0.5719	0.5360	0.6063
Gluc371 (M1)	0.2172	0.2216	0.2243	0.2315	0.2220	0.2177	0.2236	0.2249	0.2320	0.2252
Gluc372 (M2)	0.1195	0.1421	0.1404	0.1549	0.1175	0.1186	0.1410	0.1407	0.1561	0.1218
Gluc373 (M3)	0.0355	0.0484	0.0457	0.0545	0.0332	0.0345	0.0466	0.0462	0.0548	0.0357
Gluc374 (M4)	0.0087	0.0131	0.0123	0.0159	0.0080	0.0085	0.0124	0.0125	0.0161	0.0086
Gluc375 (M5)	0.0019	0.0035	0.0032	0.0043	0.0017	0.0019	0.0031	0.0032	0.0043	0.0020
Gluc376 (M6)	0.0003	0.0005	0.0005	0.0006	0.0003	0.0003	0.0005	0.0005	0.0007	0.0003
Gluc377 (M7)	0.0001	0.0001	0.0001	0.0001	0.0001	0.0001	0.0001	0.0001	0.0001	0.0001

Table D.16 Mass isotopomer distributions of intracellular metabolites at [U-^{13}C]glycerol experiments (Flask #1 and #2). They were measured by MOX-TBDMS derivatization and GC-MS and used for MID analysis and flux estimation. (data not corrected for natural isotope abundances)

	Con	Dex	Dib	8Br	Ins	Con	Dex	Dib	8Br	Ins
	Flask #1	Flask #1	Flask #1	Flask #1	Flask #1	Flask #2	Flask #2	Flask #2	Flask #2	Flask #2
Pyr174 (M0)	0.8292	0.7711	0.8333	0.8400	0.8313	0.8340	0.7810	0.8365	0.8425	0.8270
Pyr175 (M1)	0.1082	0.1093	0.1080	0.1116	0.1059	0.1072	0.1079	0.1063	0.1097	0.1087
Pyr176 (M2)	0.0427	0.0446	0.0407	0.0404	0.0407	0.0403	0.0427	0.0400	0.0402	0.0410
Pyr177 (M3)	0.0170	0.0659	0.0158	0.0070	0.0195	0.0163	0.0603	0.0151	0.0068	0.0205
Pyr178 (M4)	0.0019	0.0063	0.0016	0.0007	0.0019	0.0016	0.0056	0.0015	0.0007	0.0020
Pyr179 (M5)	0.0010	0.0029	0.0006	0.0003	0.0008	0.0006	0.0025	0.0006	0.0002	0.0008
Lact233 (M0)	0.7601	0.7593	0.7595	0.7603	0.7584	0.7603	0.7593	0.7602	0.7604	0.7586
Lact234 (M1)	0.1604	0.1606	0.1606	0.1604	0.1606	0.1603	0.1607	0.1606	0.1604	0.1612
Lact235 (M2)	0.0682	0.0686	0.0685	0.0680	0.0693	0.0680	0.0686	0.0678	0.0680	0.0687
Lact236 (M3)	0.0096	0.0097	0.0096	0.0096	0.0098	0.0096	0.0097	0.0096	0.0095	0.0098
Lact237 (M4)	0.0018	0.0018	0.0018	0.0017	0.0019	0.0018	0.0018	0.0017	0.0017	0.0018
Lact261 (M0)	0.7503	0.7493	0.7495	0.7507	0.7486	0.7502	0.7487	0.7496	0.7499	0.7483
Lact262 (M1)	0.1665	0.1662	0.1665	0.1664	0.1664	0.1665	0.1671	0.1669	0.1667	0.1669
Lact263 (M2)	0.0699	0.0707	0.0705	0.0699	0.0709	0.0700	0.0702	0.0699	0.0703	0.0703
Lact264 (M3)	0.0110	0.0114	0.0112	0.0107	0.0116	0.0110	0.0116	0.0112	0.0108	0.0119
Lact265 (M4)	0.0021	0.0021	0.0021	0.0020	0.0022	0.0021	0.0021	0.0021	0.0020	0.0022
Lact266 (M5)	0.0003	0.0003	0.0003	0.0002	0.0003	0.0003	0.0003	0.0003	0.0002	0.0003
Ala232 (M0)	0.7564	0.7560	0.7557	0.7560	0.7542	0.7556	0.7551	0.7478	0.7561	0.7546
Ala233 (M1)	0.1646	0.1649	0.1651	0.1647	0.1653	0.1648	0.1648	0.1635	0.1647	0.1649
Ala234 (M2)	0.0676	0.0676	0.0677	0.0679	0.0688	0.0682	0.0685	0.0751	0.0678	0.0689
Ala235 (M3)	0.0097	0.0097	0.0097	0.0097	0.0100	0.0098	0.0099	0.0112	0.0097	0.0099
Ala236 (M4)	0.0017	0.0017	0.0017	0.0017	0.0018	0.0017	0.0017	0.0023	0.0017	0.0017
Ala260 (M0)	0.7492	0.7483	0.7486	0.7495	0.7471	0.7488	0.7476	0.7408	0.7490	0.7465
Ala261 (M1)	0.1688	0.1686	0.1687	0.1686	0.1688	0.1687	0.1691	0.1675	0.1691	0.1695
Ala262 (M2)	0.0690	0.0698	0.0694	0.0693	0.0703	0.0695	0.0699	0.0691	0.0692	0.0701
Ala263 (M3)	0.0109	0.0111	0.0110	0.0106	0.0115	0.0109	0.0112	0.0183	0.0106	0.0115
Ala264 (M4)	0.0019	0.0020	0.0019	0.0018	0.0020	0.0019	0.0020	0.0033	0.0018	0.0020
Ala265 (M5)	0.0003	0.0003	0.0003	0.0002	0.0003	0.0002	0.0003	0.0009	0.0002	0.0003
Gly218 (M0)	0.6533	0.6646	0.6607	0.7189	0.5997	0.6485	0.6655	0.6607	0.7195	0.5996
Gly219 (M1)	0.2506	0.2414	0.2449	0.1969	0.2943	0.2543	0.2402	0.2440	0.1964	0.2940
Gly220 (M2)	0.0787	0.0774	0.0776	0.0716	0.0846	0.0794	0.0777	0.0783	0.0716	0.0850
Gly221 (M3)	0.0174	0.0166	0.0168	0.0126	0.0214	0.0178	0.0166	0.0170	0.0125	0.0214

Table D.16 continued

Gly246 (M0)	0.6452	0.6571	0.6533	0.7094	0.5927	0.6404	0.6559	0.6505	0.7097	0.5874
Gly247 (M1)	0.1421	0.1459	0.1451	0.1554	0.1373	0.1414	0.1461	0.1448	0.1551	0.1372
Gly248 (M2)	0.1714	0.1592	0.1627	0.1113	0.2157	0.1757	0.1600	0.1651	0.1112	0.2198
Gly249 (M3)	0.0302	0.0278	0.0286	0.0184	0.0392	0.0311	0.0281	0.0291	0.0183	0.0402
Gly250 (M4)	0.0111	0.0099	0.0103	0.0056	0.0151	0.0115	0.0100	0.0106	0.0056	0.0154
Pro258 (M0)	0.7383	0.7377	0.7377	0.7390	0.7329	0.7378	0.7377	0.7219	0.7394	0.7317
Pro259 (M1)	0.1781	0.1779	0.1780	0.1776	0.1791	0.1781	0.1783	0.1746	0.1779	0.1797
Pro260 (M2)	0.0698	0.0706	0.0706	0.0695	0.0733	0.0702	0.0703	0.0686	0.0693	0.0735
Pro261 (M3)	0.0111	0.0112	0.0112	0.0109	0.0119	0.0112	0.0112	0.0125	0.0109	0.0121
Pro262 (M4)	0.0023	0.0022	0.0022	0.0024	0.0024	0.0023	0.0021	0.0176	0.0022	0.0025
Pro263 (M5)	0.0003	0.0003	0.0003	0.0004	0.0003	0.0003	0.0003	0.0033	0.0003	0.0003
Pro264 (M6)	0.0001	0.0001	0.0001	0.0001	0.0001	0.0001	0.0001	0.0013	0.0001	0.0001
Pro286 (M0)	0.7305	0.7309	0.7308	0.7318	0.7251	0.7302	0.7299	0.7145	0.7322	0.7237
Pro287 (M1)	0.1815	0.1813	0.1814	0.1816	0.1826	0.1818	0.1819	0.1782	0.1817	0.1828
Pro288 (M2)	0.0720	0.0723	0.0723	0.0718	0.0749	0.0724	0.0725	0.0709	0.0714	0.0755
Pro289 (M3)	0.0121	0.0122	0.0123	0.0117	0.0139	0.0122	0.0124	0.0122	0.0118	0.0143
Pro290 (M4)	0.0032	0.0026	0.0026	0.0024	0.0029	0.0025	0.0024	0.0044	0.0023	0.0030
Pro291 (M5)	0.0005	0.0004	0.0004	0.0004	0.0004	0.0004	0.0004	0.0153	0.0004	0.0005
Pro292 (M6)	0.0002	0.0002	0.0002	0.0002	0.0001	0.0003	0.0004	0.0032	0.0001	0.0001
Pro293 (M7)	0.0001	0.0001	0.0001	0.0001	0.0001	0.0001	0.0001	0.0013	0.0001	0.0001
Suc289 (M0)	0.7332	0.7315	0.7333	0.7379	0.7260	0.7344	0.7316	0.7289	0.7374	0.7256
Suc290 (M1)	0.1740	0.1744	0.1744	0.1732	0.1763	0.1740	0.1745	0.1719	0.1735	0.1765
Suc291 (M2)	0.0758	0.0772	0.0762	0.0737	0.0803	0.0755	0.0773	0.0745	0.0738	0.0801
Suc292 (M3)	0.0122	0.0126	0.0123	0.0117	0.0135	0.0123	0.0127	0.0132	0.0117	0.0135
Suc293 (M4)	0.0024	0.0025	0.0024	0.0022	0.0029	0.0024	0.0026	0.0087	0.0022	0.0029
Suc294 (M5)	0.0021	0.0015	0.0011	0.0011	0.0008	0.0011	0.0011	0.0022	0.0012	0.0011
Suc295 (M6)	0.0004	0.0003	0.0003	0.0002	0.0002	0.0003	0.0002	0.0007	0.0003	0.0002
Fum287 (M0)	0.7265	0.7241	0.7262	0.7324	0.7152	0.7279	0.7256	0.6330	0.7317	0.7190
Fum288 (M1)	0.1784	0.1779	0.1780	0.1764	0.1797	0.1776	0.1779	0.1618	0.1773	0.1794
Fum289 (M2)	0.0769	0.0783	0.0773	0.0750	0.0817	0.0761	0.0776	0.1575	0.0748	0.0804
Fum290 (M3)	0.0146	0.0157	0.0149	0.0130	0.0184	0.0147	0.0150	0.0341	0.0130	0.0167
Fum291 (M4)	0.0030	0.0033	0.0030	0.0026	0.0041	0.0030	0.0032	0.0115	0.0026	0.0037
Fum292 (M5)	0.0005	0.0006	0.0005	0.0005	0.0008	0.0005	0.0005	0.0018	0.0005	0.0007
Fum293 (M6)	0.0001	0.0001	0.0001	0.0001	0.0001	0.0001	0.0001	0.0003	0.0001	0.0002
Ser302 (M0)	0.6076	0.6256	0.6201	0.6786	0.5477	0.6053	0.6244	0.6136	0.6786	0.5379
Ser303 (M1)	0.1656	0.1693	0.1678	0.1796	0.1580	0.1637	0.1687	0.1666	0.1800	0.1564
Ser304 (M2)	0.1856	0.1683	0.1739	0.1178	0.2391	0.1891	0.1698	0.1799	0.1175	0.2489
Ser305 (M3)	0.0413	0.0368	0.0382	0.0240	0.0551	0.0420	0.0371	0.0399	0.0240	0.0568

Table D.16 continued

Ser306 (M4)	0.0000	0.0000	0.0000	0.0000	0.0000	0.0000	0.0000	0.0000	0.0000	0.0000
Ser362 (M0)	0.4736	0.5042	0.4939	0.5850	0.4015	0.4707	0.5021	0.4966	0.5847	0.3918
Ser363 (M1)	0.2948	0.2833	0.2867	0.2538	0.2994	0.2936	0.2848	0.2760	0.2542	0.2967
Ser364 (M2)	0.1763	0.1631	0.1680	0.1268	0.2262	0.1797	0.1635	0.1745	0.1268	0.2358
Ser365 (M3)	0.0552	0.0495	0.0515	0.0343	0.0729	0.0560	0.0497	0.0528	0.0343	0.0756
Ser366 (M4)	0.0000	0.0000	0.0000	0.0000	0.0000	0.0000	0.0000	0.0000	0.0000	0.0000
Ser390 (M0)	0.4578	0.4900	0.4825	0.5700	0.3830	0.4518	0.4812	0.4740	0.5665	0.3702
Ser391 (M1)	0.2383	0.2349	0.2363	0.2305	0.2346	0.2374	0.2347	0.2289	0.2305	0.2309
Ser392 (M2)	0.1554	0.1488	0.1492	0.1281	0.1598	0.1550	0.1515	0.1465	0.1296	0.1593
Ser393 (M3)	0.1041	0.0891	0.0929	0.0517	0.1548	0.1092	0.0933	0.1057	0.0530	0.1667
Ser394 (M4)	0.0328	0.0278	0.0291	0.0153	0.0489	0.0343	0.0293	0.0330	0.0157	0.0526
Ser395 (M5)	0.0116	0.0095	0.0101	0.0045	0.0188	0.0123	0.0101	0.0120	0.0045	0.0203
AKG346 (M0)	0.7117	0.7094	0.7104	0.7160	0.7000	0.7129	0.7084	0.7118	0.7161	0.7009
AKG347 (M1)	0.1882	0.1868	0.1880	0.1875	0.1888	0.1873	0.1874	0.1877	0.1876	0.1894
AKG348 (M2)	0.0807	0.0825	0.0815	0.0790	0.0864	0.0806	0.0830	0.0809	0.0788	0.0854
AKG349 (M3)	0.0156	0.0165	0.0160	0.0140	0.0194	0.0154	0.0165	0.0155	0.0140	0.0190
AKG350 (M4)	0.0032	0.0035	0.0032	0.0027	0.0042	0.0031	0.0035	0.0031	0.0027	0.0042
AKG351 (M5)	0.0005	0.0008	0.0006	0.0005	0.0008	0.0005	0.0007	0.0006	0.0005	0.0008
AKG352 (M6)	0.0001	0.0002	0.0001	0.0001	0.0002	0.0001	0.0002	0.0001	0.0001	0.0001
AKG353 (M7)	0.0001	0.0003	0.0002	0.0001	0.0001	0.0001	0.0002	0.0001	0.0002	0.0001
Mal391 (M0)	0.6408	0.6418	0.6416	0.6458	0.6344	0.6420	0.6400	0.6422	0.6455	0.6344
Mal392 (M1)	0.2201	0.2187	0.2201	0.2182	0.2207	0.2188	0.2203	0.2194	0.2192	0.2222
Mal393 (M2)	0.1051	0.1058	0.1045	0.1024	0.1084	0.1051	0.1057	0.1046	0.1030	0.1076
Mal394 (M3)	0.0248	0.0247	0.0244	0.0232	0.0269	0.0250	0.0247	0.0245	0.0232	0.0267
Mal395 (M4)	0.0061	0.0065	0.0063	0.0059	0.0069	0.0062	0.0062	0.0060	0.0058	0.0068
Mal396 (M5)	0.0032	0.0026	0.0030	0.0046	0.0028	0.0029	0.0031	0.0033	0.0033	0.0023
Mal419 (M0)	0.6317	0.6305	0.6318	0.6359	0.6232	0.6331	0.6308	0.6335	0.6359	0.6260
Mal420 (M1)	0.2241	0.2227	0.2235	0.2234	0.2234	0.2231	0.2235	0.2232	0.2239	0.2239
Mal421 (M2)	0.1081	0.1090	0.1081	0.1066	0.1119	0.1074	0.1087	0.1078	0.1063	0.1105
Mal422 (M3)	0.0272	0.0280	0.0273	0.0256	0.0305	0.0272	0.0275	0.0269	0.0255	0.0293
Mal423 (M4)	0.0069	0.0072	0.0069	0.0063	0.0082	0.0069	0.0070	0.0067	0.0062	0.0077
Mal424 (M5)	0.0013	0.0014	0.0013	0.0011	0.0018	0.0013	0.0014	0.0012	0.0011	0.0016
Mal425 (M6)	0.0007	0.0013	0.0010	0.0011	0.0011	0.0010	0.0011	0.0008	0.0012	0.0010
Asp390 (M0)	0.6292	0.6350	0.6374	0.6412	0.6318	0.6380	0.6363	0.6214	0.6411	0.6318
Asp391 (M1)	0.2303	0.2257	0.2246	0.2239	0.2252	0.2245	0.2253	0.2182	0.2241	0.2261
Asp392 (M2)	0.1068	0.1059	0.1054	0.1039	0.1078	0.1051	0.1058	0.1034	0.1039	0.1076
Asp393 (M3)	0.0263	0.0258	0.0254	0.0243	0.0272	0.0252	0.0254	0.0416	0.0242	0.0266
Asp394 (M4)	0.0063	0.0064	0.0061	0.0058	0.0068	0.0061	0.0062	0.0116	0.0057	0.0066

Table D.16 continued

Asp395 (M5)	0.0011	0.0012	0.0011	0.0010	0.0013	0.0011	0.0011	0.0039	0.0010	0.0012
Asp418 (M0)	0.6232	0.6250	0.6295	0.6310	0.6232	0.6297	0.6292	0.6142	0.6339	0.6232
Asp419 (M1)	0.2288	0.2265	0.2262	0.2260	0.2255	0.2257	0.2256	0.2200	0.2255	0.2265
Asp420 (M2)	0.1108	0.1107	0.1084	0.1085	0.1112	0.1087	0.1092	0.1058	0.1069	0.1114
Asp421 (M3)	0.0283	0.0286	0.0274	0.0264	0.0301	0.0274	0.0274	0.0279	0.0260	0.0293
Asp422 (M4)	0.0072	0.0075	0.0069	0.0066	0.0080	0.0070	0.0070	0.0227	0.0064	0.0077
Asp423 (M5)	0.0014	0.0015	0.0013	0.0012	0.0017	0.0013	0.0013	0.0065	0.0011	0.0016
Asp424 (M6)	0.0003	0.0003	0.0003	0.0002	0.0003	0.0003	0.0003	0.0029	0.0002	0.0003
PEP453 (M0)	0.4272	0.4836	0.4724	0.5865	0.3095	0.4208	0.4700	0.5019	0.5837	0.2855
PEP454 (M1)	0.1491	0.1795	0.1643	0.2015	0.1177	0.1474	0.1743	0.1747	0.2015	0.1081
PEP455 (M2)	0.0771	0.0983	0.0850	0.1004	0.0704	0.0765	0.0947	0.0883	0.0997	0.0644
PEP456 (M3)	0.2385	0.1650	0.1921	0.0789	0.3446	0.2445	0.1802	0.1627	0.0811	0.3707
PEP457 (M4)	0.0726	0.0502	0.0582	0.0229	0.1059	0.0745	0.0552	0.0493	0.0235	0.1147
PEP458 (M5)	0.0354	0.0234	0.0280	0.0099	0.0519	0.0364	0.0257	0.0232	0.0105	0.0566
Glu432 (M0)	0.6218	0.6233	0.6233	0.6279	0.6125	0.6254	0.6212	0.6187	0.6283	0.6119
Glu433 (M1)	0.2311	0.2279	0.2293	0.2296	0.2292	0.2294	0.2288	0.2288	0.2298	0.2301
Glu434 (M2)	0.1102	0.1103	0.1099	0.1079	0.1144	0.1089	0.1114	0.1100	0.1076	0.1149
Glu435 (M3)	0.0281	0.0291	0.0284	0.0266	0.0326	0.0277	0.0291	0.0280	0.0264	0.0320
Gln435 (M4)	0.0070	0.0075	0.0072	0.0065	0.0088	0.0069	0.0075	0.0075	0.0064	0.0086
Gln436 (M5)	0.0014	0.0015	0.0014	0.0012	0.0020	0.0013	0.0015	0.0050	0.0012	0.0019
Gln437 (M6)	0.0002	0.0003	0.0003	0.0002	0.0004	0.0003	0.0003	0.0014	0.0002	0.0004
Gln438 (M7)	0.0001	0.0001	0.0001	0.0001	0.0001	0.0001	0.0001	0.0006	0.0001	0.0001
DHAP484 (M0)	0.3786	0.4527	0.4382	0.5560	0.2634	0.3713	0.4224	0.4238	0.5641	0.2529
DHAP485 (M1)	0.1575	0.1859	0.1673	0.2135	0.1180	0.1516	0.1874	0.1656	0.2080	0.1031
DHAP486 (M2)	0.0765	0.1034	0.0828	0.1007	0.0682	0.0740	0.1002	0.0803	0.0983	0.0614
DHAP487 (M3)	0.2596	0.1771	0.2129	0.0886	0.3700	0.2706	0.1917	0.2223	0.0891	0.3945
DHAP488 (M4)	0.0883	0.0564	0.0683	0.0293	0.1241	0.0918	0.0689	0.0749	0.0289	0.1287
DHAP489 (M5)	0.0394	0.0245	0.0305	0.0120	0.0562	0.0408	0.0295	0.0331	0.0116	0.0594
Gln431 (M0)	0.6280	0.6292	0.6290	0.6297	0.6290	0.6289	0.6303	0.6264	0.6288	0.6300
Gln432 (M1)	0.2322	0.2320	0.2325	0.2316	0.2321	0.2321	0.2305	0.2307	0.2320	0.2311
Gln433 (M2)	0.1066	0.1059	0.1057	0.1058	0.1061	0.1063	0.1063	0.1057	0.1062	0.1060
Gln434 (M3)	0.0258	0.0256	0.0256	0.0255	0.0255	0.0255	0.0256	0.0254	0.0257	0.0256
Gln435 (M4)	0.0061	0.0060	0.0060	0.0060	0.0060	0.0059	0.0060	0.0061	0.0060	0.0060
Gln436 (M5)	0.0010	0.0010	0.0010	0.0011	0.0010	0.0010	0.0011	0.0040	0.0011	0.0010
Gln437 (M6)	0.0002	0.0002	0.0002	0.0002	0.0002	0.0002	0.0002	0.0011	0.0002	0.0002
Gln438 (M7)	0.0001	0.0001	0.0001	0.0001	0.0001	0.0001	0.0001	0.0005	0.0001	0.0001
GLP571 (M0)	0.4183	0.4342	0.4301	0.4968	0.3465	0.4178	0.4313	0.4350	0.4969	0.3434
GLP572 (M1)	0.1921	0.2006	0.1983	0.2283	0.1646	0.1924	0.1993	0.2007	0.2285	0.1623

Table D.16 continued

GLP573 (M2)	0.1053	0.1113	0.1091	0.1239	0.0952	0.1054	0.1102	0.1100	0.1236	0.0935
GLP574 (M3)	0.1773	0.1590	0.1644	0.0979	0.2427	0.1774	0.1622	0.1595	0.0980	0.2467
GLP575 (M4)	0.0714	0.0636	0.0658	0.0369	0.1000	0.0715	0.0651	0.0637	0.0368	0.1018
GLP576 (M5)	0.0355	0.0312	0.0324	0.0163	0.0510	0.0356	0.0320	0.0312	0.0163	0.0522
Cit459 (M0)	0.6157	0.6101	0.6127	0.6171	0.6046	0.6152	0.6090	0.5925	0.6172	0.6047
Cit460 (M1)	0.2305	0.2292	0.2308	0.2313	0.2308	0.2314	0.2311	0.2244	0.2318	0.2323
Cit461 (M2)	0.1131	0.1146	0.1143	0.1119	0.1175	0.1126	0.1140	0.1096	0.1117	0.1167
Cit462 (M3)	0.0299	0.0312	0.0304	0.0287	0.0339	0.0300	0.0308	0.0496	0.0285	0.0333
Cit463 (M4)	0.0080	0.0085	0.0082	0.0075	0.0095	0.0079	0.0084	0.0153	0.0075	0.0094
Cit464 (M5)	0.0017	0.0018	0.0017	0.0015	0.0022	0.0017	0.0019	0.0053	0.0015	0.0022
Cit465 (M6)	0.0004	0.0005	0.0004	0.0003	0.0005	0.0004	0.0005	0.0014	0.0004	0.0005
Cit466 (M7)	0.0003	0.0006	0.0005	0.0005	0.0004	0.0004	0.0006	0.0008	0.0005	0.0005
Cit467 (M8)	0.0004	0.0036	0.0009	0.0012	0.0004	0.0005	0.0037	0.0010	0.0010	0.0005
3PG585 (M0)	0.3641	0.4080	0.3960	0.4991	0.2542	0.3488	0.3995	0.4224	0.4957	0.2354
3PG586 (M1)	0.1693	0.2013	0.1851	0.2307	0.1277	0.1640	0.1965	0.1966	0.2303	0.1184
3PG587 (M2)	0.0971	0.1202	0.1056	0.1281	0.0834	0.0947	0.1166	0.1100	0.1273	0.0771
3PG588 (M3)	0.2265	0.1687	0.1927	0.0907	0.3227	0.2362	0.1781	0.1676	0.0925	0.3394
3PG589 (M4)	0.0947	0.0683	0.0796	0.0351	0.1378	0.1010	0.0728	0.0684	0.0364	0.1472
3PG585 (M5)	0.0483	0.0335	0.0410	0.0164	0.0742	0.0553	0.0365	0.0350	0.0179	0.0824

Duplicate experiments at each condition were analyzed by MOX-TBDMS derivatization and GC-MS. The measurement error of mass isotopomer distribution by MS analysis was less than 0.2 mo%.

Table D.17 Mass isotopomer distributions of intracellular metabolite, G6P/Glucose and F6P at [U-^{13}C]glycerol experiments (Flask #3). They were measured by dephosphorylation, MOX-TMS derivatization and GC-MS and used for MID analysis and flux estimation. (data not corrected for natural isotope abundances)

	Con	Dex	Dib	8Br	Ins
Isotopomer	Flask #3	Flask #3	Flask #3	Flask #3	Flask #3
G6P217 (M0)	0.4778	0.6704	0.5194	0.6368	0.4067
G6P218 (M1)	0.1567	0.1480	0.1587	0.1582	0.1475
G6P219 (M2)	0.1037	0.0719	0.0974	0.0785	0.1191
G6P220 (M3)	0.1503	0.0122	0.1247	0.0479	0.1854
G6P221 (M4)	0.0847	0.0797	0.0759	0.0610	0.1009
G6P222 (M5)	0.0269	0.0179	0.0240	0.0176	0.0403
G6P205 (M0)	0.5533	0.7357	0.5851	0.6885	0.4872
G6P206 (M1)	0.1674	0.1557	0.1564	0.1539	0.1472
G6P207 (M2)	0.2225	0.0872	0.2069	0.1272	0.2838
G6P208 (M3)	0.0404	0.0163	0.0361	0.0220	0.0580
G6P209 (M4)	0.0164	0.0051	0.0155	0.0084	0.0239
G6P319 (M0)	0.4005	0.5178	0.4399	0.5899	0.3617
G6P320 (M1)	0.2207	0.2197	0.2255	0.2161	0.1996
G6P321 (M2)	0.0922	0.0977	0.0951	0.0981	0.0870
G6P322 (M3)	0.1440	0.0938	0.1308	0.0639	0.1539
G6P323 (M4)	0.0982	0.0486	0.0743	0.0220	0.1400
G6P324 (M5)	0.0324	0.0167	0.0257	0.0079	0.0427
G6P325 (M6)	0.0120	0.0057	0.0087	0.0021	0.0151
F6P307 (M0)	0.4839	0.5027	0.5134	0.6264	0.3739
F6P308 (M1)	0.1464	0.1616	0.1516	0.1816	0.1207
F6P309 (M2)	0.0790	0.0928	0.0800	0.0930	0.0708
F6P310 (M3)	0.2102	0.1758	0.1847	0.0715	0.3089
F6P311 (M4)	0.0537	0.0454	0.0470	0.0190	0.0798
F6P312 (M5)	0.0267	0.0218	0.0233	0.0084	0.0460
F6P364 (M0)	0.3071	0.3253	0.3399	0.5024	0.2137
F6P365 (M1)	0.2324	0.2536	0.2461	0.2347	0.2003
F6P366 (M2)	0.1653	0.1613	0.1526	0.1225	0.1581
F6P367 (M3)	0.1390	0.1302	0.1273	0.0533	0.1663
F6P368 (M4)	0.0846	0.0640	0.0676	0.0188	0.1471
F6P369 (M5)	0.0321	0.0280	0.0295	0.0172	0.0544
F6P370 (M6)	0.0395	0.0376	0.0370	0.0511	0.0601

G6P fragments were mixtures with intracellular G6P and glucose. (SD, < 0.2 mol%)

Table D.18 Mass isotopomer distributions of media glucose and glycerol for [U-^{13}C]glycerol experiments (Flask #1). They were measured by aldonitrile pentapropionate and di-O-isopropylidene propionate derivatization and GC-MS. (data not corrected for natural isotope abundances)

	Con	Dex	Dib	8Br	Ins
Isotopomer	Flask #1	Flask #1	Flask #1	Flask #1	Flask #1
Glyc173 (M0)	0.0893	0.1219	0.1204	0.1011	0.0516
Glyc174 (M1)	0.0145	0.0173	0.0171	0.0151	0.0128
Glyc175 (M2)	0.8300	0.7971	0.7991	0.8183	0.8526
Glyc176 (M3)	0.0575	0.0552	0.0550	0.0567	0.0710
Glyc177 (M4)	0.0089	0.0086	0.0085	0.0089	0.0120
Gluc173 (M0)	0.6174	0.6790	0.6640	0.7979	0.4803
Gluc174 (M1)	0.0653	0.0696	0.0685	0.0769	0.0598
Gluc175 (M2)	0.2916	0.2311	0.2459	0.1143	0.4216
Gluc176 (M3)	0.0208	0.0166	0.0175	0.0083	0.0310
Gluc177 (M4)	0.0049	0.0037	0.0040	0.0025	0.0074
Gluc259 (M0)	0.6006	0.6538	0.6392	0.7624	0.4931
Gluc260 (M1)	0.0921	0.0960	0.0947	0.1068	0.0818
Gluc261 (M2)	0.0228	0.0244	0.0237	0.0215	0.0265
Gluc262 (M3)	0.2521	0.2007	0.2154	0.0965	0.3536
Gluc263 (M4)	0.0273	0.0212	0.0230	0.0108	0.0376
Gluc264 (M5)	0.0052	0.0039	0.0040	0.0021	0.0074
Gluc284 (M0)	0.3268	0.3957	0.3752	0.5890	0.2279
Gluc285 (M1)	0.2977	0.2997	0.3008	0.2528	0.2709
Gluc286 (M2)	0.1965	0.1718	0.1805	0.1019	0.2364
Gluc287 (M3)	0.1240	0.0960	0.1029	0.0396	0.1687
Gluc288 (M4)	0.0444	0.0279	0.0316	0.0087	0.0808
Gluc289 (M5)	0.0067	0.0050	0.0053	0.0033	0.0110
Gluc290 (M6)	0.0039	0.0039	0.0037	0.0048	0.0043
Gluc370 (M0)	0.2896	0.3611	0.3384	0.5567	0.1799
Gluc371 (M1)	0.1814	0.1964	0.1957	0.2023	0.1440
Gluc372 (M2)	0.2426	0.2309	0.2371	0.1576	0.2322
Gluc373 (M3)	0.1597	0.1298	0.1379	0.0585	0.2080
Gluc374 (M4)	0.0740	0.0517	0.0569	0.0174	0.1293
Gluc375 (M5)	0.0445	0.0254	0.0288	0.0060	0.0905
Gluc376 (M6)	0.0069	0.0040	0.0044	0.0012	0.0137
Gluc377 (M7)	0.0014	0.0008	0.0009	0.0004	0.0023
Gluc301 (M0)	0.3015	0.3663	0.3423	0.5780	0.1916

Table D.18 continued

Gluc302 (M1)	0.1784	0.1928	0.1905	0.1877	0.1429
Gluc303 (M2)	0.1268	0.1251	0.1280	0.0866	0.1189
Gluc304 (M3)	0.2044	0.1848	0.1903	0.1046	0.2097
Gluc305 (M4)	0.0872	0.0685	0.0750	0.0269	0.1360
Gluc306 (M5)	0.0583	0.0395	0.0453	0.0115	0.1091
Gluc307 (M6)	0.0379	0.0206	0.0256	0.0042	0.0806
Gluc308 (M7)	0.0041	0.0020	0.0024	0.0004	0.0087
Gluc309 (M8)	0.0012	0.0003	0.0004	0.0001	0.0023

Glycerol and glucose mass fragments were derivatized by aldonitrile pentapropionate method and only Gluc301 fragments was analyzed by di-O-isopropylidene propionate method.

Table D.19 Mass isotopomer distributions of media glucose and glycerol for [U-^{13}C]glycerol experiments (Flask #2 and #3). They were measured by aldonitrile pentapropionate and di-O-isopropylidene propionate derivatization and GC-MS. (data not corrected for natural isotope abundances)

Isotopomer	Con Flask #2	Dex Flask #2	Dib Flask #2	8Br Flask #2	Ins Flask #2	Con Flask #3	Dex Flask #3	Dib Flask #3	8Br Flask #3	Ins Flask #3
Glyc173 (M0)	0.0898	0.1191	0.1165	0.1033	0.0516	0.0968	0.1141	0.1148	0.1061	0.0527
Glyc174 (M1)	0.0145	0.0172	0.0168	0.0152	0.0129	0.0152	0.0169	0.0168	0.0153	0.0128
Glyc175 (M2)	0.8295	0.8000	0.8032	0.8161	0.8545	0.8219	0.8050	0.8046	0.8133	0.8536
Glyc176 (M3)	0.0574	0.0552	0.0551	0.0566	0.0693	0.0572	0.0556	0.0553	0.0565	0.0691
Glyc177 (M4)	0.0089	0.0085	0.0085	0.0089	0.0116	0.0089	0.0086	0.0086	0.0089	0.0116
Gluc173 (M0)	0.6194	0.6753	0.6732	0.7982	0.4495	0.6186	0.6814	0.6683	0.7986	0.4814
Gluc174 (M1)	0.0651	0.0695	0.0691	0.0765	0.0599	0.0647	0.0700	0.0689	0.0763	0.0591
Gluc175 (M2)	0.2899	0.2349	0.2370	0.1142	0.4502	0.2899	0.2288	0.2416	0.1142	0.4209
Gluc176 (M3)	0.0207	0.0168	0.0169	0.0084	0.0326	0.0210	0.0163	0.0171	0.0084	0.0302
Gluc177 (M4)	0.0049	0.0036	0.0038	0.0026	0.0079	0.0058	0.0035	0.0041	0.0025	0.0084
Gluc259 (M0)	0.6015	0.6479	0.6444	0.7631	0.4690	0.6000	0.6566	0.6391	0.7629	0.4919
Gluc260 (M1)	0.0903	0.0956	0.0953	0.1071	0.0817	0.0904	0.0958	0.0946	0.1066	0.0829
Gluc261 (M2)	0.0233	0.0246	0.0238	0.0214	0.0284	0.0234	0.0240	0.0241	0.0213	0.0275
Gluc262 (M3)	0.2532	0.2058	0.2102	0.0955	0.3711	0.2542	0.1988	0.2152	0.0963	0.3503
Gluc263 (M4)	0.0268	0.0220	0.0223	0.0108	0.0407	0.0270	0.0210	0.0228	0.0108	0.0389
Gluc264 (M5)	0.0050	0.0041	0.0040	0.0021	0.0092	0.0050	0.0038	0.0041	0.0021	0.0085
Gluc284 (M0)	0.3309	0.3910	0.3843	0.5908	0.2090	0.3286	0.4018	0.3774	0.5907	0.2286
Gluc285 (M1)	0.2964	0.2991	0.2982	0.2508	0.2687	0.2985	0.2960	0.2978	0.2511	0.2740
Gluc286 (M2)	0.1956	0.1735	0.1761	0.1010	0.2412	0.1977	0.1696	0.1784	0.1008	0.2343
Gluc287 (M3)	0.1223	0.0981	0.1013	0.0402	0.1758	0.1217	0.0953	0.1043	0.0403	0.1662
Gluc288 (M4)	0.0442	0.0291	0.0308	0.0089	0.0882	0.0431	0.0282	0.0324	0.0089	0.0798
Gluc289 (M5)	0.0067	0.0052	0.0054	0.0034	0.0122	0.0066	0.0051	0.0056	0.0033	0.0116
Gluc290 (M6)	0.0040	0.0040	0.0040	0.0050	0.0049	0.0038	0.0040	0.0041	0.0049	0.0054
Gluc370 (M0)	0.2920	0.3536	0.3512	0.5616	0.1557	0.2905	0.3673	0.3483	0.5571	0.1771
Gluc371 (M1)	0.1815	0.1949	0.1953	0.2009	0.1385	0.1833	0.1958	0.1941	0.2001	0.1462
Gluc372 (M2)	0.2398	0.2332	0.2331	0.1550	0.2342	0.2427	0.2288	0.2316	0.1581	0.2372
Gluc373 (M3)	0.1589	0.1322	0.1337	0.0578	0.2151	0.1583	0.1270	0.1344	0.0594	0.2074
Gluc374 (M4)	0.0748	0.0541	0.0541	0.0171	0.1375	0.0732	0.0510	0.0562	0.0176	0.1273
Gluc375 (M5)	0.0446	0.0271	0.0276	0.0061	0.1010	0.0434	0.0254	0.0297	0.0062	0.0888
Gluc376 (M6)	0.0070	0.0041	0.0042	0.0012	0.0154	0.0071	0.0038	0.0046	0.0012	0.0136
Gluc377 (M7)	0.0013	0.0008	0.0008	0.0003	0.0026	0.0015	0.0008	0.0010	0.0004	0.0025

Table D.19 continued

Gluc301 (M0)	0.3031	0.3586	0.3566	0.5747	0.1652	0.3022	0.3708	0.3484	0.5747	0.1943
Gluc302 (M1)	0.1770	0.1912	0.1885	0.1899	0.1352	0.1795	0.1906	0.1870	0.1897	0.1438
Gluc303 (M2)	0.1260	0.1263	0.1252	0.0878	0.1172	0.1274	0.1231	0.1261	0.0871	0.1205
Gluc304 (M3)	0.2002	0.1852	0.1875	0.1046	0.2124	0.2000	0.1821	0.1891	0.1051	0.2060
Gluc305 (M4)	0.0895	0.0706	0.0716	0.0270	0.1447	0.0894	0.0681	0.0741	0.0271	0.1349
Gluc306 (M5)	0.0606	0.0422	0.0434	0.0113	0.1201	0.0595	0.0406	0.0458	0.0115	0.1092
Gluc307 (M6)	0.0390	0.0233	0.0246	0.0041	0.0934	0.0376	0.0222	0.0265	0.0043	0.0815
Gluc308 (M7)	0.0038	0.0022	0.0023	0.0004	0.0095	0.0037	0.0021	0.0026	0.0004	0.0080
Gluc309 (M8)	0.0008	0.0004	0.0004	0.0001	0.0025	0.0007	0.0003	0.0004	0.0001	0.0018